PROCEEDINGS OF THE THIRTEENTH WORKSHOP ON GENERAL RELATIVITY AND GRAVITATION in JAPAN

Osaka City University Media Center, Osaka City University,

Sugimoto Campus, Osaka, Japan

December 1 – 4, 2003

Edited by

H. Ishihara, K. Nakao, N. Kanda, H. Nakano

T. Nakamura, K. Tomita

PREFACE

The thirteenth workshop on General Relativity and Gravitation in Japan was held at Osaka City University Media Center, Osaka City University located in the Sugimoto Campus from 1 to 4 December 2003. The main purpose of this workshop was to review the latest progress in the field of general relativity, gravitation, general relativistic astrophysics, and the detection of gravitational waves as well as to promote interaction between researchers working in these field.

The workshop was organized as an international conference and composed of 11 invited talks, and 78 contributed talks (oral presentation: 44 and poster presentation: 34). Among them, 9 were presented by the researcheres from overseas. The workshop was attended by about 150 researcheres. We appreciate very much all the participants for their contribution to the workshop.

We would like to thank Ms. K. Yokota, the secretary at the Department of Physics, Kyoto University, for her devoted transaction of various official works. We are also grateful to the members (E. Sakane, I. Tanaka, H. Kozaki, K. Ogawa, C. Yoo, K. Matsuno and S. Saito) of the research group for theoretical astrophysics and theory of gravity in the Department of Mathematics and Physics, Osaka City University for their cooperation in management of the workshop. Finally we appreciate very much the Osaka City University Media Center for providing a conference room without any charge. The workshop was financially supported by Monbukagakusho Grands for scientific researches, Nos. 12440063 (PI: K. Tomita) and 14047212 (PI: T. Nakamura).

H. Ishihara, N. Kanda, K. Nakao and H. Nakano July 2004

Organizing Committees

Table of Contents

Invited talks

Contributed talks

LIGO: S1 Science Results and Plans Beyond

B. Abbott,[13] R. Abbott,[16] R. Adhikari,[14] A. Ageev,[21,28] B. Allen,[40] R. Amin,[35] S. B. Anderson,[13] W. G. Anderson,[30] M. Araya,[13] H. Armandula,[13] F. Asiri,[13,a] P. Aufmuth,[32] C. Aulbert,[1] S. Babak,[7] R. Balasubramanian,[7] S. Ballmer,[14] B. C. Barish,[13] D. Barker,[15] C. Barker-Patton,[15] M. Barnes,[13] B. Barr,[36] M. A. Barton,[13] K. Bayer,[14] R. Beausoleil,[27,b] K. Belczynski,[24] R. Bennett,[36,c] S. J. Berukoff,[1,d] J. Betzwieser,[14] B. Bhawal,[13] I. A. Bilenko,[21] G. Billingsley,[13] E. Black,[13] K. Blackburn,[13] B. Bland-Weaver,[15] B. Bochner,[14,e] L. Bogue,[13] R. Bork,[13] S. Bose,[41] P. R. Brady,[40] V. B. Braginsky,[21] J. E. Brau,[38] D. A. Brown,[40] S. Brozek,[32,f] A. Bullington,[27] A. Buonanno,[6,g] R. Burgess,[14] D. Busby,[13] W. E. Butler,[39] R. L. Byer,[27] L. Cadonati,[14] G. Cagnoli,[36] J. B. Camp,[22] C. A. Cantley,[36] L. Cardenas,[13] K. Carter,[16] M. M. Casey,[36] J. Castiglione,[35] A. Chandler,[13] J. Chapsky,[13,h] P. Charlton,[13] S. Chatterji,[14] Y. Chen,[6] V. Chickarmane,[17] D. Chin,[37] N. Christensen,[8] D. Churches,[7] C. Colacino,[32,2] R. Coldwell,[35] M. Coles,[16,i] D. Cook,[15] T. Corbitt,[14] D. Coyne,[13] J. D. E. Creighton,[40] T. D. Creighton,[13] D. R. M. Crooks,[36] P. Csatorday,[14] B. J. Cusack,[3] C. Cutler,[1] E. D'Ambrosio,[13] K. Danzmann,[32,2,20] R. Davies,[7] E. Daw,[17,j] D. DeBra,[27] T. Delker,[35,k] R. DeSalvo,[13] S. Dhurandhar,[12] M. Díaz,[30] H. Ding,[13] R. W. P. Drever,[4] R. J. Dupuis,[36] C. Ebeling,[8] J. Edlund,[13] P. Ehrens,[13] E. J. Elliffe,[36] T. Etzel,[13] M. Evans,[13] T. Evans,[16] C. Fallnich,[32] D. Farnham,[13] M. M. Fejer,[27] M. Fine,[13] L. S. Finn,[29] É. Flanagan,[9] A. Freise,[2,1] R. Frey,[38] P. Fritschel,[14] V. Frolov,[16] M. Fyffe,[16] K. S. Ganezer,[5] J. A. Giaime,[17] A. Gillespie,[13,m] K. Goda,[14] G. González,[17] S. Goßler,[32] P. Grandclément,[24] A. Grant,[36] C. Gray,[15] A. M. Gretarsson,[16] D. Grimmett,[13] H. Grote,[2] S. Grunewald,[1] M. Guenther,[15] E. Gustafson,[27,n] R. Gustafson,[37] W. O. Hamilton,[17] M. Hammond,[16] J. Hanson,[16] C. Hardham,[27] G. Harry,[14] A. Hartunian,[13] J. Heefner,[13] Y. Hefetz,[14] G. Heinzel,[2] I. S. Heng,[32] M. Hennessy,[27] N. Hepler,[29] A. Heptonstall,[36] M. Heurs,[32] M. Hewitson,[36] N. Hindman,[15] P. Hoang,[13] J. Hough,[36] M. Hrynevych,[13,o] W. Hua,[27] R. Ingley,[34] M. Ito,[38] Y. Itoh,[1] A. Ivanov,[13] O. Jennrich,[36,p] W. W. Johnson,[17] W. Johnston,[30] L. Jones,[13] D. Jungwirth,[13,q] V. Kalogera,[24] E. Katsavounidis,[14] K. Kawabe,[20,2] S. Kawamura,[23] W. Kells,[13] J. Kern,[16] A. Khan,[16] S. Killbourn,[36] C. J. Killow,[36] C. Kim,[24] C. King,[13] P. King,[13] S. Klimenko,[35] P. Kloevekorn,[2] S. Koranda,[40] K. Kötter,[32] J. Kovalik,[16] D. Kozak,[13] B. Krishnan,[1] M. Landry,[15] J. Langdale,[16] B. Lantz,[27] R. Lawrence,[14] A. Lazzarini,[13] M. Lei,[13] V. Leonhardt,[32] I. Leonor,[38] K. Libbrecht,[13] P. Lindquist,[13] S. Liu,[13] J. Logan,[13,r] M. Lormand,[16] M. Lubinski,[15] H. Lück,[32,2] T. T. Lyons,[13,r] B. Machenschalk,[1] M. MacInnis,[14] M. Mageswaran,[13] K. Mailand,[13] W. Majid,[13,h] M. Malec,[32] F. Mann,[13] A. Marin,[14,s] S. Márka,[13] E. Maros,[13] J. Mason,[13,t] K. Mason,[14] O. Matherny,[15] L. Matone,[15] N. Mavalvala,[14] R. McCarthy,[15] D. E. McClelland,[3] M. McHugh,[19] P. McNamara,[36,u] G. Mendell,[15] S. Meshkov,[13] C. Messenger,[34] V. P. Mitrofanov,[21] G. Mitselmakher,[35] R. Mittleman,[14] O. Miyakawa,[13] S. Miyoki,[13,v] S. Mohanty,[1,w] G. Moreno,[15] K. Mossavi,[2] B. Mours,[13,x] G. Mueller,[35] S. Mukherjee,[1,w] J. Myers,[15] S. Nagano,[2] T. Nash,[10,y] H. Naundorf,[1] R. Nayak,[12] G. Newton,[36] F. Nocera,[13] P. Nutzman,[24] T. Olson,[25] B. O'Reilly,[16] D. J. Ottaway,[14] A. Ottewill,[40,z] D. Ouimette,[13,q] H. Overmier,[16] B. J. Owen,[29] M. A. Papa,[1] C. Parameswariah,[16] V. Parameswariah,[15] M. Pedraza,[13] S. Penn,[11] M. Pitkin,[36] M. Plissi,[36] M. Pratt,[14] V. Quetschke,[32] F. Raab,[15] H. Radkins,[15] R. Rahkola,[38] M. Rakhmanov,[35] S. R. Rao,[13] D. Redding,[13,h] M. W. Regehr,[13,h] T. Regimbau,[14] K. T. Reilly,[13] K. Reithmaier,[13] D. H. Reitze,[35] S. Richman,[14,aa] R. Riesen,[16] K. Riles,[37] A. Rizzi,[16,bb] D. I. Robertson,[36] N. A. Robertson,[36,27] L. Robison,[13] S. Roddy,[16] J. Rollins,[14] J. D. Romano,[30,cc] J. Romie,[13] H. Rong,[35,m] D. Rose,[13] E. Rotthoff,[29] S. Rowan,[36] A. Rüdiger,[20,2] P. Russell,[13] K. Ryan,[15] I. Salzman,[13] G. H. Sanders,[13] V. Sannibale,[13] B. Sathyaprakash,[7] P. R. Saulson,[28] R. Savage,[15] A. Sazonov,[35] R. Schilling,[20,2] K. Schlaufman,[29] V. Schmidt,[13,dd] R. Schofield,[38] M. Schrempel,[32,ee] B. F. Schutz,[1,7] P. Schwinberg,[15] S. M. Scott,[3] A. C. Searle,[3] B. Sears,[13] S. Seel,[13] A. S. Sengupta,[12] C. A. Shapiro,[29,ff] P. Shawhan,[13] D. H. Shoemaker,[14] Q. Z. Shu,[35,gg] A. Sibley,[16] X. Siemens,[40] L. Sievers,[13,h] D. Sigg,[15] A. M. Sintes,[1,33] K. Skeldon,[36] J. R. Smith,[2] M. Smith,[14] M. R. Smith,[13] P. Sneddon,[36] R. Spero,[13,h] G. Stapfer,[16] K. A. Strain,[36] D. Strom,[38] A. Stuver,[29] T. Summerscales,[29] M. C. Sumner,[13] P. J. Sutton,[29,y] J. Sylvestre,[13] A. Takamori,[13] D. B. Tanner,[35] H. Tariq,[13] I. Taylor,[7] R. Taylor,[13] K. S. Thorne,[6] M. Tibbits,[29] S. Tilav,[13,hh] M. Tinto,[4,h] K. V. Tokmakov,[21] C. Torres,[30] C. Torrie,[13,36] S. Traeger,[32,ii] G. Traylor,[16] W. Tyler,[13] D. Ugolini,[31] M. Vallisneri,[6,jj] M. van Putten,[14] S. Vass,[13] A. Vecchio,[34] C. Vorvick,[15] S. P. Vyachanin,[21] L. Wallace,[13] H. Walther,[20] H. Ward,[36] B. Ware,[13,h] K. Watts,[16] D. Webber,[13] A. Weidner,[20,2] U. Weiland,[32] A. Weinstein,[13] R. Weiss,[14] H. Welling,[32] L. Wen,[13] S. Wen,[17] J. T. Whelan,[19] S. E. Whitcomb,[13] B. F. Whiting,[35] P. A. Willems,[13] P. R. Williams,[1,kk] R. Williams,[4] B. Willke,[32,2] A. Wilson,[13] B. J. Winjum,[29,d] W. Winkler,[20,2] S. Wise,[35] A. G. Wiseman,[40] G. Woan,[36] R. Wooley,[16] J. Worden,[15] I. Yakushin,[16] H. Yamamoto,[13] S. Yoshida,[26] I. Zawischa,[32,ll] L. Zhang,[13] N. Zotov,[18] M. Zucker,[16] and J. Zweizig[13]

(The LIGO Scientific Collaboration, http://www.ligo.org)
[1] *Albert-Einstein-Institut, Max-Planck-Institut für Gravitationsphysik, D-14476 Golm, Germany*
[2] *Albert-Einstein-Institut, Max-Planck-Institut für Gravitationsphysik, D-30167 Hannover, Germany*
[3] *Australian National University, Canberra, 0200, Australia*
[4] *California Institute of Technology, Pasadena, CA 91125, USA*
[5] *California State University Dominguez Hills, Carson, CA 90747, USA*
[6] *Caltech-CaRT, Pasadena, CA 91125, USA*
[7] *Cardiff University, Cardiff, CF2 3YB, United Kingdom*
[8] *Carleton College, Northfield, MN 55057, USA*
[9] *Cornell University, Ithaca, NY 14853, USA*
[10] *Fermi National Accelerator Laboratory, Batavia, IL 60510, USA*
[11] *Hobart and William Smith Colleges, Geneva, NY 14456, USA*
[12] *Inter-University Centre for Astronomy and Astrophysics, Pune - 411007, India*
[13] *LIGO - California Institute of Technology, Pasadena, CA 91125, USA*
[14] *LIGO - Massachusetts Institute of Technology, Cambridge, MA 02139, USA*
[15] *LIGO Hanford Observatory, Richland, WA 99352, USA*
[16] *LIGO Livingston Observatory, Livingston, LA 70754, USA*
[17] *Louisiana State University, Baton Rouge, LA 70803, USA*
[18] *Louisiana Tech University, Ruston, LA 71272, USA*
[19] *Loyola University, New Orleans, LA 70118, USA*
[20] *Max Planck Institut für Quantenoptik, D-85748, Garching, Germany*
[21] *Moscow State University, Moscow, 119992, Russia*
[22] *NASA/Goddard Space Flight Center, Greenbelt, MD 20771, USA*
[23] *National Astronomical Observatory of Japan, Tokyo 181-8588, Japan*
[24] *Northwestern University, Evanston, IL 60208, USA*
[25] *Salish Kootenai College, Pablo, MT 59855, USA*
[26] *Southeastern Louisiana University, Hammond, LA 70402, USA*
[27] *Stanford University, Stanford, CA 94305, USA*
[28] *Syracuse University, Syracuse, NY 13244, USA*
[29] *The Pennsylvania State University, University Park, PA 16802, USA*
[30] *The University of Texas at Brownsville and Texas Southmost College, Brownsville, TX 78520, USA*
[31] *Trinity University, San Antonio, TX 78212, USA*
[32] *Universität Hannover, D-30167 Hannover, Germany*
[33] *Universitat de les Illes Balears, E-07071 Palma de Mallorca, Spain*
[34] *University of Birmingham, Birmingham, B15 2TT, United Kingdom*
[35] *University of Florida, Gainsville, FL 32611, USA*
[36] *University of Glasgow, Glasgow, G12 8QQ, United Kingdom*
[37] *University of Michigan, Ann Arbor, MI 48109, USA*
[38] *University of Oregon, Eugene, OR 97403, USA*
[39] *University of Rochester, Rochester, NY 14627, USA*
[40] *University of Wisconsin-Milwaukee, Milwaukee, WI 53201, USA*
[41] *Washington State University, Pullman, WA 99164, USA*
(Dated: January 28, 2004)

LIGO held its first science run (S1) from 23 August to 09 September 2002. During the 17-day period, the three km-scale LIGO interferometers (4 km and 2 km in WA and 4 km in LA) and the 600m GEO interferometer (outside Hannover, Germany) operated as a network of detectors for part of the time. The strain sensitivity of the LIGO interferometers during this observational period was $h(f) \sim 3 - 20 \times 10^{-21}\,\mathrm{Hz}^{-\frac{1}{2}}$ near $f \sim 300\,\mathrm{Hz}$. Their useful instrumental bandwidth spanned the decade $100\,\mathrm{Hz} \lesssim f \lesssim 1000\,\mathrm{Hz}$. During S1, LIGO interferometers had better broadband sensitivities than any prior gravitational wave detector. In addition, the number of interferometers operating simultaneously was unprecedented.

The LIGO Scientific Collaboration have completed analyses of the S1 data for a number of classes of sources of gravitational waves (*GW*). These included: (i) inspiral and merger of compact binary systems; (ii) continuous wave sources, the GW counterparts to radio pulsars; (iii) burst or transient sources, such as GW emissions from SNe; (iv) a stochastic gravitational wave background. The emphasis in this first science run was to develop the analysis techniques and software pipelines that will be used to analyze data during periods of extended observation in future science runs. At the same time, the S1 data quality were such that it was be possible to provide improved *direct observational* limits on gravitational radiation for a number of sources with these fundamentally new instruments.

PACS numbers:

I. INTRODUCTION

During the last few years a number of new gravitational wave detectors, using long-baseline laser interferometry, are being commissioned and have been entering into operation. These include the Laser Interferometer Gravitational Wave Observatory - *LIGO* [1] - detectors located in Hanford, WA and Livingston, LA, built by a Caltech-MIT collaboration; the GEO-600 detector near Hannover, Germany, built by an UK-German collaboration [1]; the VIRGO detector near Pisa, Italy, built by an Italian-French collaboration [2]; and the Japanese TAMA-300 detector in Tokyo [3]. While none of these instruments is yet performing at its design sensitivity, many have begun making dedicated data collecting runs and performing gravitational wave search analyses on the data.

In particular, from 23 August 2002 to 9 September 2002, the LIGO Hanford and LIGO Livingston Observatories [4] [5] took coincident science data (referred to hereafter as S1). The LHO site contains two, identically oriented interferometers: one having 4 km long measurement arms (referred to as H1), and one having 2 km long arms (H2); the LLO site contains a single, 4 km long interferometer (L1). These interferometers each have one arm aligned parallel to the great circle connecting the sites, thus providing optimal alignment to the same GW polarization. GEO also took data in coincidence with the LIGO detectors during that time, although with significantly poorer sensitivity.

The LIGO Scientific Collaboration[6] have completed analyses of the S1 data set for evidence of signatures coming from four classes of gravitational wave (GW) sources. These include: (i) inspiral and coalescence of compact binary systems; (ii) continuous wave sources, GW counterparts to radio pulsars; (iii) burst or transient sources, such as GW emissions from SNe; (iv) a stochastic gravitational wave background. The emphasis in this first science run was to develop the analysis techniques and software pipelines that will be used to analyze data continuously during periods of extended observation in future science runs. While no detections were made, the S1 data quality are such that it was possible to provide improved direct observational limits on GW from a number of sources with these fundamentally new instruments.

Fig. 1 presents a composite graph showing the amplitude spectral densities for the three LIGO interferometers taken during the S1 run. The LA 4 km machine was the most sensitive, achieving strain sensitivities of h(300 Hz) ~

---

[a]Currently at Stanford Linear Accelerator Center
[b]Permanent Address: HP Laboratories
[c]Currently at Rutherford Appleton Laboratory
[d]Currently at University of California, Los Angeles
[e]Currently at Hofstra University
[f]Currently at Siemens AG
[g]Permanent Address: GReCO, Institut d'Astrophysique de Paris (CNRS)
[h]Currently at NASA Jet Propulsion Laboratory
[i]Currently at National Science Foundation
[j]Currently at University of Sheffield
[k]Currently at Ball Aerospace Corporation
[l]Currently at European Gravitational Observatory
[m]Currently at Intel Corp.
[n]Currently at Lightconnect Inc.
[o]Currently at Keck Observatory
[p]Currently at ESA Science and Technology Center
[q]Currently at Raytheon Corporation
[r]Currently at Mission Research Corporation
[s]Currently at Harvard University
[t]Currently at Lockheed-Martin Corporation
[u]Currently at NASA Goddard Space Flight Center
[v]Permanent Address: University of Tokyo, Institute for Cosmic Ray Research
[w]Currently at The University of Texas at Brownsville and Texas Southmost College
[x]Currently at Laboratoire d'Annecy-le-Vieux de Physique des Particules
[y]Currently at LIGO - California Institute of Technology
[z]Permanent Address: University College Dublin
[aa]Currently at Research Electro-Optics Inc.
[bb]Currently at Institute of Advanced Physics, Baton Rouge, LA
[cc]Currently at Cardiff University
[dd]Currently at European Commission, DG Research, Brussels, Belgium
[ee]Currently at Spectra Physics Corporation
[ff]Currently at University of Chicago
[gg]Currently at LightBit Corporation
[hh]Currently at University of Delaware
[ii]Currently at Carl Zeiss GmbH
[jj]Permanent Address: NASA Jet Propulsion Laboratory
[kk]Currently at Shanghai Astronomical Observatory
[ll]Currently at Laser Zentrum Hannover

TABLE I: Operational duty cycles of different coincidence modes during S1.

	Locked Time (Hr)	Duty Cycle (%)
	Single	
H1 (4 km)	235	57.6
H2 (2 km)	298	73.1
L1(4 km)	170	41.7
	Double Coincidence	
H1+L1	116	28.4
H2+L1	131	32.1
H1+H2	188	46.1
	Triple Coincidence	
H1+H2 +L1	95.7	23.4

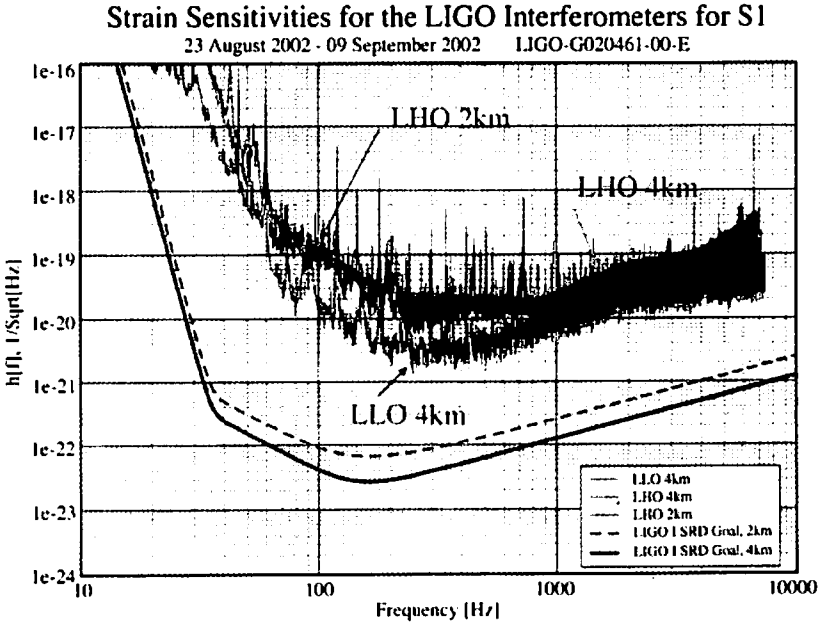

FIG. 1: Spectra of instrumental sensitivities for the three LIGO interferometers during the S1 science run. The solid curve corresponds to the design goal for the 4 km long interferometers in WA and LA. The dashed curve gives the goal for the shorter, 2 km long instrument in WA.

$3 \times 10^{-21}\,\mathrm{Hz}^{-\frac{1}{2}}$. Table I presents the operational duty cycles for the different coincidence modes during S1. During S1, LIGO interferometers had better broadband sensitivities than any prior gravitational wave detector. In addition, the number of machines operating simultaneously was unprecedented.

II. DISCUSSION

Searches for the four classes of GW sources described above have been conducted with the S1 data. In all cases, the primary emphasis of the analyses was to define, develop, and implement data analysis pipelines to provide production capability for processing data end-to-end. These efforts included support for Monte Carlo simulations to validate and calibrate the search efficiencies. Fig. 2 presents a block diagram schematic of the analysis flow for the burst event search. It is representative of a prototypical analysis pipeline for an event-based search.

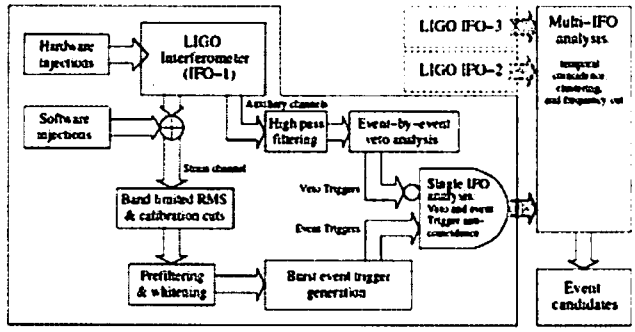

FIG. 2: The burst analysis pipeline as a prototypical analysis technique. Notation: DSO - a search algorithm library; LDAS - LIGO Data Analysis System environment; DB - relational database used to archive event metadata; DMT - data monitoring tool suite used to look at non-strain channel data in near real time; IFO - interferometer; LHO - LIGO Hanford Observatory ; LLO - LIGO Livingston Observatory.

Data streams from each interferometer were processed through a pipeline that generated candidate events. These events were subsequently analyzed for coincidence among as many interferometers as were operating at the epoch when the candidate event was produced. The gravitational wave (strain) channel was processed by *event trigger generator* filter(s) that perform optimal filtering of the strain channel using either template waveforms based on astrophysical source models or parametrizable waveforms (e.g., wavelets) that were correlated continuously against the interferometer output. When the event trigger exceeds a threshold determined by Monte Carlo calibration of the pipeline, a putative event is identified for further postprocessing downstream.

A variety of auxiliary channels were used to monitor instrumental and environmental characteristics at the same time the strain channel is analyzed. Transient or off-nominal behavior of these other channels is used to *veto* candidate events during epochs of detection when the instrument was not operating in its quiescent state. Candidates that survive these vetoes were then processed for coincidence among the several interferometers. Further, consistency checks were enforced to verify, for example, that the coincident events were consistent among all interferometers: for example, comparable signal amplitude, duration, and frequency content were required of a coincidence for it to be considered a possible astrophysical event.

Interpretation of the results requires that models of source distributions, source strengths and waveform characteristics be injected into the data stream using Monte Carlo techniques. In this way the detection efficiency could be determined for different classes of signals.

A. Searches for compact binary inspirals

Waveforms associated with the inspiral of $M_1 + M_2 \lesssim 6M_\odot$ compact binary systems are the most well-studied sources that can be detected in the LIGO band. What is much less well known is the *rate* with which such events occur in Nature. Information on binary systems is inferred from observations of radio pulsars. The most probable rate of NS+NS coalescences were recently revised *upward* by almost a factor $10\times$ [8][9] compared to rate estimates of even a few years ago [7]. The improved prospect for detection by the initial generation of km-scale interferometer results from the recent discovery of the most relativistic pulsar binary system to date, PSR J0737-3039. The present understanding of the population of these systems suggest that NS+NS merger rates within the local cosmic spacetime volume enclosing the Virgo cluster may approach ~ 1 per $1-2$ years at the upper end of the 95% confidence bound[8].

Unfortunately, there are no known NS/BH binaries in which the NS is also a pulsar. Therefore, it is necessary to rely on much less certain estimates based on simulations of the evolution of a population of progenitor binary systems to determine the number of systems that lead to compact NS/BH binaries. It is important to note that the uncertainties in the predicted rates of mergers span *three* orders of magnitude. A one year observation with current LIGO interferometers is likely to not observe these types of events.

The detection technique employs optimal Wiener filtering with matched templates in the frequency domain [10]. Specific details of the implementation of the analysis technique to the LIGO S1 data are provided elsewhere[11] and will only be summarized here. The interferometer strain data are correlated with theoretically derived signal

waveforms (*templates*), weighted by the reciprocal of the instrument noise spectral density to produces a time series of signal-to-noise ratio. Let the detector's calibrated strain data be $s(t) = n(t) + h(t)$, where $n(t)$ is the instrumental strain noise and $h(t)$ is a gravitational wave signal (if present). The strain produced in the instrument is written as

$$h(t) = \frac{1\ \mathrm{Mpc}}{D_{\mathrm{eff}}}\left[\sin\alpha\, h_s^I(t - t_c) + \cos\alpha\, h_c^I(t - t_c)\right], \tag{1}$$

where α depends on the orbital phase and orientation of the binary system, t_c is the time (at the detector) when the binary reaches its inner-most stable circular orbit, and $h_{s,c}^I(t - t_c)$ are the two polarizations of the gravitational waveform produced by an inspiralling binary normalized to the amplitude produced by an optimally oriented source at a distance of 1 Mpc. The two waveforms are related by $\tilde{h}_c^I(f) = -i\tilde{h}_s^I(f)$. The binary inspiral waveform can thus be parameterized (for a single detector) in terms of the component masses $I = (m_1, m_2)$, the effective distance, and the signal phase. D_{eff} includes the combined effect antenna pattern and source position. The matched filter output for given masses I then is the complex time series,

$$z(t:I) = x(t) + iy(t) \;=\; 4\int_0^\infty \frac{\tilde{h}_c^I(f)\tilde{s}^*(f)}{S_n(f)}\, e^{2\pi i f t} df \;\;:\;\; \sigma_z^2 = 4\int_0^\infty \frac{|\tilde{h}_c^I(f)|^2}{S_n(f)} df. \tag{2}$$

$$\rho(t) \;=\; \frac{|z(t)|}{\sigma_z}. \tag{3}$$

$S_n(f)$ is the one-sided strain noise power spectral density. In this expression, $x(t)$ is the matched filter response to the $\alpha = 0$ waveform, h_c^I, while $y(t)$ is the matched filter response to the $\alpha = \pi/2$ waveform, h_s^I. σ_z^2 is the variance of the matched filter output due to detector noise. The signal-to-noise ratio (SNR) of the matched filter output is given by ρ. For stationary and Gaussian noise, ρ is the optimal detection statistic for a single detector.

A powerful χ^2 discriminant against events generated by non Gaussian detector noise can be formulated by considering the frequency-time distribution of SNR as the signal evolves over time. The total SNR is divided into p contiguous frequency bins each of which is chosen to contain equal contribution to ρ. Thus the bins will differ in width.

$$\chi_p^2(t) \;=\; \frac{p}{\sigma^2}\sum_{l=1}^{p} |z_l(t) - z(t)/p|^2. \tag{4}$$

If a putative signal $h(t)$ has masses which do not exactly match any template in the bank, then χ^2 has a non-central chi-squared distribution with $2p - 2$ degrees of freedom and a non-central parameter $\lambda = 2\rho^2\varepsilon^2$, where ρ is the SNR for the signal and ε is the fractional loss of SNR due to parameter mismatch. The analysis imposed a maximum allowable, ρ-dependent threshold on χ^2 for putative inspiral events. This is referred to as the χ^2-veto:

$$\chi^2 < 5(p + 0.03\rho^2). \tag{5}$$

$p = 8$ bins were used throughout the S1 analysis. Since the detector noise was not Gaussian, the threshold was selected based on performance in a playground data set used to tune the analysis

Fig. 3 shows the dependence of coalescence signals on frequency. The ordinate gives the so-called "characteristic" strain of an inspiral signal. This quantity is the square root of the signal power spectral density multiplied by the number of cycles in the waveform at that frequency: it is a measure of the total power radiated at any given frequency during a coalescence event. This shows that the S1 search had adequate sensitivity to detect coalescence events for NS+NS systems to $D \sim 100$ kpc. In fact, the most sensitive L1 interferometer could detect with SNR = 8 an optimally oriented $1.4M_\odot + 1.4M_\odot$ merger to $D = 176$ kpc; H1 had a corresponding range of $D = 46$ kpc. The mass range $1M_\odot \le m_1 \le m_2 \le 4M_\odot$ and $(m_1 + m_2) \le 4M_\odot$ required a total of 2110 *non-spinning* second order post-Newtonian templates to ensure a minimum match of 97% everywhere within this parameter space. The analysis was performed with an SNR threshold $\rho > 6.5$ and $\chi^2 \lesssim 40$ (cf. to Eq. 5).

Putative merger events had to originate from data segments having suitable RMS noise performance as determined by analyzing the playground data set. In addition, coincidences between detectors had to occur within an 11 ms time window and correspond to the same set of template parameters to within 1%. *No coincident events were detected that met these criteria.*

Consequently, an upper limit could be set by considering the highest SNR event detected in the L1 detector ($\rho = 15.9$). A detailed population model was developed that included the Milky Way and the neighboring satellite Small and Large Magellenic Clouds (SMC and LMC, respectively). The number of potential sources within the Milky Way was used as a population unit - the Milky Way Equivalent Galaxy or MWEG. The total available source population was then 1.13 MWEG. A detection efficiency of $\epsilon(\rho) = 0.53$ for $\rho = 15.9$ was determined by Monte Carlo,

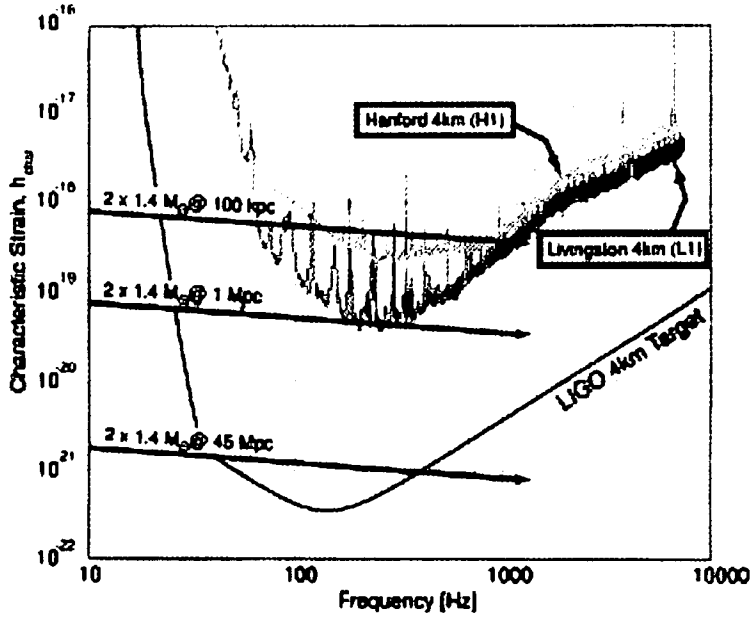

FIG. 3: Plot comparing sensitivity curves of the three LIGO interferometers during S1 and the ultimate design sensitivity for the 4 km instruments. The trajectories correspond to the power spectra for signals arising from the indicated sources. S1 provided galactic coverage for detection of inspiral coalescences.

which implied that $1.13 \times 0.53 = 0.60$ MWEG of the potential sources within the immediate galactic neighborhood would have been observable. Revising this estimate downward to account for systematic calibration uncertainties by 0.1 MWEG, an estimated 0.50 MWEG was within detection range during S1. Using an observation period of $T = 236$ h, this results in a 90% upper confidence bound on the merger rate of $\mathcal{R}_{90\%} \leq 1.7 \times 10^2 \mathrm{y}^{-1}\mathrm{MWEG}^{-1}$.

B. Searches for periodic sources of GW

Periodic sources are narrowband coherent signals that extend over the entire period of observation. For sufficiently long observations, the deterministic and well-characterized frequency modulations (FM) imposed by the barycentric motion of the Earth around the sun can be exploited to verify the extraterrestrial nature of such a source. On the scale of the S1 run, only a portion of the yearly FM cycle is detectable and the FM signatures correspond to monotonic drifts in signal frequency upon which is superimposed the daily modulations caused by Earth rotation. In addition, there may also be superimposed more complex frequency modulations due to intrinsic source characteristics. If these are not known *a priori*, they correspond to a parameter space over which searches must be executed.

The first analysis of LIGO and GEO data concentrated on the search for GW emission from a specific source with a known radio pulsar counterpart, PSR1939+2134 ($f_{GW} = 1283.86$ Hz). Fig. 4 presents a "landscape" of sensitivities achieved during S1 and possible sources of GW associated with known radio pulsar counterparts. In the near future, broadband interferometers will allow simultaneous observation and parallel analysis of many sources – something not previously possible with resonant cryogenic bars.

The search for GWs from PSR1939+2134 was conducted with two independent methods: a time domain Bayesian analysis and a frequency-domain frequentist analysis. The details of both searches are provided elsewhere[12]. Results are summarized below for the time domain only. *No evidence of periodic GWs from this source was observed.* The two techniques resulted in concordant upper limits.

The data from the four interferometers were analyzed separately because timing jitter during the run prevented coherent multidetector analysis in this first analysis. The time domain technique relies on the precisely known $\{f, \dot{f}\}$ characteristics of the source from radio pulsar data. The data were heterodyned in two steps using the doppler and spindown model for this source, thereby reducing the raw data stream by a factor $\sim \times 10^{-6}$ to 1 sample

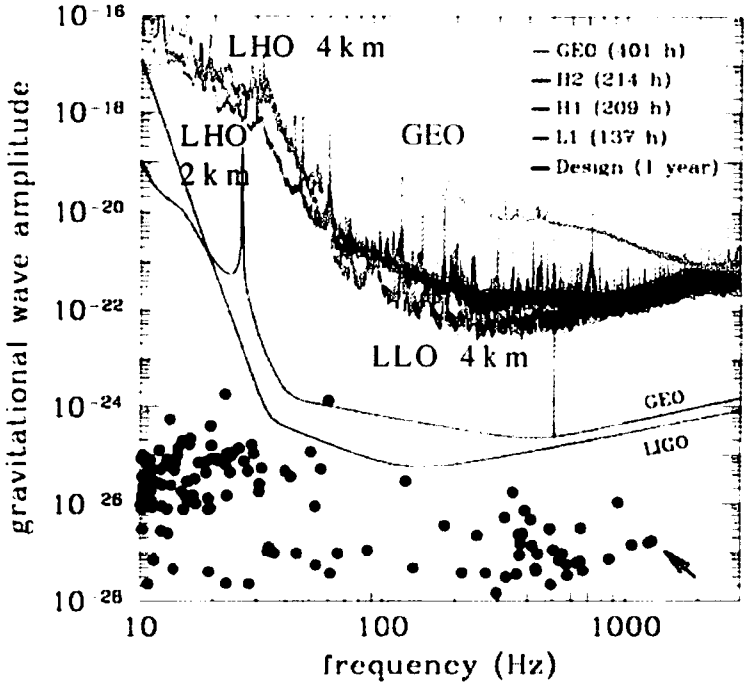

FIG. 4: Composite graph showing the S1 strain sensitivities of the four interferometers used during S1 to search for periodic waves. The labeled smooth curves correspond to design sensitivities. Data and curves are scaled to show the critical amplitude, $h_0(f) \equiv 11.4\sqrt{S_h(f)/T_{obs}}$, that is detectable with 99% confidence and 10 % false dismissal rate during the observation period of S1, $T_{obs} \approx 17$d. The interferometers operated with different duty cycles, leading to the actual observation times noted in the legend. The filled circles correspond to known millisecond radio pulsars. The abscissa is twice the radio pulsar frequency. The ordinate corresponds to the signal that would be generated *if* observed spin-down were attributable entirely to GW emission. This provides an astrophysical upper limit derived from energy conservation arguments. The arrow at the lower right indicates the location of PSR1939+2134. If a rapidly rotating neutron star exhibits an equatorial ellipticity the associated dynamic quadrupole will generate GW with characteristic strength $h_0 = \frac{4\pi^2 G}{c^4}\frac{I_{zz} f_{GW}^2}{r}\epsilon$, where r is the distance to the NS, I_{zz} is its principal moment of inertia about the rotation axis, $\epsilon \equiv (I_{xx} - I_{yy})/I_{zz}$ is the ellipticity, and the gravitational wave signal frequency, f_{GW}, is twice the rotation frequency, f_r. G is Newton's constant, and c is the speed of light. This is the emission mechanism that was assumed to produce the GW signal from targeted sources. Observational limits on h_0 yield limits on ϵ.

per minute. A χ^2 analysis between the data (time dependence of signal frequency and amplitude) and a physical model combining source characteristics and expected antenna pattern-induced signal modulation yielded a probability distribution function (PDF) for a signal in the presence of Gaussian noise. The left panel of Fig. 5 shows the PDFs for each detector. Nuisance parameters associated with the source are: ι, inclination of the spin axis with respect to observation direction, ϕ, rotational phase offset of the ellipticity, and ψ, the GW polarization of the source. It is possible to marginalize the four-dimensional PDF over the angle parameters, resulting in a PDF depending solely on wave amplitude, h_0. The resulting marginalized PDFs are shown in the right panel of Fig. 5. Referring to Fig. 5, the best constraint on h_0 from this source is obtained from L1: $h_0 \leq 1.4 \pm 0.1 \times 10^{-22}$. This yields a constraint on the source equatorial ellipticity, $\epsilon \leq 2.9 \times 10^{-4}\left(\frac{10^{45} gcm^2}{I_{zz}}\right)$.

C. Searches for burst sources of GW

Burst sources have no deterministic phase or frequency evolution and thus template-based modeling of source properties is not applicable. Instead, techniques predicated on *novelty detection* have been applied. By novelty detection is meant a search algorithm which employs statistical methods to characterize the data stream over periods of time that are much longer than the expected duration of a burst event, then to use these prior characteristics of

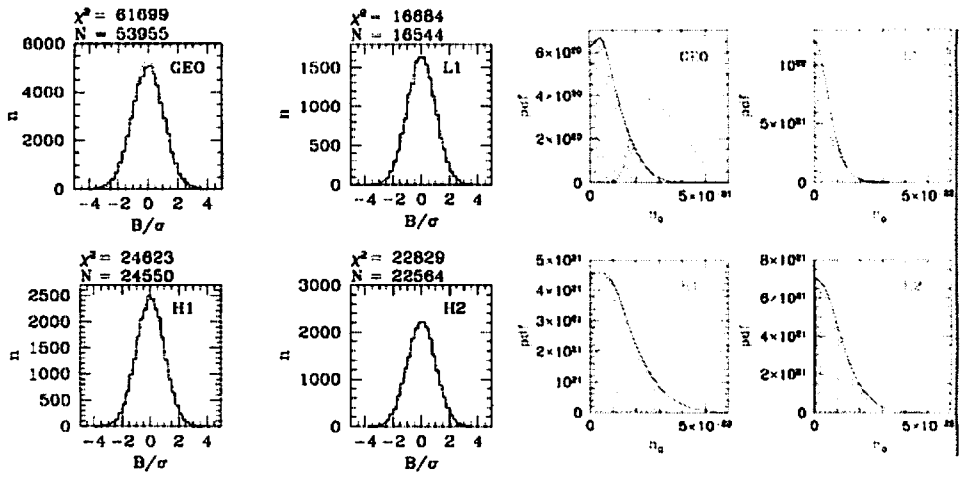

FIG. 5: **Left panel:** normalized residuals between the time-domain heterodyned data and the physical model of signal frequency and amplitude variations caused from the known source characteristics. The residuals are Gaussian to a high degree and exhibit a χ^2 per degree of freedom (DOF) very close to unity, as expected for well behaved Gaussian noise. These are the PDFs of the data including the four parameters: $\{h_0, \iota, \phi, \psi\}$ (cf. text for details). **Right panel:** marginalized PDFs for h_0. The bounds on the shaded regions give the 95% CL for an upper limit on h_0 for each of the four detectors. L1 provided the smallest upper limit by virtue of its greater sensitivity (cf. discussion on inspirals).

the data to set thresholds looking for excess signal power on time scales of fractions of a second.

For the S1 run, two techniques were implemented. One approach searched in the time domain to detect the amplitude fluctuations of the signal on short time scales. The other approach utilized the time-frequency map of the strain channel to look for clustering of contiguous pixels that exceeded a predetermined threshold. The former approach implemented an algorithm, termed *slope filter*, which could detect large changes of slope over short periods of time. The algorithm is a subset of a more general algorithm developed by the Orsay group [13].

The latter time-frequency approach had two similar implementations. The first of these, termed *excess power* [14][15], tessellated the *t-f* plane into "postage-stamp" patches of constant $\Delta f \Delta t$ and looked for excess power fluctuations over time . A second algorithm, termed *tfclusters* [16], used a clustering algorithm that was able to identify and detect groups of contiguous pixels having arbitrary shapes. Both approaches were shown capable of detecting excess power embedded in a noisy signal. These techniques are also suitable for detecting black hole ringdowns. A detailed discussion of both time-domain and f-t methods is provided elsewhere[17]. The excess power technique was not fully implemented for the S1 search Here a summary of the *tfcluster* approach is provided.

Referring to Fig. 2, only those stretches of data for which the RMS in four bands (320 – 400 Hz, 400 – 600 Hz, 600 – 1600 Hz, and 1600 – 3000 Hz) were below a predefined threshold were considered. Whenever the RMS over a six-minute interval for any detector in any of these bands exceeded a threshold of 3 times the 68th percentile level for the entire run (10 times for the 320–400 Hz band), the data from that six-minute period were excluded from further analysis.

Calibration of the algorithm efficiency for detection and false alarm was determined using extensive Monte Carlo simulations of injected bursts. The simulated bursts were of two types: (i) sine-Gaussians, two-parameter narrowband transients characterized by a central frequency, f_0, and duration of the Gaussian amplitude envelope, τ; and (ii) broadband limited duration Gaussian bursts characterized by τ. Fig. 6 shows the dependence of the 50% detection threshold on central frequency for a specific set of sine-Gaussians.

The tfcluster algorithm had a time resolution of $\sim$ 500 ms. This is $\sim 50\times$ the maximum physical time delay for bursts between the two LIGO sites (baseline distance of 3002 km). With such a large coincidence window, the background rate even for a threefold coincidence among the LIGO interferometers was non-zero. The background was estimated by repeating the coincidence analysis for a large number of different time shifts in the interval $\Delta t = \{-100s, 100s\}$ of the L1 data stream relative to the H1 and H2 data streams. Fig. 7 shows these results. The estimated background was found to be $B = 10.1 \pm 0.6$ events for threefold coincidence during the S1 run. The six measured events at zero time offset could be explained by the measured background. *Therefore no transient events were detected during the S1 run using the* tfcluster *search algorithm.* Using the unified approach of Feldman and Cousins[18], the 90%

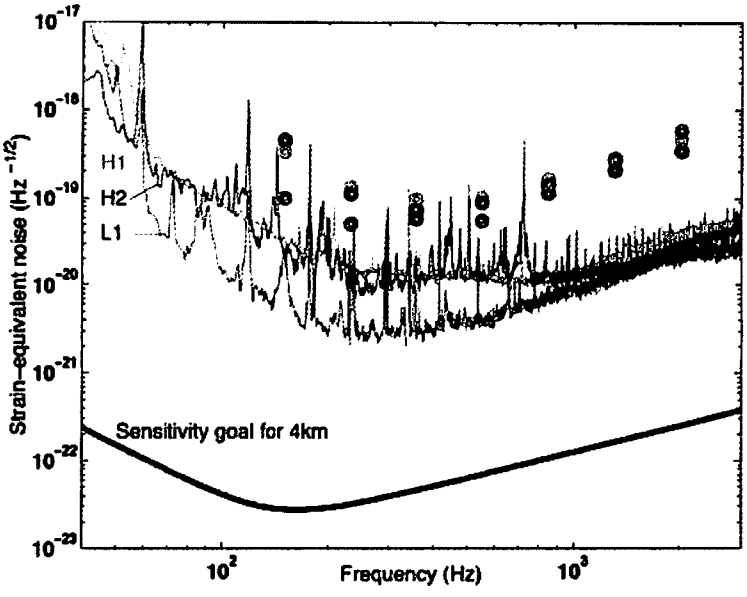

FIG. 6: The behavior of the *tfcluster* algorithm 50% detection efficiency for sine-Gaussians with $Q \equiv \sqrt{2}\pi\tau f_0 \simeq 8.9$ of various central frequencies, f_0. The amplitude for 50% detection efficiency tracks the interferometer sensitivity curves a factor $\gtrsim 10\times$ above the respective noise floors.

confidence bound on true coincident events which includes zero is $0 \leq \mathcal{R}_{90\%} \leq 2.3$. Using this result and folding in the amplitude-dependent detection sensitivity for threefold coincidences leads to an exclusion region at the 90% confidence level in the rate-vs-amplitude plane, shown in Fig. 8. For example, the tightest constraint resulting from the search for sine-Gaussians with $f_0 = 361$ Hz is near the knee in the curve, for which it was found that $\mathcal{R}_{90\%}[h_{rss} \sim 4 \times 10^{-19})] \leq 3$ per day

A subgroup of the burst search team is also developing search methodologies for so called *externally* triggered searches, whereby astrophysical triggers (e.g., GRB events) can be used to localize in time searches for coincidences among multiple interferometers. By such techniques, it is possible to provide upper limits, in lieu of detection, of the amount of GW energy associated with externally triggered events seen by other detectors [19].

D. Searches for a stochastic gravitational wave background

Gravitational waves of cosmological origin produce a stochastic background analogous to the relic microwave background radiation, but arising at a much earlier epoch. The search for such a signal is performed by cross-correlating the strain signals from pairs of interferometers and introducing an optimal Wiener filter to maximize detection signal-to-noise [20][21][22][23].

The background is stochastic and thus its properties are only statistically characterized. Its spectral properties are described by the dimensionless quantity

$$\Omega_{\rm gw}(f) \equiv \frac{f}{\rho_{\rm critical}} \frac{d\rho_{\rm gw}}{df} , \tag{6}$$

where $\rho_{\rm gw}$ is the energy density in gravitational waves, and

$$\rho_{\rm critical} = \frac{3c^2 H_0^2}{8\pi G} , \tag{7}$$

is the energy density required (today) to close the universe. H_0 is the Hubble expansion rate in the present epoch

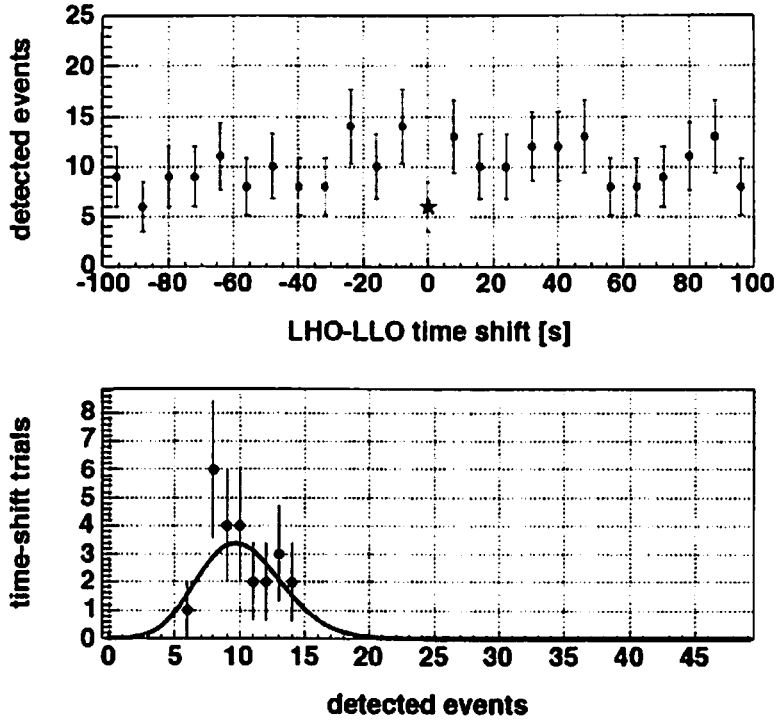

FIG. 7: **Upper panel**: The threefold coincidences over the entire S1 run for the *tfcluster* algorithm with a number of different (unphysical) time shifts spanning the time offset $\Delta t = \pm 100$ s. The star at $\Delta t = 0$ corresponds to the result from this search. **Lower panel**: Best fit Poissonian background to the histogrammed data in the upper panel. The estimated background is $B = 10.1 \pm 0.6$ events over the entire S1 run.

[24]:

$$H_0 \equiv h_{100} \cdot 100 \frac{\text{km}}{\text{sec} \cdot \text{Mpc}} \approx 3.24 \times 10^{-18}\, h_{100} \frac{1}{\text{sec}}\,, \tag{8}$$

$$= 71^{+4}_{-3}\ \text{km/s/Mpc} = 0.71\, h_{100} \tag{9}$$

$\Omega_{\rm gw}(f)\, h^2_{100}$ is independent of the actual Hubble expansion rate, and has been used extensively in the literature when H_0 was not known very accurately. $\Omega_{\rm gw}(f)$ is related to the one-sided power spectral density of gravitational wave strain $S_{\rm gw}(f)$ via[32]

$$S_{\rm gw}(f) = \frac{3H_0^2}{10\pi^2}\, f^{-3} \Omega_{\rm gw}(f)\,. \tag{10}$$

Thus, for a stochastic gravitational wave background with $\Omega_{\rm gw}(f) = \text{const}$, the power in gravitational waves falls off as $1/f^3$.

The spectrum $\Omega_{\rm gw}(f)$ completely specifies the statistical properties of a stochastic background of gravitational radiation provided we make several additional assumptions. Namely, we assume that the stochastic background is: (i) isotropic, (ii) unpolarized, (iii) stationary, and (iv) Gaussian. Anisotropic or non-Gaussian backgrounds (e.g., due to an incoherent superposition of gravitational waves from a large number of unresolved white dwarf binary star systems in our own galaxy, or a "pop-corn" stochastic signal produced by gravitational waves from supernova explosions [25][26] will require different data analysis techniques than those used for the S1 analysis [27][28].

Cross-correlating interferometer signals with an optimal Wiener filter allows one to detect the presence of a correlated signal at levels several orders of magnitude weaker than the noise spectral density. Fig. 9 presents theoretical predictions for the magnitudes of stochastic signals arising from a $\Omega_{GW} = \text{const}$ background that was at the limits of

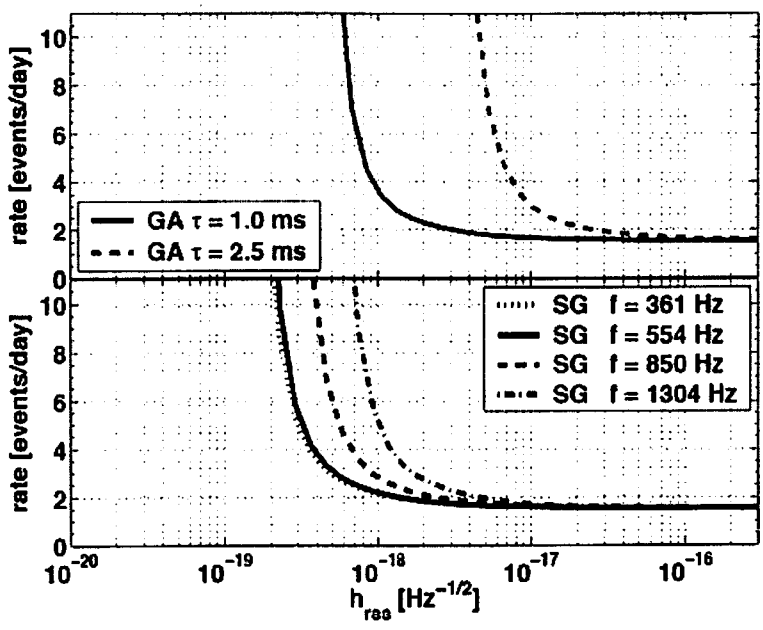

FIG. 8: Exclusion graph in the rate-vs-amplitude plane for events as determined during S1. Rates and amplitudes above and to the right of the curves are excluded at the 90% confidence limit. The limits depended upon both signal type (upper panel: Gaussians, lower panel: sine-Gaussians) and their frequency content.

detectability during S1. Details of the S1 search for a stochastic background are provided elsewhere[29]. Here these will be only briefly summarized.

Under the assumptions discussed above, the optimally filtered estimate of the stochastic background is:

$$\Omega_{GW}^{estimate} \sim \int_0^\infty df \, \frac{\gamma(|f|)\tilde{s}_1^*(f)\tilde{s}_2(f)}{|f|^3 \tilde{S}_{n1}(|f|)\tilde{S}_{n2}(|f|)}, \tag{11}$$

where $\tilde{s}_i(f)$ are the strain signals from the interferometers and $\tilde{S}_{ni}(f)$ are their noise spectral densities. The function $\gamma(|f|)$ is a geometrical form factor describing frequency-dependent response of an antenna pair due to their space-time separation[22]. The response is for an isotropic, unpolarized irradation by a stochastic GW background. Refer to Fig. 10 which shows $\gamma(|f|)$ for a number of interferometer pairs and also for the LA 4 km interferometer + ALLEGRO cryogenic bar. This figure shows that the long transcontinental baseline between the LIGO sites imposes a constraint on the maximum frequency over which such searches can be performed. In general, best sensitivity is obtained when the following conditions are met: (i) relative orientation is such that both interferometers of a pair respond to the same gravitational wave polarization; (ii) both instruments must have well-matched instrumental frequency responses; (iii) the spacetime overlap of the GW on to isolated detectors imposes a further constraint, $\lambda_{GW} \gtrsim 2D_{\rm baseline} \rightarrow f_{GW} \lesssim 40$Hz. The interplay of the function $\gamma(|f|)$ in the numerator and the noise spectra in the denominator of Eq. 11, $S_{n1}(|f|)\tilde{S}_{n2}(|f|)$, leads to the distribution of total SNR that is shown in Fig. 11.

Using the L1-H2 pair of interferometers, the S1 run produced a limit for Ω_{GW} that is better than previous direct determinations of this quantity in the frequency band 40 Hz $\lesssim$ f $\lesssim$ 300 Hz: $\Omega_{gw}h_{100}^2 \leq 23 \pm 4.6$ (90% CL). The uncertainty derives from systematic errors associated with the calibration of the strain information. Fig. 12 shows some intermediate results that go into the final estimate of Ω_{GW}. The L1-H1 result is statistically consistent, although $\sim 2\times$ larger. The H1-H2 correlations exhibit *negative* instrumental cross-correlations due primarily to acoustic couplings between the two interferometers sharing a common room where the detection benches are located. These instrumental artifacts precluded using this pair during S1.

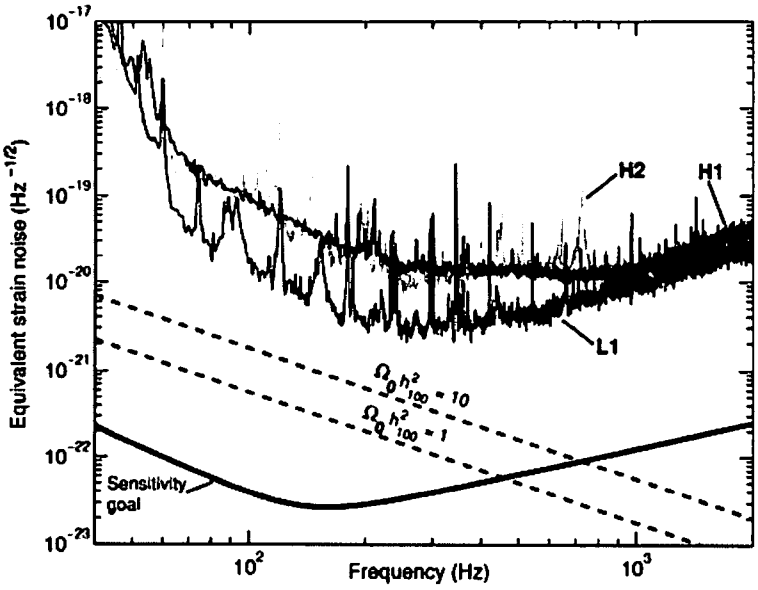

FIG. 9: Superposition of the S1 sensitivities of the three LIGO interferometers with predicted sensitivities of different interferometer pairs to an $\Omega_{GW}(f)$ = const stochastic background. By cross-correlating pairs of detectors the sensitivity can be improved two to three orders of magnitude beyond that of the individual interferometers.

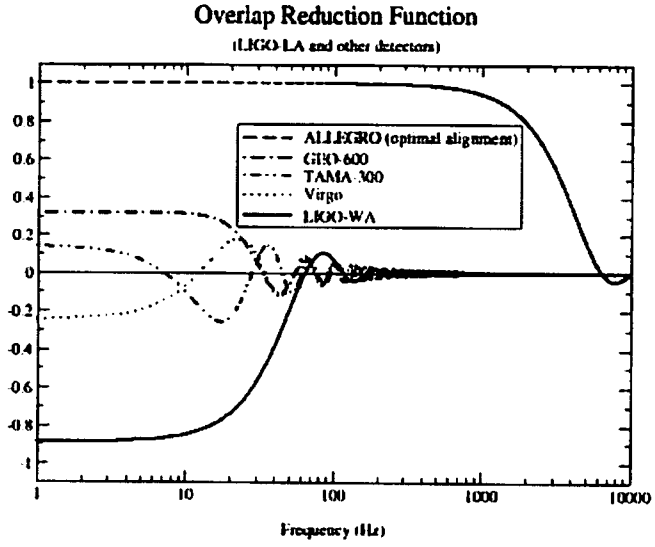

FIG. 10: Overlap reduction function between LIGO Livingston and the other major interferometers plus the LSU cryogenic resonant bar detector ALLEGRO (in an optimal alignment of 72° East of North).

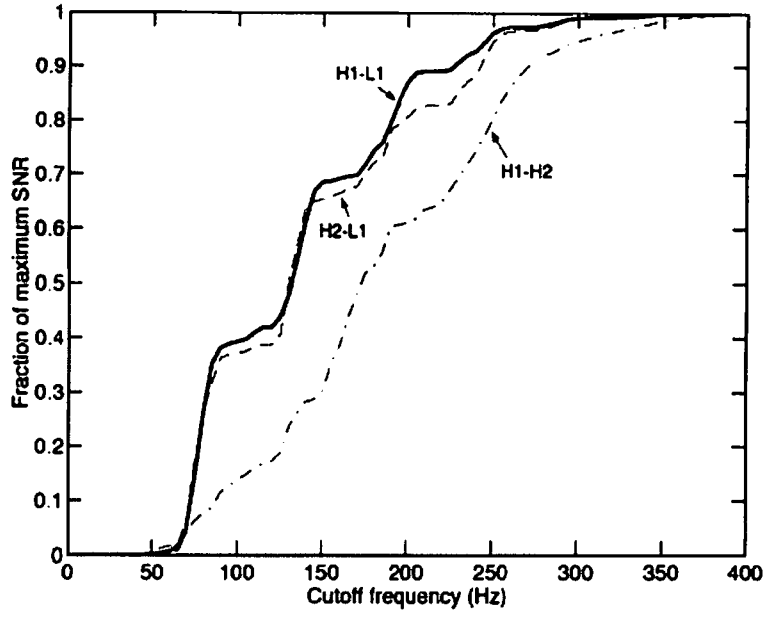

FIG. 11: Distribution of SNR over frequency for the measurement of Ω_{GW} using the LIGO interferometers. The interferometer pairs involving a transcontinental baseline are similar. The theoretical sensitvity for the co-located pair H1-H2 is better since $\gamma(|f|) = 1$ for all frequencies.

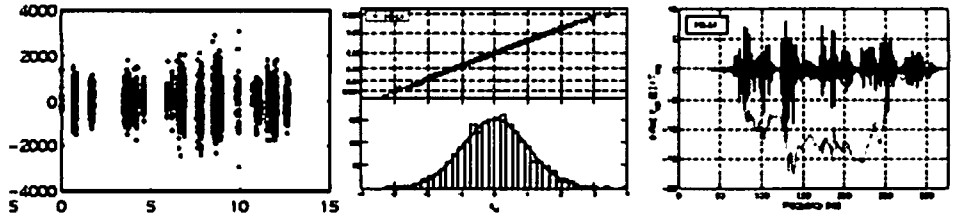

FIG. 12: Results from S1 analysis for the H2-L1 detector pair. **Left panel**: scatter plot of the individual estimates of Ω_{GW} taken over 14 days of coincident operation during S1. **Center panel**: normalized residuals for each point in the right panel from the average best estimate of Ω_{GW}. Upper graph is a "normal plot" wherein a Gaussian PDF maps into a straight line. This indicates the residuals are well-described by zero-mean unit deviates. **Right panel**: Black graph is the run-averaged cross-correlation spectrum (i.e., the kernel of the integral in Eq. 11). Each dot in the left panel contributes a spectrum to the average. Silver/gray graph shows the cumulative integral. The end point at the highest frequency corresponds to the result of the S1 measurement.

III. SUMMARY AND PROSPECTS

LIGO has begun scientific operation and the results for the first science run, S1, have been submitted for publication by the collaboration. The primary focus of the S1 run was to develop the analysis pipelines that will be used to process the strain data for a variety of GW sources. At the same time, the results provided *direct* observational limits on the flux of gravitational radiation from CW and stochastic source classes that improve on presently published limits. TAMA results from a 1000 h search [30][31] for binary mergers improve upon results obtained by LIGO for S1.

At the time of this writing, two longer science runs, S2 and S3, each of approximately 8 weeks duration, have been completed and the data are being analyzed. The instruments performed $\gtrsim 10\times$ *better* than S1. Over the past 20 months there has been significant improvement in the sensitivity of the machines (refer to Fig. 13). The LIGO H1 instrument completed the S3 run with sensitivity within a factor $\sim 2 \times -3\times$ of design sensitvity.

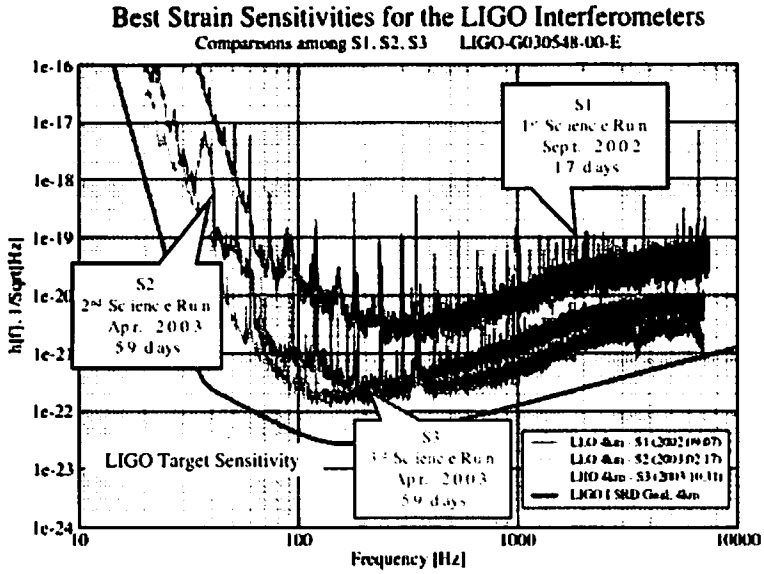

FIG. 13: Cascade plot of strain sensitivity improvements for the HA and LA 4 km interferometers showing progress in performance over the past ~20 months. The data sets represent sensitivities achieved during the S1, S2, and S3 science runs.

During S2 and S3 all three instruments were better matched in sensitivity, increasing prospects of multiple coincidence operation without the serious degradation of detection range seen during S1. The limiting sensitivities for all classes of searches have been dramatically improved, especially in the low-frequency regime, $f \lesssim 300$Hz. The collaboration is in the process of analyzing these data at the present time. The $\sim 5\times$ combined longer observation time of S2 & S3 will improve rate-limited observations as $\propto 1/T_{obs}$ and background-limited observations as $\propto 1/\sqrt{T_{obs}}$. The detectors exhibited better stationarity, allowing for greater operational duty cycles and less severe data cuts than had to be applied during S1. The experience gained during S1 analysis will be applied to the S2 & S3 analyses, leading to better techniques and earlier results.

After S3, a planned retrofit of several subsystems will be carried out in order to prepare for a much longer ($\sim$ 6 month) S4 run starting the last quarter of 2004. First, the seismic isolation systems at Livingston, LA are being upgraded to provide additional active seismic isolation that will reduce the residual motion at the top of the isolation systems by $\sim 30\times$, thereby allowing much higher duty cycles and allowing the interferometers to approach their design sensitivities within the year. In addition, a thermal lensing compensation subsystem based on a CO_2 laser will be introduced in order to correct the optical figure of the recycling cavity mirror. This will improve the shot noise limited sensitivity at high laser power. Finally, the digital control system for length and alignment will be enhanced by modifying the optical plant model in the server control loop. The modification will take into account the quantum radiation pressure-induced cavity alignment instabilities which, if not controlled, limit the sensitivity and duty cycle of the interferometers.

IV. ACKNOWLEDGMENTS

The author is indebted to his colleagues within LIGO Laboratory and the LIGO Scientific Collaboration, without whose collective participation the S1 run and the subsequent results could not have been achieved. The following agencies have made this work possible. The United States National Science Foundation provided funding for the construction and operation of the LIGO Laboratory and the Particle Physics and Astronomy Research Council of the United Kingdom, the Max-Planck-Society and the State of Niedersachsen/Germany provided support for the construction and operation of the GEO600 detector. Support for the research was provided by these agencies and by the Australian Research Council, the Natural Sciences and Engineering Research Council of Canada, the Council of Scientific and Industrial Research of India, the Department of Science and Technology of India, the Spanish Ministerio de Ciencia y Tecnologia, the John Simon Guggenheim Foundation, the David and Lucile Packard Foundation, the

Research Corporation, and the Alfred P. Sloan Foundation.
This document has been assigned the LIGO Laboratory document number LIGO-P040001-00.

---

[1] LIGO Scientific Collaboration, Abbott et al., Nucl. Inst. & Meth. A517 154 (2004).
[2] Caron, B. et al., in Gravitational Wave Experiments, proceedings of the Edoardo Amaldi Conference, World Scientific, 86 (1995).
[3] Tsubono, K. et al., in Gravitational Wave Experiments, proceedings of the Edoardo Amaldi Conference, World Scientific, 112 (1995).
[4] `http://www.ligo-wa.caltech.edu`
[5] `http://www.ligo-la.caltech.edu`
[6] `http://www.ligo.org`
[7] Kalogera, V. et al., Ap. J. 556 340 (2001).
[8] Burgay, M. et al., Nature 426 531 (2003).
[9] Kalogera, V. et al., astro-ph/0312101 (2003).
[10] Wainstein, L. A. & Zubakov, V. D., **Extraction of signals from noise**, Prentice-Hall, Englewood Cliffs, NJ (1962).
[11] LIGO Scientific Collaboration, Abbott et al., gr-qc/0308069, submitted to Phys. Rev. D (2004).
[12] LIGO Scientific Collaboration, Abbott et al., gr-qc/0308050, in press Phys. Rev. D (2004).
[13] Pradier, T., et al., Phys.Rev. D, 63, 042002 (2001).
[14] Anderson, W., et al., Int.J.Mod.Phys. D, 9 303 (2000).
[15] Anderson, W., et al., Phys. Rev. D, 63, 042003 (2001).
[16] Sylvestre, J., Phys. Rev. D, 66, 102004 (2002).
[17] LIGO Scientific Collaboration, Abbott et al., gr-qc/0312056, in press Phys. Rev. D (2004).
[18] G. J. Feldman & R. D. Cousins, Phys. Rev. D 57, 3873 (1998).
[19] Finn, L.S. , Mohanty, S.D., Romano, J.D., Phys.Rev. D, 60, 121101 (1999).
[20] Michelson, P. F., Mon. Not. R. Astron. Soc., 227, 933 (1987).
[21] Christensen, N., Phys. Rev. D. 46, 5250 (1992).
[22] Flanagan, É. É., Phys. Rev. D, 48, 2389 (1993).
[23] Allen, B. & Romano, J. D., Phys. Rev. D, 59, 102001 (1999).
[24] Bennett, C.L. et al., "First Year Wilkinson Microwave Anisotropy Probe (WMAP1) Observations: Preliminary Maps and Basic Results," astro-ph/0302207, submitted to Ap. J. (2003).
[25] Blair, D.G. & Ju, L., *Mon. Not. R. Astron. Soc.*, "A cosmological background of gravitational waves produced by supernovae in the early universe" (1996).
[26] Blair, D.G. , Burman, R. , Ju, L. , Woodings, S. , Mulder, M. , Zadnik, M.G., preprint, University of Western Australia, "The supernova cosmological background of gravitational waves" (1997).
[27] Allen, B. & Ottewill, A.C., Phys. Rev. D, 56, 545 (1997).
[28] Drasco, S. & Flanagan, É.É., in *Proceedings of the Ninth Marcel Grossmann Meeting on General Relativity*, edited by V. G. Gurzadyan, R.T. Jantzen and R. Ruffini, World Scientific, "Detecting a non-Gaussian Stochastic Background of Gravitational Radiation" (2002).
[29] LIGO Scientific Collaboration, Abbott et al., gr-qc/0312088, submitted to Phys. Rev. D (2004).
[30] TAMA Collaboration, Kanda et al., 28th International Cosmic Ray Conference Proc. 3059 (2003).
[31] TAMA Collaboration, Ando et al., Japanese General Relativity and Gravitation Workshop (these proceedings, 2003).
[32] $S_{gw}(f)$ is defined by $\lim_{T\to\infty} \frac{1}{T}\int_0^T |h(t)|^2\,dt = \int_0^\infty S_{gw}(f)\,df$, where $h(t)$ is the gravitational wave strain in a single detector due to the stochastic background signal.

Are Supersymmetric Compactifications Unstable?

Kengo Maeda[1]

Yukawa Institute for Theoretical Physics,
University of Kyoto, Kyoto, Japan, 606-8502

Abstract

Supersymmetric compactifications of string theory or M-thoery consist of higher-dimensional product spacetimes with a compact manifold. All supersymmetric solutions are believed to be stable against linear perturbations due to the supersymmetry. In this article we investigate non-linear perturbations of such a higher-dimensional product spacetime. First of all, we show that cosmic censorship is violated generically in $D = 5$, $\mathcal{N} = 8$ supergravity, which is believed to be a consistent truncation of ten dimensional IIB supergravity on S^5. We next show that cosmic censorship is violated in a wide class of gravity model coupled to a scalar field with a negative false vacuum even though a positive energy theorem is satisfied. We finally show that a large class of higher dimensional spacetimes with a compact Ricci-flat manifold has the property that there are configurations with negative energy density (from a four dimensional perspective). These results suggest that a large class of supersymmetric compactifications of string theory or M-theory is unstable.

1 Introduction

Cosmological models of higher-dimensional spacetime are now widely accepted among relativists or even astrophysicists. One of the reason is that they naturally arise as a supergravity model in the low energy limit of superstring theory or M-theory. Furthermore, a new compactification model [1] proposed a way how to resolve a hierarchy problem by reducing the fundamental Planck energy scale to TeV scale. So, it might be possible to produce a black hole by a future collider [2].

Motivated by these facts, it is worth while examining the stability issues of higher dimensional spacetimes in detail. Based on the singularity theorem, Penrose [3] argued that higher dimensional spacetime is unstable against a particular perturbation or possibly more general perturbations as follows: Let us consider a perturbation of a product vacuum spacetime of the form $M_4 \times K$, where M_4 is four dimensional Minkowski spacetime and K is a compact, Ricci flat manifold. Because of large degrees of freedom to choose initial data, we can perturb it in such a way that the macroscopic $\mathbf{R}^3$ space remains flat. So, the perturbed spacetime looks like a product spacetime of a closed compact universe and the flat $\mathbf{R}^3$ space. By applying the singularity theorem to the closed universe, we can show that a singularity inevitably appears in the product spacetime. We cannot,

[1]E-mail:kmaeda@yukawa.kyoto-u.ac.jp

however, immediately conclude that the product vacuum spacetime is unstable since the perturbation is unphysical in the sense that the amplitude cannot decay at infinity. So, we need to require that the perturbed region has a compact support B (outside of B, the amplitude is exactly zero). In this case the initial data would include a trapped surface on the boundary ∂B to connect smoothly the inside to the outside (for example, see [4]) and thus it is no more surprising that a singularity appears after evolution. As a result, we cannot say anything definite about stability issues of higher dimensional spacetime by applying the singularity theorem.

In this article, we explore non-linear instability issues of supersymmetric compactifications. Especially we give a counter example for cosmic censorship in five-dimensional $\mathcal{N} = 8$ gauged supergravity model. $\mathcal{N} = 8$ supergravity models are believed to arise as the low energy limit of string theory or M theory with boundary conditions $AdS_4 \times S^7$ [5] or $AdS_5 \times S^5$. For these boundary conditions, we have the powerful AdS/CFT correspondence which relates string theory to a dual field theory [6].

In section II, we first construct initial data with negative gravitational mass unbounded from below, even though it satisfies a positive energy theorem [7]. At first glance, there seems to be a contradiction. We can resolve, however, this problem by introducing a modified energy which is indeed always positive. The modified energy is given in section III. Section IV is devoted to showing that the time evolution of the initial data leads to the formation of a naked singularity.

The five-dimensional $\mathcal{N} = 8$ supergravity is believed to be a consistent truncation of ten dimensional IIB supergravity on S^5. This means that it is possible to lift our five dimensional solution to ten dimensions. At the linearized level, the fields which saturate the BF bound [8] correspond to $\ell = 2$ modes on S^5. Even though it is not known how to lift a general solution of the $\mathcal{N} = 8$ supergravity to ten dimensions, this is known for solutions that only involve the metric and scalars that saturate the BF bound [9]. So we can immediately conclude that the ten dimensional analog of the solution also evolves to naked singularities.

In general it is very hard to test cosmic censorship in each supergravity model. However, we can say more about a gravity model minimally coupled to a scalar field with a general potential satisfying a positive energy theorem. In section V we consider asymptotically Anti de Sitter spacetime where the scalar field approaches a negative false vacuum. It is shown that cosmic censorship is also violated for some potentials.

The standard supersymmetric compactifications of string theory consist of solutions of the form $M_4 \times K$ where K is a compact, Ricci flat manifold admitting a covariantly constant spinor. Familiar examples of K include T^n, $K3$, Calabi-Yau spaces, and manifolds with G_2 holonomy. So, the next question is: are there any non-linear instabilities in such a supersymmetric asymptotically flat spacetime? In section VI we show that a large class, including all simply connected Calabi-Yau and G_2 manifolds, has the surprising property that there are configurations with negative energy density. In other words, from a four dimensional perspective, there can be finite regions of space with negative energy. In fact, the energy density is unbounded from below! In contrast, these properties do not hold - at least not in the same way - for T^n or $K3$ compactifications. This may indicate that a class of asymptotically flat supersymmetric compactifications is also unstable, although we cannot say anything about cosmic censorship.

2 $\mathcal{N} = 8$ gauged supergravity model

$\mathcal{N} = 8$ gauged supergravity in five dimensions [10, 11] is thought to be a consistent truncation of ten dimensional type IIB supergravity on S^5. The spectrum of this compactification involves 42 scalars parameterizing the coset $E_{6(6)}/USp(8)$. The fields which saturate the BF bound correspond to a subset that parameterizes the coset $SL(6,R)/SO(6)$. From the higher dimensional viewpoint, these arise from the $\ell = 2$ modes on S^5 [12]. The relevant part of the action for our discussion involves five scalars α_i and takes the form [13]

$$S = \int \sqrt{-g}\left[\frac{1}{2}R - \sum_{i=1}^{5}\frac{1}{2}(\nabla\alpha_i)^2 - V(\alpha_i)\right] \tag{2.1}$$

where we have set $8\pi G = 1$.[2] The potential for the scalars α_i is given in terms of a superpotential $W(\alpha_i)$ via

$$V = \frac{g^2}{4}\sum_{i=1}^{5}\left(\frac{\partial W}{\partial \alpha_i}\right)^2 - \frac{g^2}{3}W^2 \quad , \tag{2.2}$$

W is most simply expressed as

$$W = -\frac{1}{2\sqrt{2}}\sum_{i=1}^{6} e^{2\beta_i} \tag{2.3}$$

where the β_i sum to zero, and are related to the five α_i's with standard kinetic terms as follows [13],

$$\begin{pmatrix}\beta_1\\ \beta_2\\ \beta_3\\ \beta_4\\ \beta_5\\ \beta_6\end{pmatrix} = \begin{pmatrix} 1/2 & 1/2 & 1/2 & 0 & 1/2\sqrt{3}\\ 1/2 & -1/2 & -1/2 & 0 & 1/2\sqrt{3}\\ -1/2 & -1/2 & 1/2 & 0 & 1/2\sqrt{3}\\ -1/2 & 1/2 & -1/2 & 0 & 1/2\sqrt{3}\\ 0 & 0 & 0 & 1/\sqrt{2} & -1/\sqrt{3}\\ 0 & 0 & 0 & -1/\sqrt{2} & -1/\sqrt{3}\end{pmatrix}\begin{pmatrix}\alpha_1\\ \alpha_2\\ \alpha_3\\ \alpha_4\\ \alpha_5\end{pmatrix} \tag{2.4}$$

The potential reaches a negative local maximum when all the scalar fields α_i vanish. This is the maximally supersymmetric AdS state, corresponding to the unperturbed S^5 in the type IIB theory. At linear order around the AdS solution, the five scalars each obey the free wave equation with a mass saturating the BF bound. Nonperturbatively, the fields couple to each other and it is generally not consistent to set only some of them to zero. The exception is α_5, which does not act as a source for any of the other fields.

We now find a class of negative energy solutions that only involve α_5, so $\alpha_i = 0$, $i = 1,..4$ in our solutions. Writing $\alpha_5 = \phi$ and setting $g^2 = 4$ so that the AdS radius is equal to one, the action (2.1) further reduces to

$$S = \int \sqrt{-g}\left[\frac{1}{2}R - \frac{1}{2}(\nabla\phi)^2 + \left(2e^{2\phi/\sqrt{3}} + 4e^{-\phi/\sqrt{3}}\right)\right] \tag{2.5}$$

[2] Our formula's differ slightly from [13], since they use $4\pi G = 1$.

We construct the solutions by first solving the constraint equations on a spacelike surface Σ. We consider initial data with all time derivatives set to zero. For time symmetric initial data the constraint equations reduce to

$$^{(4)}\mathcal{R} = g^{ij}\phi_{,i}\phi_{,j} + 2V(\phi) \tag{2.6}$$

For spherically symmetric configurations the spatial metric can be written as

$$ds^2 = \left(1 - \frac{m(r)}{3\pi^2 r^2} + r^2\right)^{-1} dr^2 + r^2 d\Omega_3^2. \tag{2.7}$$

The normalization is chosen so that the total mass is simply the asymptotic value of $m(r)$

$$M = \lim_{r\to\infty} m(r) \tag{2.8}$$

The constraint (2.6) yields the following equation for $m(r)$

$$m_{,r} + \frac{1}{3}mr(\phi_{,r})^2 = 2\pi^2 r^3 \left[(V(\phi)+6) + \frac{1}{2}(1+r^2)(\phi_{,r})^2\right] \tag{2.9}$$

The general solution for arbitrary $\phi(r)$ is

$$m(r) = 2\pi^2 \int_0^r e^{-\int_{\tilde{r}}^r \tilde{r}(\phi_{,r})^2/3\, d\tilde{r}} \left[(V(\phi)+6) + \frac{1}{2}(1+r^2)(\phi_{,r})^2\right] \tilde{r}^3 d\tilde{r}. \tag{2.10}$$

We now specify initial data for $\phi(r)$ on Σ. We consider a simple class of configurations with a constant density inside a sphere of radius R_0:

$$\phi(r) = \frac{A}{R_0^2} \qquad (r \le R_0), \qquad\qquad \phi(r) = \frac{A}{r^2} \quad (r > R_0) \tag{2.11}$$

The fall-off of ϕ is motivated as follows. If $\phi \to 0$ slowly, we decrease the contribution to the energy from the positive gradient terms and increase the contribution from the negative potential term. Since we want to try to construct a solution with negative energy, we clearly want ϕ to vanish as slowly as possible. It is easy to verify that $1/r^2$ is the slowest fall-off that yields finite total energy. In addition, this behavior is the same as the fall-off of the mode solutions of the free wave equation when BF bound is saturated. One can now easily show that for these initial data, the negative contribution to the mass from the potential more than compensates for the positive contribution from the gradient terms. If we take $0 < A \ll R_0^2$ so that the field is everywhere small then (5.12) gives

$$M \approx -\pi^2 A^2 \tag{2.12}$$

Since we can make R_0 and therefore A arbitrarily large, it is clear that the total energy can be arbitrarily negative. For $A > R_0^2$, ϕ is not small inside the sphere, but by using the fact that $V(\phi) < -6 - 2\phi^2 - \frac{2}{3\sqrt{3}}\phi^3$ for all $\phi > 0$, one can obtain a general upper limit to the total mass, $M < -\pi^2 A^2/\sqrt{3}$.

We have found that there exist non-singular configurations in $\mathcal{N} = 8$ supergravity with negative total mass. In section 4 we study the evolution of our initial data, but first we explain why this result is not in conflict with the positive energy theorem [7].

3 Positive energy theorem

How are our negative energy solutions compatible with the fact that there is a positive energy theorem for supergravity? How are they compatible with the AdS/CFT correspondence since the gauge theory Hamiltonian is bounded from below? To answer these questions, we first review the argument for positive energy of test fields originally given in [8, 14], and then discuss the full nonlinear proof of the positive energy theorem.

3.1 Positive energy for test fields

Consider a test field of mass $m^2 = -4$ which saturates the BF bound in AdS_5. We start with the action

$$\begin{aligned} S &= \frac{1}{2}\int[-(\nabla\phi)^2 + 4\phi^2]r^3 dt dr d\Omega_3 \\ &= \frac{1}{2}\int\left[\frac{\dot{\phi}^2}{(1+r^2)} - (D\phi)^2 + 4\phi^2\right] r^3 dt dr d\Omega_3 \end{aligned} \tag{3.1}$$

where D is the spatial derivative on a constant t surface. Since the background is static, one can compute the Hamiltonian in the usual way and obtain

$$E = \frac{1}{2}\int\left[\frac{\dot{\phi}^2}{(1+r^2)} + (D\phi)^2 - 4\phi^2\right] r^3 dr d\Omega_3 \tag{3.2}$$

This energy density is not positive definite due to the negative m^2. However, if we write $\phi = \psi/(1+r^2)$, substitute into (3.2) and integrate by parts we obtain

$$E = \frac{1}{2}\int\left[(\dot{\psi})^2 + (1+r^2)(D\psi)^2 + 4\psi^2\right]\frac{r^3}{(1+r^2)^3} dr d\Omega_3 - \oint_\infty \psi^2 d\Omega_3 \tag{3.3}$$

The volume term is now manifestly positive. The surface term vanishes provided ψ goes to zero asymptotically, which means that ϕ falls off *faster* than $1/r^2$. But we are interested in solutions that fall off precisely as $1/r^2$. In this case, the surface term is nonzero and manifestly negative. So there need not be a positive energy theorem and indeed, as we have seen, negative energy solutions can occur. Notice that this is possible only for fields which saturate the BF bound. If $m^2 > -4$, then the total energy of any configuration that falls-off as $1/r^2$ diverges. Finite energy configurations must fall-off faster, so the surface term vanishes and the energy is always positive. It is the delicate cancellation between the $m^2\phi^2$ term and the gradient term in (3.2) which allows fields with $m^2 = -4$ to have $1/r^2$ fall-off and finite energy.

One might have thought that the reaction to this would be to claim that one has positive energy only for $m^2 > m^2_{BF}$. Instead Breitenlohner and Freedman [8] proposed to include the limiting case $m^2 = m^2_{BF}$ and modify the definition of the energy[3]. In the

[3]In [14], Mezincescu and Townsend note that a perturbative analysis is not sufficient to prove stability if the bound is saturated. Later, Townsend [7] performed a nonperturbative analysis in spacetimes of arbitrary dimension, following the approach of Boucher [15], in which he claims to establish a positive energy theorem (and stability) even when the bound is saturated. However, as we will discuss in section 3.2, the proof given in [7] does not apply to the usual AdS energy if $m^2 = m^2_{BF}$.

original papers from the early 1980's, this was described in terms of an "improved stress tensor" which corresponds to adding a $\beta R\phi^2$ term to the Lagrangian. In AdS, R is a constant, so this indeed looks like a mass term for a test field. But as soon as one goes beyond the linearized approximation, adding a term like this changes the theory. In the context we have been considering, $\mathcal{N} = 8$ gauged supergravity in five dimensions, there is no $\beta R\phi^2$ term in the action, so this is not an option.

However, one still has the possibility of adding a surface term to the action (3.1) to get

$$\begin{aligned} \tilde{S} &= \frac{1}{2}\int [\phi\nabla^2\phi + 4\phi^2] r^3 dt dr d\Omega_3 \\ &= S + \frac{1}{2}\oint \phi\nabla_\mu\phi dS^\mu \end{aligned} \tag{3.4}$$

Now if one derives the Hamiltonian, one finds an extra surface term in the expression for the energy which exactly cancels the surface term in (3.3). This is possible since if n is the unit radial normal to the sphere at infinity, $\phi n \cdot \nabla\phi = -2\phi^2$. So starting with this modified action, the energy is indeed positive.

3.2 Nonlinear positive energy theorem

We now turn to the full positive energy theorem for AdS. This is a generalization of the spinorial proof for asymptotically flat spacetimes given by Witten [16]. We will follow the approach in [7]. The boundary conditions needed to apply this proof do not seem to have been clearly spelled out. In AdS, there are no covariantly constant spinors, but there are "supercovariantly" constant spinors ϵ_0 satisfying

$$\nabla_\mu\epsilon_0 + \frac{1}{2}\gamma_\mu\epsilon_0 = 0 \tag{3.5}$$

where γ^μ are the five dimensional gamma matrices. For the theory we are considering (2.5), the scalar potential is derivable from a superpotential $W(\phi)$ via $V = W'^2 - (4/3)W^2$ (2.2). One now defines a modified derivative $\hat{\nabla}_\mu \equiv \nabla_\mu - \frac{1}{3\sqrt{2}}W(\phi)\gamma_\mu$ and the Nester two-form [17]

$$E^{\mu\nu} \equiv \bar{\epsilon}\gamma^{\mu\nu\sigma}\hat{\nabla}_\sigma\epsilon + \text{h.c.} \tag{3.6}$$

where $\gamma^{\mu\nu\sigma} \equiv \gamma^{[\mu}\gamma^\nu\gamma^{\sigma]}$ and ϵ is an arbitrary spinor that asymptotically approaches ϵ_0.

Let Σ be a nonsingular spacelike surface with boundary at infinity, and let ϵ be a solution to $\gamma^i\hat{\nabla}_i\epsilon = 0$ (where i runs only over directions tangent to Σ) which asymptotically approaches ϵ_0. Then the integral of $\nabla_\mu E^{\mu\nu}$ over Σ is nonnegative, and vanishes if and only if the spacetime is AdS everywhere. (If there is matter in addition to the scalar field, its stress tensor must satisfy the dominant energy condition.) Hence

$$\oint_\infty E_{\mu\nu}dS^{\mu\nu} \geq 0 \tag{3.7}$$

(Note that the volume element picks out the components orthogonal to the three-sphere at infinity.) If W is constant, this reduces to the usual definition of mass in asymptotically

AdS spacetimes. However, in our case W is not constant, and for small ϕ, $\frac{W}{3\sqrt{2}} \approx -1/2 - \phi^2/6$. So there is an additional surface term

$$\oint_\infty \phi^2(\bar{\epsilon}_0\gamma_{\mu\nu}\epsilon_0)dS^{\mu\nu} \tag{3.8}$$

Since the area of the S^3 at infinity grows like r^3, $\phi \sim 1/r^2$, and ϵ_0 is supercovariantly constant at infinity, one might have thought that this surface term would always vanish. But it doesn't. Supercovariantly constant spinors grow like $r^{1/2}$ in AdS (see e.g. [18]). In retrospect this is not surprising since the square of a supercovariantly constant spinor is a Killing vector, and a timelike Killing vector in AdS has norm proportional to r. So in order for this surface term to vanish and recover the usual positive energy theorem, one needs ϕ to vanish faster than $1/r^2$ at infinity. We have seen that this boundary condition is too strong for fields which saturate the BF bound. In general dimension d, the required boundary condition on ϕ in order to apply the positive energy theorem is that ϕ must vanish faster than $r^{-(d-1)/2}$. A natural way out of this conundrum is to modify the definition of energy to include the extra surface term (3.8). We have seen that the combination of this with the usual energy cannot be negative and vanishes only for AdS.

Supersymmetry implies that the square of the supercharge should be positive. Although we have not checked it, we believe that the supercharge also has an extra contribution in this case, so that the positive quantity is indeed the entire surface term (3.7). It would be interesting to verify this by extending the work of [19] to $\mathcal{N} = 8$ supergravity. Since the Hamiltonian of the dual field theory must be positive (or at least bounded from below if one includes Casimir energy) it should be identified with this modified energy.

4 Evolution and Naked Singularities

In this section, we consider the evolution of the negative energy initial data constructed in section 2, and show that they evolve to naked singularities. But first, we point out another interesting difference between the usual energy and the modified energy, which arises in evolution.

4.1 Is the energy time dependent?

For fields behaving as $\phi = A/r^2 + O(1/r^3)$ at large r, the usual energy is time dependent if A is a function of t. There is a nonzero flux of energy at infinity. The modified energy, on the other hand, is always time independent. To see this, it suffices to consider the linearized theory, since ϕ is very small asymptotically. In terms of the conserved stress tensor

$$T_{\mu\nu} = \nabla_\mu\phi\nabla_\nu\phi - \frac{1}{2}g_{\mu\nu}[(\nabla\phi)^2 + 2V(\phi)] \tag{4.1}$$

the usual energy (3.2) is just the integral of $T_{\mu\nu}\xi^\mu$ over a spacelike surface, where ξ^μ is the timelike Killing field. The local flux of energy at infinity is thus $T_{\mu\nu}\xi^\mu n^\nu$ where n^ν is an asymptotic unit radial vector. Integrating this flux between t_1 and t_2 yields

$$E(t_2) - E(t_1) = \lim_{r\to\infty}\int_{t_1}^{t_2} r^4 dt d\Omega_3\ \dot{\phi}(r\partial_r)\phi = -\int [A^2(t_2) - A^2(t_1)]d\Omega_3 \tag{4.2}$$

It is now clear that if we add to the definition of the energy a surface term $\int A^2 d\Omega_3$, the modified energy will be time-independent. This is precisely the same surface term which makes the energy positive.

Of course, if one wants the usual energy to be time independent, one can require that A be independent of time. This can be achieved by imposing boundary conditions at a large but finite R and requiring $\phi = A/R^2$ (with fixed A) at this radius. (This is automatically implemented in most numerical evolution schemes.) The radius R is like a cut-off, and in principle should be taken to infinity to obtain the true solution.

The fact that the total energy may be time dependent holds only for fields which saturate the BF bound. If $m^2 > m^2_{BF}$, then finite energy requires fields to fall off faster than $1/r^2$ and then the flux always vanishes at infinity.

4.2 Cosmic censorship violation

Recall that our initial data consisted of a constant field $\phi = A/R_0^2$ inside a sphere of radius R_0. The proper size of this sphere initially is

$$L \approx \int_0^{R_0} \frac{dr}{[1+(Hr)^2]^{1/2}} \approx H^{-1} \ln R_0 \tag{4.3}$$

where $H^2 = -V(A/R_0^2)/6$. So for large R_0 there is a large region $r < R_0$ of constant energy density and we can model the evolution inside its domain of dependence by a $k = -1$ Robertson-Walker universe,

$$ds^2 = -dt^2 + a^2(t) d\sigma^2 \tag{4.4}$$

where $d\sigma^2$ is the metric on the four dimensional unit hyperboloid. The field equations are

$$\frac{\ddot{a}}{a} = \frac{1}{6}[V(\phi) - \frac{3}{2}\dot{\phi}^2] \tag{4.5}$$

$$\ddot{\phi} + \frac{4\dot{a}}{a}\dot{\phi} + V_{,\phi} = 0. \tag{4.6}$$

and the constraint equation is

$$\dot{a}^2 - \frac{a^2}{6}\left[\frac{1}{2}\dot{\phi}^2 + V(\phi)\right] = 1 \tag{4.7}$$

It is well known that a homogeneous scalar field, rolling down a negative potential, produces a singularity in finite time [21, 22]. The argument is the following. We start with $\phi = A/R_0^2 \ll 1$ and $\dot{\phi} = 0$, so initially we have

$$\phi(t) = \frac{A}{R_0^2}\cosh 2t\ , \qquad a(t) = H^{-1}\cos Ht. \tag{4.8}$$

By (4.5), $\ddot{a}/a$ is always less than its initial value $-H^2$ (which is close to one). So the scale factor must vanish in a time less than $\pi/2H$. Since $\dot{\phi} \neq 0$, the vanishing of the scale factor causes the energy in the scalar field to diverge, resulting in a curvature singularity. More

precisely, after a certain time T_0 the potential term in (4.6) is unimportant and the field behaves as $\dot{\phi} = c/a^4$, where c is a constant. Matching at T_0 gives $c \approx A/R_0^2$. From (4.7) it follows that the change in ϕ induces a change in the form of the scale factor when $a^2\dot{\phi}^2$ is of order one, which occurs when $a^3 \approx c$. Assuming the potential term is negligible compared to the kinetic term (which can be confirmed after the solution is found) (4.7) reduces to $\dot{a}^2 - c^2/(12a^6) \approx 0$, which implies $a(t) \propto (T_s - t)^{1/4}$ and hence $\phi(t) \propto -\ln(T_s - t)$. Actually, (4.7) also determines the coefficient so that $\phi = -\frac{\sqrt{3}}{2}\ln(T_s - t)$. Since the scalar field diverges, one has a curvature singularity.

Before one can claim that our initial data evolve to a singularity, one must check that the homogeneous approximation is valid all the way to the singularity. This is not completely obvious since the boundary of the domain of dependence is a null surface, and in pure AdS, a radial light ray can travel an infinite distance in finite time. So we need to calculate the proper distance on the initial surface traveled by the inward going radial light ray from the border of the homogeneous region at $r = R_0$ to the singularity. From the Robertson-Walker form of the metric, this is $l = a(0)\int_0^{T_s} dt/a(t)$. In pure AdS the distance l diverges. But, as we have seen, in our case $a(t)$ changes its form near the singularity resulting in finite l. If $\phi(R_0) \approx c \ll 1$ then the cutoff on t where $a(t)$ changes its form occurs close to the maximum value $\pi/2H$, yielding $l \propto -\ln c^{1/3} > 1$ (for instance for $c = .01$ one has $l \approx 2.3$). Since the proper distance is proportional to $\ln r$ this implies that the homogeneous approximation is good all the way to the singularity for radii less than $e^{-l}R_0$. This is much smaller than R_0 but it can easily be made arbitrarily large by increasing R_0 keeping $\phi(R_0)$ fixed. If $\phi(R_0)$ is of order one, then the size of the singular region is $\sim R_0$, for large R_0.

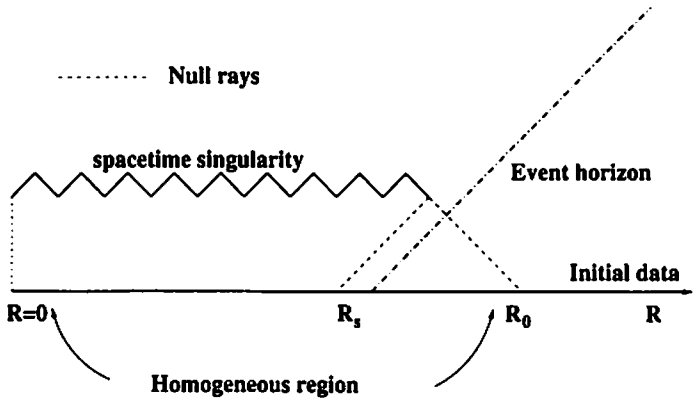

Figure 1: If an event horizon encloses the singularity, it must have an initial size greater than R_s.

If the total mass could not increase, one could easily show that a black hole could not enclose this singularity as follows. If this singularity lies inside a black hole, then we can trace the null geodesic generators of the event horizon back to the initial surface, where they will form a sphere of radius at least $R_s = e^{-2l}R_0$ (one factor of l is for the reduced size of the domain of dependence at the singularity and the second is because the event horizon is an outgoing null surface (see Fig.1)). The area theorem for black holes only requires the null convergence condition and hence still holds even in theories with

$V(\phi) < 0$. Since the area of the event horizon cannot decrease during evolution and we are assuming the mass cannot increase, the initial mass M must be large enough to support a static black hole of size R_s. Clearly it is impossible to produce a Schwarzschild AdS black hole, since this requires a positive mass $M_{BH} \propto R_s^4$, and our mass is negative. One could imagine the formation of a black hole with scalar hair, with $\phi(r) \sim r^{-2}$ at large r so that the hair renders the total mass finite and negative. However we have numerically verified that with our potential all black hole solutions with scalar hair have $\phi(r) \sim \ln r/r^2$ at large r. Thus our finite mass initial data can not evolve to a black hole with scalar hair.

We have seen that the total mass is not conserved, so it might increase during evolution. If it increases enough, a black hole could form. To ensure that a naked singularity is produced, we can impose a large radius cut-off as mentioned above. This is discussed in more detail in [20]. Since the cut-off can be at an arbitrarily large radius, we will continue the following discussion ignoring the cut-off.

Inside the domain of dependence of the homogeneous region the singularity will be spacelike, like a big crunch. The singularity is likely to extend somewhat outside this domain of dependence (so our estimate for R_s is really a lower limit), but not reach infinity. So the singularity will either end or become timelike. In both cases, one has naked singularities. In fact, there is really no way to distinguish these two cases since the evolution ends at the first moment that a naked singularity appears. To see a timelike singularity, one would have to know the appropriate boundary conditions to impose at the singularity, which is not possible classically. If the singularity did reach infinity, it would cut off all space, producing a disaster much worse than naked singularities. But this is unlikely since there would then be a radius R_c on the initial surface such that the outgoing null surfaces for $r > R_c$ expand indefinitely and reach infinity, while those with $r < R_c$ hit the singularity and (probably) contract to a point. This indicates that the surface with $r = R_c$ would reach a finite radius asymptotically, just like the stationary horizons which are ruled out.[4] A similar argument allows us to say something about the geometry near the naked singularity. Consider the area of the spherical cross-sections on an outgoing null surface which hits the naked singularity. If the areas shrink to zero as one reaches the singularity, then a nearby null surface starting at slightly larger radius will have the areas decrease near the naked singularity and then increase as the surface reaches infinity. This contradicts the Raychaudhuri equation and the null convergence condition. We conclude that the area of spheres near the naked singularity remain of nonzero size. The naked singularity is metrically a sphere and not a point. We have seen that inside the domain of dependence of the homogeneous region, the singularity is a strong curvature singularity and all spatial distances shrink to zero. This shows that as the singularity extends outside this region, it becomes weaker, and when it ends, the two sphere remains a finite size. The curvature, however, still diverges.

The above arguments assumed spherical symmetry, but that was not essential. In the central region, the collapsing Robertson-Walker metric develops trapped surfaces. We can clearly perturb our initial data and construct nearby initial data (which need not

[4]There is also the possibility that the singularity could become null. If the null singularity reached infinity, it would again cut off all space, and be worse than a naked singularity. If it remained inside a finite region, it would be like a static black hole with singular horizon. Numerical evidence suggests that even these solutions do not exist.

be time-symmetric) which will still produce trapped surfaces. The singularity theorem guarantees that a singularity must form. On the other hand, the energy will still remain negative, so the singularity cannot be enclosed inside a black hole. Thus cosmic censorship is generically violated in the theory (2.5). In fact, cosmic censorship is generically violated in $D = 5$, $\mathcal{N} = 8$ supergravity, since one can also perturb the other fields in the theory and still produce naked singularities.

The fact that the naked singularity is not a point holds even for general, nonspherical solutions. To see this, consider the boundary of the past of infinity in the maximal evolution of our initial data. (We are assuming boundary conditions at infinity, so the fact that infinity is timelike is not a problem for evolution.) This is a null surface which ends on the naked singularity. Standard arguments show that this surface is generated by null geodesics which cannot be converging. So the area of any crosssection increases into the future.[5]

5 Generalized potential case

As an attempt to generalize the previous result, we shall consider four dimensional gravity coupled to a single scalar field with a potential $V(\phi)$. We take V to have a global minimum at $\phi = 0$ and a local minimum at $\phi = \phi_1 > 0$ (see Fig. 2). We assume $V(0) = -3V_0$ and $V(\phi_1) = -3V_1$ are both negative and we consider solutions that asymptotically approach the local (AdS) minimum at ϕ_1. We require that V satisfies the positive energy theorem (PET) for solutions with this boundary condition. While some formulations of this theorem assume a local energy condition stating that V is never less than its asymptotic value, it has been shown that this is not necessary [7, 15]. Generally speaking, the PET holds if the barrier separating the extrema is high enough, but it does not hold if the barrier is too low [6]. By adjusting the height of the barrier to be close to the transition point, one decreases the mass of nontrivial configurations that probe the region of V around the true minimum. We will show that although the positive energy theorem holds in such theories, cosmic censorship does not. We demonstrate this by first constructing initial data with a large approximately homogeneous region in the interior where $V < -3V_1$, but with $\phi \to \phi_1$ asymptotically. The central region evolves to a singularity, since a homogeneous scalar field rolling down a potential to a negative minimum will generically become singular. We then show that if the barrier is close to the transition point, the total mass is too small to produce a black hole large enough to enclose the entire singular region, so the singularity must be naked.

This violation of cosmic censorship in AdS is quite general since for a large class of potentials, one only has to adjust one parameter. Even though the naked singularity in black hole critical phenomena [23] also arises from adjusting one parameter, the implication here is completely different. This is because we are adjusting a parameter in the

[5] One can view this null surface as a type of event horizon since the points inside cannot communicate with infinity. However this event horizon becomes singular and does not correspond to a standard black hole.

[6] There exist potentials that admit the PET even if $V(\phi_1)$ is a local maximum. For example, if $V(\phi) \geq 2W'^2 - 3W^2$ for any function $W(\phi)$, the PET holds [15]. However, if ϕ_1 is small enough, or $V_0 - V_1$ is big enough, the PET will be violated unless a sufficiently high barrier separates both extrema.

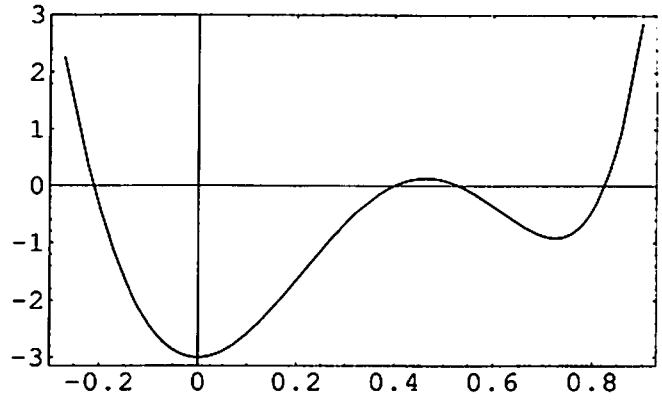

Figure 2: A potential $V(\phi)$ that satisfies the positive energy theorem for solutions that asymptotically approach the local (AdS) minimum at ϕ_1, but which violates cosmic censorship.

potential, not the initial data. For a given theory, there is an open set of initial data which produce naked singularities. Furthermore, in our case one does not even have to fix the parameter exactly, it only has to be close to some critical value.

It may also be possible to violate cosmic censorship for asymptotically flat initial data, using potentials of the above form with the local minimum at $V = 0$. However it is much easier in the asymptotically AdS case. This is because a large black hole of radius R_s in AdS requires a mass $M_{BH} = (R_s^3 + R_s)/2$ (where we have set the AdS radius to one). This is much larger than the mass of a Schwarzschild black hole of size R_s. For this reason, the asymptotically flat case is much more delicate. We will see that this can be explored with $1+1$ dimensional numerical relativity and hence provides a feasible new test of cosmic censorship.

To begin, we find the precise condition for potentials of the above type to admit a PET. To minimize the mass, we consider initial data with all time derivatives set to zero. For time symmetric initial data the constraint equations reduce to

$$^{(3)}\mathcal{R} = g^{ij}\phi_{,i}\phi_{,j} + 2V(\phi) \tag{5.9}$$

where we set $8\pi G = 1$. Since spatial gradients raise the energy, we first restrict attention to spherically symmetric configurations with metric

$$ds^2 = \left(1 - \frac{m(r)}{4\pi r}\right)^{-1} dr^2 + r^2 d\Omega_2^2. \tag{5.10}$$

The constraint then yields the following equation for the "mass" m as a function of the radius,

$$m_{,r} + \frac{1}{2} m r (\phi_{,r})^2 = 4\pi r^2 \left[V(\phi) + \frac{1}{2}(\phi_{,r})^2\right]. \tag{5.11}$$

The general solution for arbitrary $\phi(r)$ is

$$m(r) = 4\pi \int_0^r e^{-\int_{\tilde{r}}^r \tilde{r}(\phi_{,r})^2/2\, d\tilde{r}} \left[V(\phi) + \frac{1}{2}(\phi_{,r})^2\right] \tilde{r}^2 d\tilde{r}. \tag{5.12}$$

The total ADM mass is defined to be

$$M = \lim_{r\to\infty}[m(r) + 4\pi V_1 r^3] \tag{5.13}$$

We require that $\phi \to \phi_1$ faster than $1/r^{3/2}$ since this is required for finite mass. In fact, it suffices to consider configurations where $\phi(r)$ reaches ϕ_1 at a (possibly large) finite radius $r = R_1$, and in this case $M = m(R_1) + 4\pi V_1 R_1^3$. This is because one can always perturb ϕ to have finite R_1, keeping the change in the mass arbitrarily small.

To identify the criterion on V for the PET to hold, we first minimize

$$m_V = 4\pi \int_0^{R_1} e^{-\int_r^{R_1} \hat{r}(\phi,_r)^2/2\, d\hat{r}} V(\phi) r^2 dr \tag{5.14}$$

over a suitable class of ϕ. Introducing a new radial variable $y = r/R_1$ and writing $\tilde{\phi}(y) = \phi(R_1 y)$ it is easy to see that m_V/R_1^3 is independent of R_1. Let $\mathcal{S}$ be the set of all $\tilde{\phi}(y)$ with $\tilde{\phi}(0) = \phi_0 \geq 0$, $V(\phi_0) < -3V_1$ and $\tilde{\phi}(1) = \phi_1$. The boundary condition at the origin is chosen so that if V admits any negative energy configurations, then it admits some in $\mathcal{S}$. We define

$$\rho_V \equiv \min_{\tilde{\phi}\in\mathcal{S}} \frac{m_V}{4\pi R_1^3} = \min_{\tilde{\phi}\in\mathcal{S}} \int_0^1 e^{-\int_y^1 d\hat{y}\hat{y}\tilde{\phi}'^2/2} V y^2 dy \tag{5.15}$$

where $\tilde{\phi}' = \tilde{\phi}_{,y}$. The minimum clearly exists since the integral is bounded below by $-V_0$. Clearly ρ_V is a continuous function of V, and R_1 is now a free parameter that acts like an overall scale. If $\rho_V < -V_1$ then the PET does not hold, since the contribution to the mass from the $(\phi_{,r})^2$ term is proportional to R_1 while the contribution from V is proportional to R_1^3. So for large R_1, the mass will be negative. However, if $\rho_V \geq -V_1$, then the PET will hold since this minimal configuration has positive mass. (When the PET holds, the true minimal configuration has zero mass and corresponds to $\phi(r) = \phi_1$ for all r. Our minimal configuration has positive mass, since it is required to have $V(\phi(0)) < -3V_1$.)

To compute ρ_V for a given theory we take the variation $\delta\phi$ of the integral (5.15), to find the lowest mass configuration subject to the boundary conditions discussed above. This yields the following integro-differential equation for the 'optimal' paths $\tilde{\phi}(y)$,

$$\int_0^{\bar{y}} dy\, y^2 V(\tilde{\phi}) e^{-\int_y^1 d\hat{y}\,\hat{y}\tilde{\phi}'^2/2} = \tag{5.16}$$

$$-\frac{e^{-\int_0^1 d\hat{y}\,\hat{y}\tilde{\phi}'^2/2}\left(\bar{y}^2 V_{,\tilde{\phi}} + \bar{y}^3\tilde{\phi}' V(\tilde{\phi})\right)}{\bar{y}\tilde{\phi}'' + \tilde{\phi}'}$$

where all derivatives on the right hand side are evaluated at $\bar{y}$. Notice that the left hand side is precisely $m_V(\bar{y})/4\pi R_1^3$, so equation (5.16) expresses the density ρ_V of the optimal paths in terms of field derivatives at $y = 1$.

To give a concrete example, we numerically solve eq. (5.16) and compute ρ_V for the following one-parameter family of potentials (shown in Fig. 2 for $\alpha = 45.9$),

$$V(\phi) = -3 + 50\phi^2 - 81\phi^3 + \alpha\phi^6. \tag{5.17}$$

We have chosen the parameter α to control the height of the barrier between both extrema. For $\alpha = 45.928$ we have $\rho_V = -V_1$. For this potential, $V_0 = 1$, $V_1 = .305$, and $\phi_1 = .725$. The solution for the optimal path in the theory at the transition point is shown in Fig. 3. The solution starts at the global minimum at the origin $y = 0$, climbs very slowly out the true vacuum and reaches the false vacuum at $y = 1$.

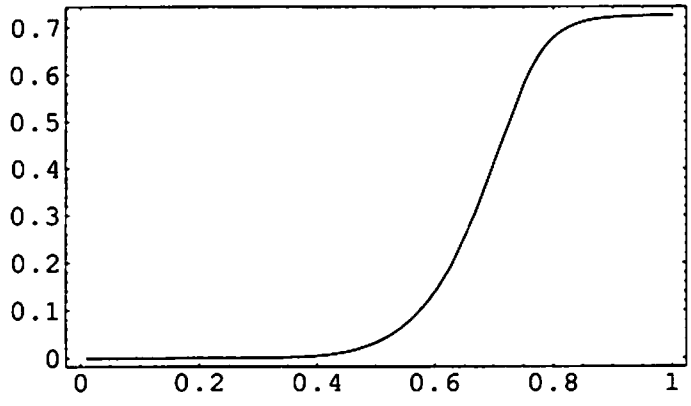

Figure 3: The lowest mass configuration $\tilde{\phi}(y)$, subject to the boundary conditions discussed in the text, for the potential shown in figure 2.

At the transition point, $\rho_V + V_1 = 0$, the potential contribution to the mass vanishes. In terms of the area coordinate $r = yR_1$, the total ADM mass of the minimal configuration $\phi(r)$ is then given by

$$M = 2\pi \int_0^{R_1} e^{-\int_r^{R_1} \tilde{r}(\phi,_r)^2/2\, d\tilde{r}} (\phi,_r)^2 r^2 dr \propto R_1 \ . \tag{5.18}$$

So, let us assume that cosmic censorship holds. Then, there would a black hole with size $R_s \sim e^{-2l} R_1$ since the large approximately homogeneous region ($y \leq 0.58$) collapses to a singularity, where l is a large positve constant independent of R_1 (see [24] in details). However, the mass of the black hole would be proportional to $R_s^3 \sim e^{-6l} R_1^3 >> R_1$ in the limit $R_1 \to \infty$, which leads to a contradiction.

6 Asymptotically flat supersymmetric compactification

Until now we have shown that cosmic censorship is violated in asymptotically anti de Sitter spacetime, including $\mathcal{N} = 8$ gauged supergravity. So, a simple question naturally arises: can we also show that cosmic censorship is violated in asymptotically flat higher-dimensional spacetime? Unfortunately, we will not come to a definite conclusion, as we mentioned earlier. We can say, however, that a class of asymptotically flat higher dimensional spacetime admits an arbitrary large negative curvature along the macroscopic direction!

The key mathematical fact is as follows: As shown in [25], all simply connected compact manifolds of dimension five, six, or seven admit Riemannian metrics with positive

scalar curvature. Other manifolds, such as T^n and $K3$ do not. Positive scalar curvature on K leads to negative energy density as follows. Vacuum solutions can be characterized by their initial data on $\mathbf{R}^3 \times K$. Since we want to minimize the energy, we set the time derivatives of the metric to zero. For time symmetric initial data, the Einstein constraint equations reduce to the vanishing of the scalar curvature, $\mathcal{R} = 0$. For a product metric on $\mathbf{R}^3 \times K$, $\mathcal{R} = \mathcal{R}_3 + \mathcal{R}_K$ where $\mathcal{R}_3$ is the scalar curvature on $\mathbf{R}^3$ and $\mathcal{R}_K$ is the scalar curvature on K. If $\mathcal{R}_K > 0$, we must take $\mathcal{R}_3 < 0$. But negative scalar curvature on $\mathbf{R}^3$ is just like negative energy density. (Recall that the usual constraint of $3+1$ dimensional general relativity says[7] $\mathcal{R}_3 = 2\rho$ in the time symmetric case.) Therefore, from an effective four dimensional standpoint, positive scalar curvature on K acts like negative energy density. In other words, ten dimensional vacuum gravity has configurations with effective negative energy density! Of course, we must require that the metric on K approaches the standard Ricci flat metric at infinity, so we cannot keep the metric a product everywhere. However, one can satisfy this boundary condition and keep the region of negative energy density by taking the metric to be product inside a large ball of radius R_0. In a finite transition region, $R_0 < r < R_1$, one can change the metric on K to the standard Ricci flat metric.

Not only is there negative energy density in four dimensions, but this energy can be arbitrarily negative. This follows immediately from the fact that there is no upper bound on the scalar curvature $\mathcal{R}_K$. Given a metric on K with $\mathcal{R}_K > 0$, one can clearly rescale it by a constant factor and make the scalar curvature arbitrarily large. This shows that the negative energy density is unbounded from below.

To describe this more in details, let us consider the metric

$$ds^2 = \left(1 - \frac{2m(r)}{r}\right)^{-1} dr^2 + r^2 d\Omega_2^2 + g_{mn}(r,y) dy^m dy^n \tag{6.19}$$

where the indices m, n label the extra compact dimensions. The metric $g_{mn}(r,y)$ denotes a one parameter family of metrics on K. The Ricci scalar of (6.19) is

$$\begin{aligned} \mathcal{R} &= -\left(1 - \frac{2m(r)}{r}\right)\left[-\frac{1}{4}\partial_r g^{mn}\partial_r g_{mn} + g'' + \frac{2}{r}g' + \frac{1}{4}(g')^2\right] \\ &\quad + \mathcal{R}_K + \partial_r m\left(\frac{4}{r^2} + \frac{g'}{r}\right) - \frac{m}{r^2}g' \end{aligned} \tag{6.20}$$

where $g' \equiv g^{mn}\partial_r g_{mn}$, $g'' = \partial_r g'$, and $\mathcal{R}_K$ is the scalar curvature of $g_{mn}(r,y)$ at fixed r.

Inside some region $r < R_0$, we choose $g_{mn}(r,y)$ to be independent of r, and equal to some metric with $\mathcal{R}_K = 2V_0$, a positive constant. In this case, the contraint $\mathcal{R} = 0$ reduces to $\partial_r m = -V_0 r^2/2$ which is easily solved for $m(r)$ yielding a region of constant negative energy density. We now pick a radius $R_1 > R_0$ and choose any path in the space of metrics which connects our positive scalar curvature metric $g_{mn}(R_0, y)$ to a metric on the moduli space, $g_{mn}(R_1, y)$. In general, we cannot solve $\mathcal{R} = 0$ for $m(r)$ because there is nontrivial y dependence. However, we can find an $m(r)$ so that $\mathcal{R} \geq 0$. We can either view this as non vacuum initial data for string theory, by adding say a dilaton with $\varphi = 0$

[7] We set $8\pi G = 1$.

and $\dot{\varphi}^2 = \mathcal{R}$. Or we can obtain vacuum initial data by a subsequent conformal rescaling of the nine dimensional metric (6.19). Let $\widetilde{ds}^2 = e^{4\psi/7} ds^2$, then the change in the scalar curvature is given by

$$\tilde{\mathcal{R}} = \psi^{-4/7} \left[\mathcal{R} - \frac{32}{7} \psi^{-1} \nabla^2 \psi \right]. \tag{6.21}$$

So if ψ is a solution to the conformally invariant Laplace equation in nine dimensions

$$-\nabla^2 \psi + \frac{7}{32} \mathcal{R} \psi = 0 \tag{6.22}$$

then the rescaled scalar curvature vanishes. In order for the rescaled metric to be nonsingular and asymptotically flat, we need a solution ψ which is nonvanishing and goes to one at infinity. One can show that such solutions always exist when $\mathcal{R} \geq 0$. This conformal rescaling can only decrease the total energy since the ADM mass changes by

$$\Delta M \propto - \oint \nabla \psi \propto - \int \mathcal{R} \psi < 0. \tag{6.23}$$

From the four dimensional viewpoint, the metric on K is like a collection of scalar fields with potential $-\mathcal{R}_K$. Qualitatively, this potential has a local minimum at zero when g_{mn} is on the moduli space. There is then a finite positive barrier separating this minimum from a region where the potential is negative. Since the potential is just the scalar curvature, the height of the barrier is roughly $1/L_K^2$ where L_K is a characteristic size of K. Thus large Calabi-Yau spaces have small potential barriers. The width of the potential is harder to estimate since it depends on mathematical details about the space of metrics on K which are not yet known. For example, a key open question is: How close does the moduli space of Ricci flat metrics come to the region of positive scalar curvature metrics? The positive energy theorems we discuss later can be used to give some information about this distance.

Once one reaches a metric of constant scalar curvature $\mathcal{R}_K = 2V_0 > 0$, one can always rescale the metric by a conformal factor which is constant on K, to increase the curvature and make the effective three dimensional energy density more negative. We can easily compute the effective potential for this mode. Let us start with a product metric on $\mathbf{R}^3 \times K$, $ds^2 = ds_3^2 + ds_K^2$. Let ϕ be a function depending only on $\mathbf{R}^3$. The scalar curvature of the metric

$$ds^2 = e^{-n\phi} ds_3^2 + e^{2\phi} ds_K^2 \tag{6.24}$$

is

$$\mathcal{R} = e^{n\phi} [\mathcal{R}_3 + 2V_0 e^{-(2+n)\phi} - \frac{n(n+2)}{2} (\nabla \phi)^2] \tag{6.25}$$

where n is the dimension of K. The second term on the right is just the scalar curvature of the rescaled metric on K. The vacuum constraint is $\mathcal{R} = 0$, and in $3+1$ dimensions, the energy density is $\rho = \mathcal{R}_3/2$. So we obtain

$$\rho = \frac{n(n+2)}{4} (\nabla \phi)^2 - V_0 e^{-(2+n)\phi}. \tag{6.26}$$

Rescaling ϕ to have a standard kinetic term we get

$$\rho = \frac{1}{2}(\nabla\tilde{\phi})^2 - V_0 e^{-\alpha\tilde{\phi}} \tag{6.27}$$

where

$$\alpha^2 = \frac{2(n+2)}{n}. \tag{6.28}$$

So the potential is not only negative, but falls off exponentially fast. Notice that for more than one extra dimension, $2 < \alpha^2 < 6$.

7 Discussion

We explored a non-linear instability in supersymmetric compactifications. We first showed that cosmic censorship is violated in $D = 5$, $\mathcal{N} = 8$ supergravity, which is the low energy limit of string theory with $AdS_5 \times S^5$ boundary conditions. With $AdS_4 \times S^7$ boundary conditions, one obtains $D = 4$, $\mathcal{N} = 8$ supergravity. Although we have focused on five dimensions, this theory also has fields which saturate the BF bound. So, it will also have negative energy solutions and violate cosmic censorship. We next showed that cosmic censorship is violated in certain theories with a positive energy theorem in asymptotic AdS space. The mechanism for producing a naked singularity is not sensitive to the configuration of the potential. This implies that a large class of potentials may produce a naked singularity in asymptotic AdS.

It is an open question whether the cosmic censorship hypothesis holds in string theory with asymptotically flat boundary conditions. We finally showed, however, that a large class of Calabi-Yau compactifications of the form $M_4 \times K$ contains four-dimensional potentials which become negative. In this case the positive energy theorem guarantees the positivity of the ADM energy for all solutions that tend asymptotically to the supersymmetric vacuum. However one might imagine there exist certain configurations that have a large central region with negative energy density which develops a singularity, but with a positive total mass that is too small to enclose the singular region by an event horizon. It would be worth investigating this more in details.

In $\mathcal{N} = 8$ gauged supergravity model, it is believed that AdS/CFT correspondence exists. This implies that string theory must resolve the naked singularities, indicating that *classical* string theory should resolve these singularities. This can be viewed as saying that the α' corrections prevent the curvature from diverging, but another interpretation is simply that the spacetime metric is not well defined near the singularity.

Since the singularities are spacelike in the central region, the resolution of the singularity in the gauge theory should determine whether the the universe can "bounce". There are two possibilities. After the formation of the singularity in AdS, the field theory state could correspond to a bulk metric which is semiclassically well defined only outside a finite region, or it could correspond to a metric which is well defined everywhere. In the first case, the classical naked singularity would continue for a while. (It might continue for all time, or eventually the metric could become well defined again and the naked singularity would disappear.) In the second case, the naked singularity would only last an instant. This would be analogous to passing through cosmological singularities in

quantum gravity. There has been considerable debate recently about this possibility. We now have a new concrete approach for settling this issue.

Acknowledgments

This work was supported in part by a Yukawa fellowship.

References

[1] L. Randall and R. Sundrum, "A Large Mass Hierarchy from a Small Extra Dimension," Phys. Rev. Lett. **83** (1999) 3370; "An Alternative to Compactification," Phys. Rev. Lett. **83** (1999) 4690.

[2] D. M. Eardley and S. B. Giddings, "Classical Black Hole Production in High-Energy Collisions," Phys.Rev. D66 (2002) 044011.

[3] R. Penrose, "On the instability of extra space dimensions," in *The future of theoretical physics and cosmology*, Festschrift in honor of S. W. Hawking's 60th birthday, G. W. Gibbons, S. Rankin and P. Shellard eds., to appear.

[4] J. Geddes, "The collapse of large extra dimensions," Phys. Rev. D **66**(2002)023507

[5] B. de Wit, H. Nicolai, "The Consistency of the S^7 Truncation in $D = 11$ Supergravity," Nucl. Phys. **B281** (1987) 211.

[6] J. M. Maldacena, "The large N limit of superconformal field theories and supergravity," Adv. Theor. Math. Phys. **2** (1998) 231 [Int. J. Theor. Phys. **38** (1999) 1113] [arXiv:hep-th/9711200].

[7] P. K. Townsend, "Positive Energy And The Scalar Potential In Higher Dimensional (Super)Gravity Theories," Phys. Lett. B **148** (1984) 55.

[8] P. Breitenlohner and D. Z. Freedman, "Stability In Gauged Extended Supergravity," Annals Phys. **144** (1982) 249; "Positive Energy In Anti-De Sitter Backgrounds And Gauged Extended Supergravity," Phys. Lett. B **115** (1982) 197.

[9] M. Cvetic, H. Lu, C. N. Pope, A. Sadrzadeh, T. A. Tran, "Consistent $SO(6)$ Reduction Of Type IIB Supergravity on S^5," Nucl. Phys. **B586** (2000) 275 [arXiv:hep-th/0003103].

[10] M. Gunaydin, L. J. Romans, N. P. Warner, "Gauged $N = 8$ Supergravity in Five Dimensions," Phys. Lett. **154B** (1985) 268; "Compact and Noncompact Gauged Supergravity Theories in Five Dimensions," Nucl. Phys. **272** (1986) 598.

[11] M. Pernici, K. Pilch, P. van Nieuwenhuizen, "Gauged $N = 8$ $D = 5$ Supergravity,"Nucl. Phys. **B259** (1985) 460.

[12] O. DeWolfe, D. Z. Freedman, S. S. Gubser, G. T. Horowitz, I. Mitra, "Stability of $AdS_p \times M_q$ Compactifications Without Supersymmetry," Phys. Rev. D **65** (2002) 064033 [arXiv:hep-th/0105047].

[13] D. Z. Freedman, S. S. Gubser, K. Pilch, N. P. Warner, "Continuous Distributions of D3-Branes and Gauged Supergravity," JHEP **0007** (2000) 038 [arXiv:hep-th/9906194].

[14] L. Mezincescu, P. K. Townsend, "Stability at a Local Maximum in Higher Dimensional Anti-de Sitter Space and Applications to Supergravity," Ann. Phys. **160** (1985) 406.

[15] W. Boucher, "Positive Energy Without Supersymmetry," Nucl. Phys. B **242** (1984) 282.

[16] E. Witten, "A Simple Proof Of The Positive Energy Theorem," Commun. Math. Phys. **80** (1981) 381.

[17] J. M. Nester, "A New Gravitational Energy Expression with a Simple Positivity Proof," Phys. Lett. **83A** (1981) 241.

[18] B. Ghosh and S. Mukhi, "Killing spinors and supersymmetric AdS orbifolds," JHEP **9910** (1999) 021 [arXiv:hep-th/9908192].

[19] M. Henneaux, C. Teitelboim, "Asymptotically Anti-de Sitter Spaces," Comm. Math. Phys. **98** (1985) 391.

[20] T. Hertog, G. T. Horowitz, and K. Maeda, "Negative Energy in String Theory and Cosmic Censorship Violation," hep-th/0310054, to appear in Phys. Rev. D.

[21] S. R. Coleman and F. De Luccia, "Gravitational Effects On And Of Vacuum Decay," Phys. Rev. D **21** (1980) 3305.

[22] T. Banks, "T C P, Quantum Gravity, The Cosmological Constant And All That..," Nucl. Phys. B **249** (1985) 332.

[23] M. W. Choptuik, "Universality and scaling in gravitational collapse of a massless scalar field," Phys. Rev. Lett. **70**(1993)9.

[24] T. Hertog, G. T. Horowitz, K. Maeda, "Generic Cosmic Censorship Violation in anti de Sitter Space," [arXiv:gr-qc/0307102].

[25] T. Hertog, G. T. Horowitz and K. Maeda, "Negative energy density in Calabi-Yau compactifications," JHEP **0305** (2003) 060 [arXiv:hep-th/0304199].

The Curvaton Mechanism and Its Implications to Particle Cosmology

Takeo Moroi[†]

Department of Physics, Tohoku University, Sendai 980-8578, Japan

Abstract

I will describe basic features of the curvaton scenario where the primordial fluctuation of a late-decaying scalar field, called "curvaton," becomes the dominant source of the cosmic density fluctuations. I will also discuss its implications to the particle cosmology.

1 Introduction

In the study of the evolution of the universe, it is important to understand the origin of the cosmic density fluctuations. The most conventional scenario is inflation [1] where quantum fluctuation of the inflaton field during the inflation becomes the origin of the cosmic density fluctuations. From the particle-physics point of view, it is desirable to construct a model of inflation which is testable by collider (or other laboratory) experiments; if it is possible, we can test the mechanism of the cosmological density fluctuations with collider experiments. It is, however, difficult to construct such a testable model of inflation since the requirements on the inflaton potential is very stringent.[#1]

Recently, a new mechanism of generating the cosmic density fluctuations has been attracting many attentions, where a late-decaying scalar condensation provides the dominant source of the cosmic density fluctuations. In this scenario, dominant part of the cosmic density fluctuations originate from the primordial fluctuation of a new scalar field, called "curvaton," which is different from the inflaton field [3, 4, 5]. Even though, in a large class of the curvaton scenario, inflation is assumed as a solution to the horizon and flatness problems as well as to generate the primordial fluctuation of the curvaton field, constraints on the inflaton potential can be relaxed in the curvaton scenario. In addition, since the requirements on the curvaton is not so stringent, it is possible to use (some of the) well-motivated particles as the curvaton; for example, scalar fields in the minimal supersymmetric standard model (MSSM) may play the role of the curvaton. In such a case, it may be possible to study the properties of the fields responsible for the structure formation by collider experiments. (For detailed studies of the curvaton scenario, see [6].)

Here, I will review the curvaton scenario and discuss some of its implications to particle cosmology. Organization of the rest of this article is as follows. In Section 2, I introduce the scenario I consider and discuss the mechanism of generating the cosmological density fluctuations via the curvaton mechanism. Then, in Section 3, behaviors of the Cosmic Microwave Background (CMB) anisotropy in the curvaton scenario are studied. Implications to some classes of cosmological scenarios are discussed in Section 4. Section 5 is devoted for the conclusions and discussion.

2 Mechanism

2.1 Thermal history

I first discuss the scenario we consider. In the curvaton scenario, there are two scalar fields which play important roles; one is the inflation χ and the other is the curvaton field ϕ.[#2] The most important

[†]E-mail:moroi@tuhep.phys.tohoku.ac.jp

[#1]Within the minimal supersymmetric standard model, however, it may be possible to use some of the scalar quarks and Higgs bosons as the inflaton. For detail, see [2].

[#2]I assume the inflation to solve the horizon and flatness problems. The curvaton mechanism may be implemented in the pre-big-bang [7] and the ekpyrotic [8] scenarios. In this article, however, I will not discuss those cases.

aspects of the curvaton scenario do not depend on the details of the inflation. Thus, I do not assume any specific form of the inflaton potential. On the contrary, resultant density fluctuations depend on the potential of the curvaton field. Here, for simplicity, I adopt the simplest form of the curvaton potential, i.e., the parabolic one:

$$V(\phi) = \frac{1}{2} m_\phi^2 \phi^2, \tag{2.1}$$

where m_ϕ is smaller than the expansion rate of the universe during the inflation $H_{\rm inf}$. In addition, the curvaton field is assumed to have non-vanishing initial amplitude $\phi_{\rm init}$.

In the scenario, the universe starts with the inflationary epoch and, after the inflation, the universe is reheated by the decay of the inflaton. Then, the universe is dominated by the radiation (which I call γ_χ). I call the radiation-dominated epoch filled with radiation generated from the decay products of the inflaton as the first radiation dominated epoch, or RD1 epoch, since, in the curvaton scenario, there are two radiation-dominated epochs. Denoting the decay rate of the inflaton as Γ_χ, reheating temperature after the inflation is given by[#3]

$$T_{\rm R1} \sim \sqrt{M_* \Gamma_\chi}, \tag{2.2}$$

where M_* is the reduced Planck scale. In the early stage of the RD1 epoch, slow-roll condition is satisfied for the curvaton field. As the universe expands, however, the curvaton field starts to oscillate. (See Fig. 1.) When $\Gamma_\phi \lesssim H \lesssim m_\phi$ (with Γ_ϕ being the decay rate of ϕ), energy density of ϕ behaves as that of non-relativistic matter. Then, the energy density of the curvaton ρ_ϕ is proportional to a^{-3} while the energy density of γ_χ is proportional to a^{-4}, where a is the scale factor. Thus, as the universe expands, curvaton dominates the universe (if the lifetime of the curvaton is long enough). I call this epoch as curvaton-dominated epoch, or ϕD epoch. The curvaton field decays when the expansion rate becomes comparable to the decay rate of the curvaton. The reheating temperature due to the curvaton decay is given by

$$T_{\rm R2} \sim \sqrt{M_* \Gamma_\phi}. \tag{2.3}$$

Schematic picture of the evolutions of the energy densities of various components in the universe is given in Fig. 2.

2.2 Evolutions of the fluctuations

In the curvaton scenario, ϕ also acquires the primordial fluctuation during the inflation. Denoting the curvaton field (with comoving momentum coordinate $\vec{x}$) as[#4]

$$\phi(t, \vec{x}) = \phi(t) + \delta\phi(t, \vec{x}), \tag{2.4}$$

let us consider the two-point correlation function of the fluctuation:

$$\langle 0|\delta\phi(t,\vec{x})\delta\phi(t,\vec{y})|0\rangle = \int \frac{dk}{k} \frac{d\Omega_{\vec{k}}}{4\pi} |\delta\phi(t,\vec{k})|^2 e^{i\vec{k}(\vec{x}-\vec{y})}. \tag{2.5}$$

Then, the Fourier amplitude generated during the inflation is given by

$$\delta\phi(t,\vec{k}) = \left(\frac{k}{2aH_{\rm inf}}\right)^{m_\phi^2/3H_{\rm inf}^2} \left[\frac{H_{\rm inf}}{2\pi}\right]_{k=aH_{\rm inf}}, \tag{2.6}$$

where the subscript "$k = aH_{\rm inf}$" implies that the quantity is evaluated at the time of the horizon-exit during the inflation. As I discuss below, the primordial fluctuation of ϕ given in Eq. (2.6) becomes the origin of the cosmic density fluctuations in the curvaton scenario.

[#3] In the following discussions, I neglect $O(1)$ coefficients which are not important.

[#4] Here, I use the same notation for the zero-mode and for the total amplitude since there should be no confusion.

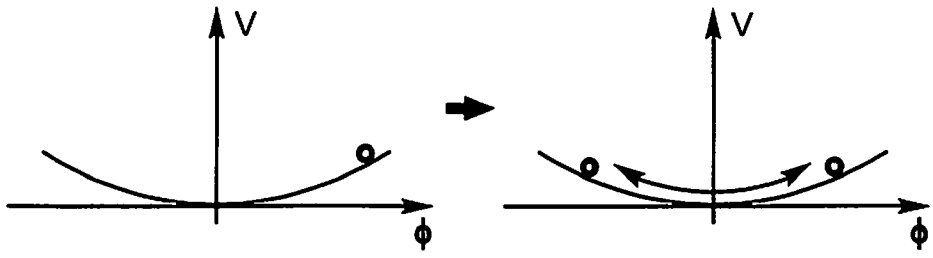

Figure 1: Behavior of the curvaton field in the early universe.

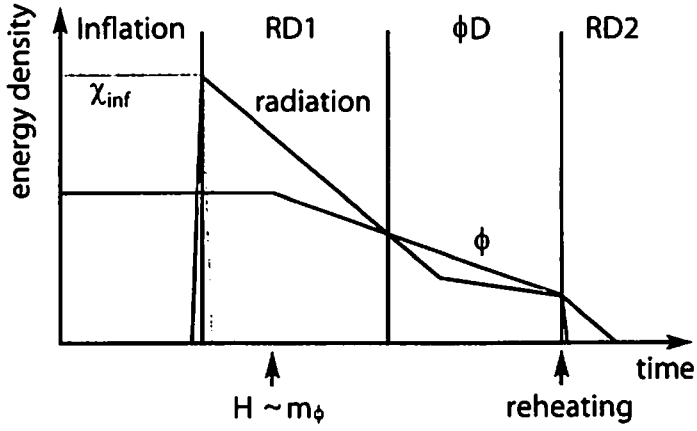

Figure 2: Evolutions of the energy densities of various components in the universe. Here, I adopt the instantaneous decay approximation for the inflaton decay, and hence the epoch where the universe is dominated by the inflaton oscillation just after the inflation is not shown in this figure.

Now, we are at the position to discuss the evolutions of the cosmological density fluctuations generated from $\delta\phi_{\rm init}$. For this purpose, I use the Newtonian gauge where the line element is described with the metric perturbations Ψ and Φ as[#5]

$$ds^2 = -(1+2\Psi)dt^2 + a^2(1+2\Phi)d\vec{x}^2 = a^2\left[-(1+2\Psi)d\tau^2 + (1+2\Phi)d\vec{x}^2\right], \tag{2.7}$$

where τ is the conformal time. In addition, the variable δ_X is defined as

$$\delta_X \equiv \delta\rho_X/\rho_X, \tag{2.8}$$

where the subscript X denotes the individual components (like radiation, cold dark matter (CDM), baryon, and so on) and $\delta\rho_X$ is the fluctuation of the energy density of X.

Substituting Eq. (2.7) into the Einstein equation, we obtain the generalized Poisson equation for Φ:

$$k^2\Phi = \frac{1}{2M_*^2}\left(\frac{a}{a_0}\right)^2 \rho_{\rm tot}\left[\delta_{\rm tot} + \frac{3\mathcal{H}}{k}(1+\omega_{\rm tot})V_{\rm tot}\right]. \tag{2.9}$$

Here, "tot" denotes the total matter and the variable V_X denotes the velocity perturbation of the component X. Furthermore, $\omega_{\rm tot} \equiv \rho_{\rm tot}/p_{\rm tot}$ the equation-of-state parameter for the total matter, and

$$\mathcal{H} \equiv \frac{1}{a}\frac{da}{d\tau}. \tag{2.10}$$

[#5]Here, I use the notation and convention of [9] unless otherwise mentioned.

In addition, I consider the situation where the temperature of the universe is so high that the momentum-exchange of relativistic particles are efficient enough. In this case, perturbation of the radiation becomes locally isotropic and the anisotropic stress perturbation vanishes, resulting in $\Psi + \Phi = 0$.

When the perturbation of the radiation becomes locally isotropic, the equations for the density and velocity perturbations of the radiation are given by

$$\delta_\gamma' = -\frac{4}{3}kV_\gamma - 4\Phi', \tag{2.11}$$

$$V_\gamma' = \frac{1}{4}k\delta_\gamma + k\Psi, \tag{2.12}$$

where the "prime" denotes the derivative with respect to the conformal time τ. In addition, if a very weakly interacting non-relativistic component exists, its perturbations obey the following equations:

$$\delta_m' = -kV_m - 3\Phi', \tag{2.13}$$

$$V_m' = -\mathcal{H}V_m + k\Psi, \tag{2.14}$$

where the subscript "m" is for non-relativistic matters. Notice that, when a scalar field is oscillating, the equation-of-state parameter of the scalar condensation vanishes and hence the density and velocity perturbations of the scalar field also obey Eqs. (2.13) and (2.14).

In the curvaton scenario, it is assumed that the primordial fluctuation $\delta\phi_{\rm init}$ becomes the dominant source of the cosmic density fluctuations. Thus, hereafter, I will discuss the density fluctuations generated from $\delta\phi_{\rm init}$. When $\Gamma_\phi \lesssim H \lesssim m_\phi$, then, the situation is like the case with isocurvature fluctuation in non-relativistic matter component [10]. In the curvaton case, as in the conventional isocurvature case, it is convenient to define the (primordial) entropy fluctuation between ϕ (and its decay products) and the photon from the inflaton γ_χ:

$$S_{\phi\chi} \equiv \left[\delta_\phi - \frac{3}{4}\delta_{\gamma_\chi}\right]_{\rm RD1}. \tag{2.15}$$

In the curvaton scenario, cosmological density fluctuations are parameterized by using $S_{\phi\chi}$.

In order to discuss the evolutions of the fluctuations, it is important to know the equation-of-state parameters of individual components in the universe. If all the components behave as the relativistic or the non-relativistic matter, evolutions of the perturbations are described by Eqs. (2.11) – (2.14). In this case, it is convenient to distinguish the photon (or any other components) from the decay product of ϕ from that from the inflaton field, which I call γ_ϕ and γ_χ, respectively.[#6] In order to consider δ_{γ_ϕ} in the RD2 epoch, we can neglect γ_χ since the CMB radiation at this epoch is dominantly from the ϕ field. Then, we find that, in the RD2 epoch, Ψ and δ_{γ_ϕ} become constant while $V_{\gamma_\phi} = O(k\tau)$ up to higher order corrections. Indeed, combining Eq. (2.9) with Eqs. (2.11) and (2.12), and using $\delta_{\rm tot} = \delta_{\gamma_\phi}$ and $V_{\rm tot} = V_{\gamma_\phi}$, we obtain $V_{\gamma_\phi}^{(\delta\phi)} = -\frac{1}{2}k\tau\Psi_{\rm RD2}^{(\delta\phi)}$ and

$$\delta_{\gamma_\phi}^{(\delta\phi)} = -2\Psi_{\rm RD2}^{(\delta\phi)}, \tag{2.16}$$

where $\Psi_{\rm RD2}^{(\delta\phi)}$ is the metric perturbation induced by the primordial fluctuation of the amplitude of ϕ. (In the following, the superscript "$(\delta\phi)$" is for perturbations generated from the primordial fluctuation of ϕ.) As I mentioned, $\Psi_{\rm RD2}^{(\delta\phi)}$ is constant up to a correction of $O(k^2\tau^2)$.

Behavior of $\delta_{\gamma_\chi}^{(\delta\phi)}$ is also easily understood. In discussing the effects of the primordial fluctuation of ϕ, we neglect the initial fluctuation of the inflaton field and hence $\delta_{\gamma_\chi}^{(\delta\phi)} \to 0$ in the deep RD1 epoch. In addition, from Eqs. (2.11) and (2.12), $V_{\gamma_\chi}^{(\delta\phi)}$ becomes higher order in $k\tau$ than $\delta_{\gamma_\chi}^{(\delta\phi)}$ and $\Psi^{(\delta\phi)}$. Thus, we obtain

$$\delta_{\gamma_\chi}^{(\delta\phi)} = 4\Psi^{(\delta\phi)}. \tag{2.17}$$

[#6] In fact, these photons are mixed each other and they cannot be defined separately. In other words, their velocity perturbations should be the same since they form a single fluid. Even so, the following arguments are unchanged as far as we consider the leading terms in the density perturbations since the velocity perturbation is at most $O(k\tau)$. In the following discussion, γ_ϕ and γ_χ should be understood as representatives of the components which are and are not generated from the decay product of ϕ, respectively.

The above relation holds in the RD1, ϕD, and RD2 epochs up to corrections of $O(k^2\tau^2)$.

$\Psi_{\rm RD2}^{(\delta\phi)}$ can be related to $S_{\phi\chi}^{(\delta\phi)}$. Using the fact that the entropy fluctuation is a conserved quantity for superhorizon mode, the following relation holds:

$$S_{\phi\chi}^{(\delta\phi)} = \left[\frac{3}{4}\delta_{\gamma_\phi}^{(\delta\phi)} - \frac{3}{4}\delta_{\gamma_\chi}^{(\delta\phi)}\right]_{\rm RD2} = \left[\delta_\phi^{(\delta\phi)} - \frac{3}{4}\delta_{\gamma_\chi}^{(\delta\phi)}\right]_{\phi{\rm D,RD1}}. \tag{2.18}$$

With this relation, in particular, we obtain

$$\Psi_{\rm RD2}^{(\delta\phi)} = -\frac{2}{9}S_{\phi\chi}^{(\delta\phi)}. \tag{2.19}$$

Density fluctuations of various components are also parameterized by $S_{\phi\chi}^{(\delta\phi)}$. Detailed properties of the density fluctuations, however, depends on how the various components in the universe are produced. If a component X is generated from the decay product of ϕ, then there is no entropy between the photon (i.e., γ_ϕ) and X. On the contrary, if some other scalar field ψ generates X, the entropy between the photon and X is the same as $S_{\phi\chi}^{(\delta\phi)}$. Thus, if all the components in the universe are generated from ϕ, the density fluctuations become purely adiabatic and

$$\left[\delta_\gamma^{(\delta\phi)}\right]_{\rm RD2} = \frac{4}{3}\left[\delta_b^{(\delta\phi)}\right]_{\rm RD2} = \frac{4}{3}\left[\delta_c^{(\delta\phi)}\right]_{\rm RD2} = -2\Psi_{\rm RD2}^{(\delta\phi)}, \tag{2.20}$$

where the subscripts γ, b, and c are for the photon, baryon, and CDM, respectively. In this case, the isocurvature perturbation in the ϕ field is converted to the purely adiabatic density perturbation after the decay of ϕ. On the contrary, if the baryon asymmetry is generated by the scalar field ψ, the entropy between the radiation and the baryon becomes $S_{\phi\chi}^{(\delta\phi)}$ and hence [5, 11]

$$\left[\delta_\gamma^{(\delta\phi)}\right]_{\rm RD2} = \frac{4}{3}\left[\delta_c^{(\delta\phi)}\right]_{\rm RD2} = -2\Psi_{\rm RD2}^{(\delta\phi)}, \quad \left[\delta_b^{(\delta\phi)}\right]_{\rm RD2} = \frac{3}{4}\left[\delta_\gamma^{(\delta\phi)}\right]_{\rm RD2} + \frac{9}{2}\Psi_{\rm RD2}^{(\delta\phi)}, \tag{2.21}$$

and in the case where ψ is responsible for the CDM while the baryon number is somehow generated from the decay product of ϕ,

$$\left[\delta_\gamma^{(\delta\phi)}\right]_{\rm RD2} = \frac{4}{3}\left[\delta_b^{(\delta\phi)}\right]_{\rm RD2} = -2\Psi_{\rm RD2}^{(\delta\phi)}, \quad \left[\delta_c^{(\delta\phi)}\right]_{\rm RD2} = \frac{3}{4}\left[\delta_\gamma^{(\delta\phi)}\right]_{\rm RD2} + \frac{9}{2}\Psi_{\rm RD2}^{(\delta\phi)}. \tag{2.22}$$

In addition, if the baryon and the CDM are both generated from sources other than ϕ, we obtain

$$\left[\delta_\gamma^{(\delta\phi)}\right]_{\rm RD2} = -2\Psi_{\rm RD2}^{(\delta\phi)}, \quad \left[\delta_b^{(\delta\phi)}\right]_{\rm RD2} = \left[\delta_c^{(\delta\phi)}\right]_{\rm RD2} = \frac{3}{4}\left[\delta_\gamma^{(\delta\phi)}\right]_{\rm RD2} + \frac{9}{2}\Psi_{\rm RD2}^{(\delta\phi)}. \tag{2.23}$$

It is important to notice that, for the cases given in Eqs. (2.21) – (2.23), the isocurvature perturbation is correlated with the adiabatic perturbation.

So far, we have seen that the primordial fluctuation of the curvaton field may generate the metric and density fluctuations. Before closing this section, we should compare the size of the curvaton contribution with the inflaton contribution. Even with the curvaton, there is also a contribution from the inflaton fluctuation since I assume inflation as a solution to the horizon and flatness problems. If we consider the situation where there is no entropy fluctuation, inflaton contribution to the metric perturbation (in the RD2 epoch) is given by [15]

$$\Psi_{\rm RD2}^{(\rm inf)}(k) = \frac{2}{3}\left[\frac{3H_{\rm inf}^2}{V'_{\rm inf}} \times \frac{H_{\rm inf}}{2\pi}\right]_{k=aH}, \tag{2.24}$$

while the curvaton contribution is

$$\Psi_{\rm RD2}^{(\delta\phi)}(k) = -\frac{4}{9}\left[\frac{1}{\phi_{\rm init}} \times \frac{H_{\rm inf}}{2\pi}\right]_{k=aH}. \tag{2.25}$$

(Here and hereafter, the superscript "(inf)" is for quantities generated from the inflaton fluctuation.) As one can see, the curvaton contribution to Ψ is inversely proportional to $\phi_{\rm init}$ and hence, if $\phi_{\rm init}$ is small enough, curvaton contribution dominates over the inflaton contribution.

Thus, in the curvaton scenario, there are two conflicting requirements on the initial amplitude of the curvaton field. One is the upper bound on $\phi_{\rm init}$; upper bound on $\phi_{\rm init}$ for $\Psi^{(\delta\phi)} \gtrsim \Psi^{(\rm inf)}$ depends on the model of the inflation. For the case of the chaotic inflation, for example, the curvaton contribution becomes larger than the inflaton contribution if $\phi_{\rm init} \lesssim M_*$. The other is the lower bound on the $\phi_{\rm init}$, since the ϕD epoch cannot be realized if $\phi_{\rm init}$ is too small. Lower bound depends on the reheating temperatures $T_{\rm R1}$ and $T_{\rm R2}$ given in Eqs. (2.2) and (2.3), respectively. In Fig. 3, I plot the lower bound on $\phi_{\rm init}$ to realize the ϕD epoch.

3 CMB Angular Power Spectrum

3.1 Spectral index

Now, we are at the position to discuss the CMB angular power spectrum in the curvaton scenario. One of the most important consequences of the curvaton scenario is that, if all the components in the universe are generated only from the decay products of ϕ, no entropy fluctuation is generated and the primordial density fluctuations (after the RD2 epoch) becomes purely adiabatic. Let us first consider such a case.

One important check point is that the scale dependence of the primordial density fluctuations. In the case where the cosmic density fluctuations are generated from the primordial fluctuation of the inflaton, scale-dependence originates from the change of the slope of the inflaton potential as well as the expansion rate during the inflation. As can be seen from Eq. (2.25), on the contrary, scale-dependence of the curvaton contribution is only from the change of the expansion rate (as far as $m_\phi \ll H_{\rm inf}$). Thus, even though both the curvaton and inflation contributions are from primordial fluctuations of some scalar fields, their scale-dependences are different. Defining the spectral index $n_{\rm S}$ as

$$\frac{d}{d\ln k}\ln[\Psi_{\rm RD2}^{(\rm inf,\delta\phi)}]^2 \simeq n_{\rm s}^{(\rm inf,\delta\phi)} - 1, \tag{3.1}$$

the spectral indices for the inflaton and curvaton contributions are calculated as

$$n_{\rm s}^{(\rm inf)} = 1 - 6\epsilon + 2\eta, \tag{3.2}$$

$$n_{\rm s}^{(\delta\phi)} = 1 - 2\epsilon, \tag{3.3}$$

where ϵ and η are slow-roll parameters which are given by

$$\epsilon = \frac{1}{2}M_*^2\left(\frac{V'_{\rm inf}}{V_{\rm inf}}\right)^2, \quad \eta = M_*^2\frac{V''_{\rm inf}}{V_{\rm inf}}.$$

Due to the change of the scale-dependence, we can see that the observational constraints on inflation models are relaxed in the curvaton scenario. For example, for the case of the chaotic inflation with the inflaton potential $V_{\rm inf} \propto \chi^{p_{\rm inf}}$, spectral indices for the inflaton and curvaton contributions are estimated as $n_{\rm s}^{(\rm inf)} \simeq 0.96$ and $n_{\rm s}^{(\delta\phi)} \simeq 0.98$ for $p_{\rm inf} = 2$, $n_{\rm s}^{(\rm inf)} \simeq 0.95$ and $n_{\rm s}^{(\delta\phi)} \simeq 0.97$ for $p_{\rm inf} = 4$, and $n_{\rm s}^{(\rm inf)} \simeq 0.94$ and $n_{\rm s}^{(\delta\phi)} \simeq 0.95$ for $p_{\rm inf} = 6$. Thus, using currently available constraint on the spectral index $n_{\rm s} = 0.99 \pm 0.04$ [12] from the WMAP, simple chaotic inflation model with $p_{\rm inf} = 6$ is excluded by the observations while, with the curvaton mechanism, $p_{\rm inf} = 6$ becomes consistent with the observational constraints. For other class of inflation models, change of the constraint may be more drastic.

3.2 Entropy fluctuations

Next, let us discuss the effects of the possible entropy fluctuation in the curvaton scenario. As mentioned in the previous section, in the curvaton scenario, correlated mixture of the adiabatic and isocurvature fluctuations may be generated. In order to discuss effects of the entropy fluctuation to the CMB angular power spectrum, it is convenient to parameterize the density fluctuation of the non-relativistic matter as

$$\left[\delta_m^{(\delta\phi)}\right]_{\rm RD2} \equiv \left[(\Omega_b/\Omega_m)\delta_b^{(\delta\phi)} + (\Omega_c/\Omega_m)\delta_c^{(\delta\phi)}\right]_{\rm RD2} = \frac{3}{4}\left[\delta_\gamma^{(\delta\phi)}\right]_{\rm RD2} + \kappa_m\Psi_{\rm RD2}^{(\delta\phi)}, \tag{3.4}$$

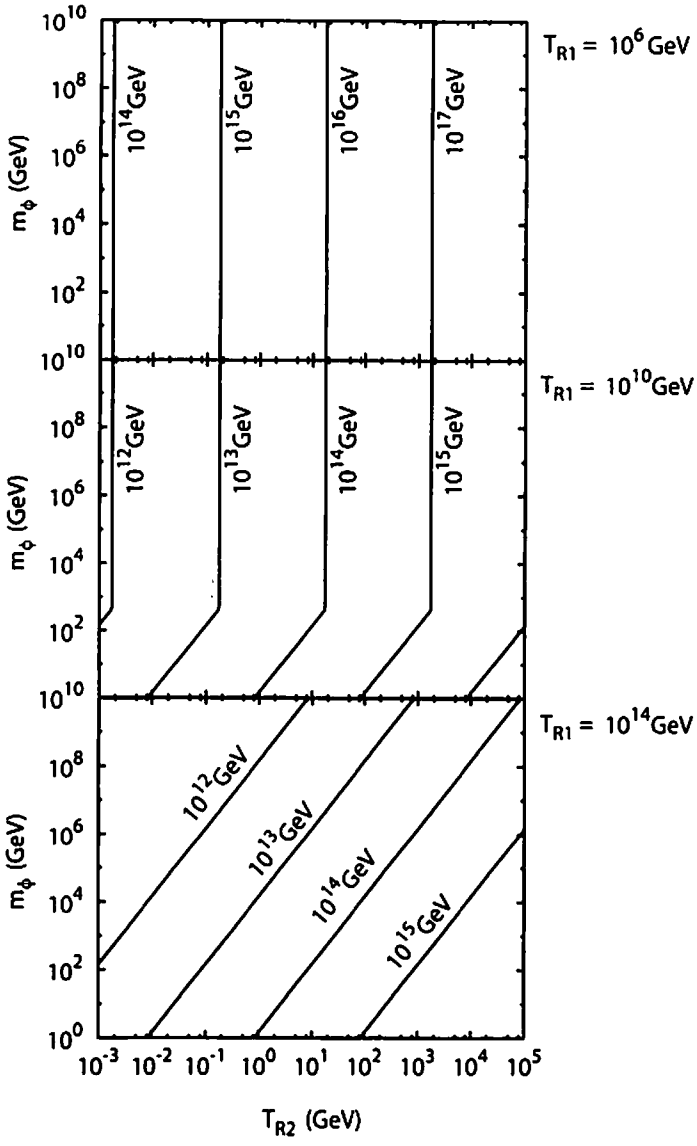

Figure 3: Lower bound on $\phi_{\rm init}$ to realize the ϕD epoch on T_{R2} vs. m_ϕ plane. T_{R1} is taken to be $T_{R1} = 10^6$GeV, $T_{R1} = 10^{10}$GeV and $T_{R1} = 10^{14}$GeV from the top.

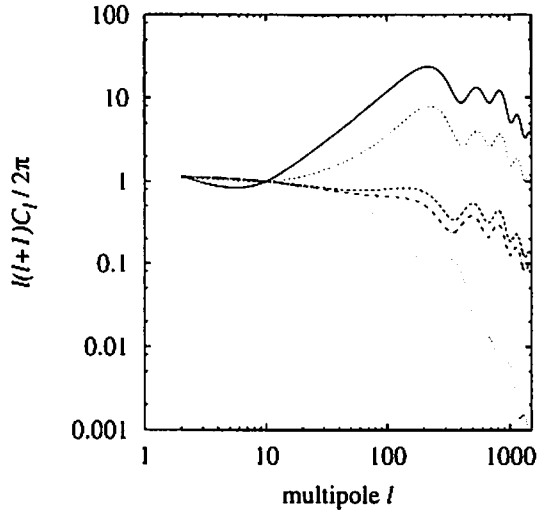

Figure 4: The angular power spectrum with correlated mixture of the adiabatic and isocurvature perturbations in the baryonic sector (solid line), in the CDM sector (long-dashed line), and in the baryonic and CDM sectors (dot-dashed line). (See Eqs. (2.21), (2.22), and (2.23), respectively.) I also show the CMB angular power spectrum for the purely adiabatic (i.e., $\kappa_m = 0$) and purely isocurvature ($\kappa_m = \infty$) cases with short-dashed and dotted lines, respectively. The overall normalizations are taken as $[l(l+1)C_l/2\pi]_{l=10} = 1$.

where Ω_b, Ω_c and Ω_m are the (present) density parameters of the baryon, the CDM, and the non-relativistic component (and hence $\Omega_m = \Omega_b + \Omega_c$). Although the density fluctuations for the baryon and the CDM are independent, shape of the CMB angular power spectrum is determined once κ_m is fixed. For the purely adiabatic case, $\kappa_m = 0$. With the relations (2.21), (2.22), and (2.23), κ_m becomes $\frac{9}{2}(\Omega_b/\Omega_m)$, $\frac{9}{2}(\Omega_c/\Omega_m)$, and $\frac{9}{2}$, respectively.

In Fig. 4, I show how the CMB angular power spectrum depends on the κ_m parameter. As one can see, C_l strongly depends on κ_m and, if $|\kappa_m| \gtrsim O(0.1)$, deviation of the CMB angular power spectrum from the adiabatic result (i.e., C_l with $\kappa_m = 0$) becomes sizable. Importantly, the WMAP results strongly suggest that the primordial density fluctuations be (almost) purely adiabatic; with the WMAP data, $\kappa_m < 0.1$ is obtained [13]. Thus, the WMAP results impose stringent constraint on the curvaton scenario. A possible small contamination of the entropy fluctuation in some case will be discussed in the next section.

4 Implications to Particle Cosmology

4.1 Case of D-term inflation

So far, we have discussed some generic features of the curvaton scenario. As can be imagined, the curvaton scenario has important connection with particle cosmology. Thus, in this section, I would like to show some examples of the applications and implications of the curvaton scenario to several specific cases.

The first topics is the case with D-term inflation in supersymmetric models [14]. One of the strong motivation to consider the D-term inflation is to eliminate the dangerous Hubble-induced mass term; in supergravity, it is often the case that all the scalar fields acquire effective mass during inflation as large as $\sim \pm H_{\rm inf}$ and, if such a large mass is generated for the inflaton, the conventional slow-roll inflation cannot proceed. The dangerous Hubble-induced mass term is generated from expectation value of the F-term potential. In the scenario of the D-term inflation, however, the inflation is driven by the D-term potential and hence we may evade the problem of the Hubble-induced mass.

The primary purpose here is to discuss the application of the curvaton scenario to the D-term inflation, but not to study the detail of the scenario of the D-term inflation. Thus, let us take a simple model of D-term inflation; here, we consider the model with (new) U(1) gauged symmetry and introduce three chiral superfields, $S(0)$, $\bar{Q}(-1)$ and $Q(+1)$ where we denote the U(1) charges of the superfields in the parenthesis. With the superpotential

$$W = \lambda S \bar{Q} Q, \tag{4.1}$$

and adopting non-vanishing Fayet-Illiopoulos D-term parameter ξ, the scalar potential is given by

$$V = \lambda^2 \left(|S\bar{Q}|^2 + |SQ|^2 + |\bar{Q}Q|^2 \right) + \frac{1}{2} g^2 \left(-|\bar{Q}|^2 + |Q|^2 - \xi \right)^2, \tag{4.2}$$

where g is the gauge coupling constant.[#7] In our study, we take ξ to be positive (although the final result is independent of the sign of ξ). Minimizing the potential, the true vacuum is given by

$$\langle S \rangle = 0, \quad \langle \bar{Q} \rangle = 0, \quad \langle Q \rangle = \sqrt{\xi}. \tag{4.3}$$

Although the true vacuum is given by (4.3), there is a (quasi) flat direction, that is, $S \to \infty$ with $\bar{Q}$ and Q being vanished. Indeed, in this limit, the scalar potential becomes $V = \frac{1}{2} g^2 \xi^2$ and hence, at the tree level, the scalar potential becomes constant. This flat direction is used as the inflaton. Thus, in this scenario, inflation proceeds in the symmetric phase of U(1) while the vacuum is in the broken phase, and hence the cosmic string is formed. The mass per unit length of the string is given by

$$\mu = 2\pi\xi. \tag{4.4}$$

Once the cosmic-string network is formed, it affects the cosmic density fluctuations. In particular, an important constraint is obtained by studying its effects on the CMB anisotropy. The perturbations induced by cosmic strings are non-Gaussian and decoherent isocurvature, which leads to characteristic spectrum of the CMB anisotropy, which is distinguished from that induced by inflation.

To study this issue, let us consider the evolution of the inflation field a little bit more carefully. Once the radiative corrections are taken into account, the flat direction is slightly lifted. When the scalar field S takes large amplitude, $\bar{Q}$ and Q become massive and decouple from the effective theory at the energy scale λS. This fact means that the gauge coupling constant in this case should be evaluated at the scale λS and hence, for $S \gg g\sqrt{\xi}/\lambda$, $V(S) = \frac{1}{2} g^2(\lambda S)\xi^2$. Using one-loop renormalization group equation, and defining

$$S = \frac{1}{\sqrt{2}} \sigma e^{i\theta}, \tag{4.5}$$

the potential for the real scalar field σ is given by

$$V(\sigma) = \frac{g^2}{2}\xi^2 + \frac{g^4 \xi^2}{8\pi^2} \ln \frac{\sigma}{\sigma_0}, \tag{4.6}$$

where σ_0 is some constant.

Since the scalar field σ has a very flat potential when σ is large, the σ field can be used as an inflaton; inflation occurs if σ has large enough amplitude. Assuming the slow-roll condition, evolution of the σ field during the inflation is described as

$$\sigma^2 = \sigma_{\rm end}^2 + \frac{g^2}{2\pi^2} N_e M_*^2, \tag{4.7}$$

where N_e is the e-folds of the inflation and $M_* \simeq 2.4 \times 10^{18}$ GeV is the reduced Planck scale. The cosmic density fluctuations responsible for the CMB anisotropy measured by the WMAP (and other) experiment are generated when $N_e \sim 30 - 50$. (Hereafter, we take $N_e = 50$ in evaluating C_l.) In addition, $\sigma_{\rm end}$ is

[#7] Here and hereafter, we use the same notation for the scalar fields and for the chiral superfields since there should be no confusion.

the inflaton amplitude at the end of the inflation. In order to realize the D-term inflation, σ should be large enough so that (i) the slow-roll condition is satisfied and (ii) the effective mass squared of the Q field becomes positive. Inflation ends one of these conditions are violated and hence $\sigma_{\rm end}$ is estimated as

$$\sigma_{\rm end} = \max(\sigma_{\rm s.r.}, \sigma_{\rm inst}), \tag{4.8}$$

where

$$\sigma_{\rm s.r.} \simeq \frac{g}{2\pi} M_*, \quad \sigma_{\rm inst} \simeq \frac{\sqrt{2}g}{\lambda}\sqrt{\xi}. \tag{4.9}$$

Notice that $\sigma_{\rm s.r.}$ and $\sigma_{\rm inst}$ are derived from the slow-roll condition and the instability of the potential of Q, respectively.

Once the evolution of the inflaton field is understood, we can calculate the metric perturbation Ψ generated from the primordial fluctuation of the inflaton field. The metric perturbation from the inflaton fluctuation is given in Eq. (2.24), and hence[#8]

$$\Psi_{\rm RD}^{(\rm inf)}(k) = \left[\frac{2\sqrt{2\pi}}{3\sqrt{3}}\frac{\xi}{gM_*^3}\sigma\right]_{k=aH}. \tag{4.10}$$

Importantly, $\Psi_{\rm RD}^{(\rm inf)}$ changes its behavior at $\lambda \sim \lambda_{\rm crit}$ with

$$\lambda_{\rm crit} \equiv \frac{2\pi}{\sqrt{N_e}}\frac{\sqrt{\xi}}{M_*}. \tag{4.11}$$

When $\lambda \gg \lambda_{\rm crit}$, the second term in the right-hand side of Eq. (4.7) dominates over the first term and hence σ for corresponding N_e is given by $gM_*\sqrt{N_e}/\sqrt{2\pi}$. On the contrary, if $\lambda \ll \lambda_{\rm crit}$, the first term wins and $\sigma \simeq \sigma_{\rm inst}$. As a result, we obtain

$$\Psi_{\rm RD}^{(\rm inf)} \simeq \frac{2}{3\sqrt{3}}\frac{\xi}{M_*^2}\sqrt{N_e} \times \begin{cases} 1 & : \ \lambda \gg \lambda_{\rm crit} \\ (\lambda/\lambda_{\rm crit})^{-1} & : \ \lambda \ll \lambda_{\rm crit} \end{cases}. \tag{4.12}$$

When $\lambda \gg \lambda_{\rm crit}$, $\Psi_{\rm RD}^{(\rm inf)}$ is proportional to ξ and is independent of λ. On the contrary, if $\lambda \ll \lambda_{\rm crit}$, $\Psi_{\rm RD}^{(\rm inf)}$ is proportional to $\xi^{3/2}/\lambda$. This fact implies that, for a fixed value of ξ, the metric perturbation generated from the inflaton fluctuation is enhanced for sufficiently small value of λ.

Because of the cosmic string formation, the CMB angular power spectrum in the D-term inflation scenario contains two contributions: one is the adiabatic one from the primordial fluctuation of the inflaton and the other is from the cosmic string. (So far, we have not introduced the curvaton yet.) Assuming no correlation between these two contributions, we obtain

$$C_l = C_l^{(\rm inf)} + C_l^{(\rm str)}, \tag{4.13}$$

where $C_l^{(\rm inf)}$ and $C_l^{(\rm str)}$ are contributions from primordial inflaton fluctuation and cosmic string, respectively. The adiabatic part $C_l^{(\rm inf)}$ can be calculated with the conventional method. Since $C_l^{(\rm inf)}$ is from the two point correlation function, the CMB angular power spectrum is second order in $\Psi^{(\rm inf)}$. In particular, $C_l^{(\rm inf)}$ is proportional to ξ^2 and ξ^3/λ^2 for $\lambda \gg \lambda_{\rm crit}$ and $\lambda \ll \lambda_{\rm crit}$, respectively. In addition, the cosmic string contribution $C_l^{(\rm str)}$ is proportional to $\mu^2 \propto \xi^2$ [16].

The important point is that the l-dependence of the cosmic string contribution $C_l^{(\rm str)}$ is different from that of $C_l^{(\rm inf)}$, although the detailed shape of the cosmic string contribution depends on the analysis. (For example, Refs. [17] suggest that the combination $l(l+1)C_l^{(\rm str)}$ is almost independent of l, while another class of studies result in "tilted" behavior [18] where the function $\sqrt{l(l+1)C_l^{(\rm str)}}$ approximately has a

[#8]The spectral index n_S is very close to 1 in the D-term inflation and hence we neglect the scale dependence of the primordial metric perturbation.

linear dependence on $\ln l$ up to $l \sim 400 - 600$ then it steeply decreases. In any case, $C_l^{(\rm str)}$ does not have oscillatory behavior as $C_l^{(\rm inf)}$ and the constraints on the D-term inflation in the following discussion do not change qualitatively.

Since $C_l^{(\rm str)}$ and $C_l^{(\rm inf)}$ have different l-dependence, the total angular power spectrum becomes inconsistent with the observation if the size of $C_l^{(\rm str)}$ is comparable to that of $C_l^{(\rm inf)}$. Indeed, if $\lambda \geq \lambda_{\rm crit}$, the ratio $C_l^{(\rm str)}/C_l^{(\rm inf)}$ becomes independent with ξ. In [19], it has been seen that the shape of the total angular power spectrum becomes inconsistent with the observation in such a case. In addition, in order to suppress the ratio $C_l^{(\rm str)}/C_l^{(\rm inf)}$, λ should be smaller than $O(10^{-4} - 10^{-5})$.

A consistent scenario of the D-term inflation with $\lambda \sim 1$ can be constructed by adopting the curvaton mechanism. In the case of D-term inflation with the curvaton, the curvaton contribution to the metric perturbation is calculated as

$$\Psi_{\rm RD}^{(\delta\phi)} = -\frac{4}{9}\frac{\delta\phi_{\rm init}}{\phi_{\rm init}} = -\frac{2}{9\sqrt{6\pi}}\frac{g\xi}{M_*\phi_{\rm init}}. \tag{4.14}$$

Since there is no correlation between the primordial fluctuations in the inflaton and curvaton fields, the total CMB angular power spectrum is now given in the form

$$C_l = C_l^{(\rm inf)} + C_l^{(\rm str)} + C_l^{(\delta\phi)}, \tag{4.15}$$

where $C_l^{(\delta\phi)}$ is the curvaton contribution. As we emphasized, the density fluctuations associated with $\delta\phi_{\rm init}$ are purely adiabatic. In addition, $\Psi^{(\delta\phi)}$ is almost scale-invariant since the expansion rate during the D-term inflation is almost constant. As a result, the total CMB angular power spectrum may become well consistent with the WMAP observation if the curvaton contribution dominates over the inflaton contribution. We can see that such a hierarchy is relatively easily realized; using the fact that $C_l^{(\rm inf)}$ and $C_l^{(\rm str)}$ are proportional to $[\Psi^{(\rm inf)}]^2 \propto \mu^2$ when $\lambda \sim 1$ while $C_l^{(\delta\phi)}$ is proportional to $[\Psi^{(\delta\phi))}]^2$, the curvaton contribution dominates when $\phi_{\rm init} \lesssim gM_*$ since $\Psi^{(\rm inf)} \sim O(\xi/M_*^2)$.

To be more quantitative, we calculate the χ^2 variable to derive constraints on the parameters in the scenario. Now the total angular power spectrum has the form

$$C_l = [C_l^{(\rm adi)}]_{\Psi_{\rm RD}=1}\Psi_{\rm RD}^2 + [C_l^{(\rm str)}]_{G\mu=1}(G\mu)^2, \tag{4.16}$$

where

$$\Psi_{\rm RD}^2 = [\Psi_{\rm RD}^{(\rm inf)}]^2 + [\Psi_{\rm RD}^{(\delta\phi)}]^2, \tag{4.17}$$

and $C_l^{(\rm adi)}$ is the CMB angular power spectrum generated from purely adiabatic density fluctuations. The χ^2 variable is minimized when the cosmic-string contribution is negligibly small and $\Psi_{\rm RD} \simeq 3.0 \times 10^{-5}$. The latter condition can be satisfied by tuning the curvaton contribution (as far as the inflaton contribution to $\Psi_{\rm RD}$ is not too large.) In order to realize hierarchy between the adiabatic and cosmic-string contributions, it is necessary to make μ small by suppressing ξ. Requiring that $\Delta\chi^2 < 4$, we obtain the upper bound on μ for the case of $\lambda \sim 1$ as

$$G\mu \lesssim O(10^{-6}), \tag{4.18}$$

and hence, using Eq. (4.4), the upper bound on ξ is given by

$$\sqrt{\xi}/M_* \lesssim O(10^{-3}). \tag{4.19}$$

In addition, using the best-fit value of $\Psi_{\rm RD}$ given above, we can estimate the required value of the initial amplitude of the curvaton field. Importantly, in order to realize the adiabatic-like CMB angular power spectrum, $\Psi^{(\delta\phi)} \gg \Psi^{(\rm inf)}$ since $C_l^{(\rm str)}$ and $C_l^{(\rm inf)}$ are of the same order if $\lambda \sim 1$. Thus, requiring $\Psi_{\rm RD}^{(\delta\phi)} \simeq 3.0 \times 10^{-5}$, we obtain

$$\phi_{\rm init}/M_* \simeq 9.5 \times 10^2 \times g\left(\frac{\sqrt{\xi}}{M_*}\right)^2. \tag{4.20}$$

Finally, I would like to make a brief comment on the cases of hybrid inflation. In many classes of hybrid inflation models, gauged U(1) symmetry exists which is spontaneously broken after the inflation. With such a U(1) symmetry, cosmic string is also formed, which also affects the CMB anisotropy. The dynamics of the hybrid inflation and the mass of the string per unit length are almost the same as the D-term inflation [20]. Therefore, the result obtained in the present work can apply to the hybrid inflation. Of course, for general hybrid inflation models where the cosmic string affects the CMB anisotropy too much to be consistent with the observations, the curvaton mechanism can solve the difficulty as in the D-term inflation case.

4.2 Case of the right-handed sneutrino as the curvaton

The next possibility I would like to discuss is the case where the curvaton field is also responsible for the scenario of baryogenesis. Among various scenarios, there are some cases where the baryon asymmetry of the universe is generated from scalar-field condensations. In those scenarios, scalar fields often dominate the universe at some epoch and hence, if they have primordial fluctuations, they may play the role of the curvaton. Probably, two of the most famous examples of the possible scalar fields responsible for the baryon asymmetry are right-handed sneutrino [21, 22] and the Affleck-Dine field [23].

Here, we consider the case where the right-handed sneutrino, which becomes the origin of the baryon asymmetry of the universe [21], plays the role of the curvaton [24]. First, I briefly summarize the model and the thermal history. Here, the relevant part of the superpotential is given by

$$W = \hat{h}_{N,i\alpha} N_i L_\alpha H_u + \frac{1}{2}\hat{M}_{N,ij} N_i N_j, \tag{4.21}$$

where $\hat{h}_N$ is the Yukawa matrix for the neutrino while $\hat{M}_N$ is the Majorana mass matrix for the right-handed (s)neutrinos. Here, i and j are generation indices of the right-handed neutrino N while α is that of the left-handed lepton doublet L. In addition, H_u is the up-type Higgs field. I work in the basis where the matrix $\hat{M}_N$ is diagonalized. For simplicity, let us consider the case where the lightest right-handed sneutrino $\tilde{N} = \tilde{N}_1$ has non-vanishing initial amplitude. (Hereafter, mass of $\tilde{N}$ is denoted as M_N.)

With a non-vanishing primordial amplitude, $\tilde{N}$ starts to oscillate when $H \sim M_N$ and decays when $H \sim \Gamma_N$, where Γ_N is the decay rate of $\tilde{N}$. Since the Majorana mass term breaks the lepton-number symmetry, lepton-number asymmetry may be generated at the time of the sneutrino decay if non-vanishing CP violation exists. Such a lepton-number asymmetry becomes the source of the baryon-number asymmetry of the universe with the sphaleron process.

The mechanism of generating the baryon-number asymmetry is basically the supersymmetric version of the Fukugita-Yanagida mechanism [25]. Expression for the resultant amount of the baryon asymmetry is, however, rather complicated since, in this case, the primordial abundance of the right-handed sneutrino has non-thermally determined. Assuming $\Gamma_N < \Gamma_\chi$, we obtain [22]

$$\frac{n_B}{s} \simeq 0.24 \times 10^{-10} f_{\gamma_N} \delta_{\rm eff} \left(\frac{T_N}{10^6 {\rm GeV}}\right) \left(\frac{m_{\nu_3}}{0.05{\rm eV}}\right), \tag{4.22}$$

where T_N is the temperature at the epoch of the decay of $\tilde{N}$, m_{ν_3} the mass of the heaviest (left-handed) neutrino mass. (So, if $\tilde{N}$ decays after dominating the universe, T_N becomes the reheat temperature due to the decay of $\tilde{N}$.) In addition, in the basis where the Majorana mass matrix for the right-handed neutrinos $\hat{M}$ is real and diagonalized, the effective CP violating phase is given by

$$\delta_{\rm eff} = \frac{(H_u)^2}{m_{\nu_3}} \frac{{\rm Im}[\hat{h}\hat{h}^\dagger \hat{M}^{-1} \hat{h}^* \hat{h}^T]_{11}}{[\hat{h}\hat{h}^\dagger]_{11}}. \tag{4.23}$$

Notice that, with maximum CP violation, $\delta_{\rm eff} \sim 1$. In addition, f_γ is the energy fraction of the radiation generated from the decay product of $\tilde{N}$. With the relation $\Gamma_N < \Gamma_\chi$, $\tilde{N}$ decays after the inflaton decay. In this case, it is convenient to define the following quantity:

$$\tilde{N}_{\rm eq} \sim \begin{cases} (\Gamma_N/M_N)^{1/4} M_* & : \quad M_N < \Gamma_\chi \\ (\Gamma_N/\Gamma_\chi)^{1/4} M_* & : \quad M_N > \Gamma_\chi \end{cases}. \tag{4.24}$$

If $\tilde{N}_{\rm init} \sim \tilde{N}_{\rm eq}$, $\rho_{\gamma_\chi} \sim \rho_{\tilde{N}}$ is realized when $H \sim \Gamma_{\tilde{N}}$. Thus, when $\tilde{N}_{\rm init} \lesssim \tilde{N}_{\rm eq}$, $\tilde{N}$ decays in the γ_χ-dominated universe and hence

$$f_{\gamma_{\tilde{N}}} \sim \frac{(\tilde{N}_{\rm init}/\tilde{N}_{\rm eq})^2}{1+(\tilde{N}_{\rm init}/\tilde{N}_{\rm eq})^2} \quad : \quad \tilde{N}_{\rm init} \lesssim \tilde{N}_{\rm eq}. \tag{4.25}$$

On the contrary, if $\tilde{N}_{\rm init} \gtrsim \tilde{N}_{\rm eq}$, the right-handed sneutrino decays after it dominates the universe and we obtain

$$f_{\gamma_{\tilde{N}}} \sim \frac{(\tilde{N}_{\rm init}/\tilde{N}_{\rm eq})^{8/3}}{1+(\tilde{N}_{\rm init}/\tilde{N}_{\rm eq})^{8/3}} \quad : \quad \tilde{N}_{\rm eq} \lesssim \tilde{N}_{\rm init}. \tag{4.26}$$

Thus, as is easily seen, energy fraction of $\gamma_{\tilde{N}}$ becomes close to 1 when $\tilde{N}_{\rm init} \gg \tilde{N}_{\rm eq}$ while, in the opposite limit, most of the radiation are generated from the decay product of the inflaton.

Now, we are at the position to discuss the cosmological density fluctuations in this scenario. In particular, we consider the case where the condensation of the right-handed sneutrino plays the role of the curvaton. (Thus, in this case, the epoch after the decay of $\tilde{N}$ is identified as the RD2 epoch.) The scenario is basically the same as the curvaton scenario which I have explained before.

In the previous discussion, we have considered the cases where the all the components in the universe are generated from the decay product of the curvaton, which corresponds to the case of $f_{\gamma_{\tilde{N}}} \simeq 1$. As is explained above, however, (small) contamination of the radiation from the decay product of the inflaton may always exist. If the baryon asymmetry is generated from thermally produced particles after the RD2 epoch is realized, then entropy fluctuations vanish and the primordial density fluctuations become purely adiabatic.

In the scenario we consider, however, the situation is quite different since the baryon asymmetry is generated from the decay product of $\tilde{N}$. In particular, if the energy fraction of the radiation from the decay product of the inflaton becomes sizable, non-vanishing baryonic entropy fluctuation may be generated.

Evolution of the density fluctuations in this case is also understood by solving the Einstein and Boltzmann equations for the fluctuations given in the previous section. We calculate the entropy in the radiation-dominated universe after the decay of both χ and $\tilde{N}$. In the radiation-dominated universe [9]

$$\Delta_{\rm tot} = O(k^2\tau^2), \quad \delta_{\rm tot} = -2\Psi_{\rm RD2}, \quad V_{\rm tot} = \frac{1}{2}\Psi_{\rm RD2}k\tau. \tag{4.27}$$

Then, with the relation

$$\Delta_{\rm tot} = f_{\gamma_\chi}\Delta_{\gamma_\chi} + f_{\gamma_{\tilde{N}}}\Delta_{\gamma_{\tilde{N}}}, \tag{4.28}$$

with $\Delta_{\gamma_X} = \delta_{\gamma_X} + 4(a'/a)V_{\rm tot}/k$, we obtain

$$\Delta_{\gamma_{\tilde{N}}}^{(\delta\tilde{N})} = -\frac{f_{\gamma_\chi}}{f_{\gamma_{\tilde{N}}}}\Delta_{\gamma_\chi}^{(\delta\tilde{N})} = -6\frac{f_{\gamma_\chi}}{f_{\gamma_{\tilde{N}}}}\Psi_{\rm RD2}^{(\delta\tilde{N})}. \tag{4.29}$$

Using the fact that the entropy between any component produced from $\tilde{N}$ and that from the inflaton field is conserved, we can relate $\Psi_{\rm RD2}^{(\delta\tilde{N})}$ with $S_{\tilde{N}\chi}^{(\delta\tilde{N})}$; with the relation $S_{\tilde{N}\chi}^{(\delta\tilde{N})} = \frac{3}{4}(\Delta_{\gamma_{\tilde{N}}}^{(\delta\tilde{N})} - \Delta_{\gamma_\chi}^{(\delta\tilde{N})})$, we obtain

$$\Psi_{\rm RD2}^{(\delta\tilde{N})} = -\frac{2}{9}f_{\gamma_{\tilde{N}}}S_{\tilde{N}\chi}^{(\delta\tilde{N})} = -\frac{4}{9}f_{\gamma_{\tilde{N}}}\frac{\delta\tilde{N}_{\rm init}}{\tilde{N}_{\rm init}}. \tag{4.30}$$

Thus, if $\tilde{N}$ decays much after it dominates the universe, $f_{\gamma_{\tilde{N}}} \simeq 1$ and hence the metric perturbation becomes comparable to the primordial entropy perturbation. On the other hand, if $f_{\gamma_{\tilde{N}}} \ll 1$, the metric perturbation becomes negligibly small. Since the baryon asymmetry is generated from $\tilde{N}$, the density fluctuation in the baryonic component is given by

$$\Delta_b^{(\delta\tilde{N})} = \frac{3}{4}\Delta_{\gamma_{\tilde{N}}}^{(\delta\tilde{N})} = -\frac{9}{2}\frac{f_{\gamma_\chi}}{f_{\gamma_{\tilde{N}}}}\Psi_{\rm RD2}^{(\delta\tilde{N})}. \tag{4.31}$$

Thus, the entropy between the baryon and the radiation is given by

$$S_{b\gamma}^{(\delta\tilde{N})} = \Delta_b^{(\delta\tilde{N})} - \frac{3}{4}\Delta_{\rm tot}^{(\delta\tilde{N})} = -\frac{9}{2}\frac{f_{\gamma_\chi}}{f_{\gamma_{\tilde{N}}}}\Psi_{\rm RD2}^{(\delta\tilde{N})} = -\frac{9(1-f_{\gamma_{\tilde{N}}})}{2f_{\gamma_{\tilde{N}}}}\Psi_{\rm RD2}^{(\delta\tilde{N})}, \tag{4.32}$$

and defining

$$\kappa_b^{(\delta\tilde{N})} \equiv \frac{S_{b\gamma}^{(\delta\tilde{N})}}{\Psi_{\rm RD2}^{(\delta\tilde{N})}}, \tag{4.33}$$

we obtain

$$\kappa_b^{(\delta\tilde{N})} = -\frac{9(1-f_{\gamma_{\tilde{N}}})}{2f_{\gamma_{\tilde{N}}}}. \tag{4.34}$$

If the right-handed sneutrino once dominates the universe, $f_{\gamma_{\tilde{N}}} \to 1$ and hence the perturbation becomes adiabatic. (Thus, the situation is like the case discussed in the previous section.)

It is interesting if a sizable amount of the energy density of the radiation is from the inflaton. In this case, $f_{\gamma_{\tilde{N}}}$ becomes smaller than 1 and correlated mixture of the adiabatic and isocurvature fluctuations is generated. As mentioned in the previous section, WMAP data suggests that the baryonic and CDM entropy fluctuations should be very small; $|\kappa_b| < 0.5$ [13]. If $f_{\gamma_{\tilde{N}}} \sim 0.1$, however, $|\kappa_b|$ can be smaller than the present upper bound but the deviation of the CMB angular power spectrum from the adiabatic result may still be within the reach of the future precise observations. Thus, it is desirable to find the signal from the (correlated) entropy fluctuation in the future precise observations of the CMB anisotropy for the test of the curvaton scenario.

Finally, let me comment on the case where the curvaton also generates the baryon asymmetry of the universe via Affleck-Dine mechanism. If the primordial fluctuation of the Affleck-Dine field becomes the dominant source of the cosmological density fluctuations, large baryonic entropy fluctuation is generated even if the universe is once completely dominated by the Affleck-Dine field. This is due to the fact that the Affleck-Dine field is a complex scalar field and also that the resultant baryon asymmetry of the universe is sensitive to the initial value of the Affleck-Dine field. If the Affleck-Dine field acquires primordial fluctuation, its initial phase as well as the initial amplitude is expected to have fluctuations.

5 Conclusions and Discussion

Here, I have discussed the basic features of the curvaton scenario and its implications to particle physics. In particular, I have discussed that the cosmic density fluctuations can be dominantly originate from the primordial fluctuation of the "curvaton" field, which is a late-decaying scalar condensation other than the inflaton. In the curvaton scenario, scale-dependence of the cosmic density fluctuation becomes different from the case of the simple inflation, and in many cases, the spectral index n_s becomes close to 1 compared to the simple inflation case. Thus, given the fact that the CMB anisotropy observed by the WMAP suggests (almost) scale-invariant primordial density fluctuations, observational constraints on the inflaton potential can be relaxed by adopting the curvaton scenario.

One of the important feature of the curvaton scenario is the possible contamination of the (correlated) entropy fluctuation in the non-relativistic matter. The CMB angular power spectrum is sensitive to the entropy fluctuation. Thus, if such correlated entropy fluctuation is sizable, it affects the shape of the CMB angular power spectrum and hence it will be interesting and important to try to find its consequence in particular in the CMB anisotropy at future precision observations of the universe.

Acknowledgments T.M. is supported by the Grant-in-Aid for Scientific Research from the Ministry of Education, Science, Sports, and Culture of Japan, No. 15540247.

References

[1] A. H. Guth, Phys. Rev. D **23** (1981) 347; K. Sato, MNRAS **195** (1981) 467.

[2] S. Kasuya, T. Moroi and F. Takahashi, arXiv:hep-ph/0312094.

[3] K. Enqvist and M. S. Sloth, Nucl. Phys. B **626** (2002) 395.

[4] D. H. Lyth and D. Wands, Phys. Lett. B **524** (2002) 5.

[5] T. Moroi and T. Takahashi, Phys. Lett. B **522** (2001) 215 [Erratum-ibid. B **539** (2002) 303].

[6] N. Bartolo and A. R. Liddle, Phys. Rev. D **65** (2002) 121301; T. Moroi and T. Takahashi, Phys. Rev. D **66** (2002) 063501; D. H. Lyth, C. Ungarelli and D. Wands, Phys. Rev. D **67** (2003) 023503; M. S. Sloth, Nucl. Phys. B **656** (2003) 239; R. Hofmann, arXiv:hep-ph/0208267; K. Dimopoulos and D. H. Lyth, arXiv:hep-ph/0209180; T. Moroi and H. Murayama, Phys. Lett. B **553** (2003) 126; K. Enqvist, S. Kasuya and A. Mazumdar, Phys. Rev. Lett. **90** (2003) 091302; F. Di Marco, F. Finelli and R. Brandenberger, Phys. Rev. D **67** (2003) 063512; K. A. Malik, D. Wands and C. Ungarelli, Phys. Rev. D **67** (2003) 063516; M. Postma, Phys. Rev. D **67** (2003) 063518; C. Gordon and A. Lewis, arXiv:astro-ph/0212248; K. Dimopoulos, Phys. Rev. D **68** (2003) 123506; A. R. Liddle and L. A. Urena-Lopez, Phys. Rev. D **68** (2003) 043517; J. McDonald, Phys. Rev. D **68** (2003) 043505; K. Dimopoulos, G. Lazarides, D. Lyth and R. Ruiz de Austri, JHEP **0305** (2003) 057; K. Enqvist, A. Jokinen, S. Kasuya and A. Mazumdar, Phys. Rev. D **68** (2003) 103507; K. Dimopoulos, D. H. Lyth, A. Notari and A. Riotto, JHEP **0307** (2003) 053 M. Endo, M. Kawasaki and T. Moroi, Phys. Lett. B **569** (2003) 73; M. Postma and A. Mazumdar, arXiv:hep-ph/0304246; M. Postma, arXiv:astro-ph/0305101; S. Kasuya, M. Kawasaki and F. Takahashi, Phys. Lett. B **578** (2004) 259; D. H. Lyth and D. Wands, Phys. Rev. D **68** (2003) 103515; D. H. Lyth and D. Wands, Phys. Rev. D **68** (2003) 103516; K. Dimopoulos, G. Lazarides, D. Lyth and R. R. de Austri, Phys. Rev. D **68** (2003) 123515; K. Hamaguchi, M. Kawasaki, T. Moroi and F. Takahashi, arXiv:hep-ph/0308174. D. H. Lyth, Phys. Lett. B **579** (2004) 239; N. Bartolo, S. Matarrese and A. Riotto, Phys. Rev. D **69** (2004) 043503; J. McDonald, JCAP **0312** (2003) 005; J. McDonald, arXiv:hep-ph/0310126; C. Gordon and K. A. Malik, arXiv:astro-ph/0311102; M. Bastero-Gil, V. Di Clemente and S. F. King, arXiv:hep-ph/0311237; S. Gupta, K. A. Malik and D. Wands, arXiv:astro-ph/0311562; L. Pilo, A. Riotto and A. Zaffaroni, arXiv:astro-ph/0401302; E. J. Chun, K. Dimopoulos and D. Lyth, arXiv:hep-ph/0402059.

[7] G. Veneziano, Phys. Lett. B **265** (1991) 287; M. Gasperini and G. Veneziano, Astropart. Phys. **1** (1993) 317; M. Gasperini and G. Veneziano, Phys. Rev. D **50** (1994) 2519; M. Gasperini and G. Veneziano, Phys. Rep. **373** (2003) 1.

[8] J. Khoury, B. A. Ovrut, P. J. Steinhardt and N. Turok, Phys. Rev. D **64** (2001) 123522; J. Khoury, B. A. Ovrut, N. Seiberg, P. J. Steinhardt and N. Turok, Phys. Rev. D **65** (2002) 086007; J. Khoury, B. A. Ovrut, P. J. Steinhardt and N. Turok, Phys. Rev. D **66** (2002) 046005.

[9] W. T. Hu, Ph. D Thesis (arXiv:astro-ph/9508126).

[10] S. Mollerach, Phys. Rev. D **42** (1990) 313.

[11] T. Moroi and T. Takahashi, in [6].

[12] D. N. Spergel *et al.*, Astrophys. J. Suppl. **148** (2003) 175.

[13] K. Hamaguchi, M. Kawasaki, T. Moroi and F. Takahashi, in Ref. [6].

[14] E. Halyo, Phys. Lett. B **387** (1996) 43; P. Binetruy and G. R. Dvali, Phys. Lett. B **388** (1996) 241.

[15] J. M. Bardeen, P. J. Steinhardt and M. S. Turner, Phys. Rev. D **28** (1983) 679.

[16] See, for example, A. Vilenkin and E.P.S. Shellard, "Cosmic Strings and Other Topological Defects" (Cambridge University Press, 1994).

[17] B. Allen, R.R. Caldwell, E.P.S. Shellard, A. Stebbins and S.Veeraraghavan, Phys. Rev. Lett. **77** (1996) 3061; B. Allen, R.R. Caldwell, S. Dodelson, L. Knox, E.P.S. Shellard and A. Stebbins, Phys. Rev. Lett. **79** (1997) 2624; M. Landriau, E.P.S. Shellard, astro-ph/0302166.

[18] C.R. Contaldi, M. Hindmarsh and J. Magueijo, Phys. Rev. Lett. **82** (1999) 679; A. Albrecht, R.A. Battye and J. Robinson, Phys. Rev. **D59** (1999) 023508; L.Pogosian and T.Vachaspati, Phys. Rev. **D60** (1999) 083504; E.J. Copeland, J. Magueijo and D.A.Steer, Phys. Rev. **D61** (2000) 063505.

[19] M. Endo, M. Kawasaki and T. Moroi, in [6].

[20] T. Asaka, K. Hamaguchi, M. Kawasaki and T. Yanagida, Phys. Rev. D **61** (2000) 083512.

[21] H. Murayama, H. Suzuki, T. Yanagida and J. Yokoyama, Phys. Rev. Lett. **70** (1993) 1912.

[22] K. Hamaguchi, H. Murayama and T. Yanagida, Phys. Rev. D **65** (2002) 043512.

[23] I. Affleck and M. Dine, Nucl. Phys. B **249** (1985) 361.

[24] T. Moroi and H. Murayama, in [6].

[25] M. Fukugita and T. Yanagida, Phys. Lett. B **174** (1986) 45.

Creation of a brane world

Koh-suke Aoyanagi[1], Kei-ichi Maeda[2]

Department of Physics, Waseda University, Okubo 3-4-1, Shinjuku, Tokyo 169-8555, Japan

Abstract

We study a creation of a brane world using an instanton solution. We analyze two models: one is a brane model with a bulk scalar field and the other is that with a bulk Gauss-Bonnet term. We construct instanton solutions with branes for those models, and calculate the values of the actions to discuss an initial state of a brane universe.

1 Introduction

New paradigm of cosmology based on a superstring/M-theory, which is the so-called "brane world", has been proposed for last several years. One of the most interesting approach was given by Randall and Sundrum [1]. They considered a pure 5-dimensional (5D) Einstein gravity in a bulk only with a cosmological constant. Whereas, in a string/M-theory context, one would also expect some scalar fields, associated with the many moduli fields. Those fields will, in principle, also propagate in the bulk. For example, Lukas, Ovrut and Waldram [2] derived an effective 5D action by a dimensional reduction from 11-dimensional M theory. It contains a scalar fields in the 5D bulk, which correspond to moduli associated with compactification of six dimensions on a Calabi-Yau space. The other possible modification is to add higher curvature correction terms to the Einstein gravity. These are, in fact, derived from low energy limit of a string theory. The first correction term would be a ghost-free Gauss-Bonnet combination : $\mathcal{L}_{GB} = \alpha\left(R^2 - 4R_{AB}R^{AB} + R_{ABCD}R^{ABCD}\right)$. It was shown that a massless graviton mode at low energy is localized in the brane model with Gauss-Bonnet term as well as in the RS II model. Rather, a correction for the Newton's law becomes milder by including the Gauss-Bonnet term [6]. Using these models, we study creation of a brane universe[4]. We consider creation of a brane world using an instanton solution which is given by solving the 5D Euclidean Einstein equations. In order to construct a compact Euclidean manifold, we have to glue two copies of a finite patch of a bulk spacetime with a brane boundary by use of the Israel's junction condition. Garriga and Sasaki [3] first constructed a brane instanton in the Randall-Sundrum model. Here we discuss two models of brane instantons which contains either a bulk scalar field or a Gauss-Bonnet term in a bulk.

2 Creation of a brane world with a bulk scalar field

As for a brane world with a bulk scalar field ϕ, the Euclidean action of this model is given by

$$S_E = -\frac{1}{2\kappa_5^2}\left\{\int d^5x\sqrt{g}\left[R - \frac{1}{2}\partial_a\phi\partial^a\phi - V(\phi)\right] - \sum_i \int_{r=r_i} d^4x\sqrt{g_{(i)}}\left[K^{\pm}_{(i)} - \lambda_{(i)}(\phi)\right]\right\}, \tag{1}$$

where κ_5^2 denotes the five dimentional gravitational constant and $K^{\pm}_{(i)}$ denotes the extrinsic curvatur. We consider a model with a bulk potential $V(\phi) = (\beta^2 - 2/3)v^2\exp(-2\beta\phi)$, where β and v are parameters. This model includes the Hořava-Witten theory ($\beta = 1$) [2] and the Randall-Sundrum model ($\beta = 0$). The tension of a brane is assumed to be $\lambda(\phi) = \pm 2\sqrt{2}v\exp(-\beta\phi)$. Note that for this choice of potential and tension, the 3-curvature of a brane vanishes. Hence, a boundary brane in this instanton solution must be flat. We assume the Euclidean metric $ds^2 = dr^2 + b(r)^2\gamma_{ij}dx^idx^j$, where γ_{ij} is the metric of 4-dimensional torus in order that Euclidean solution (instanton) is compact.

[1]E-mail:aoyanagi@gravity.phys.waseda.ac.jp
[2]E-mail:maeda@gravity.phys.waseda.ac.jp

The equations of motion are

$$b'^2 = \frac{1}{12}b^2\left(\frac{1}{2}\phi'^2 - \left(\beta^2 - \frac{2}{3}\right)v^2 e^{-2\beta\phi}\right), \tag{2}$$

$$\phi'' + 4\frac{b'}{b}\phi' = -2\beta\left(\beta^2 - \frac{2}{3}\right)v^2 e^{-2\beta\phi}, \tag{3}$$

with the junction condition on a brane located at $r = r_i$ being

$$b'(r_i) = \mp\frac{\sqrt{2}}{6}b(r_i)ve^{-\phi}\Big|_{r=r_i}, \quad \phi'(r_i) = \mp\sqrt{2}ve^{-\phi}\Big|_{r=r_i}. \tag{4}$$

Here we use the notation $r_i (i = 0, 1, 2)$ where i means the number of a brane. For 2-brane model, $i = 1$ and $i = 2$ stand for a negative tension brane and a positive one, respectively. For a single brane model, we apply the upper case at $r = r_0$. Then we construct an instanton solution with two boundary branes at $r = r_1$ and $r = r_2$. The instanton solutions are

$$ds_E^2 = dr^2 + b_0^2 r^{\frac{1}{3\beta^2}}\gamma_{ij}dx^i dx^j, \tag{5}$$

and

$$\phi(r) = \frac{1}{\beta}\ln\left(\sqrt{2}v\beta^2 r\right), \tag{6}$$

where b_0 is a constant. The location of the branes ($r = r_1$ and $r = r_2$) are arbitrary Calculating the action for this solution, we find it vanishes : $S_E = 0$. Because the action has no minimum value with respect to the distance between two branes, we are not able to predict the initial state of the brane universe.

For a single brane model, the instanton solution (5) has a singularity at the origin ($r = 0$). However the action for this instanton is finite for $\beta < \sqrt{2/3}$, and then the action also vanishes. This is just like a Hawking-Turok singular instanton[5].

3 Creation of a brane world with a Gauss-Bonnet term

Next we analyze a brane model with a Gauss-Bonnet term and a negative cosmological constant Λ in the bulk. The action is given by

$$S_E = S_E^{bulk} + S_E^{brane}, \tag{7}$$

where

$$S_E^{bulk} = -\frac{1}{2\kappa_5^2}\int_{\mathcal{M}} dx^5\sqrt{g}\left[R - 2\Lambda + \alpha(R^2 - 4R_{AB}R^{AB} + R_{ABCD}R^{ABCD})\right], \tag{8}$$

Λ is a negative cosmological constant, R, R_{AB} and R_{ABCD} are the five dimetional scalar curvatuer, Ricci tensor and Riemann tensor ,respectively, and α is coupling constant. The induced four dimentional metric $h_{\mu\nu}$ on a 3-brane is defined by $h_{AB} = g_{AB} - n_A n_B$, where n_A is the spacelike unit-vector field which normal to the brane hypersurface. The action is given by the following form :

$$S_E^{brane} = -\frac{1}{\kappa_5^2}\sum_i \int_{\partial\mathcal{M}_i} d^4x\sqrt{h}\left[L_{surface} - \lambda_i\right], \tag{9}$$

where

$$L_{surface} = K + 2\alpha(J - 2G^{\rho\sigma}K_{\rho\sigma}) \tag{10}$$

is surface term. λ_i is a tension on the i-th brane, $K_{\mu\nu}$ is the extrinsic curvature of $\partial\mathcal{M}_i$, $K = K^\mu_\mu$, and $G_{\mu\nu}$ is the Einstein tensor of the induced metric $h_{\mu\nu}$. J is the combination of the extrinsic curvature given by

$$J = \frac{1}{3}\left(2KK_{\rho\sigma}K^{\rho\sigma} + K_{\rho\sigma}K^{\rho\sigma}K - 2K_{\mu\rho}K^{\rho\sigma}K^\mu_\sigma - K^3\right) \tag{11}$$

The total action gives the field equations as

$$\mathcal{G}_{AB} + \alpha\mathcal{H}_{AB} = -\Lambda g_{AB} - \lambda g_{AB}\delta(\partial\mathcal{M}_i), \tag{12}$$

where

$$\mathcal{G}_{AB} = R_{AB} - \frac{1}{2}g_{AB}R, \tag{13}$$

$$\mathcal{H}_{AB} = 2\left[RR_{AB} - 2R_{AC}R^C_{\ B} - 2R^{CD}R_{ACBD} + R_A^{\ CDE}R_{BCDE}\right] - \frac{1}{2}g_{AB}\mathcal{L}_{GB}. \tag{14}$$

We assume that the metric is $O(5)$-invariant, which gives the Euclidean metric as

$$ds_E^2 = dr^2 + b(r)^2\gamma_{\mu\nu}dx^\mu dx^\nu, \tag{15}$$

where $\gamma_{\mu\nu}$ is the metric of 4-sphere.

The equations of motion are now

$$3\left(\frac{b''}{b} - \frac{k - b'^2}{b^2}\right) + 12\alpha\frac{(k - b'^2)}{b^3}b'' = -\Lambda - \lambda_i\delta(r - r_i), \tag{16}$$

$$6\frac{k - b'^2}{b^2} + 12\alpha\frac{(k - b'^2)^2}{b^4} = \Lambda, \tag{17}$$

where the prime denotes the derivative with respect to r.

By integrating the first equation for a small interval $(r_i - \varepsilon, r_i + \varepsilon)$ including a brane, one obtain the junction condition at $r = r_i$ as

$$\frac{3b'b^2 - 4\alpha b'^3 + 12\alpha kb'}{b^3} = \mp\frac{\lambda_i}{2}, \tag{18}$$

where the upper (lower) sign is applied at r_2 (at $r = r_1$) for two brane model. Also for single brane model we apply the upper case at $r = r_0$.

We construct an instanton solution by cutting the above solution at $r = r_i$ and gluing two copies on the surface of the excising point in order that the Euclidean manifold (instanton) is a compact. On that surface we impose Israel's junction condition (18) with $k = 1$. For a single brane instanton we impose "no boundary boundary condition" at the origin [7]. For a 2-brane model we impose the junction condition at $r = r_i$ $(i = 1, 2)$.

We find a brane instanton only for $-3/4\alpha \leq \Lambda < 0$, which is

$$b(r) = \frac{1}{\sqrt{-X_\pm}}\sinh\sqrt{-X_\pm}r, \tag{19}$$

where

$$X_\pm = \frac{-3 \pm \sqrt{9 + 12\alpha\Lambda}}{12\alpha}. \tag{20}$$

The tension of the i-th brane is determined by the junction condition on the brane.

$$\lambda_i^{(\pm)} = (-1)^i\frac{1}{l}\left[\frac{2}{3}(6 \pm \beta)\frac{\cosh(r_i/l)}{\sinh(r_i/l)} + \frac{3}{4}(3 \mp \beta)\left(\frac{\cosh(r_i/l)}{\sinh^3(r_i/l)}\right)\right], \tag{21}$$

where $l_\pm = 1/\sqrt{-X_\pm}$, and $\beta = \sqrt{9+12\alpha\Lambda}$. The range of β is restricted as from the condition for $0 \leq \beta < 3$.

Here we note a 'critical tension'. In the limit of $r \to \infty$, the curvature of the brane vanishes because the radius of the brane ($b(r)$) (S^4 manifold) become infinitely large. In this limit the tension of a brane (??) is

$$\lambda_i^{cri} = (-1)^i \frac{2}{3l}(6 \pm \beta) = \frac{2}{l}(3 + 4\alpha X_\pm). \tag{22}$$

We rewrite it with α and Λ as

$$\alpha\lambda_{cri}^2 = 1 - 4\alpha\Lambda \mp \left(1 + \frac{4}{3}\alpha\Lambda\right)^3, \tag{23}$$

which is consistent with generalized Randall-Sundrum tuning condition for a flat brane in the model with Gauss-Bonnet term, derived by Maeda and Torii [8]. The tension of a positive brane is divided into two parts $\lambda = \lambda_{cri} + \lambda'$. λ' is always positive because λ decrease monotonically with respect to r for $0 \leq \beta < 3$. Hence this brane has always a positive effective cosmological constant, that is, de Sitter brane.

Next we calculate the action. The total Eudlidean action for this solution is given by

$$S_E = -\frac{V_4^\gamma}{\kappa_5^2}\left\{\left[(6 \mp \beta)\sinh\left(\frac{r_2}{l}\right)\cosh\left(\frac{r_2}{l}\right) + (6 \mp 3\beta)\left(\frac{r_2}{l}\right)\right] - [r_2 \to r_1]\right\}, \tag{24}$$

where V_4^γ is a volume of manifold with the metric $\gamma_{\mu\nu}$, i.e., $V_4^\gamma = 8\pi^2/3$ for S^4.

Again, we do not find the action minimum. Then, the initial size of a brane universe is not fixed.

4 Conclusion

We have presented instanton solutions for models with a scalar field and a Gauss-Bonnet term respectively. For the former case, we construct 2-brane and single (singular) brane instantons with flat 3-curvature. However we cannot predict the initial state of the brane universe because there is no action minimum. For the model with Gauss-Bonnet term, we also construct 2-brane and single (non-singular) de Sitter brane instantons. Again the initial size of brane universe is not fixed. In order to predict the initial state of created brane universe, we need to include other mechanisms such as the Casimir effect. This issue is left for further study.

References

[1] L. Randall and R. Sundrum, Phys. Rev. Lett. **83** (1999) 4690; *ibid.* **83** (1999) 3370.

[2] A. Lukas, B. Ovrut, and D. Waldram, Phys. Rev. D. **60** (1999) 086001; *ibid.* **61** (2000) 023506

[3] J. Garriga and M. Sasaki, Phys. Rev. D **62**, 043523 (2000).

[4] K. Aoyanagi and K. Maeda, in preparation.

[5] S. W. Hawking and N. Turok, Phys. Lett. B **425** (1988) 25.

[6] N. Deruelle and M. Sasaki Prog.Theor.Phys. **110**(2003) 441.

[7] J. B. Hartle and S. W. Hawking, Phys. Rev. D **28**, (1983) 2960.

[8] K. Maeda and T. Torii, Phys. Rev. D **69**, (2004) 024002.

Amplification of Super Horizon Scale Magnetic Fields During Preheating

Youhei Araki[1] and Yasusada Nambu[2]

Department of Physics, Graduate School of Science,
Nagoya University, chikusa, Nagoya 464-8602, Japan

Abstract

We investigate the evolution of power spectrum of large-scale fluctuations during preheating phase by using 'separate universe approach' proposed by Tanaka and Bassett[1]. We show that on the super-Hubble scale, scalar field's fluctuations with all wave number k are amplified by the effect of parametric resonance and their power spectrum become flat like white noise. We think the interpretation of these spectrum and we also comment on large scale magnetic field.

1 Introduction

During reheating inflaton decays into another particles and standard big bang phase is set. So reheating is a crucial part of inflationary cosmology. Reheating can occur through the process of parametric resonance which cause an exponential growth of another fields induced by coherent oscillation of inflaton field. Such a phase is called 'preheating' era.

It has been argued that preheating can amplify super-Hubble scale fluctuations and so it may alter standard predictions of inflationary cosmology. To investigate these effects, the dynamics of inflaton fields and other created particles must be known. But the dynamics of preheating has not been clearly understood yet because there are two difficulties to analysis. The one is we must take into account metric backreaction because we are interesting in structures on today's cosmological scale (several kilo or mega parsecs) which is much larger than horizon scale at preheating (several meters). So we need general relativistic treatment. The other is nonlinearity of this problem. Preheating usually ends due to backreaction of amplified fields against oscillating inflaton field. This can't be understood with linear perturbation approach that often used in inflationary cosmology. One of means to overcome these difficulties is solving linearized equation involve Hartree terms[2]. But this is hard to deal with computing power spectrum because this include only scattering events that does not change the momentum of field so this ignores 'rescattering' which deforms spectrum.

So it seems that full general relativistic and nonlinear treatment is needed to get power spectrum and such a full treatment require numerical computation[3]. But to compute spectrum on the scale from horizon size at preheating to cosmological scale has to use vast computer resources so it is difficult to know spectrum at the end of preheating on cosmological scale.

Tanaka and Bassett recently propose a new treatment to calculate the dynamics of preheating based on so-called 'separate universe approach' which seems reasonable to manage cosmological scale fluctuations. In this formalism, we think regions separate over distance lager than horizon scale at that time as independent and as having no interaction each other. Each regions are represented by each homogeneous universe and they evolve independently and as a result, super large scale inhomogeneity are generated. In this paper, we use the model same as Tanaka. In this model, inflaton's energy is transferred to conformaly coupled massless scalar by parametric resonance. And they also have a chaos[4].

We calculate large-scale fluctuation's spectrum in this model. This has a very characteristic flat spectrum like white noise because of chaotic motion. And we think interpretation of this spectrum. We also calculate the dynamics of large-scale magnetic filed.

[1]E-mail:yaraki@allegro.phys.nagoya-u.ac.jp
[2]E-mail:nambu@allegro.phys.nagoya-u.ac.jp

2 Model and basic equations

We consider universe with two scalar fields , the one is the inflaton (ϕ) and the other is the massless scalar fields (χ). And their potential is given by

$$V = \frac{\lambda}{4}\phi^4 + \frac{1}{2}g^2\phi^2\chi^2. \tag{1}$$

In this paper, we think the case $g^2 = 2\lambda$ where χ field has an instability on long wave length mode up to $k = 0$. Therefore, χ field grows exponentially as long as inflaton oscillates coherently.

And we introduce quasi-isotropic metric

$$ds^2 = -N(t,x)^2 ds^2 + a(t,x)^2 dx^2. \tag{2}$$

When we neglect the spatial differential terms for the reason that we explained above, Einstein equations are

$$\frac{\dot{H}}{N} = -\frac{1}{2}\Big((\frac{\dot{\phi}}{N})^2 + (\frac{\dot{\chi}}{N})^2\Big), \tag{3}$$

$$\frac{1}{N}\Big(\frac{\dot{\chi}}{N}\Big)^{\cdot} + 3H\Big(\frac{\dot{\chi}}{N}\Big) + g^2\phi^2\chi = 0, \tag{4}$$

$$\frac{1}{N}\Big(\frac{\dot{\phi}}{N}\Big)^{\cdot} + 3H\Big(\frac{\dot{\phi}}{N}\Big) + \lambda\phi^3 + g^2\chi^2\phi = 0, \tag{5}$$

where $H \equiv \frac{\dot{a}}{aN}$ and $\cdot \equiv \frac{\partial}{\partial t}$. These are the same equations as homogeneous ones but here we think inhomogeneous system so each values depend on position x.

And we have Hamiltoinian and momentum constraint.

$$3H^2 = \frac{1}{2}\Big(\frac{\dot{\phi}}{N}\Big)^2 + \frac{1}{2}\Big(\frac{\dot{\chi}}{N}\Big)^2 + \frac{\lambda}{4}\phi^2 + \frac{g^2}{2}\chi^2\phi^2 \tag{6}$$

$$\frac{\partial H}{\partial x} = -\frac{1}{2}\Big(\frac{\dot{\phi}}{N}\frac{\partial\phi}{\partial x} + \frac{\dot{\chi}}{N}\frac{\partial\chi}{\partial x}\Big) \tag{7}$$

In this formalism, we solve Einstein equations without spatial differential terms. Nevertheless, both of two constraints are satisfied in any time if only they are satisfied at initial.

3 Time evolution of the spectrum

In order to discuss the modification of spectrum during preheating , we need to set initial data which represents ones at the end of inflation. In the case $\lambda = 2g^2$, χ field behave like as massless scalar during most of inflation, so the effective mass ($\sim g^2\phi^2$) are almost negligible. Thus we can set the initial value of χ in k-space on large scale same as massless scalar

$$\chi_k \propto \frac{e^{i\theta}}{k^{n/2}}, \tag{8}$$

where θ is taken randomly from the interval [0,1], and n is an index of power spectrum which is usally taken to 3 on large scale.

Initial data of other values which satisfies two constraints can be chosen as

$$H, \phi = const, \dot{\chi} = 0, \dot{\phi} = \sqrt{6H^2 - 2V(\phi,\chi)}. \tag{9}$$

We use these initial data, and solve equation (3)~(5) numericaly. We choose symcronous slice condition $N = 1$. In order to compare this result with perturbation approach, we define "homogeneous background" of quantity X as $X_0 = \langle X \rangle$ and "inhomogeneity" as $\delta X(x) = X(x) - \langle X \rangle$ where $\langle\cdot\rangle$ denotes volume average. We empathize that δX must not be small compared with X_0 because we don't use perturbation approach.

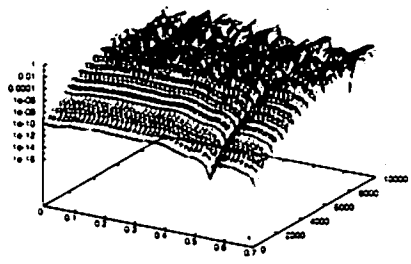

Figure 1: Time development of spatial distribution of χ. Initial structure is modified by chaotic motion of fields and structure become

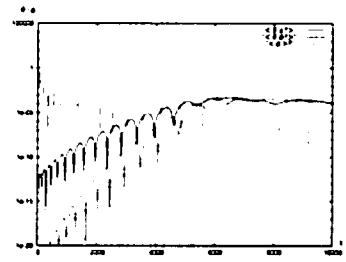

Figure 2: The amplitude of fields as a function of time. We also plot homogeneous part of inflaton ϕ.

Figure 1 shows time development of spatial distribution of χ and Figure 2 shows time development of amplitude of fluctuations of each fields. Each of them are represented in unit $\phi(t = 0) = 1, \lambda = 1$. We can find that fluctuation of χ grows exponentially due to parametric resonance. When χ becomes same order to ϕ backreaction effect changes instability condition of χ and so χ ceases to grow. These behaviors are in good agreement with analysis based on linear and Hartree approximation.

Now we pay an attention to the spatial distribution of χ. Figure 3 shows snap shot of special distribution of χ at each moment. In this case we choose spectrum index $n = 1$. Initial distribution is kept untill backreaction become important. But when it becomes important, chaotic motion of each fields make spatial distribution more complex and finally that becomes random distribution. Thus initial spectrum is modified and become flat spectrum like white noise. This is common in all n and characteristic in separate universe approach. Whether spectrum become flat or not depends on both duration time of preheating and the ratio of initial amplitude of ϕ to one of χ. Unless parametric resonance is disturbed by some process (Born decay of inflaton to other particles, for example) before χ become comparable to inflaton, large scale spectrum become flat in this model.

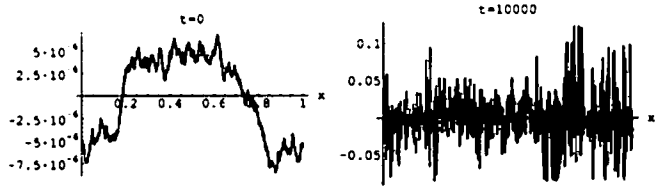

Figure 3: Spatial distribution of χ at initial and late time. Left figure is ploted at $t = 0$, and right one is ploted at $t = 10000$.

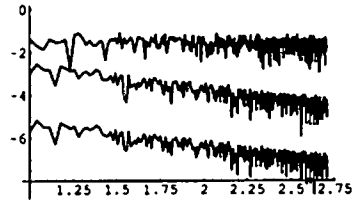

Figure 4: The power spectrum $\ln |\chi_k|^2$ aganist $\ln k$. Spectrums are ploted at t=0,4000,10000, respectively.

4 Discussion

To know whether flat spectrum obtained above is really random white noise, we manipulate Gaussian filter to these spectrums and compare these with distribution of random number. Because if spatial distribution of χ is really random, initial data set during inflation are washed out and such a initial data fail to explain the origin of large scale structure.

Figure 5 shows filtered above result and filtered random number. Each of them is ensemble averaged over ten samples in order to obtain more accurate spectrum. We can't distinguish these. So we think

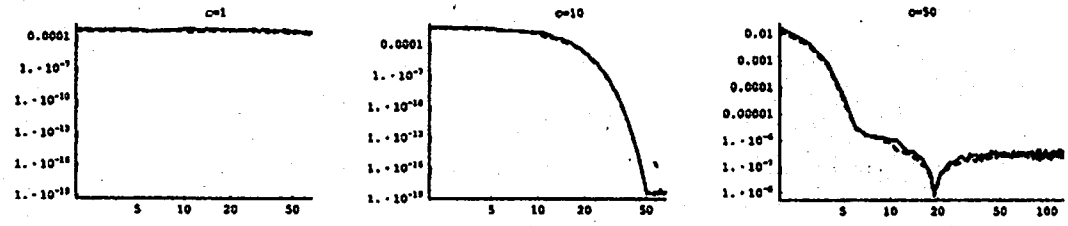

Figure 5: Filtered power spectrum of χ_k. Solid line denotes above result at $t = 10000$ and dashed line denotes white noise obteined from random numbers. Left figure is caluculated at filter width 0.01, middle one is at 0.1 and right one is at 0.5, respectively.

chaos of this system has erased the information about the initial spectrum. If initial spectrum made during inflation are lost during preheating, then models with preheating are constraint because they are in conflict with large scale structure.

Now we mention to the case $g^2 \neq 2\lambda$. If g^2/λ is not between the integer values $g^2/\lambda = n(n+1)/2$ with n integer, then χ field has no instability at $k = 0$[2]. In that case, large scale mode grows only by mode coupling with small scale mode. Such a growth can't be not considered in separate universe approach because we think only $k = 0$ mode in each universe in that approach. Therefore, in order to discuss such a effect, we need a full treatment which is difficult to deal with.

If g^2/λ is between $g^2/\lambda = n(n+1)/2$, $k = 0$ mode has an instability. But in the case $g^2 > 2\lambda$, damping of χ field due to mass during inflation is not negligible and spectrum is suppressed on large scale[5]. In this case, the growth of cosmological-scale modes will stop due to small-scale modes that are less suppressed during inflation and cosmological-scale modes are not amplified very much. But even in this case the chaotic motion of two field occur because backreaction becomes important. So spectrum will also be flat if preheating continues enough, and it will be a problem again.

We note about the amplification of the primordial magnetic field during preheating. In this model, metric is no longer conformaly flat, so large scale magnetic field can be producted. These effects can be computed by Maxwell equaiton in curved spacetime

$$\ddot{A}_i + H\dot{A}_i = 0, \tag{10}$$

here we neglect spatial differential term again, and we also neglect conductibity. Magnetic field can be amplified by metric fluctuations but their spectrum also become flat. So amplification large scale magnetic field means overproduction of small scale magnetic field. This may be avoid by conductivity and this is one of future works.

5 Summary

We calculate super-horizon scale spectrum in conformaly coupled two scalar fields. The spectrum become flat like white noise because of chaotic motion. This behavior is not depend on initial spectrum index n. If chaos occur during preheating, initial condition set during inflation is washed out and such a distribution may be in conflict with large scale structure.

References

[1] T. Tanaka and B. Bassett, astro-ph/0302544 (2003).

[2] P. Greene, L. Kofman, A. Linde and A. Starobinsky, Phys. Rev. **D56**, 6175 (1997).

[3] R. Easther and M. Parry, Phys. Rev. **D62**, 103503 (2000).

[4] R. Easther and K. Maeda, Class. Quantum Grav. **16**, 1637 (1999).

[5] J. Zibin, R. Brandenberger and D. Scott, Phys. Rev. **D63**, 043511 (2001).

Generation of large-scale magnetic fields in inflationary cosmology

Kazuharu Bamba, J. Yokoyama

Department of Earth and Space Science, Graduate School of Science, Osaka University, Toyonaka 560-0043, Japan

Abstract

The generation of large-scale magnetic fields is studied in dilaton electromagnetism in inflationary cosmology, taking into account the dilaton's evolution throughout inflation and reheating until it is stabilized with possible entropy production. It is shown that the amplitude of the generated magnetic field could be sufficiently large even in the case that a huge amount of entropy is produced with the dilution factor $\sim 10^{24}$ as the dilaton decays if the conformal invariance of the Maxwell theory is broken through the coupling between the dilaton and electromagnetic fields in such a way that the resultant quantum fluctuations in the magnetic field have a nearly scale-invariant spectrum.

1 Introduction

It is well established that magnetic fields with the field strength $\sim 10^{-6}$G, ordered on $1-10$kpc scale, exist in our galaxy and other galaxies. Furthermore, in recent years magnetic fields in clusters of galaxies have been observed by means of the Faraday rotation measurements (RMs) of polarized electromagnetic radiation passing through an ionized medium. In general, the strength and the scale are estimated on $10^{-7}-10^{-6}$G and 10kpc$-$1Mpc, respectively. It is very interesting and mysterious that magnetic fields in clusters of galaxies are as strong as galactic ones and that the coherence scale may be as large as $\sim$Mpc. The most natural origin of such a large-scale magnetic field would be electromagnetic quantum fluctuation generated in the inflationary stage [1]. This is because inflation naturally produces effects on very large scales, larger than Hubble horizon, starting from microphysical processes operating on a causally connected volume. However, there is a serious obstacle on the way of this nice scenario as argued below.

The Friedmann-Robertson-Walker (FRW) metric usually considered is conformally flat. Moreover, the electrodynamics is conformally invariant. Hence large-scale electromagnetic fluctuations could not be generated quantum mechanically in cosmological background. In other words, if the origin of large-scale magnetic fields in clusters of galaxies is electromagnetic quantum fluctuations generated and amplified in the inflationary stage, the conformal invariance must have been broken at that time. Several breaking mechanisms therefore have been proposed.

In the present paper [2], in addition to the inflaton field ϕ we assume the existence of the dilaton field Φ and introduce the coupling of it to electromagnetic fields. Such coupling is reasonable in the light of indications in higher-dimensional theories, *e.g.*, string theories. The coupling was first suggested by Ratra [3]. In his model, however, the inflaton and the dilaton were identified and the case the dilaton freezes at the end of inflation was considered. We therefore consider a more realistic case that the dilaton continues its evolution with the exponential potential after inflation until it is stabilized after oscillating around its potential minimum and then decays into radiation with or without entropy production. We use units in which $k_{\rm B} = c = \hbar = 1$ and denote the gravitational constant $8\pi G$ by κ^2 so that $\kappa^2 \equiv 8\pi/{M_{\rm Pl}}^2$ where $M_{\rm Pl} = G^{-1/2} = 1.2 \times 10^{19}$GeV is the Planck mass. Moreover, in terms of electromagnetism we adopt Heaviside-Lorentz units. The suffixes 'R' and '0' represent the quantities at the end of inflation (namely, the instantaneous reheating stage) $t_{\rm R}$ and the present time t_0, respectively.

2 Model

Our model Lagrangian $\mathcal{L} = \mathcal{L}_{\rm inflaton} + \mathcal{L}_{\rm dilaton} + \mathcal{L}_{\rm EM}$ consists of the following three parts.

$$\mathcal{L}_{\rm inflaton} = -\frac{1}{2}g^{\mu\nu}\partial_\mu\phi\partial_\nu\phi - U[\phi], \tag{1}$$

$$\mathcal{L}_{\rm dilaton} = -\frac{1}{2}g^{\mu\nu}\partial_\mu\Phi\partial_\nu\Phi - V[\Phi], \quad V[\Phi] = \tilde{\Gamma}\exp(-\tilde{\lambda}\kappa\Phi), \tag{2}$$

$$\mathcal{L}_{\rm EM} = -\frac{1}{4}f(\Phi)F_{\mu\nu}F^{\mu\nu}, \quad f(\Phi) = \exp(\lambda\kappa\Phi), \tag{3}$$

where $U[\phi]$ and $V[\Phi]$ are the inflaton and dilaton potentials, $\tilde{\Gamma}$ is a constant, and f is the coupling between the dilaton and electromagnetic fields with λ and $\tilde{\lambda}\,(>0)$ being dimensionless constants. The form of the dilaton potential in Eq. (2) and that of the coupling between the dilaton and electromagnetic fields in Eq. (3) can be motivated by higher-dimensional theories reduced to four dimensions. Moreover, $F_{\mu\nu} = \partial_\mu A_\nu - \partial_\nu A_\mu$ is the electromagnetic field-strength tensor, where A_μ is the U(1) gauge field.

We assume the spatially flat FRW space-time with the metric

$$ds^2 = g_{\mu\nu}dx^\mu dx^\nu = -dt^2 + a^2(t)d\boldsymbol{x}^2, \tag{4}$$

where $a(t)$ is the scale factor.

Since we are interested in the specific case where the background space-time is inflating, we assume that the spatial derivatives of ϕ and Φ are negligible compared to the other terms. Hence the equations of motion for the background homogeneous scalar fields read

$$\ddot{\phi} + 3H\dot{\phi} + \frac{dU[\phi]}{d\phi} = 0, \quad \ddot{\Phi} + 3H\dot{\Phi} + \frac{dV[\Phi]}{d\Phi} = 0, \tag{5}$$

together with the background Friedmann equation

$$H^2 = \left(\frac{\dot{a}}{a}\right)^2 = \frac{\kappa^2}{3}(\rho_\phi + \rho_\Phi), \tag{6}$$

$$\rho_\phi = \frac{1}{2}\dot{\phi}^2 + U[\phi], \quad \rho_\Phi = \frac{1}{2}\dot{\Phi}^2 + V[\Phi], \tag{7}$$

where a dot denotes a time derivative. Here ρ_ϕ and ρ_Φ are the energy density of the inflaton and that of the dilaton.

We consider the case that during slow-roll inflation the cosmic energy density is dominated by $U[\phi]$ and the energy density of the dilaton is negligible, that is, $\rho_\phi \gg \rho_\Phi$. During inflation H therefore reads

$$H^2 \approx \frac{\kappa^2}{3}U[\phi] \equiv {H_{\rm inf}}^2, \tag{8}$$

where $H_{\rm inf}$ is the Hubble constant in the inflationary stage.

We consider the evolution of the gauge field in this background. Its equation of motion in the Coulomb gauge, $A_0(t,\boldsymbol{x}) = 0$ and $\partial_j A^j(t,\boldsymbol{x}) = 0$, becomes

$$\ddot{A}_i(t,\boldsymbol{x}) + \left(H_{\rm inf} + \frac{\dot{f}}{f}\right)\dot{A}_i(t,\boldsymbol{x}) - \frac{1}{a^2}\partial_j\partial_j A_i(t,\boldsymbol{x}) = 0. \tag{9}$$

It follows from the form of f in (3) and the approximate solution of the equation of motion for Φ in (5) that f can be practically expressed by the following approximate form.

$$f(\Phi) = f[\Phi(t)] = f[\Phi(a(t))] \equiv \tilde{f}a^{\beta-1}, \tag{10}$$

Reciprocity – a test for the new generation

Bruce A. Bassett, Martin Kunz

Department of Physics, Kyoto University, Japan & ICG, University of Portsmouth, UK

Astronomy Centre, University of Sussex, Brighton, UK

Abstract

In cosmology, distances based on standard candles (e.g. supernovae) and standard rulers (e.g. baryon oscillations) agree as long as three conditions are met: (1) photon number is conserved, (2) gravity is described by a metric theory with (3) photons travelling on unique null geodesics. This is the content of the reciprocity relation which can be violated by exotic physics. Here we analyse the implications of the latest cosmological data sets for reciprocity. While broadly in agreement and confirming acceleration we find a 2-σ violation of reciprocity caused by excess brightening of SN-Ia at $z > 0.5$. Nevertheless, our results rule out significant SN-Ia evolution, extinction and axion-photon mixing.

1 Introduction

In 1933 Etherington [1, 2, 3] proved a beautiful and general duality that implies that distances in cosmology based on a metric theory of gravity are unique: whether one uses the apparent luminosity of standard candles (yielding the luminosity distance, $d_L(z)$) or the apparent size of standard rulers (the angular-diameter distance $d_A(z)$), does not matter since they are linked by the reciprocity relation:

$$\frac{d_L(z)}{d_A(z)(1+z)^2} = 1\,. \tag{1}$$

where z is redshift. Reciprocity holds for general metric theories of gravity in any background (not just FLRW) in which photons travel on unique null geodesics and is essentially equivalent to Liouville's theorem in kinetic theory. While it is impervious to gravitational lensing (for infinitesimal geodesic bundles) it depends crucially on photon conservation. Our aim is to discuss how reciprocity may become a powerful test of a wide range of both exotic and fairly mundane physics and to present a general analysis of what constraints on violations of reciprocity arise from current data as well as critically analysing the conclusions drawn from recent type-Ia supernovae data [4].

To test reciprocity we use the latest combined type Ia supernovae (SNIa) data [4] together with earlier data [7, 6, 5] as a measure of the luminosity distance, $d_L(z)$ [8]. This data includes a significant number of $z > 1$ observations. On the other hand, our estimates of the angular-diameter distance, $d_A(z)$, come from several different sources including FRIIb radio galaxies [9, 10], compact radio sources [11, 12, 13] and X-ray clusters [14].

All these data sets give broadly the same picture of an accelerating, high-Ω_Λ cosmology. Nevertheless, there are a few observations in disagreement with the accelerating 'concordance' model (e.g. [17]), there are suggestions that SNIa may suffer from significant extinction [18], evolution [19] or axion-photon mixing [21]. There are also radical alternatives to general relativity, such as MOND [20]. Reciprocity gives us a way to test all of these possibilities.

2 Distance-duality violations

Since our aim is to promote reciprocity as a powerful test of fundamental physics it seems appropriate to begin by describing some phenomena that could be detected through violations of reciprocity. Perhaps the most likely source of reciprocity is non-conservation of photon number. This could have a mundane origin (scattering from dust or free electrons) or an exotic origin (e.g. photon decay or photon mixing

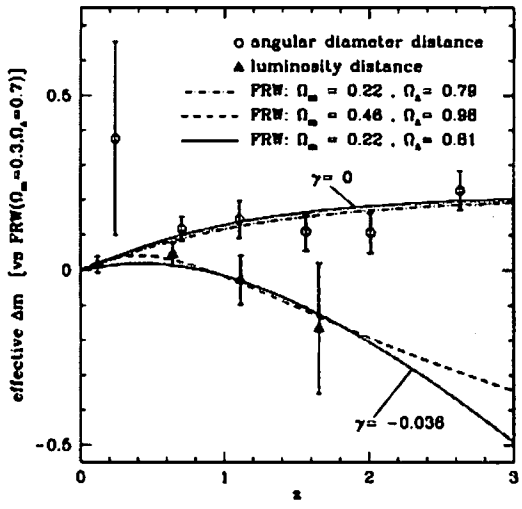

Figure 1: **Graphic evidence for violation of reciprocity.** The binned data for $d_L(z)$ (blue circles, SN-Ia) and $d_A(z)$ (red triangles, radio sources) are shown in equivalent magnitudes relative to the flat concordance model ($\Omega_\Lambda = 0.7, \Omega_m = 0.3$) with 1σ error bars. They should coincide if the reciprocity relation holds but they differ significantly at $z > 0.7$. The dashed curves are the best-fit FLRW models to the $d_A(z)$ data (top) and $d_L(z)$ (bottom) separately with no loss of photons ($\gamma = 0$). The solid curves have the same underlying FLRW model ($\Omega_\Lambda = 0.81$, $\Omega_m = 0.22$) but the lower curve includes the best-fit brightening ($\gamma = -0.036$, see eq. 2) with $\alpha = -2, \beta = 1$. Since the violation of the reciprocity relation increases exponentially when $\gamma \neq 0$ more high redshift data and/or smaller error bars will significantly improve constraints.

with other light states such as the dark energy, dilaton or axion [21, 22]). However, all of these effects tend to reduce the number of photons in a light bundle and therefore *reduce* the apparent luminosity of a source. If unaccounted for, this dimming makes the source appear more distant, i.e. increases d_L. Since d_A is typically unaffected (or negligibly altered) by such effects, this rather generally implies that the ratio in equation (1) becomes greater than unity. The case of axion-photon mixing has been studied in [22].

We consider a 3-parameter (α, β, γ) extension of equation (1), viz [23]:

$$\frac{d_L(z)}{d_A(z)(1+z)^2} = (1+z)^{\beta-1} \exp\left(-\gamma \int_0^z \frac{dz'}{E(z')(1+z')^\alpha}\right) \tag{2}$$

where $E(z) \equiv H(z)/H_0$; γ, α control the scattering/decay cross-section of the photon. H_0 is the current value of the Hubble constant. $\alpha = -2$ corresponds to a scattering cross-section $\propto \rho_{cdm} \propto (1+z)^3$, as in the case of Compton scattering from free-electrons. The case of photon decay corresponds to $\alpha = 1$. Loss of photons should therefore generically imply $\gamma > 0$. In fact $\gamma \neq 0$ leads to a violation of reciprocity that grows roughly exponentially with redshift, see Fig (1).The reciprocity relation corresponds to $(\beta, \gamma) = (1, 0)$ (in which case α is arbitrary).

3 Constraints from Current Data

Here we use the standard FLRW equations to calculate the theoretical distance $d_A(z)$ as a function of the cosmic parameters $(\Omega_M, \Omega_\Lambda)$ (over which we then marginalise, as they are determined by the angular diameter distance data) and use (2) to infer $d_L(z)$ given (α, β, γ). We use a standard Markov-Chain Monte Carlo method to sample the likelihood. More details of our data sets and method are given in [23]. In Figure (1) we show the binned $d_L(z)$ and $d_A(z)$ data as a function of redshift converted to

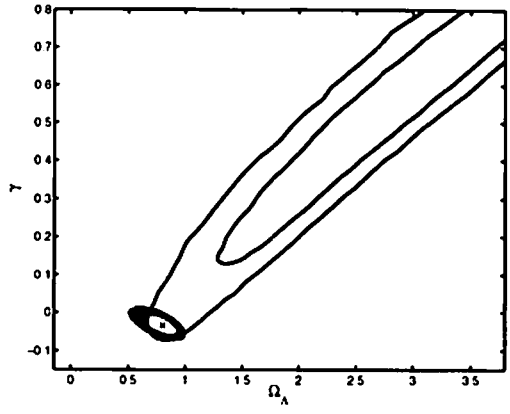

Figure 2: **Supernovae are brighter relative to d_A data.** γ-Ω_Λ likelihood plot in the case $\alpha = -2, \beta = 1$ which corresponds to a photon scattering probability $\propto (1+z)^3$. The best fit corresponds to $\gamma = -0.036$, i.e. brightening of SNIa relative to the d_A data, as required from figure 1. The diagonal solid (blue) contours are the very weak 1 and 2σ constraints found using only the SN-Ia data. This illustrates the power of blending d_L and d_A data as a consistency check of existing data and as a test of new physics.

magnitude (relative to the flat concordance model) assuming the reciprocity relation holds, in which case both data sets *should lie on the same curve.* The shaded regions shows the effect of the best-fit $\gamma = -0.036$ ($\alpha = -2, \beta = 1$) on the underlying $d_A(z)$ showing how it is possible to simultaneously fit the d_L and d_A data with a single model. Also shown are the very different best-fits to the d_L and d_A data taken separately. While the d_A data favour a flat universe, the SN-Ia data favour a very closed model (ruled out from the CMB) due to the unexpected brightening at $z > 0.5$.

Figure (2) shows the joint $\gamma - \Omega_\Lambda$ likelihood that follows when one imposes $\beta = 1$ and $\alpha = -2$ by assuming scattering from objects whose number density scales as $(1+z)^3$ (such as Compton scattering by free-electrons) we find that the best fit for the absorption coefficient is $\gamma = -0.036$ with $\chi^2_{min} = 219$ and $-0.07 < \gamma < 0$ at 95% confidence. Surprisingly, the best-fit corresponds not to absorption but brightening, as is clear from figure (1) since the $d_A(z)$ data lies above the d_L points.

The magnitude of the effect corresponds to an increase of about 5% in the number of photons per Hubble time, a very large violation of photon conservation. We can put this into perspective by comparing it with the expected loss of photons due to Compton scattering by the free electrons in the ionised intergalactic medium. At $z < 3$ helium is expected to be doubly ionised ($f_Y = 0.5$), leading to a free-electron density $n_e = \Omega_b \rho_{crit}(1 - Y f_Y)/m_N$ where $Y = 0.24$ is the primordial helium abundance. We therefore find a scattering amplitude of $\gamma_{Compton} = \sigma_T n_e/(2H_0) \sim 10^{-3}$, a factor of about 50 less than the best-fit (and of opposite sign).

4 Conclusions

In this paper we have emphasised reciprocity as a test of fundamental and exotic physics related to the metric nature of gravity and photon conservation on cosmic scales. Although stringent constraints will arise in the next few years the test is already proving powerful. In particular we are able to essentially rule-out non-accelerating models of the universe which explain the supernova dimming by grey-dust scattering, extinction or evolution. Interestingly, current data suggests a small (2-σ) discrepancy, corresponding to brightening of supernovae over their d_A counterparts [22, 23]. The definitive test of reciprocity will come from combining large galaxy surveys (such as KAOS) measuring d_A via baryon oscillations and the SNAP satellite measuring d_L.

BB is supported by the Royal Society & JSPS. MK is supported by PPARC.

References

[1] J.M.H. Etherington, Phil. Mag. **15**, 761 (1933)

[2] G.F.R. Ellis, in Proc. School "Enrico Fermi", Ed. R. K. Sachs, New York (1971)

[3] P. Schneider, J. Ehlers and E.E. Falco, *Gravitational Lenses*, Springer (1992)

[4] A. G. Riess *et al*, to appear in Astrophys. J., astro-ph/0402512 (2004)

[5] J. L. Tonry *et al.*, Astrophys. J. **594**, 1 (2003)

[6] B. J. Barris, *et al.*, to appear in Astrophys. J., astro-ph/0310843 (2003)

[7] R. A. Knop, *et al.*, to appear in Astrophys. J., astro-ph/0309368 (2003)

[8] S. Perlmutter and B. P. Schmidt, In Supernovae & Gamma Ray Bursts, K. Weiler, Ed., Springer, Lecture Notes in Physics; astro-ph/0303428.

[9] R. A. Daly, & S. G. Djorgovski, Astrophys. J.**597**, 9 (2003).

[10] R.A. Daly, E. J. Guerra, Astron.J. **124**, 1831 (2002)

[11] L.I. Gurvitis, 1994, Astrophys. J. **425**, 442

[12] J.C. Jackson and M. Dodgson, Mon.Not.Roy.Astron.Soc. **285**, 806 (1997)

[13] J.C. Jackson, astro-ph/0309390 (2003).

[14] S.W. Allen, R.W. Schmidt, A.C. Fabian and H. Ebeling, Mon.Not.Roy.Astron.Soc. **342**, 287 (2003).

[15] P.J. Outram *et al.*, Mon.Not.Roy.Astron.Soc. **348** 745 (2004)

[16] J. L. Mitchell, C. R. Keeton, J. A Frieman, R. K. Sheth, astro-ph/0401138 (2004).

[17] S. C. Vauclair, *et al.*, A&A **412**, L37 (2003)

[18] M. Rowan-Robinson, Mon.Not.Roy.Astron.Soc., **332**, 352 (2002)

[19] P. S. Drell, T. J. Loredo and I. Wasserman, Astrophys.J. **530**, 593 (2000)

[20] M. Milgrom, Astrophys.J. **270**, 365 (1983)

[21] C. Csaki, N. Kaloper and J. Terning, Phys. Rev. Lett. **88**, 161302, (2002)

[22] B. A. Bassett and M. Kunz, astro-ph/0311495, to appear in Astrophys. J. (2004)

[23] B. A. Bassett and M. Kunz, astro-ph/0312443 (2004) Astrophys. J **561** 106 (2001); erratum ibid **589**, 1089 (2003)

[24] B.P. Schmidt *et al.*, Ap. J, **432**, 42 (1994)

[25] J.A. Cardelli, G.C. Clayton and J.S. Mathis, Astrophys. J. **345**, 245 (1989).

[26] B.A. Bassett, M. Kunz, M., J. Silk, & C. Ungarelli, Mon.Not.Roy.Astron.Soc., **336**, 1217 (2003)

[27] B.A. Bassett, M. Kunz, D. Parkinson, & C. Ungarelli, Phys. Rev. D **68**, 043504 (2003)

Null hypersurfaces in general relativity

Ewa Czuchry[1], Jacek Jezierski[2] Jerzy Kijowski[3]

Yukawa Institute for Theoretical Physics, Kyoto University, Kitashirakawa-Oiwake-Cho, Sakyo-ku, Kyoto 606-8502, Japan

Department of Mathematical Methods in Physics, University of Warsaw, ul. Hoża 69, 00-682 Warszawa, Poland

Center for Theoretical Physics, Polish Academy of Sciences, Al. Lotników 32/46; 02-668 Warszawa, Poland

Abstract

Basic geometric tools describing the structure of a null-like surface S are reviewed. Problems arising from degeneracy of the induced three-dimensional metric are discussed in detail, with attention focused on the ambiguity of the derivative operator and the impossibility of its unique definition. The notion of external curvature for a null-like hypersurface is introduced. Gauss-Codazzi constraint equations in terms of this object are given.

1 Introduction

A null hypersurface in a Lorentzian space-time M is a three-dimensional submanifold $S \subset M$ such that the restriction g_{ab} of the space-time metrics $g_{\mu\nu}$ to S is degenerate. There are several problems arising in connection with this degeneracy.

Geometry of a hypersurface $S \subset M$ in a Riemannian manifold (M, g) may be described by two objects: the restriction g_{ab} of the metric tensor to S (called its "first fundamental form") and the external curvature (called its "second fundamental form"). For many purposes it is useful to represent the latter by the so called Arnowitt-Deser-Misner momentum-density $Q^a{}_b$. In a pseudo-Riemannian (Lorentzian) manifold M, the analogous quantity may be easily defined for any submanifold S whose first fundamental form is non-degenerate – see [1] and [2].

Yet this is not true if S is a wave front, i.e. null manifold. In this case the induced metric is degenerate, and the standard construction of external curvature does not make any sense. For a non-degenerate (time-like or space-like) hypersurface, the extrinsic curvature may be described in many equivalent ways: by tensors or tensor densities, both of them in the contravariant, covariant or mixed version. In a null-like case, the degenerate metric on S does not allow us to convert tensors into tensor densities and *vice versa*. Also, we are not allowed to rise covariant indices, whereas lowering the contravariant indices is not an invertible operator and leads to information losses.

However it turns out that the mixed tensor densities have the appropriate null-like limit and that the divergence of such tensor densities (fulfilling some additional algebraic properties) is a well defined geometrical object. Luckily enough, basic quantities used for description of the geometric properties of null-like hypersurfaces, and further for dynamics of light-like shell – external curvature and energy-momentum tensor density – are of such type, and the basic equations which are to be fulfilled by these quantities, contain only divergence operator.

The structure of the paper is the following. In Sec. 2 we introduce some geometric tools describing intrinsic geometry of the null hypersurface. Then in Sec. 3 we review problems with definition of derivative operator with respect to the three-dimensional null geometry and propose the definition of the divergence operator, which occurs to be well behaving geometric object. In the next section we introduce the analog of the external curvature which is used for description of the extrinsic geometry of the wave front and is to fulfil the null version of Gauss-Codazzi constraint equations.

[1]E-mail:eczuchry@yukawa.kyoto-u.ac.jp
[2]E-mail:jjacekj@fuw.edu.pl
[3]E-mail:kijowski@cft.edu.pl

In this paper we use adapted coordinates: Cauchy surfaces V_t corresponding to constant value of the "time-like" coordinate $x^0 = t$ are space-like and the x^3 coordinate is constant on S. Space coordinates will be labelled by $k, l = 1, 2, 3$; coordinates on S will be labelled by $a, b = 0, 1, 2$; finally, coordinates on $S_t := V_t \cap S$ will be labelled by $A, B = 1, 2$. Space-time coordinates will be labelled by Greek characters α, β, μ, ν.

2 Geometry of null hypersurfaces

The non-degeneracy of the space-time metric implies that the metric g_{ab} induced on S from the spacetime metric $g_{\mu\nu}$ has signature $(0, +, +)$. This means that there is a non-vanishing null-like vector field X^a on S, such that its four-dimensional embedding X^μ to M (in adapted coordinates $X^3 = 0$) is orthogonal to S. Hence, the covector $X_\nu = X^\mu g_{\mu\nu} = X^a g_{a\nu}$ vanishes on vectors tangent to S and, therefore, the following identity holds:

$$X^a g_{ab} \equiv 0 \,. \tag{1}$$

It is easy to prove (cf. [3]) that integral curves of X^a, after a suitable reparameterization, are geodesic curves of the space-time metric $g_{\mu\nu}$. Moreover, any null hypersurface S may always be embedded in a 1-parameter congruence of null hypersurfaces.

We assume that topologically we have $S = \mathbb{R}^1 \times S^2$. Since our considerations are purely local, we fix the orientation of the $\mathbb{R}^1$ component and assume that null like vectors X describing degeneracy of the metric g_{ab} of S will be always compatible with this orientation. Moreover, we shall always use coordinates such that the coordinate x^0 increases in the direction of X, i.e. inequality $X(x^0) = X^0 > 0$ holds. In these coordinates degeneracy fields are of the form $X = f(\partial_0 - n^A \partial_A)$, where $f > 0$, $n_A = g_{0A}$ and we rise indices with the help of the two-dimensional matrix $\overset{\circ}{g}{}^{AB}$, inverse to g_{AB}.

If by λ we denote the two-dimensional volume form on each surface $x^0 = \text{const.}$:

$$\lambda := \sqrt{\det g_{AB}} \,, \tag{2}$$

then for any degeneracy field X of g_{ab}, the following object

$$v_X := \frac{\lambda}{X(x^0)}$$

is a scalar density on S. Its definition does not depend upon the coordinate system (x^a) used in the above definition. To prove this statement it is sufficient to show that the value of v_X gets multiplied by the determinant of the Jacobi matrix when we pass from one coordinate system to another. This means that $\mathbf{v}_X := v_X dx^0 \wedge dx^1 \wedge dx^2$ is a coordinate-independent differential three-form on S. However, v_X depends upon the choice of the field X.

It follows immediately from the above definition that the following object:

$$\Lambda = v_X \, X \,,$$

is a well defined (i.e. coordinate-independent) vector-density on S. Obviously, it *does not depend* upon any choice of the field X:

$$\Lambda = \lambda(\partial_0 - n^A \partial_A) \,. \tag{3}$$

Hence, it is an intrinsic property of the internal geometry g_{ab} of S. The same is true for the divergence $\partial_a \Lambda^a$, which is, therefore, an invariant, X-independent, scalar density on S. Mathematically (in terms of differential forms), the quantity Λ represents the two-form:

$$\mathbf{L} := \Lambda^a \left(\partial_a \rfloor \, dx^0 \wedge dx^1 \wedge dx^2\right) \,,$$

whereas the divergence represents its exterior derivative (a three-from): $\mathrm{d}\mathbf{L} := (\partial_a \Lambda^a)\, dx^0 \wedge dx^1 \wedge dx^2$. In particular, a null surface with vanishing $\mathrm{d}\mathbf{L}$ is called a *non-expanding horizon* (see [4]).

3 Problems with a derivative operator

The degenerate metric g_{ab} on S does not allow to define *via* the compatibility condition $\nabla g = 0$, any natural connection, which could apply to generic tensor fields on S. Nevertheless, there is one exception: the degenerate metric defines *uniquely* a certain covariant, first order differential operator. This operator may be applied only to mixed (contravariant-covariant) tensor-density fields $\mathbf{H}^a{}_b$, satisfying the following algebraic identities:

$$\mathbf{H}^a{}_b X^b = 0 \ , \quad \mathbf{H}_{ab} = \mathbf{H}_{ba} \ , \tag{4}$$

where $\mathbf{H}_{ab} := g_{ac}\mathbf{H}^c{}_b$. Its definition cannot be extended to other tensorial fields on S. Fortunately the extrinsic curvature of a null-like surface and the energy-momentum tensor of a null-like shell are described by tensor-densities of this type.

The operator, which we denote by $\overline{\nabla}_a$, could be defined by means of the four dimensional metric connection in the ambient space-time M in the following way. Given $\mathbf{H}^a{}_b$, take any its extension $\mathbf{H}^{\mu\nu}$ to a four-dimensional, symmetric tensor density, "orthogonal" to S, i.e. satisfying $\mathbf{H}^{\perp\nu} = 0$ ("$\perp$" denotes the component transversal to S). Define $\overline{\nabla}_a \mathbf{H}^a{}_b$ as the restriction to S of the four-dimensional covariant divergence $\nabla_\mu \mathbf{H}^\mu{}_\nu$. The ambiguities which arise when extending three dimensional object $\mathbf{H}^a{}_b$ living on S to the four dimensional one, cancel finally and the result is unambiguously defined as a covector-density on S. It turns out, however, that this result does not depend upon the space-time geometry and may be defined intrinsically on S.

In case of a non-degenerate metric, the covariant divergence of a symmetric tensor $\mathbf{H}$ density may be calculated by the following formula:

$$\nabla_a \mathbf{H}^a{}_b = \partial_a \mathbf{H}^a{}_b - \mathbf{H}^a{}_c \Gamma^c_{ab} = \partial_a \mathbf{H}^a{}_b - \frac{1}{2}\mathbf{H}^{ac} g_{ac,b} \ , \tag{5}$$

with $g_{ac,b} := \partial_b g_{ac}$. In case of our degenerate metric, we want to mimic the last formula, but here rising of indices of $\mathbf{H}^a{}_b$ makes no sense. Nevertheless, formula (5) may be given a unique sense also in the degenerate case, if applied to a tensor density $\mathbf{H}^a{}_b$ satisfying identities (4). Namely, we take as $\mathbf{H}^{ac}$ *any* symmetric tensor density, which reproduces $\mathbf{H}^a{}_b$ when lowering an index:

$$\mathbf{H}^a{}_b = \mathbf{H}^{ac} g_{cb} \ . \tag{6}$$

It is easily seen, that such a tensor-density always exists due to identities (4), but reconstruction of $\mathbf{H}^{ac}$ from $\mathbf{H}^a{}_b$ is not unique, because $\mathbf{H}^{ac} + CX^a X^c$ also satisfies (6) if $\mathbf{H}^{ac}$ does. Conversely, two such symmetric tensors $\mathbf{H}^{ac}$ satisfying (6) may differ only by $CX^a X^c$. This non-uniqueness does not influence the value of (5), because of the following identity implied by (1):

$$0 \equiv (X^a X^c g_{ac})_{,b} = X^a X^c g_{ac,b} + 2X^a g_{ac} X^c{}_{,b} = X^a X^c g_{ac,b} \, . \tag{7}$$

Hence, the following definition makes sense:

$$\overline{\nabla}_a \mathbf{H}^a{}_b := \partial_a \mathbf{H}^a{}_b - \frac{1}{2}\mathbf{H}^{ac} g_{ac,b} \ . \tag{8}$$

The right-hand-side does not depend upon any choice of coordinates (i.e. transforms like a genuine covector-density under change of coordinates). The proof is straightforward and does not differ from the standard case of formula (5), when metric g_{ab} is non-degenerate.

The above definition of the operator $\overline{\nabla}$ uses only the intrinsic metric of S. We want to prove now that it coincides with the definition given in terms of the four dimensional space-time metric-connection. For that purpose observe, that the only non-uniqueness in the reconstruction of the four-dimensional tensor density of $\mathbf{H}^{\mu\nu}$ is of the type $CX^\mu X^\nu$. Indeed, any such reconstruction may be obtained from a reconstruction of $\mathbf{H}^{ac}$ by putting $\mathbf{H}^{3\nu} = 0$ in a coordinate system adapted to S (i.e. such that the coordinate x^3 remains constant on S). Now, calculate the four-dimensional covariant divergence $\mathbf{H}_\nu := \nabla_\mu \mathbf{H}^\mu{}_\nu$. Due to the geodesic character of integral curves of the field X, the only non-uniqueness which remains after this operation is of the type $\tilde{C}X_\nu$. Hence, the restriction $\mathbf{H}_b$ of $\mathbf{H}_\nu$ to S is already unique. Due to (5), it equals:

$$\nabla_\mu \mathbf{H}^\mu{}_b = \partial_\mu \mathbf{H}^\mu{}_b - \frac{1}{2}\mathbf{H}^{\mu\lambda} g_{\mu\lambda,b} = \partial_a \mathbf{H}^a{}_b - \frac{1}{2}\mathbf{H}^{ac} g_{ac,b} = \overline{\nabla}_a \mathbf{H}^a{}_b \ . \tag{9}$$

4 Extrinsic geometry of a null hypersurface

To describe extrinsic geometry of S begin with covariant derivatives *along* S of the "orthogonal vector X". Consider the tensor $\nabla_a X^\mu$. Unlike in the non-degenerate case, there is no unique "normalization" of X and, therefore, such an object does depend upon a choice of the field X. The length of X is constant (because vanishes). Hence, the tensor is again orthogonal to S, i.e. the components corresponding to $\mu = 3$ vanish identically in adapted coordinates. This means that $\nabla_a X^b$ is a purely three dimensional tensor living on S.

For general purposes it is useful to use the "ADM-like" version of this object, defined in the following way:

$$Q^a{}_b(X) := -s\left\{v_X\left(\nabla_b X^a - \delta^a{}_b \nabla_c X^c\right) + \delta^a{}_b \partial_c \Lambda^c\right\}\ , \tag{10}$$

where $s := \operatorname{sgn} g^{03} = \pm 1$. Due to above convention, the "extrinsic curvature" $Q^a{}_b(X)$ feels only *external orientation* of S and does not feel any internal orientation of the field X.

The last term in (10) is X-independent. It has been introduced in order to correct algebraic properties of the quantity $v_X\left(\nabla_b X^a - \delta^a{}_b \nabla_c X^c\right)$: we prove in the paper [5] that $Q^a{}_b$ satisfies identities (4) and, therefore, its covariant divergence with respect to the degenerate metric g_{ab} on S is uniquely defined. This divergence enters into the Gauss-Codazzi equations which relate the divergence of Q with the transversal component $\mathcal{G}^\perp_b$ of the Einstein tensor-density $\mathcal{G}^\mu{}_\nu = \sqrt{|\det g|}\left(R^\mu{}_\nu - \delta^\mu{}_\nu \frac{1}{2} R\right)$. The transversal component of such a tensor-density is a well defined three-dimensional object living on S. In coordinate system adapted to S, i.e. such that the coordinate x^3 is constant on S, we have $\mathcal{G}^\perp_b = \mathcal{G}^3{}_b$. Due to the fact that $\mathcal{G}$ is a tensor-density, components $\mathcal{G}^3{}_b$ *do not change* with changes of the coordinate x^3, provided it remains constant on S. These components describe, therefore, an intrinsic covector-density living on S.

Proposition. *The following null-like-surface version of the Gauss-Codazzi equation is true:*

$$\overline{\nabla}_a Q^a{}_b(X) + s v_X \partial_b\left(\frac{\partial_c \Lambda^c}{v_X}\right) \equiv -\mathcal{G}^\perp_b\ . \tag{11}$$

The proof of the above proposition is given in the paper [5]. We only remind the reader that the ratio between two scalar densities: $\partial_c \Lambda^c$ and v_X, is a scalar function. Its gradient is a co-vector field. Finally, multiplied by the density v_X, it produces an intrinsic co-vector density on S. This proves that also the left-hand-side is a well defined geometric object living on S.

The quantity $Q^a{}_b$ defined above enables us to consider spacetimes with singular (distribution-like) curvature confined to a null-like hypersurface. Such spacetimes are a natural arena for the theory of a null-like matter shell. Such shells, carrying a self-gravitating light-like matter, are of the special interest as toys models in different quantum gravity theories. In the paper [5] we gave a complete classical, Lagrangian and Hamiltonian, description of a physical system composed of a gravitational field interacting with a light-like matter shell. It is worth to mention that null hypersurfaces also arise in the other physical situation – they describe the so called nonexpanding horizons in the theory of black holes.

References

[1] R. Arnowitt, S. Deser, and C. Misner, in *Gravitation: an Introduction to Current Research*, edited by L. Witten (Wiley, New York, 1962), p. 227.

[2] C. W. Misner, K. S. Thorne, and J. A. Wheeler, *Gravitation*, (Freeman, San Francisco, 1973).

[3] J. Jezierski, J. Kijowski, E. Czuchry, Rep. Math. Phys. **46** (2000) pp. 397–418.

[4] A. Ashtekar, C. Beetle, O. Dreyer, S. Fairhurst, B. Krishnan, J. Lewandowski, and J. Wisniewski, Phys. Rev. Lett. **85**, 3564 (2000); A. Ashtekar, S. Fairhurst, and B. Krishnan, Phys. Rev. D **62**, 104025 (2000).

[5] J. Jezierski, J. Kijowski, E. Czuchry, Phys. Rev. D **65** (2002), p. 064036.

Spacetime singularity in massive gravity

Hiroki Emoto [1]

High Energy Accel. Res. Organization
1-1 Oho, Tsukuba-shi, Ibaraki-ken 305-0801, Japan

Abstract

We discussed the property two type of classical solution of massive gravity with non-Fierz Pauli mass term which was investigated in [4] although definite results have not reached. Attention is paying to the generating condition of closed trapped surface and energy condition.

1 Introduction

Spacetime singularity is one of the most famous problem in general relativity and many people have been investigating this topic by quatum gravity, string theory, or realistic model of gravitational collapse and so on. Among them, most simple type of singularity, Schwartzschild black hole seems to be difficult to understand. On the other hand, the choice of the different type of theory, modified gravity, would be another possibility. General relativity is massless spin 2 (helicity 2) field theory perturbatively although quantum field theory has not established completely. On the other hand, There has been many discussion about "massive gravity", which have many forms of theory.In recent interest, they are discussed in the context of extra, multi dimensional, brane world [1],[2], or string thoery [3], or field theory formulation of gravity [4], [6]. Although whole picture is not so clear , their perturbative (linearized) theory is 2-rank tensor field theory which has finite mass. This field theoretical degree consist of spin 2 (5 degree) and spin 0 (1 degree) component and spin 0 component has been considered as negative norm (or energy) state. Many authors has killed this spin 0 component by giving infinite mass (Fierz-Pauli mass) from the biginning in their action ,and solve the wave equation with 5 degree which has led to famous discontinuity in the massless, general relativity limit(VDVZ discontinuity) [7]. The possibile recovery of continuity has been expected in non-linear effect [9] or discussed in extra dimensional set-up [1]. Another approach would be covariantly (BRST) quantization with 5 or 6 degree and appropriate selection of physical state [10] but non-linear order is obscure. In elementary particle physics, most established understanding for massive gauge theory (vector field, Yang-Mills) is Higgs mechanism. As for gravity, recent study was carried out along this line [2], [11].

In this poster, I concentrate on the analysis of classical solution which was analyzed already in [4]. Especially I choose the formulation of "finite-range gravity" based on the field theoretical formulation of gravity which is equivalent to general relativity in the limit of massless graviton. Since I hope to discuss and understand the spacetime property of this theory as generally as possible, I would study some conditions of generating spacetime singularity in general relativity and report some results.

2 Finite-range gravity and energy condition

We take the theory of finitee-range(massive) gravity [4] here based on the field theoretical forumulation [5]. This theory is constructed on flat spacetime (metric is $\gamma^{\mu\nu}$) and has covariant energy-momentum tensor of gravitational field on this background. The flatness of the background spacetime is assumption and constraint.Another assumption is the universal coupling of all other fields ro gravity field $h^{\mu\nu}$. The variation of this action leads to the field equation

$$R_{\mu\nu} - \frac{1}{2}g_{\mu\nu}R - M_{\mu\nu} = 8\pi G T_{\mu\nu} \tag{1}$$

[1] E-mail:emo@post.kek.jp

by changing variables "Riemann metric $g^{\mu\nu}$" through $\sqrt{-g}g^{\mu\nu} = \sqrt{-\gamma}(\gamma^{\mu\nu} + h^{\mu\nu})$, where

$$\begin{aligned} M_{\mu\nu} &= \Big(\delta^\alpha_\mu\delta^\beta_\nu - \frac{1}{2}g^{\alpha\beta}g_{\mu\nu}\Big)(2k_1h_{\alpha\beta} + 2k_2\gamma_{\alpha\beta}h) \\ &= 2\gamma_{\rho\alpha}\gamma_{\sigma\beta}\Big(\delta^\alpha_\mu\delta^\beta_\nu - \frac{1}{2}g^{\alpha\beta}g_{\mu\nu}\Big)\Big[k_1\Big(\frac{\sqrt{-g}}{\sqrt{-\gamma}}g^{\rho\sigma} - \gamma^{\rho\sigma}\Big) + k_2\gamma^{\rho\sigma}\Big(\frac{\sqrt{-g}}{\sqrt{-\gamma}}g^{\tau\psi}\gamma_{\tau\psi} - 4\Big)\Big] \end{aligned} \tag{2}$$

is the general mass term of gravity. This is the quasigeometric form and written in bi-metric. The case of $k_1 = -k_2$ is "Pauli-Fierz mass".Conservation law for energy momntum tensor and Bianchi identity holds, so

$$M^\mu_{\nu|\mu} = 0 \tag{3}$$

here, $|\mu$ is covariantderivative with respect to $g_{\mu\nu}$.

In this theory, dynamics of geodesics deviation is the same derivation from geodesic equation of general relativity, and Raychaudhuri's equation is the same form

$$\frac{d\theta}{d\lambda} = -\frac{1}{2}\theta^2 - \sigma_{\mu\nu}\sigma^{\mu\nu} + \omega_{\mu\nu}\omega^{\mu\nu} - R_{\mu\nu}k^\mu k^\nu \tag{4}$$

where,θ is expansion, shear $\sigma_{\mu\nu}$, twist $\omega_{\mu\nu}$.But in this case, $R_{\mu\nu}k^\mu k^\nu$, 4th term of right hand side of this equation which is important for determining the sign of expansion rate $d\theta/d\lambda$ is modified by "graviton mass"

$$R_{\mu\nu}k^\mu k^\nu = \kappa T_{\mu\nu}k^\mu k^\nu - 2(k_1h_{\mu\nu} + k_2\gamma_{\mu\nu}h)k^\mu k^\nu \geq 0 \tag{5}$$

So We have to evaluate the effect of mass term by this equation around the geodesics of classical solution. I had some set-up for this calculation, in Spherically symmetric static backgraoun and the cosmological background. These work is still undergoing and I briefly explain this strategy as following sections.

3 Spherically symmetric static solution

This spacetime is described as

$$ds^2 = -f(r)dt^2 + \frac{1}{X'^2F}dr^2 + R^2d\Omega^2 = -f(R)dt^2 + \frac{1}{F(R)}dR^2 + R^2d\Omega^2 \tag{6}$$

where $r = r(R) \equiv X$, and $X' = dX/dR$.The authors of [4] solved field equations of this spacetime numerically, and found asymptotic forms of function by extrapolation.Their result shows that this spacetime has no "event horizon",$f \to o$ as $R \to 0$, F decreces as $R \to 2M$ and starts to increase near the $2M$, Schwarzschild radius in GM. In addition there is a curvature singularity at the center. Near the center $R = 0$ they evaluate numerically

$$F(R) = C_F(\frac{R}{2M})^{-1-\nu} + \frac{1}{1+\nu}, \qquad f(R) = C_f(\frac{R}{2M})^{-1+\nu} + \frac{C_f}{(1+\nu)C_F}(\frac{R}{2M})^{2\nu} \tag{7}$$

here,C_F, C_f are arbitrary constant and $\nu = 4.62977 \times 10^5$. tangent vector k^μ of the radial null geodesics of this spacetime is

$$k^\mu = \Big(\frac{1}{f}, \pm\sqrt{\frac{X'^2F}{f}}, 0, 0\Big), \qquad \theta = g^{\mu\nu}k_{\mu|\nu} = \pm\frac{2}{R}\sqrt{\frac{F}{f}} \tag{8}$$

up to constant.+ is outward,− is inward solution. If this θ is negative for both signs, there exists closed trapped surface. By the results of autors [4], there seems no zero point of f except at $R = 0$, So this expression can be used all region of R (which is diferrnt from Schwawarzschild case in GR), but just for that reason, there seems to be no trapped surface in this spacetime. From the form of asymptotic solution, we have checked that asymptotic behaviour of this spacetime near $R = 0$ is a naked type singularity which is similar to negative mass Schwawrtzschild. But this case is attractive force aganist test particle not repelling effect by negative mass solution.

Although we have not checked yet definitely, this solution would have no trapped surface. The authors of [4] commented that this "singularity" only the reflection of point mass assumption, and realistic

extended object would resolve it. But we must investigate internal stellar solution practically. That is future work.

Besides, It may be useful to calculate the quantity of "energy condition"

$$R_{\mu\nu}k^\mu k^\nu = -2\frac{1}{f^2}\Big[-\frac{3}{2}\zeta+\frac{3}{2}\zeta(\frac{R}{X})^2\frac{1}{\sqrt{X'^2Ff}}+\frac{2\zeta+1}{2}\sqrt{\frac{f}{X'^2F}}\Big(1-X'^2Ff\Big) \\ +\frac{3}{2}\zeta X'^2Ff+\frac{3}{2}(\frac{R}{X})^2X'^2Ff\sqrt{X'^2Ff}\Big] \tag{9}$$

here,ζ is the ratio,$\beta^2=\zeta\alpha^2$, and α,β are each mass of spin 2, spin 0 component.

4 Homogeneous isotropic universe

For the time being, only $K=0$(sapce flat) case being considered[4].Another topology ($K=\pm1$) is under work now. This spacetime is

$$ds^2=-b^2(t)dt^2+a^2(t)dr^2+r^2(d\theta^2+\sin^2\theta) \tag{10}$$

As is the case of ordinary cosmology, we assumed matter source as $T^0_0=-\epsilon(t),T^1_1=T^2_2=T^3_3=p(t)$. From the conservation law $T^\mu_{\nu|\mu}=0$, we get $\epsilon'+3(a'/a)(p+\epsilon)=0$ here $'\equiv d/dt$. Equation of motion was also studied by [4] and found initial no singular (bounce) solution. As spherically symmtric solution, we have solved the null tangent vector k^μ in this case. Here we extend to the case of spacelike open and closed universe case as

$$ds^2=-b^2(t)dt^2+a^2(t)dr^2+f(r)^2(d\theta^2+\sin^2\theta) \tag{11}$$

where $f(r)=\sin r,r,\sinh r$ for $K=1,0,-1$.

The results are

$$k^\mu=\frac{b}{a}\exp\Big(\pm2\frac{ab'}{b^2}r\Big)\Big(-1,\pm\frac{b}{a},0,0\Big) \tag{12}$$

is the null geodesic tangent vector,for + outgoing,− ingoing.Expansion rate is

$$\theta=\frac{2}{a^2}\exp\Big(\pm2\frac{ab'}{b^2}r\Big)\Big(-a'b\mp\frac{a^2b''-aa'b'}{b^3}r\pm\frac{b^2}{f}\frac{df}{dr}\Big) \tag{13}$$

and we have checked the energy condition $R_{\mu\nu}k^\mu k^\nu$ in the case of $K=0,\zeta=0$ numerically. Results is that $R_{\mu\nu}k^\mu k^\nu>0$ always holds around "bouncing era". So we anticipate the trapped surface is not generated in this solution although we wil check this near future.

5 Current status and future problems

Although introducing graviton mass have not realized in enough widely accepted manner, this kind of theoretical challenge have been done in some direction such as Higgs-like condensation, or brane-setup. Although most strategy is subject to extracting spin 0 component mass (Fierz-Pauli type), there would be still needs of studying more wide class of non-Fierz-Pauli type mass because unitarity is closely connected gauge symmetry and this type mass has more smooth limit to general relativity.

In this poster, we only study some situation of two type of classical solutions with non-Fierz Pauli mass term and saw the symptom of no closed trapped surface but more close study is needed. Moreover we need to know the equilibrium equation of internal stellar solution in the black hole type solution. We hope to report near future these situation with field theoretical property to which was not referred in detail.

Acknowledgements: I hope to thank sincerely all people who discuss with me about this poster or shows hospitality and the organizers of JGRG13.

References

[1] C. Deffayet, G. Dvali, G. Gabadadze. A. Vainshtein, Phys. Rev. **D65**, 044026 (2002).

[2] T. Damour, I. I. Kogan, A. Papazoglou, Phys. Rev. **D67**, 064009 (2003).

[3] M. B. Green, C. B. Thorn, Nucl. Phys. **B367**, 462 (1991); W. Siegel, Phys. Rev. **D49**, 4144(1994).

[4] S. V. Babak, L. P. Grishchuk, arXiv:gr-qc/0209006.

[5] S. V. Babak, L. P. Grishchuk, Phys. Rev. **D61**, 024038,(2000).

[6] A. A. Logunov, arXiv:gr-qc/0210005.

[7] H. van Dam, M. Veltman, Nucl. Phys. **B22**, 397 (1970).

[8] D. G. Boulware, S. Deser, Phys. Rev. **D6**, 3368 (1972).

[9] A. I. Vainshtein, Phys. Lett. **B39**, 393 (1972).

[10] S. Hamamoto, Prog.Theor.Phys.**96**, 639 (1996); C. Fronsdal, W. F. Heidenreich, Annals. Phys. **215**, 51 (1992).

[11] N. Arkani-Hamed, H. Georgi, M. D. Schwartz, Annals. Phys.**305**, 96 (2003); N. Arkani-Hamed, H-C. Cheng, M. A. Luty, S. Mukohyama, arXiv:hep-th/0312099,

Gravitational waves from a particle orbiting a Kerr black hole

Ryuichi Fujita[1], Hideyuki Tagoshi[2], Misao Sasaki[3],

Department of Earth and Space Science, Graduate School of Science, Osaka University, Toyonaka, Osaka 560-0043, Japan
Yukawa Institute for Theoretical Physics, Kyoto University, Kyoto 606-8502, Japan

Abstract

Gravitational radiation from compact stars orbiting and falling into a supermassive black hole is one of the most important sources for the space laser interferometer detectors such as the Laser Interferometer Space Antenna (LISA). Gravitational waves from such systems are calculated by the Teukolsky equation. We develop highly accurate numerical codes to calculate such gravitational waves. The method is based on the formalism by Mano, Suzuki and Takasugi in which the homogeneous solutions of the Teukolsky equation is described in terms of series of hypergeometric functions and Coulomb wave functions. Although the application of this formalism are limited to the analytical calculation of gravitational waves previously, we find that it is also useful for the numerical calculation. As a test, we calculate the energy flux of the gravitational waves from a particle in circular orbit on the equatorial plane around a Kerr black hole.

1 Introduction

Recently, there has been great progresses in the project of the gravitational wave detectors. Ground-based detectors, TAMA300, began to operate in 1999 and has operated several times since them. LIGO and GEO600 began to operate 2002. VIRGO are expected to begin the operation soon.

On the other hand, the project of the space-based detectors, LISA, have also been in progress. In LISA project, it is planned to launch the satellite in the early 2010's. One of the main targets of the LISA is the gravitational waves from compact stars orbiting around a supermassive black hole. Compact stars around a supermassive black hole are evolving due to the emission of gravitational radiation while they orbit around the hole. They lose the energy and the angular momentum by gravitational radiation reaction, and their orbital radius gradually shrink. Such situation is often called "extreme mass ratio inspiral".

Observations of the gravitational waves from such systems will bring us interesting information such as mass, spin and higher multipole moments of supermassive black holes, by which we may be able to test the general relatively. They will also bring us astrophysically interesting information which can not be obtained by observation of the electromagnetic radiation.

In order to obtain such physical information, we must predict the wave forms with sufficiently good accuracy. The gravitational waves from the extreme mass ratio inspirals can be calculated by the black hole perturbation method. At the first order of the perturbation, the compact object with the mass can be assumed to move along the geodesic of the background spacetime, which is governed by the supermassive black hole with the mass. With this assumption, we solve the Teukolsky equation which describes the evolution of the perturbation . Conventional approach to solve the Teukolsky equation is Green's function method. Solutions of the Teukolsky equation is obtained by the integration of Green's function multiplied by the source term. Since the source term is given by specifying the orbit of the point particle. If the orbit of the point particle are complicated, as in the case of the sources for LISA, the integration of the Green's function with source terms takes much computation time and become difficult to establish good accuracy. Thus, it is important to develop highly accurate computational method to compute the Green's function and the source terms.

[1]E-mail:draone@vega.ess.sci.osaka-u.ac.jp
[2]E-mail:tagoshi@vega.ess.sci.osaka-u.ac.jp
[3]E-mail:misao@yukawa.kyoto-u.ac.jp

In this paper, we focus only on the Green's function.

The Green's function is expressed by the homogeneous solutions of the Teukolsky equation. We adopt a formalism, developed by Mano, Suzuki and Takasugi [5, 6], to obtain the homogeneous solutions of the Teukolsky equation. In Mano, Suzuki and Takasugi formalism (MST formalism), the homogeneous solutions are expressed in series of special functions. The asymptotic amplitudes of the homogeneous solutions, which are needed for constructing the Green's function, are also given algebraically. We develop numerical code to compute the homogeneous solutions of the Teukolsky equation using MST formalism. As a test calculation, we calculate the gravitational wave flux induced by a particle in a circular orbit on the equatorial plane around a Kerr black hole.

Throughout this paper we use units with $G = c = 1$.

2 Teukolsky formalism

The radial Teukolsky equation is given by [1]

$$\Delta^2 \frac{d}{dr}\left(\frac{1}{\Delta}\frac{dR_{\ell m\omega}}{dr}\right) - V(r)R_{\ell m\omega} = T_{\ell m\omega}. \tag{1}$$

The potential $V(r)$ is given by

$$V(r) = -\frac{K^2 + 4i(r-M)K}{\Delta} + 8i\omega r + \lambda. \tag{2}$$

where M is the black hole mass, aM is the angular momentum of the black hole, $\Delta = r^2 - 2Mr + a^2$, $K = (r^2+a^2)\omega - ma$ and λ is the eigenvalue of the angular Teukolsky equation. In this paper, we consider a homogeneous solution, $R^{\rm in}_{lm\omega}$, of the homogeneous Teukolsky equation which has purely ingoing wave property at the horizon, but has both ingoing wave property and outgoing property at infinity.

$$R^{\rm in}_{lm\omega} \rightarrow \begin{cases} B^{\rm trans}_{lm\omega}\Delta^2 e^{-ikr^*} & \text{for } r \rightarrow r_+, \\ r^3 B^{\rm ref}_{lm\omega} e^{i\omega r^*} + r^{-1} B^{\rm inc}_{lm\omega} e^{-i\omega r^*} & \text{for } r \rightarrow +\infty, \end{cases} \tag{3}$$

where $k = \omega - ma/2Mr_+$ and r^* is the tortoise coordinate.

3 Mano-Suzuki-Takasugi formalism

In MST method, the solution of the homogeneous Teukolsky equation is expressed by two kinds of series of special functions [5, 6]. One is expressed by series of the hypergeometric functions, and another is expressed by series of Coulomb wave functions. The former is convergent at horizon and the latter at infinity. The solution in series of Coulomb wave functions is originally formulated by Leaver [4]. The MST formalism is an elegant reformulation of the one by Leaver.

In MST method, the solution $R^{\rm in}_{lm\omega}$ is expressed by series of hypergeometric functions

$$\begin{cases} R^{\rm in} = e^{i\epsilon\kappa x}(-x)^{-s-i(\epsilon+\tau)/2}(1-x)^{i(\epsilon-\tau)/2}p_{\rm in}(x), \\ p_{\rm in}(x) = \sum_{n=-\infty}^{\infty} a_n F(n+\nu+1-i\tau, -n-\nu-i\tau; 1-s-i\epsilon-i\tau; x). \end{cases} \tag{4}$$

where, $x = \omega(r_+ - r)/\epsilon\kappa$, $\epsilon = 2M\omega$, $\kappa = \sqrt{1-q^2}$, $q = \frac{a}{M}$, $\tau = \frac{\epsilon - mq}{\kappa}$ and $F(\alpha,\beta;\gamma;x)$ is hypergeometric function. We note that ν is a parameter, does not exist in the Teukolsky equation. This parameter is introduced to converge series and actually represent a solution of the Teukolsky equation.

The solution in series of Coulomb wave functions is also expressed in the similar form of Eq.(4). Inserting the series Eq.(4) and series of Coulomb wave functions into the homogeneous Teukolsky equation respectively, we find that the expansion coefficients a_n satisfy the three-term recurrence relations [5].

$$\alpha^\nu_n a_{n+1} + \beta^\nu_n a_n + \gamma^\nu_n a_{n-1} = 0. \tag{5}$$

where

$$\alpha_n^\nu = \frac{i\epsilon\kappa(n+\nu+1+s+i\epsilon)(n+\nu+1+s-i\epsilon)(n+\nu+1+i\tau)}{(n+\nu+1)(2n+2\nu+3)},$$

$$\beta_n^\nu = -\lambda - s(s+1) + (n+\nu)(n+\nu+1) + \epsilon^2 + \epsilon(\epsilon - mq) + \frac{\epsilon(\epsilon-mq)(s^2+\epsilon^2)}{(n+\nu)(n+\nu+1)},$$

$$\gamma_n^\nu = -\frac{i\epsilon\kappa(n+\nu-s+i\epsilon)(n+\nu-s-i\epsilon)(n+\nu-i\tau)}{(n+\nu)(2n+2\nu-1)}.$$

In MST formalism, solving the Teukolsky equation is reduced to determine a parameter ν. Dividing Eq(5) by a_n and setting $n = 0$, we obtain the following equation that determine a parameter ν,

$$f(\nu) \equiv \beta_0^\nu + \alpha_0^\nu R_1 + \gamma_0^\nu L_{-1} = 0, \tag{6}$$

where R_1 and L_{-1} are expressed by the continued fractions,

$$R_n(\nu) \equiv \frac{a_n}{a_{n-1}} = -\frac{\gamma_n^\nu}{\beta_n^\nu + \alpha_n^\nu R_{n+1}} = \cfrac{-\gamma_n^\nu}{\beta_n^\nu - \cfrac{\alpha_n^\nu\gamma_{n+1}^\nu}{\beta_{n+1}^\nu - \cfrac{\alpha_{n+1}^\nu\gamma_{n+2}^\nu}{\beta_{n+2}^\nu - \cdots}}}, \tag{7}$$

$$L_n(\nu) \equiv \frac{a_n}{a_{n+1}} = -\frac{\alpha_n^\nu}{\beta_n^\nu + \gamma_n^\nu L_{n-1}} = \cfrac{-\alpha_n^\nu}{\beta_n^\nu - \cfrac{\alpha_{n-1}^\nu\gamma_n^\nu}{\beta_{n-1}^\nu - \cfrac{\alpha_{n-2}^\nu\gamma_{n-1}^\nu}{\beta_{n-2}^\nu - \cdots}}}. \tag{8}$$

We note that when ν is a root of (6), $\nu + k$ ($k = \pm1, \pm2, \cdots$) are also roots of (6) since ν only appears as $\nu+n$ in the continued fractions of (6). In Fig.1, we show plots of $f(\nu)$ for $\ell = 2, m = 2, q = 0.1, \omega = 0.1$.

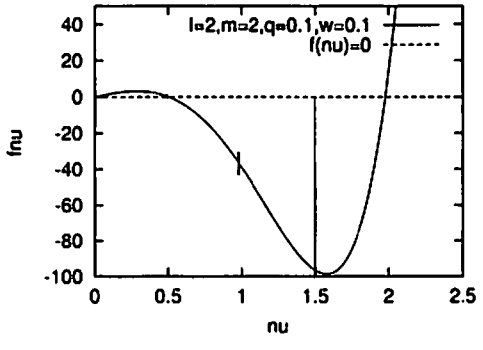

Figure 1: Plots of $f(\nu)$ for $\ell = 2, m = 2, q = 0.1, \omega = 0.1$

In order to search for a root of this implicit equation $f(\nu) = 0$, we adopt so called *Brent's algorithm* which are explained in [7] in detail. In any algorithm to search for a root of implicit equations, we need an initial guess of a root of this equation. In the case when $M\omega$ is not large, we can use an analytic expression of ν for the initial value given in series of $M\omega$ [5].

4 Energy flux

We calculate the energy flux of the gravitational waves induced by a test particle orbiting in circular and equatorial plane around a Kerr black hole in order to check the performance of our numerical code. In Table 1, we show the gravitational energy flux, where multipoles up to $\ell = 6$, for the various spin parameter a and orbital radius r. We compare our results with the past works. We find that our numerical results agree with that of [2, 3] for 4-5 digits.

r	a=-0.9	a=-0.6	a=-0.3	a=0	a=0.3	a=0.6	a=0.9
6	2.004135e-03	1.508195e-03	1.170599e-03	9.361914e-04	7.706536e-04	6.521290e-04	5.664521e-04
8	2.911242e-04	2.521389e-04	2.209621e-04	1.959297e-04	1.757686e-04	1.595008e-04	1.463718e-04
10	7.926031e-05	7.237431e-05	6.650463e-05	6.149856e-05	5.722916e-05	5.359075e-05	5.049533e-05
12	2.909290e-05	2.728628e-05	2.569303e-05	2.428878e-05	2.305233e-05	2.196525e-05	2.101153e-05
14	1.279326e-05	1.218970e-05	1.164609e-05	1.115697e-05	1.071745e-05	1.032317e-05	9.970235e-06
16	6.361251e-06	6.123441e-06	5.906160e-06	5.707866e-06	5.527154e-06	5.362747e-06	5.213484e-06
18	3.459836e-06	3.354129e-06	3.256539e-06	3.166550e-06	3.083689e-06	3.007517e-06	2.937630e-06
20	2.015492e-06	1.963962e-06	1.916013e-06	1.871449e-06	1.830088e-06	1.791761e-06	1.756309e-06
40	6.094897e-08	6.044684e-08	5.996449e-08	5.950151e-08	5.905753e-08	5.863216e-08	5.822505e-08
60	8.027815e-09	7.992990e-09	7.959204e-09	7.926444e-09	7.894699e-09	7.863957e-09	7.834209e-09
80	1.910004e-09	1.904717e-09	1.899561e-09	1.894536e-09	1.889640e-09	1.884873e-09	1.880233e-09
100	6.274268e-10	6.261980e-10	6.249959e-10	6.238203e-10	6.226712e-10	6.215484e-10	6.204517e-10
120	2.526754e-10	2.523019e-10	2.519357e-10	2.515768e-10	2.512251e-10	2.508806e-10	2.505433e-10
140	1.171053e-10	1.169688e-10	1.168347e-10	1.167030e-10	1.165737e-10	1.164469e-10	1.163225e-10
160	6.015022e-11	6.009307e-11	6.003687e-11	5.998162e-11	5.992731e-11	5.987395e-11	5.982152e-11
180	3.341910e-11	3.339259e-11	3.336649e-11	3.334081e-11	3.331553e-11	3.329067e-11	3.326621e-11
200	1.975372e-11	1.974038e-11	1.972723e-11	1.971429e-11	1.970153e-11	1.968898e-11	1.967662e-11
400	6.205909e-13	6.204450e-13	6.203006e-13	6.201576e-13	6.200162e-13	6.198763e-13	6.197378e-13
600	8.189537e-14	8.188495e-14	8.187462e-14	8.186438e-14	8.185423e-14	8.184416e-14	8.183417e-14
800	1.945607e-14	1.945447e-14	1.945288e-14	1.945130e-14	1.944974e-14	1.944818e-14	1.944664e-14
1000	6.379870e-15	6.379495e-15	6.379123e-15	6.378753e-15	6.378385e-15	6.378020e-15	6.377657e-15

Table 1: The gravitational energy flux, up through $\ell = 6$, for various spin parameters and orbital radius

5 Concluding remarks

The convergence of the series of the hypergeometric functions is usually very rapid. Thus, the MST formalism is a powerful method to compute the homogeneous solution numerically. Our preliminary estimate of the accuracy of our code is at least 10 digits by the double precision computation. Currently, this accuracy is limited by the accuracy of ν and the accuracy of the routine of the hypergeometric functions. We will improve these points and apply this method to compute the gravitational waves from a compact star in generic orbits around a supermassive black hole in the future.

We thank D. Kennefick to kindly provide us his numerical data based on his work [2]. This work is supported in part by Monbukagaku-sho Grant-in-Aid for Scientific Research No. 14047214 and 12640269.

References

[1] Teukolsky, S.A., Astrophys. J. **185**, 635 (1973).

[2] Glampedakis, K. and Kennefick, D., Phys. Rev. D **66**, 044002 (2002).

[3] M.Shibata, Phys. Rev. D **48**, 663 (1993).

[4] Leaver, E.W., J. Math. Phys. **27**, 1238 (1986).

[5] Mano, S., Suzuki, H., and Takasugi, E., Prog. Theor. Phys. **95**, 1079 (1996).

[6] Mano, S., and Takasugi, E., Prog. Theor. Phys. **97**, 213 (1996).

[7] Press, W.H.,and Teukolsky, S.A., Vetterling, W.T. and Flannery, B.P., *Numerical Recipes* (Cambridge University Press, Cambridge, England, 1992)

Accelerating Expansion of the Present Universe in a Generalized Scalar-Tensor Cosmology

Takao Fukui[1]

Department of Language and Culture,
Dokkyo University, 1-1 Gakuencho, Soka, Saitama 340-0042, Japan

Abstract

Two types of the expansion of the Universe are obtained in a generalized scalar-tensor (GST) cosmology. The GST cosmology is applied to the supernovae magnitude-redshift relation. It fits the observational data quite well.

1 Introduction

In the present GST cosmology obtained by modifying the original GST theory [1], the cosmological term depends on not only the scalar field ϕ but also its gradient $\phi_{,\kappa}\phi^{,\kappa}$ [2]. The model enables us to draw reasonable results to the cosmological "constant" and flatness problems. We can write a scenario to expect a late-time inflation by applying one of the solutions for the scale factor, to the present era too.

Then in the present work, we compare the scenario in the GST model with the observational data of the Type Ia supernovae.

2 Variational Principle

The field equation is obtained by the following variational principle,

$$0=\delta\int\left\{\phi[R+2\Lambda(\phi,\phi_{,\kappa}\phi^{,\kappa})]+\frac{16\pi}{c^4}L_M-\omega(\phi)\frac{\phi_{,\kappa}\phi^{,\kappa}}{\phi}\right\}\sqrt{-g}d\Omega. \tag{1}$$

The field equation for the metric tensor field $g_{\mu\nu}$ is

$$R_{\mu\nu}-\frac{1}{2}g_{\mu\nu}R=\frac{8\pi}{\phi c^4}(T_{\mu\nu}+T^{\phi}_{\mu\nu}). \tag{2}$$

$T^{\phi}_{\mu\nu}$ is the energy-momentum tensor of the scalar field and is defined as

$$\frac{8\pi}{\phi c^4}T^{\phi}_{\mu\nu}\equiv\frac{\omega}{\phi^2}\left(\phi_{,\mu}\phi_{,\nu}-\frac{1}{2}g_{\mu\nu}b\right)+\frac{1}{\phi}(\phi_{,\mu;\nu}-g_{\mu\nu}\phi^{,\kappa}{}_{;\kappa})+g_{\mu\nu}\Lambda-2\frac{\partial\Lambda}{\partial b}\phi_{,\mu}\phi_{,\nu}, \tag{3}$$

where $b\equiv\phi_{,\kappa}\phi^{,\kappa}$. The field equation for ϕ is

$$R+2\Lambda+2\phi\frac{\partial\Lambda}{\partial\phi}-4\frac{\partial}{\partial x^{\kappa}}\left(\phi\frac{\partial\Lambda}{\partial b}\right)\phi^{,\kappa}-4\phi\frac{\partial\Lambda}{\partial b}\phi^{,\kappa}{}_{;\kappa}=\frac{\omega}{\phi^2}b-\frac{2\omega}{\phi}\phi^{,\kappa}{}_{;\kappa}-\frac{b}{\phi}\frac{d\omega}{d\phi}. \tag{4}$$

Eq.(4) ensures that the conservation law $T^{\kappa}_{\mu;\kappa}=0$ holds.

3 Robertson-Walker Metric

The time-time component of the metric tensor field equation is

$$\left(\frac{\dot{a}}{a}\right)^2+\frac{kc^2}{a^2}-\frac{\Lambda c^2}{3}+\frac{2}{3}\frac{\partial\Lambda c^2}{\partial\dot{\phi}^2}\dot{\phi}^2=\frac{8\pi}{3\phi c^2}\epsilon+\frac{\omega}{6}\left(\frac{\dot{\phi}}{\phi}\right)^2-\frac{\dot{a}}{a}\frac{\dot{\phi}}{\phi}, \tag{5}$$

[1]E-mail:tfukui@dokkyo.ac.jp

while the space-space components yield

$$2\frac{\ddot{a}}{a}+\left(\frac{\dot{a}}{a}\right)^2+\frac{kc^2}{a^2}-\Lambda c^2=-\frac{8\pi}{\phi c^2}p-\frac{\omega}{2}\left(\frac{\dot{\phi}}{\phi}\right)^2-\frac{\ddot{\phi}}{\phi}-2\frac{\dot{a}}{a}\frac{\dot{\phi}}{\phi}, \tag{6}$$

where $p=(\gamma-1)\epsilon$, and $\epsilon=\epsilon_\gamma a^{-3\gamma}$ which is derived from $T^{\kappa}_{\mu;\kappa}=0$.

The scalar field equation yields the following wave equation for ϕ,

$$\begin{aligned}\frac{\ddot{a}}{a} &+ \left(\frac{\dot{a}}{a}\right)^2+\frac{kc^2}{a^2}-\frac{\Lambda c^2}{3}-\frac{\phi}{3}\frac{\partial\Lambda c^2}{\partial\phi}+\frac{2}{3}\frac{\partial}{\partial t}\left(\phi\frac{\partial\Lambda c^2}{\partial\dot{\phi}^2}\right)\cdot\dot{\phi}+\frac{2}{3}\phi\frac{\partial\Lambda c^2}{\partial\dot{\phi}^2}\left(\ddot{\phi}+3\frac{\dot{a}}{a}\dot{\phi}\right)\\ &= \omega\frac{\dot{a}}{a}\frac{\dot{\phi}}{\phi}+\frac{\omega}{3}\frac{\ddot{\phi}}{\phi}+\frac{1}{6}\frac{d\omega}{d\phi}\frac{\dot{\phi}^2}{\phi}-\frac{\omega}{6}\left(\frac{\dot{\phi}}{\phi}\right)^2.\end{aligned} \tag{7}$$

Eqs.(5)-(7) are the basic equations to be solved for the scale factor $a(t)$, the scalar field $\phi(t)$ and the cosmological term $\Lambda(\phi,\dot{\phi})$. Here we assume that $a(t)$ proper to $g_{\mu\nu}$, and $\phi(t)$ should be separable in Eq.(7). The assumption leads to the following relation,

$$\frac{\partial\Lambda c^2}{\partial\dot{\phi}^2}=\frac{\omega}{2\phi^2}. \tag{8}$$

Then Eq.(7) reduces to the separable form,

$$\frac{\ddot{a}}{a}+\left(\frac{\dot{a}}{a}\right)^2+\frac{kc^2}{a^2}=\frac{1}{3}\left[\Lambda c^2+\phi\frac{\partial\Lambda c^2}{\partial\phi}-\frac{1}{2}\frac{d\omega}{d\phi}\frac{\dot{\phi}^2}{\phi}+\frac{\omega}{2}\left(\frac{\dot{\phi}}{\phi}\right)^2\right]=const.(\equiv K). \tag{9}$$

Eq.(9) can be solved for a as follows,

$$K = 0; \quad a=\sqrt{-kc^2t^2+\alpha t+\beta}, \tag{10}$$

$$K \neq 0; \quad a=\sqrt{C_1e^{\sqrt{2K}t}+C_2e^{-\sqrt{2K}t}+\frac{kc^2}{K}}, \tag{11}$$

where α, β, C_1 and C_2 are integration constants.

The cosmological term is obtained from Eq.(8),

$$\Lambda c^2=\frac{\omega}{2}\left(\frac{\dot{\phi}}{\phi}\right)^2+\frac{f_\Lambda}{\phi}+3K, \tag{12}$$

where f_Λ is a constant. Eqs.(5) and (6) give an identical equation for ϕ on the assumption, Eq.(8), and can be solved in each γ [2]. In the case of $k=0$, for example, the scalar field is solved as,

$$K = 0,\ \gamma=1; \quad \phi=\frac{16\pi\epsilon_1 t}{3\alpha c^2 a}+\frac{4f_\Lambda}{15\alpha^2}a^4+\frac{\phi_{k0}}{a}, \tag{13}$$

$$K \neq 0; \quad \phi=-\frac{16\pi\epsilon_\gamma}{3Kc^2(3\gamma+1)}a^{-3\gamma}-\frac{2f_\Lambda}{3K}+\psi_{k0}a. \tag{14}$$

4 Accelerating Universe

The observation of Type Ia supernovae suggests an accelerating expansion of the present Universe [3]. By attributing the acceleration to the vacuum energy of the cosmological constant, we take a scenario that we are now in the late-time inflation era ($\gamma=0$) of a flat ($k=0$) expanding ($C_2=0$) Universe again. Hereafter $\psi_{k0}=0$ is taken in Eq.(14) because ϕ should be separable from a. Therefore a and ϕ in the present late-time inflation era are given as follows,

$$a = \sqrt{C_1e^{\sqrt{2K_p}t}}, \tag{15}$$

$$\phi = -\frac{16\pi\epsilon_{0p}}{3K_pc^2}-\frac{2f_\Lambda}{3K_p}=const., \tag{16}$$

where K_p is that of the present K and is different from that of the early-time inflation era. From Eq.(12), the cosmological term in the present era turns out to be constant.

5 Magnitude-Redshift Relation

The magnitude-redshift relation in a flat Universe is given as follows,

$$m = M + 5log_{10}(1+z)a_R(r_R - r_E) + K(z) + const., \tag{17}$$

where $K(z)$ is an effect of a shift of the spectrum in frequency on a magnitude.

(I) Small Reshift Source: Light signals are both emitted at t_E and received at t_R in the present late-time inflation era (Eq.(15) for a). The radial comoving distance $r_R - r_E$ is obtained as follows,

$$r_R - r_E = \int_{t_E}^{t_R} \frac{c}{a} dt = \frac{cz}{H_R a_R}, \tag{18}$$

where the Hubble parameter at t_R is $H_R = \sqrt{2K_p}/2$, and $a_R/a_E = 1 + z$.

(II) Large Redshift Source: Light signals are received in the present late-time inflation era (Eq.(15) for a) but emitted in the matter era (Eq.(10) with $k = 0$ for a).

$$\begin{aligned} r_R - r_E &= \int_{t_E}^{t_i} \frac{c}{\sqrt{\alpha t + \beta}} dt + \int_{t_i}^{t_R} \frac{c}{\sqrt{C_1 e^{\sqrt{2K_p}t}}} dt \\ &= \frac{c}{H_R a_R} \left\{ 2\frac{a_R}{a_i} - \left(\frac{a_R}{a_i}\right)^2 \frac{1}{1+z} - 1 \right\}, \end{aligned} \tag{19}$$

where a_i is the scale factor at the interface between the matter era and the late-time inflation era. Since $\epsilon_M \propto a^{-3}$ and $\epsilon_\Lambda = const.$ from the conservation law, the ratio a_R/a_i is given as

$$\frac{a_R}{a_i} = \left(\frac{\Omega_\Lambda}{\Omega_M}\right)^{1/3}. \tag{20}$$

We take the values of $\Omega_\Lambda = 0.75$ and $\Omega_M = 0.25$ for evaluation of Eq.(17). Since Eq.(17) itself, however, contains complicated factors, especially in $K(z)$ which is the same in all models, here we plot residuals, i.e. the differences $\Delta m(z)$ between our $m(z)$ and the form of the current "standard" ΛCDM cosmology [4].

$$\Delta m(z) \equiv m(z) - m_{\Lambda CDM}. \tag{21}$$

We show below only the plots of $\Delta m(z)$ in the cases of GST cosmology with $\gamma = 0$ and of the other standard cosmologies, together with the observational data [4].

6 Comments

The figure shows that the scenario in the GST cosmology fits the observational data quite well. But we have not studied yet whether or not it fits better than the fiducial ΛCDM model.

In the present work, we explore only the case of $k = 0$, $C_2 = 0$ and $\gamma = 0$. In order to make the plot be complete, the other cases, $k \neq 0$ and/or $C_2 \neq 0$ should be explored further.

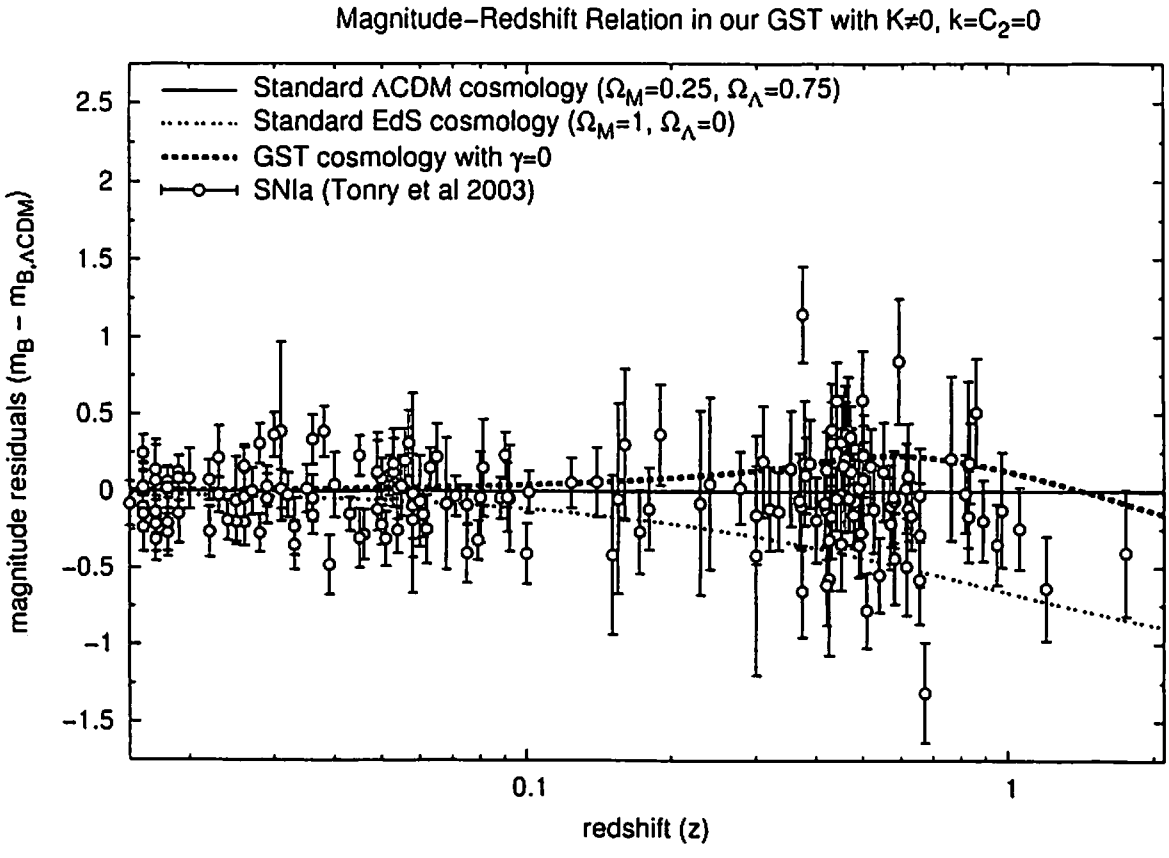

Acknowledgment

The author is grateful to James M. Overduin for his work of producing the plot, $\Delta m(z) - z$ relation.

References

[1] P. G. Bergmann, Int. J. Theor. Phys. 1, 25 (1968); R. V. Wagoner, Phys. Rev. D1, 3209 (1970).

[2] T. Fukui, K. Arai and M. Hashimoto, Class. Quantum Grav. 18, 2087 (2001); T. Fukui and J. M. Overduin, Int. J. Theor. Phys. 11, 669 (2002).

[3] S. Perlmutter et al., Astrophys. J. 517, 565 (1999).

[4] J. L. Tonry et al., Astrophys. J. 594, 1 (2003).

Instability of massive scalar fields in Kerr-Newman space times

Hironobu Furuhashi[1], Yasusada Nambu[2]

Department of Physics, Graduate School of Science,
Nagoya University, chikusa, Nagoya 464-8602, Japan

Abstract

We investigate the instability of charged massive scalar fields in Kerr-Newman spacetime. Due to the super-radiant effect of the background geometry, the bound state of the scalar field suffers from instability and its amplitude grows in time. By solving the Klein-Gordon equation of the scalar field as an eigen-value problem, we numerically obtain the growing rate of the instability of the scalar field. Although the dependence of the scalar field mass and the scalar field charge on the growing rate fairly agrees with the result of the analytic approximation, the maximum value of the growing rate is three times larger than that of the analytic approximation. We also discuss the effect of the electric charge on the instability of the scalar field.

1 Introduction

The propagation of waves in black hole spacetime have been studied by many researchers in the context of black hole perturbations [1]. The super-radiance is one of the interesting phenomena in this subject [2]. As an application of the super-radiance, Press and Teukolsky proposed the black hole bomb[3]; they considered the situation that mirrors surround a Kerr black hole. The scattered wave with the super-radiant amplification is reflected back to the black hole by mirrors and the wave is amplified again. Then the amplitude of the wave grows exponentially in time and becomes unstable. Damour *et al.*[4] have shown that the black hole bomb can be realized by using a charged massive scalar field in Kerr-Newman spacetime. The effective potential of the massive scalar field has a local minimum and the scalar field wave can be confined in this potential well. Hence the mass of the scalar field plays a role of the mirrors which is necessary to cause the instability of the scalar field. According to their analysis, the instability of the scalar field occurs if the bound state and the super-radiant condition are both satisfied.

To evaluate the growing rate of the instability, we must solve the Klein-Gordon equation in the black hole geometry. By imposing the ingoing condition at the black hole horizon and the regular condition at infinity, the problem of obtaining the unstable mode reduces to an eigen-value problem. For Kerr spacetime, the growing rate of the unstable modes for the scalar field with the small mass $\mu \ll 1/M$ (M is the mass of a black hole) was obtained by using the asymptotic matching method [5], and that for the large mass $\mu \gg 1/M$ was obtained by using the WKB approximation [6]. However, these analysis do not cover the parameter region $\mu M \sim 1$ where the growing rate is expected to have a maximum value.

In this paper, we aim to obtain the growing rate of the charged massive scalar field with the mass $\mu M \lesssim 1$ in Kerr-Newman spacetime by solving the eigen-value problem numerically. The paper is organized as follows. In Sec. 2, we estimate the growing rate of the scalar field with $\mu M \ll 1$ and $qQ \ll 1$ in Kerr-Newman spacetime using the method of Detweiler[5]. Then in Sec. 3, we introduce our numerical method and obtain the growing rate of the instability and its parameter dependence for $\mu M \lesssim 1$. Sec. 4 is devoted to summary and conclusion.

We use the unit in which $G = c = \hbar = 1$ throughout the paper.

2 Analytic Approach

In this section, we calculate the growing rate of the instability of the scalar field using the asymptotic matching method used by Detweiler [5] in Kerr-Newman spacetime.

[1]E-mail:hironobu@allegro.phys.nagoya-u.ac.jp
[2]E-mail:nambu@allegro.phys.nagoya-u.ac.jp

The Kerr-Newman metric in the Boyer-Lindquist coordinate is

$$ds^2 = -\left(1 - \frac{2Mr-Q^2}{\Sigma}\right)dt^2 - \frac{(2Mr-Q^2)2a\sin^2\theta}{\Sigma}dtd\phi + \frac{\Sigma}{\Delta}dr^2 + \Sigma d\theta^2 + \frac{A\sin^2\theta}{\Sigma}d\phi^2, \tag{1}$$

$$\Delta = r^2 - 2Mr + a^2 + Q^2, \quad \Sigma = r^2 + a^2\cos^2\theta, \quad A = \left(r^2+a^2\right)^2 - a^2\Delta\sin^2\theta,$$

where M is the mass, a is the angular momentum and Q is the electric charge of the black hole, respectively. The location of horizons $r_\pm$ are given by roots of $\Delta = 0$. The Klein-Gordon equation for the charged scalar field with mass μ is

$$(\nabla^\alpha - iqA^\alpha)(\nabla_\alpha - iqA_\alpha)\Psi = \mu^2\Psi, \qquad A_\alpha = \left(-\frac{rQ}{\Sigma}, 0, 0, \frac{aQr}{\Sigma}\sin^2\theta\right), \tag{2}$$

where ∇^α is the covariant derivative in the Kerr-Newman geometry and q is the charge of the scalar field. Equation (2) is separable using the spheroidal harmonics $S(\theta)$:

$$\Psi = \psi(r)S(\theta)\exp(i(-\omega t + m\phi)). \tag{3}$$

The radial function $\psi(r)$ satisfies

$$\Delta\frac{d}{dr}\Delta\frac{d\psi}{dr} + \left[-\Delta(\mu^2r^2 + \lambda) + \left\{(r^2+a^2)\omega - ma - qQr\right\}^2\right]\psi = 0, \tag{4}$$

$$\lambda = l(l+1) - 2ma\omega + (a\omega)^2 + O(a^2(\mu^2-\omega^2)) \overset{\omega\sim\mu}{\longrightarrow} \lambda = l(l+1) - 2ma\omega + (a\omega)^2,$$

where l, m are integers and $|m| \leq l$. We assume $l \geq 1$; for $l = 0$, there is no centrifugal force and the bound state of the scalar field does not exit. As we are interested in the eigen-mode of which frequency is nearly equal to the mass of the scalar field $\omega \sim \mu$, it is possible to set $O(a^2(\mu^2 - \omega^2)) = 0$. We solve Eq. (4) with the boundary condition of an outgoing wave at infinity and an ingoing wave at the black hole horizon. To apply the asymptotic matching method, we need to assume that parameters satisfies the condition $O(\omega M) = O(\mu M) = O(qQ) \equiv O(\epsilon)$, $\epsilon \ll 1$, and they can be treated as small parameters. The angular momentum of the black hole is assumed to be $O(a/M) = 1$. As we are interested in the unstable mode, the scalar field must be in the bound state and the following bound state condition is required:

$$M\mu \gtrsim qQ. \tag{5}$$

For large value of $r \gg M$, the solution of Eq. (4) which becomes regular at infinity is proportional to the confluent hypergeometric functions . For the region near the black hole horizon $r \sim r_+$, the solution of Eq. (4) is given by the function which is proportional to the Gauss hypergeometric function. Then, matching two solutions at the matchable region, we obtain the eigen-value ω : $(\omega \equiv \sigma + i\gamma)$.

If the imaginary part γ of ω is positive, the considering mode is unstable and γ represents the growing rate of the instability. The condition of instability is

$$P = \frac{1}{2\kappa}(m\Omega^H + q\Phi^H - \omega) > 0, \tag{6}$$

where the surface gravity κ, the angular velocity Ω^H, and the electric potential Φ^H for the Kerr-Newman black hole are introduced as follows:

$$\kappa = \frac{1}{2}\left(\frac{r_+ - r_-}{a^2 + r_+^2}\right), \quad \Omega^H = \frac{a}{a^2+r_+^2}, \quad \Phi^H = \frac{Qr_+}{a^2+r_+^2}. \tag{7}$$

This condition of instability (6) coincides with that of the super-radiance. If the super-radiant condition is compatible with the condition of bound state (5), the scalar field becomes unstable. These features of the unstable mode are consistent with the analysis by Damour *et al* [4]. The most unstable mode corresponds to $l = m = 1$, $n = 0$ and the value γ of this mode is given by

$$\gamma = \frac{\mu^4}{24}|M\mu - qQ|^5(a^2+r_+^2)^3(\Omega^H + q\Phi^H - \mu)(\kappa^2 + (\Omega^H + q\Phi^H - \mu)^2). \tag{8}$$

We show the mass and the charge dependence of γ in Fig. 1. The maximum value is $\gamma \approx 3 \times 10^{-8}$ at $\mu M \approx 0.3$, $qQ \approx -0.08$. The positive values of γ appear in the region where both the super-radiant condition $P > 0$ and the bound state condition $Mq \gtrsim qQ$ are satisfied. Let us consider the region $\mu M \ll 1, |qQ| \ll 1$ where our approximation is expected to be good. In this region, by keeping on the leading terms of the small parameters, (μ, q) dependence of γ is determined by the factor $\mu^4|M\mu - qQ|^5$.

For a fixed value of q, γ is an increasing function of μ. For a fixed value of μ, γ is an decreasing function of qQ. The formula shows that the main effect of the scalar field charge q is to change the depth of the potential well which is necessary to bound the scalar field. As the charge q increases, the depth of the well of the scalar field effective potential decreases and the scalar field becomes less bounded. Thus the increase of the charge reduces the growing rate of the scalar field.

For the positive charge $q > 0$, P can be positive for the negative azimuthal quantum number $m < 0$. This is contrasted with the Kerr black hole case, which requires $m > 0$ to be $P > 0$. This indicates the possibility of the unstable mode with $m < 0$. However for $m < 0$, the condition $P > 0$ can not be compatible with the bound state condition (5). Thus for $q > 0$ and $m \leq 0$ in Kerr-Newman spacetime, the super-radiance occurs but the scalar field can not be in the bound state and the mode becomes stable. For Reissner-Nordström spacetime $a = 0$, $P > 0$ gives $\mu < \frac{qQ}{r_+}$. This condition also can not be compatible with the bound state condition (5) and we conclude that there is no unstable mode of the scalar field in Reissner-Nordström spacetime. From these results, the super-radiance caused by the rotation of the black hole is essential to make the scalar field unstable.

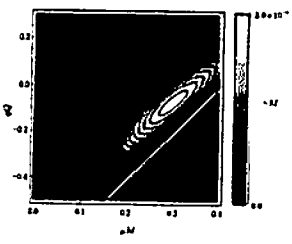

Figure 1: The dependence of the mass μ and the charge q of the scalar field on the growing rate γ. The parameters are $a = 0.98M$, $Q = 0.01M$, $l = m = 1$, $n = 0$. The solid line corresponds to $P = 0$ and the dotted line corresponds to $M\mu - qQ = 0$.

3 Numerical Approach

Method To investigate the instability of the scalar field for the wide range of parameters, we perform numerical calculation. We rewrite Eq. (4) using the tortoise coordinate

$$x = \int dr \frac{r^2}{\Delta} = r + \frac{1}{r_+ - r_-}\left[r_+^2 \ln(r - r_+) - r_-^2 \ln(r - r_-)\right], \tag{9}$$

and a new radial function $u = r\psi$:

$$\frac{d^2u}{dx^2} = V_{\rm eff}(r)u, \qquad V_{\rm eff}(r) = \frac{\Delta}{r^2}\left[\mu^2 + \frac{\lambda}{r^2} + \frac{2M}{r^3} - \frac{2(a^2+Q^2)}{r^4}\right] - \frac{1}{r^4}\left[(r^2+a^2)\omega - am - qQr\right]^2. \tag{10}$$

The shape of the effective potential $V_{\rm eff}$ for $a = 0.98M$, $Q = 0.01M$, $\mu M = 0.35$, $qQ = -0.08$, $l = m = 1$ is shown in Fig. 2. Due to the mass of the scalar field, the effective potential has a well and the wave can be trapped in this well.

We use the solutions that the incoming solution of Eq. (10) in the region near the horizon and the regular solution of Eq. (10) in the far region to impose the boundary condition for numerical integration of Eq. (10). We prepare the inner numerical boundary $x = x_1$ near the horizon r_+ and the outer numerical boundary $x = x_2$. By integrating Eq. (10) from $x = x_1$ with the boundary condition, we obtain a mode function $u^{(1)}$. In the same way, we obtain $u^{(2)}$ with the boundary condition imposed at the far region $x = x_2$. For a given complex value of ω, if the Wronskian : $W(u^{(1)}, u^{(2)}) = u^{(1)}\frac{du^{(2)}}{dx} - u^{(2)}\frac{du^{(1)}}{dx}$ evaluated at the mid point $x = x_m (x_1 < x_m < x_2)$ becomes zero, two solutions $u^{(1)}$ and $u^{(2)}$ are linearly dependent and ω gives an eigen-value of the considering equation. We search the zero point of the complex function $W(\omega)$ numerically in complex ω plane.

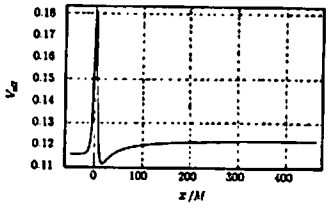

Figure 2: The effective potential $V_{\rm eff}(x)$ of the scalar field .

Result We have performed the numerical calculation to search the mode of the scalar field with $l = m = 1$ and $\omega \sim \mu$, for which the growing rate of the unstable mode is expected to have the largest value. We choose the parameters of the black hole as $a = 0.98M$, $Q = 0.01M$ and used the 4th order Runge-Kutta integrator. We obtained the value of the growing rate γ as the function of the scalar field mass μ and the scalar field charge q. The calculated parameter points in (μ, q)-space are shown in Fig.3.

The obtained growing rate is shown is Fig. 4. The shape of the numerically obtained function $\gamma(\mu, q)$ is almost same as that of the analytically obtained one (see Fig. 1). The left panel in Fig. 5 shows μ

dependence of γ for different values of q. The plus points represent the maximum values of γ for each μ and the cross points represent γ for $q = 0$. The solid line is values of γ for $q = 0$ predicted by the analytic approximation. The right panel in Fig. 5 shows q dependence of γ. The solid line is γ by the analytic approximation for $\mu M = 0.2$ and the approximation is good for $-0.2 \lesssim qQ$.

The growing rate has the maximum value $\gamma M \simeq 1.13 \times 10^{-7}$ at $\mu M \simeq 0.35, qQ \simeq -0.08$. The obtained minimum value of the growing rate is 7.6×10^{-11} at $\mu M = 0.20, qQ = 0.1$. Although the shape of the function $\gamma(\mu, q)$ fairly agrees with the analytically obtained result Fig. 1, its maximum value is three times larger. We can confirm that the instability occurs in the region in (μ, q)-space where both the super-radiant condition $P > 0$ and the bound state condition $M\mu \gtrsim qQ$ are satisfied. This parameter region is also shown in Fig. 3. For all numerically obtained modes, the growing rates are positive and they are contained in the region bounded by two lines $P = 0$ and $M\mu - qQ = 0$. As the parameter point (μ, q) approaches these lines, the growing rate decreases. Hence the function $\gamma(\mu, q)$ has the maximum value in this region. We could not obtain the stable mode with negative γ because the value γ for the stable mode is small compared to that of the unstable mode, it was not possible to get the definite value within the accuracy of our numerical calculation.

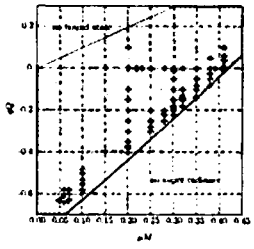

Figure 3: The calculated parameters in (μ, q)-space is shown as plus points. The solid line is $P = 0$ and the dotted line is $M\mu - qQ = 0$. The scalar field is expected to become unstable for the parameters in the grey region.

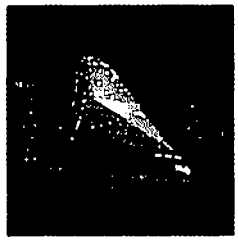

Figure 4: The numerically obtained value of the growing rate γ. Spheres represent obtained values of γ. This is the bird-eyes view of $\gamma(\mu, q)$.

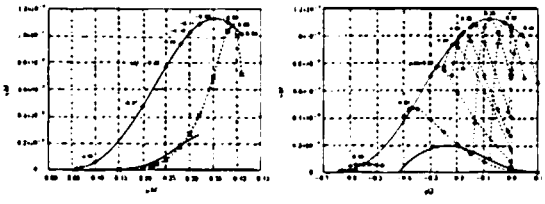

Figure 5: The left panel is μ dependence of the growing rate γ for different values of q. The dashed line is the numerical solution for $q = 0$ and the solid line is the analytic approximation (8) for $q = 0$. The right panel is q dependence of the growing rate γ for different values of μ. The dashed lines are γ for $\mu = 0.1 \sim 0.41$. The solid line is the analytic approximation for $\mu M = 0.20$.

4 Summary and Discussion

In this paper, we study the unstable modes of the massive scalar field in Kerr-Newman spacetime. We obtain the growing rate for $\mu M \ll 1$, $qQ \ll 1$ by using the asymptotic matching method and for $\mu M \lesssim 1$ by numerical method. For the black hole with $a = 0.98M, Q = 0.01M$, we obtained the maximum value of the growing rate of the unstable mode $\gamma M \simeq 1.13 \times 10^{-7}$ at $\mu M \simeq 0.35, qQ \simeq -0.08$. The location of the maximum value in (μ, q)-space fairly agrees with the result of the analytic method, but its numerical value is three times larger than that of the analytic result.

Acknowledgements We would like to thank Tomoyuki Hanawa for his suggestion on the numerical method of the eigen-value problem and Akira Tomimatsu for valuable discussions on this subject.

References

[1] K. D. Kokkotas, Living Rev. Rel. **2**, 2 (1999).

[2] V. P. Frolov and I. D. Novikov, *Black Hole Physics* (Kluwer Academic Publishers, 1998).

[3] W. H. Press and S. A. Teukolsky, Nature **238**, 211 (1072).

[4] T. Damour, N. Deruelle, and R. Ruffini, Lett. Nuovo cimento **15**, 257 (1976).

[5] S. Detweiler, Phys. Rev. D **22**, 2323 (1980).

[6] T. J. M. Zouros and D. M. Eardley, Ann. Phys. **118**, 139 (1979).

A New Analytical Method for Self-force Regularization

Wataru Hikida[a1], Sanjay Jhingan[b2], Hiroyuki Nakano[c3], Norichika Sago[d,e4], Misao Sasaki[a5], Takahiro Tanaka[e6]

[a] *Yukawa Institute for Theoretical Physics, Kyoto University, Kyoto 606-8502, Japan*
[b] *Departamento de Física Teórica, Universidad del País Vasco, Apdo. 644, 48080, Bilbao, Spain*
[c] *Department of Mathematics and Physics, Graduate School of Science, Osaka City University, Osaka 558-8585, Japan*
[d] *Department of Physics, Graduate School of Science, Kyoto University, Kyoto 606-8502, Japan*
[e] *Department of Earth and Space Science, Graduate School of Science, Osaka University, Toyonaka 560-0043, Japan*

Abstract

We formulate a new analytical method for regularizing the self-force acting on a particle of small mass μ orbiting a black hole of mass M, where $\mu \ll M$. There are a lot of regularization methods for the gravitational self-force problem, but this proposed method is more analytic for the time-domain calculation. Here we present our new regularization method and the result of the regularized self-force in the simple case of a plunge orbit by using new formulation.

1 Introduction

Due to the recent technological advance, we are now at the dawn of gravitational wave astronomy/astrophysics. The observation of gravitational waves is absolutely a new window to observe our universe. We also expect that the observation of gravitational waves provides a direct experimental test of general relativity. The interferometric gravitational wave detectors, LIGO, TAMA300 and GEO600 are currently in the early stage of their operations. Furthermore, R&D studies of a space-based interferometer project, the Laser Interferometer Space Antenna (LISA), are in rapid progress. These interferometers, after their final sensitivity goals are achieved, are expected to detect gravitational waves from compact star binaries or compact stars orbiting super-massive black holes at galactic centers.

To fully utilize the information contained in the observed gravitational wave data, particularly for the purpose of a precision test of general relativity, we have to know accurate theoretical predictions of the waveforms. When the mass ratio of the objects composing a binaries is extremely large, the black hole perturbation approach is very effective. Here we consider the corrections to the force acting on the small mass body (which is treated as a point-particle) that are induced by the field generated by the particle itself, the so-called self-force corrections. The self-force, however, diverges at the location of the particle, and hence should be regularized. It is known that the properly regularized self-force is given by the tail part (or the R -part) of the self-field, obtained by subtracting the direct part (or the S-part) from the full self-field[1, 2, 3]. The most successful method of regularization relies on the spherical harmonic decomposition of the self-force, the so-called mode-sum regularization or mode decomposition regularization[4].

So far the regularized self-force has been calculated only for special orbits. This is primarily due to mismatch in the domain used for evaluating the full self-field and the S-part. The full field is calculated with either the Regge-Wheeler-Zerilli or Teukolsky formalism, which heavily relies on the Fourier decomposition of time-dependence, so the full field is calculated in the frequency domain. On the other hand, the S-part can be given only in the time domain. So we have to integrate the full field over ω.

[1] E-mail:hikida@yukawa.kyoto-u.ac.jp
[2] E-mail:wtpsaxxj@lg.ehu.es
[3] E-mail:denden@sci.osaka-cu.ac.jp
[4] E-mail:sago@scphys.kyoto-u.ac.jp
[5] E-mail:misao@yukawa.kyoto-u.ac.jp
[6] E-mail:tama@scphys.kyoto-u.ac.jp

In this time, we formulate a new analytical method for regularizing the self-force acting on a particle of small mass μ orbiting a black hole of mass M, where $\mu \ll M$, and utilizing a new decomposition (the $\tilde{S}$ and $\tilde{R}$-part) of the retarded Green function in the frequency domain, we have shown a systematic method for the computation of the self-force[5, 6]. This decomposition is found from the construction of the homogeneous solutions by the Mano-Suzuki-Takasugi's analytical method [7]. Here, for simplicity, we focus on the case of a scalar charge in order to avoid the gauge problem [8, 9].

2 Regularization

We consider a point scalar charged particle (charge: q) moving in the Schwarzschild background. The full scalar field induced by this charged particle is given, using the retarded Green function, as

$$\psi^{\rm full}(x) = q\int d\tau\, G^{\rm full}(x, z(\tau)), \tag{1}$$

where $z(\tau)$ is the trajectory of the particle, τ is the proper time along this trajectory, and $G^{\rm full}(x,x')$ satisfies the Klein-Gordon equation

$$\nabla^\alpha\nabla_\alpha G^{\rm full}(x,x') = -\frac{\delta^{(4)}(x-x')}{\sqrt{-g}}, \tag{2}$$

with the retarded boundary condition. The retarded Green function is represented in terms of the Fourier-harmonic decomposition as

$$G^{\rm ret}(x,x') = \int\frac{d\omega}{2\pi}e^{-i\omega(t-t')}\sum_{\ell m} g^{\rm full}_{\ell m\omega}(r,r')Y_{\ell m}(\theta,\phi)Y^*_{\ell m}(\theta',\phi'). \tag{3}$$

Here $Y_{\ell m}(\theta,\phi)$ are the ordinary spherical harmonics and $(^*)$ indicates complex conjugation. Then, Eq. (2) reduces to an ordinary differential equation for the radial Green function as

$$\left[\left(1-\frac{2M}{r}\right)\frac{d^2}{dr^2}+\frac{2(r-M)}{r^2}\frac{d}{dr}+\left(\frac{\omega^2}{1-\frac{2M}{r}}-\frac{\ell(\ell+1)}{r^2}\right)\right] g^{\rm full}_{\ell m\omega}(r,r') = -\frac{1}{r^2}\delta(r-r'). \tag{4}$$

The radial part of the full Green function is expressed in terms of homogeneous solutions of Eq. (4), which can be obtained by a systematic analytic method developed in Ref. [7], as

$$\begin{aligned} g^{\rm full}_{\ell m\omega}(r,r') &= \frac{-1}{W_{\ell m\omega}(\phi^\nu_{\rm in},\phi^\nu_{\rm up})}\left(\phi^\nu_{\rm in}(r)\phi^\nu_{\rm up}(r')\theta(r'-r)+\phi^\nu_{\rm up}(r)\phi^\nu_{\rm in}(r')\theta(r-r')\right), \\ W_{\ell m\omega}(\phi^\nu_{\rm in},\phi^\nu_{\rm up}) &= r^2\left(1-\frac{2M}{r}\right)\left[\left(\frac{d}{dr}\phi^\nu_{\rm up}(r)\right)\phi^\nu_{\rm in}(r)-\left(\frac{d}{dr}\phi^\nu_{\rm in}(r)\right)\phi^\nu_{\rm up}(r)\right]. \end{aligned} \tag{5}$$

Here the in-going and up-going homogeneous solutions are denoted, respectively, by $\phi^\nu_{\rm in}$ and $\phi^\nu_{\rm up}$, and ν is called the renormalized angular momentum [7], which is equal to ℓ in the limit $M\omega\to 0$.

We express the homogeneous solutions $\phi^\nu_{\rm in}$ and $\phi^\nu_{\rm up}$ in terms of the solutions $\phi^\nu_{\rm c}$ and $\phi^{-\nu-1}_{\rm c}$, which can be expressed in terms of a series of the Coulomb wave functions [7], as

$$\phi^\nu_{\rm in} = \phi^\nu_{\rm c}+\tilde{\beta}_\nu\,\phi^{-\nu-1}_{\rm c}, \qquad \phi^\nu_{\rm up} = \tilde{\gamma}_\nu\,\phi^\nu_{\rm c}+\phi^{-\nu-1}_{\rm c}, \tag{6}$$

Using these homogeneous solutions, we divide the Green function into two parts in the previous work [5].

$$g^{\rm full}_{\ell m\omega}(r,r') = g^{\tilde{S}}_{\ell m\omega}(r,r')+g^{\tilde{R}}_{\ell m\omega}(r,r'), \tag{7}$$

where

$$\begin{aligned} g^{\tilde{S}}_{\ell m\omega}(r,r') &= \frac{1}{W_{\ell m\omega}(\phi^\nu_{\rm c},\phi^{-\nu-1}_{\rm c})}\left[\phi^\nu_{\rm c}(r)\phi^{-\nu-1}_{\rm c}(r')\theta(r'-r)+\phi^{-\nu-1}_{\rm c}(r)\phi^\nu_{\rm c}(r')\theta(r-r')\right], \\ g^{\tilde{R}}_{\ell m\omega}(r,r') &= \frac{1}{(1-\tilde{\beta}_\nu\tilde{\gamma}_\nu)W_{\ell m\omega}(\phi^\nu_{\rm c},\phi^{-\nu-1}_{\rm c})} \\ &\quad\times\left[\tilde{\beta}_\nu\tilde{\gamma}_\nu\left(\phi^\nu_{\rm c}(r)\phi^{-\nu-1}_{\rm c}(r')+\phi^{-\nu-1}_{\rm c}(r)\phi^\nu_{\rm c}(r')\right)+\tilde{\gamma}_\nu\phi^\nu_{\rm c}(r)\phi^\nu_{\rm c}(r')+\tilde{\beta}_\nu\phi^{-\nu-1}_{\rm c}(r)\phi^{-\nu-1}_{\rm c}(r')\right]. \end{aligned} \tag{8}$$

The $\tilde{S}$-part $g^{\tilde{S}}_{\ell m\omega}$ is singular and symmetric, and it satisfies the same inhomogeneous equation as the Green function. The $\tilde{R}$-part $g^{\tilde{R}}_{\ell m\omega}$ is regular, and it satisfies the source free equation. It is noted that the $\tilde{S}$-part is need to take care in the regularization of the self-force. On the other hand, there is no divergence associated with the remaining $\tilde{R}$-part. So, in order to obtain the R-part, we consider the following regularization,

$$F^R_\alpha = (F^{\tilde{S}}_\alpha - F^S_\alpha) + F^{\tilde{R}}_\alpha . \tag{9}$$

The important fact is that the $\tilde{S}$-part in the frequency domain is given in the form of a simple Taylor series with respect ω multiplied by $\exp[-i\omega(t-t')]$. Therefore, the integration over ω just produces $\delta(t-t')$ and its derivatives. Using this technique we can obtain the $\tilde{S}$-part in the time domain relativity easily. The details are given in [5, 6].

3 Application: Plunge orbit

We can calculate the part which needs to be regularized ($F^{\tilde{S}}_\alpha - F_S$) and the residual part ($F^{\tilde{R}}_\alpha$) actually. The former is represented by the local quantities (the energy $\mathcal{E}$, angular momentum $\mathcal{L}$ and distance r), while the latter can not do. So we divide the regularized self-force into two parts, which consist of the part that can be represented by $\mathcal{E}$, $\mathcal{L}$ and r ($F^{\mathrm{R.pow}}_\alpha$) and the rest that is obtained from the Green function including the logarithmic term, $\ln\omega$, ($F^{\mathrm{R.ln}}_\alpha$).

In this section, we calculate the regularized scalar self-force on a particle which is falling radially into a Schwarzschild black hole, by using the above regularization scheme.

When we assume the angular coordinates of the particle location as $z^\theta(t) = \pi/2$ and $z^\varphi(t) = 0$, the plunge orbit is given by using the parameter η as the following [10].

$$\tau = \frac{R}{2}\left(\frac{R}{2M}\right)^{1/2}(\eta + \sin\eta), \quad z^r = \frac{R}{2}(1+\cos\eta). \tag{10}$$

Here we consider the free fall of a particle from rest, starting from $z^r = R$ at $z^t = 0$.

For the part $F^{R,\mathrm{pow}}_\alpha$, we can calculate just by substituting

$$\mathcal{E} = \sqrt{1-\frac{2M}{R}}, \quad \mathcal{L} = 0, \quad u^r = -\sqrt{\frac{2M}{R}}\frac{\sin\eta}{1+\cos\eta}. \tag{11}$$

On the other hand, the calculation for the part $F^{R,\mathrm{ln}}_\alpha$ needs to be calculated by numerical integration. It is, however, easy to do numerical calculation by using the following formulas;

$$F^{R,\mathrm{ln}}_{\alpha\ell} = q^2 P_\alpha{}^\beta \sum_{mkj} i^k \lim_{x\to z(t)} \nabla_\beta \frac{\partial^k}{\partial t^k}\left[-f(0)\ln(t) - \int_0^t dt' f'(t')\ln(t-t') - \left(\gamma - \frac{i\pi}{2}\right) f(t)\right], \tag{12}$$

where the function $f(t)$ is given by

$$f(t) = \frac{1}{\mathcal{E}}\left(1-\frac{2M}{z^r(t)}\right)\mathcal{G}^{\mathrm{ln}(j)}_{\ell mk}(r, z^r(t))Y_{\ell m}(\theta,\varphi)Y^*_{\ell m}(\pi/2, 0), \quad g^{\mathrm{ln}}_{\ell m\omega} = \sum_{k=2}^{\infty}\sum_{j=1}^{\infty}\omega^k \mathcal{G}^{\mathrm{ln}(j)}_{\ell mk}(r, r')(\ln\omega)^j,$$

and $g^{\mathrm{ln}}_{\ell m\omega}$ is the part, including $\ln\omega$, of the Green function.

In Fig. 1, we show the case of the free fall from rest, starting from $R^* = 40M$ where $R^* = R + 2M\ln[(r-2M)/(2M)]$, and in the numerical calculation we set $q = M = 1$.

4 Conclusion

We present a more realistic analytic scheme for the radiation reaction problem and the result of the regularized self-force acting on the particle orbiting plunge.

We are going to solve the geodesic equation by $O(\mu)$ and extend to the Kerr black hole case. And we would like to derive the gravitational self-force on a point particle and calculate the orbit including the correction of self-force.

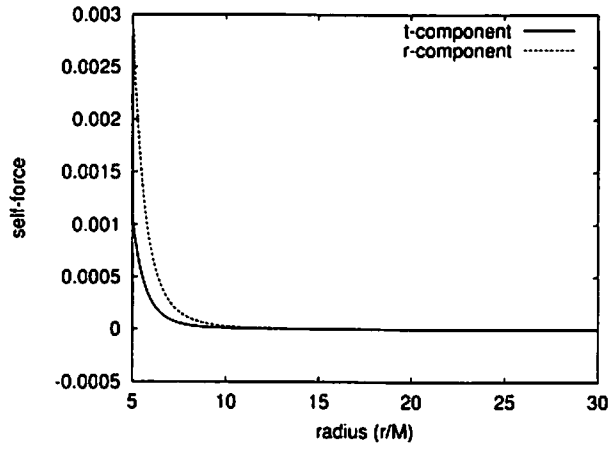

Figure 1: The scalar self-force in the case of the free fall from rest, starting from $R^* = 40$ ($R \sim 34$) by third post-Newtonian (3PN). The line and dotted line are t-component and r-component of self-force respectively.

Acknowledgments

We would like to thank Y. Mino, T. Nakamura for useful discussions. We also thank all the participants of the 6th Capra meeting and the Post Capra meeting at Yukawa Institute, Kyoto University (YITP-W-03-02). HN is supported by JSPS Research Fellowships for Young Scientists, No. 5919. SJ acknowledges support under a Basque govt postdoctoral fellowship. This work was supported in part by Monbukagakusho Grant-in-Aid for Scientific Reasearch, Nos. 14047212, 14047214 and 12640269.

References

[1] Y. Mino, M. Sasaki and T. Tanaka, Phys. Rev. D **55**, 3457 (1997)

[2] T. C. Quinn and R. M. Wald, Phys. Rev. D **56**, 3381 (1997)

[3] S. Detweiler and B. F. Whiting, Phys. Rev. D **67**, 024025 (2003)

[4] L. Barack, Y. Mino, H. Nakano, A. Ori and M. Sasaki, Phys. Rev. Lett. **88**, 091101 (2002)

[5] W. Hikida. et.al., arXiv:gr-qc/0308068

[6] web page: http://www2.yukawa.kyoto-u.ac.jp/~misao/BHPC/

[7] S.Mano, H.Suzuki and E.Takasugi, Prog. Theor. Phys. **95**, 1079 (1996)

[8] N. Sago, H. Nakano and M. Sasaki, Phys. Rev. D **67**, 104017 (2003). [arXiv:gr-qc/0208060].

[9] H. Nakano, N. Sago and M. Sasaki, arXiv:gr-qc/0308027.

[10] C. W. Misner, K. S. Thorne and J. A. Wheeler, *Gravitation* (Freeman, San Francisco, 1973)

Evolution of gravitational waves from inflationary brane-world

Takashi Hiramatsu[1], Kazuya Koyama[2], Atsushi Taruya[3]

Department of Physics, School of Science,
University of Tokyo, Hongo 7-3-1, Bunkyo-ku, Tokyo 113-0033, Japan

Abstract

We study the evolution of gravitational waves(GWs) after inflation in a brane-world cosmology embedded in five-dimensional anti-de Sitter (AdS) spacetime [1]. Contrary to the standard four-dimensional results, the GWs at the high-energy regime in brane-world model suffer from the effects of the non-standard cosmological expansion and the excitation of the Kaluza-Klein modes(KK-modes), which can affect the amplitude of stochastic gravitational wave background significantly. To investigate these two high-energy effects quantitatively, we numerically solve the wave equation of the GWs in the radiation dominated epoch at relatively low-energy scales. We show that the resultant GWs are suppressed by the excitation of the KK modes which escape away from the brane to the bulk gravitational field. The results are also compared to the semi-analytic prediction from the low-energy approximation and the evolved amplitude of GWs on the brane reasonably matches the numerical simulations.

1 Introduction

The stochastic gravitational wave background (stochastic GWB) generated during the inflationary era is a promising source for the low-frequency gravitational waves and this can provide a direct way to probe the extremely early Universe. In particular, such GWs are expected to have information about the extra dimensions. In the case of the single-brane model proposed by Randall & Sundrum [2], the scale of the extra dimension is well below the length $l \lesssim 0.1\mathrm{mm}$ according to the current experiments of the Newton gravity. Therefore, the effect of the extra-dimension can be imprinted on the GWB at the low-frequency band, $f \gtrsim f_{\mathrm{crit}} \sim 2 \times 10^{-4}\,(0.1\mathrm{mm}/l)^{1/2}$ Hz.

Theoretically, the evolution of GWs in the brane-world cosmology is expected to deviate from the standard four-dimensional theory in the following two aspects: 1) the non-standard cosmological expansion due to the bulk gravity and 2) the excitation of the Kaluza-Klein mode(KK-mode) of graviton. The former may enhance the amplitude of GWs and the latter may suppress or modulate the GW form on a brane relative to the prediction from the four-dimensional theory. These effects are particularly significant in the high-energy regime of the universe. To investigate these effects in a realistic situation of the cosmological brane-world, we solve the wave equation of GWs numerically in the Randal-Sundrum type single-brane model. It has been shown that the excitation of KK-modes are suppressed during inflation and zero-mode remains constant after inflation at super-horizon scale [3]. Thus we will consider the evolution of the GWs starting from an initially zero-mode state at super-horizon scales and focus on the behavior just after the horizon-crossing time. Additionally, to understand the numerical results, we perform the low-energy approximation for the wave equation.

2 Basic equations

We specifically treat the single-brane model embedded in a five-dimensional anti-de Sitter (AdS) space, in which the matter content on brane is simply given by a homogeneous and isotropic perfect fluid satisfying the equation of state $p = w\rho$. Using the Gaussian normal coordinate to the brane, the metric including the tensor perturbation is given by

$$ds^2 = -n^2(t,y)dt^2 + a^2(t,y)(\delta_{ij} + E_{ij})dx^i dx^j + dy^2. \tag{1}$$

[1]E-mail:hiramatsu@utap.phys.s.u-tokyo.ac.jp
[2]E-mail:kazuya@utap.phys.s.u-tokyo.ac.jp
[3]E-mail:ataruya@utap.phys.s.u-tokyo.ac.jp

where the brane is located at $y = 0$. The lapse function $n(t, y)$ and the scale factor $a(t, y)$ for the background space-time are determined from the five-dimensional Einstein equation. In absence of the dark radiation, these quantities are written as follows [3][4]:

$$a(t,y) = a_0(t)\left\{\cosh(\mu y) - \left(1 + \frac{\rho(t)}{\lambda}\right)\sinh(\mu y)\right\}, \quad n(t,y) = e^{-\mu y} + (2+3w)\frac{\rho(t)}{\lambda}\sinh(\mu y), \tag{2}$$

where $\lambda > 0$ denotes the tension of the brane and $\mu^{-1} = \sqrt{6/\kappa_4^2\lambda}$ represents the curvature scale of the AdS bulk. The scale factor $a_0(t)$ and the energy density on the brane $\rho(t)$ are determined from the effective Friedmann equations [4]:

$$H^2 \equiv \left(\frac{\dot{a}_0}{a_0}\right)^2 = \frac{\kappa_4^2}{3}\rho(t)\left(1 + \frac{\rho(t)}{2\lambda}\right), \qquad \dot{\rho} = -3H(1+w)\rho(t), \tag{3}$$

The solution of the above equations is easily obtained and can be expressed in terms of the dimensionless variables $\tau = t/l_*$ and $\epsilon = \rho/\lambda$:

$$a_0(\tau) = a_*\left(\tau^2 + 2c\tau - 2c\right)^{\frac{1}{3(1+w)}}, \qquad \rho(\tau) = \rho_*\left(\tau^2 + 2c\tau - 2c\right)^{-1}, \tag{4}$$

where the subscript $*$ means the quantity evaluated at the time $\tau = 1$ and $c \equiv \sqrt{1 + \epsilon_*/2} - 1$. Note that the Gaussian-normal coordinate has a coordinate singularity at $y = y_c$, defined by $a(\tau, y_c(\tau)) = 0$.

The perturbed quantity E_{ij} in the metric (1) satisfies the transverse and the traceless conditions, which is automatically gauge-invariant. Decomposing the perturbation in spatial Fourier modes as $E_{ij} = E(t, y; \mathrm{k})e^{i\mathbf{k}\cdot\mathbf{x}}\hat{e}_{ij}$, where $\hat{e}_{ij}$ is transverse-traceless polarization tensor, the wave equation for the Fourier component E becomes [3]:

$$\frac{\partial^2 E}{\partial t^2} + \left(3\frac{\dot{a}}{a} - \frac{\dot{n}}{n}\right)\frac{\partial E}{\partial t} + \frac{n^2}{a^2}k^2 E - n^2\left\{\frac{\partial^2 E}{\partial y^2} + \left(3\frac{a'}{a} + \frac{n'}{n}\right)\frac{\partial E}{\partial y}\right\} = 0. \tag{5}$$

Ignoring the anisotropic stress tensor π_{ij} on brane, the perturbed Israel condition is [3]:

$$\left.\frac{\partial E}{\partial y}\right|_{y=0} = 0. \tag{6}$$

Hereafter, we will focus on the time evolution of the tensor perturbation in the radiation-dominated epoch($w = 1/3$) and solve the wave equation (5) numerically.

3 Numerical analysis

To solve the wave equation (5) numerically, we use a Tchebychev collocation method with the Gauss-Lobbatto collocation points, $y_\ell = \cos(\ell\pi/N)$ with $\ell = 0, 1, \cdots, N$. With this method, the quantity $E(\tau, y)$ is first transformed to a set of variables $E_\ell(\tau)$ defined in the Tchebychev space, and the equation (5) can be regarded as the ordinary differential equations for E_ℓ. Then, the time evolution of E_ℓ is followed by the Predictor-Corrector method based on the Adams-Bashforth-Moulton finite-difference scheme.

As mentioned in section 1, the initial condition for the quantity E is set to the zero-mode solution in the inflationary era, i.e., $E(\tau_0, y) =$ constant. The calculations are then started before the wavelength of the zero-mode crosses the Hubble horizon. For convenience, we set the comoving wave number k to $k = a_* H_*$, that is, the GW mode just crosses the Hubble horizon when $\tau = 1$.

Since the computational domain should be finite, and the Gaussian normal coordinate (1) has a coordinate singularity, we must introduce another boundary in the bulk and impose another boundary condition at this boundary for numerical purpose. Therefore, we put a regulator brane at $y_{\mathrm{reg}}(\tau) = \gamma\, y_c(\tau)$ inside the coordinate singularity and impose the Neumann boundary condition:

$$n^\mu \left.\frac{\partial E}{\partial x^\mu}\right|_{y=y_{\mathrm{reg}}(\tau)} = 0, \tag{7}$$

where n^μ is the normal vector to the boundary trajectory. Thus, provided the location of the boundaries $y = 0$ and $y = y_{\rm reg}(\tau)$, the only physical parameter is ϵ_*, i.e., the dimensionless energy density ρ/λ at the horizon-crossing time, which is directly related to the scale of the GW concerned. For large ϵ_*, the proper distance between the physical brane and regulator brane becomes small. The results will crucially depend on the regulator brane. Hence, we restrict our analysis to the the small ϵ_* case.

In Fig.1, the resultant waveform on the brane is depicted as function of time in the case with $\epsilon_* = 0.2$, $\gamma = 0.8$. Apart from the overall damping $1/a_0(t)$ due to the cosmological expansion, the amplitude of the numerical solution on the brane (*solid*) becomes smaller than that of the solution in the four-dimensional theory (*long-dashed*). This result simply reflects the fact that the localization of gravity is not fulfilled in presence of the ρ^2-term (see Eq.(3)) and the GW can easily escape from the brane.

If the regulator brane is located sufficiently far away from the physical brane, we expect that we can safely neglect the effect of the regulator brane. To confirm this, in Fig.2, we plot the damping factor, i.e., the ratio of the amplitude obtained from the numerical solution to that from the four-dimensional theory in the case of $\epsilon_* = 0.05$, 0.2 and 0.3. The damping factor depends linearly on small ϵ_*, and tends to converge for $\gamma \to 1$.

4 Result from low-energy expansion

In order to understand the behavior of the numerical results in previous section, we employ a low energy expansion scheme to solve the wave equation approximately. In this treatment, the term $\epsilon = \rho/\lambda$ in effective Friedmann equation (3) is assumed to be small. Thus, treating the dimensionless quantity ϵ as small expansion parameter, we expand the tensor perturbation $E(\tau, y)$:

$$E(\tau, y) = E_0(\tau) + E_1(\tau, y) + E_2(\tau, y) + \cdots, \qquad E_k(\tau, y) = \mathcal{O}(\epsilon^k). \tag{8}$$

The scale factor $a_0(\tau)$ and the Hubble parameter $H(\tau)$ are expanded in the same way. Note further the fact that in the low energy approximation, since the time-derivative is the order of the Hubble parameter and the y-derivative is the order of the bulk scale μ, there is a hierarchical relation of the derivatives $\dot{E}/E' \sim \mathcal{O}(\epsilon^{1/2})$. Keeping the relation in mind, one can expand the wave equation (5) in terms of ϵ and find the higher-order solutions iteratively. Then, imposing boundary conditions, we derive an ordinary differential equations for $E_0(\tau)$:

$$\begin{aligned} &\frac{d^2E_0}{d\tau^2} + 3\left(1 + \frac{H_1}{H_0} + 4\frac{\rho(\tau)}{\lambda}|1 - 2B(y_0)|\right) H_0 \frac{dE_0}{d\tau} \\ &\quad + \left(\frac{k}{a_0^{(0)}}\right)^2 \left(1 - 2\frac{a_0^{(1)}}{a_0^{(0)}} + 4\frac{\rho(\tau)}{\lambda}|1 - 2B(y_0)|\right) E_0 = 0 \end{aligned} \tag{9}$$

in the case of the static boundary. Here, we defined $B(y_0) \equiv \mu y_0/(1 - e^{-2\mu y_0})$. The variable y_0 denotes the position of the boundary determined at an initial time $\tau = \tau_0$, i.e., $y_0 = \gamma y_c(\tau_0)$. If the regulator brane is moving, the equation contains the term proportional to $\dot{y}_{\rm reg}(t)$ and it becomes rather complicated. Note also that this approximation will break down if the regulator brane becomes far away from our brane $e^{\mu y_{\rm reg}} > \rho/\lambda$, since the low energy approximation breaks down on the regulator brane.

In spite of the above limitations of this approximation, the solution quite well reproduces the numerical results for $E_0(\tau)$ even in the case of the moving boundary (see *short-dashed* in Fig.1). Thus, at least in a qualitative level, we can use this approximation to understand the behavior of perturbations on the brane. The second terms in the coefficients of $H_0\dot{E}_0$ and E_0 come from the modification of background Friedmann equation, that is, ρ^2-term in Eq. (3). The third terms arise from the non-separable nature of the metric (1) or the time-dependant Hubble parameter $\dot{H} \neq 0$, which excite KK-modes in the bulk and cause the dissipation of the perturbations on the brane.

In the long wavelength limit $k \to 0$, the zero-mode solution $E_0 = $ const. is the solution for the effective equation (9). However, if the perturbation crosses the horizon, the zero-mode solution cannot be a solution and then KK-modes are inevitably excited. The effects of the non-standard cosmological expansion tend to enhance the amplitude of the perturbation compared to the four-dimensional theory (note that the quantity H_1/H_0 is negative for the late time). On the other hand, both the numerical results

and the low energy approximation show that the amplitude of the perturbations decreases, which implies that the influence of the excitation of KK-modes overcomes the effects of the non-standard cosmological expansion. Therefore, the suppression of the amplitude of GWs can be understood as the consequence of the excitation of the KK-modes due to the non-separable nature of the bulk metric in the Gaussian normal coordinate defined with respect to the physical brane.

5 Conclusion

We have numerically investigated the evolution of GWs during the radiation dominated epoch in the Randall-Sundrum type single-brane model. Especially focusing on the behavior after the horizon-crossing time, we found that the amplitude of GWs on brane is suppressed compared to that of the four-dimensional theory. From the analysis using the low-energy approximation, the suppression of GWs can be understood as a consequence of the excitation of KK-modes. The influence of the KK-modes on GWs overcomes the effect of the non-standard cosmological expansion arising from the ρ^2-term. The suppression of GWs becomes significant as increasing the energy scales ϵ_*. Therefore, contrary to the four-dimensional prediction, the intensity of the stochastic GWB around the frequency $f \sim f_{\rm crit}$ tends to decrease as increasing the frequency, which might provide an important clue to check for the extra-dimensions.

In order to investigate the degree of this effect precisely, however, the boundary condition imposed on the regulator brane might be inadequate. Instead of using the Neumann condition (7), a suitable choice of the boundary condition such as the non-reflecting boundary condition should be considered. Further, to impose a realistic boundary condition, the Poincaré coordinate, which covers the wider region of the AdS spacetime than the Gaussian normal coordinate, would be crucial in our numerical calculation. The implementation of these technical points is straightforward and the analysis is now in progress.

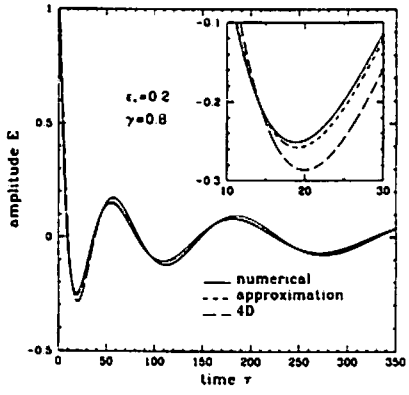

Figure 1: Numerical solution of GW on brane (*solid*), together with the 4-dimensional GW (*long-dashed*) and the result from the low-energy approximation (*short-dashed*).

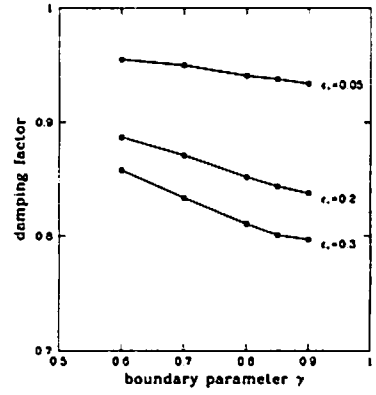

Figure 2: Damping factor of the GW amplitude on brane as function of boundary parameter γ

References

[1] T. Hiramatsu, K. Koyama and A. Taruya, Phys. Lett. **B578**, 269 (2004).

[2] L. Randall and R. Sundrum, Phys. Rev. Lett. **83**, 4690 (1999).

[3] D. Langlois, R. Maartens and D. Wands, Phys. Lett. **B489**, 259 (2000).

[4] P. Binétruy, C. Deffayet, U. Ellwanger and D. Langlois, Phys. Lett. **B477**, 285 (2000).

Causal Structure and Gravitational Waves in Brane World Cosmology

Kiyotomo Ichiki[1,a,b] and Kouji Nakamura[2,c]

[a] *Department of Astronomy, University of Tokyo, 7-3-1 Hongo, Bunkyo-ku, Tokyo 113-0033, Japan*

[b] *Division of Theoretical Astrophysics, National Astronomical Observatory, 2-21-1, Osawa, Mitaka, Tokyo 181-8588, Japan*

[c] *Department of Astronomical Science, the Graduate University for Advanced Studies, 2-21-1, Osawa, Mitaka, Tokyo 181-8588, Japan*

Abstract

We investigate the causal structure of the flat brane universe of RSII type to clarify the boundary conditions for stochastic gravitational waves. Based upon the causal structure, we discuss the boundary conditions for gravitational waves in the bulk. Introducing a null coordinate, we propose a procedure to solve gravitational waves with appropriate initial conditions and avoid the problems in setting boundary conditions in the bulk. The problem in the choice of the initial condition for gravitational waves is briefly discussed.

1 Introduction

Since the proposal of a brane world model of our spacetime by Randall and Sundrum [1] (RS), the phenomenology of brane world cosmological models has been the subject of intensive investigations in recent years. In these brane world models, our universe is regarded as a four dimensional boundary (brane) in a higher dimensional spacetime (bulk). Many authors have found more realistic models which include realistic matter fields on the brane and realize the cosmic expansion [2] , and tried to constrain on these models by the observational data.

The stochastic gravitational waves will be a promising candidate which provides a direct and deep test of such cosmologies. In order to give theoretical predictions of stochastic gravitational waves, many authors have adopted the Gaussian normal (GN) coordinate system in the neighborhood of the brane. The equation of gravitational waves takes the same form as that of the five-dimensional massless scalar field:

$$\Box_5 h = 0. \tag{1}$$

To obtain the theoretical spectrum of stochastic gravitational waves, we just solve this equation with appropriate boundary conditions. However, Eq. (1) in terms of the GN coordinate system includes a singularity at finite coordinate values in the bulk, where the metric function vanishes. The treatment of Eq. (1) near the singularity is one of difficulties when we obtain the evolution of stochastic gravitational waves [3]. In fact, this singularity corresponds to the "seam singularity" discussed by Ishihara [4].

The aim of this paper is to propose a procedure to solve the evolution of cosmological gravitational waves avoiding the above difficulty in GN coordinate system. The procedure proposed here is based on the characteristic initial value problem according to the causal structure of the entire spacetime. We use a null coordinate instead of the proper time on the brane. In this procedure, the boundary conditions in the bulk are replaced by the initial condition on a null hypersurface and the above difficulty in the treatment of Eq. (1) near the singularity is resolved if we simply specify the initial spectrum on a null hypersurface. The details are found in [5].

[1] E-mail:ichiki@th.nao.ac.jp
[2] E-mail:kouchan@th.nao.ac.jp

2 GN coordinate system in AdS_5 bulk

In this section, we first relate GN coordinate system to the flat chart in AdS_5, and then find where the singularity of the equation (1) in the bulk in the closed chart of AdS_5 which covers the entire ADS_5.

We consider a brane universe embedded in the AdS_5 with a negative cosmological constant $\Lambda_5 = -4/l^2$. In terms of the static charts of AdS_5, the metric on AdS_5 is given by

$$ds^2 = -f_K(r_K)dt_K^2 + f_K(r_K)^{-1}dr_K^2 + r_K^2 d\Sigma_K^2, \tag{2}$$

where K takes the values $-1, 0$, and $+1$, corresponding to the negative, zero, and positive constant curvature of a maximally symmetric three dimensional space, respectively . The function $f_K(r_K)$ in this metric is defined by $f_K(r_K) := K + \frac{r_K^2}{l^2}$, and the metric $d\Sigma_K^2$ is given by

$$d\Sigma_K^2 = \begin{cases} d\chi_+^2 + \sin^2\chi_+\{d\theta^2 + \sin^2\theta d\phi^2\} & (K=+1), \\ d\chi_0^2 + \chi_0^2\{d\theta^2 + \sin^2\theta d\phi^2\} & (K=0), \end{cases}$$

respectively. In these static charts, a trajectory of three brane is given by $r_K = r_K(t_K) := a(\tau)$ and $t_K = t_K(\tau)$, where τ is the proper time of the world volume of the brane and $a(\tau)$ is a cosmological scale factor on the brane. The equation of the brane motion is given by the generalized Friedmann equation [2].

Cosmological solutions of the RS type brane world in terms of GN coordinate system were found by several authors (for example, see [2]), which is given by

$$ds^2 = -\frac{\psi^2(\tau,w)}{\varphi(\tau,w)}d\tau^2 + \varphi(\tau,w)a^2(\tau)d\Sigma_K^2 + dw^2. \tag{3}$$

For explicit expressions of functions ψ and φ, we refer readers to Ref. [6]. We have chosen the coordinate w so that $w = 0$ on the brane. As noted in Sec. 1, this coordinate system has a coordinate singularity at $w = w_h = \frac{l}{2}\log((A+1)/(A-1))$. Here w_h is determined by the equation $\varphi(\tau, w_h) = 0$ for each τ and $A := \sqrt{1 + l^2H^2}$ where $H := \dot{a}/a$ is well known Hubble parameter. This is nothing but the singularity in Eq. (1). Explicit coordinate transformations between the metrics (2) and (3) with $K = 0$ are given by,

$$r_0^2 = \varphi(\tau,w)a^2(\tau), \tag{4}$$

$$t_0 - t_b = \frac{l^2}{a}\sqrt{\frac{A+1}{A-1}}\left[1 - \frac{2}{(1-A)e^{2\frac{w}{l}} + 1 + A}\right], \tag{5}$$

where $t_b(\tau)$ is chosen so that $t_0 = t_b(\tau)$ on the brane ($w = 0$) for any τ [5, 6]. Clearly, the singularity in the equation (1) is just on the region $r_0 = 0$ in the flat chart. To find where is the singularity in Eq. (1) in the bulk, we first see the region of $r_0 = 0$ in the entire AdS_5 using the closed chart. On this closed chart, we can easily specify the point of the singularity in Eq. (1) in AdS_5 bulk by tracing the spacelike geodesic which normal to the brane for each τ.

Now, we consider the relation between the flat chart and the closed chart of AdS_5. This was already given by Ishihara[4] and we followed his arguments to fine the event $\varphi(\tau, w_h) = 0$ for each τ in the closed chart. Fixing the proper time τ on the brane, the coordinate functions r_+, t_+, and χ_+ behave as

$$\begin{aligned} r_+ &= \frac{l^2}{a(\tau)}\frac{A}{\sqrt{A^2-1}} + t_b, \\ \frac{t_+}{l} &= \arctan\left[\frac{r_+}{l}\right] = \frac{r_*}{l}, \\ \cos\chi_+ &= -1 \end{aligned} \tag{6}$$

in the limit $w \to w_h$ ($\varphi(\tau, w) \to 0$). This shows that the coordinate singularity at which $\varphi(\tau, w_h) = 0$ is just on the "seam singularity" $t_+/l = r_*/l = \arctan(r_+/l)$, $\cos\chi_+ = -1$ (see Fig. 1).

Note that the seam singularity can be replaced by the other regular portion of a spacetime according to the creation scenario of the brane universe. In this sense, we do not have to be afraid of this singularity, or equivalently, the singularity in Eq. (1), seriously. Moreover, when we consider the characteristic initial value problem, the initial conditions are chosen on the future light cone $\partial\mathcal{D}(\tau_c)$ and the seam singularity is shaded by this light cone (see Fig. 2). Therefore, the difficulties in the treatment of the singularity in Eq. (1) are simply reduced to the choice of initial conditions for gravitational waves.

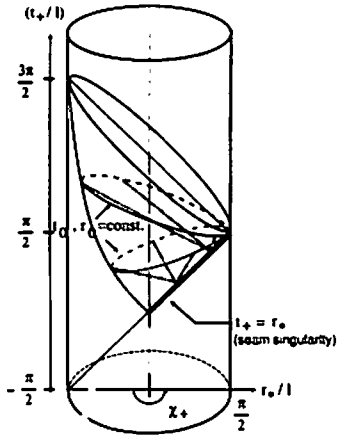

Figure 1: Geodesics normal to the brane for each τ (dot-dashed lines) in the entire AdS_5 spacetime. The geodesics converge to the seam singularity $t_+ = r_*$ at which $\varphi(\tau, w) = 0$. This figure is from Ref. [5].

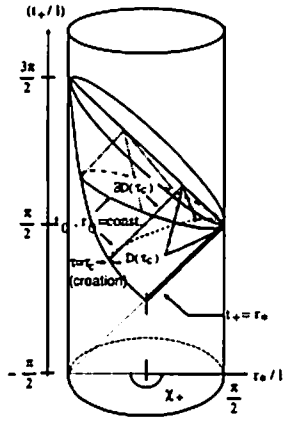

Figure 2: Brane trajectory (lines) and future light cone from the brane (dot-dashed lines). Singularity where $\varphi(\tau, w_h) = 0$ is shown as a thick line and it is completely hidden by the future light cone $\partial\mathcal{D}(\tau_c)$. Gravitational waves in a shaded region are determined by the scenario of the creation of the flat FRW brane.

3 Null Coordinate and Gravitational Wave Equation

At this point, we have a clear strategy to tackle the problem the evolution of gravitational waves in the brane universe. The singularities $\varphi(\tau, w_h) = 0$ in Eq. (1) are completely shaded by the future light cone $\partial\mathcal{D}(\tau_c)$ (Fig. 2). Thus, we do not have to care the singularity $\varphi(\tau, w_h) = 0$ any more and there is no need to introduce any artificial boundaries in the bulk to impose boundary conditions at bulk infinity. In order to develop the characteristic initial value problem associated with the light cone $\partial\mathcal{D}(\tau)$, let us introduce the function u by

$$u = t_0 - \frac{l^2}{r_0} - t_b' + \frac{l^2}{r_b'} \ , \tag{7}$$

where (t_b', r_b') determine the zero point of this function u. The function u is constant on the light cone $\partial\mathcal{D}(\tau)$ for each τ. We can easily confirm that the one-form $(du)_a$ is null through the metric (2) with $K = 0$. In terms of the new coordinate system u and $\overline{w} = w$, we found that the five-dimensional metric (3) on AdS_5 can be written as

$$ds^2 = -F(\tau, \overline{w})du^2 - 2F(\tau, \overline{w})du d\overline{w} + r^2(\tau, \overline{w})d\Sigma_0^2, \tag{8}$$

where $F(\tau, w) = \frac{r_0^2/l^2}{\sqrt{r_0^2/l^2 + \dot{a}^2} + \dot{a}}$. As mentioned in Sec. 1, the equation for gravitational waves in the bulk is simply given by that for the five-dimensional massless scalar field Eq. (1). In terms of the coordinate system $(u, \overline{w})$ Eq. (1) is given by

$$\left[\partial_{\overline{w}}^2 - \frac{2}{F}\partial_{\overline{w}}\partial_u - \frac{3}{Fr}\left(\left(\frac{\partial r}{\partial u}\right)_{\overline{w}}\partial_{\overline{w}} + \left(\frac{\partial r}{\partial \overline{w}}\right)_u \partial_u\right) + \left(\frac{1}{F}\left(\frac{\partial F}{\partial \overline{w}}\right)_u + \frac{3}{r}\left(\frac{\partial r}{\partial \overline{w}}\right)_u\right)\partial_{\overline{w}} - \frac{k^2}{r^2}\right] h(u, \overline{w}; k) = 0 \ , \tag{9}$$

where $-k^2$ is the eigen value of the Laplacian of $d\Sigma_0$. The above equation can be formally integrated to give

$$\partial_u h(u, \overline{w}) = r^{-3/2}(\tau, \overline{w}) \times \left(\int^{\overline{w}} S(w')r^{3/2}dw' + C(u)\right), \tag{10}$$

where $S(\overline{w}) = \frac{F}{2}\left(\partial_{\overline{w}}^2 h - \frac{k^2}{r^2}h\right) + \left(\frac{1}{2}\frac{\partial F}{\partial \overline{w}} + \frac{3F}{2}\frac{\partial \ln r}{\partial \overline{w}} - \frac{3}{2}\frac{\partial \ln r}{\partial u}\right)\partial_{\overline{w}} h$ and it is given by know functions. These equations are the main result of this work. The function $C(u)$ in Eq. (10) is determined by the

boundary condition at the brane ($\overline{w} = 0$). When the anisotropic stress on the brane is not induced due to matter fields on the brane, the boundary condition for gravitational waves h at the brane is the Neumann type.This is accomplished by imposing

$$\partial_u h(u,0) = -\left(\frac{\partial u}{\partial w}\right)_\tau^{-1} \partial_{\overline{w}} h = F(\tau,0)\partial_{\overline{w}} h \quad , \tag{11}$$

at the brane. Eq. (10) with the boundary condition (11) are easier to solve than Eq. (1) and enough to predict the cosmological evolution of gravitational waves. Of course, as the initial condition, we should specify spectrum of gravitational waves on the light cone $\partial\mathcal{D}(\tau_c)$ according to the creation scenario of the flat FRW brane.

4 Summary and Discussion

In this paper, we have carefully investigated the causal structure of the flat FRW model of RS type II brane world and proposed the single null coordinate system to solve the cosmological evolution of gravitational waves. We have explicitly seen that in this null coordinate system, we do not have to care the singularity in Eq. (1). Further, it is not necessary to introduce any artificial boundaries to impose some boundary conditions at the bulk infinity.

The initial conditions for gravitational waves in brane world cosmologies crucially depend on the creation scenario of the FRW brane. There are some scenarios where the FRW brane is created after the inflationary phase. If we adopt these brane inflationary scenarios, it might be natural to consider that the initial spectrum of gravitational waves is determined in this inflationary phase. The spectrum of gravitational waves under the deSitter evolution of the brane is discussed by several authors [7, 8, 9]. It was pointed out that gravitational waves decay away except but the zero-mode, and it approaches to a constant amplitude in the inflationary phase. These discussions are based on the GN coordinate system. Since GN coordinate system does not cover the entire bulk space, these discussions seem inappropriate to specify the initial spectrum of gravitational waves. However, it was also shown that the vacuum defined on the deSitter slicing asymptotically approaches to the vacuum defined in terms of the Poincare coordinates on AdS_5 [8]. This will imply that the vacuum state on the static AdS_5 frame is appropriate as the bulk initial spectrum of gravitational waves when we consider these inflationary scenarios.

If we do not adopt the inflationary scenarios, we have to specify the initial spectrum according to the other creation scenario of the FRW brane. However, in any case, once given the initial configuration on a null hypersurface, our method can be applied to solve the evolution of gravitational waves. The final spectrum of the stochastic gravitational waves can be a powerful probe to investigate the existence of extra-dimensions by comparison with the spectrum in the four-dimensional standard cosmology. Therefore, it is interesting to discuss the evolution of gravitational waves with an appropriate initial conditions. This is our future work.

References

[1] L. Randall and R. Sundrum, Phys. Rev. Lett. **83**, 4690 (1999).

[2] P. Binetruy, C. Deffayet, U. Ellwanger and D. Langlois, Phys. Lett. B **477**, 285 (2000).

[3] T. Hiramatsu, K. Koyama and A. Taruya, hys. Lett. B **578**, 269 (2004).

[4] H. Ishihara, Phys. Rev. D **66**, 023513 (2002).

[5] K. Ichiki and K. Nakamura, arXiv:hep-th/0310282.

[6] S. Mukohyama, T. Shiromizu and K. i. Maeda, Phys. Rev. D **62**, 024028 (2000)

[7] T. Kobayashi, H. Kudoh and T. Tanaka, Phys. Rev. D **68**, 044025 (2003).

[8] D. S. Gorbunov, V. A. Rubakov and S. M. Sibiryakov, JHEP **0110**, 015 (2001).

[9] D. Langlois, R. Maartens and D. Wands, Phys. Lett. B **489**, 259 (2000).

Gravitational waves from slightly nonspherical stellar collapse to a black hole

Hideo Iguchi[1], Tomohiro Harada[2], Masaru Shibata[3]

[1] *Department of Physics, Tokyo Institute of Technology, Meguro, Tokyo 152-8550, Japan*
[2] *Astronomy Unit, School of Mathematical Science, Queen Mary, Mile End Road, London E1 4NS, UK*
[3] *Department of Earth Science and Astronomy, Graduate School of Arts and Sciences, University of Tokyo, Meguro, Tokyo 153-8902, Japan*

Abstract

We numerically study gravitational waves from slightly nonspherical stellar collapse to a black hole in the linearized Einstein theory in which we adopt a spherically collapsing star to a black hole as the zeroth-order solution and gravitational waves are computed in the perturbation theory on the spherical background. Here, we report on the results of odd-parity modes perturbations for the collapses of supermassive star.

1 Introduction

In our paper [1], we present a new implementation in the linearized Einstein theory in which the spherical background spacetimes are computed with Hernandez-Misner scheme, and the nonspherical linear perturbations are with the single-null coordinate system. With the Hernandez-Misner scheme, it is possible to compute the spherical stellar collapse to a black hole until almost all the matter collapse into the event horizon. Furthermore, the null coordinate system is well-suited for computation of gravitational waves emitted near the event horizon. We performed simulations for the collapses of a supermassive star and investigate qualitative natures of gravitational waves from the collapses. We show that the waveform depends strongly on the perturbation profile that we initially give. Next section we briefly present the results of our analyses. We skip formulations for evolution equations and explanations about notations. Please refer the article [1] for details.

2 Collapse of a supermassive star and gravitational radiation

2.1 spherical collapse

We adopted a model with $\Gamma_a = (4/3) + 0.00142$ to model a supermassive star of mass $10^6 M_\odot$. In the numerical simulation, we typically take 1000 grid points to cover the supermassive star. For the collapse of model B, with the May-White scheme, apparent horizon was located near the center in a late time of collapse, but soon after the formation, numerical accuracy deteriorates and as a result computation crashed before the event horizon swallowed all the fluid elements. On the other hand, the computation can be continued until the null hypersurface reaches the event horizon with the Hernandez-Misner scheme; i.e., the whole region outside the event horizon is computed numerically. This clearly indicates the robustness of the Hernandez-Misner scheme.

In Fig. 1(a), we display the snapshots of the density profile at selected timesteps. In this simulation, the spacetime settles down to a static one at $\bar{u} \simeq 176780M$. Since the equation of state of supermassive stars is soft, the mass is highly concentrated around the center. In the late stage of the collapse, the increase of the central density is accelerated, and hence the collapse proceeds in a runaway manner. (This makes the simulation without null formulation technically difficult). Figure 1(b) shows the trajectories of mass shells for $\bar{u} \lesssim 176400M$. Each mass shell asymptotically approaches a constant value $> 2m$ because the lapse function decreases to zero. This figure shows that the central region collapses earlier, while the outer envelope accretes slowly after the evolution of the central region is almost frozen. We find that 80%

[1] E-mail:iguchi@th.phys.titech.ac.jp

of the stellar mass is swallowed into the high-redshift region within the time interval $\Delta\bar{u} \sim 15M$. After the inner region collapses, surrounding atmosphere falls into this high-redshift region spending a much longer time $\lesssim 230M$.

2.2 gravitational radiation

For computation of the nonspherical perturbations, a static initial condition for $\bar{\beta}$ should be given. However, the realistic perturbation profile of the initial data set is not clear for the odd-parity perturbation. The purpose of this paper is to study the gravitational waveforms during the formation of a black hole qualitatively. Thus, to investigate the dependence of the gravitational waveforms on the initial perturbation profile, we gave three kinds of the initial data sets as (1) with $\bar{\beta}_{\rm init}$ =const, (2) with $\bar{\beta}_{\rm init} = \exp[-(R/R_{\rm c})^2]$, and (3) with $\bar{\beta}_{\rm init} = \exp[-((R - R_{\rm s})/R_{\rm c})^2]$, where the scale length of the inhomogeneity, $R_{\rm c}$, for the matter perturbation is chosen to be $R_{\rm c} = R_{\rm s}/3$. For (1), the perturbation is uniformly distributed. For (2), the amplitude of the perturbation in the inner region is larger than that in the outer region. For (3), the amplitude of the perturbation is the largest near the stellar surface. In all these cases, the matching is done on the mass-shell near the stellar surface within which 99.7% of the total mass is enclosed.

We show the waveform of quadrupole ($l = 2$) gravitational waves for different initial perturbations (1)-(3) in Fig. 2. In all three cases, the amplitude of the perturbation is normalized so that $q = 2M$. Here, we display the results with $N = 1000$.

As seen in Fig. 2, the gravitational waveform depends strongly on the perturbation profile initially given. For case (2), as seen in Fig. 2(b), gravitational waves of high amplitude are emitted around $\bar{u} \simeq 176510M$, approximately at the same time as the formation of the high-redshift region. The waveform is characterized mainly by a quasinormal mode of the formed black hole. The duration of this major emission is roughly $\sim 50M$, i.e., approximately equal to a few wavelength and/or the damping time of the quasinormal mode. Indeed, the waveform for $\bar{u} \lesssim 176520M$ is well fitted by a damped oscillation of the complex frequency $2M\omega \approx 0.74 + 0.19i$ which agrees with the theoretically predicted value $2M\omega = 0.74734 + 0.17792i$ [2] within a few % error.

For case (1), as seen in Fig. 2(a), gravitational waves look as the linear combination of a quasinormal mode of a black hole and a long-timescale and nonoscillative component (note that the amplitude of gravitational waves does not settle down to zero for a long-time duration $\simeq 230M$ after $\bar{u} \simeq 176510M$). The long-timescale component is produced due both to the perturbation profile initially given and to the nature of the collapse of the background spherical star: In the collapse of supermassive stars, the central region collapses first and subsequently, the outer envelope gradually falls into the black hole spending a long time duration $\simeq 230M$. Since $\bar{\beta}_{\rm init}$ =const, the outer envelope retains a considerable fraction of the perturbation for case (1). As a result, the quasinormal modes are likely to be continuously excited for the duration $\simeq 230M$ during which the matter falls into a black hole. However, the quasinormal modes continuously excited should cancel each other due to the phase cancellation effect [3]. This suppresses the amplitude of gravitational waves and produces a long-timescale component, which results in the suppression of radiated energy

For case (3), in which the matter perturbation is retained mainly near the stellar surface, as seen in Fig. 2(c), the effect of the phase cancellation is more outstanding. In this case, the amplitude of gravitational waves is highly suppressed and the amplitude of the quasinormal mode ringing is much smaller than that of the long-timescale component. We note that the timescale of the long-timescale component is in approximate agreement with the time duration in which the accretion of the surrounding envelope continues.

To explain why the long-timescale and nonoscillative component appears, we artificially superimpose the waveform $\Phi(t)$ obtained for case (2) displayed in Fig. 2(b), which is characterized by quasinormal ringing, with the weight factor $w(t)$ as

$$\int_{-\infty}^{\infty} dt' w(t') \Phi(t - t'), \tag{1}$$

where $w(t)$ is chosen by trial as

$$w(t) = \begin{cases} 8\left(\frac{t}{t_c}\right)\exp\left(-\frac{t}{t_c}\right) + \left(\frac{t}{t_a/4}\right)\left[\left(\frac{t}{t_a/4}\right)^3 + 1\right]^{-1} & \text{for } 0 \le t \le t_a, \\ 0 & \text{for } t < 0, t_a < t, \end{cases} \tag{2}$$

and we set $t_c = 2.95M$ and $t_a = 236M$. The t_c and t_a correspond to the timescales of the collapse of the inner region and of the accretion of the outer envelope, respectively. See Fig. 2(f) for the shape of this function. In the above functional form, the first and second terms imitate the effects of inner collapse and subsequent accretion of the outer envelope, respectively. In Fig. 2(d), we display the result for the superimposed waveform. This result is qualitatively the same as that obtained for case (1) displayed in Fig. 2(a). We note that the long-timescale and nonoscillative component is produced by the long-term superposition of quasinormal ringing including a precursory "burst" wave.

Next we choose another weight factor $w(t)$ defined as

$$w(t) = \begin{cases} \left(\frac{t}{t_a/4}\right)\left[\left(\frac{t}{t_a/4}\right)^3 + 1\right]^{-1} & \text{for } 0 \le t \le t_a, \\ 0 & \text{for } t < 0, t_a < t, \end{cases} \tag{3}$$

and we again set $t_a = 236M$. See Fig. 2(f) for the shape of this function. This functional form imitates the effect of accretion of the outer envelope alone. In Fig. 2(e), we display the result for the superimposed waveform. This result is qualitatively the same as that obtained for case (3) displayed in Fig. 2(c). It should be again emphasized that the superposition not of the pure damped oscillation but of the full waveform for case (2), including the precursory burst wave, produces the long-timescale component. The above consideration confirms our speculation.

References

[1] T. Harada, H. Iguchi and M. Shibata, Phys. Rev. D **68**, 024002 (2003).

[2] S. Chandrasekhar and S. Detweiler, Proc. Roy. Soc. London **344**, 441 (1975).

[3] T. Nakamura and M. Sasaski, Phys. Lett. **106B**, 69 (1981).

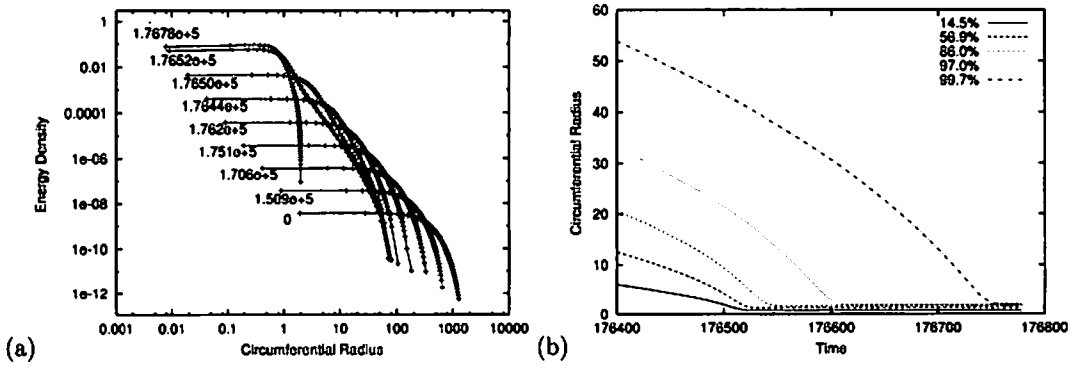

Figure 1: (a) Snapshots of the density profile, (b) trajectories of mass shells and for gravitational collapse with $\Gamma_a = (4/3) + 0.00142$. We extract 1 % of the internal energy from the equilibrium configuration to induce the collapse. In (a), the label for each curve denotes the observer time $\bar{u}$. In (b), the vertical and horizontal axes denote the circumferential radius and observer time, respectively. The labels denote the mass fractions enclosed by mass shells. All the quantities are shown in units of $M = 1$.

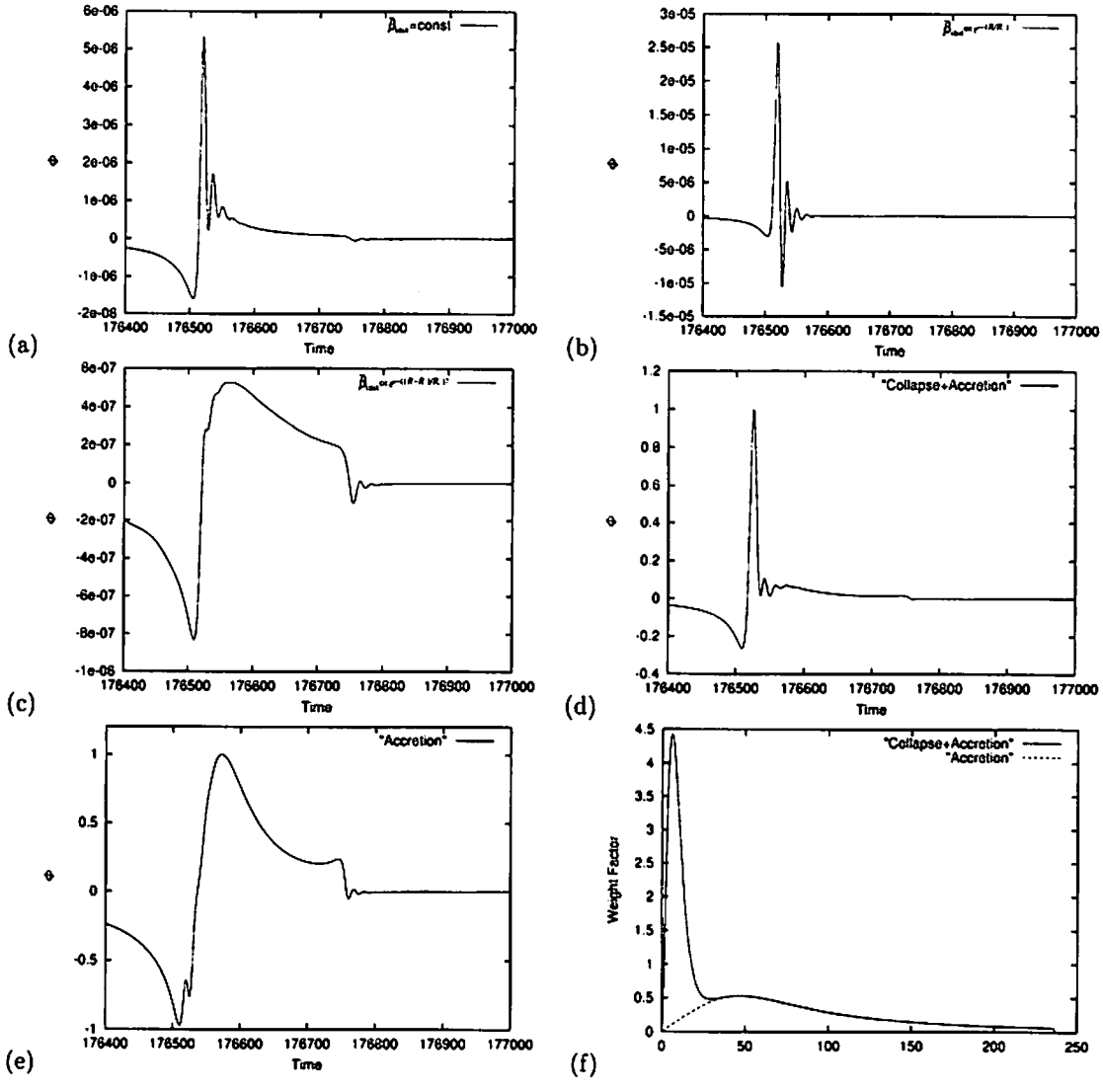

Figure 2: [(a), (b), (c)] Waveform of gravitational waves for $l = 2$ radiated from the collapse with $\Gamma_a = (4/3) + 0.00142$. Gravitational waves are extracted at $R = 2000M$. The momentarily static initial perturbation is given. The amplitude of the perturbation is normalized so that $q = 2M$. [(d), (e)] Waveforms made by superimposing the waveform obtained for case (2). The shape of weight factors are displayed in (f). (d) and (e) show the waveforms for the weight factor labelled "Collapse+Accretion" and for that labelled "Accretion". The waveforms are normalized so that the maximum amplitude is unity. See text for details All the quantities are shown in units of $M = 1$.

Linearized Stability Analysis for Black Brane Backgrounds

Gungwon Kang[1]

School of Physics, Korea Institute for Advanced Study,
207-43 Cheongryangri-dong, Dongdaemun-gu, Seoul 130-012, Korea

Abstract

Classical linearized stability behaviors of various static black brane backgrounds have been summarized. It includes black strings in AdS_5 space, charged black p-brane solutions in the type II supergravity, and the BTZ black string in four-dimensions. The relationship between dynamical stability and local thermodynamic stability - the so-called Gubser-Mitra conjecture - has also been checked for those cases.

1 Introduction

It is well known that the four-dimensional Schwarzschild black hole in Einstein gravity is stable classically under linearized perturbations. Recently, Ishibashi and Kodama [1] have shown that this stable behavior extends to hold for higher dimensional cases. Some static black hole solutions in higher dimensions have hypercylindrical horizons instead of compact hyperspherical ones. Such black holes are called black strings or branes. Gregory and Laflamme [2] have investigated the stability of a black p-brane that is a product of the $(D-p)$-dimensional Schwarzschild black hole with the p-dimensional flat space, and found that such background is unstable as the compactification scale of extended directions becomes larger than the order of the horizon radius - the so-called Gregory-Laflamme instability. Gregory and Laflamme [3] also considered a class of magnetically charged black p-brane solutions for a stringy action containing the NS5-brane of the type II supergravity. For horizons with infinite extent, they have shown that the instability persists to appear but decreases as the charge increases to the extremal value. On the other hand, branes with extremal charge turned out to be stable [4]. Since their discovery of such linearized instability, black strings or branes have been believed to be generically unstable classically under small perturbations except for the cases of extremal or suitably compactified ones, and the Gregory-Laflamme instability has been used to understand physical behaviors of various systems involving black brane configurations as in string theory.

In the context of string theory, however, black branes that Gregory and Laflamme considered are those having magnetic charges with respect to Neveu-Schwarz gauge fields only. Recently a wider class of black string or brane backgrounds has been studied in order to see whether or not the stability behavior drastically changes. In this talk I briefly summarize some of interesting results obtained so far, and report some new result for black $D3$-branes.

2 Linearized stability behaviors of black strings/branes

In order to check the classical stability of a given black string or brane background under small perturbations, we seek any unstable linearized solution that grows in time and is regular spatially outside the event horizon. In the viewpoint of the Kaluza-Klein (KK) dimensional reduction, such unstable solution can be expanded in terms of KK modes along the extra directions characterized by the KK mass parameter m. In particular, s-wave perturbations that are spherically symmetric in the submanifold perpendicular to the space in extra directions are believed to be the strongest instability for most cases. The existence of such s-wave unstable mode can be checked by analyzing the so-called threshold mode that is static and the onset of instability. The number of unknown functions in the analysis can be further reduced by suitably choosing gauge conditions allowed in the system. If the set of coupled linearized equations allows a solution with the non-vanishing threshold KK mass m^* for certain parameter values characterizing the background fields, the corresponding black brane is unstable.

[1] E-mail: gwkang@kias.re.kr

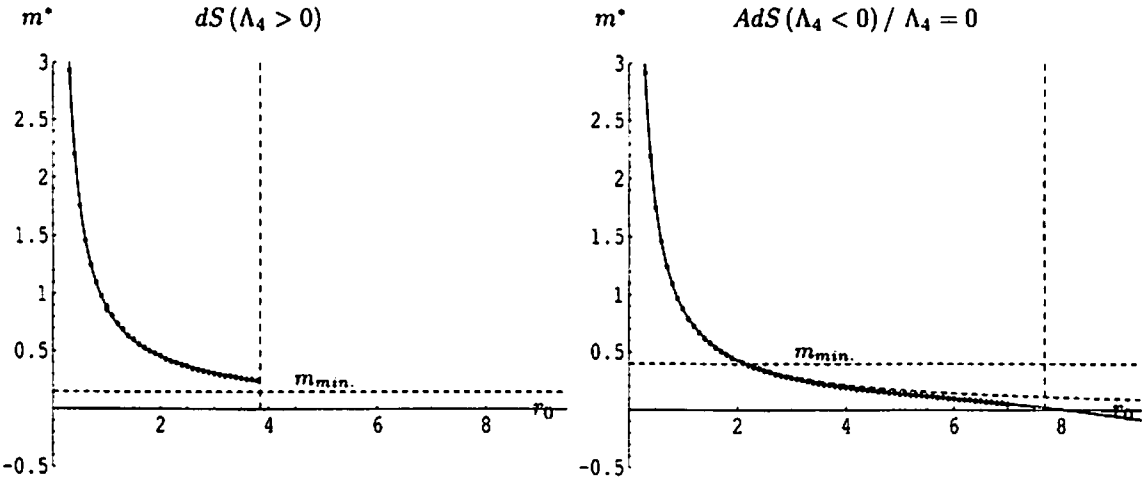

Figure 1: The lefthand side: threshold masses for varying r_0 with given $l_4 = 10$ in the dS_4-Schwarzschild black strings. The vertical dotted line denotes the maximum possible value (Nariai limit), $r_0 \simeq 3.85$. Note that all threshold masses are larger than the lowest value in the KK mass spectrum (*i.e.*, $m_*(r_0 \simeq 3.85) = 0.29 > m_{\rm min.} \simeq 0.15$). The righthand side: For the case of Schwarzschild black strings threshold masses (dotted curve) never cross the horizontal axis ($m_{\rm min} = 0$). For AdS_4-Schwarzschild black strings, however, the threshold mass becomes smaller than the lowest allowed KK mass at a certain value of $r_0(\simeq 2.1)$, implying no unstable solution for r_0 larger than such critical value.

2.1 Black strings in AdS space

In five-dimensional AdS space, one has three types of static black string solutions characterized by the parameter r_0 that is related to the mass density and the four-dimensional cosmological constant $\Lambda_4 = \pm 3/l_4^2$. They are Schwarzschild ($\Lambda_4 = 0$), dS_4-Schwarzschild ($\Lambda_4 > 0$), and AdS_4-Schwarzschild ($\Lambda_4 < 0$) black strings. As shown in Fig. 1 for varying r_0 with a given value of Λ_4 [5], there always exist non-vanishing threshold masses for cases of Schwarzschild [6] and dS_4-Schwarzschild black strings, implying instability as usual. For the case of AdS_4-Schwarzschild black strings, however, the s-wave instability disappears as the horizon radius is larger than the order of the AdS_4 radius.

2.2 Black branes in type II string theory

Recently, Hirayama, Kang, and Lee [7] have analyzed the linearized stability of a wider class of magnetically charged black p-brane solutions for the string gravity action given by

$$\mathrm{I} = \int d^D x \sqrt{-g} \left[R - \frac{1}{2}(\partial\phi)^2 - \frac{1}{2n!} e^{a\phi} F_n^2 \right]. \tag{1}$$

It turns out that the stability of these black p-branes behaves very differently depending on the coupling parameter a. That is, there exists a critical value of the coupling parameter $a_{\rm cr}(D,p)$ to be determined by the full spacetime dimension D and the dimension of the spatial worldvolume $p = D - 2 - n$. The case that Gregory and Laflamme studied is precisely when $a = a_{\rm cr}$. Black branes with horizons of infinite extent in this case are always unstable as explained above, and magnetically charged NS5-branes of the type II supergravity belong to this class. When $0 \leq a < a_{\rm cr}$, black branes with small charge are unstable as usual. As the charge increases, however, the instability decreases and eventually disappears at a certain critical value of the charge density which could be even far from the extremal point. Magnetically charged black D0, F1, D1, D2, D4 branes of the type II string theory belong to this class for instance. When $a > a_{\rm cr}$, on the other hand, the instability persists all the way down to the extremal point. Magnetically charged black D5 and D6 branes are in this case for example. However it is shown that all black branes mentioned above are stable at the extremal point, which might be expected due to the BPS nature of

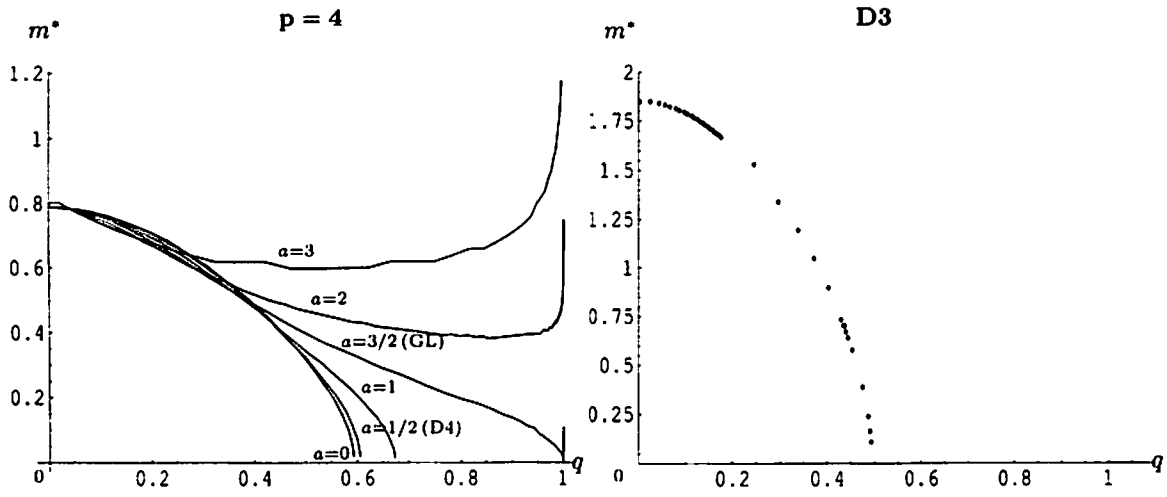

Figure 2: The lefthand side: behavior of threshold masses for black 4-branes in $D = 10$ at various values of a with fixed mass density $M = 2^5$. $m^* \simeq 1.581/r_H \simeq 0.791$ with $r_H = 2$ for uncharged black branes (*i.e.*, $q = 0$). The extremality parameter $q = 1$ for extremal branes. Critical values at which the instability disappears are $q_{cr} \simeq 0.593, 0.606, 0.674$ for cases of $a = 0, 1/2, 1$, respectively. The righthand side: behavior of threshold masses for black $D3$-branes with mass density $M = 5$. The critical value is $q_{cr} \simeq 0.49$.

extremal solutions in string theory. On the lefthand side of Fig. 2 behaviors of threshold masses are illustrated for some black 4-branes as the charge increases.

2.3 Black $D3$-branes

The case of $n = D/2$ (*i.e.*, $a = 0$) with a self-dual n-form field strength $\mathbf{F} = {}^*\mathbf{F}$ in Eq. (1) is treated separately for some technical reasons. This case includes black D3-branes in the type II supergravity for which the AdS/CFT correspondence has been understood very well in string theory. In contrast to previous cases mentioned above, the fluctuation of the dilaton field is completely decoupled and can be set to be zero, but the s-wave perturbation of the field strength should not be frozen in order to be consistent with the metric perturbation as a black brane in this case gets charged. As shown in the numerical results on the righthand side of Fig. 2 for black $D3$-branes, a black brane in this class is unstable when it has small charge density. As the charge density increases for given mass density, however, the instability decreases down to zero at a certain finite value of the charge density, and then the black brane becomes stable all the way down to the extremal point [8, 9].

2.4 Black strings in $D \leq 4$

It is possible to have stationary black string or brane solutions even in four dimensions when a negative cosmological constant is present. Interestingly it is likely that all known stationary black branes in four dimensions are stable. In particular, the case of BTZ black strings has been checked to be stable under small perturbations explicitly [10].

3 Thermodynamic stability behavior

One of naive explanations for the occurrence of the Gregory-Laflamme instability is that a hyperspherical black hole configuration is entropically preferred to the configuration of a black string with the same mass. Recently, Gubser and Mitra [11] refined such entropy comparison argument, and proposed a conjecture that a black brane with a non-compact translational symmetry is classically stable if and only if it is

locally thermodynamically stable. The proof of this Gubser-Mitra (GM) conjecture has been argued for a certain class of black brane systems by Reall [12]. This interesting relationship between the classical dynamical stability and the local thermodynamic stability has been explicitly checked to hold for various black string or brane systems [13, 11, 10, 7, 9, 8]. When the translational symmetry along the horizon is broken, one can see some disagreements for onset points of instability as shown in the stability analysis for AdS_4-Schwarzschild black strings in AdS space [5]. It also should be pointed out that the GM conjecture simply gives the information about when a black string or brane becomes stable or unstable. It does not explain or predict other details of classical stability behaviors [7].

4 Discussion

To conclude, black string or brane backgrounds are not always unstable under small perturbations. Some of them could be stable due to the AdS nature of spacetime or the presence of a charge. Further work is required in order to have deeper understandings of such diverse stability behaviors. Some of interesting open questions are

1. What are special around the critical point in the parameter space at which the stability changes?
2. How does the Gregory-Laflamme instability evolve when it is present?
3. General proof of the stability when the s-wave instability is absent.
4. Is it possible to extend the GM conjecture to the case of static non-uniform black branes?

References

[1] A. Ishibashi and H. Kodama, Prog. Theor. Phys. **110**, 901 (2003) [arXiv:hep-th/0305185].

[2] R. Gregory and R. Laflamme, Phys. Rev. Lett. **70**, (1993) 2837.

[3] R. Gregory and R. Laflamme, Nucl. Phys. B **428**, 399 (1994) [arXiv:hep-th/9404071].

[4] R. Gregory and R. Laflamme, Phys. Rev. D **51**, 305 (1995) [arXiv:hep-th/9410050].

[5] T. Hirayama and G. Kang, Phys. Rev. D **64**, 064010 (2001) [arXiv:hep-th/0104213].

[6] R. Gregory, Class. Quant. Grav. **17**, L125 (2000) [arXiv:hep-th/0004101].

[7] T. Hirayama, G. Kang and Y. Lee, Phys. Rev. D **67**, 024007 (2003) [arXiv:hep-th/0209181].

[8] G. Kang and J. Lee;"Classical Stability of Black D3-branes," preprint KIAS-P03062, hep-th/0401225.

[9] S. S. Gubser and A. Ozakin, JHEP **0305**, 010 (2003) [arXiv:hep-th/0301002].

[10] G. Kang, *Proceedings of the 11th Workshop on General Relativity and Gravitation* held at Tokyo, Japan, Jan. 9-12, 2002, arXiv:hep-th/0202147; G. Kang and Y. Lee;"Lower Dimensional Black Strings/Branes Are Stable," preprint KIAS-P03063 (2003).

[11] S. S. Gubser and I. Mitra, arXiv:hep-th/0009126; JHEP **0108**, 018 (2001) [arXiv:hep-th/0011127].

[12] H. S. Reall, Phys. Rev. D **64**, 044005 (2001) [arXiv:hep-th/0104071].

[13] T. Prestidge, Phys. Rev. D **61** (2000) 084002 [arXiv:hep-th/9907163]; J. P. Gregory and S. F. Ross, Phys. Rev. D **64**, 124006 (2001) [arXiv:hep-th/0106220].

Gravitational Waves from Rotating Black Strings

Sugumi Kanno[1], Jiro Soda[2]

Department of Physics, Kyoto University, Kyoto 606-8501, Japan

Abstract

In the Randall-Sundrum two-brane model (RS1), a Kerr black hole on the brane can be naturally identified with a section of rotating black string. To estimate Kaluza-Klein (KK) corrections on gravitational waves emitted by perturbed rotating black strings, we give the effective Teukolsky equation on the brane which is separable equation and hence numerically manageable. In this process, we derive the master equation for the electric part of the Weyl tensor $E_{\mu\nu}$ which would be also useful to discuss the transition from black strings to localized black holes triggered by Gregory-Laflamme instability.

1 Introduction

The recent progress of superstring theory has provided a new picture of our universe, the so-called braneworld. The evidence of the extra dimensions in this scenario should be explored in the early stage of the universe or the black hole. In particular, gravitational waves are key probes because they can propagate into the bulk freely. Cosmology in this scenario has been investigated intensively. While, gravitational waves from black holes have been less studied so far. In this paper, we shall take a step toward this direction.

Here, we will concentrate on a two-brane model which is proposed by Randall and Sundrum as a simple and phenomenologically interesting model [1]. In this RS1 model, the large black hole on the brane is expected to be black string. Hence, it would be important to clarify how the gravitational waves are generated in the perturbed black string system and how the effects of the extra dimensions come into the observed signal of the gravitational waves. It is desired to have a basic formalism for analyzing gravitational waves generated by perturbed rotating black string.

It is well known in general relativity that the perturbation around Kerr black hole is elegantly treated in the Newman-Penrose formalism. Indeed, Teukolsky derived a separable master equation for the gravitational waves in the Kerr black hole background [2]. The main purpose of this paper is to extend the Teukolsky formalism to the braneworld context and derive the effective Teukolsky equation.

The organization of this paper is as follows. In sec.II, we present the model and demonstrate the necessity of solving $E_{\mu\nu}$ in deriving the effective Teukolsky equation. In sec.III, a perturbed equation and the junction conditions for $E_{\mu\nu}$ are obtained. In sec.IV, we give the explicit solution for $E_{\mu\nu}$ using the gradient expansion method. Then, the effective Teukolsky equation is presented. The final section is devoted to the conclusion.

2 Teukolsky Equation on the Brane

Based on the Newmann-Penrose (NP) null-tetrad formalism, in which the tetrad components of the curvature tensor are the fundamental variables, a master equation for the curvature perturbation was developed by Teukolsky for a Kerr black hole with source. The master equation is called the Teukolsky equation, and it is a wave equation for a null-tetrad component of the Weyl tensor $\Psi_0 = -C_{pqrs}\ell^p m^q \ell^r m^s$ or $\Psi_4 = -C_{pqrs}n^p \bar{m}^q n^r \bar{m}^s$, where C_{pqrs} is the Weyl tensor and $\ell, n, m, \bar{m}$ are null basis in the NP formalism. All information about the gravitational radiation flux at infinity and at the event horizon can be extracted from Ψ_0 and Ψ_4. The Teukolsky equation is constructed by combining the Bianchi identity with the Einstein equations. The Riemann tensor in the Bianchi identity is written in terms of the Weyl

[1] E-mail:sugumi@tap.scphys.kyoto-u.ac.jp
[2] E-mail:jiro@tap.scphys.kyoto-u.ac.jp

tensor and the Ricci tensor. The Ricci tensor is replaced by the matter fields using the Einstein equations. In this way, the Bianchi identity becomes no longer identity and one can get a master equation in which the curvature tensor is the fundamental variable.

It is of interest to consider the four-dimensional effective Teukolsky equation in braneworld to investigate gravitational waves from perturbed rotating black strings. We consider an S_1/Z_2 orbifold space-time with the two branes as the fixed points. In this RS1 model, the two 3-branes are embedded in AdS_5 with the curvature radius ℓ and the brane tensions given by $\sigma_\oplus = 6/(\kappa^2\ell)$ and $\sigma_\ominus = -6/(\kappa^2\ell)$. Our system is described by the action

$$S = \frac{1}{2\kappa^2}\int d^5x\sqrt{-\overset{(5)}{g}}\left(\mathcal{R}+\frac{12}{\ell^2}\right) - \sum_{i=\oplus,\ominus}\sigma_i\int d^4x\sqrt{-g^{i\text{-brane}}} + \sum_{i=\oplus,\ominus}\int d^4x\sqrt{-g^{i\text{-brane}}}\,\mathcal{L}^i_{\text{matter}}\,, \quad (1)$$

where $\overset{(5)}{g}_{\mu\nu}$, $\mathcal{R}$, $g^{i\text{-brane}}_{\mu\nu}$, and κ^2 are the 5-dimensional metric, the 5-dimensional scalar curvature, the induced metric on the i-brane, and the 5-dimensional gravitational constant, respectively.

Since the Bianchi identity is independent of dimensions, what we need is the projected Einstein equations on the brane derived by Shiromizu, Maeda and Sasaki [3]. The first order perturbation of the projected Einstein equation is

$$G_{\mu\nu} = 8\pi G T_{\mu\nu} - \delta E_{\mu\nu}\,, \quad (2)$$

where $8\pi G = \kappa^2/\ell$. If we replace the Ricci curvature in the Bianchi identity to the matter fields and $E_{\mu\nu}$ using Eq. (2), then the projected Teukolsky equation on the brane is written in the following form,

$$\begin{aligned}
&[(\Delta+3\gamma-\gamma^*+4\mu+\mu^*)(D+4\epsilon-\rho)-(\delta^*-\tau^*+\beta^*+3\alpha+4\pi)(\delta-\tau+4\beta)-3\Psi_2]\delta\Psi_4\\
&\quad=\frac{1}{2}(\Delta+3\gamma-\gamma^*+4\mu+\mu^*)\\
&\quad\times[(\delta^*-2\tau^*+2\alpha)(8\pi G T_{nm^*}-\delta E_{nm^*})-(\Delta+2\gamma-2\gamma^*+\mu^*)(8\pi G T_{m^*m^*}-\delta E_{m^*m^*})]\\
&\quad+\frac{1}{2}(\delta^*-\tau^*+\beta^*+3\alpha+4\pi)\\
&\quad\times[(\Delta+2\gamma+2\mu^*)(8\pi G T_{nm^*}-\delta E_{nm^*})-(\delta^*-\tau^*+2\beta^*+2\alpha)(8\pi G T_{nn}-\delta E_{nn})]\,. \quad (3)
\end{aligned}$$

Here our notation follows that of [2]. We see the effects of a fifth dimension, $\delta E_{\mu\nu}$, is described as a source term in the projected Teukolsky equation. It should be stressed that the projected Teukolsky equation on the brane Eq. (3) is not a closed system yet. One must solve the gravitational field in the bulk to obtain $\delta E_{\mu\nu}$.

3 Master Equation for $\delta E_{\mu\nu}$

Starting with the 5-dimensional Bianchi identities, we can derive the perturbed equation for $\delta E_{\mu\nu}$. The background we consider is a Ricci flat string without source ($T_{\mu\nu}=0$) whose metric is written as

$$ds^2 = dy^2 + e^{-2\frac{y}{\ell}}g_{\mu\nu}(x^\mu)dx^\mu dx^\nu\,, \quad (4)$$

where $g_{\mu\nu}(x^\mu)$ is supposed to be the Ricci flat metric. The equation of motion for $\delta E_{\mu\nu}$ in the bulk is found as

$$\left(\partial_y^2-\frac{4}{\ell}\partial_y+\frac{4}{\ell^2}\right)\delta E_{\mu\nu} \;=\; -e^{2\frac{y}{\ell}}\hat{\mathcal{L}}_{\mu\nu}{}^{\alpha\beta}\delta E_{\alpha\beta} \equiv -e^{2\frac{y}{\ell}}\hat{\mathcal{L}}\delta E_{\mu\nu}\,, \quad (5)$$

where $\hat{\mathcal{L}}_{\mu\nu}{}^{\alpha\beta}$ stands for the Lichnerowicz operator,

$$\hat{\mathcal{L}}_{\mu\nu}{}^{\alpha\beta} = \Box\delta^\alpha_\mu\delta^\beta_\nu + 2R_\mu{}^\alpha{}_\nu{}^\beta\,. \quad (6)$$

Here, the covariant derivative and the Riemann tensor are constructed from $g_{\mu\nu}(x)$.

On the other hand, the junction conditions on each branes become

$$e^{2\frac{Y}{\ell}}\left[e^{-2\frac{Y}{\ell}}\delta E_{\mu\nu}\right]_{,Y}\Big|_{y=0} = -\frac{\kappa^2}{6}\overset{\oplus}{T}_{|\mu\nu} - \frac{\kappa^2}{2}\hat{\mathcal{L}}_{\mu\nu}{}^{\alpha\beta}\left(\overset{\oplus}{T}_{\alpha\beta} - \frac{1}{3}g_{\alpha\beta}\overset{\oplus}{T}\right) , \tag{7}$$

$$e^{2\frac{Y}{\ell}}\left[e^{-2\frac{Y}{\ell}}\delta E_{\mu\nu}\right]_{,Y}\Big|_{y=d} = \frac{\kappa^2}{6}\overset{\ominus}{T}_{|\mu\nu} + \frac{\kappa^2}{2}\hat{\mathcal{L}}_{\mu\nu}{}^{\alpha\beta}\left(\overset{\ominus}{T}_{\alpha\beta} - \frac{1}{3}g_{\alpha\beta}\overset{\ominus}{T}\right) . \tag{8}$$

Let $\overset{\oplus}{\phi}(x)$ and $\overset{\ominus}{\phi}(x)$ be the scalar fields on each branes which satisfy

$$\Box\overset{\oplus}{\phi} = \frac{\kappa^2}{6}\overset{\oplus}{T} , \quad \Box\overset{\ominus}{\phi} = \frac{\kappa^2}{6}\overset{\ominus}{T} , \tag{9}$$

respectively. In the Ricci flat space-time, the identity

$$(\Box\phi)_{|\mu\nu} = \hat{\mathcal{L}}_{\mu\nu}{}^{\alpha\beta}\left(\phi_{|\alpha\beta}\right) \tag{10}$$

holds. Thus, Eqs.(7) and (8) can be rewritten as

$$e^{2\frac{Y}{\ell}}\left[e^{-2\frac{Y}{\ell}}\delta E_{\mu\nu}\right]_{,Y}\Big|_{y=0} = -\hat{\mathcal{L}}\left(\overset{\oplus}{\phi}_{|\mu\nu} - g_{\mu\nu}\Box\overset{\oplus}{\phi}\right) - \frac{\kappa^2}{2}\hat{\mathcal{L}}\overset{\oplus}{T}_{\mu\nu} \equiv \hat{\mathcal{L}}\overset{\oplus}{S}_{\mu\nu} , \tag{11}$$

$$e^{2\frac{Y}{\ell}}\left[e^{-2\frac{Y}{\ell}}\delta E_{\mu\nu}\right]_{,Y}\Big|_{y=d} = \hat{\mathcal{L}}\left(\overset{\ominus}{\phi}_{|\alpha\beta} - g_{\mu\nu}\Box\overset{\ominus}{\phi}\right) + \frac{\kappa^2}{2}\hat{\mathcal{L}}\overset{\ominus}{T}_{\mu\nu} \equiv -\hat{\mathcal{L}}\overset{\ominus}{S}_{\mu\nu} . \tag{12}$$

The scalar fields $\overset{\oplus}{\phi}$ and $\overset{\ominus}{\phi}$ can be interpreted as the brane fluctuation modes.

4 Effective Teukolsky Equation

Now, we solve Eq.(5) under the boundary conditions (11) and (12) using the gradient expansion method.

4.1 Gradient Expansion Method

It is known that the Gregory-Laflamme instability occurs if the curvature length scale of the black hole L is less than the Compton wavelength of KK modes $\sim \ell\exp(d/\ell)$. As we are interested in the stable rotating black string, we assume

$$\epsilon = \left(\frac{\ell}{L}\right)^2 \ll 1 . \tag{13}$$

This means that the curvature on the brane can be neglected compared with the derivative with respect to y. Our iteration scheme consists in writing the Weyl tensor $E_{\mu\nu}$ in the order of ϵ [4]. Hence, we will seek the Weyl tensor as a perturbative series

$$\delta E_{\mu\nu}(y,x^\mu) = \overset{(1)}{\delta E}_{\mu\nu}(y,x^\mu) + \overset{(2)}{\delta E}_{\mu\nu}(y,x^\mu) + \overset{(3)}{\delta E}_{\mu\nu}(y,x^\mu) + \cdots . \tag{14}$$

Substituting this Eq.(14) into Eq.(5), we can obtain $\delta E_{\mu\nu}$ perturbatively.

4.2 Effective Teukolsky Equation

As a result, Teukolsky equation takes the following form

$$\hat{P}\delta\Psi_4 = \hat{Q}\left(8\pi G T_{nm\bullet} - \delta E_{nm\bullet}\right) + \cdots , \tag{15}$$

where $\hat{P}$ and $\hat{Q}$ are operators defined in (3). What we needed is $\delta E_{\mu\nu}$ in the above equation. We can write down $\delta E_{\mu\nu}$ on the brane up to the second order as [5]

$$\begin{aligned}\delta E_{\mu\nu}\Big|_{y=0} &= \frac{2}{\ell}\frac{\Omega^2}{1-\Omega^2}\left[\overset{\oplus}{S}_{\mu\nu} + \Omega^2\overset{\ominus}{S}_{\mu\nu}\right] \\ &\quad + \left[\frac{1}{2} + \frac{d}{\ell}\frac{1}{\Omega^2-1}\right]\frac{\ell}{1-\Omega^2}\left[\hat{\mathcal{L}}\overset{\oplus}{S}_{\mu\nu} + \Omega^4\hat{\mathcal{L}}\overset{\ominus}{S}_{\mu\nu}\right] + \frac{\ell}{4}\left[\hat{\mathcal{L}}\overset{\oplus}{S}_{\mu\nu} + \Omega^2\hat{\mathcal{L}}\overset{\ominus}{S}_{\mu\nu}\right] ,\end{aligned} \tag{16}$$

where

$$\overset{\oplus}{S}_{\mu\nu} = -\overset{\oplus}{\phi}_{|\mu\nu} + g_{\mu\nu}\Box\overset{\oplus}{\phi} - \frac{\kappa^2}{2}\overset{\oplus}{T}_{\mu\nu} , \tag{17}$$

$$\overset{\ominus}{S}_{\mu\nu} = -\overset{\ominus}{\phi}_{|\mu\nu} + g_{\mu\nu}\Box\overset{\ominus}{\phi} - \frac{\kappa^2}{2}\overset{\ominus}{T}_{\mu\nu} . \tag{18}$$

Substituting this $\delta E_{\mu\nu}$ into (3), we get the effective Teukolsky equation on the brane. From Eq. (16), we see KK corrections give extra sources to Teukolsky equation. To obtain quantitative results, we must resort to numerical calculations. It should be stressed that the effective Teukolsky equation is separable like as the conventional Teukolsky equation. Therefore, it is suitable for numerical treatment.

Notice that our result in this section assume only Ricci flatness. If we do not care about separability, we can study the gravitational waves in the general Ricci flat background. Moreover, we can analyze other types of waves using $\delta E_{\mu\nu}$. As $\delta E_{\mu\nu}$ has 5 degrees of freedom which corresponds to the degrees of freedom of the bulk gravitational waves, one expect the scalar gravitational waves and vector gravitational waves. Without KK effects, no vector gravitational waves exist and the scalar gravitational waves can be described as the Brans-Dicke scalar waves. However, KK effects produce new effects which might be observable.

5 Conclusion

We formulated the perturbative formalism around the Ricci flat two-brane system. In particular, the master equation for $\delta E_{\mu\nu}$ is derived. The gradient expansion method is utilized to get a series solution. This gives the closed system of equations which we call the effective Teukolsky equations in the case of type D induced metric on the brane. This can be used for estimating the Kaluza-Klein corrections on the gravitational waves emitted from the perturbed rotating black string. Our effective Teukolsky equation is completely separable, hence the numerical scheme can be developed in a similar manner as was done in the case of 4-dimensional Teukolsky equation.

Acknowledgements
This work was supported in part by Grant-in-Aid for Scientific Research Fund of the Ministry of Education, Science and Culture of Japan No. 155476 (SK) and No.14540258 (JS) and also by a Grant-in-Aid for the 21st Century COE "Center for Diversity and Universality in Physics".

References

[1] L. Randall and R. Sundrum, Phys. Rev. Lett. **83**, 4690 (1999) [arXiv:hep-th/9906064]; *ibid.*, 3370 (1999) [arXiv:hep-th/9905221].

[2] S. A. Teukolsky, Astrophys. J. **185**, 635 (1973).

[3] T. Shiromizu, K. Maeda and M. Sasaki, Phys. Rev. D **62**, 024012 (2000) [arXiv:gr-qc/9910076].

[4] S. Kanno and J. Soda, Phys. Rev. D **66**, 083506 (2002) [arXiv:hep-th/0207029];
ibid., 043526 (2002) [arXiv:hep-th/0205188];
S. Kanno and J. Soda, Astrophys. Space Sci., **283**, 481 (2003), [arXiv:gr-qc/0209087];
J. Soda and S. Kanno, *ibid.*, 639 (2003) [arXiv:gr-qc/0209086];
S. Kanno and J. Soda, arXiv:hep-th/0303203.

[5] S. Kanno and J. Soda, arXiv:gr-qc/0311074.

Dynamically unstable modes in differentially rotating stars

Shigeyuki Karino[1], Yoshiharu Eriguchi[2]

Department of Earth Science and Astronomy,
Graduate school of Arts and Sciences,
University of Tokyo
Komaba, Meguro, Tokyo 153-8902, JAPAN

Abstract

The results of linear stability analysis about dynamical instabilities of rapidly and differentially rotating Newtonian polytropes are presented. We found that when we consider strong differential rotations, the critical limit where dynamical instability sets in will decrease considerably. Additionally, when the effect of differential rotation is so large, the star will suffer from the instability, even if the stellar rotation rate is small.

It is well known that the rotating self-gravitating fluids will be unstable when the rotation rates are sufficiently large. This rotational instabilities of stars can be divided into two types; secular instability and dynamical instability. The secular instability is the instability which grows in the time-scale of the energy dissipation mechanisms, while the dynamical instability grows in the dynamical time-scale of the system. In this study, we are interested in the dynamical instability of rotating stars. For simple models called the Maclaurin spheroids (the rigidly rotating uniform density stellar models), the critical rotation rates where those instabilities will appear have been studied. Namely, stars will be secularly unstable (due to gravitational waves) when $T/|W| \gtrsim 0.14$, and also they will be dynamically unstable when $T/|W| \gtrsim 0.27$. Here, a parameter $T/|W|$ is the ratio between the rotational kinetic energy T, and the potential energy W, and we often use this parameter to describe the stellar rotation rates.

In actual situations, however, it is difficult to approximate real objects by using such simple models. For example, typical main targets of the study of rotational instabilities are nascent compact stars since they will be accompanied with rapid rotations, but such young compact stars will have soft equations of state and non-uniform rotation laws. Therefore, it is unknown whether the stability criteria given from classical analysis can be applied in the cases of realistic young compact objects. In fact, recently some authors have claimed that in differentially rotating stars, the stability criteria will be changed significantly. Hence, in order to confirm the stability of such differentially rotating stars, we systematically investigate the secular and dynamical stability of differentially rotating Newtonian polytropes by using linear stability analysis method.

In this study, as the stellar models, we assume axisymmetric stars in the framework of Newtonian gravity. We use polytropic relations as the equations of state. When we consider the linear perturbations, we assume the adiabatic perturbations. The perturbed quantities (say, f) can be expanded as $\delta f \propto \exp(-i\sigma t + im\varphi)$. Here, we only investigate about the oscillation modes which have $m = 2$. By solving the linearized equations of perturbed fluid numerically, we can obtain the eigenvalue of the mode, σ. By using this σ, we can know the dynamic stability of rotating stars. That is, if the eigenvalue, σ, has finite imaginary part, such a mode will grow exponentially, hence we can label it "unstable".

From the linear analysis, we found a lot of new properties of rotational instabilities in differentially rotating stars. In the investigation of the stability of differentially rotating compressible stars, we show that the stability will strongly depend on the degree of the differential rotation. When we consider sufficiently steep rotation laws, the critical rotation rate where the dynamical instability sets in will decrease considerably. That is, under the effects of differential rotation, stars will be dynamically unstable even when $T/|W| < 0.27$ (see, Karino & Eriguchi 2003, Shibata, Karino & Eriguchi 2002).

The numerical results are shown in the table. In this table, the critical limit of $T/|W|$ where dynamical instability starts to appear in differentially rotating polytropes with $N = 1.0$ and 1.5. Here, we use the

[1] E-mail:karino@provence.c.u-tokyo.ac.jp
[2] E-mail:eriguchi@esa.c.u-tokyo.ac.jp

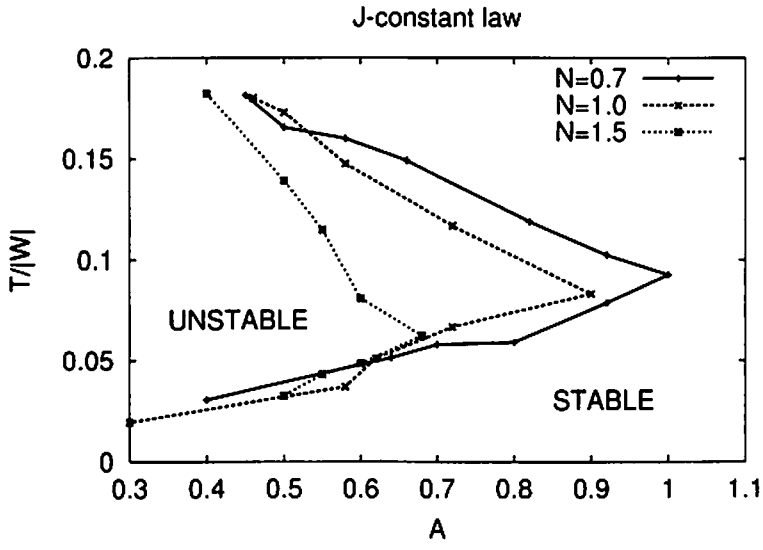

Figure 1: The unstable parameter region. The stellar model is $N = 0.7, 1.0$, and 1.5 polytrope. The central-left region bounded by lines denote the newly found unstable zone.

differential rotation law: $\Omega \propto A^2/(R^2 + A^2)$, where R is the distance from the rotation axis and A is the parameter to decide the effects of differential rotation (we call this rotation law as the "J-constant law"). A model with small value of A corresponds to a star with steep differential rotation in this case. As shown in the table, when we consider strong differential rotations (i.e. small A), the critical limit of dynamical instability tends to decrease for both polytropic indices. In the extreme case, even if $T/|W| \approx 0.2$, the differentially rotating star will suffer from dynamical instability.

Critical Limit of Dynamical Instability

$N = 1.0$		$N = 1.5$	
A	$T/\|W\|_{\rm crit}$	A	$T/\|W\|_{\rm crit}$
1.00	2.646E-01	0.75	2.480E-01
0.90	2.553E-01	0.70	2.421E-01
0.80	2.456E-01	0.60	2.263E-01
0.70	2.350E-01	0.55	2.176E-01
0.65	2.287E-01	0.50	2.100E-01
0.60	2.218E-01	0.45	2.004E-01
0.55	2.135E-01		
0.50	2.065E-01		

Additionally, we found that when the degrees of the differential rotations is significantly large, new branches of dynamical instabilities will appear, even when the stellar rotation rates are small. According to our computations, when we consider enough strong differential rotations, stars with small rotation rates as $T/|W| \approx 0.05$ will be also unstable dynamically. Rotational instabilities appear in slowly rotating stars have been known in restricted cases as like the Papaloizou-Pringle instability or the shear instability, but the present instability will be different type with them. These results about the dynamical stability of rotating stars strongly suggest that the classical critical limits where instabilities appear can not be applied in realistic stars no longer (see, Shibata, Karino & Eriguchi 2003).

In the figure, the critical boundary of dynamical instability which we found is plotted in A vs $T/|W|$ plane, when we choose $N = 0.7, 1.0$ and 1.5 as the polytropic index. The triangular region where extends from the left to the center corresponds to the previous unstable region. This newly found dynamically

unstable parameter region which has a vertex at $(A, T/|W|) \simeq (0.9, 0.08)$ for $N = 1.0$ case, extends on quite broad region when the degree of differential rotation gets stronger. Particularly when $A \simeq 0.4$, almost regions become dynamically unstable independently from the rotation rate of the star. Also it is clear that the stability against the present mode depends on the equations of state strongly, and it is shown that the mode becomes unstable in broader parameter region when the equations of state is stiffer, i.e. when the value of N is smaller. Especially in the case of $N = 0.7$, the mode tends to become unstable even if the degree of differential rotation is relatively large ($A \approx 1.0$).

Those rotational instabilities will be important in the actual astronomical situations. For example, rapidly rotating objects will lose their angular momentum and make their spins down in consequence of the growth of the dynamical instability. This process will affect drastically in the spin evolutions of nascent objects, as like nascent neutron stars, young stellar cores, and so on. Also when we consider compact stars as the target of the instabilities, the growth of instabilities will cause the quasi-periodic gravitational wave emissions, therefore, it is also important to investigate the stability properties from the standpoint of gravitational wave astronomy.

In this presentation, we suggest that the rotational instability will occur even if the stellar rotation rate is much smaller than the level we have believed. This conclusion means that rotational instabilities will be much more important in realistic astrophysical events than we thought.

References

[1] S. Karino and Y. Eriguchi, ApJ, 592, 1119 (2003).

[2] M. Shibata, S. Karino, and Y. Eriguchi, MNRAS, 334L, 27 (2002).

[3] M. Shibata, S. Karino, and Y. Eriguchi, MNRAS, 343, 619 (2003).

Algebraic approach to binary gravitational lens

Masumi Kasai[1]

Faculty of Science and Technology, Hirosaki University
Bunkyo-cho 3, Hirosaki, Aomori 036-8561, Japan

Abstract

An algebraic approach to the binary gravitational lens system is shown. It is shown that the lens equation for the binary lens, which is a set of coupled nonlinear equation, is reduced to a single, real quintic equation. Some useful information on the number and the positions of the images are also given.

1 Introduction

In this paper, we show an algebraic, non-numerical approach towards binary gravitational lens system.

1.1 Why binary lens?

There are many binary objects in the universe. For example, there are many binary stars. From the viewpoint of the gravitational radiation research, study of compact object binaries of neutron stars, black holes, etc., has been investigated. Furthermore, recent searches for extra-solar planets have discovered more than a hundred planets. Most of them can be regarded as the binary system of a star and a giant planet. These binary systems are likely to behave as the gravitational lenses.

1.2 Why algebraic approach?

Analytical study of the gravitational lensing has been limited to the cases of a few, simple lens models, e.g., the spherically symmetric lenses. We need numerical approach for more generic lens models. Even if the numerical study is necessary in such cases, if would be nice if we can have some, hopefully useful information on the lensed image properties, before performing numerical computations. We will show an algebraic (non numerical) approach can tell such useful information on the properties of the binary gravitational lens system.

1.3 Previous works

The lens equation for the binary system is a set of coupled, non-linear equations for the image position $\vec{\theta} = (x, y)$. Witt[1] has shown the lens equation reduces to a single, quintic equation for a complex variable $z \equiv x + i\,y$ with complex coefficients. It follows that the maximum number of the solutions, i.e., the number of images is 5. However, the complex formalism does not give other informations such as the condition of getting 3 images, the positions of the images, and so on.

Recently, Asada[2] and Asada et al.[3] have shown that the binary lens equation can reduce to a single, real polynomial equation. Asada's formulation is based on taking the polar coordinates. Therefore, we have to be a little bit careful in treating the lens equation. Imagine we have the lens equation as a single polynomial equation of the angular coordinates $\varphi \equiv y/x$. The number of the solution for φ does not always equal to the number of the images. (Consider the case that the images are on the same straight line crossing the origin.)

1.4 The purpose of this paper

Inspired by Asada's work, we develop a systematic, algebraic approach to derive a single, real equation for the binary lens, using the usual Cartesian coordinates. We will give some useful information on the number and positions of the lensed images, before performing numerical computations.

[1] E-mail: kasai@phys.hirosaki-u.ac.jp

2 The binary lens

2.1 The lens equation

After a suitable normalization, the lens equation for the binary lens system is

$$\vec{\beta} = \vec{\theta} - \left((1-\nu)\frac{\vec{\theta}}{|\vec{\theta}|^2} + \nu \frac{\vec{\theta} - \vec{\ell}}{|\vec{\theta} - \vec{\ell}|^2} \right), \tag{1}$$

where $\vec{\beta} = (\beta_x, \beta_y)$ and $\vec{\theta} = (x, y)$ represent the position of the source and the image, respectively, $\nu \equiv M_2/(M_1 + M_2)$ is the relative mass ratio, and $\vec{\ell} = (\ell, 0)$ is the lens separation. If we wright down

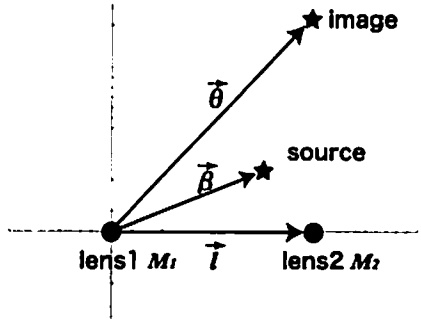

Figure 1: The binary gravitational lens system.

each components explicitly,

$$\beta_x = x - \left((1-\nu)\frac{x}{x^2+y^2} + \nu \frac{x-\ell}{(x-\ell)^2+y^2} \right), \tag{2}$$

$$\beta_y = y - \left((1-\nu)\frac{y}{x^2+y^2} + \nu \frac{y}{(x-\ell)^2+y^2} \right). \tag{3}$$

It is a set of non-linearly coupled equations for x and y, with given lens parameters β_x, β_y, ν and ℓ. Usual technique of eliminating one variable, e.g., x, seems hopeless.

2.2 The lens equation as a set of polynomial equations

We can regard the the lens equation as a set of two polynomial equations,

$$\begin{aligned} f_5(x^5, y^4, ...) &= 0 \qquad \text{quintic eq. of } x \\ f_4(x^4, y^5, ...) &= 0 \qquad \text{quartic eq. of } x \end{aligned} \tag{4}$$

Then the following theorem of algebra can be applied: the condition for the two equations $f_5(x^5, ...) = 0, f_4(x^4, ...) = 0$ to have common roots is that the resultant vanishes:

$$\texttt{Resultant}\,[f_5(x^5, y^4, ...),\ f_4(x^4, y^5, ...),\ \texttt{x}] = 0. \tag{5}$$

After a straightforward calculation and a suitable factorization, we obtain the quintic equation of y;

$$F_5(y) \equiv \sum_{i=0}^{5} a_i\, y^i = 0. \tag{6}$$

The coefficients a_i are completely written in terms of the lens parameters β_x, β_y, ν and ℓ. The explicit form of a_i will be given elsewhere[4].

Once the roots for y are given, the corresponding solutions for x are obtained by using the Euclidean algorithm for polynomials:

$$\begin{aligned} f_5(x^5,...) &= q_3(x)\, f_4(x^4,...) + f_3(x^3,...), \\ f_4(x^4,...) &= q_2(x)\, f_3(x^3,...) + f_2(x^2,...), \\ f_3(x^3,...) &= q_1(x)\, f_2(x^2,...) + f_1(x). \end{aligned}$$

In the above way, $f_5(x^5,...) = 0$, $f_4(x^4,...) = 0$ reduce to $f_1(x) = A(y)\,x + B(y) = 0$, from which we have $x = -B(y)/A(y)$.

2.3 How many images?

It is straightforward that the real quintic equation $F_5(y) = 0$ has either 5, 3, or 1 real roots, depending on the signature of the discriminant D_5. We obtain 5 images for $D_5 > 0$, and 3 images for $D_5 < 0$. (The single root case does not appear in our lens model.) Moreover, $D_5 = 0$ directly corresponds to the caustics, which is explicitly written in terms of the source position β_x and β_y.

2.4 Where are the images?

Since the lens equation is now the quintic equation $F_5(y) = 0$, is not in general solved analytically. However, without performing numerical computations, we can obtain a bit useful information on the position of the images.

Let us consider the case $\beta_y > 0$. (From Figure.1, it is sufficient to consider the "upper half plane" case.) Next, check the sign of the coefficients a_i of $F_5(y)$. Then Descartes' sign rule in algebra tells the number of the positive roots for $F_5(y) = 0$. The result is that the we have only one positive root. It should be emphasized that this result does not depend on the values of the lens parameters.

3 Summary

We have shown a systematic, algebraic approach to binary gravitational lens. The non-linearly coupled lens equations reduce to the single polynomial equation. The discriminant D_5 of the equation determines the number of the lensed images. In particular, $D_5 = 0$ directly corresponds to the caustics. Concerning the image positions, Descartes' sign rule tells that only one image appears in the same side as of the source, with respect to the lens symmetry axis.

Finally, it should be mentioned that the algebraic approach we showed here is quite general and applicable to other generic lens models.

References

[1] H. J. Witt, Astron. Astrophys. **236** (1990), 311.

[2] H. Asada, Astron. Astrophys. **390** (2002), L11.

[3] H. Asada, T. Kasai, and M. Kasai, Prog. Theor. Phys. **108** (2002), 1031.

[4] H. Asada, T. Kasai, and M. Kasai, (2004), in preparation.

Dynamical D-branes in closed string field theory

Shinpei Kobayashi[1]

Graduate School of Human and Environment Studies, Kyoto University, Kyoto 606-8501, Japan

Tsuguhiko Asakawa [2]

Yukawa Institute for Theoretical Physics, Kyoto University, Kyoto 606-8502, Japan

So Matsuura [3]

Theoretical Physics Laboratory, RIKEN (The Institute of Physical and Chemical Research), Wako, Saitama 351-0198, Japan

Abstract

We consider a closed string field theory with an arbitrary matter current as a source of the closed string field. We find that the source must satisfy a constraint equation as a consequence of the BRST invariance of the theory. We see that it corresponds to the covariant conservation law for the matter current, and the equation of motion together with this constraint equation determines the classical behavior of both the closed string field and the matter. We then consider the boundary state (D-brane) as an example of a source. We see that the ordinary boundary state cannot be a source of the closed string field when the string coupling g turns on. By perturbative expansion, we derive a recursion relation which represents the bulk backreaction and the D-brane recoil. We also make a comment on the rolling tachyon boundary state. This proceeding is based on [1].

1 Introduction

Throughout the recent studies of the (super)string theories, we have obtained deep insights into the off-shell structure of the string theories. Especially, D-branes have played extremely important roles. For example, it was conjectured that unstable D-brane systems decay into the vacuum or lower dimensional D-branes through the tachyon condensation [2], and analysis using various methods supports the correctness of this conjecture. The rolling tachyon solution was also proposed, which is a time dependent background representing the rolling down of the open string tachyon field towards the bottom of its potential [3].

Another important feature of D-brane is that it is thought to be a soliton of closed string theory. This is well understood by expressing the D-brane as the boundary state [4][5]. D-brane is originally defined as an object on which open strings can attach their end points. The corresponding boundary condition is determined so that it does not break the conformal symmetry of the world-sheet with the disk topology (the boundary CFT), and this symmetry enable us to transform the boundary condition for open strings into that for closed stings. The obtained state $|B\rangle$ is the boundary state which satisfies the boundary condition in terms of closed strings. Then, it can be viewed as a source in closed string theory [4][5]. Namely, adding a boundary to the world-sheet is equivalent to adding a boundary state to the equation of motion for the closed string field as

$$Q|\Phi\rangle = -|B\rangle, \tag{1}$$

where Q is the BRST charge of the closed string. The nilpotency $Q^2 = 0$ implies that the admissible boundary states are characterized by the condition,

$$Q|B\rangle = 0, \tag{2}$$

[1]E-mail:shinpei@phys.h.kyoto-u.ac.jp
[2]E-mail:asakawa@yukawa.kyoto-u.ac.jp
[3]E-mail:matsu@riken.jp

that is, BRST invariant boundary states give conformal backgrounds.

Open string dynamics on the D-brane can also be expressed by inserting an appropriate boundary interaction in the boundary state and they correctly describes the tachyon condensation which is mentioned above (see e.g. [6]). The rolling tachyon background can be also described in the same way [3]. Through the study of this rolling tachyon boundary state, it is found that the final state of this decay is not the closed string vacuum but a state with finite energy density and no pressure, which is called the tachyon matter [7]. However, in spite of many studies on the rolling tachyon and the tachyon matter [8, 9, 10], the relation between the closed string emission from the decaying D-brane and the tachyon condensation is not clear yet. This would be because the effect of closed string interactions are not taken into account in (1).

One of our main purposes is to give a general formalism to deal with D-branes in a closed string field theory (closed SFT). In other words, we will see what happens to (1) by turning on the closed string coupling g. Here, we regard the boundary state as a matter current which couples to the closed string field. We first give a general formalism to determine the classical behavior of the closed string field when there is an arbitrary matter current which couples to the closed string field. Starting with adding a source term to the action of a closed SFT, we find a constraint equation that the source must satisfy and we see that the constraint equation plays an important role in this formalism. Although we adopt HIKKO's closed SFT [11] as an example of a closed SFT because of its simplicity, we emphasize here that our argument does not depend on the detail of the theory but applicable to any kind of closed SFTs that is consistent at least at the tree level in the sense of BRST invariance, because our argument relies only on the BRST invariance of the theory in the tree level. One of our most interesting results is that the ordinary boundary state does not satisfy the constraint equation but must be modified so that it can be a consistent source of the closed string. We see that it is quite natural to expect that the modification is caused by open string excitations on the D-brane, which give dynamical degrees of freedom to the source.

2 Source Term in Closed String Field Theory

We start with the action of HIKKO's closed SFT [11], which is invariant under the BRST transformation and gauge transformation. We then add to it a source term as

$$S = \frac{1}{2}\Phi \cdot Q\Phi + \frac{g}{3}\Phi \cdot \Phi * \Phi + \Phi \cdot J. \tag{3}$$

Here J is considered to be some (yet unknown) matter current.

Applying the variational principle to the action (3), the equation of motion of this system is obtained:

$$Q\Phi + g\Phi * \Phi + J = 0. \tag{4}$$

From this equation, although the BRST transformation for the current J has not been defined, we can symbolically rewrite this as

$$\delta_B J \equiv QJ + 2g\Phi * J = 0, \tag{5}$$

which corresponds to the covariant conservation law for the current.

Furthermore, using the definition of the BRST transformation

$$\delta_B \Phi = Q\Phi + g\Phi * \Phi, \tag{6}$$

and the fact that (4) can be written as $\delta_B \Phi = -J$, we obtain (4) as the consequence of the nilpotency of the BRST transformation.

3 Boundary State as A Source

Then we restrict our attention to boundary states and regard them as sources for the closed string field. To be more precise, we consider the boundary state $|B_p\rangle$ which describes a (bosonic) Dp-brane, extended in x^α ($\alpha = 0, \cdots, p$) direction and sitting at $x^i = 0$ ($i = p+1, \cdots, 25$). As explained in the introduction,

the boundary state is obtained by performing the modular transformation for the boundary condition of open strings. In the above case, we impose the Neumann boundary conditions for X^α and the Dirichlet boundary conditions for X^i. The boundary conditions for the ghost fields are determined so as the total boundary state is BRST- invariant,

$$Q\,|\,B_p\,\rangle = 0. \tag{7}$$

Then, the obtained state is (see, *e.g.*, Ref. [12])

$$|\,B_p\,\rangle \equiv \frac{T_p}{2}\delta^{25-p}(x^i)\exp\left\{\sum_{n=1}^{\infty}\left(\frac{-1}{n}\alpha^\mu_{-n}S_{\mu\nu}\tilde{\alpha}^\nu_{-n} + c_{-n}\tilde{b}_{-n} + \tilde{c}_{-n}b_{-n}\right)\right\}c_0^+c_1\tilde{c}_1\,|\,0\,\rangle\,, \tag{8}$$

where T_p is the tension of the Dp-brane and $S_{\mu\nu} \equiv (\eta_{\alpha\beta}, -\delta_{ij})$. It is a state in the closed string Hilbert space with ghost number 3. In order to regard the boundary state as a source for the physical sector of the closed string field $|\,\phi\,\rangle$, it is first required to multiply c_0^- to (8);

$$|\,J\,\rangle \equiv c_0^-\,|\,B_p\,\rangle\,. \tag{9}$$

Then, it has the correct ghost number 4 and we can prove easily that J is also BRST invariant:

$$QJ = 0\,. \tag{10}$$

Comparing this to the equation (5), it is obvious that the boundary state $|\,B_p\,\rangle$ is a source of the closed string field only when the closed string coupling constant vanishes. In other words, when $g \neq 0$, the usual BRST invariant boundary state cannot be a source for the closed string field (unless $B_p * \Phi = 0$). This means that, if the closed string coupling is turned on, the boundary state must be modified so that it satisfies the condition,

$$\delta_B J = 0. \tag{11}$$

We can then regard this J as a matter current that truly describes a D-brane. The necessity of this modification is not surprising. In fact, it is consistent with the usual picture of the string perturbation theory: Since a D-brane is a non-perturbative object and has mass $\sim 1/g$, it is infinitely heavy in the limit $g \to 0$ so that it behaves as a rigid hyperplane in the space-time and this defines a conformal background. When small g is turned on, it is still heavy but can receive some recoil effect from the bulk and behaves as a non-relativistic object moving in the space-time. To maintain the unitarity, there should be collective coordinates for the D-brane [13] and they give the dynamical degrees of freedom for the source. Therefore, it is quite natural to assume that this modification is due to the open string excitation: it is schematically written as

$$|\,J\,\rangle = e^{-S_b[X]}\,|\,B_p\,\rangle\,, \tag{12}$$

where $S_b[X]$ is an appropriate boundary interaction [4]. In the presence of the boundary state $|\,B_p\,\rangle$ alone, the space-time symmetry such as the translational symmetry in the x^i direction is generally broken. On the other hand, since the modified current J contains the collective coordinate for the broken symmetry, e.g., the scalar fields on the D-brane, it can keep the global gauge symmetry. As a result, the current becomes a dynamical source and the equation (11) would effectively describes the behavior of the open string excitations on the D-brane. In the next subsection, we will discuss this point in more detail.

4 Conclusion

In this proceeding, we presented a general framework for the closed strings in the presence of an arbitrary matter current. Starting with a closed string field theory with an arbitrary source term, we derived a couple of equations, one is the equation of motion for the closed string field, and the other is a constraint equation which expresses the covariant conservation law for the matter current.

Then we applied our argument to D-branes. We claimed that the usual BRST invariant boundary state is not a consistent source, but it should be modified by turning on dynamical degrees of freedom so that it satisfies the constraint equation.

Another interesting issue is to apply our argument to a time dependent matter source. It is a fascinating issue to decide whether the modified boundary state starting from the rolling tachyon boundary state correctly describes the decaying process of non-BPS D-branes. Our argument could also apply to gravity theories. For example, if we find a solution that describes the decaying process of some extended object, the low energy limit might express the classical solution for the black hole evaporation.

Applying our argument to the superstring theories is also one of the important future works. For instance, our setting seems quite useful to understand the AdS/CFT correspondence at the more fundamental level. The essence of the AdS/CFT correspondence is the duality between the open string theory on a D-brane and the closed string theory in the background of the classical geometry made by the D-brane.

References

[1] T. Asakawa, S. Kobayashi and S. Matsuura, "Closed string field theory with dynamical D-branes," JHEP **0310** (2003) 023 [arXiv:hep-th/0309074].

[2] A. Sen, "Tachyon condensation on the brane antibrane system," JHEP **9808** (1998) 012 [arXiv:hep-th/9805170].

[3] A. Sen, "Rolling tachyon," JHEP **0204** (2002) 048 [arXiv:hep-th/0203211];

[4] C. G. Callan, C. Lovelace, C. R. Nappi and S. A. Yost, "Adding Holes And Crosscaps To The Superstring," Nucl. Phys. B **293** (1987) 83; C. G. Callan, C. Lovelace, C. R. Nappi and S. A. Yost, "Loop Corrections To Conformal Invariance For Type 1 Superstrings," Phys. Lett. B **206** (1988) 41.

[5] J. Polchinski and Y. Cai, "Consistency Of Open Superstring Theories," Nucl. Phys. B **296** (1988) 91.

[6] T. Asakawa, S. Sugimoto and S. Terashima, "Exact description of D-branes via tachyon condensation," JHEP **0302** (2003) 011 [arXiv:hep-th/0212188].

[7] A. Sen, "Tachyon matter," JHEP **0207** (2002) 065 [arXiv:hep-th/0203265].

[8] K. Ohta and T. Yokono, "Gravitational approach to tachyon matter," Phys. Rev. D **66** (2002) 125009 [arXiv:hep-th/0207004].

[9] T. Okuda and S. Sugimoto, "Coupling of rolling tachyon to closed strings," Nucl. Phys. B **647** (2002) 101 [arXiv:hep-th/0208196].

[10] N. Lambert, H. Liu and J. Maldacena, "Closed strings from decaying D-branes," arXiv:hep-th/0303139.

[11] H. Hata, K. Itoh, T. Kugo, H. Kunitomo and K. Ogawa, "Covariant String Field Theory," Phys. Rev. D **34** (1986) 2360, "Covariant String Field Theory. 2," Phys. Rev. D **35** (1987) 1318.

[12] for a review, P. Di Vecchia and A. Liccardo, "D branes in string theory. I," [arXiv:hep-th/9912161]. P. Di Vecchia and A. Liccardo, "D-branes in string theory. II," [arXiv:hep-th/9912275].

[13] W. Fischler, S. Paban and M. Rozali, "Collective Coordinates for D-branes," Phys. Lett. B **381** (1996) 62 [arXiv:hep-th/9604014].

[14] V. Periwal and O. Tafjord, "D-brane recoil," Phys. Rev. D **54** (1996) 3690 [arXiv:hep-th/9603156]. I. I. Kogan, N. E. Mavromatos and J. F. Wheater, "D-brane recoil and logarithmic operators," Phys. Lett. B **387** (1996) 483 [arXiv:hep-th/9606102].

D-term inflation in type I inspired models

Tatsuo Kobayashi

Department of Physics, Kyoto University, Kyoto 606-8502, Japan

Osamu Seto

Institute of Physics, National Chiao Tung University, Hsinchu 300, Taiwan R.O.C.

Abstract

We investigate the possibility of D-term inflation within the framework of type-I string inspired models. Although the D-term inflation model has the excellent property that it is free of the so-called η- problem, two serious problems appear when we embed D-term inflation in string theory; the magnitude of the FI term and the rolling motion of the dilaton. In the present paper, we analyze the potential of D-term inflation in type-I-inspired models and study the behavior of dilaton and twisted moduli fields. Adopting the nonperturbative superpotential induced by gaugino condensation, the twisted moduli can be stabilized. If the dilaton is in a certain range, it evolves very slowly and does not run away to infinity. Thus D-term-dominated vacuum energy becomes available for driving inflation. By studying the density perturbation generated by the inflation model, we derive the constraints on model parameters and give some implications on D-term inflation in type-I-inspired models.

1 Introduction

In the success of slow-roll inflation, a sufficient flat potential for the inflaton is required. However, it is not so easy to construct a model of inflation where the corresponding scalar field has a very flat potential in the framework of supergravity. In the case that the vacuum energy is dominated by the F-term during the inflation, supergravity effects produce the soft mass of inflaton field whose magnitude is the same order of H and spoil the flatness of potential. In other words, such large inflaton mass gives $\eta \sim 1$ and violates the slow roll condition, which is often referred to as the η problem.

From this point of view, D-term inflation is one of the attractive inflation scenarios within the framework of supersymmetric models [1, 2], because the inflaton does not acquire the mass squared term of the order of H^2 and the flatness of the potential is preserved. In the D-term inflation scenario, the Fayet-Iliopoulos (FI) term is dominant during the inflation and this vacuum energy causes an accelerating expansion. The FI term comes from the anomalous $U(1)$ symmetry in the framework of string theory and is dependent on the field which plays a role in the Green-Schwarz anomaly cancellation mechanism [3] for the anomalous $U(1)$.

However, there are difficulties in the realization of D-term inflation based on heterotic string models. The first problem is the energy scale of inflation. The magnitude of the FI term is given as

$$\xi = \frac{g^2}{192\pi^2}\mathrm{Tr}(Q)M_p^2, \tag{1}$$

where g^2 is the gauge coupling, M_p is the reduced Planck mass and $\mathrm{Tr}(Q)$ is a model-dependent constant of the order of $O(10) - O(10^2)$ [4]. Eq. (1) reads $\sqrt{\xi}/M_p = O(10^{-1})$. On the other hand, the CMB anisotropy requires $\xi^{1/2} \simeq 10^{15}$ GeV. We find that the theoretical prediction is too larger to meet the observational estimation. The second problem is due to the dilaton dependence of the FI term and the anomalous $U(1)$ gauge coupling. Since $g^2 \propto 1/\mathrm{Re}S$, the D-term scalar potential, $V_D = g^2\xi^2/2$, is in proportion to $(\mathrm{ReS})^{-3}$. Hence the dilaton rolls down the potential to the infinity, $\mathrm{ReS} \longrightarrow \infty$, and the D-term potential energy goes to zero, $V_D \longrightarrow 0$. This phenomenon is the same as the dilaton runaway problem in generic string models and such runaway behavior of the dilaton prevents a viable inflation.

Now, we study behavior of dilaton and moduli fields in the D-term inflation scenario with the above two problems in mind in order to explore a way to avoid these problems at the same time [5]. Now, in particular, we will consider type-I-string inspired models. The D-term inflation in type I inspired model has been studied in Ref. [6] and it was shown that the magnitude of the FI-term is reducible to a desired value. This result arises from the facts that the FI-term is determined by the expectation value of the twisted moduli and the string scale M_s is independent of the Planck scale M_p [7] in type-I string models. However, in Ref. [6] the stabilization of the twisted moduli and the runway problem have not been discussed.

2 Behavior of dilaton and twisted moduli fields

In this section we study the behavior of dilaton and twisted moduli fields in type-I string inspired D-term inflation models. We consider the case that the anomalous $U(1)$ originates from the $D9$ brane. In this case the gauge kinetic function is obtained as [8]

$$f_9 = S + \sigma \frac{M}{M_s}, \tag{2}$$

where σ is a model-dependent constant and we define $\tilde{\sigma} = \sigma/M_s$. The corresponding gauge coupling g_9 is obtained as $g_9^2 = 1/Re(f_9)$. The Kähler potential of the dilaton field S is written as

$$K(S, \bar{S}) = -\ln(S + \bar{S}). \tag{3}$$

On the other hand, the Kähler potential of the twisted moduli field $K(M, \bar{M})$ is not clear. For small values of M, it can be expanded as [9]

$$K(M, \bar{M}) = \frac{1}{2}(M + \bar{M})^2 + \cdots. \tag{4}$$

However, the reliability of this form is not clear for large values of M, i.e. $M \geq O(1)$.

The twisted moduli field plays a role in the 4D Green-Schwarz anomaly cancellation mechanism, and the FI term is obtained as

$$\xi = \delta_{GS} K'(M, \bar{M}), \tag{5}$$

where δ_{GS} is a model-dependent constant. Thus the D-term scalar potential during inflation is obtained as

$$V_D = \frac{[\delta_{GS} K'(M, \bar{M})]^2}{S + \bar{S} + \tilde{\sigma}(M + \bar{M})}. \tag{6}$$

First, let us study behavior of S during inflation. When we suppose the twisted moduli M is stabilized somehow such that $S + \bar{S} \ll \tilde{\sigma}(M + \bar{M})$, we obtain

$$\left(\frac{1}{V_D}\frac{\partial V_D}{\partial \phi}\right)^2 \simeq 2\left(\frac{S + \bar{S}}{\tilde{\sigma}(M + \bar{M})}\right) \ll 1, \tag{7}$$

$$\frac{1}{V_D}\frac{\partial^2 V_D}{\partial \phi^2} \simeq -\frac{2\sqrt{2}(S + \bar{S})}{\tilde{\sigma}(M + \bar{M})} \ll 1, \tag{8}$$

that is, the slow-roll condition is satisfied for the dilaton field and it does not run away, where ϕ is the canonically normalized dilaton field. Note that this result is independent of the form of $K(M, \bar{M})$.

Next, we study the stabilization of M in the model. For $S + \bar{S} \ll \tilde{\sigma}(M + \bar{M})$, the potential reduces to

$$V_D = \frac{[\delta_{GS} K'(M, \bar{M})]^2}{\tilde{\sigma}(M + \bar{M})}. \tag{9}$$

Unfortunately, only the term V_D does not stabilize the twisted moduli M at a finite value with nonvanishing vacuum energy, unless we choose a special form of $K(M, \bar{M})$. Hence, another term is necessary for stabilization of M such that the D-term inflation can be realized. Now, we assume that gaugino

condensation of another non-abelian gauge group generates the nonperturbative potential. Then we can find the local minimum of the potential for the twisted moduli field at the point

$$\langle M+\bar{M}\rangle_{inf} = \left(O(10^{-2}) - O(10^{-1})\right) M_p \tag{10}$$

where $\langle ... \rangle_{inf}$ denotes the expectation value during inflation. Here we assumed $S+\bar{S} \ll \tilde{\sigma}(M+\bar{M})$ during inflation and $K(M,\bar{M}) = \frac{1}{2}(M+\bar{M})^2$. Note that the key point for stabilization is the polynomial form of the Kähler potential, in particular the canonical form. From this point, the above result that M is stabilized as a small value is favorable.

3 Dynamics and density perturbation

Now let us discuss the dynamics in this inflation model. The relevant potential including one-loop correction during inflation is given by

$$V = \frac{\delta_{GS}^2 \langle M+\bar{M}\rangle_{inf}^2}{S+\bar{S}+\tilde{\sigma}\langle M+\bar{M}\rangle_{inf}} \left[1 + \frac{1}{16\pi^2} \frac{2}{S+\bar{S}+\tilde{\sigma}\langle M+\bar{M}\rangle_{inf}} \ln \frac{\lambda^2 |X|^2}{(S+\bar{S})\Lambda^2}\right]. \tag{11}$$

Here one should notice that the stabilization of twisted moduli is achieved by the F-term potential and we can replace $M+\bar{M}$ with $\langle M+\bar{M}\rangle_{inf}$. Hereafter we will consider only the region, $S+\bar{S} \ll \tilde{\sigma}\langle M+\bar{M}\rangle_{inf}$ in order to avoid runway motion of the dilaton and obtain a successful inflation.

From the solutions of equations of motion for scalar fields under the slow roll approximation, we obtain the following equation ;

$$\left.\frac{S+\bar{S}}{\tilde{\sigma}\langle M+\bar{M}\rangle_{inf}}\right|_{t_e} = \frac{1}{\frac{\tilde{\sigma}\langle M+\bar{M}\rangle_{inf}}{S+\bar{S}} - 2N}, \tag{12}$$

where t_e denotes the time of the end of the inflation, by using the definition of the number of e-folds, $-dN \equiv Hdt$. Since the l.h.s. must be less than the order of 10^{-1}, we find that $\tilde{\sigma}\langle M+\bar{M}\rangle_{inf}/(S+\bar{S}) \sim 10^2$ for the present horizon scale. Here we estimate the following quantity

$$\left(\frac{\dot{\phi}}{\dot{X}}\right)^2 \simeq 10^{-1} \left(\frac{\tilde{\sigma}\langle M+\bar{M}\rangle_{inf}}{10^{-1}}\right) \left(\frac{\left.\frac{S+\bar{S}}{\tilde{\sigma}\langle M+\bar{M}\rangle_{inf}}\right|_{t_e}}{10^{-1}}\right)^2. \tag{13}$$

Thus we find that the ratio of kinetic energies of these scalar fields takes a value of $O(10^{-1}) - O(10^{-2})$.

Next, we turn to the density perturbation generated by this inflation model. The WMAP data shows that the adiabatic fluctuation is favored [10]. On the other hand, in general, inflation model which contains several evolving scalar fields produces also the isocurvature fluctuation. Accordingly, we estimate the contribution from the isocurvature mode and confirm this model to be consistent with observations. In this model, the power spectrum of the density perturbations at the end of inflation [11] is estimated as

$$\mathcal{P}_\zeta|_{t_e} = \left(\frac{H^2}{2\pi|\dot{X}|}\right)^2\Bigg|_{t_k} \left[1 - 2\left.\frac{\epsilon_\phi}{\epsilon_X}\right|_{t_e} + \frac{\left(\epsilon_\phi/\epsilon_X|_{t_e}\right)^2}{\epsilon_\phi/\epsilon_X|_{t_k}}\right], \tag{14}$$

where t_k is a horizon crossing time during inflation. We find that the variation of ζ on superhorizon scales by the isocurvature perturbation is suppressed by the power of $\dot{\phi}^2/\dot{X}^2 = O(10^{-1}) - O(10^{-2})$. Thus, we obtain the constraint on the model parameters,

$$\frac{\delta_{GS}\langle M+\bar{M}\rangle_{inf}}{M_p^2} \simeq 10^{-5}, \tag{15}$$

for the present horizon scale. For the GS coefficient δ_{GS}, a suppressed value is required like the heterotic case. Explicit models through type IIB orientifold construction seem to derive $\delta_{GS}/M_s = O(10^{-1}) - O(10^{-3})$ [12]. Anyway, the GS coefficient δ_{GS} is model-dependent. If we find the model that δ_{GS} is small enough like $\delta_{GS}/M_s \sim 10^{-3}$, the string scale can be almost comparable with M_p or slightly smaller. Otherwise, if the original FI terms are not small enough, we would need the mechanism to reduce the effective FI term such as a lower string scale.

4 Conclusion

We have studied D-term inflation within the framework of type-I string inspired models. In this case, the twisted moduli field plays a significant role. Stabilization of the twisted moduli during inflation is achieved with the help of the gaugino condensation potential and this stabilization mechanism does not spoil the situation that the potential is dominated by D-term. Furthermore it is a favorable property that the expectation value of the twisted moduli during inflation is enough smaller than the unity where the Kähler potential $K = (M + \bar{M})^2/2$ is valid.

At first, we found that the magnitude of thr FI term would be reducible to a desirable value within this framework even if we do not assume a hierarchically large gap between the string scale M_s and the Planck scale M_p.

Concerning the second problem, or dilaton runaway problem, we found the condition to avoid this difficulty for the initial value of the dilaton. In the potential with a fixed twisted moduli, we could find the field region where the dilaton does not run away, $S + \bar{S} \ll \tilde{\sigma}(M + \bar{M})_{inf}$. If the dilaton takes such an initial value at the pre inflation stage, it is possible that the universe undergoes the quasi de-Sitter expansion, because the dilaton can evolve slowly. Of course, at the moment, we cannot answer the question why the dilaton takes such initial value. The point we would like to emphasize is that D-term inflaton is possible in type I string inspired model under certain conditions.

Acknowledgments

T. K. is supported in part by a Grant-in-Aid for Scientific Research from the Ministry of Education, Science, Sports and Culture of Japan (No. 14540256). O. S. is supported by the National Science Council of Taiwan under the grant Nos. NSC 92-2811-M-009 -006- and -018-.

References

[1] P. Binetruy and G. Dvali, Phys. Lett. **B388** (1996) 241;
E. Halyo, Phys. Lett. **B387** (1996) 43;
For a review, see e.g. D.H. Lyth and A. Riotto, Phys. Rept. **314** (1999) 1.

[2] J. A. Casas, J. M. Moreno, C. Munoz and M. Quiros, Nucl. Phys. B **328**, 272 (1989).

[3] M. B. Green and J. H. Schwarz, Phys. Lett. B **149**, 117 (1984).

[4] E. Witten, Phys. Lett. **149B** (1984) 351;
M. Dine, N. Seiberg and E. Witten, Nucl. Phys. **B289** (1987) 589;
W. Lerche, B.E.W. Nilsson and A.N. Schellekens, Nucl. Phys. **B289** (1987) 609.

[5] T. Kobayashi and O. Seto, hep-ph/0307332.

[6] E. Halyo, Phys. Lett. B **454**, 223 (1999).

[7] E. Witten, Nucl. Phys. B **471**, 135 (1996).

[8] See for effective low-energy Lagrangian of Type I models
L. E. Ibanez, C. Munoz and S. Rigolin, Nucl. Phys. B **553**, 43 (1999) and references therein.

[9] E. Poppitz, Nucl. Phys. B **542**, 31 (1999).

[10] C. L. Bennett *et al.*, Astrophys. J. Suppl. **148**, 1 (2003); H. V. Peiris *et al.*, *ibid.* **148**, 213 (2003).

[11] J. Garcia-Bellido and D. Wands, Phys. Rev. D **53**, 5437 (1996).

[12] I. Antoniadis, E. Kiritsis and J. Rizos, Nucl. Phys. B **637**, 92 (2002).

Brane cosmological perturbations and bulk scalars from a new perspective

Tsutomu Kobayashi[1], Takahiro Tanaka[2]

Department of Physics, Kyoto University, Kyoto 606-8502, Japan

Abstract

We introduce a $(5 + m)$-dimensional vacuum description of five-dimensional bulk inflaton models with exponential potentials that makes analysis of cosmological perturbations simple and transparent. We show that various solutions, including the power-law inflation model recently discovered by Koyama and Takahashi, are generated from known $(5 + m)$-dimensional vacuum solutions of pure gravity. We derive master equations for all types of perturbations, and each of them becomes a second order differential equation for one master variable supplemented by simple boundary conditions on the brane. One exception is the case for massive modes of scalar perturbations. In this case, there are two independent degrees of freedom, and in general it is difficult to disentangle them into two separate sectors.

1 Introduction

Recent progress in particle physics suggests that the universe might be a four-dimensional subspace, called a "brane", embedded in a higher dimensional "bulk" spacetime. Various kinds of braneworld models have been proposed, and the cosmological consequences of these models have been studied (for a review see, e.g., Ref. [1]). The idea of the braneworld brings new possibilities, in particular to scenarios of the early universe.

A simple model proposed by Randall and Sundrum [2] is such that the unperturbed bulk is a five-dimensional anti-de Sitter spacetime (warped bulk) bounded by one brane or two. An empty bulk, however, seems less likely from the point of view of unified theories, which often require various fields in addition to gravity. Cosmological solutions in the context of heterotic M theory has been studied in [3, 4]. In the model discussed in Refs. [3], the scalar field has an exponential potential in the bulk and the tensions of the two branes are also exponential functions of the scalar field. In this model the power-law expansion (but not inflation) is realized on the brane. A single-brane model with such exponential-type potentials is also interesting, and it has been investigated in Ref. [4]. Very recently, an inflationary solution was found in a similar setup by Koyama and Takahashi [5]. A striking feature of their model is that cosmological perturbations can be solved analytically.

In spite of the tremendous efforts by many authors [6, 7], it is still an unsolved problem to calculate the evolution of perturbations in the braneworld models with infinite extra dimensions. This lack of knowledge constrains the predictability of this interesting class of models. Only a few cases are known where perturbation equations can be analytically solved [7]. One of them is the special class of bulk inflaton models mentioned above [5]. In this article we clarify the reason why the perturbation equations are soluble in this special case. Based on this notion, we present a new systematic method to find a wider class of background cosmological solutions and to analyze perturbations from them. For details, see Ref. [8].

2 Key Idea

The Key idea is summarized in Fig. 1. We begin with the $(n + 2 + m)[= 5 + m]$-dimensional Randall-Sundrum model which consists of an empty AdS bulk and a vacuum brane:

$$S = \frac{1}{2\kappa_{D+1}^2} \int d^{D+1}X \sqrt{-G}\,(R[G] - 2\Lambda_{D+1}) - \int d^D X \sqrt{-g}\,\sigma. \tag{1}$$

[1]E-mail:tsutomu@tap.scphys.kyoto-u.ac.jp
[2]E-mail:tama@scphys.kyoto-u.ac.jp

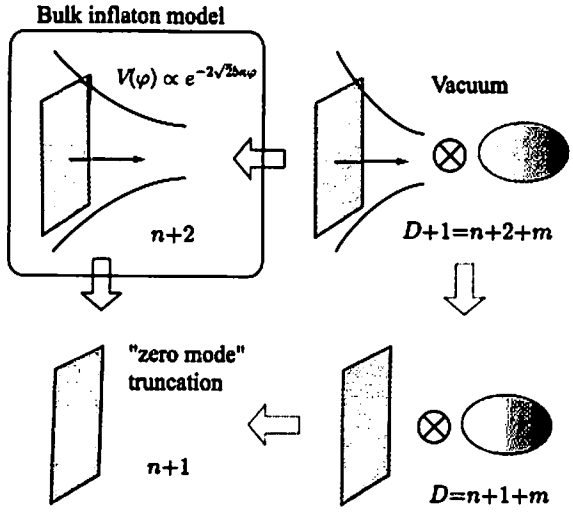

Figure 1: Schematic of the higher dimensional vacuum description of an $(n+2)$-dimensional bulk inflaton model and the derivation of the $(n+1)$-dimensional effective theory on the brane. The top-left picture represents the bulk inflaton model which we are interested in. To analyze cosmological background solutions (and "zero mode" perturbations), we use the $(n+1)$-dimensional description shown in the bottom-left corner. On the other hand, we make use of the $(D+1)$-dimensional description presented in the top-right corner to simplify the perturbation analysis.

Now we assume the metric form as $ds^2 = \mathcal{G}_{ab}(x)dx^a dx^b + e^{2\phi(x)}\gamma_{\mu\nu}dy^\mu dy^\nu$, with $\gamma_{\mu\nu}$ the metric of m-dimensional maximally symmetric space. Then, dimensional reduction to $(n+2)[=5]$ dimensions yields a braneworld model with a bulk scalar field which has exponential-type potentials both in the bulk and on the brane:

$$S^{(5)} = \int d^5x\sqrt{-\tilde{\mathcal{G}}}\left\{\frac{1}{2\kappa_5^2}R[\tilde{\mathcal{G}}] - \frac{1}{2}\tilde{\mathcal{G}}^{ab}\partial_a\varphi\partial_b\varphi - V(\varphi)\right\} - \int d^4x\sqrt{-q}\,U(\varphi), \tag{2}$$

where $\varphi := \kappa_5^{-1}\sqrt{m(m+3)/3}\,\phi$ and

$$V(\varphi) = -\frac{(m+3)(m+4)}{2\kappa_5^2\ell^2}e^{-2\sqrt{2}b\kappa_5\varphi} - \frac{Km(m-1)}{2\kappa_5^2}e^{-\sqrt{2}\kappa_5\varphi/3b}, \quad U(\varphi) = \tilde{\sigma}e^{-\sqrt{2}b\kappa_5\varphi}, \tag{3}$$

with $b := \sqrt{\frac{m}{6(m+3)}}$. Thus we see that these two models are equivalent to each other. As we will see, however, the perturbation analysis is simplified a lot by making use of the former $(5+m)$-dimensional description.

3 Cosmological Perturbations

First let us consider the following form of background metric:

$$ds^2 = e^{2\omega(z)}\left(dz^2 + g_{\hat{A}\hat{B}}dx^{\hat{A}}dx^{\hat{B}}\right) = e^{2\omega(z)}\left(dz^2 - dt^2 + e^{2\alpha(t)}\gamma_{\mu\nu}dy^\mu dy^\nu + e^{2\beta(t)}\delta_{ij}dx^i dx^j\right), \tag{4}$$

where latin and roman indices, respectively, run m and n-dimensional subspaces, and the warp factor is given by $e^{\omega(z)} = \ell H_0/\sinh(H_0 z)$. We assume that $\alpha(t)$ and $\beta(t)$ are chosen so that $g_{\hat{A}\hat{B}}$ is a solution of the $(n+1+m)$-dimensional vacuum Einstein equations with a cosmological constant,

$$m\left(\ddot{\alpha} + \dot{\alpha}^2\right) + n\left(\ddot{\beta} + \dot{\beta}^2\right) = (m+n)H_0^2, \tag{5}$$

$$\ddot{\alpha} + \dot{\alpha}\left(m\dot{\alpha} + n\dot{\beta}\right) + K(m-1)e^{-2\alpha} = (m+n)H_0^2, \tag{6}$$

$$\ddot{\beta} + \dot{\beta}\left(m\dot{\alpha} + n\dot{\beta}\right) = (m+n)H_0^2. \tag{7}$$

In the case of $K = 0$, for example, these equations are solved to give following two types of expressions:

$$\alpha = \beta = H_0 t. \tag{8}$$

and

$$e^{m\alpha+n\beta} = \sinh[(m+n)H_0 t], \quad e^{\alpha-\beta} = [\tanh((m+n)H_0 t/2)]^{\pm\sqrt{\frac{m+n-1}{mn}}}. \tag{9}$$

The de Sitter solution (8) yields a power-law inflation model which is equivalent to the model of Ref. [5], while the solution (9) gives a rather nontrivial cosmological expansion law. We can also obtain a background solution with $K = \pm 1$, $H_0 = 0$ analytically. In what follows we include more general cases with $K = \pm 1$ and $H_0 \neq 0$. Although the background solution cannot be obtained in an explicit form for such non-flat compactifications with a cosmological constant, we will find that general properties of perturbations can be explored to a great extent.

Now let us move on to the perturbations. We write the perturbed metric as

$$\begin{aligned} ds^2 = e^{2\omega}\Big\{&(1+2N)dz^2 + 2Adtdz - (1+2\Phi)dt^2 + e^{2\alpha}(1+2S)\gamma_{\mu\nu}dy^\mu dy^\nu \\ &+e^{2\beta}\left[(1+2\Psi)\delta_{ij}dx^i dx^j + 2E_{ij}dx^i dx^j + 2B_i dx^i dt + 2C_i dx^i dz\right]\Big\}, \end{aligned} \tag{10}$$

and decompose the perturbed quantities into scalar, vector and tensor components. The $(n+2+m)$-dimensional Einstein equations give the perturbation equations.

Tensor perturbations Since tensor perturbations are gauge-invariant from the beginning, they are in general easy to analyze. The equation for tensor perturbations is

$$\mathcal{L}E_{ij}^T = 0, \tag{11}$$

where we have defined a differential operator $\mathcal{L} := \partial_t^2 + \left(m\dot{\alpha} + n\dot{\beta}\right)\partial_t + e^{-2\beta}k^2 - \partial_z^2 - (m+n)(\partial_z\omega)\partial_z$. The perturbed junction condition implies that boundary conditions are Neumann on the brane, $\partial_z E_{ij}^T|_{z=z_b} = 0$. The perturbation equation is manifestly separable, and so one can easily solve it. This is not a surprise because the background of the current model is just an AdS_{m+2+n} bulk with a de Sitter brane.

Scalar perturbations Since scalar perturbations are more complicated, we begin with fixing the gauge appropriately in order to simplify the perturbed Einstein equations. We impose the Gaussian-normal gauge conditions $N = A = C = 0$. In this Gaussian-normal gauge, boundary conditions on the brane for all remaining variables become Neumann: $\partial_z\Psi|_{z=z_b} = \partial_z E|_{z=z_b} = \partial_z S|_{z=z_b} = \partial_z\Phi|_{z=z_b} = \partial_z B|_{z=z_b} = 0$.

Three of eight scalar perturbation equations are the constraint equations, and the other five are the evolution equations. Scalar perturbations have two independent physical degrees of freedom, corresponding to the bulk scalar field and the "graviscalar" mode, and with the aid of the constraint equations, these fives are simplified to give *master equations for the KK modes*,

$$\mathcal{L}\Psi = -2(n-2)\dot{\beta}\left(\dot{\alpha} - \dot{\beta}\right)\Psi + \frac{4}{n}\dot{\beta}\dot{\Phi} - 2\left\{\frac{n-2}{n}\dot{\beta}\left[(m+1)\dot{\alpha} + n\dot{\beta}\right] - (m+n)H^2\right\}\Phi, \tag{12}$$

$$\begin{aligned} \mathcal{L}\Phi = &-4\dot{\beta}\dot{\Phi} - 2\left\{(m+1)\ddot{\alpha} + n\ddot{\beta} + 2\dot{\beta}\left[(m+1)\dot{\alpha} + n\dot{\beta}\right] - (m+n)H^2\right\}\Phi \\ &-2n\left[\ddot{\alpha} - \ddot{\beta} + 2\dot{\beta}\left(\dot{\alpha} - \dot{\beta}\right)\right]\Psi. \end{aligned} \tag{13}$$

Unfortunately, except for the simplest case ($\alpha = \beta = H_0 t$) we do not know how to disentangle these two equations, although there is no problem in solving these equations numerically. Once we could solve

these coupled equations, the other variables S, B, E are easily determined just by using the constraint equations.

For the zero mode, the Einstein equations reduce to a second order differential equation for *one* master variable because the zero-mode perturbations are, just as the background metric, described by the $(n+1)[=4]$-dimensional effective theory and so the analysis is much the same as the conventional four-dimensional cosmological perturbation theory.

4 Summary

We have shown that a wide class of braneworld models with bulk scalar fields can be constructed by dimensional reduction from a higher dimensional extension of the Randall-Sundrum model with an empty bulk. The sizes of compactified dimensions translate into scalar fields with exponential potentials both in the bulk and on the brane. We have mainly concentrated on models with a single scalar field, which include the power-law inflation solution of Ref. [5].

First we have investigated the evolution of five$[=n+2]$-dimensional background cosmologies, and then we have studied cosmological perturbations in such braneworld models. Lifting the models to $(5+m)[=n+2+m]$-dimensions is a powerful technique for this purpose. The degrees of freedom of a bulk scalar field in $(n+2)$-dimensions are deduced from a purely gravitational theory in the $(n+2+m)$-dimensional Randall-Sundrum braneworld, which consists of a vacuum brane and an empty bulk. We would like to emphasize that the analysis is greatly simplified thanks to the absence of matter fields. From the $(n+2+m)$-dimensional perspective, we have derived master equations and shown that the mode decomposition is possible for all models which are constructed by using this dimensional reduction technique.

To sum up, our "embedding and reduction" approach enables systematic study of cosmological perturbations in a class of braneworld models with bulk scalar fields.

References

[1] D. Langlois, Prog. Theor. Phys. Suppl. **148**, 181 (2003), R. Maartens, "Brane-world gravity," arXiv:gr-qc/0312059.

[2] L. Randall and R. Sundrum, Phys. Rev. Lett. **83**, 3370 (1999), L. Randall and R. Sundrum, Phys. Rev. Lett. **83**, 4690 (1999).

[3] A. Lukas, B. A. Ovrut and D. Waldram, Phys. Rev. D **60**, 086001 (1999), H. S. Reall, Phys. Rev. D **59**, 103506 (1999).

[4] S. Kachru, M. B. Schulz and E. Silverstein, Phys. Rev. D **62**, 045021 (2000), M. Cvetic, H. Lu and C. N. Pope, Phys. Rev. D **63**, 086004 (2001), V. Bozza, M. Gasperini and G. Veneziano, Nucl. Phys. B **619**, 191 (2001), H. Ochiai and K. Sato, Phys. Lett. B **503**, 404 (2001), A. Feinstein, K. E. Kunze and M. A. Vazquez-Mozo, Phys. Rev. D **64**, 084015 (2001), D. Langlois and M. Rodriguez-Martinez, Phys. Rev. D **64**, 123507 (2001), C. Charmousis, Class. Quant. Grav. **19**, 83 (2002).

[5] K. Koyama and K. Takahashi, Phys. Rev. D **67**, 103503 (2003), K. Koyama and K. Takahashi, Phys. Rev. D **68**, 103512 (2003).

[6] S. Mukohyama, Phys. Rev. D **62**, 084015 (2000), H. Kodama, A. Ishibashi and O. Seto, Phys. Rev. D **62**, 064022 (2000), D. Langlois, Phys. Rev. D **62**, 126012 (2000), D. Langlois, Phys. Rev. Lett. **86**, 2212 (2001), K. Koyama and J. Soda, Phys. Rev. D **62**, 123502 (2000).

[7] D. Langlois, R. Maartens and D. Wands, Phys. Lett. B **489**, 259 (2000), D. S. Gorbunov, V. A. Rubakov and S. M. Sibiryakov, JHEP **0110**, 015 (2001), T. Kobayashi, H. Kudoh and T. Tanaka, Phys. Rev. D **68**, 044025 (2003).

[8] T. Kobayashi and T. Tanaka, "Bulk inflaton shadows of vacuum gravity," arXiv:hep-th/0311197.

Reconstructing the Primordial Spectrum from WMAP Data by the Cosmic Inversion Method

Noriyuki Kogo[1], Makoto Matsumiya[2], Misao Sasaki[3], and Jun'ichi Yokoyama[4]

[1,2,4] *Department of Earth and Space Science, Graduate School of Science, Osaka University, Toyonaka 560-0043, Japan*
[3] *Yukawa Institute for Theoretical Physics, Kyoto University, Kyoto 606-8502, Japan*

Abstract

We reconstruct the primordial spectrum of the curvature perturbation, $P(k)$, from the observational data of the Wilkinson Microwave Anisotropy Probe (WMAP) by the cosmic inversion method developed recently. In contrast to conventional parameter-fitting methods, our method can reproduce fine features in $P(k)$ with good accuracy. As a result, we obtain an oscillatory $P(k)$. We evaluate the statistical significance of nontrivial features in the reconstructed $P(k)$, performing Monte Carlo simulations for the scale-invariant spectrum. It is found that there are some possible deviations around $k \simeq 1.5 \times 10^{-2}\mathrm{Mpc}^{-1}$, while the oscillatory feature isn't significant.

1 Introduction

The Wilkinson Microwave Anisotropy Probe (WMAP) satellite has brought us much information of our Universe [1]. From their remarkably precise observation of the temperature fluctuations and the polarization of the cosmic microwave background (CMB), we have obtained invaluable information of the cosmological parameters and the properties of the primordial fluctuations. The results are almost consistent with the so-called concordance model [1, 2, 3]. However, there seems to be some discrepancies in the primordial spectrum such as running of the spectral index, lack of power on large scales, and oscillatory behaviors of the power spectrum on intermediate scales. Some attempts to reconstruct the primordial spectrum were made by [4, 5] after the WMAP data release. They all used the binning or wavelet band powers method. Although they reconstruct the primordial spectrum in a broad range, the disadvantage of these methods is that they cannot detect possible fine features. It is preferable to use a method which can restore the primordial spectrum as a continuous function without any ad hoc filtering scale. Recently, such a new method named the cosmic inversion method has been proposed by [6, 7]. The advantage of this method is that we can investigate possible fine features in the primordial spectrum by inverting the observed angular power spectrum to the primordial spectrum as an arbitrary function, given the cosmological parameters. In this presentation, we attempt to reconstruct the primordial spectrum from the WMAP data, using this method.

2 Inversion Method

First, we briefly review the cosmic inversion method. In this study, we assume the spatially flat universe and the adiabatic initial condition, both of which are generic predictions of standard inflation and have been supported by the WMAP data.

The CMB anisotropy is quantified by the angular correlation function defined as

$$C(\theta) \equiv \langle \Theta(\hat{\mathbf{n}}_1)\Theta(\hat{\mathbf{n}}_2)\rangle = \sum_{\ell=0}^{\infty} \frac{2\ell+1}{4\pi} C_\ell P_\ell(\cos\theta), \quad \cos\theta = \hat{\mathbf{n}}_1 \cdot \hat{\mathbf{n}}_2 , \tag{1}$$

[1] E-mail:kogo@vega.ess.sci.osaka-u.ac.jp
[2] E-mail:matumiya@vega.ess.sci.osaka-u.ac.jp
[3] E-mail:misao@yukawa.kyoto-u.ac.jp
[4] E-mail:yokoyama@vega.ess.sci.osaka-u.ac.jp

where $\Theta(\hat{\mathbf{n}})$ is the temperature fluctuation in the direction $\hat{\mathbf{n}}$. We decompose the Fourier components of the temperature fluctuations $\Theta(\eta, k)$ into multipole moments,

$$\Theta(\eta, k, \mu) = \sum_{\ell=0}^{\infty} (-i)^{\ell} \Theta_{\ell}(\eta, k) P_{\ell}(\mu), \tag{2}$$

where $\mu \equiv \hat{\mathbf{k}} \cdot \hat{\mathbf{n}}$, k is the comoving wavenumber, and η is the conformal time with its present value being η_0. The angular power spectrum is expressed as

$$\frac{2\ell+1}{4\pi} C_{\ell} = \frac{1}{2\pi^2} \int_0^{\infty} \frac{dk}{k} \frac{k^3 \langle |\Theta_{\ell}(\eta_0, k)|^2 \rangle}{2\ell+1}. \tag{3}$$

Theoretically, $\Theta_{\ell}(\eta, k)$ is given by solving the Boltzmann equation. When we attempt to invert Eq. (3), we adopt the thin last scattering surface (LSS) taking its thickness into account. Then, we find the approximated multipole moments as

$$\Theta_{\ell}^{\rm app}(\eta_0, k) = (2\ell+1) \left[f(k) j_{\ell}(kd) + g(k) j_{\ell}'(kd) \right] \Phi(0, \mathrm{k}), \tag{4}$$

where d is the conformal distance from the present to the LSS and $f(k)$, $g(k)$ are the transfer functions which depend only on the cosmological parameters. From Eq. (4) via Eq. (1), (3), we write down the approximated angular correlation function as

$$C^{\rm app}(r) = \sum_{\ell=\ell_{\rm min}}^{\ell_{\rm max}} \frac{2\ell+1}{4\pi} C_{\ell}^{\rm app} P_{\ell} \left(1 - \frac{r^2}{2d^2} \right), \tag{5}$$

where r is defined as $r = 2d \sin(\theta/2)$ on the LSS. Using the Fourier sine formula, we obtain a first-order differential equation for the primordial power spectrum of the curvature perturbation, $P(k) \equiv \langle |\Phi(0, \mathrm{k})|^2 \rangle$,

$$-k^2 f^2(k) P'(k) + \left[-2k^2 f(k) f'(k) + k g^2(k) \right] P(k) = 4\pi \int_0^{\infty} dr \frac{1}{r} \frac{\partial}{\partial r} \{ r^3 C^{\rm app}(r) \} \sin kr \equiv S(k). \tag{6}$$

Since $f(k)$ and $g(k)$ are oscillatory functions around zero, we can find values of $P(k)$ at the zero-points of $f(k)$ as

$$P(k_s) = \frac{S(k_s)}{k_s g^2(k_s)} \quad \text{for} \quad f(k_s) = 0, \tag{7}$$

assuming that $P'(k)$ is finite at the singularities, $k = k_s$. We can calculate $f(k)$, $g(k)$ by using a numerical code such as CMBFAST [8]. If the cosmological parameters and the angular power spectrum are given, we can solve Eq. (6) as a boundary value problem between the singularities.

However, the errors caused by the approximation, or the differences between the approximated angular spectrum $C_{\ell}^{\rm app}$ and the exact angular spectrum $C_{\ell}^{\rm ex}$ for the same initial spectrum are as large as about 30%. Thus, we should not use the observed power spectrum $C_{\ell}^{\rm obs}$ directly in Eq. (5). In fact, we find that the ratio,

$$b_{\ell} \equiv \frac{C_{\ell}^{\rm ex}}{C_{\ell}^{\rm app}}, \tag{8}$$

is almost independent of $P(k)$. Using this fact, we first calculate the ratio, $b_{\ell}^{(0)} = C_{\ell}^{\rm ex(0)} / C_{\ell}^{\rm app(0)}$, for a known fiducial initial spectrum $P^{(0)}(k)$ such as the scale-invariant one. Then, inserting $C_{\ell}^{\rm obs} / b_{\ell}^{(0)}$, which is much closer to the actual $C_{\ell}^{\rm app}$, into Eq. (5), we may solve for $P(k)$ with good accuracy.

In this study, we use a modified CMBFAST code with much finer resolutions than the original one in both k and ℓ. We limit C_{ℓ} in the range $20 \leq \ell \leq 700$ in order not to use the data which have large observational errors due to the cosmic variance at small ℓ and the detector noise at large ℓ. We adopt the fiducial initial spectrum, $P^{(0)}(k)$ as the scale-invariant spectrum and the fiducial cosmological parameter set as $\tau = 0.17$, $h = 0.72$, $\Omega_b = 0.047$ and $\Omega_{\Lambda} = 0.71$, which are the best-fit values to the WMAP data for the scale-invariant spectrum, $k^3 P(k) = A$. In this case, the positions of the singularities (7) are at $kd \simeq 70, 430, 680, \cdots$, where $d \simeq 1.34 \times 10^4$Mpc. Because the reconstructed $P(k)$ around the singularities has large numerical errors which are amplified by the observational errors, we can obtain $P(k)$ with good accuracy in the limited range $120 \lesssim kd \lesssim 380$ or $9.0 \times 10^{-3}\mathrm{Mpc}^{-1} \lesssim k \lesssim 2.8 \times 10^{-2}\mathrm{Mpc}^{-1}$. Note that kd corresponds roughly to ℓ.

3 Results and Discussion

We show $P(k)$ reconstructed from the WMAP data for the fiducial cosmological parameter set in Fig. 1. We can see the oscillation whose amplitude is about $20-30\%$ of the mean value. To check whether our method works correctly, we recalculate C_ℓ from the obtained $P(k)$ in the range $120 \lesssim kd \lesssim 380$, assuming the scale-invariance outside of this range, and compare it with the observational data of WMAP. Then, we find that the recalculated C_ℓ agrees with the binned WMAP data whose bin size is $\Delta\ell = 5$ as shown in Fig. 1. This is because our method has a finite resolution in $P(k)$, which is caused by the Fourier sine transform in the inversion. In practice, this is determined by a cutoff scale of the integration in the source term of Eq. (6) as $r_{\rm cut} \simeq 0.5d$ which leads to $\Delta\ell \sim \Delta kd \simeq \pi d/r_{\rm cut} \simeq 6$.

To examine whether the oscillatory feature is real, we perform Monte Carlo simulations for the scale-invariant $P(k)$. Then, we find a similar oscillatory feature in the resultant $P(k)$'s, which is purely caused by the scatter of the data. Therefore, to evaluate the statistical significance of nontrivial features, we quantify the deviation from the scale-invariance in $P(k)$ as

$$D(k_1, k_2) \equiv \int_{k_1}^{k_2} dk \left[k^3 P(k) - A\right]^2, \tag{9}$$

where k_1, k_2 are chosen by hand, and estimate the probability that the value of $D(k_1, k_2)$ for the simulation exceeds its observed value in a certain range for 10,000 realizations. We show the results of this analysis in Table 1. We find only 0.39% in the range $175 \leq kd \leq 225$, from which we conclude that there are some possible deviations around $kd \simeq 200$. On the other hand, the low probability near the second singularity $kd \simeq 430$, namely, 2.23% in the range $350 \leq kd \leq 400$, may be due to inappropriate choice of the cosmological parameters [7]. According to them, if the different cosmological parameters from actual values are adopted in the inversion, the reconstructed $P(k)$ is distorted from the real one, especially around the singularities. As for the oscillatory feature, since significant deviations are not found in the other ranges, we conclude that it has no significance.

We also examine the dependence of the reconstructed $P(k)$ on the cosmological parameters as shown in Fig. 2. It is found that the oscillatory feature remains, but the global amplitude and especially the sharpness of the oscillation around the second singularity change. Thus, there may be more appropriate choice of the cosmological parameters. This issue is currently under study.

4 Conclusion

We have reconstructed the shape of the primordial spectrum, $P(k)$, applying the cosmic inversion method to the WMAP data. As a result, we have confirmed that the reconstruction is successful and found that there are some possible deviations from the scale-invariance around $kd \simeq 200$ or $k \simeq 1.5 \times 10^{-2}\mathrm{Mpc}^{-1}$. In the future work, we should constrain the cosmological parameters systematically and extend the formalism to include the CMB polarization which will constrain $P(k)$ more severely.

References

[1] C. L. Bennett et al., 2003, Astrophys. J. Suppl., 148, 1

[2] D. N. Spergel et al., 2003, Astrophys. J. Suppl., 148, 175

[3] H. V. Peiris et al., 2003, Astrophys. J. Suppl., 148, 213

[4] S. L. Bridle, A. M. Lewis, J. Weller, and G. Efstathiou, 2003, Mon. Not. Roy. Astron. Soc., 342, L72

[5] P. Mukherjee and Y. Wang, astro-ph/0303211

[6] M. Matsumiya, M. Sasaki, and J. Yokoyama, 2002, Phys. Rev. D, 65, 083007

[7] M. Matsumiya, M. Sasaki, and J. Yokoyama, 2003, JCAP, 0302, 003

[8] http://www.cmbfast.org/

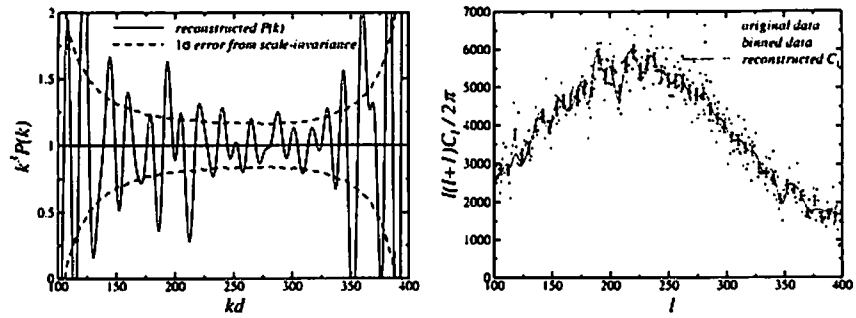

Figure 1: The left panel shows the reconstructed $P(k)$ from the WMAP data for $\tau = 0.17$, $h = 0.72$, $\Omega_b = 0.047$, $\Omega_\Lambda = 0.71$. The right panel shows the comparison of the recovered C_ℓ and the WMAP data binned by $\Delta\ell = 5$.

Table 1: Statistical significance of the deviations from the scale-invariance.

range $[k_1 d, k_2 d]$	[100,150]	[150,200]	[200,250]	[250,300]	[300,350]	[350,400]
probability	18.20%	9.72%	3.08%	83.31%	16.52%	2.23%

range $[k_1 d, k_2 d]$	[100,400]	[150,350]	[175,225]
probability	1.41%	4.48%	0.39%

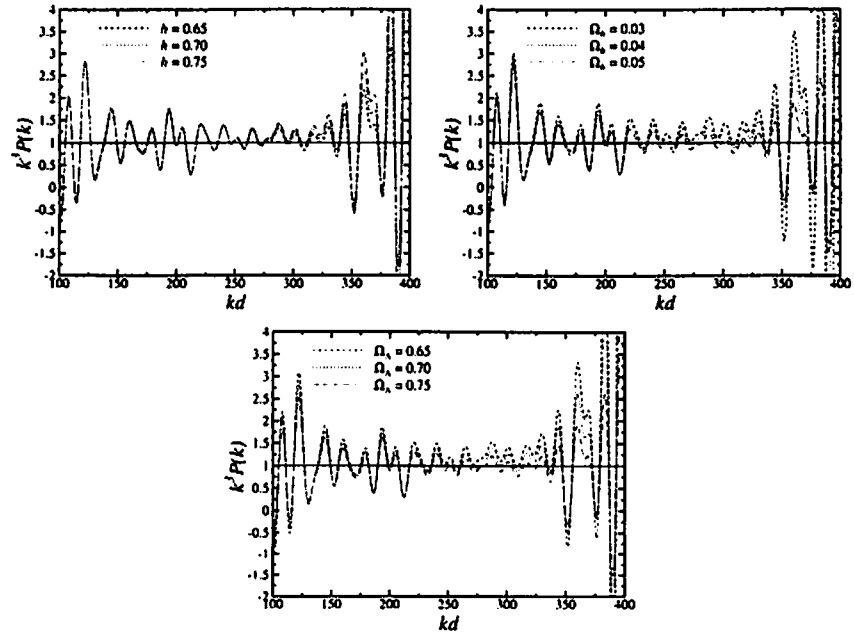

Figure 2: The reconstructed $P(k)$ from the WMAP data for (a) $h = 0.65, 0.70, 0.75$, $\Omega_b = 0.04$, $\Omega_\Lambda = 0.70$ (top-left panel), (b) $h = 0.70$, $\Omega_b = 0.03, 0.04, 0.05$, $\Omega_\Lambda = 0.70$ (top-right panel), (c) $h = 0.70$, $\Omega_b = 0.04$, $\Omega_\Lambda = 0.65, 0.70, 0.75$ (bottom panel), respectively.

Hadronic decay of SUSY particle and destruction of light elements

Kazunori Kohri[1]

Department of Earth and Space Science, Graduate School of Science Osaka University, Toyonaka OSAKA 560-0043

Masahiro Kawasaki

Research Center for the Early Universe (RESCEU), School of Science, The University of Tokyo, 7-3-1 Hongo, Bunkyo-ku, Tokyo 113-0033, Japan

Takeo Moroi

Department of Physics, Tohoku University, Sendai 980-8578, Japan

Abstract

In this talk, we consider the effects on big bang nucleosynthesis (BBN) of the hadronic decay of a long-lived massive particle in supergravity. If high-energy hadrons are emitted during/after the BBN epoch ($t \sim 10^{-2} - 10^{12}$ sec), they may change the abundances of the light elements through the destruction processes caused by such high energy hadrons, which may result in a significant discrepancy between standard BBN and observation. So far, these types of hadronic decay process in BBN have not been studied well without a few papers whose treatments were simple, because of severe shortage of hadron experimental data. However, recently the experiments of the high energy physics have been widely developed. Now we can obtain a lot of experimental informations of the hadron fragmentation in the high energy region and also simulate the process even in the higher energies where we have no experimental data by executing the numerical code of the hadron fragmentation, e.g. JETSET 7.4 Monte Carlo event generator. In addition, we have more experimental data of the hadron-nucleon cross sections. One of the candidates of the long-lived massive particle would be gravitino which appears in supergravity. If we consider general particle physics models in supergravity, it possibly decays during/after big-bang nucleosynthesis epoch. Compared with observational light element abundances, for the successful nucleosynthesis, we can obtain severe upper bound on reheating temperature after the primordial inflation which controls the primordial abundance of gravitinos. We discuss the implications of that result for cosmology, particle physics and nuclear physics.

[1] E-mail:kohri@vega.ess.sci.osaka-u.ac.jp

Big bang nucleosynthesis (BBN) is one of the most important tools to probe the early universe because it is sensitive to the condition of the universe from 10^{-2} sec to 10^{12} sec, for the review, see Ref. [1]. Therefore, from the theoretical predictions we can indirectly check the history of the universe in such an early epoch and impose constraints on hypothetical particles by observational light element abundances. Now we have a lot of models of modern particle physics beyond the standard model, e.g., supergravity or superstring theory, which predict unstable massive particles with masses of $O(100)$ GeV - $O(100)$ TeV, such as gravitinos, Polonyi fields, or moduli. They have long lifetimes because their interactions are suppressed by inverse powers of the gravitational scale ($\propto 1/M_{\rm pl}$). These exotic particles may necessarily decay during/after the BBN epoch ($T \lesssim O(1)$ MeV) if they have already existed in earlier stages.

If the massive particles X decay into quarks or gluons (see Fig. 1), during/after the BBN epoch $10^{-2} \lesssim t \lesssim 10^{12}$ sec. it is expected that non-standard effects are induced. If once the high-energy quarks or gluons are emitted, they quickly fragment into a lot of hadrons. Then, such high-energy hadrons are injected into the electromagnetic thermal bath which is constituted by photons, electrons, and nucleons (protons and nucleons) at that time.

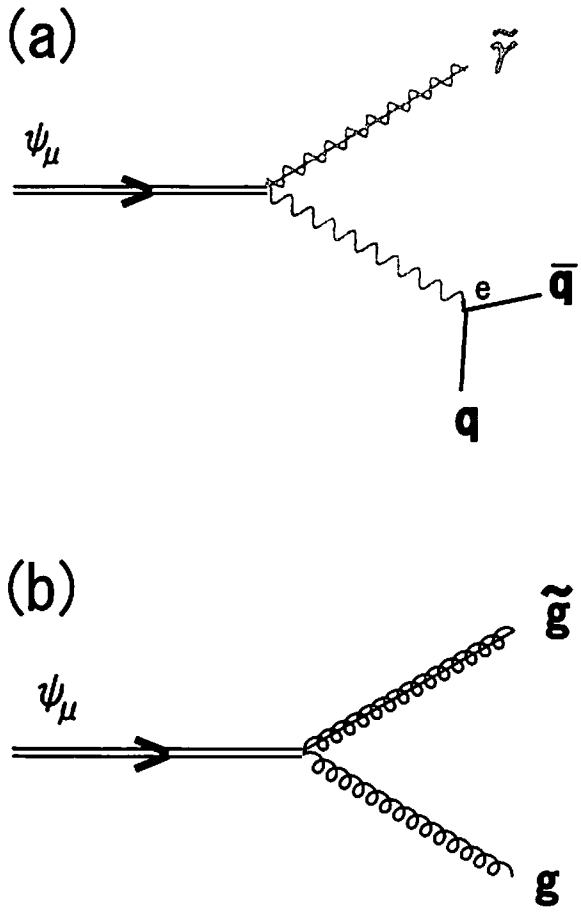

Figure 1: Feynman diagrams of the decay of a gravitino ψ_μ into (a) a photino $\tilde{\gamma}$ and a quark-antiquark pair $q\bar{q}$, and (b) a gluino $\tilde{g}$ and a gluon g.

For relatively short lifetime ($\lesssim 10^4$ sec), the emitted high-energy hadrons scatter off the background

photons and electrons because they are more abundant than the background nucleons. Then, almost all kinetic energy of the hadrons are transfered into the thermal bath through the electromagnetic interaction. As a result, they are completely stopped and reach to the kinetic equilibrium. After that time, they scatter off the background p or n through the strong interaction, and they inter-convert the background p and n each other even after the normal freeze-out time of the neutron to proton ratio n/p of the weak interaction. This effect extraordinarily tends to increase n/p. Therefore, the produced ^{4}He would be increased in the hadron injection scenario compared to standard big-bang nucleosynthesis (SBBN) [2].

On the other hand, for relatively longer lifetime ($\gtrsim 10^4$ sec), the other important effects occur. The emitted high-energy nucleons are no longer stopped in the electromagnetic plasma and directly scatter off the background nuclei such as proton or ^{4}He. Then ^{4}He is destroyed through strong interactions and produces many lighter nuclei and nucleons. The produced nuclei and nucleons still have high energies and induce the further hadronic showers, for the schematic picture, see Fig. 2. Namely this hadron showers produce a lot of light elements, and that may result in a significant discrepancy between SBBN and observations.

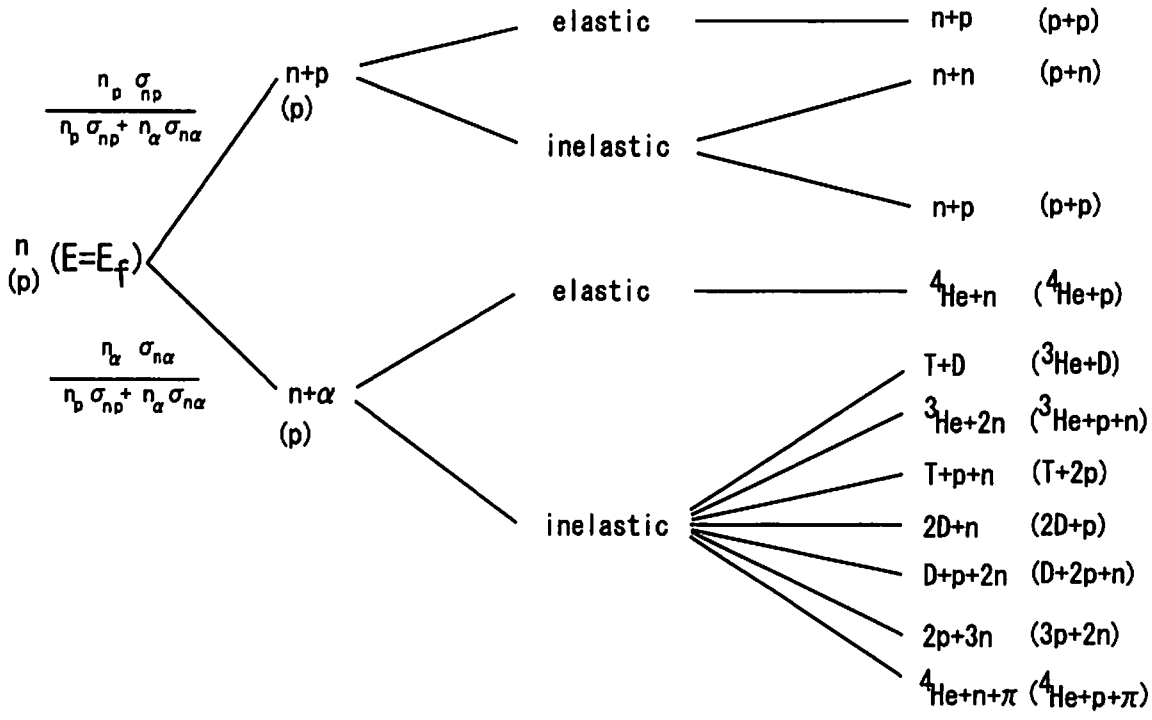

Figure 2: Schematic picture of hadron shower induced by a high energy neutron (proton) which scatters off the background proton or the background ^{4}He (α) with its energy $E = E_f$.

In this situation, we have obtained upper bounds on the abundance n_X/s as a function of the lifetime τ_X to agree with the observations for the wide range of the mass m_X = 100 GeV - 100 TeV which are relevant for various models of supergravity or superstring theory. We have also applied the results obtained by a generic hadronic decaying particle to gravitino $\psi_{3/2}$. Then we have got the upper bound on the reheating temperature after primordial inflation as a function of the mass. The details will be shown in Ref. [3].

References

[1] K. Hagiwara *et al.* [Particle Data Group Collaboration], Phys. Rev. D **66**, 010001-162 (2002).

[2] K. Kohri, Phys Rev D64, 043515 (2001) [astro-ph/0103411], and references therein.

[3] M. Kawasaki, K. Kohri and T. Moroi, in preparation.

Stationary Electromagnetic Fields around a Slowly Rotating Magnetized Neutron Stars

Yasufumi Kojima

Department of Physics,
Hiroshima University. Higashi-Hiroshima 739-8526, Japan
E-mail:kojima@theo.phys.sci.hiroshima-u.ac.jp

Abstract

Electromagnetic fields exterior to a slowly rotating relativistic star are solved. The analytic expression for the stationary fields is impossible in the presence of the spacetime dragging, but approximate one applicable to a wide range of parameters is given.

1 Introduction

Rich observational properties of neutron stars have unveiled gradually. In particular, enormously intense magnetic fields are inferred from recent observation associated with magnetars, i.e. magnetized neutron stars with $B = 10^{13} - 10^{15}$ Gauss. Violent dynamical events may be realized in compact stars as a consequence of both intense gravity and magnetic fields. In this paper, we consider stationary electromagnetic fields outside a rotating relativistic star. The effect of dense plasma is also important in constructing pulsar magnetosphere, since the electromagnetic fields strongly depend on charge density and current flow. This problem is one of difficult problems, and inherently requires highly numerical calculations for the coupled system of plasma and electromagnetic fields. We here neglect the plasma effect, but consider the general relativistic effect on the exterior fields in vacuum. The curved spacetime produced by a rotating relativistic star is important near the surface. Rotation of the magnetic dipole field induces the electric quadrupole field by imposing perfect conductivity condition at the surface. The analytic solutions are known for the flat spacetime, i.e. Deutsch solution[1]. The problem is straightforwardly extended to the curved spacetime, but there are no longer analytic expressions due to spacetime curvature and dragging. This problem was considered previously, but here a new method is developed [2], in which no low frequency approximation is used in solving the Maxwell equation. This is remarkably different from the previous work in solving for oblique rotator. In the previous work, the applicable range is limited within the light cylinder. An approximate method, useful solutions and the validity are discussed briefly. Details are given in Ref.[2]. We use the units of $c = G = 1$.

2 Stationary electromagnetic fields in vacuum

The general form of axially symmetric spacetime is given by

$$ds^2 = -\alpha^2 dt^2 + e^{2\psi}(d\phi - \omega dt)^2 + e^{2\mu}dr^2 + e^{2\eta}d\theta^2. \tag{1}$$

In this paper, the electromagnetic fields $\vec{E}$ and $\vec{B}$ are denoted by the values measured by "zero angular momentum observers", i.e. ZAMOs [3], and their components projected to a locally orthonormal tetrad frame are expressed as $\vec{E} = (E^{\hat{r}}, E^{\hat{\theta}}, E^{\hat{\phi}})$ and $\vec{B} = (B^{\hat{r}}, B^{\hat{\theta}}, B^{\hat{\phi}})$. We shall impose stationary condition on these fields. The stationarity means that a scalar function f should depend on the time t and the azimuthal angle ϕ in the combination $\phi' = \phi - \Omega t$. In the corotating frame with angular velocity Ω, the function is expressed as $f(r, \theta, \phi')$. The function is constant along the direction $\partial_t + \Omega\partial_\phi$. For vector fields, the condition can be described by the Lie derivative. Using the stationarity, the time derivative of a vector is eliminated and equations involving 'rotation $\nabla\times$' in the Maxwell equation are solved by scalar potentials for vacuum case. The electromagnetic fields are expressed by two functions, G and H:

$$\vec{E} = -\frac{1}{\alpha\Lambda}\left[e^{-\mu}G_{,r} + \varpi e^{\psi-\eta}\alpha^{-1}H_{,\theta},\ e^{-\eta}G_{,\theta} - \varpi e^{\psi-\mu}\alpha^{-1}H_{,r},\ e^{-\psi}\Lambda G_{,\phi}\right], \tag{2}$$

$$\vec{B} = -\frac{1}{\alpha\Lambda}\left[e^{-\mu}H_{,r} - \varpi e^{\psi-\eta}\alpha^{-1}G_{,\theta},\ e^{-\eta}H_{,\theta} + \varpi e^{\psi-\mu}\alpha^{-1}G_{,r},\ e^{-\psi}\Lambda H_{,\phi}\right], \tag{3}$$

where

$$\Lambda = 1 - \varpi^2 e^{2\psi}\alpha^{-2} = 1 - (\Omega - \omega)^2 e^{2\psi}\alpha^{-2}. \tag{4}$$

These functions should satisfy the equations $\vec{\nabla}\cdot\vec{E} = 0$ and $\vec{\nabla}\cdot\vec{B} = 0$. They are explicitly written as

$$\begin{aligned}&\Lambda\left[\alpha\left(e^{-\mu+\eta+\psi}\alpha^{-1}G_{,r}\right)_{,r} + \alpha\left(e^{\mu-\eta+\psi}\alpha^{-1}G_{,\theta}\right)_{,\theta} + e^{\mu+\eta-\psi}\Lambda G_{,\phi,\phi}\right]\\ &\quad - e^{-\mu+\eta+\psi}\Lambda_{,r}G_{,r} - e^{\mu-\eta+\psi}\Lambda_{,\theta}G_{,\theta} + K_r H_{,\theta} - K_\theta H_{,r} = 0,\end{aligned} \tag{5}$$

$$\begin{aligned}&\Lambda\left[\alpha\left(e^{-\mu+\eta+\psi}\alpha^{-1}H_{,r}\right)_{,r} + \alpha\left(e^{\mu-\eta+\psi}\alpha^{-1}H_{,\theta}\right)_{,\theta} + e^{\mu+\eta-\psi}\Lambda H_{,\phi,\phi}\right]\\ &\quad - e^{-\mu+\eta+\psi}\Lambda_{,r}H_{,r} - e^{\mu-\eta+\psi}\Lambda_{,\theta}H_{,\theta} - K_r G_{,\theta} + K_\theta G_{,r} = 0,\end{aligned} \tag{6}$$

where

$$K_j = \alpha\left(\frac{\varpi e^{2\psi}}{\alpha^2}\right)_{,j} + \frac{\varpi^2 e^{4\psi}}{\alpha^3}(\varpi)_{,j} \qquad (\text{for } j = r,\theta). \tag{7}$$

These equations (5) and (6) are symmetric under the transformation between $\vec{E}$ and $\vec{B}$, i.e. $\vec{E}\to\vec{B}$, by changing $G\to H$ and $H\to -G$. This property is generic one in the source-free Maxwell equations.

There is a singular surface, light cylinder for eqs.(5) and (6) as well as the poloidal components defined in eqs.(2) and (3). The velocity of corotating frame measured by ZAMOs becomes the light speed at the light cylinder, which corresponds to $\Lambda = 0$. The singularity is not physical, but mathematical drawback. We need special treatment at the surface. For example, in the direct numerical calculation eqs.(5) and (6) are solved in each side of the light cylinder so as to be continuously matched.

3 A method by series expansion

For the spacetime exterior to a slowly rotating star with spin angular momentum J, the metric functions are simplified. In particular, the light cylinder is expressed simply by

$$0 = \Lambda = 1 - b^2\sin^2\theta, \tag{8}$$

where

$$b = \frac{\varpi r}{\alpha}, \quad \varpi = \Omega - \frac{2J}{r^3}, \quad \alpha = \left(1 - \frac{2M}{r}\right)^{1/2}. \tag{9}$$

The light cylinder $r(\theta)$ is expressed by solving $b^{-2} = \sin^2\theta$ for r. In this case, there is a nice method using a series expansion to remove the problem associated with the light cylinder. The following expansion forms with respect to angular variables are useful:

$$\begin{cases} G(r,\theta) = \displaystyle\sum_{n=0}^{\infty} g_n(r)(\sin\theta)^{2n}, \\ H(r,\theta) = \cos\theta\left(\displaystyle\sum_{n=0}^{\infty} h_n(r)(\sin\theta)^{2n}\right) \end{cases} \tag{10}$$

for axially symmetric case (azimuthal wave number $m = 0$) and

$$\begin{cases} G(r,\theta,\phi,t) = e^{i(\phi-\Omega t)}\sin\theta\cos\theta\left(\displaystyle\sum_{n=0}^{\infty} g_n(r)(\sin\theta)^{2n}\right), \\ H(r,\theta,\phi,t) = e^{i(\phi-\Omega t)}\sin\theta\left(\displaystyle\sum_{n=0}^{\infty} h_n(r)(\sin\theta)^{2n}\right) \end{cases} \tag{11}$$

for non-axially symmetric case (azimuthal wave number $m = 1$).

We require that the poloidal fields given by eqs.(2) and (3) should be regular at the light cylinder. The numerators of these equations should vanish because the denominator, i.e. Λ goes to zero. Substituting $\sin^2\theta = b^{-2}$ in the numerators, we have two independent conditions. They are relations among the radial functions g_n, h_n. These regularity conditions should hold for $b \geq 1$, equivalently $r \geq r_c$, where r_c is defined by $b(r_c) = 1$. The value r_c becomes Ω^{-1} in the flat spacetime. It is not necessary for the radial functions to satisfy the regularity conditions in the inner region $r < r_c$. It may be possible to construct a global solution by smoothly matching the radial functions across the radius r_c. which are solved with and without the regularity conditions for each side. We however look for the solution satisfied or approximately satisfied with the constraints in the whole space exterior to the star. This method may restrict a class of solutions, but is free from the location of r_c. If there is no solution with the strong constraints in entire region outside the star, we should look for the solutions under weaker conditions.

We look for the Deutsch-type solutions in a curved spacetime, that is, electromagnetic fields originated from a rotating magnetic dipole in a fixed curved spacetime. It is possible to truncate the expansion series (10) and (11) up to $n = 1$ for the flat spacetime. We shall truncate them up to $n = 1$ for the spacetime around a slowly rotating star. The truncation leads to overdetermined system in the presence of spacetime dragging[2]. Therefore, the truncation is possible only in an approximate meaning. After obtained the solutions, we can check the approximation, e.g. by increasing order n.

4 Electromagnetic fields exterior to aligned rotator

The electromagnetic field are axially symmetric, when the dipole moment is parallel to the rotating axis. We consider the system described by $g_n, h_n (n = 0, 1)$. From the expansion coefficients in the divergence of electromagnetic fields, eqs.(5) and (6), we have three differential equations for the radial functions. Combined with two regularity conditions, there are five equations for four functions. These five equations are independent unless $\varpi' = 0$, i.e. except for non-rotating case. The system of equations is overdetermined. If the term $\mathcal{E}_1 = \frac{\varpi'}{\varpi} h_1$ is neglected, the system is reduced to four independent equations. In this case, we can solve the function $g_n, h_n (n = 0, 1)$. They are solutions in an approximate meaning, and the validity can be checked below. The analytic solutions for them are known in the literature. Using the solutions, the electromagnetic fields are given by

$$\bar{B} = \left[-h_0' \cos\theta, \frac{h_0}{\alpha r} \sin\theta, 0 \right], \tag{12}$$

$$\bar{E} = \left[\frac{2h_1}{\varpi r^2} P_2(\cos\theta), \frac{q_1}{\alpha r} \sin\theta\cos\theta, 0 \right], \tag{13}$$

where h_0, h_1 and q_1 are functions of r. See Ref.[2]. The neglected quantity is expressed as

$$\mathcal{E}_1 = \frac{\varpi'}{\varpi} h_1 \sim -\frac{9}{10} \left(4M^6 c_1 + 5J \right) \frac{\mu\omega}{Mr^3} \quad \propto r^{-6} \qquad (\text{for } r \gg M). \tag{14}$$

This value (14) can be regarded as an 'error' for the consistency of our method. The actual value of the 'error' is quite small, and therefore the analytic expressions are applicable to almost every case.

We have so far considered the lowest approximation by truncating the series expansion at $n = 1$. Within the approximation, the system was overdetermined. One might think that this drawback may be recovered by extending n to a larger value. The answer is no unless n is finite. The system is still overdetermined. For example, we increase the degree of freedom up to $n = 2$. In this case, we have five differential equations from the divergence of electromagnetic fields. In addition, there are two regularity conditions. Therefore, we have seven equations for six radial functions $g_n, h_n (n = 0, 1, 2)$. The seven equations are reduced to six independent ones for $\varpi' = 0$. The 'error' term becomes

$$\mathcal{E}_2 = \frac{\varpi'}{\varpi} h_2. \tag{15}$$

This term is smaller than $\mathcal{E}_1$, that is, the accuracy significantly increases compared with the first-order case.

5 Electromagnetic fields exterior to perpendicular rotator

In this section, the axis of the magnetic dipole is assumed to be perpendicular to the rotational axis. The resultant electromagnetic fields are non-axially symmetric, and depend on $e^{i\phi}$, (or $e^{-i\phi}$). The method to solve the Maxwell equation is almost the same as done in the axially symmetric case.

We consider the case described by $g_n, h_n (n = 0, 1)$. These radial functions should satisfy five equations if $\varpi' \neq 0$. The system is overdetermined. If an inconsistency term is neglected, then we have solution in an approximate meaning. The electromagnetic fields are governed by a pair of coupled equations for radial functions, F_1 and F_2:

$$\alpha^2(\alpha^2 F_1')' + \left(\varpi^2 - \frac{2\alpha^2}{r^2}\right) F_1 + \frac{1}{3}\alpha^2 \varpi' F_2 = 0, \tag{16}$$

$$\alpha^2(\alpha^2 F_2')' + \left(\varpi^2 - \frac{6\alpha^2}{r^2}\right) F_2 - 3\alpha^2 \varpi' F_1 = 0. \tag{17}$$

These equations are reduced to Regge-Wheeler wave-equations F_l $(l = 1, 2)$ in the limit of non-rotating case. Using functions F_1 and F_2, the electromagnetic fields are expressed as

$$\vec{B} = \left[-\frac{1}{r^2} F_1 \sin\theta e^{i\phi'}, \quad -\left(\frac{\alpha}{2r} F_1' + \frac{\varpi}{6\alpha r} F_2\right) \cos\theta e^{i\phi'}, \quad -i\left(\frac{\alpha}{2r} F_1' + \frac{\varpi}{6\alpha r} F_2 \cos 2\theta\right) e^{i\phi'}\right], \tag{18}$$

$$\vec{E} = \left[-\frac{1}{2r^2} F_2 \sin 2\theta e^{i\phi'}, \quad \left(\frac{\varpi}{2\alpha r} F_1 - \frac{\alpha}{6r} F_2' \cos 2\theta\right) e^{i\phi'}, \quad i\left(\frac{\varpi}{2\alpha r} F_1 - \frac{\alpha}{6r} F_2'\right) \cos\theta e^{i\phi'}\right]. \tag{19}$$

In case of flat spacetime, eqs.(16) and (17) are decoupled, and their analytic solutions are possible. In the presence of curvature $\alpha \neq 1$, there are no analytic solutions due to backscatter. Furthermore, the presence of spacetime dragging causes the coupling of two equations with the coefficient $\varpi' = 6J/r^4$.

The 'error' term involving our method is estimated as

$$\mathcal{Y} = -\frac{2J}{r^4} F_2. \tag{20}$$

This does not vanish in general, but rapidly decreases to zero with the radius because of the factor $2J/r^4$. In fact, we can find

$$\mathcal{Y} \sim -\frac{6\mu J \Omega R^2}{r^6} \quad \text{(near the light cylinder)}, \tag{21}$$

$$\sim \frac{2\mu J \Omega^3 R^2 \exp\{i\Omega(r + 2M\ln(r/2M - 1))\}}{r^4} \quad \text{(beyond the light cylinder)}. \tag{22}$$

Since the function F_2 describes the induced electromagnetic fields by rotating perfect conductor, it is regarded as the first order quantity with respect to the low frequency expansion. The term (20) was therefore neglected in the previous approximation. There are some analytic expressions near the stellar surface derived by the low frequency approximation [4]. Their analytic result becomes invalid roughly before the light cylinder[2].

References

[1] Deutsch A.J., 1955, Annales d'astrophysique, 18, 1

[2] Kojima Y., Matsunaga N., Okita, T., 2004, MNRAS in press

[3] Thorne K.S., Price R.H., Macdonald D.A., 1986, *Black Hole: The Membrane Paradigm.* Yale University Press, New Haven

[4] Rezzolla L., Ahmedov B.J., Miller J.C., 2001, MNRAS, 322, 723

Gravitational Radiation from the Collapse of Massive Stars

Kei Kotake[1], Shoichi Yamada[2], Katsuhiko Sato[3]

[1]*Department of Physics, School of Science, The University of Tokyo, 7-3-1 Hongo, Bunkyo-ku, Tokyo 113-0033, Japan, email: kkotake@utap.phys.s.u-tokyo.ac.jp*
[2]*Science & Engineering, Waseda University, 3-4-1 Okubo, Shinjuku, Tokyo, 169-8555, Japan*
[3]*Research Center for the Early Universe (RESCEU), School of Science, The University of Tokyo, 7-3-1 Hongo, Bunkyo-ku, Tokyo 113-0033, Japan*

Abstract

We have done a series of two-dimensional hydrodynamic simulations of the rotational collapse of a supernova core in axisymmetry. We have employed a realistic equation of state (EOS) and taken into account electron captures and neutrino transport by the so-called leakage scheme. It is an important progress to apply the realistic EOS coupled with the microphysics to 2-D simulations for computing gravitational radiation in rotational core collapse. We have used the quadrupole formula to calculate the amplitudes and the waveforms of gravitational wave assuming the Newtonian gravity. From these computations, we have extended the conventional category of the gravitational waveforms. Our results have shown that the peak amplitudes of gravitational wave are mostly within the sensitivity range of the laser interferometers such as TAMA and first LIGO for a source at a distance of 10 kpc. Furthermore we have found that the amplitudes of the second peaks are within the detection limit of first LIGO for the source and first pointed out the importance of the detections, since they will give us the information as to the angular momentum distribution of evolved massive stars.

1 Introduction

Asymmetric core collapse and supernova have been supposed to be one of the most plausible source of gravitational radiation for the long-baseline laser interferometers (GEO600, LIGO, TAMA, VIRGO). The detection of the gravitational signal is important not only for the direct confirmation of general relativity but also for the understanding of supernovae themselves because the gravitational wave is only a window that enables us to see directly the innermost part of an evolved star, where the angular momentum distribution and the equation of state are unknown.

Observationally, the asymmetric aspects of the dynamics of supernovae are evident because they are confirmed by many observations of SN 1987A and by the kick velocity of pulsars. On the other hand, there is no consensus of the origin of asymmetry theoretically. However, provided the facts that the progenitors of collapse-driven supernovae are a rapid rotator on the main sequence and that the recent theoretical studies suggest a fast rotating core prior to the collapse [1], rotation should play an important role as the origin of the asymmetric motions in the core collapse. It is noted that anisotropic neutrino radiations induced by rotation [2] could induce a jet-like explosion [3] as suggested by the observations of SN 1987A.

So far there have been works devoted to study the gravitational radiation in the rotational core collapse (see [4] for a review). To say rigorously, reliable core collapse simulations should require the implementation of a realistic equation of state (EOS), an adequate treatment of microphysics (electron captures and other weak interactions) and neutrino transport, and a relativistic treatment of gravitation. However it is difficult to incorporate all of them at the same time. Therefore previous investigations have neglected or approximated the above requirements partially. So far most of the computations have oversimplified the microphysics. In addition, it has been reported that general relativity does not alter the significant features of gravitational radiation compared with those obtained in Newtonian approximation such as the range of gravitational wave amplitudes and frequencies. This situation motivates us to employ a realistic EOS and treat microphysics adequately in the Newtonian gravity. In this paper, we will study

the wave forms of gravitational radiation elaborately by performing the improved rotational core collapse simulations and will discuss what information can be extracted from the analysis.

We describe the numerical models in the next section. In the third section, we show the main numerical results. Conclusion is given in the last section.

2 Initial Models and Numerical Methods

We know little of angular momentum distributions in a core of evolved massive stars. Although it is supposed that some instabilities grow and transport angular momentum during the quasi-static evolutions, which mode prevails in what time scale is not understood very well at present. Therefore, we assume in this study the following two possible rotation profiles, which are the shell-type or cylindrical. We have computed twelve models changing the combination of the total angular momentum, the rotation law, and the degree of differential rotation. We will choose some representative models, which clearly illustrates the effects of rotation on the gravitational signals in this contribution. For more detailed information, see the paper [5]. The numerical method for hydrodynamic computations employed in this paper is based on the ZEUS-2D code [6]. We have made several major changes to the base code to include the microphysics. First we have added an equation for electron fraction to treat electron captures, which is solved separately. We have approximated electron captures and neutrino transport by the so-called leakage scheme. Second, we have incorporated the tabulated equation of state (EOS) based on the relativistic mean field theory [7] instead of the ideal gas EOS assumed in the original code. It is noted that the implementation of the recent realistic EOS to 2-D simulations is an important progress beyond the previous calculations. For a more detailed description of the methods, see Kotake et al. [2].

3 Results

3.0.1 The Properties of the Waveform

We first show the general properties of the waveform with collapse dynamics. We choose model A, which is based on the recent stellar evolution calculation [1]. The time evolution of the amplitude of gravitational wave are shown in the left panel of Figure 1. As the inner core shrinks, the central density increases and a core bounce occurs when the central density reaches its peak at $t_b \cong 243$ msec with $2.65\ 10^{14}$ g cm^{-3}. At this time, the absolute value of the amplitude becomes maximum. After the core bounce, the core slightly re-expands and oscillates around its equilibrium. As a result, the gravitational wave shows several small bursts and begins to decay. These gross properties are common to all other models. However, there exist some important differences when we compare them in more detail. We will discuss the differences in the following.

In the right panel of Figure 1, the time evolution of the amplitude of gravitational wave for model B, which has a cylindrical rotation law with strong differential rotation, are given. By comparing the left with the right panel of Figure 1, the oscillation period of the inner core for model B is clearly longer than for model A. In other words, the pronounced peaks can be seen distinctively in this case. This is because the central density becomes more smaller after the distinct bursts by the strong differential rotation. This effect increases with the initial angular momentum. It is also found that the signs of the values of the second peaks are negative for model B, on the other hand, positive for model A. Note that we will speak of the second peak where the absolute amplitude is second largest. The above characteristics are common to the models for strongly differential rotation with cylindrical rotation law.

3.0.2 Maximum Amplitude and Second Peak

The values of maximum amplitude for all our models range from $5 \times 10^{-21} \leq h^{TT} \leq 3 \times 10^{-20}$, which is almost the same as the results by Zwerger et al. [8] and Mönchmeyer et al. [9]. On the other hand, the values of the standard models by Yamada & Sato [10] are about an order of magnitude lower. This is understood as follows. They employed a parametric EOS by which the effects of microphysical and transport processes were assumed to be expressed. Since they found that the maximum amplitude is most sensitive to the adiabatic index at the subnuclear density by their parametric surveys, we pay attention

to this. Compared to their EOS, our realistic EOS is rather soft for the subnuclear density regime. At the regime, our realistic EOS can express the softening of EOS by the effect that the nuclear interactions become attractive. Due to this effect, the inner core can shrink more compact at core bounce, which results in the larger maximum amplitude. It is naturally suggested that we may get the information about the subnuclear matter if we can detect the gravitational wave from the rotationally collapsing cores. We hope it can be realized in the near future since the maximum amplitudes for our models are mostly within the detection limit for TAMA and first LIGO which are now in operation if a source is located at a distance of 10 kpc (see Figure 2).

As pointed earlier, we find that the signs of the values of the second peaks are negative for the models for strongly differential rotation with cylindrical rotation law and positive for the others. The absolute amplitudes of the second peak are also presented in Figure 2. As shown, they are within the detection limit of first LIGO for a source at a distance of 10 kpc. In addition, it seems quite possible for the detectors in the next generation such as advanced LIGO and LCGT to detect the difference. Therefore if we can find the difference of the signs of the second peaks by observations of gravitational wave, we will obtain the information about the angular momentum distribution of evolved massive stars. Since there is no way except for the detection of the gravitational wave to obtain the information, it is of great importance to detect the second peaks in the future.

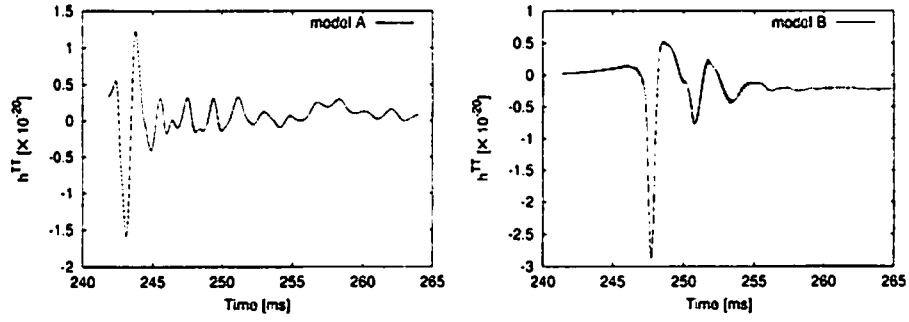

Figure 1: Time evolutions of the amplitude of gravitational wave for model A (left panel) and B (right panel). Note that the distance of the source is assumed to be located at the distance of 10 kpc.

4 Conclusion

We have done a series of two-dimensional hydrodynamic simulations of the rotational collapse of a supernova core and calculated gravitational waveforms using the quadrupole formula. We have employed a realistic EOS and taken into account electron captures and neutrino transport in an approximated method. We have found the following:

1. The peak amplitudes of gravitational wave obtained in this study are mostly within the detection limits of the detectors of TAMA and first LIGO which are now in operation if a source is located at a distance of 10 kpc. In addition, the peak amplitude becomes extrema for the models whose initial rotation rate is moderate.

2. The waveforms are categorized into the criteria by Zwerger et al. [8]. In addition, we further find that type II does not occur for models with shellular rotation law, on the other hand, does occur regardless of the initial rotation rate in case of strong differential rotation with cylindrical rotation law, and that the type III does not occur if a realistic EOS is employed.

3. At the subnuclear density regime, our realistic EOS can express the softening of EOS by the effect that the nuclear interactions become attractive. Therefore the inner core can shrink more compact at core bounce than the other work [10] in which EOS is expressed in a parametric manner. Subsequently, this results in the larger maximum amplitude. It follows that we may get the information about the

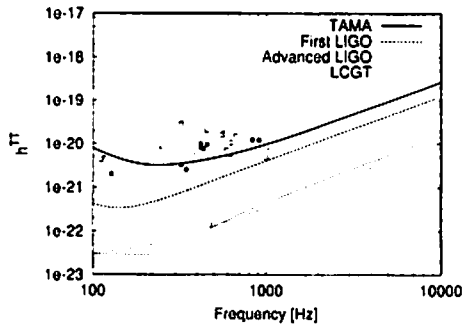

Figure 2: Detection limits of TAMA, first LIGO, advanced LIGO, and LCGT with the expected amplitudes from numerical simulations. The open squares represent the maximum amplitudes for all the models. On the other hand, the pluses and the closed squares represent the amplitudes of second peaks for models with strong differential rotation with cylindrical rotation law and for the other models, respectively. We estimate the characteristic frequencies by the inverse of duration periods of the corresponding peaks. Note that the source is assumed to be located at the distance of 10 kpc.

subnuclear matter if we can detect the gravitational wave from the rotationally collapsing cores.

4. The signs of the values of the second peaks are negative for the models with strong differential rotation with the cylindrical rotation law, on the contrary, positive for the other models. The absolute amplitudes of the second peaks are within the detection limit of first LIGO. Therefore if we can detect the signs of the second peaks, it will give us the information as to the angular momentum distribution of massive evolved stars when a supernova occurs at our galactic center.

As stated earlier, the detection of gravitational wave is likely for the models whose initial rotation rate is moderate. According to the study of rotational core collapse by Kotake et al. [2], the anisotropic neutrino radiation is well induced by such a rotation rate. Noting that the anisotropic neutrino radiation can induce the globally asymmetric explosion [3], the detection of gravitational wave will be a good tool to help understand the explosion mechanism itself. We are currently preparing for a sequel of this work, in which the effects of the magnetic fields on the gravitational wave are investigated. This will be presented in the forthcoming paper [11].

References

[1] A. Heger, N. Langer and S. E. Woosley, Astrophys. J. **528**, 368, (2000).

[2] K. Kotake, S. Yamada, and K. Sato, Astrophys. J. **595**, 304, (2003).

[3] T. M. Shimizu, T. Ebisuzaki, K. Sato, and S. Yamada, Astrophys. J. **552**, 756, (2001).

[4] K. S. New, accepted for publication in Living Reviews in Relativity, gr-qc/0206041.

[5] K. Kotake, S. Yamada, and K. Sato, Phys. Rev. D. **68**, 044023, (2003).

[6] J. M. Stone and M. L. Norman, Astrophys. J. Supl. **80**, 753, (1992).

[7] H. Shen, H. Toki, K. Oyamatsu, and K. Sumiyoshi, Nucl. Phys. **A637**, 43, (1998).

[8] T. Zweger and E. Müller, Astron. Astrophys. **320**, 209, (1997).

[9] R. Mönchmeyer, G. Schäfer, E. Müller, and R. E. Kates, Astron. Astrophys. **246**, 417, (1991).

[10] S. Yamada and K. Sato, Astrophys. J. **450**, 245, (1995).

[11] K. Kotake, S. Yamada, K. Sato, K. Sumiyoshi, H. Ono, and H. Suzuki, Phys. Rev. D (2004) in press.

The three-point correlation functions in the non-linear gravitational clustering regime

Hiroko Koyama[1], Taihei Yano[2]

National Astronomical Observatory, Mitaka, Tokyo 181-8588, Japan

Abstract

The connection between the two-point and the three-point correlation functions in the non-linear gravitational clustering regime is studied. We derive a new formula about the relationship between these correlation functions under the scaling hypothesis. In particular, if the Fourier phases keep correlated through the non-linear effects, we find that the three-point correlation function ζ obeys the scaling law, $\zeta \propto \xi^{\frac{3m+4w}{2m+2w}}$, where ξ is the two-point correlation function, m is the power index of the power spectrum in the non-linear gravitational clustering regime and w is the spatial dimension.

1 Introduction

Formation of large-scale structures of the Universe is one of the most important and interesting problems in cosmology. It is generally believed that these structures have developed by a process of gravitational instability from small initial fluctuations in the density of a largely homogeneous early Universe. Hence, it is very important to clarify physical mechanism of the evolution of density fluctuations by a gravitational instability.

The inflationary scenario predicts a random Gaussian field possessing the properties of statistical homogeneity and isotropy as the primordial fluctuations. The statistical properties of the Gaussian field are completely characterized by the two-point correlation function (hereafter 2PCF) or the power spectrum, since higher order correlations vanish although the two-point correlation function 2PCF has a certain value. However, the non-linear gravitational clustering gives rise to non-zero values of the higher-order correlations, even if the primordial density fluctuations were indeed Gaussian. When we consider the evolution is governed by non-linear gravitational clustering, in other words, higher order statistics, like the three-point correlation function (hereafter 3PCF), become essential. Therefore it is a quite important subject for understanding the non-linear evolution to investigate the property of the 3PCF.

Generally, it is hard to deal with the exact formula of the 3PCF both theoretically and numerically, since it is much more lengthy and complicated than 2PCF. Historically an assumption had proposed[2, 1]; The 3PCF can be expressed by the product of the 2PCF as

$$\zeta_{abc} = Q[\xi_a\xi_b + \xi_b\xi_c + \xi_c\xi_a], \tag{1}$$

where ζ, ξ, and Q are the 3PCF, the 2PCF, and a certain constant, respectively. The expression (1) or $\zeta \propto \xi^2$ is often called "hierarchical form". The data from the Zwicky and Shane-Wirtanen catalogs are in good agreement with the model when we choose $Q \simeq 0.85$ for Zwicky and $Q \simeq 1.24$ for Shane-Wirtanen [2, 1].

However there is a serious fault about the proposal (1). It has no theoretical ground, although some observational or numerical data may be well-fitted. One explanation may be that the form of Eq. (1) for ζ with $Q = 1$ resembles the Kirkwood superposition approximation occasionally used in liquid physics and turbulence theory, if $\xi_a\xi_b\xi_c \ll 1$. However this approximation is not appropriate for the non-linear regime, since the distribution of the gravitational sources is strongly correlated, $\xi \gg 1$, in such regimes. Hence this resemblance is helpless to excuse the theoretical defect.

[1]E-mail:hiroko.koyama@nao.ac.jp
[2]E-mail:yano.t@nao.ac.jp

Indeed, there were many theoretical investigations about the 3PCF. Nevertheless their analyses are based on the "hierarchical form" assumption; The coefficient Q under the "hierarchical form" was estimated by assuming self-similarity. The BBGKY hierarchy was analyzed by assuming the "hierarchical form" as well as self-similarity. In the first place, however, there is no reason why the 3PCF should necessarily depend only on the second power of the 2PCF, even if we accept the self-similarity. Indeed, the possibility of solutions which do not satisfy the "hierarchical form" on the bases of the BBGKY equations has been suggested. Therefore investigating physical adequacy for "hierarchical form" itself and more reliable and useful formulae for the 3PCF are required pressingly.

In this paper we study the connection between the 2PCF and the 3PCF in the non-linear gravitational clustering regime. Since the gravity is scale free, we assume the time evolution of the statistics obeys also some self-similar rules. The power spectrum in the non-linear regime is assumed to obey a power law. In addition, phases between Fourier modes in the bispectrum are considered to be also correlated in the non-linear regime, where galaxies or galaxy groups are strongly clustered each other. We suppose the self-similarity where the bispectrum obeys also self-similar rules as well as the power spectrum. What is unique is that we never assume the "hierarchical form". Consequently, we obtain the new formula between the 2PCF and the 3PCF, focusing to their power indices. The relevance to the "hierarchical form" is also discussed. In Sec.2 we obtain the new connection with these statistics under the scaling hypothesis. The final section is devoted to summary.

2 The connection between the 2PCF and the 3PCF under the scaling hypothesis

In this section we derive the connection between the 2PCF and the 3PCF, under the scaling hypothesis. This assumption is adequate, since we consider that fluctuations evolve due to purely gravity.

Let us denote by $\bar{\rho}$ the mean density and take $\rho(\boldsymbol{x})$ to be the density at a point specified by the position vector $\boldsymbol{x}$ with respect to some arbitrary origin. As usual, we define the fluctuation to be

$$\delta(\boldsymbol{x}) = \frac{\rho(\boldsymbol{x}) - \bar{\rho}}{\bar{\rho}}. \tag{2}$$

We assume this to be expressible as a Fourier series:

$$\delta_{\boldsymbol{k}} = \frac{1}{L^w} \int \delta(\boldsymbol{x}) e^{i\boldsymbol{k}\cdot\boldsymbol{x}} d^w x, \tag{3}$$

$$\delta(\boldsymbol{x}) = \int_{-\infty}^{\infty} \delta_{\boldsymbol{k}} e^{-i\boldsymbol{k}\cdot\boldsymbol{x}} \frac{L^w}{(2\pi)^w} d^w k, \tag{4}$$

where $\delta_{\boldsymbol{k}}$ is a Fourier amplitude, and w is the number of spatial dimension.

Firstly, we assume the power spectrum in the non-linear regime obeys a power law as

$$\begin{aligned} P(k) &= \langle |\delta_k|^2 \rangle \\ &\propto k^m, \end{aligned} \tag{5}$$

where the index is a value in the non-linear regime. Substituting Eq.(5) into Eq.(??) gives

$$\begin{aligned} \xi(r) &\propto \int k^m d^w k \\ &\propto r^{-(m+w)}. \end{aligned} \tag{6}$$

Next, the bispectrum in Eq. (??) is decomposed by

$$B(k, k') = \left\langle |\delta_k||\delta_{k'}||\delta_{-k-k'}| e^{i(\phi_k + \phi_{k'} + \phi_{-k-k'})} \right\rangle, \tag{7}$$

where ϕ_k is the Fourier phase of the modes with a wave number k.

Now we consider the Fourier phases in Eq.(7) in the non-linear regime. Let the initial fluctuations are a random Gaussian field whose phases are distributed randomly. Induced by the gravitational instability, however, the density fluctuations become more and more strong, which means the phases between Fourier modes become distributed non-randomly. That is, the Fourier phases are also correlated due to the gravitational clustering. It is not difficult to imagine that the phases are extremely assemble in the case of the gravitational collapse like a pancake, for example.

Generally, the 3PCF or the bispectrum depend on the shape of the configuration. If we fix the shape of the triangle, however, the 3PCF and the bispectrum are determined by one parameter. Here we assume the bispectrum in the strong non-linear regime obeys a scaling law as well as the power spectrum. Hence the expectation value of the Fourier phase in the bispectrum (7) is described as

$$\langle e^{i(\phi_{kt}+\phi_{k't}+\phi_{-kt-k't})}\rangle \propto t^{-\alpha}\langle e^{i(\phi_k+\phi_{k'}+\phi_{-k-k'})}\rangle \tag{8}$$

in the strongly non-linear regime. Assuming the scaling hypothesis corresponds to considering the following two characteristic possibilities physically; First, the Fourier phases keep correlated, and the expectation value converges to some non-zero constant value through the non-linear gravitational clustering. In this case the value of α in Eq. (8) is zero. Second, the Fourier phase correlations disappear finally due to non-linear gravitational clustering, although the phases may be correlated by gravitational instability at once. In this case the expectation value of the Fourier-phase correlations converges to zero, and the value of α in Eq. (8) is some finite value which is depend on the way to converge. That is, the constant α should be a non-negative value. Similarly, other terms in Eq. (7) are also assumed to obey some scaling laws.

The 3PCF is reduced to

$$\begin{aligned}
\zeta(r,s) &\propto \iint B(k,k')d^wkd^wk' \\
&\propto t^{-(\frac{3}{2}m+2w-\alpha)}\iint\langle|\delta_{tk}|\rangle\langle|\delta_{tk'}|\rangle\langle|\delta_{-tk-tk'}|\rangle\langle e^{i(\phi_{tk}+\phi_{tk'}+\phi_{-tk-tk'})}\rangle d^w(tk)d^w(tk') \\
&\quad +t^{-(\frac{3}{2}m+2w-\beta-\gamma_{4y})}\iint\langle|\delta_{tk}|\rangle\langle|\delta_{tk'}|\rangle\langle|\delta_{-tk-tk'}|\rangle\langle\delta e^{i(\phi_{tk}+\phi_{tk'}+\phi_{-tk-tk'})}\rangle d^w(tk)d^w(tk') \\
&\quad +\cdots .
\end{aligned} \tag{9}$$

Where β and γ is the scaling factors of variance and other constants. Each value of these factors should be positive or zero so that the 3PCF should not diverge. Then the 3PCF can be approximated by

$$\zeta(r,s) \propto t^{-(\frac{3}{2}m+2w-\epsilon)}\zeta\left(\frac{r}{t},\frac{s}{t}\right), \tag{10}$$

that is,

$$\zeta(rt,st) \propto t^{-(\frac{3}{2}m+2w-\epsilon)}, \tag{11}$$

where ϵ is defined as

$$\epsilon \equiv min(\alpha,\ \beta+\gamma_{2y},\ \beta+\gamma_{3y},\ \beta+\gamma_{4y}). \tag{12}$$

From Eqs.(6) and (11), we finally obtain a new connection between ζ and ξ as

$$\zeta \propto \xi^{\frac{3m+4w-2\epsilon}{2m+2w}}. \tag{13}$$

The formula (13) states that the 3PCF is proportional to the power of the 2PCF. The power index depends on the power index of the power spectrum in the non-linear regime, m, and the scaling factors of the bispectrum, ϵ. The formula clarifies the source of the power index of the 3PCF, for the first time, under the scaling hypothesis.

Now we consider the case where the Fourier phases keep correlated through the non-linear effects. In this case the expectation value of the phase correlations converges to a finite constant value, $\alpha = 0$. Then the power index of the formula (13) depends only on the index of the power spectrum and the number of the spatial dimension,

$$\zeta \propto \xi^{\frac{3m+4w}{2m+2w}}. \tag{14}$$

Accordingly, the 3PCF can be described as the closed form only by the 2PCF. In addition, if the power index of the power spectrum is zero, $m = 0$, the 3PCF is proportional to the second power of the 2PCF. Remind that the index of the power spectrum is around zero in the transitional region from the linear regime to the non-linear regime, if the power index of the power spectrum of the initial random Gaussian field is not negative value. Considering these facts, we suppose the "hierarchical form" is realized accidentally around such quasi-linear scales. On the other hand, it is proper from our formula that the power index of the 3PCF deviates from the second power of the 2PCF in the strongly non-linear regime, if the phases keep correlated.

3 Summary

In this paper we have studied the connection between the 2PCF and the 3PCF in the non-linear gravitational clustering regime. Under the scaling hypothesis to the bispectrum as well as the power spectrum, we have obtained new formula about the 3PCF. It is striking that the origin of the power index of the 3PCF has been revealed for the first time.

Under the scaling hypothesis, there remain two characteristic possibilities for the phases of the Fourier modes; they keep correlated or tend to become uncorrelated in the strongly non-linear regime. Our analytical formula says that if the phases of the Fourier modes keep correlated in the strongly non-linear regime, the power index of the 3PCF can be expressed as the closed form by the 2PCF. If the Fourier phases become distributed randomly asymptotically due to the non-linear gravitational clustering, on the other hand, the power index of the 3PCF consists not only of the information of 2PCF, but also of that of the higher statistics. However, our numerical simulations supports that phases keep correlated in the highly non-linear regime, since the numerical results agree to the analytical formula in the case where phases of the Fourier modes keep correlated, Eq. (14) rigorously. Therefore it is Eq. (14) that new and reliable formula between the 2PCF and the 3PCF in the non-linear gravitational clustering regime. In the strict sense, the "hierarchical form", $\zeta \propto \xi^2$, is reproduced only when the power index of the power spectrum is zero. As results, we have achieved more comprehensive understanding for the hierarchy of the higher-order statistics than before.

It is believed generally that the power index of the power spectrum in the non-linear regime, m, depends on the initial power spectrum. Combining this fact and our formula, Eq. (14), we can claim that the power index of the 3PCF originates from the initial power spectrum. Therefore, it is an important future work to clarify the relationship between the power spectrum in the non-linear regime and the initial one.

Radical progress of recent observations needs increasingly advanced and practical formalism for analyses containing the higher-order statistics. Standing on such circumstances, our new formula is expected to be a good indicator to understand the non-linear gravitational clustering. For the purpose it is a succeeding subject to check if the new formula is consistent with the BBGKY hierarchy. In addition, it will be also important to complete the formula by investigating the coefficients as well as the power indices, in order to inspect the adjustment with the "hierarchical form" and to understand the origin of the parameter Q. We hope the new formula become a very useful instrument for analysis of the large-scale structure.

References

[1] Groth, E. J., & Peebles, P. J. E. 1977, APJ, 217, 385.

[2] Peebles, P. J. E., & Groth, E. J. 1975, APJ, 196,1.

[3] Koyama, H., & Yano, T. 2003, astro-ph/0308454

Inflation in brane models with radion stabilization

Kazuya Koyama [1],

Department of Physics, Tokyo University, Japan

Abstract

The low energy effective theory in a stabilized Randall-Sundrum model is derived. Then a stable configuration of the inflationary branes is constructed. Difficulties in constructing a realistic inflationary model are addressed.

1 Introduction

The hierarchy problem is one of the most serious problems in particle physics. Why is the Planck scale $M_{pl} \sim 10^{18}$ GeV much higher than the electroweak scale $M_{ew} \sim 10^3$ GeV ? Why is such a large hierarchy stable under radiative corrections? One way to solve this problem is to introduce the supersymmetry which prevents the electroweak scale from receiving radiative corrections. Supersymmetric theories predict the existence of superpartner particles but, so far, none of the superpartner particles is detected. Thus it would be important to consider an alternative way to explain the hierarchy problem.

Recently, according to the development of brane world ideas, an interesting possibility is proposed. The key aspect of brane world ideas is that the dimensionality could be different for matter fields and the gravity. The gravity can propagate into the whole higher dimensional spacetime. On the other hand, matter fields are confined to the lower dimensional brane. The scale for the gravity is determined by the higher dimensional Planck scale, say M_*. If this scale is of the same order as M_{ew}, there is no hierarchy problem. Of course, we should explain why the Planck scale in 4D spacetime is M_{pl} not M_{ew}. This can be explained by that fact that the higher dimensional gravity couples to matter fields very weakly on the brane.

Randall and Sundrum proposed an interesting model based on this idea [1]. They consider the 5D AdS spacetime bounded by two branes. The 5D spacetime is described by the metric

$$ds^2 = dy^2 + e^{-2ky}\eta_{\mu\nu}dx^\mu dx^\nu, \tag{1}$$

where k is the curvature scale of the AdS spacetime. The branes are located at $y = 0$ and $y = d_0$ respectively. The tension of the branes is positive and negative respectively and we are assumed to live in negative tension brane located at $y = d_0$. The 4D planck scale on the negative tension brane is given by

$$M_{pl}^2 = (e^{2kd_0} - 1)M_*^3/k. \tag{2}$$

So, if $kd_0 \sim 37$, M_{pl} can be 10^{18} GeV even if k and 5D Placnk scale M_* are of the order M_{ew}.

In order to realize this scenario, the stabilization of the distance between two branes (so called radion) is essential. It is of course needed to stabilize the hierarchy between M_{pl} and M_{ew}, but also it is essential to recover the Einstein gravity on the brane. If we do not stabilize the radion, the linearized gravity is described by Brance Dicke (BD) gravity with a BD parameter that contradicts solar-system observations [2]. This is because the radion is massless if the stabilization mechanism is not included. The stabilization mechanism that gives a mass to the radion is necessary.

It has been pointed out that the radion mass is affected by the curvature of the brane [3]. If the branes are de Sitter branes, the radion mass is give by formula

$$m_r^2 = -4H^2 + m_0^2(H), \tag{3}$$

where H is the Hubble parameter on the brane and m_0 is the mass which comes from the stabilization mechanism [4]. This formula tells us that if we do not include the stabilization mechanism, the radion

[1] E-mail:kazuya@utap.phys.s.u-tokyo.ac.jp

is tachyonic and the configuration of two de Sitter branes is unstable. Because the radion mass that comes from the stabilization mechanism $m_0(H)$ also depends on H, it is not so obvious that we do have a tachyonic mode if we include the stabilization mechanism. The purpose of this article is to investigate the effect of the curvature of the brane on the stabilization mechanism and investigate whether the stable configuration for inflationary brane world is possible or not.

2 Stabilization mechanism

The easiest way to stabilize the radion is to include the scalar field in the bulk [5]. The action for the model is

$$S = \int d^5x\sqrt{-g}\left(\frac{1}{2\kappa^2}\,{}^{(5)}R - \frac{1}{2}(\partial\varphi)^2 - V(\varphi)\right) - \int d^4x\sqrt{-h_+}\lambda_+(\varphi) - \int d^4x\sqrt{-h_-}\lambda_-(\varphi), \quad (4)$$

where $\kappa^2 = M_*^{-3}$ and $h_\pm$ are induced metric on the branes. We take the potential for the scalar field in the bulk $V(\varphi)$ and on the brane $\lambda(\varphi)$ so that we can derive the analytic solution for the scalar field [6];

$$V(\varphi) = -\frac{6k^2}{\kappa^2} + \left(\frac{u^2}{2} + 2ku\right)\varphi^2 - \frac{\kappa^2}{6}u^2\varphi^4, \quad (5)$$

$$\lambda_\pm = \pm\frac{6k}{\kappa} \mp u\varphi_\pm^2 \mp 2u\varphi_\pm(\varphi - \varphi_\pm) + \gamma_\pm^2(\varphi - \varphi_\pm)^2. \quad (6)$$

Then we can derive the solution for 5D Einstein equation

$$\begin{aligned} ds^2 &= dy^2 + e^{-2A(y)}\eta_{\mu\nu}dx^\mu dx^\nu, \quad A(y) = ky + \frac{\kappa^2\varphi_+^2}{12}e^{-2uy}, \\ \varphi(y) &= \varphi_+ e^{-uy}. \end{aligned} \quad (7)$$

The junction condition for the scalar field gives

$$\frac{\varphi_-}{\varphi_+} = e^{-ud_0}. \quad (8)$$

Then the radion d_0 is fixed by the scalar field.

3 Low energy effective equations

Now we include the effect of the matter on the brane. It is rather difficult to derive the solution for 5D Einstein equation if the scalar field has time dependence. Here we will use low energy expansion scheme [7]. We begin with the 0-th order solution given by

$$\begin{aligned} A(y,x) &= kd_0(x)y + \frac{\kappa^2\varphi_0(x)^2}{12}e^{-2ud_0(x)y}, \\ \varphi(y,x) &= \varphi_0(x)e^{-ud_0(x)y}, \end{aligned} \quad (9)$$

where branes are located at $y = 0$ and $y = k^{-1}$ respectively. These are the solutions for 5D Einstein equation for $D\varphi_0(x) \ll k\varphi_0, Dd_0(x) \ll kd_0(x)$, where D is the covariant derivative with respect to induced metric h_- on the negative tension brane. And also they can satisfy the junction conditions if $\kappa^2\varphi_+(\varphi_- - \varphi_0 e^{-ud_0}) < 1$ and $\kappa^2 k^{-1}T^\mu_{\pm\ \nu} < 1$ where $T^\mu_{\pm\ \nu}$ is the energy-momentum tensor on the brane. We assume that these conditions are satisfied and solve the 5D Einstein equation perturbatively.

In the next order, we can derive the equations that determine φ_0 and d_0. The resultant theory becomes a very complicated scalar-tensor theory coupled to the scalar field. It is too complicated to write it down here, so we use further approximations. First, the potentials on the branes are very steep $\gamma_\pm \to 0$ so that the scalar field is exactly pinned down at $\varphi_\pm$ on the branes. Then the solution for φ_0 is just

$$\varphi_0 = \varphi_+. \quad (10)$$

And also we assume that the backreaction of the scalar field is weak, so we neglect the terms proportional to $\kappa^2\varphi_+^2 \ll 1$. Then the resultant effective Einstein equation on the negative tension (visible) brane is given by

$$\begin{aligned} G^\mu_\nu &= -\kappa^2 k T^\mu_{-\ \nu} - \kappa^2 u(u+2k)\varphi_+(\varphi_- - \varphi_+ e^{-ud_0})e^{-ud_0}\delta^\mu_\nu - E^\mu_\nu, \\ -E^\mu_\nu &= \frac{2k}{1-e^{-2kd_0}}\left(\frac{\kappa^2}{2}(e^{2kd_0}T^\mu_{+\ \nu} + T^\mu_{-\ \nu}) + (D^\mu D_\nu d_0 - \delta^\mu_\nu D^2 d_0) - k\left(D^\mu d_0 D_\nu d_0 + \frac{1}{2}\delta^\mu_\nu (Dd_0)^2\right)\right) \\ &\quad +\kappa^2 u(u+2k)\varphi_+(\varphi_- - \varphi_+ e^{-ud_0})e^{-ud_0}\delta^\mu_\nu. \end{aligned} \tag{11}$$

The equation for the radion d_0 is given by the traceless condition for E^μ_ν;

$$D^2 d_0 + k(Dd_0)^2 - U(d_0) = \frac{\kappa^2}{6}(e^{2kd_0}T_+ + T_-), \quad U(d) = \frac{2\kappa^2}{3}\frac{u}{k}(u+2k)\varphi_+(\varphi_- - \varphi_+ e^{-ud_0})e^{-ud_0}(1-e^{-2kd_0}), \tag{12}$$

where $T_\pm$ is the tarce of the energy-momentum tensor.

We first check that the effective equation recovers the result for the linearized gravity. We consider the stabilized two Minkowski branes. The radion potential has a minimum at

$$d_0 = d_*, \quad \frac{\varphi_-}{\varphi_+} = e^{-ud_*}. \tag{13}$$

Let us consider the perturbation around this minimum $d_0 = d_* + \delta d$. Then the equation for δd becomes

$$D^2\delta d - m_r^2 \delta d = 0, \quad m_r^2 \equiv m_0^2(d_*) = \frac{2\kappa^2}{3}\frac{u^2}{k}(u+2k)\varphi_+^2 e^{-2ud_*} = \frac{2\kappa^2}{3}e^{2kd_*}\frac{\int_0^{k^{-1}} dy e^{2A}}{\int_0^{k^{-1}} dy e^{4A}\varphi'^2} \tag{14}$$

This precisely recovers the result for linearized gravity [8]. For the scale lower than m_r, radion is massive, so it is easy to show that the 4D linearized Einstein gravity is recovered.

4 De sitter branes

Now we consider the de Sitter brane. The stating point is the equation of motion for the radion (12). The first possibility to have the stabilized radion is to chose

$$T_+ = -T_- e^{2kd_*}, \quad \varphi_- = \varphi_+ e^{-ud_*}. \tag{15}$$

Then the radion mass around this minimum becomes

$$m_r^2 = -4H^2 + m_0^2. \tag{16}$$

Because m_0 is of the order TeV if we want to solve the hierarchy problem, this solution is unstable for $H > TeV$. However, this solution is not natural phenomenologically. The effective Einstein equation becomes

$$H^2 = -\frac{\kappa^2 k \rho_-}{3}, \quad (T_- = -4\rho_-). \tag{17}$$

Thus the energy density on the visible brane should be negative. And also we need the fine tuning between the energy densities on the positive tension brane and the negative tension brane.

Hence, we seek another possibility. We assume the hidden brane is vacuum, thar is $T_+ = 0$. Then the equation for the radion has a solution

$$d = d_H < d_*, \quad \rho_- = \frac{u}{k}(u+2k)(\varphi_- - \varphi_+ e^{-ud_H})\varphi_+ e^{-ud_H}(1-e^{-2kd_H}). \tag{18}$$

Note that the above solution exists only for

$$\rho_- < \rho_{max} = \frac{u}{4k}(u+2k)\varphi_-^2. \tag{19}$$

The radion mass is given by

$$m_r^2 = m_0^2(d_H) - \frac{2\kappa^2}{3}\frac{u^2}{k}(u+2k)\varphi_+(\varphi_- - \varphi_+ e^{-ud_H})e^{-ud_H} - 4H^2 \tag{20}$$

The effective Einstein equation gives

$$H^2 = \frac{\kappa^2 k}{e^{2kd_H}-1}\frac{\rho_-}{3}. \tag{21}$$

The energy density on the brane is positive and the Friedmann equation is completely the same as the 4D Einstein gravity where the 4D Placnk scale is given by $M_{pl}^2 = (e^{2kd_H}-1)M_*^3/k$. In order to solve the hierarchy problem, we assume k and u are M_{ew} scale. Then the energy density ρ_- cannot exceed $\rho_{\max} \sim M_{ew}^4$ and the Hubble parameter should be

$$H^2 < \frac{M_{ew}^4}{M_{pl}^2}. \tag{22}$$

Hence the tachyonic mass $-4H^2$ in m_r^2 can be neglected. And also the second term should be small because of our assumption $\kappa^2\varphi_+(\varphi_- - \varphi_0 e^{-ud_0}) < 1$. Thus we conclude that the radion mass squared is positive

$$0 < m_r^2 < m_0^2. \tag{23}$$

Therefore, in this case, a configuration of inflationary two branes is stable.

5 Conclusion

In this article, we derived the low energy effective theory in the stabilized Randall-Sundrum brane world. We have shown that a stable configuration of inflationary two branes is realized. However, phenomenologically, this model has a crucial problem. The Hubbel scale is very low so it is quite difficult to produce the correct amplitude of the density fluctuations. It is a common problem in TeV gravity scenario where the energy density cannot exceed M_{ew}^4. And also, the minimum of the radion is different from true minimum d_* during inflation. Then there could be a moduli problem.

A possible way to avoid the problem of the low Hubble scale is to include the energy density on the hidden brane. However, even in this case, the Hubble scale cannot exceed TeV because for $H >$ TeV the tachyonic mass $-4H^2$ appeared in radion mass becomes important and it becomes difficult to construct the stable configuration [4]. Moreover, in this case inflaton is living on the hidden brane, we need a mechanism to convert the energy density of the inflaton to the radiation on the visible brane. Careful investigations are needed in order to construct an inflation model in the stabilized Randall-Sundrum model.

References

[1] L. Randall, R. Sundrum, Phys. Rev. Lett. 83 (1999) 3370

[2] J. Garriga and T. Tanaka, Phys. Rev. Lett. 84 (2000) 2778

[3] U. Gen, M. Sasaki, Prog. Theor. Phys. 105 (2001) 591

[4] A.V. Frolov, L. Kofman, hep-th/0309002

[5] W.D. Goldberger, M.B. Wise, Phys. Rev. Lett. 83 (1999) 4922

[6] O. DeWolfe, D.Z. Freedman, S.S. Gubser, A. Karch, Phys. Rev. D62 (2000) 046008

[7] S. Kanno, J. Soda, Phys. Rev. D66 (2002) 083506; T. Shiromizu K. Koyama, Phys. Rev. D67 (2003) 084022.

[8] T. Tanaka and X. Montes, Nucl. Phys. B 582 (2000) 259

CFT description of three-dimensional Hawking-Page phase transition

Yasunari Kurita[1], Masa-aki Sakagami[2]

Graduate School of Human and Environmental Studies,
Kyoto University, Yoshidanihonmatsu-cho, Sakyo-ku, Kyoto 606-8501, Japan

Abstract

We construct a conformal field theory(CFT) model which describes the three-dimensional Hawking-Page phase transition. We find that the free fermion CFT on the boundary torus has a good description for it. Around the critical temperature where semi-classical approximation does not work, the modular invariant free fermion model predicts that the transition will smoothly occur through the conical spaces and small black holes phase, which means Hawking-Page transition is not phase transition. However we also find that the free fermion model which do not have modular invariance predicts that the three-dimensional Hawking-Page transition is the second order phase transition.

1 Introduction

The Hawking-Page phase transition is a transition between thermal anti-de Sitter space and AdS black holes spacetime with thermal radiation[1]. The original argument is based on the semi-classical approximation of the Euclidean path integral. However this approximation will break down around the critical temperature, and we have to consider the quantum correction between two classical solutions.

We consider the three-dimensional Hawking-Page transition and construct the phenomenological boundary conformal field theory model which describes it. The boundary CFT can be regarded as the quantum theory of asymptotically AdS_3 gravity so that it can predict the thermodynamical behavior even for the temperature around the critical one. The free fermion CFT on the torus which is the boundary topology of asymptotically thermal AdS_3 spacetime gives us a good description of the transition for the temperature $T \gg T_c$ and $T \ll T_c$ in comparison with the result of the semi-classical approximation. The modular invariant free fermion model predicts that the three-dimensional Hawking-Page phase transition will occur smoothly through a conical space and small black holes phase, which means the Hawking-Page phase transition is not a phase transition. On the other hand, the free fermion models which do not have modular invariance may predict that the Hawking-Page transition is the second order hase transition. Thus it seems to have some relation with modular invariance of the boundary conformal field theory whether the Hawking-Page transition is phase transition or not.

2 The three-dimensional Hawking-Page transition

We consider canonical ensemble of a black hole, that is, the situation in which a black hole is in equilibrium with thermal radiation in the bulk at the Hawking temperature. The partition function of this system is defined by a path integral over metric fields which tends asymptotically to anti-de Sitter space identified periodically in a Euclidean time with the period $\beta = 1/T_H$. The partition function can be evaluated by the semi-classical approximation:

$$Z = \int_{t_E \sim t_E + 1/T} \mathcal{D}g \, e^{-I_E[g]} \sim e^{-I[\bar{g}]} \tag{1}$$

[1] E-mail:kurita@phys.h.kyoto-u.ac.jp
[2] E-mail:sakagami@phys.h.kyoto-u.ac.jp

where $\hat{g}$ is the metric of the classical solutions. Thus we can obtain the free energy of each thermal spacetime[2].

$$F = -T\log Z = TI_E[\hat{g}] = \begin{cases} -(2\pi lT)^2 & (\text{BTZ}) \\ -1 & (AdS_3) \end{cases} \tag{2}$$

The expectation values of the energy in each space are

$$\langle E\rangle_{BTZ} = -\frac{\partial}{\partial\beta}\log Z = \partial_\beta(-\frac{4\pi^2l^2}{\beta}) = M = (2\pi lT)^2 \tag{3}$$

$$\langle E\rangle_{AdS_3} = -1. \tag{4}$$

At the temperature $T = T_c := (2\pi l)^{-1}$, the free energy of thermal radiation accords with that of a BTZ black hole. For temperatures $T < T_c$, the free energy of thermal radiation is lower than that of a BTZ black hole which means that a BTZ black hole is less possible than pure thermal radiation. On the other hand, if $T > T_c$, the free energy of the BTZ black hole will be less than that of pure radiation. Then pure radiation will tend to tunnel to the BTZ black hole configuration. This is the Hawking-Page transition, which means the most dominant classical solution (or state) changes as temperature does.

At the critical temperature $T = T_c$, the energy of spacetime seems to change discontinuously. However, the evaluation of the partition function in this argument is only depends on the semi-classical approximation which will be broken near the critical temperature because, at the ctirital temperature, two classical solution contribute to the partition function equally, and some Euclidean solution interpolating these two classical solution will be impertant. Therefore we have to consider alternative approach in order to investigate this transition near the critical temperature.

3 CFT description of the three- dimensional Hawking-Page transition.

There are some features of asymptotically AdS_3 spacetime which imply the quantum theory of asymptotic AdS_3 is the boundary conformal field theory. First, there is no local gravitational degrees of freedom in bulk. Only pure gauge exists there. It becomes physical on the boundary. The second feature is the asymptotic symmetry including quantum fluctuation of metric fields is the Virasoro symmetry which is two-dimensional conformal symmetry. The central charge of it is also given as $c = \frac{3l}{2G}$. The third feature is topology of the Euclidean boundary is a torus T^2 with the modular parameter $\tau = \frac{i}{2\pi lT}$. These facts strongly suggest that quantum gravity of asymptotically AdS_3 is the CFT on the boundary T^2 with $c = \frac{3l}{2G}$.

In terms of CFT, the mass gap between AdS_3 and BTZ spacetime at zero temperature can be explained as the casimir energy of CFT[3]. Furthermore, Strominger related the entropy of a large BTZ black holes to the number of microscopic states in conformal field theory through the Cardy's formula[4]. Thus we can expect that the boundary CFT can also describe the Hawking-Page transition.

We consider pure fermionic CFT on the boundary torus, because, at the finite temperature, there is no supersymmetry and bosonic fields contribute finite correction to the specific heat in low temperature limit where it should be zero. The modular invariant partition function of pure fermion CFT on the boundary torus with the modular parameter τ is

$$Z_f(\tau) = \left(\frac{\theta_2(\tau)}{\eta(\tau)}\right)^{2c} + \left(\frac{\theta_3(\tau)}{\eta(\tau)}\right)^{2c} + \left(\frac{\theta_4(\tau)}{\eta(\tau)}\right)^{2c}.$$

It behaves as;

$$Z_f(T) \to \begin{cases} e^{-I_{AdS_3}} & (T \to 0) \\ e^{-I_{BTZ}} & (T \to \infty) \end{cases}$$

Thus the Hawking-Page transition can be described in this model. The turning point of the partition function is $\tau = -\frac{1}{\tau}$ where $T = T_c$. The expectation value of energy in low and high tenperature limit

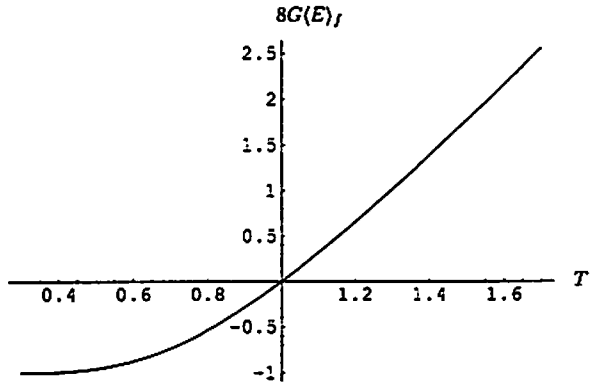

Figure 1: This figure shows the behavior of the energy (5) in classical limit around the critical temperature $T = T_c$. We set $\ell = 1/2\pi$, so $T_c = 1$. This is the result of the modular invariant free fermion model.

behaves as

$$\begin{aligned} \langle E\rangle_f &= M_{AdS_3} + \mathcal{O}(e^{-\frac{1}{2lT}}), \qquad (T \to 0) \\ \langle E\rangle_f &= M_{BTZ}(T) + \mathcal{O}(T^2 e^{-2\pi^2 lT}), \quad (T \to \infty) \end{aligned}$$

where M_{AdS_3}, M_{BTZ} are the mass of AdS_3 space and a BTZ black hole respectively. For $T \sim T_c$, in classical limit ($G_3 \to 0$),

$$8G_3\langle E\rangle_f \sim -24l\left(\frac{\partial_\beta\theta_3}{\theta_3} - \frac{\partial_\beta\eta}{\eta}\right),$$

which means the contribution comes only from the NS-NS sector in this model. Around the critical temperature, this model predicts the transition occur smoothly, passing through the conical space phase ($-\frac{1}{8G_3} < M < 0$) and small black holes phase ($0 < M < \frac{1}{8G_3}$).

If one can be allowed to break the modular invariance, the partition function consisting only of R-NS and NS-R sectors can be considered.

$$Z(\tau) = \left(\frac{\theta_2(\tau)}{\eta(\tau)}\right)^{2c} + \left(\frac{\theta_4(\tau)}{\eta(\tau)}\right)^{2c} \tag{5}$$

Then the expectation value of energy and the specific heat are:

$$8G\langle E\rangle_{\mathrm{NS,R}} = -24l\left[\frac{\theta_2^{2c}}{\theta_2^{2c}+\theta_4^{2c}}\left(\frac{\theta_2'}{\theta_2} - \frac{\eta'}{\eta}\right) + \frac{\theta_4^{2c}}{\theta_2^{2c}+\theta_4^{2c}}\left(\frac{\theta_4'}{\theta_4} - \frac{\eta'}{\eta}\right)\right], \tag{6}$$

$$\begin{aligned} 8G\, C_{\mathrm{NS,R}} &= \frac{24l}{T^2}\frac{\theta_2^{2c}}{\theta_2^{2c}+\theta_4^{2c}}\left[\sum_{i=2,4}\left(\frac{\theta_i''}{\theta_i} - \frac{\eta''}{\eta} - (\frac{\theta_i'}{\theta_i})^2 + (\frac{\eta'}{\eta})^2\right)\right] \\ &\quad + 24l\frac{2c}{T^2}\frac{(\theta_2\theta_4)^{2c}}{(\theta_2^{2c}+\theta_4^{2c})^2}\left(\frac{\theta_2'}{\theta_2} - \frac{\theta_4'}{\theta_4}\right)^2, \end{aligned} \tag{7}$$

The behavior of the specific heat are shown in the figure 2. There is discontinuity in the specific heat and therefore the Hawking-Page transition in this case can be interpreted as a second order phase transition.

4 Summary

We show that the Hawking-Page phase transition which is originally predicted in the Euclidean semi-classical gravity can also be described in boundary CFT by identifying the boundary CFT partition

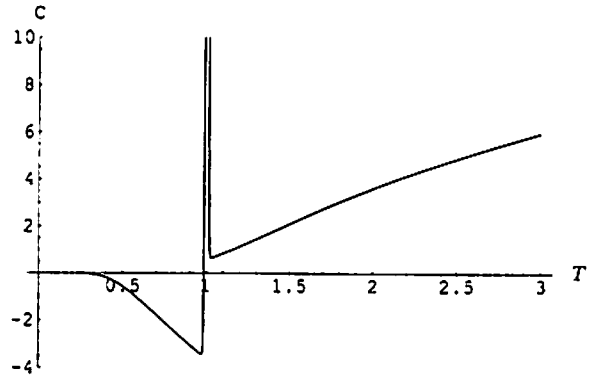

Figure 2: This shows (7). We set $l = (2\pi)^{-1}$ so that $T_c = 1$. It diverges at the critical temperature.

function with that of Euclidean asymptotic AdS_3 gravity. In the semi-classical gravity, we can not discuss thermodynamics near the critical temperature in terms of semi-classical gravity because two classical solution equally contribute to the partition function. In this work, we treat the boundary CFT as an effective quantum theory which can predict the thermodynamical behavior even at the critical temperature.

For a CFT model, we consider a free fermion model. The partition function of this CFT behaves as that of the gravitational instanton of AdS_3 and a BTZ black hole in low and high temperature limit respectively. This fact means the Hawking-Page transition can be described by the boundary CFT, and the critical temperature can be determined as the self dual point under the boundary modular transformation $\tau \to -\frac{1}{\tau}$, giving the same temperature as in the Euclidean semi-classical result. This model has a good description for temperature not around the critical temperature.

Unlike the transition predicted in the Euclidean semi-classical approach, the modular invariant fermions model seems to have smooth transition between the AdS_3 phase and the BTZ phase even in classical limit. It is a new prediction from this fermions model. In classical limit, the dominant contribution to the partition function around the critical temperature comes only from the NS-NS sector in this model.

If one can be allowed to break modular invariance, only R-NS and NS-R sectors will also be considered. These sectors are also invariant under the boundary modular transformation $\tau \to -\frac{1}{\tau}$. The contributions from these sectors are much like the case of the Euclidean semi-classical approach in classical limit. Around the critical temperature, this model shows that there is discontinuity in the specific heat at the critical temperature, which means that the Hawking-Page transition is the second order phase transition. Therefore, it seems to have some relation with modular invariance of the boundary conformal field theory whether the Hawking-Page transition is a phase transition or not.

References

[1] S.W. Hawking and D.N. Page, Commun.Math.Phys. **87**, 577 (1983).

[2] M. Banados, C. Teitelboim and J. Zanelli, Phys.Rev.Lett. **69**, (1992) 1849.

[3] O. Coussaert and M. Henneaux, Phys.Rev.Lett. **72**, 183 (1994).

[4] A. Strominger, JHEP, 9802(1998)009.

Stability criterion for self-similar solutions with a scalar field and those with a stiff fluid

Hideki Maeda[1]

Advanced Research Institute for Science and Engineering, Waseda University, Okubo 3-4-1, Shinjuku, Tokyo 169-8555, Japan

Tomohiro Harada[2]

Astronomy Unit, School of Mathematical Sciences, Queen Mary, University of London. Mile End Road, London E1 4NS, UK

Abstract

A stability criterion is derived in general relativity for self-similar solutions with a scalar field and those with a stiff fluid, which is a perfect fluid with the equation of state $P = \rho$. A wide class of self-similar solutions turn out to be unstable against kink mode perturbation. Several interesting applications are discussed, one of which is related to critical behaviour for these two systems.

1 Introduction

Scale-invariant nature of gravity implies that there exists a class of scale-invariant solutions for the gravitational field equations, which are called *self-similar solutions*. Recently, self-similar solutions have been watched with keen interest and intensively investigated because of their importance among more general non-self-similar solutions in dynamical situations. It has been reported that a class of self-similar solutions is realized as an *attractor* in generic situations. The suggestion that solutions might naturally evolve to a self-similar form is called *self-similarity hypothesis* [1]. In fact, Harada and Maeda [2] numerically found that a self-similar solution is an attractor in the spherically symmetric collapse of a perfect fluid with the equation of state $P = k\rho$ $(0 < k < 1)$ at least for $0 < k \lesssim 0.03$.

Spherically symmetric self-similar solutions have been also studied in the context of *critical behaviour* in gravitational collapse, in which a self-similar solution, which is called a critical solution, is not an attractor but an *intermediate attractor*. The critical behaviour was numerically discovered by Choptuik [3] in the spherical system of a massless scalar field. In this case, the critical solution is a *discretely self-similar solution*. This phenomenon has been understood by Koike, Hara and Adachi by using a renormalization group approach [4]. They found that a critical solution is identified with possessing a single unstable mode. Evans and Coleman [5] studied the spherical system of a radiation fluid ($P = \rho/3$) and found similar phenomena although the observed critical solution is a *continuously self-similar solution*. Several authors [5, 6, 7, 2] have extended the work to perfect fluids with the equation of state $P = k\rho$ $(0 < k \leq 1)$ although the observed critical solution is a *continuously self-similar solution*. For a *stiff fluid* $(k = 1)$, it is interesting because the stiff fluid is known to be equivalent to a massless scalar field in certain circumstances [8]. Neilsen and Choptuik [7] studied the stiff-fluid system and found that the critical behaviour can be regarded as a continuous limit of that for a perfect fluid with $P = k\rho$ $(0 < k < 1)$ as $k \to 1$. The critical solution is continuously self-similar and we refer to the critical solution found by Neilsen and Choptuik as the Evans-Coleman stiff-fluid solution. Brady *et al.* [8] numerically found a *continuous self-similar solution* for which the solution has regular centre and analytic similarity horizon in the spherical system of a massless scalar field. We refer to this self-similar solution as the Brady-Choptuik-Gundlach-Neilsen (BCGN) solution. They found that this solution has a single unstable mode which is analytic at the similarity horizon and studied the mystery of why the critical behaviour for a stiff fluid is different from that for a scalar field.

[1] E-mail:hideki@gravity.phys.waseda.ac.jp
[2] E-mail:T.Harada@qmul.ac.uk

The present article concerns *weak discontinuity* around self-similar solutions. If we insert a perturbation with a sufficiently small weak discontinuity, it may grow too large to neglect as time proceeds. This instability has been called *kink instability*. Harada [9] investigated the kink instability of self-similar solutions for the spherical system of a perfect fluid with the equation of state $P = k\rho$ $(0 < k < 1)$ in general relativity. In this article we derive a stability criterion against the kink mode perturbation for both self-similar solutions with a scalar field and those with a stiff fluid in general relativity. Several interesting applications are discussed, one of which is related to critical behaviour for these two systems.

This article is based on [10] and organized as follows. In Sec. 2, we derive the basic equations for the spherically symmetric Einstein-scalar-field system and those for self-similar solutions. Also in this section we introduce the kink mode for the self-similar scalar-field solutions, derive the equations for this mode and obtain the stability criterion for self-similar scalar-field solutions. In Sec. 3, the stability criterion for self-similar stiff-fluid solutions is mentioned. In Sec. 4, we discuss the applications of the present result, in particular, to critical behaviour of gravitational collapse. We adopt units such that $G = c = 1$.

2 Stability criterion for self-similar solutions with a scalar field

2.1 Equations for a self-gravitating massless scalar field

In this section, we basically follow the notation given by Brady *et al.* [8]. We consider a massless scalar field ϕ as a matter field, for which the stress-energy tensor is given by

$$T^{ab} = \nabla^a\phi\nabla^b\phi - \frac{1}{2}g^{ab}(\nabla_c\phi\nabla^c\phi). \tag{1}$$

We adopt the Bondi coordinates for a spherically symmetric spacetime as

$$ds^2 = -g\bar{g}du^2 - 2gdudR + R^2(d\theta^2 + \sin^2\theta d\phi^2), \tag{2}$$

where $g = g(u, R)$ and $\bar{g} = \bar{g}(u, R)$. For later convenience we define a new function $\bar{h}(u, R)$ as

$$\phi = \bar{h}(u, R) - \kappa \ln|u|, \tag{3}$$

where κ is an arbitrary constant, and we define the following variables:

$$x \equiv -\frac{R}{u}, \quad X \equiv \ln|x|, \quad T \equiv -\ln|u|. \tag{4}$$

Then the Einstein equation and the equation of motion for the scalar field reduce to

$$(\ln g)' = 4\pi\bar{h}'^2, \tag{5}$$

$$\bar{g}' = g - \bar{g}, \tag{6}$$

$$g\left[\left(\frac{\bar{g}}{g}\right)^{\cdot} + \left(\frac{\bar{g}}{g}\right)'\right] = 8\pi(\dot{\bar{h}} + \bar{h}' + \kappa)[x(\dot{\bar{h}} + \bar{h}' + \kappa) - \bar{g}\bar{h}'], \tag{7}$$

$$(\bar{g}\bar{h}')^{\cdot} + \bar{g}\bar{h}' = 2x[(\dot{\bar{h}} + \bar{h}') + (\dot{\bar{h}} + \bar{h}')' + \kappa], \tag{8}$$

where the dot and prime denote the partial derivatives with respect to T and X, respectively. We refer to $u < 0$ and $u > 0$ as early times and late times, respectively. It is noted that the present definition of prime is different from that in Brady *et al.* [8].

2.2 Self-similar scalar-field solutions

For self-similar solutions, we assume that $g = g(X)$, $\bar{g} = \bar{g}(X)$ and $\bar{h} = \bar{h}(X)$. The ordinary differential equations for g, $\bar{g}$ and $\bar{h}$ are given by

$$(\ln g)' = 4\pi j^2, \tag{9}$$

$$\bar{g}' = g - \bar{g}, \tag{10}$$

$$g - \bar{g} = 4\pi[2\kappa^2 x - (\bar{g} - 2x)(j^2 + 2\kappa j)], \tag{11}$$

$$\bar{h}' = j, \tag{12}$$

$$(2x - \bar{g})j' = -2\kappa x + j(g - 2x). \tag{13}$$

where the prime denotes the differentiation with respect to X.

These equations are singular when $\bar{g} = 2x$, which is called a *similarity horizon*. We denote the value of x at the similarity horizon as x_s and also the value of X as $X_s \equiv \ln|x_s|$. This line corresponds to a radial ingoing (outgoing) null curve for early-time (late-time) solutions because

$$\frac{dX}{dT} = 1 - \frac{\bar{g}}{2x}. \tag{14}$$

along a radial ingoing (outgoing) null curve. We consider self-similar scalar-field solutions with finite values of functions g, $\bar{g}$, $\bar{h}$ and j and their gradients with respect to X at the similarity horizon. Then we find at $X = X_s$

$$g = 2x_s(4\pi\kappa^2 + 1), \quad \bar{g} = 2x_s, \quad j = \frac{1}{4\pi\kappa}, \tag{15}$$

for $\kappa \neq 0$ and

$$g = \bar{g} = 2x_s, \quad j = j_s, \tag{16}$$

for $\kappa = 0$. For $\kappa = 0$, similarity horizons are parametrized by j_s.

2.3 Kink instability of self-similar solutions with a scalar field

We consider perturbations which satisfy the following conditions in the background of a self-similar solution: (1) The initial perturbations vanish inside the similarity horizon for early-time solutions ($u < 0$). (For late-time solutions ($u > 0$), the initial perturbations vanish outside the similarity horizon.) (2) g, $\bar{g}$, $\bar{h}$ and $\bar{h}'$ are continuous everywhere, in particular at the similarity horizon. (3) $\bar{h}''$ and $\dot{\bar{h}}''$ are discontinuous at the similarity horizon, although they have finite one-sided limit values as $X \to X_s - 0$ and $X \to X_s + 0$.

We denote the full-order perturbations as

$$\delta g(T, X) \equiv g(T, X) - g_b(X), \quad \delta\bar{g}(T, X) \equiv \bar{g}(T, X) - \bar{g}_b(X), \quad \delta\bar{h}(T, X) \equiv \bar{h}(T, X) - \bar{h}_b(X), \tag{17}$$

where g_b, $\bar{g}_b$ and $\bar{h}_b$ denote the background self-similar solution.

By conditions (2), the perturbations satisfy $\delta\bar{h} = \delta\bar{h}' = 0$ and $\delta\bar{h}'' \neq 0$ at the similarity horizon at initial moment $T = T_0$. The evolution of the initially unperturbed region is completely described by the background self-similar solution because no information from the perturbed side can penetrate the unperturbed side by condition (1). Then, by conditions (2) and (3), we find $\delta\bar{h} = \delta\bar{h}' = 0$ and $\delta\bar{h}'' \neq 0$ at the similarity horizon for $T \geq T_0$ for early-time solutions (for $T \leq T_0$ for late-time solutions). We find $\delta g = \delta\bar{g} = \delta g' = \delta\bar{g}' = \delta\bar{g}'' = 0$ but $\delta g'' \neq 0$ and $\delta\bar{g}''' \neq 0$ from Eqs. (5), (6) and (7) for the full-order perturbations at the point of discontinuity.

After some calculations, we obtain the full-order perturbation equation for $\delta j'$ at the similarity horizon:

$$\delta\dot{j}' - (8\pi\kappa^2 - 1)\delta j' = 0. \tag{18}$$

It should be noticed that the full-order analysis results in a linear-order equation. This equation can be integrated as

$$\delta j' = \text{const} \cdot e^{\alpha T}, \tag{19}$$

where

$$\alpha = -(1 - 8\pi\kappa^2). \tag{20}$$

Therefore, for early-time solutions, it is found that the perturbation decays exponentially for $4\pi\kappa^2 < 1/2$, it is constant for $4\pi\kappa^2 = 1/2$ and it grows exponentially for $4\pi\kappa^2 > 1/2$. The situation is reversed for late-time solutions.

Here we define instability by the exponential growth of discontinuity. Then we find the following criterion: for early-time solutions, solutions with a regular similarity horizon and $4\pi\kappa^2 < 1/2$ are stable against the kink mode, while those with $4\pi\kappa^2 > 1/2$ are unstable. Solutions with $4\pi\kappa^2 = 1/2$ are marginally stable against this mode. The situation is reversed for late-time solutions.

3 Stability criterion for self-similar solutions with a stiff fluid

An irrotational stiff fluid with positive energy density is equivalent to a scalar field with a timelike gradient. When there is the equivalence between a self-similar scalar-field solution and a self-similar stiff-fluid solution, the stability against the kink mode and its growth rate coincide for both self-similar solutions.

It is noted that discontinuity grows more rapidly and blows up to infinity at a finite moment before $t = 0$ for the perfect-fluid system with $P = k\rho$ $(0 < k < 1)$ [9]. In other words, the kink instability results in the reduction of the rank of differentiability and the formation of a shock wave before the singularity formation for a perfect fluid with $0 < k < 1$, while it does not for the scalar-field system and also for the stiff-fluid ($k = 1$) system until the singularity forms.

4 Applications

These systems have recently attracted attention in the context of critical phenomena in gravitational collapse. The present result shows that both the BCGN scalar-field solution ($4\pi\kappa^2 \approx 0.577$) and Evans-Coleman stiff-fluid solution, which are both early-time solutions, are unstable against the kink mode. This implies that the latter solution, which was identified with a critical solution in the stiff-fluid collapse by Neilsen and Choptuik [7] and Brady *et al.* [8], cannot be a critical solution once we allow sufficiently small discontinuity in the density gradient field in the initial data sets; nor can the BCGN scalar-field solution be a critical solution once we allow sufficiently small discontinuity in the second-order derivative of the scalar field in the initial data sets. As another important application, we have shown the kink instability at the particle horizon of the flat Friedmann universe, which is a late-time solution, with a scalar field ($4\pi\kappa^2 = 1/3$) and with a stiff fluid, while the flat Friedmann collapse solution, which is an early-time solution, is stable against this mode.

References

[1] B.J. Carr and A.A. Coley, Class. Quantum Grav. **16**, R31-R71 (1999).

[2] T. Harada and H. Maeda, Phys. Rev. D **63**, 084022 (2001).

[3] M.W. Choptuik, Phys. Rev. Lett. **70**, 9 (1993).

[4] T. Koike, T. Hara and S. Adachi, Phys. Rev. Lett. **74**, 5170 (1995).

[5] C.R. Evans and J.S. Coleman, Phys. Rev. Lett. **72**, 1782 (1994).

[6] D. Maison, Phys. Lett. B **366**, 82 (1986);
T. Koike, T. Hara and S. Adachi, Phys. Rev. D **59**, 104008 (1999).

[7] D.W. Neilsen and M.W. Choptuik, Class. Quantum Grav. **17**, 733 (2000);
D.W. Neilsen and M.W. Choptuik, Class. Quantum Grav. **17**, 761 (2000).

[8] P.R. Brady, M.W. Choptuik, C. Gundlach and D.W. Neilsen, Class. Quantum Grav. **19**, 6359 (2002).

[9] T. Harada, Class. Quantum Grav. **18**, 4549 (2001).

[10] T. Harada and H. Maeda, Class. Quantum Grav. **21**, 371 (2004).

Local mass, Weyl charge and dark radiation in brane cosmology

Masato Minamitsuji[1,2*] and Misao Sasaki[2†]

[1] *Department of Earth and Space Science, Graduate School of Science, Osaka University, Toyonaka 560-0041, Japan*

[2] *Yukawa Institute for Theoretical Physics, Kyoto University, Kyoto 606-8502, Japan*

Abstract

In the context of the Randall-Sundrum braneworld scenario, we consider the bulk dynamics and brane cosmology in terms of the local energy conservation law which is satisfied in a spacetime with constant curvature 3-space. The local conservation law enables us to define the local mass in the bulk. We show that on the brane the local mass gives the generalization of the dark radiation term. We find there also is a conserved current associated with the bulk Weyl tensor, thus the corresponding local charge, which we call "Weyl charge". The Weyl charge is given by the sum of the local mass and a linear combination of some components of the bulk energy momentum tensor. On the brane, the Weyl charge gives the non-trivial component of projected Weyl tensor in the geometrical formalism. This gives the unique decomposition of the projected Weyl tensor into the generalized dark radiation and the remaining bulk-induced energy-momentum tensor.

1 Introduction

In braneworld scenarios, our universe is assumed to be on a membrane embedded in a higher dimensional spacetime. In this paper, we focus our attention on a single brane scenario with negative bulk cosmological constant, the so-called second Randall-Sundrum (RS2) scenario [1].

In many cases, the 5-dimensional bulk geometry is assumed to be AdS-Schwarzschild:

$$ds^2 = -\left(K + \frac{r^2}{\ell^2} - \frac{M_0}{r^2}\right)dt^2 + \left(K + \frac{r^2}{\ell^2} - \frac{M_0}{r^2}\right)^{-1} dr^2 + r^2 d\Omega^2_{(K.3)}, \tag{1}$$

where $\ell := \sqrt{-6/\Lambda_5}$ is the AdS curvature radius, M_0 is the black hole mass, and $d\Omega^2_{(K.3)}$ is the maximally symmetric (constant curvature) 3-space with $K = -1$, 0 or $+1$. The brane trajectory in the bulk, $(t, r) = (t(\tau), r(\tau))$, is determined by the junction condition. As usual, we impose the reflection symmetry with respect to the brane. Then, we obtain the effective Friedmann equation on the brane as

$$\left(\frac{\dot{r}}{r}\right)^2 + \frac{K}{r^2} = \left(\frac{\kappa_5^4}{36}\sigma^2 - \frac{1}{l^2}\right) + \frac{\kappa_5^4}{18}\left(2\sigma\rho + \rho^2\right) + \frac{M_0}{r^4}, \tag{2}$$

where σ and ρ are the brane tension and energy density of the matter on the brane, respectively, and $\dot{r} = dr/d\tau$ with τ being the proper time on the brane. The final term proportional to the mass of the bulk black hole is often called the "dark radiation" since it behaves as the ordinary radiation. Geometrically, it comes from the projected Weyl tensor in the bulk, denoted commonly by $E_{\mu\nu}$ [2].

When the bulk ceases to be pure AdS-Schwarzschild, or when there exists a dynamical degree of freedom other than the metric, the parameter M_0 is no longer constant in general, but becomes dynamical. In this paper, we investigate the case when there is non-trivial dynamics in the bulk, and clarify the relation between the bulk geometry and the dynamics of the brane. We focus on the case of isotropic and homogeneous branes, hence assume the existence of slicing by the maximally symmetric 3-space as in Eq. (1). In this case, we can derive a local energy conservation law in the bulk, in analogy with spherical

*E-mail:masato@yukawa.kyoto-u.ac.jp

†E-mail:misao@yukawa.kyoto-u.ac.jp

symmetric spacetimes in 4-dimensions [3]. Then, this conservation law can be used to relate the brane dynamics with the geometrical properties of the bulk, especially with the projected Weyl tensor in the bulk.

In this paper, we derive the local energy conservation law in the bulk and discuss the general property of the bulk geometry and cosmology on the brane. We show that there exists a unique generalization of the dark radiation that is directly related to the local mass in the bulk. We also find that there exists another conserved current associated with the Weyl tensor, as a non-linear version of what was found in [4]. We call it the Weyl charge. The difference between the local mass and Weyl charge is given by the linear combination of certain components of the bulk energy-momentum tensor, and the projected Weyl tensor that appears in the effective Friedmann equation on the brane is indeed given by this Weyl charge. Thus we have a unique decomposition of the projected Weyl tensor term into the part due to the bulk mass that generalizes the dark radiation term and the part due to the bulk energy-momentum tensor.

2 Local Conservation Law and Brane Cosmology

2.1 Local conservation law and the Weyl charge

We assume the bulk has the 3-space with constant curvature. The bulk metric is

$$ds^2 = \frac{4r_{,u}r_{,v}}{\Phi}dudv + r(u,v)^2 d\Omega^2_{(K,3)}, \tag{3}$$

where we refer to v and u as the advanced and retarded time coordinates, respectively. The 5-dimensional Einstein equations are given by

$$G_{ab} + \Lambda_5 g_{ab} = \kappa_5^2 T_{ab} + S_{ab}\delta(y - y_0), \tag{4}$$

where the indices $\{a, b\}$ run from 0 to 3, and 5, and Λ_5 and κ_5^2 are the 5-dimensional cosmological constant and gravitational constant, respectively. The brane is introduced as a singular hypersurface locates at $y = y_0$, where y denotes a Gaussian normal coordinate in the vicinity of the brane, and S_{ab} denotes the energy-momentum tensor on the brane. The spacetime is assumed to be reflection symmetric with respect to the brane.

In this system, it is easy to show that a vector field

$$\xi^a = \frac{1}{2}\Phi\left(-\frac{1}{r_{,v}}\frac{\partial}{\partial v} + \frac{1}{r_{,u}}\frac{\partial}{\partial u}\right)^a. \tag{5}$$

is locally conserved, i.e. $\xi^a{}_{;a} = 0$. The vector field ξ^a corresponds to the asymptotically timelike Killing vector in an asymptotically constant curvature spacetime. Using the vector field ξ^a, we define another conserved vector field

$$\tilde{S}^a = \xi^b\left(T_b{}^a - \frac{1}{\kappa_5^2}\Lambda_5\delta^a_v\right) \quad \tilde{S}^a{}_{;a} = 0. \tag{6}$$

The corresponding charge, which is so-called "local mass", is

$$\tilde{M} = r^2\Big(K - \Phi\Big). \tag{7}$$

For convention, we often use the bulk matter part

$$M := \tilde{M} - \frac{1}{6}\Lambda_5 r^4. \tag{8}$$

Using the relation $C_{abcd}{}^{;d} = J_{abc}$, where J_{abc} is given by a linear combination of $T_{ab;c}$ [5], we also find one more locally conserved vector field Q^a associated with the bulk Weyl tensor,

$$Q^a = r\,\ell_b n_c J^{bca}; \quad Q^a{}_{;a} = 0, \tag{9}$$

where ℓ_a and n_a are a set of two normalized, hypersurface orthogonal null vectors [6]. The corresponding charge is clearly $r^4 C_{vu}{}^{vu}$, which we call the "Weyl charge".

The local mass and the Weyl charge are uniquely related to

$$r^4 C_{vu}{}^{vu} = 3\tilde{M} + \frac{r^4}{6}\Big(6G^v{}_v - G^i{}_i\Big) = 3M + \frac{r^4}{6}\kappa_5^2\Big(6T^v{}_v - T^i{}_i\Big). \tag{10}$$

2.2 Brane cosmology

We now consider the dynamics of the brane in the bulk discussed in the previous subsection. The brane trajectory is parameterized as $(v,u) = (v(\tau), u(\tau))$. The parameter τ is assumed to be the proper time on the brane and given by

$$4\frac{r_{,u}r_{,v}}{\Phi}\dot{u}\dot{v} = -1 \tag{11}$$

on the brane, where $\dot{u} = du/d\tau$ and so on. The junction condition under the reflection symmetry determines the brane trajectory

$$r_{,u}\dot{u} = -\frac{r}{2}\Big[\frac{\kappa_5^2}{6}\Big(\rho+\sigma\Big) - H\Big], \tag{12}$$

$$r_{,v}\dot{v} = \frac{r}{2}\Big[\frac{\kappa_5^2}{6}\Big(\rho+\sigma\Big) + H\Big], \tag{13}$$

where $H = \dot{r}/r$. From these equations, we obtain the effective Friedmann equation on the brane

$$H^2 + \frac{K}{r^2} = \Big(\frac{\kappa_5^4}{36}\sigma^2 - \frac{1}{l^2}\Big) + \frac{\kappa_5^4}{18}\Big(2\sigma\rho + \rho^2\Big) + \frac{M}{r^4}. \tag{14}$$

For a dynamical bulk, M varies in time. The evolution of M on the brane is given

$$\begin{aligned}\dot{M} &= M_{,v}\dot{v} + M_{,u}\dot{u} \\ &= \frac{2}{3}\kappa_5^2 r^4\Big[T_{vv}\Big(\frac{1}{6}\kappa_5^2(\rho+\sigma) - H\Big)\dot{v}^2 - T_{uu}\Big(\frac{1}{6}\kappa_5^2(\rho+\sigma) + H\Big)\dot{u}^2\Big] - \frac{2}{3}\kappa_5^2 r^4 H T^v{}_v.\end{aligned} \tag{15}$$

From the Codacci equation on the brane [2], we obtain the equation for the energy transfer of the matter on the brane to the bulk,

$$\dot{\rho} + 3H(\rho+p) = 2\Big(-T_{vv}\dot{v}^2 + T_{uu}\dot{u}^2\Big). \tag{16}$$

Equations (14), (15) and (16) determine the cosmological evolution on the brane, once the bulk geometry is solved.

Next, we relate the above result with the geometrical formalism developed in [2], in particular with the $E_{\mu\nu}$ term on the brane. The projected Weyl tensor

$$E_{\mu\nu} = C_{a\mu b\nu}\, n^a n^b, \tag{17}$$

has only one non-trivial component as

$$E_{\tau\tau} = C_{abcd}n^a n^c v^b v^d = 4\, C_{uvuv}\dot{u}^2\dot{v}^2 = -C_{vu}{}^{vu}. \tag{18}$$

Using Eq. (10), this can be uniquely decomposed into the part proportional to M and the part due to the projection of the bulk energy-momentum tensor on the brane:

$$E_{\tau\tau} = -\frac{3\tilde{M}}{r^4} + \frac{1}{6}\Big(G^i{}_i - 6G^v{}_v\Big) = -\frac{3M}{r^4} + \frac{\kappa_5^2}{6}\Big(T^i{}_i - 6T^v{}_v\Big). \tag{19}$$

Finally, from the brane point of view, the expressions for the effective total energy density and pressure on the brane are given:

$$\rho^{(\mathrm{tot})} = \rho^{(\mathrm{brane})} + \rho^{(\mathrm{bulk})}, \quad p^{(\mathrm{tot})} = p^{(\mathrm{brane})} + p^{(\mathrm{bulk})}, \tag{20}$$

where

$$\kappa_4^2\rho^{(\mathrm{brane})} = 3\Big[\frac{1}{6}\kappa_5^2\Big(\rho+\sigma\Big)\Big]^2, \quad \kappa_4^2 p^{(\mathrm{brane})} = \frac{1}{12}\kappa_5^4(\rho+\sigma)(\rho-\sigma+2p).$$
$$\kappa_4^2\rho^{(\mathrm{bulk})} = \frac{3\tilde{M}}{r^4}, \quad \kappa_4^2 p^{(\mathrm{bulk})} = \frac{\tilde{M}}{r^4} + \frac{1}{3}\kappa_5^2\Big(-\frac{\dot{u}}{\dot{v}}\tilde{T}^v{}_u - \frac{\dot{v}}{\dot{u}}\tilde{T}^u{}_v + 2\tilde{T}^v{}_v\Big). \tag{21}$$

where both $\tilde{M}$ and $\tilde{T}$ contain the contribution from the bulk cosmological constant. It may be noted that, unlike the effective energy density, the effective pressure contains a part coming from the bulk that cannot be described by the local mass alone. The contracted Bianchi identity implies the conservation law for the total effective energy-momentum on the brane:

$$\dot{\rho}^{(\mathrm{bulk})} + 3H\Big(\rho^{(\mathrm{bulk})} + p^{(\mathrm{bulk})}\Big) = -\dot{\rho}^{(\mathrm{brane})} - 3H\Big(\rho^{(\mathrm{brane})} + p^{(\mathrm{brane})}\Big). \tag{22}$$

This is mathematically equivalent to Eq. (15). However, these two equations have different interpretations. From the bulk point of view, Eq. (15) is more relevant, which describes the energy exchange between the brane and the bulk, whereas a natural interpretation of Eq. (22) is that it describes the energy exchange between two different matters on the brane; the intrinsic matter on the brane and the bulk matter induced on the brane. The important point is, as mentioned above, that the pressure of the bulk matter has contributions not only from the local mass but also from a projection of the bulk energy-momentum tensor, which makes the equation of state different from $p^{(\mathrm{bulk})} = \rho^{(\mathrm{bulk})}/3$, i.e., that of a simple dark radiation.

3 Summary

In the context of the RS2-type brane cosmology, we focused on a dynamical bulk with maximally symmetric 3-space and derived two local conservation laws in the bulk. One of which is just the local energy conservation law and the corresponding charge is the local mass, the existence of which is known for spherically symmetric spaces in 4 dimensions. The other, which is newly found, is associated with the Weyl tensor, hence we call the corresponding charge the Weyl charge.

We found that the bulk geometry is completely described by the local mass M and it is directly related to the generalized dark radiation term in the effective Friedmann equation. We also found that, on the brane, the Weyl charge is directly related to the time-time component of the projected Weyl tensor that appears in the geometrical approach, and it can be expressed in terms of M and a certain linear combination of the components of the bulk energy-momentum tensor. Further details and applications to a null dust fluid and the bulk inflaton model are discussed in [6].

Finally, let us briefly comment on future issues. As a more realistic situation, it will be interesting to consider a bulk scalar field such as a dilaton or a moduli field. In this case, it will be necessary to solve the bulk and brane dynamics numerically in general. Another interesting issue will be to study the evaporation of a bulk black hole by the Hawking radiation and its effect on the brane dynamics.

References

[1] L. Randall and R. Sundrum, Phys. Rev. Lett. **83**, 4690 (1999).

[2] T. Shiromizu, K. i. Maeda and M. Sasaki, Phys. Rev. D **62**, 024012 (2000).

[3] H. Kodama, Prog. Theor. Phys. **63**, 1217 (1980).

[4] M. Minamitsuji, Y. Himemoto and M. Sasaki, Phys. Rev. D **68**, 024016 (2003).

[5] S.W. Hawking and G.F.R. Ellis, *The large scale structure of space-time* (Cambridge University Press. Cambridge, 1973).

[6] M. Minamitsuji and M. Sasaki, arXiv:gr-qc/0312109.

Comments on Generalized Weyl Solutions

Takashi Mishima[1]

Laboratory of Physics, College of Science and Technology, Nihon University, Narashinodai, Funabashi, Chiba 274-0063, Japan

Abstract

Modified Weyl's canonical coordinates are introduced to the higher dimensional generalization of Weyl solutions developed by Emparan and Reall. It is shown that four dimensional Laplace equation with two independent rotational symmetries in a hypothetical Euclidean space is derived, instead of three dimensional one in the treatment of Emparan and Reall. In five dimensional case especially, the metrics corresponding to the modified Weyl's canonical coordinates asymptotically approach a simple Minkowski metric which shows apparent flatness. We also discuss how five dimensional black hole solutions are described using the modified version of the generalized Weyl formalism.

1 Introduction

In the long history of the study of four dimensional Einstein gravity, Weyl's axisymmetric solutions of Einstein equations[1] have continued to play important roles to deepen understanding of general relativity the same as the familiar Schwarzschild or Kerr solutions[2].

Through the investigations of the Weyl solutions, we can acquire the knowledge of general features of four dimensional gravity which could never be grasped only with the Schwarzschild or Kerr solutions.

In the case of higher dimensional gravity, recently Emparan and Reall tried to generalize Weyl's treatment of axisymmetric solutions to higher dimensions[3]. For the study of spacetimes in higher dimensional gravitational theories have become more and more important rapidly owing to the recent remarkable development of fundamental theories including brane world models, so that deeper understanding of higher dimensional gravity should be needed for further development.

Following the pioneering work by Emparan and Reall, rotating black ring solution in five dimensions was presented by themselves simultaneously[4] and recently Tan and Teo proposed multi-black hole solutions as corresponding five-dimensional solutions[5] to the Israel-Khan solution[6] in four dimensions, and also Ida and Uchida gave higher dimensional treatment of Maxwell-Einstein system with the same symmetry as the generalized Weyl formalism [7].

Emparan and Reall showed that by adopting the original Weyl's canonical coordinates, D-dimensional Einstein equations in the case with $D-2$ orthogonal commuting Killing vector fields, where one is timelike and others are spacelike, can be reduced essentially to axisymmetric Laplace equation represented with circular cylindrical coordinates in three-dimensional flat space. However the three-dimensional flat space which the Laplace equation is defined has no direct connection to any real spacetime, so that metrics derived as the generalized Weyl solutions have rather complicated forms especialy near spacelike infinity. Only in the original four dimensional case treated by Weyl, the spacelike portion of the metrics happens to have the form corresponding to the metric of three-dimensional flat space in circular cylindrical coordinates. Emparan and Reall also showed that the metrics of five-dimensional black holes in asymtotically flat spacetimes are derived from the solutions of the three-dimensional Laplace equation corresponding to the Newton potentials produced by several finite rods and two semi-infinite rods with mass line density $1/2$, which are appropriately arranged along z axis (see the paper by Tan and Teo[5] in more details).

In this place we reconsider the generalized Weyl formalism by Emparan and Reall. Modification of their formalism is done by introducing another choice of coordinates in place of Weyl's original canonical ones. It is shown that four dimensional Laplace equation with two independent rotational symmetries in a

[1] E-mail:tmishima@phys.ge.cst.nihon-u.ac.jp

hypothetical Euclidean space is derived in place of three dimensional one, and especially in five dimensions the metrics corresponding to the modified Weyl's canonical coordinates asymptotically approach a simple Minkowski spacetime metric which shows apparent flatness. We also discuss how the five dimensional black hole solutions are described using the modified version of the generalized Weyl formalism.

2 Modification of Generalized Weyl Formalism

Here we consider general D-dimensional spacetimes with $D-2$ orthogonal commuting Killing vector fields, where one is timelike and others are spacelike. Following the argument by Emparan and Reall[3], as a starting point we can adopt the metric form,

$$ds^2 = -e^{2U_0}(dx^0)^2 + \sum_{i=1}^{D-3} e^{2U_i}(dx^i)^2 + e^{2C}dZd\bar{Z} \tag{1}$$

where U_0, U_i and C are functions of Z and $\bar{Z}$.

The vacuum Einstein equations are reduced to the following,

$$U_0 + \sum_{i=1}^{D-3} U_i = \log\left[w(Z) + \bar{w}(\bar{Z})\right] + const. \tag{2}$$

$$\begin{cases} \nu(Z,\bar{Z}) := C(Z,\bar{Z}) - \dfrac{1}{2}\log(\partial_Z w \partial_{\bar{Z}}\bar{w}) \\ \partial_Z \nu = -\dfrac{(w+\bar{w})}{\partial_Z w}\Sigma_{I<J}\partial_Z U_I \partial_Z U_J \\ \partial_{\bar{Z}} \nu = -\dfrac{(w+\bar{w})}{\partial_{\bar{Z}}\bar{w}}\Sigma_{I<J}\partial_{\bar{Z}} U_I \partial_{\bar{Z}} U_J \quad (I,J = 0 \sim D-3) \end{cases} \tag{3}$$

$$2(w+\bar{w})\partial_Z\partial_{\bar{Z}}U_i + \partial_Z w \partial_{\bar{Z}} U_i + \partial_{\bar{Z}}\bar{w}\partial_Z U_i \quad (i = 1 \sim D-3), \tag{4}$$

where $w(Z)$ and $w(\bar{Z})$ are an arbitrary function of Z and its complex conjugate respectively.

When the following Weyl's canonical coordinates are introduced

$$w(Z) = Z \ \ (= r + iz), \tag{5}$$

the equation (2) becomes

$$\sum_{I=0}^{D-3} U_I = \log r \tag{6}$$

and the equation (4) changes into

$$\partial_r^2 U_I + \frac{1}{r}\partial_r U_I + \partial_z^2 U_I = 0. \tag{7}$$

From these equations (6) snd (7), the following statment is deduced that U_I are given as some three-dimensional Newton potential and the total sum of U_I must be Newton potential corresponding to an infinite rod of zero thickness lying along z-axis with mass line density $1/2$.

Now we introduce the following modified Weyl's canonical coordinates,

$$w(Z) = \frac{1}{2i}Z^2 \ = \chi\rho + i\frac{\rho^2 - \chi^2}{2} \qquad (Z = \chi + i\rho), \tag{8}$$

in place of the Weyl's original ones. Then the basic equations (2) and (4) are reduced to

$$\sum_{I=0}^{D-3} U_I = \log\rho + \log\chi, \tag{9}$$

$$\partial_\chi^2 U_I + \frac{1}{\chi}\partial_\chi U_I + \partial_\rho^2 U_I + \frac{1}{\rho}\partial_\rho U_I = 0. \tag{10}$$

In this case, U_I is given as some *four*-dimensional Newton potential and the total sum of U_I must be Newton potential corresponding to the homogeneous mass distribution on orthogonal two flat planes in an auxiliary four-dimensional Euclidean space.

3 The Five-dimensional Schwarzschild Black Hole solution

We restrict our concern to five dimensional black holes. In the case of the original generalized Weyl formalism, the five-dimensional Schwarzschild metric takes the form [3]

$$ds^2 = -e^{2U_0}dt^2 + e^{2U_1}d\phi^2 + e^{2U_2}d\psi^2 + e^{2\nu}(dr^2 + dz^2). \tag{11}$$

$$\begin{aligned} U_1 &= \frac{1}{2}\log\left(\sqrt{r^2 + (z + \mu/4)^2} + (z + \mu/4)\right) \\ U_2 &= \frac{1}{2}\log\left(\sqrt{r^2 + (z - \mu/4)^2} - (z - \mu/4)\right) \\ U_0 &= \log r - U_1 - U_2. \end{aligned}$$

where the coordinates (x^0, x^1, x^2) are replaced with (t, ϕ, ψ). The function ν is omitted for want of space. The Source for U_0 is a finite rod with mass line density $1/2$ on z axis and the sources for U_1 and U_2 are two semi-infinite rods with mass line density $1/2$ extending to different directions along z axis, respectively. About the spacelike infinity, the metric above can be approximately written in the form

$$ds^2 \sim -dt^2 + \left\{\sqrt{r^2 + z^2} + z\right\}d\phi^2 + \left\{\sqrt{r^2 + z^2} - z\right\}d\psi^2 + \frac{1}{2\sqrt{r^2 + z^2}}(dr^2 + dz^2). \tag{12}$$

The right hand side of the equation (13) is a Minkowski metric represented in a four-dimensional coordinates similar to the two dimensional orthogonal curvilinear coordinates based on hyperbolas. This form is not so convenient for the analysis of the spacetime, because the z axis ($r = 0$) can be actually considered a pair of orthogonal two dimensional planes in the slice of constant time, if we take the large scale viewpoint. See Fig.1.

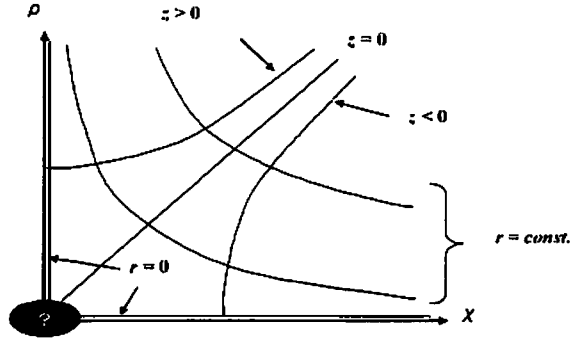

Figure 1: The relation between the coordinates (r, z) and (χ, ρ) is depicted. The black shaded region at the origin includes the region of strong gravity.

On the other hand, in the case of the modified weyl's canonical coordinates, using new functions $\tilde{U}_0 := U_0$, $\tilde{U}_1 := U_1 - \log\rho$, and $\tilde{U}_2 := U_2 - \log\chi$, the metric form is written as

$$ds^2 = -e^{2\tilde{U}_0}dt^2 + e^{2\tilde{U}_1}\rho^2 d\phi^2 + e^{2\tilde{U}_2}\chi^2 d\psi^2 + e^{2\nu}(d\rho^2 + d\chi^2), \tag{13}$$

and the relation corresponding to the equation (10) changes into $\tilde{U}_0 + \tilde{U}_1 + \tilde{U}_2 = 0$.

In this coordinates, the five-dimensional Schwarzschild Black Hole solution is described with the following $\tilde{U}_I$,

$$\begin{aligned} \tilde{U}_1 &= \frac{1}{2}\log\left[\frac{1}{\rho^2}\left(\sqrt{4\rho^2\chi^2 + (\rho^2 - \chi^2 + \mu/2)^2} + (\rho^2 - \chi^2 + \mu/2)\right)\right] \\ \tilde{U}_2 &= \frac{1}{2}\log\left[\frac{1}{\rho^2}\left(\sqrt{4\rho^2\chi^2 + (\rho^2 - \chi^2 - \mu/2)^2} - (\rho^2 - \chi^2 - \mu/2)\right)\right] \\ \tilde{U}_0 &= -\tilde{U}_1 - \tilde{U}_2, \end{aligned}$$

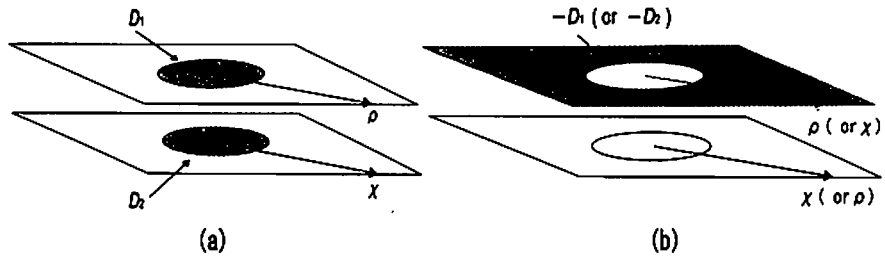

Figure 2: (a) is for $\tilde{U}_0$ and (b) is for $\tilde{U}_1$ or $\tilde{U}_2$. The white colored portions correspond to no matter distribution. The gray ones mean existence of matters.

which can be derived from U_I just performing the coordinate transformation $r = \chi\rho$ and $z = (\rho^2 - \chi^2)/2$ and correspond to homogeneous disk sources (for example, see Ida and Nakao[8]). .

As depicted in Fig.2, the function $\tilde{U}_0$ is given as four-dimensional Newton potential generated by two disk sources D_1 and D_2 with surface mass density $1/2$ which are put on two orthogonal flat planes in an auxiliary four-dimensional Euclidean space. On the other hand the functions $\tilde{U}_1$ and $\tilde{U}_2$ are generated by the homogeneous mass distribution on a flat plane where the same disk mentioned above is taken away.

The asymptotic form of the metric (13) is given by

$$ds^2 \sim -dt^2 + d\rho^2 + \rho^2\, d\phi^2 + d\chi^2 + \chi^2\, d\psi^2, \tag{14}$$

which shows that the spacetime approaches to five-dimensional Minkowski Spacetime explicitly. See Fig.1.

4 Summary

Modification of the generalized Weyl formalism was done by introducing another Weyl's coordinate system. It was shown that the solutions of the modified version have natural behavior of metric form about spacelike infinity, and also the disc sources in E^4 of the modified version correspond to the rods in E^3 in the original generalized Weyl formalism. The modification introduced here is just a coordinate transformation, but opening of new perspective of higher dimensional gravity may be expected. For introducing new coordinates has often resolved important problems in the study of general relativity.

For some interesting problems like global structure of spacetime with multi-black holes, or higher dimensional generalization of Zipoy-Voorhees spacetimes[9], the modification considered here may be useful to the study of these problems, which open up the rich structure of higher dimensional gravities.

References

[1] H. Weyl, Ann. Phys.(Leipzig)**54**, 117 (1917).

[2] D. Kramer *et al*, *Exact Solutions of Einstein's Field Equations, 2nd ed.* (Cambridge University Press, Cambridge, 2003).

[3] R. Emparan, H.S. Reall, Phys. Rev. **D65**, 084025 (2002).

[4] R. Emparan, H.S. Reall, Phys. Rev. Lett. **88**, 101101 (2002).

[5] H.S. Tan, E. Teo, Phys. Rev. **D68**, 044021 (2003).

[6] W. Israel, K.A. Khan, Nuovo Cimento **33**, 331 (1964).

[7] D. Ida, Y. Uchida, Phys. Rev. **D68**, 104014 (2003).

[8] D. Ida, K. Nakao, Phys. Rev. **D66**, 064026 (2002).

[9] D.M. Zipoy, J. Math. Phys. **8**, 1137 (1966); B.H. Voorhees, Phys. Rev. **D2**, 2119 (1970).

Electromagnetic radiation from naked singularities in self-similar gravitational collapse

Eiji Mitsuda[1], Hirotaka Yoshino[2], and Akira Tomimatsu[3]

Department of Physics, Graduate School of Science,
Nagoya University, Chikusa, Nagoya 464-8602, Japan

Abstract

We study behaviors of electromagnetic radiation emitted at the moment of naked singularity formation during spherically symmetric self-similar gravitational collapses of an isothermal gas with small circular currents. Consequently, it is found that the energy flux has various behaviors depending on internal conditions of the collapsing star.

1 Introduction

While Penrose proposes cosmic censorship conjecture, many counterexamples to this conjecture have been found over the past three decades. For example, Lemaître-Tolman-Bondi (LTB) spacetime, which describes a spherically symmetric inhomogeneous dust collapse, spherically symmetric perfect fluid self-similar spacetime [1], which describe a spherically symmetric inhomogeneous isothermal gas collapse, critical phenomena, which are behaviors of collapse solutions at a critical point which is threshold of black hole formation for a one-parameter family of initial data sets, and so on. These counterexamples predict that a naked singularity appears during the gravitational collapse of an inhomogeneous massive star and give us an expectation that one can gain information around the singularity. Unknown phenomena may happen at the singularity because of divergence of the density and the strong gravity, and so the information may lead to a breakthrough of high-energy physics.

In practice, this may be possible if we can observe the radiation emitted during the gravitational collapse to a naked singularity. And then, one can expect that peculiarities of the radiation are observed near the Cauchy horizon. Hence, many researchers have been examined u-dependence, where u is a retarded null coordinate, of the energy flux of the radiation just before the Cauchy horizon by giving linear perturbations to spacetimes including a naked singularity and determined ξ if the energy flux is proportional to $(u - u_{\rm ch})^{-\xi}$ there, where the Cauchy horizon sits on $u = u_{\rm ch}$ line. The energy flux is finite at the Cauchy horizon when $\xi = 0$ and then it is regretted that observation of efficiencies of the naked singularity may be difficult. It is noted that howbeit, from the viewpoint of stability of the Cauchy horizon, this is meaningful because then the Cauchy horizon is stable and the naked singularity still alive. When ξ is a positive value, it is expected that the energy flux grows unboundedly as the Cauchy horizon is approached and that the growing power ξ has information of the dynamics of the collapse. This means that we may be able to observe a burst phenomenon due to effects of the strong gravity, and so is significant for astrophysics although efficiencies of backreaction to the background spacetime due to the radiation should be taken into consideration in more accurate arguments. Previous works for this problem are summarized in Table.1. From these works, ξ seems to be different for the different radiation and the different gravitational collapse to a naked singularity. However, the following three points are not obvious in these works. (1) LTB solutions have parameter functions. In previous works for LTB spacetime, the energy flux was investigated only for restricted range of these parameters. More rigorous parameter-dependence of the energy flux must be clarified in order to know how it reflects internal information. (2) In previous works for semi-classical radiation, the 1st order WKB approximation was used. This means that "particle" propagation along null geodesics rather than "wave" propagation was discussed in these works. It is not obvious how the radiation reflects internal information as "wave". (3) In previous works for semi-classical radiation, two-dimensional form obtained by removing the angular degrees of freedom

[1]E-mail:emitsuda@allegro.phys.nagoya-u..ac.jp
[2]E-mail:hyoshino@allegro.phys.nagoya-u..ac.jp
[3]E-mail:atomi@allegro.phys.nagoya-u..ac.jp

researchers	background spacetime	kind of radiation	ξ
Iguchi, Nakao, and Harada [2,3]	LTB	gravitational radiation	0
Harada, Iguchi, and Nakao [4]	LTB	semi-classical radiation	$\frac{2}{3}$ or 1
Miyamoto and Harada [5]	self-similar	semi-classical radiation	2

Table 1: The value of ξ, power of $(u-u_{\rm ch})$, in previous works for the energy flux of the radiation near the Cauchy horizon associated with a naked singularity. In the second line, $\xi = 2/3$ for a minimally coupled massless scalar field, $\xi = 1$ for a conformally coupled massless scalar field.

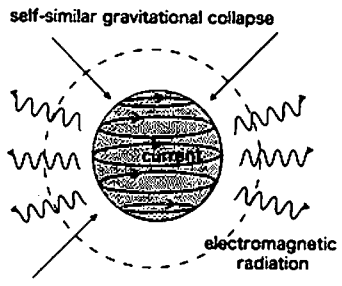

Figure 1: The physical model underlying our analysis. Note that we consider only inside a collapsing star.

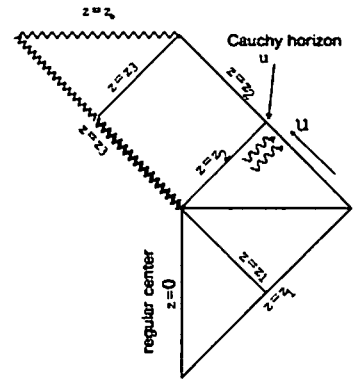

Figure 2: Penrose diagram of self-similar collapse solutions. In our analysis, the wavy line is focused on.

was used. That is to say scattering due to centrifugal force was not considered in these works. Wave scattered by the effective potential may evidently reflect features of the background spacetime such as quasi-normal modes.

Given the above points, we decide to examine the energy flux of electromagnetic radiation just before the Cauchy horizon in spherically symmetric perfect fluid self-similar gravitational collapse. We can introduce naturally effects of scattering due to centrifugal force by considering electromagnetic radiation because $l = 1$ mode, where l is multipole modes, of the radiation become conspicuous at infinity. And one of the main reason for the choice of the background spacetime is the fact that there is no classical analysis in self-similar spacetime. Additionally, Harada's and Maeda's numerical simulations [6] suggest that one of the self-similar solutions is the asymptotic behavior of a more general non-self-similar collapse, and so self-similar spacetime is more than mere solutions of Einstein equation and have a realistic possibility. Mathematically speaking, we give an electromagnetic odd-parity perturbation to spherically symmetric perfect fluid self-similar gravitational collapse solutions. Thus, the physical model underlying our analysis is that of inside a self-similar collapsing isothermal gas with small circular conserved currents to a naked singularity (see Fig.1). We derive an evolution equation for the amplitude of the perturbation and solve this equation analytically by *Green function technique* under the *3rd order* WKB approximation in order to observe "wave" propagation. By doing this, we can find poles in Fourier space of Green function. It will be shown that the existence of these poles significantly affects u-dependence of the energy flux. Our results can be applies to a *whole* range of parameters of self-similar solutions.

2 Background spacetime

We consider spherically symmetric perfect fluid self-similar gravitational collapse (comoving) :

$$ds^2 = -e^{2\nu(z)}dt^2 + e^{2\lambda(z)}dr^2 + r^2S^2(z)d\theta^2 + r^2S^2\sin^2\theta d\phi^2, \tag{1}$$

$$T^{ab} = (\rho + P)U^aU^b + Pg^{ab}, \quad P = \alpha\rho, \quad 0 \le \alpha \le 1, \tag{2}$$

where $z \equiv r/t$ is a self-similar variable. Penrose diagram of this spacetime is shown in Fig.2. Naked singularity appears at the center and $t = 0$, and the center is regular before the singularity appears. We introduce a function $V(z) \equiv ze^{\lambda-\nu}$ which is the velocity of z-const surface relative to fluid and $V(z_1) = -1$, $V(z_2) = 1$. In this spacetime, $z = z_1$ line is the past Cauchy horizon and the past null infinity and $z = z_2$ line is the future Cauchy horizon and the future null infinity. We construct null coordinates $(u,\ v)$, which are retarded and advanced null coordinate respectively, so that the neighborhood of the Cauchy horizon is locally flat. In these coordinates, the Cauchy horizon is $u = 0$ line.

This solution is parameterized by the central density parameter which is defined by

$$D \equiv 4\pi\rho(t,0)t^2. \tag{3}$$

3 Energy flux of electromagnetic radiation

We give the following currents as a perturbation to the above spacetime :

$$j_a = \left(0,\ 0,\ 0,\ j_l(t,z)\sin\theta\frac{\partial Y_{l0}}{\partial\theta}\right), \quad j_l(t,z) = \frac{j_c\delta(r-r_0)}{S^2r^2}. \tag{4}$$

This means that axisymmetric circular currents are only on a single sphere $r = r_0$ and are conserved in this sphere. Under the Lorentz gauge, the vector potential can be written as

$$A_a = \left(0,\ 0,\ 0,\ a(t,z)\sin\theta\frac{\partial Y_{l0}}{\partial\theta}\right), \tag{5}$$

where a is gauge invariant and a wave function which must be solved. Using the above form, Maxwell equation $\nabla_b F^{ab} = 4\pi j^a$ ($F_{ab} = \partial_b A_a - \partial_a A_b$) is

$$t^2\frac{\partial^2 a}{\partial t^2} - 2zt\frac{\partial^2 a}{\partial t\partial z} - \left(e^{2(\nu-\lambda)} - z^2\right)\frac{\partial^2 a}{\partial z^2} + \left\{2z + z^2(\lambda' - \nu') - e^{2(\nu-\lambda)}(\nu' - \lambda')\right\}\frac{\partial a}{\partial z}$$
$$-(\lambda' - \nu')zt\frac{\partial a}{\partial t} + \frac{e^{2\nu}l(l+1)}{z^2S^2}a = -4\pi t^2 e^{2\nu}j_l, \tag{6}$$

where $' \equiv d/dz$. We try the following Fourier expansion for a and $J_l \equiv t^2 j_l$:

$$a(t,z) = \int_{-\infty}^{\infty} f(z,k)e^{ik\log(-t)}dk, \qquad J_l(t,z) = \int_{-\infty}^{\infty} \hat{J}_l(z,k)e^{ik\log(-t)}dk. \tag{7}$$

By doing this, we find Eq. (6) to be reduced to the following ordinary differential equation :

$$f'' + p(z,k)f' + q(z,k)f = 4\pi b(z,k). \tag{8}$$

We don't explicitly write $p(z,k), q(z,k)$ and $b(z,k)$ here. To solve this equation, we impose the following boundary conditions on f : (1) f is regular at $z = 0$. (2) f has no ingoing mode at the past null infinity. By condition (2), we can purely observe effects of scattering due to the strong gravitational field around the center. We introduce two homogeneous solutions of Eq. (8) f_0 and f_1 which satisfy the condition (1) and (2) respectively and construct Green function with these homogeneous solutions. To know specific k-dependence of f_0 and f_1, we use the high frequency (WKB) approximation. In the approximation, the 3rd order of $1/k$ is taken into consideration. This consideration leads us to Wronskian W written as the following form for $l = 1$:

$$W(k,z) = f_1f_0' - f_0f_1' \simeq (k + i\gamma)(k - i\gamma)F(z), \quad \gamma^2 = 1 - \frac{2(2+3\alpha)}{3}D < 1. \tag{9}$$

We don't explicitly write $F(z)$. The above equation means that $k = \pm i\gamma$ are poles in k-space. These poles significantly contribute u-dependence of the energy flux of the radiation just before the Cauchy horizon. Note that γ can be real or imaginary number depending on D and α.

After some calculations, we obtain the following results for the energy flux of the electromagnetic radiation ($l = 1$) just before the Cauchy horizon :

1. In the case $\gamma(>0)$ is real number i.e. $D \leq 3/\{2(2+3\alpha)\}$,

$$\text{Flux} \propto u^{-2\xi}, \tag{10}$$

where ξ is defined by ($V_i' \equiv V'(z_i)$)

$$\xi \equiv 1 - \frac{\tau}{z_2 V_2'}, \quad \tau \equiv \min(\gamma, \ -z_1 V_1', \ z_2 V_2'). \tag{11}$$

This means that ξ has both possibility $\xi = 0$ and $\xi > 0$ indirectly depending on D and α.

2. In the case γ is imaginary number i.e. $D > 3/\{2(2+3\alpha)\}$,

$$\text{Flux} \propto u^{-2} \sin^2\left(\frac{\hat{\gamma}}{z_2 V_2'} \log u + c\right), \tag{12}$$

where c is constant and $\hat{\gamma} \equiv \gamma/i$. This u-dependence of the energy flux has *not* been discovered.

4 Discussion

To clarify parameter-dependence of those behaviors of the energy flux, we examine the above results in the dust self-similar solution and the general relativistic Larson-Penston solution.

In dust self-similar solution, D is determined : $D = 2/3$. Therefore, $\gamma = 1/3$ from Eq. (9) and so Flux $\propto u^{-2\xi}$. Instead of D, the solution is parameterized by the density gradient parameter κ. There exists κ^* so that a naked singularity appears in $\kappa^* > \kappa$ and don't in $\kappa^* < \kappa$. In $\kappa^* > \kappa$, we find κ_c so that $z_2 V_2' < \gamma < z_1 V_1'$ in $\kappa^* < \kappa < \kappa_c$ and $\gamma < z_2 V_2' < z_1 V_1'$ in $\kappa_c < \kappa$. Hence, From Eq. (10) and Eq. (11), the energy flux remains finite in $\kappa^* < \kappa < \kappa_c$ and grows unboundedly in $\kappa_c < \kappa$ as the Cauchy horizon is approached. This fact suggests that there is a relation between the naked singularity formation and the behaviors of the energy flux just before the Cauchy horizon.

In the general relativistic Larson-Penston solution, D is determined for given α because of analyticity on the sonic point. We found that $D > 3/\{2(2+3\alpha)\}$ for a whole range of α where a naked singularity appears in this solution. Therefore, from Eq. (12), the energy flux grows unboundedly with oscillation as the Cauchy horizon is approached.

5 Summary

We gave an odd-parity electromagnetic perturbation to spherically symmetric perfect fluid self-similar gravitational collapse solutions. Our analytic calculations based on the high frequency approximation show that the energy flux of the electromagnetic radiation due to the perturbation remains finite, grows unboundedly with inverse power-law or grows unboundedly with oscillation as the Cauchy horizon is approached depending on the central density and the equation of state. In particular, the oscillation is *new* behavior. This results indicate that the radiation emitted during the gravitational collapse to a naked singularity evidently reflects internal conditions of the collapsing star. Moreover, our results is significant for astrophysics because they predict an electromagnetic burst phenomenon during the gravitational collapse.

References

[1] A. Ori, and T. Piran, Phys. Rev. **D42**, 1068 (1990).

[2] H. Iguchi, T. Harada, and K. Nakao, Prog. Theor. Phys. **101**, 1235 (1999).

[3] H. Iguchi, T. Harada, and K. Nakao, Prog. Theor. Phys. **103**, 53 (2000).

[4] T. Harada, H. Iguchi, and K. Nakao, Phys. Rev. **D62**, 084037 (2000).

[5] U. Miyamoto, and T. Harada, gr-qc/0312080 (2003)

[6] T. Harada, and H. Maeda, Phys. Rev. **D63**, 084022 (2001)

Can semi-classical effect recover the cosmic censorship?

Umpei Miyamoto[1]

Department of Physics, Waseda University, Okubo 3-4-1, Shinjuku, Tokyo 169-8555, Japan

Tomohiro Harada[2]

Astronomy Unit, School of Mathematical Sciences, Queen Mary, Mile End Road, London E1 4NS, UK

Abstract

We are concerned with the particle creation during naked-singularity formation in spherically symmetric self-similar collapse without specifying the collapsing matter. In generic case, the power of quantum emission is found to be proportional to the inverse square of the remaining time to the Cauchy horizon. Moreover, the constant of proportion can be arbitrarily large in the limit to marginally naked singularity. Therefore, the unbounded power is especially striking in the case that a event horizon is very close to the Cauchy horizon because the emitted energy can be arbitrarily large in spite of a cutoff expected from quantum gravity. The divergence of the redshift of emitted particles is found to cause the divergence of the power to positive or negative infinity, depending on the coupling manner of scalar fields to gravity. Above results suggest the instability of the Cauchy horizon in spherically symmetric self-similar collapse from quantum field theory and seem to support the existence of a semiclassical cosmic censor.

1 Introduction

It is known that generic spherically symmetric self-similar collapse results in strong naked-singularity formation [1]. Among such self-similar spacetimes, the general relativistic Larson-Penston (GRLP) solution [2], which describes the collapse of a perfect fluid, is interesting because the existence of pressure does not prevent the formation of naked singularity completely. Moreover, the convergence of more general spherically symmetric collapse of a perfect fluid to the GRLP solution has been reported both numerically and analytically [3] as a realization of the *self-similarity hypothesis* proposed by Carr [4]. From the above, the GRLP solution will be a strongest known counterexample against the *cosmic censorship hypothesis* [5]. The discovery of the black hole critical behavior also shed light on a self-similar solution as a critical solution (see [6] for a review). We can say with fairy certainty that self-similar solutions play important roles near spacetime singularities.

Ford and Parker first gave attention to the possibility that such semiclassical effects such as particle creation would prevent the formation of a naked singularity [7]. Subsequently, these semiclassical phenomena were investigated in the collapse of self-similar null dust [8, 9], self-similar dust [10], and analytic dust [11]. Typically, the power of quantum emission from a shell-focusing singularity diverges as the Cauchy horizon (CH) is approached. For a recent review of quantum/classical emission during naked-singularity formation, see [12].

Motivated from the above, we are intended for the investigation of particle creation during the naked-singularity formation in generic self-similar collapse without specifying the collapsing matter and for the resulting instability of the CH. Our analysis is regarded as a semiclassical counterpart of [13], in which the stability of the CH in self-similar collapse was tested by a classical scalar field. For the derivation of some formulae used in this article and the application of the generic results to concrete models of self-similar collapse, see [14].

[1] E-mail:umpei@gravity.phys.waseda.ac.jp
[2] E-mail:T.Harada@qmul.ac.uk

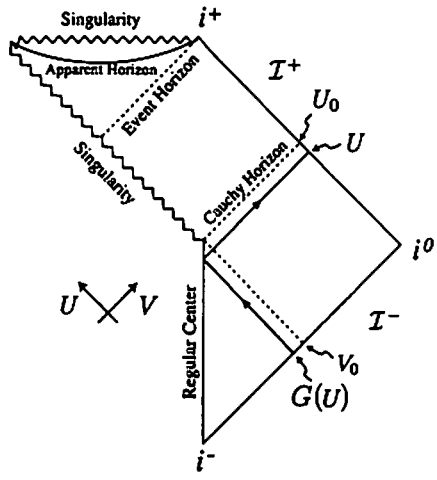

Figure 1: One of the possible causal structures considered in this article. A singularity occurs at the spacetime point (U_0, V_0) and is visible from $\mathcal{I}^+$, where (U, V) are suitable double null coordinates. An outgoing null ray $U = \text{const.}$ can be traced backward in time from $\mathcal{I}^+$ to $\mathcal{I}^-$, which turn out to be an incoming null ray $V = G(U)$. The outgoing null ray $U = U_0$ and incoming null ray $V = V_0$ represent the CH and the null ray that terminates at the NS.

2 Power, Energy, and Redshift

We consider spherically symmetric self-similar collapse with a globally naked singularity. The existence of a regular center before the occurrence of a central naked singularity and an asymptotically flat region, which is realized by a suitable cutoff of the self-similar region, is assumed. See Fig. 1 for the causal structure and a map of null ray which we define below. A map $V = G(U)$ between the moments when one incoming null ray leaves $\mathcal{I}^-$ and terminates at $\mathcal{I}^+$ after passing through the regular center plays an important role in estimating the power of emission on geometric-optics approximation. We obtain the map on the assumptions that the metric function is in C^{2-} around the CH [3] and that the curvature around the singularity causes particle creation, which was proven at least for the self-similar and analytic dust models [15], as

$$G(U) = V_0 - (U_0 - U)^\alpha G_*(U), \ \alpha > 0,$$

where $U = U_0$ and $V = V_0$ are the CH and the first incoming null ray which terminates at the naked singularity, respectively. The positive constant α is the first derivative of a metric function at the CH and the function G_* is a regular function which does not vanish at the CH.

The power can be obtained as the vacuum-expectation value of a stress-energy tensor by the point-splitting regularization [7] as

$$\begin{aligned} P &= \frac{1}{24\pi}\left[\frac{3}{2}\left(\frac{G''}{G'}\right)^2 - \frac{G'''}{G'}\right] \\ &\simeq \frac{\alpha^2 - 1}{48\pi(U_0 - U)^2}, \end{aligned} \tag{1}$$

for a minimally coupled scalar field. The emitted energy is estimated as

$$E = \int_{-\infty}^{U} P(U')dU' \simeq \frac{\alpha^2 - 1}{48\pi\,(U_0 - U)}. \tag{2}$$

[3] Weaker differentiability of the CH leads to a different map. Therefore the resulting power and energy of emission have different time dependence, although we do not look deeper into such a possibility in this article.

Deriving above expression, we assumed that $\alpha \neq 1$[4]. For a conformally coupled scalar field, the power and energy can be obtained just by replacing the factor $\alpha^2 - 1$ for $(\alpha - 1)^2$ in Eqs. (1) and (2) respectively. The power is proportional to the inverse square of the remaining time to the CH. If $\alpha > 1$, the power diverges to positive infinity for both minimally and conformally coupled scalar fields, while if $0 < \alpha < 1$, the power diverges to negative and positive infinity for minimally and conformally coupled scalar fields, respectively. The redshift of emitted particles is obtained as

$$\frac{\omega_{out}}{\omega_{in}} \propto (U_0 - U)^{\alpha - 1},$$

where ω_{in} and ω_{out} are frequencies of incoming and outgoing null rays, respectively. In terms of the redshift of particles, the case of $\alpha > 1$ ($0 < \alpha < 1$) corresponds to infinite redshift (blueshift) at the CH and the case of $\alpha = 1$ corresponds to finite amount of redshift or blueshift.

Although the power and energy diverge when the CH is approached, such divergence needs to be regarded carefully. The semiclassical approximation would cease to be valid when the curvature radius at some spacetime point inside star reaches the Planck scale. If we take into account a cutoff expected from quantum gravity, the emitted energy within the semiclassical phase can be shown to be less than the order of the Planck energy, in ordinary situations. However, there is a case that total emitted energy can be arbitrarily large, which seem to cause a crucial instability of the CH if we take into account the effect of backreaction to gravity. One can prove that the constant α can be arbitrarily large in the limit to marginally naked singularity, in which the event horizon and CH coincide [5].

3 Conclusion

We have been concerned with a quantum-mechanical particle creation by the strongly curved spacetime region which is exposed to us in generic spherically symmetric self-similar collapse. The flux of quantum emission diverges as the CH is approached except in a special class of solutions, in which the constant $\alpha = 1$. The square inverse proportion of the power to the remaining time is due to the scale invariance of self-similar spacetimes. The total energy emitted within the phase in which quantum gravitational effects could be negligible, can be arbitrarily large when the event horizon and CH are very close. We go on from this to the conclusion that if the back reaction to a gravitational field is taken into account, the semiclassical effect would cause the instability of the CH and might recover the cosmic censor in this limiting case. We have also found that the divergence of redshift or blueshift of emitted particles would be a criterion of the instability.

Due to the generality of our analysis, the results are applicable to known concrete models of self-similar collapse such as Lemaître-Tolman-Bondi, Vaidya, Roberts, GRLP solutions. Above spacetimes except Roberts solution, which describes the self-similar collapse of a massless scalar field, would be suffered from the semiclassical instability, including the GRLP solution.

Acknowledgments

This work owes to the thoughtful and helpful comments of Hideki Maeda. UM would like to thank A. Hosoya, K. Nakao, and Kengo Maeda for helpful comments at this meeting. This work was partially supported by a Grant for The 21st Century COE Program (Holistic Research and Education Center for Physics Self-Organization Systems) at Waseda University.

[4] If $\alpha = 1$, both the power and energy remain finite at the CH. For example, the power of emission of a minimally coupled scalar field is

$$P \simeq \frac{2G_*'^2(U_0) - G_*(U_0)G_*''(U_0)}{8\pi G_*^2(U_0)}.$$

[5] In the case that the event horizon and CH coincide exactly, quantum radiation reduces to the Hawking one [7, 8].

References

[1] B. Waugh and K. Lake, Phys. Rev. D **40**, 2137 (1989); K. Lake and T. Zannias, Phys. Rev. D **41**, 3866 (1990).

[2] A. Ori and T. Piran, Phys. Rev. Lett. **59**, 2137 (1987); Gen. Relat. Grav. **20**, 7 (1998); Phys. Rev. D **42**, 1068 (1990).

[3] T. Harada and H. Maeda, Phys. Rev. D **63**, 084022 (2001).

[4] B. J. Carr, in *Proceedings of the Ninth Workshop on General Relativity and Gravitation*, 1999, edited by Y. Eriguchi *et al.* (Hiroshima, Japan), p. 425, gr-qc/003009.

[5] R. Penrose, Riv. Nuovo Cime. 1, 252 (1969), reprinted in Gen. Relat. Grav. 34, 1141 (2002); in *General Relativity. An Einstein Century Survey*, edited by S. W. Hawking and W. Israel (Cambridge University Press, Cambridge, England, 1979), p. 581.

[6] C. Gundlach, Phys. Rep. **376**, 339 (2003).

[7] L. H. Ford and L. Parker, Phys. Rev. D **17**, 1485 (1987).

[8] W. A. Hiscock, L. G. Williams, and D. M. Eardley, Phys. Rev. D **26**, 751 (1982)

[9] T. P. Singh and C. Vaz, Phys. Lett. B **481**, 74 (2000).

[10] S. Barve, T. P. Singh, C. Vaz, and L. Witten, Nucl. Phys. B **532**, 361 (1998); Phys. Rev. D **58**, 104018 (1998); C. Vaz and L. Witten, Phys. Lett. B **442**, 90 (1998).

[11] T. Harada, H. Iguchi, K. Nakao, Phys. Rev. D **61**, 101502 (2000); *ibid.* **62**, 084037 (2000).

[12] T. Harada, H. Iguchi, and K. Nakao, Prog. Theor. Phys. **107**, 449 (2002).

[13] B. C. Nolan and T. Waters, Phys. Rev. D **66**, 104012 (2002).

[14] U. Miyamoto and T. Harada, gr-qc/0312080 (to be published in Phys. Rev. D).

[15] T. Tanaka and T. P. Singh, Phys. Rev. D **63**, 124021 (2001).

On uniqueness of five-dimensional rotating black holes

Yoshiyuki Morisawa[1], Daisuke Ida[2]

[1] *Yukawa Institute for Theoretical Physics, Kyoto University, Kyoto 606-8502, Japan*
[2] *Department of Physics, Tokyo Institute of Technology, Tokyo 152-8551, Japan*

Abstract

We study the boundary value problem for the stationary rotating black hole solutions to the five-dimensional vacuum Einstein equation. Assuming the two commuting rotational symmetry and the sphericity of the horizon topology, we show that the black hole is uniquely characterized by the mass, and a pair of the angular momenta.

1 Introduction

In recent years there has been renewed interest in higher dimensional black holes in the context of both string theory and brane world scenario. In particular, the possibility of black hole production in linear collider is suggested [1]. Such phenomena play a key role to get insight into the structure of space-time; we might be able to prove the existence of the extra dimensions and have some information about the quantum gravity. Since the primary signature of the black hole production in the collider will be Hawking emission from the stationary black hole, the classical equilibrium problem of black holes is an important subject. The black holes produced in colliders will be small enough compared with the size of the extra dimensions and generically have angular momenta, they will be well approximated by higher dimensional rotating black hole solutions found by Myers and Perry [2]. The Myers-Perry black hole which has the event horizon with spherical topology can be regarded as the higher-dimensional generalization of the Kerr black hole. One might expect that such a black hole solution describes the classical equilibrium state continued from the black hole production event, if it equips stability and uniqueness like the Kerr black hole in four-dimensions. The purpose of this paper is to consider the uniqueness and nonuniqueness of the rotating black holes in higher dimensions.

The uniqueness theorem states that a four-dimensional black hole with regular event horizon is characterized only by mass, angular momentum and electric charge [3]. Recently, uniqueness and nonuniqueness properties of five or higher-dimensional black holes are also studied. Emparan and Reall have found a black ring solution of the five-dimensional vacuum Einstein equation, which describes a stationary rotating black hole with the event horizon homeomorphic to $S^2 \times S^1$ [4]. In a certain parameter region, a black ring and a (Myers-Perry) black hole can carry the same mass and angular momentum. This might suggest the nonuniqueness of higher-dimensional stationary black hole solutions. For example, Reall [5] conjectured the existence of stationary, asymptotically flat higher-dimensional vacuum black hole admitting exactly two commuting Killing vector fields although all known higher dimensional black hole solutions have three or more Killing vector fields. In six or higher dimensions, Myers-Perry black hole can have an arbitrarily large angular momentum for a fixed mass. The horizon of such black hole highly spreads out in the plane of rotation and looks like a black brane in the limit where the angular momentum goes to infinity. Hence, Emparan and Myers [6] argued that rapidly rotating black holes are unstable due to the Gregory-Laflamme instability [7] and decay to the stationary black holes with rippled horizons implying the existence of black holes with less geometric symmetry compared with the Myers-Perry black holes. For supersymmetric black holes and black rings, string theoretical interpretation are given by Elvang and Emparan [8]. They showed that the black hole and the black ring with same asymptotic charges correspond to the different configurations of branes, giving a partial resolution of the nonuniqueness of supersymmetric black holes in five dimensions. On the other hand, we have uniqueness theorems for black holes at least in the static case [9]. Furthermore, the uniqueness of the stationary black holes is supported by the argument based on linear perturbation of higher dimensional

[1] morisawa@yukawa.kyoto-u.ac.jp
[2] d.ida@th.phys.titech.ac.jp

static black holes [10]. There exist regular stationary perturbations that fall off at asymptotic region only for vector perturbation, and then the number of the independent modes corresponds to the rank of the rotation group, namely the number of angular momenta carried by the Myers-Perry black holes [11]. This suggests that the higher-dimensional stationary black holes have uniqueness property in some sense, but some amendments will be required. Here we consider the possibility of restricted black hole uniqueness which is consistent with any argument about uniqueness or nonuniqueness. Though the existence of the black ring solution explicitly violates the black hole uniqueness, there still be a possibility of black hole uniqueness for fixed horizon topology [12]. Hence we restrict ourselves to the stationary black holes with spherical topology.

In this paper, we consider the asymptotically flat, black hole solution to the five-dimensional vacuum Einstein equation with the regular event horizon homeomorphic to S^3, admitting two commuting spacelike Killing vector fields and stationary (timelike) Killing vector field. Along with the argument by Carter [13], it is possible to construct a timelike Killing vector field commuting with both spacelike Killing vector fields. Hence, it is natural to assume all the three Killing vector fields are commuting with each other. The five-dimensional vacuum space-time admitting three commuting Killing vector fields is described by the nonlinear σ-model [14]. Then the Mazur identity [15] for this system is derived. We show that the five-dimensional black hole solution with regular event horizon of spherical topology is determined by three parameters under the appropriate boundary conditions.

The remainder of the paper is organized as follows. In Section 2, we give the field equations for the five-dimensional vacuum space-time admitting three commuting Killing vector fields, and introduce the matrix form of field equations to clarify the hidden symmetry of this system following Maison [14]. Then the Mazur identity which is useful to show the coincidence of two solutions is given in Section 3. In Section 4, we determine the boundary conditions. We summarize this paper in Section 5. There are detailed claculations in the full version of this paper [16].

2 Five-dimensional vacuum space-time admitting three commuting Killing vector fields

We consider the five-dimensional space-time admitting two commuting spacelike Killing vector fields $\xi_I = \partial_I$, $(I = 4, 5)$ and timelike Killing vector field $\xi_t = \partial_t$. The metric can be written in the form

$$g = f^{-1}e^{2\sigma}(d\rho^2 + dz^2) - f^{-1}\rho^2 dt^2 + f_{IJ}(dx^I + w^I dt)(dx^J + w^J dt), \tag{1}$$

where $f = \det(f_{IJ})$, all the metric functions depend only on ρ and z, $x^4 = \phi$, $x^5 = \psi$ (we will later identify ξ_4 and ξ_5 as Killing vector fields corresponding to two independent rotations in the case of asymptotically flat space-time). We define the twist potential ω_I by $\omega_{I,i} = -\rho^{-1} f f_{IJ}\epsilon_{ij\varphi}\gamma^{jk}\partial_k w^J$, where i, j run in $\{\rho, z, \varphi\}$, γ is the abstract flat three-space with the metric $\gamma = d\rho^2 + dz^2 + \rho^2 d\varphi^2$, ϵ_{ijk} denotes the totally skew-symmetric symbol such that $\epsilon_{\rho z\varphi} = 1$. Then the vacuum Einstein equation reduces to the field equations for the five scalar fields f_{IJ} and ω_I defined on the three-dimensional space:

$$D^2 f_{IJ} = f^{KL} D f_{IK} \cdot D f_{JL} - f^{-1} D\omega_I \cdot D\omega_J, \quad D^2\omega_I = f^{-1} Df \cdot D\omega_I + f^{JK} D f_{IJ} \cdot D\omega_K, \tag{2}$$

where D is the covariant derivative with respect to the three-metric γ_{ij} and the dot denotes the inner product determined by γ_{ij}. Once the five scalar fields f_{IJ}, ω_I are determined, the other metric functions σ and w^I are obtained by solving the following partial derivative equations.

Instead of the nonlinear representation by the scalar fields f_{IJ} and ω_I, we introduce the $SL(3, \mathbf{R})$ matrix field Φ as

$$\Phi = \begin{pmatrix} f^{-1} & -f^{-1}\omega_\phi & -f^{-1}\omega_\psi \\ -f^{-1}\omega_\phi & f_{\phi\phi} + f^{-1}\omega_\phi\omega_\phi & f_{\phi\psi} + f^{-1}\omega_\phi\omega_\psi \\ -f^{-1}\omega_\psi & f_{\phi\psi} + f^{-1}\omega_\phi\omega_\psi & f_{\psi\psi} + f^{-1}\omega_\psi\omega_\psi \end{pmatrix}, \tag{3}$$

which is symmetric (${}^t\Phi = \Phi$) and unimodular ($\det\Phi = 1$). When the Killing vector fields ξ_ϕ and ξ_ψ are spacelike, all the eigenvalues of Φ are real and positive. Therefore, there is an $SL(3, \mathbf{R})$ matrix field g which is a square root of the matrix field Φ, namely $\Phi = g\,{}^t g$. The current matrix defined by $J_i = \Phi^{-1}\partial_i\Phi$, which is conserved, namely every element of $D_i J^i$ independently vanishes due to the field equations (2).

3 Mazur identity

Let us consider two different sets of the field configurations $\Phi_{[0]}$ and $\Phi_{[1]}$ satisfying the field equations (2). A bull's eye $\odot$ denotes the difference between the value of functional obtained from the field configuration $\Phi_{[1]}$ and value obtained from $\Phi_{[0]}$, *e.g.*, $\overset{\odot}{J}{}^i = J^i_{[1]} - J^i_{[0]} = \Phi^{-1}_{[1]}\partial^i\Phi_{[1]} - \Phi^{-1}_{[0]}\partial^i\Phi_{[0]}$. The deviation matrix Ψ is defined by $\Psi = \overset{\odot}{\Phi}\,\Phi^{-1}_{[0]}$, which vanishes if and only if the two sets of field configurations ([1] and [0]) coincide with each other. The Mazur identity is given by

$$\oint_{\partial\Sigma} \rho\partial^a \mathrm{tr}\Psi dS_a = \int_\Sigma \rho h_{ab}\mathrm{tr}\left\{\mathcal{M}^a\,{}^t\mathcal{M}^b\right\} d\rho dz, \tag{4}$$

where h_{ab} is the flat two-dimensional metric $h = d\rho^2 + dz^2$, the relevant region is $\Sigma = \{(\rho, z)|\rho \geq 0\}$, the matrix $\mathcal{M}$ is defined by $\mathcal{M}^a = g^{-1}_{[0]}\,{}^t\overset{\odot}{J}{}^a\, g_{[1]}$. When the current difference $\overset{\odot}{J}{}^a$ is not zero, the right hand side of the identity (4) is positive. Hence we must have $\overset{\odot}{J}{}^a = 0$ if the boundary conditions under which the left hand side of Eq. (4) vanishes are imposed at $\partial\Sigma$. Then the difference Ψ is a constant matrix over the region Σ. The limiting value of Ψ is zero on at least one part of the boundary $\partial\Sigma$ is sufficient to obtain the coincidence of two solutions $\Phi_{[0]}$ and $\Phi_{[1]}$.

4 Boundary conditions and coincidence of solutions

When one use the Mazur identity, the boundary conditions for the fields Φ (*i.e.*, f_{IJ} and ω_I) are needed at the infinity, the two planes of rotation and the horizon. We will require asymptotic flatness, regularity at the two planes of rotation, and regularity at the spherical horizon. Under these conditions, the Mazur identity shows that the coincidence of the solutions. An asymptotically flat space-time with mass $M = 3\pi m/8G$, angular momenta $J_\phi = \pi ma/4G$ and $J_\psi = \pi mb/4G$ (where we restrict ourselves to the case in which $m > a^2 + b^2 + 2|ab|$) has metric as the following form:

$$\begin{aligned} g \;=\; & \left[\frac{2ma(r^2+a^2)}{r^4}\sin^2\theta + O(r^{-3})\right] dtd\phi + \left[\frac{2mb(r^2+b^2)}{r^4}\cos^2\theta + O(r^{-3})\right] dtd\psi \\ & - \left[1 - \frac{m}{r^2} + O(r^{-3})\right] dt^2 + \left[1 + \frac{m}{2r^2} + O(r^{-3})\right] \times \left[\frac{r^2 + a^2\cos^2\theta + b^2\sin^2\theta}{(r^2+a^2)(r^2+b^2)} r^2 dr^2\right. \\ & \left. + (r^2 + a^2\cos^2\theta + b^2\sin^2\theta)d\theta^2 + (r^2+a^2)\sin^2\theta d\phi^2 + (r^2+b^2)\cos^2\theta d\psi^2\right]. \end{aligned} \tag{5}$$

Here the metric (5) admits two orthogonal planes of rotation $\theta = \pi/2$ and $\theta = 0$, which are specified by the azimuthal angles ϕ and ψ, respectively. The planes $\theta = 0$ and $\theta = \pi/2$ are invariant under the rotation with respect to the Killing vector fields ∂_ϕ and ∂_ψ, respectively. Both angles ϕ and ψ have period 2π. Comparing the asymptotic form (5) with the Weyl-Papapetrou form (1), we derive boundary conditions. Since the horizon has topology of S^3, let us introduce the spheroidal coordinates on Σ as

$$z = \lambda\mu, \quad \rho^2 = (\lambda^2 - c^2)(1 - \mu^2), \tag{6}$$

where $\mu = \cos 2\theta$. Then the relevant region is $\Sigma = \{(\lambda, \mu)|\lambda \geq c, -1 \leq \mu \leq 1\}$. The boundaries $\lambda = c$, $\lambda = +\infty$, $\mu = 1$ and $\mu = -1$ correspond to the horizon, the infinity, the ϕ-invariant plane and the ψ-invariant plane, respectively. In these coordinates, the boundary conditions for f_{IJ} and ω_I are summarized as follows:

	ϕ-invariant plane $\mu \to +1$	ψ-invariant plane $\mu \to -1$	horizon $\lambda \to c$	infinity $\lambda \to +\infty$
$\tilde{f}_{\phi\phi}$	$O(1)$	$O(1)$	$O(1)$	$2\lambda + (a^2 - b^2 + m)/2 + O(\lambda^{-1/2})$
$\tilde{f}_{\phi\psi}$	$O(1)$	$O(1)$	$O(1)$	$O(\lambda^{-1/2})$
$\tilde{f}_{\psi\psi}$	$O(1)$	$O(1)$	$O(1)$	$2\lambda + (b^2 - a^2 + m)/2 + O(\lambda^{-1/2})$
$\tilde{\omega}_\phi$	$O\left((1-\mu)^2\right)$	$O(1+\mu)$	$O(1)$	$O(\lambda^{-1/2})$
$\tilde{\omega}_\psi$	$O(1-\mu)$	$O\left((1+\mu)^2\right)$	$O(1)$	$O(\lambda^{-1/2})$

where

$$f_{\phi\phi} = \frac{(1-\mu)}{2}\tilde{f}_{\phi\phi}, \quad f_{\phi\psi} = \frac{(1-\mu)(1+\mu)}{4}\tilde{f}_{\phi\psi}, \quad f_{\psi\psi} = \frac{(1+\mu)}{2}\tilde{f}_{\psi\psi}, \tag{7}$$

$$\omega_\phi = -\frac{ma}{4}\mu(2-\mu) + \tilde{\omega}_\phi, \quad \omega_\psi = -\frac{mb}{4}\mu(2+\mu) + \tilde{\omega}_\psi. \tag{8}$$

Then, the boundary integral (4) vanishes. The difference matrix Ψ is constant and vanishes at the infinity, and then Ψ is zero over Σ. Thus, the two configurations $\Phi_{[0]}$ and $\Phi_{[1]}$ coincide with each other.

5 Summary

We show uniqueness of the asymptotically flat, black hole solution to the five-dimensional vacuum Einstein equation with the regular event horizon homeomorphic to S^3, admitting two commuting spacelike Killing vector fields and stationary Killing vector field. The solution of this system is determined by only three asymptotic charges, the mass $M = 3\pi m/8G$ and the two angular momenta $J_\phi = \pi ma/4G$ and $J_\psi = \pi mb/4G$. The five-dimensional Myers-Perry black hole solution is unique in this class.

References

[1] G. 't Hooft, Phys. Lett. B **198**, 61 (1987). T. Banks and W. Fischler, arXiv:hep-th/9906038. S. B. Giddings and S. Thomas, Phys. Rev. D **65**, 056010 (2002). S. Dimopoulos and G. Landsberg, Phys. Rev. Lett. **87**, 161602 (2001).

[2] R. C. Myers and M. J. Perry, Annals Phys. **172**, 304 (1986).

[3] B. Carter, "Mathematical Foundations of the Theory of Relativistic Stellar and Black Hole Configurations," in *Gravitation in Astrophysics*, edited by B. Carter and J. B. Hartle, (Plenum Press, New York, 1987). M. Heusler, *Black Hole Uniqueness Theorems*, (Cambridge University Press, New York, 1996).

[4] R. Emparan and H. S. Reall, Phys. Rev. Lett. **88**, 101101 (2002).

[5] H. S. Reall, Phys. Rev. D **68**, 024024 (2003).

[6] R. Emparan and R. C. Myers, JHEP **0309**, 025 (2003).

[7] R. Gregory and R. Laflamme, Phys. Rev. Lett. **70**, 2837 (1993).

[8] H. Elvang and R. Emparan, JHEP **0311**, 035 (2003).

[9] S. Hwang, Geometriae Dedicata **71**, 5 (1998). G. W. Gibbons, D. Ida and T. Shiromizu, Prog. Theor. Phys. Suppl. **148**, 284 (2003). G. W. Gibbons, D. Ida and T. Shiromizu, Phys. Rev. Lett. **89**, 041101 (2002). G. W. Gibbons, D. Ida and T. Shiromizu, Phys. Rev. D **66**, 044010 (2002). M. Rogatko, Class. Quant. Grav. **19**, L151 (2002). M. Rogatko, Phys. Rev. D **67**, 084025 (2003).

[10] H. Kodama and A. Ishibashi, Prog. Theor. Phys. **110**, 701 (2003). A. Ishibashi and H. Kodama, Prog. Theor. Phys. **110**, 901 (2003).

[11] In private communication with H. Kodama.

[12] B. Kol, arXiv:hep-th/0208056.

[13] B. Carter, Commun. Math. Phys. **17**, 233 (1970).

[14] D. Maison, Gen. Rel. Grav. **10**, 717 (1979).

[15] P. O. Mazur, Phys. Lett. A **100**, 341 (1984).

[16] Y. Morisawa and D. Ida, arXiv:gr-qc/0401100.

General framework of higher order gauge invariant perturbation theory

Kouji Nakamura[1]

Department of Astronomical Science, the Graduate University for Advanced Studies, Osawa, Mitaka, Tokyo 181-8588, Japan.

Abstract

Based on the gauge invariant variables proposed in [K. Nakamura, Prog. Theor. Phys. **110** (2003), 723.], general framework of the second order gauge invariant perturbation theory on arbitrary background spacetime is considered. We derived formulae of the perturbative Einstein tensor of each order, which have the similar form as the definitions of gauge invariant variables for arbitrary perturbative fields. As a result, each order Einstein equations necessarily given in terms of gauge invariant variables.

The perturbative approach is one of the popular techniques to investigate physical systems. In particular, this approach is powerful when the construction of exactly soluble models is difficult. In general relativity, there are many exact solutions to the Einstein equation[1] but these are often too idealized to properly represent natural phenomena. In this situation, the perturbations around appropriate exact solutions are useful to investigate realistic situations. Cosmological perturbation theory[2] is now the most commonly used technique, and perturbations of black holes and stars have been widely studied to obtain descriptions of the gravitational radiation emitted from them[3].

In general relativistic perturbations, *gauge freedom*, which is unphysical degree of freedom, arises due to general covariance. To obtain physically meaningful results, we have to fix these gauge freedom or to extract *gauge invariant part of perturbations*. These situations are also senn in the recent investigations of the oscillatory behavior of gravitating Nambu-Goto membrane[4, 5], which are concerning about the dynamical degree of freedom of gravitating extended objects. In these works, it was necessary to distinguish true dynamical degree of freedom from gauge freedom in perturbations and to develop a gauge invariant treatment of general relativistic perturbations.

In Ref.[5], we discussed comparison of the oscillatory behavior of a gravitating string with that of a test string. To do this, we have developed two-parameter general relativistic gauge invariant perturbation on the Minkowski spacetime, in which one of the parameter for the perturbation is the string energy density and the other is the string oscillation amplitude. Such multi-parameter perturbations have many other physical situations to be applied. The perturbation of spherical stars[7] is one of them, in which we choose the gravitational field of a spherical star as the background spacetime for the perturbations, one of the parameters for the perturbations corresponds to the rotation of the star and another is the pulsation amplitude of it. The effects due to the rotation-pulsation coupling is described in the higher order. Even in one-parameter perturbation, it is interest to consider higher order perturbations. In particular, Gleiser et.al[8] reported that the second order perturbations predict accurate wave form of gravitational waves. Thus, there are many physical situations to which higher order gauge invariant perturbations with multi-parameter should be applied, and it is worthwhile to discuss them from general point of view.

In this article, we show our treatments of two-parameter higher order gauge invarant perturbations. In our treatments, we do not specify the physical meanings of parameters for perturbation nor background spacetime, though it is necessary to specify both of them when we apply them to some physical situations.

Though the "general covariance" is mathematically formulated in the concept of spacetime manifolds, it intuitively states that there is no preferred coordinate system in nature. Due to this general covariance, "gauge freedom" in general relativistic perturbations arises. To explain this "gauge freedom", we must remind what we are doing in perturbation theories.

In any perturbation thoery, we always treat two spacetime: one is the physical spacetime $(\mathcal{M}, g_{ab})$ which should be described by perturbations; another is the background $(\mathcal{M}_0, {}^{(0)}g_{ab})$ which is prepared

[1] E-mail:kouchan@th.nao.ac.jp

for our calculations. Keeping these two mainfolds in our mind, we always write the equation

$$Q(\text{“}p\text{”}) = Q_0(p) + \delta Q(p). \tag{1}$$

where Q is any physical field on $\mathcal{M}$. In Eq. (1), we are implicitly assuming that there exists a a map $\mathcal{X} : \mathcal{M}_0 \to \mathcal{M} : p \in \mathcal{M}_0 \mapsto \text{“}p\text{”} \in \mathcal{M}$, which is usually called a "gauge choice" in perturbation theories[9]. Namely, $Q(\text{“}p\text{”})$ in Eq. (1) is a field on $\mathcal{M}$ and $\text{“}p\text{”} \in \mathcal{M}$. On the other hand, we should regard that the background value $Q_0(p)$ of $Q(\text{“}p\text{”})$ and its deviation $\delta Q(p)$ from $Q_0(p)$ in Eq. (1) are fields on $\mathcal{M}_0$ and $p \in \mathcal{M}_0$. Since Eq. (1) is for fields, it implicitly states that the point $\text{“}p\text{”} \in \mathcal{M}$ is the same as $p \in \mathcal{M}_0$.

Note that the gauge choice $\mathcal{X}$ is not unique when we consider theories in which general covariance is imposed and this degree of freedom of $\mathcal{X}$ is "gauge freedom" of perturbations. If there is a preferred coordinate system on both $\mathcal{M}_0$ and $\mathcal{M}$, we can choose $\mathcal{X}$ using this coordinate system. However, there is no such coordiante system due to general covariance and we have no guiding principle to choose $\mathcal{X}$.

Based on this understanding of "gauge", the gauge transformation is simply the change of the map $\mathcal{X}$. To see this, we only consider the one-parameter perturbation case, because the essence of discussion for multi-parameter perturbations is same[6, 10]. We denote the perturbation parameter by ϵ and we consider the $m+1$-dim manifold $\mathcal{N} = \mathcal{M} \times \mathbb{R}$, where $m = \dim \mathcal{M}$ and $\epsilon \in \mathbb{R}$. The backgournd $\mathcal{M}_0 = \mathcal{N}|_{\epsilon=0}$ and the physical spacetime $\mathcal{M} = \mathcal{N}|_{\mathbb{R}=\epsilon} =: \mathcal{M}_\epsilon$ are submanifolds embedded in $\mathcal{N}$. On this extended manifold $\mathcal{N}$, we consider an exponential map $\mathcal{X}_\epsilon$ which is a point identification map from $\mathcal{M}_0$ to $\mathcal{M}_\epsilon$. The map $\mathcal{X}_\epsilon$ is a gauge choice discussed above. We also consider another gauge choice $\mathcal{Y}_\epsilon$. The pull-back of each gauge choice maps any field Q_ϵ on $\mathcal{M}_\epsilon$ to ${}^{\mathcal{X}}Q_\epsilon := \mathcal{X}_\epsilon^* Q_\epsilon$ and ${}^{\mathcal{Y}}Q_\epsilon := \mathcal{Y}_\epsilon^* Q_\epsilon$ on $\mathcal{M}_0$, respectively.

The gauge transformation is induced by the map $\Phi_\epsilon = \mathcal{X}_\epsilon^{-1} \circ \mathcal{Y}_\epsilon$:

$${}^{\mathcal{Y}}Q_\epsilon = \mathcal{Y}_\epsilon^* Q|_{\mathcal{M}_0} = \left(\mathcal{Y}_\epsilon^* \mathcal{X}_{-\epsilon}^* \mathcal{X}_\epsilon^* Q\right)\big|_{\mathcal{M}_0} = \Phi_\epsilon^* \left(\mathcal{X}_\epsilon^* Q\right)|_{\mathcal{M}_0} = \Phi_\epsilon^* {}^{\mathcal{X}}Q_{\lambda,\epsilon}. \tag{2}$$

The substitution of expansions ${}^{\mathcal{X}}Q_\epsilon = Q_\epsilon + \epsilon \pounds_u Q_\epsilon + (\epsilon^2/2)\pounds_u^2 Q_\epsilon + O(\epsilon^3)$, ${}^{\mathcal{Y}}Q = Q_\epsilon + \epsilon \pounds_v Q_\epsilon + (\epsilon^2/2)\pounds_v^2 Q_\epsilon + O(\epsilon^3)$, and $Q = Q_0 + \epsilon Q_1 + (\epsilon^2/2)Q_2 + O(\epsilon^3)$ into Eq. (2) leads each order gauge transforamtion rules :

$${}^{\mathcal{Y}}Q_1 - {}^{\mathcal{X}}Q_1 = \pounds_{\xi_1} {}^{\mathcal{X}}Q_0, \quad {}^{\mathcal{Y}}Q_2 - {}^{\mathcal{X}}Q_2 = 2\pounds_{\xi_1} {}^{\mathcal{X}}Q_1 + \left(\pounds_{\xi_2} + \pounds_{\xi_1}^2\right) {}^{\mathcal{X}}Q_0, \tag{3}$$

where $\xi_1^a = u^a - v^a$, $\xi_2^a = [u, v]^a$, and u^a (v^a) is the generators of $\mathcal{X}_\epsilon$ ($\mathcal{Y}_\epsilon$).

The gauge transformation $\Phi_\epsilon = \mathcal{X}_\epsilon^{-1} \circ \mathcal{Y}_\epsilon$ induces the coordinate transformation on $\mathcal{M}_\epsilon$. A chart $(\mathcal{U}, X)$ on $\mathcal{M}_0$ with a gauge choice $\mathcal{X}_\epsilon$ becomes a chart $(\mathcal{X}_\epsilon \mathcal{U}, X \circ \mathcal{X}_\epsilon^{-1})$ on $\mathcal{M}_\epsilon$ ($\{x^\mu\}$). Another gauge choice $\mathcal{Y}_\epsilon$ induces another chart $(\mathcal{Y}\mathcal{U}, X \circ \mathcal{Y}^{-1})$ on $\mathcal{M}_\epsilon$ ($\{y^\mu\}$). In the passive point of view, we obtain

$$y^\mu(q) := x^\mu(p) = \left(\left(\Phi^{-1}\right)^* x^\mu\right)(q) = x^\mu(q) - \epsilon \xi_1^\mu(q) + \frac{\epsilon^2}{2}\left\{-\xi_2^\mu(q) + \xi_1^\nu(q)\partial_\nu \xi_1^\mu(q)\right\} + O(\epsilon^3). \tag{4}$$

This includes the additional degree of freedom ξ_2^μ and this does show that the gauge freedom in perturbations is more than the usual assignment of coordiante labels.

Similarly, the gauge transformation rules in two-parameter perturbations are given by

$${}^{\mathcal{X}}Q_{\epsilon,\lambda} := \mathcal{X}_{\epsilon,\lambda}^* Q_{\epsilon,\lambda} =: \sum_{k,k'=0}^{\infty} \frac{\lambda^k \epsilon^{k'}}{k!k'!}\, \delta_{\mathcal{X}}^{(k,k')} Q, \quad \delta_{\mathcal{X}}^{(0,0)} Q = Q_0, \tag{5}$$

$$\delta_{\mathcal{Y}}^{(p,q)} Q - \delta_{\mathcal{X}}^{(p,q)} Q = \pounds_{\xi_{(p,q)}} Q_0, \qquad (p,q) = (0,1), (1,0), \tag{6}$$

$$\delta_{\mathcal{Y}}^{(p,q)} Q - \delta_{\mathcal{X}}^{(p,q)} Q = 2\pounds_{\xi_{\left(\frac{p}{2},\frac{q}{2}\right)}} \delta_{\mathcal{X}}^{\left(\frac{p}{2},\frac{q}{2}\right)} Q + \left\{\pounds_{\xi_{(p,q)}} + \pounds^2_{\xi_{\left(\frac{p}{2},\frac{q}{2}\right)}}\right\} Q_0, \qquad (p,q) = (0,2), (2,0), \tag{7}$$

$$\begin{aligned} \delta_{\mathcal{Y}}^{(1,1)} Q - \delta_{\mathcal{X}}^{(1,1)} Q = {} & \pounds_{\xi_{(1,0)}} \delta_{\mathcal{X}}^{(0,1)} Q + \pounds_{\xi_{(0,1)}} \delta_{\mathcal{X}}^{(1,0)} Q \\ & + \left\{\pounds_{\xi_{(1,1)}} + \frac{1}{2}\pounds_{\xi_{(1,0)}} \pounds_{\xi_{(0,1)}} + \frac{1}{2}\pounds_{\xi_{(0,1)}} \pounds_{\xi_{(1,0)}}\right\} Q_0. \end{aligned} \tag{8}$$

Now, we define gauge invariant variables. Our starting point to construct gauge invariant variables is the assumption, which states that we have already known the procedure to find gauge invariant variables for the linear metric perturbations. Then, linear metric perturbations ${}^{(1,0)}h_{ab}$ (${}^{(0,1)}h_{ab}$) decomposed as

$${}^{(p,q)}h_{ab} =: {}^{(p,q)}\mathcal{H}_{ab} + 2\nabla_{(a}\, {}^{(p,q)}X_{b)}, \quad (p,q) = (1,0), (0,1), \tag{9}$$

where ${}^{(p,q)}\mathcal{H}_{ab}$ (${}^{(p,q)}X_a$) is gauge invariant (variant). (We omitted the index for the gauge choice $\mathcal{X}$.)

This assumption is non-trivial. However, once we accept this assumption, we can always find gauge invariant variables for higher order perturbations[6]. In the second order, the metric perturbations are decomposed as

$$
\begin{aligned}
{}^{(p,q)}h_{ab} &=: {}^{(p,q)}\mathcal{H}_{ab} + 2\mathcal{L}_{(\frac{p}{2},\frac{q}{2})_X}{}^{(\frac{p}{2},\frac{q}{2})}h_{ab} + \left(\mathcal{L}_{(p,q)X} - \mathcal{L}^2_{(\frac{p}{2},\frac{q}{2})_X}\right){}^{(0)}g_{ab}, \ (p,q)=(2,0),(0,2); \quad (10)\\
{}^{(1,1)}h_{ab} &=: {}^{(1,1)}\mathcal{H}_{ab} + \mathcal{L}_{(0,1)X}{}^{(1,0)}h_{ab} + \mathcal{L}_{(1,0)X}{}^{(0,1)}h_{ab}\\
&\quad + \left\{\mathcal{L}_{(1,1)X} - \frac{1}{2}\mathcal{L}_{(1,0)X}\mathcal{L}_{(0,1)X} - \frac{1}{2}\mathcal{L}_{(0,1)X}\mathcal{L}_{(1,0)X}\right\}{}^{(0)}g_{ab}, \quad (11)
\end{aligned}
$$

where ${}^{(p,q)}\mathcal{H}_{ab}$ (${}^{(p,q)}X_a$) is gauge invariant (variant).

Using gauge variant parts ${}^{(p,q)}X_a$ of metric perturbations, gauge invariant variables for an arbitrary field Q other than metric[6] are given by

$$
\begin{aligned}
\delta^{(p,q)}Q &:= \delta^{(p,q)}Q - \mathcal{L}_{(p,q)X}Q_0, && (p,q)=(1,0),(0,1), \quad (12)\\
\delta^{(p,q)}Q &:= \delta^{(p,q)}Q - 2\mathcal{L}_{(\frac{p}{2},\frac{q}{2})_X}\delta^{(\frac{p}{2},\frac{q}{2})}Q - \left\{\mathcal{L}_{(p,q)X} - \mathcal{L}^2_{(\frac{p}{2},\frac{q}{2})_X}\right\}Q_0, && (p,q)=(2,0),(0,2), \quad (13)\\
\delta^{(1,1)}Q &:= \delta^{(1,1)}Q - \mathcal{L}_{(1,0)X}\delta^{(0,1)}Q - \mathcal{L}_{(0,1)X}\delta^{(1,0)}Q\\
&\quad - \left\{\mathcal{L}_{(1,1)X} - \frac{1}{2}\mathcal{L}_{(1,0)X}\mathcal{L}_{(0,1)X} - \frac{1}{2}\mathcal{L}_{(0,1)X}\mathcal{L}_{(1,0)X}\right\}Q_0. \quad (14)
\end{aligned}
$$

Next, we show the expression of the perturbative Einstein equations of each order using these gauge invariant variables defined above. We consider the pull-back $\mathcal{X}^*_{\epsilon,\lambda}\tilde{G}_a{}^b$ on $\mathcal{M}_0$ of the Einstein tensor $\tilde{G}_a{}^b$ on $\mathcal{M}$ and expand $\mathcal{X}^*_{\epsilon,\lambda}\tilde{G}_a{}^b$ as Eq. (5). In terms of gauge invariant and variant variables of metric perturbations defined above, the perturbative Einstein tensors are given by

$$
\begin{aligned}
{}^{(p,q)}G_a{}^b &= {}^{(1)}\mathcal{G}_a{}^b\left[{}^{(p,q)}\mathcal{H}_c{}^d\right] + \mathcal{L}_{(p,q)X}\ G_a{}^b, \qquad \text{for} \quad (p,q)=(0,1),(1,0), \quad (15)\\
{}^{(1,1)}G_a{}^b &= {}^{(1)}\mathcal{G}_a{}^b\left[{}^{(1,1)}\mathcal{H}_c{}^d\right] + {}^{(2)}\mathcal{G}_a{}^b\left[{}^{(1,0)}\mathcal{H}_c{}^d, {}^{(0,1)}\mathcal{H}_c{}^d\right]\\
&\quad + \mathcal{L}_{(1,0)X}\ {}^{(0,1)}G_a{}^b + \mathcal{L}_{(0,1)X}\ {}^{(1,0)}G_a{}^b\\
&\quad + \left\{\mathcal{L}_{(1,1)X} - \frac{1}{2}\mathcal{L}_{(1,0)X}\mathcal{L}_{(0,1)X} - \frac{1}{2}\mathcal{L}_{(0,1)X}\mathcal{L}_{(1,0)X}\right\}G_a{}^b, \quad (16)\\
{}^{(p,q)}G_a{}^b &= {}^{(1)}\mathcal{G}_a{}^b\left[{}^{(p,q)}\mathcal{H}_c{}^d\right] + {}^{(2)}\mathcal{G}_a{}^b\left[{}^{(p,q)}\mathcal{H}_c{}^d, {}^{(p,q)}\mathcal{H}_c{}^d\right] + 2\mathcal{L}_{(\frac{p}{2},\frac{q}{2})X}\ {}^{(\frac{p}{2},\frac{q}{2})}G_a{}^b\\
&\quad + \left\{\mathcal{L}_{(p,q)X} - \mathcal{L}^2_{(\frac{p}{2},\frac{q}{2})X}\right\}G_a{}^b \qquad \text{for} \quad (p,q)=(0,2),(2,0), \quad (17)\\
{}^{(1)}\mathcal{G}_a{}^b\left[A_c{}^d\right] &:= -2\nabla_{[a}A_{d]}{}^{bd} - A^{cb}R_{ac} + \frac{1}{2}\delta_a{}^b\left(2\nabla_{[e}A_{d]}{}^{ed} + R_{ed}{}^{(p,q)}\mathcal{H}^{ed}\right), \quad (18)\\
{}^{(2)}\mathcal{G}_a{}^b\left[A_c{}^d, B_c{}^d\right] &:= 2R_{ad}B_c{}^{(b}A^{d)c} + 2A_{[a}{}^{de}B_{d]}{}^b{}_e + 2B_{[a}{}^{de}A_{d]}{}^b{}_e\\
&\quad + 2A_e{}^d\nabla_{[a}B_{d]}{}^{be} + 2B_e{}^d\nabla_{[a}A_{d]}{}^{be} + 2A_c{}^b\nabla_{[a}B_{d]}{}^{cd} + 2B_c{}^b\nabla_{[a}A_{d]}{}^{cd}\\
&\quad - \frac{1}{2}\delta_a{}^b\left(2R_{de}B_f{}^{(d}A^{e)f} + 2A_{[f}{}^{de}B_{d]}{}^f{}_e + 2B_{[f}{}^{de}A_{d]}{}^f{}_e + 2A_e{}^d\nabla_{[f}B_{d]}{}^{fe}\right.\\
&\quad \left. + 2B_e{}^d\nabla_{[f}A_{d]}{}^{fe} + 2A^{fe}\nabla_{[f}B_{d]e}{}^d + 2B^{fe}\nabla_{[f}A_{d]e}{}^d\right), \quad (19)
\end{aligned}
$$

where $A_{abc} := \nabla_{(a}A_{b)c} - (1/2)\nabla_c A_{ab}$ and B_{abc} and ${}^{(p,q)}\mathcal{H}_{abc}$ follows the same definitions, for example ${}^{(p,q)}\mathcal{H}_{abc} := \nabla_{(a}{}^{(p,q)}\mathcal{H}_{b)c} - (1/2)\nabla_c{}^{(p,q)}\mathcal{H}_{ab}$. We note that ${}^{(1)}\mathcal{G}_a{}^b[*]$ and ${}^{(2)}\mathcal{G}_a{}^b[*,*]$ are gauge invariant parts of the perturbative Einstien tensors and each expression (15)-(17) has the same form as Eqs. (12)-(14), respectively.

Similarily, to consider the Einstein equation, we expand the energy momentum tensor as Eq. (5) and we impose the perturbed Einstein equation of each order ${}^{(p,q)}G_a{}^b = 8\pi G\ {}^{(p,q)}T_a{}^b$. We defining the each

order gauge invariant variable ${}^{(p,q)}\mathcal{T}_a{}^b$ for the perturbative energy momentum tensor by Eqs. (12)-(14). Then, perturbative Einstein equation of each order is given by

$$8\pi G\ {}^{(p,q)}\mathcal{T}_a{}^b = {}^{(1)}\mathcal{G}_a{}^b\left[{}^{(p,q)}\mathcal{H}_c{}^d\right], \quad \text{for} \quad (p,q)=(0,1),(1,0), \tag{20}$$

$$8\pi G\ {}^{(1,1)}\mathcal{T}_a{}^b = {}^{(1)}\mathcal{G}_a{}^b\left[{}^{(1,1)}\mathcal{H}_c{}^d\right] + {}^{(2)}\mathcal{G}_a{}^b\left[{}^{(1,0)}\mathcal{H}_c{}^d, {}^{(0,1)}\mathcal{H}_c{}^d\right], \tag{21}$$

$$8\pi G\ {}^{(p,q)}\mathcal{T}_a{}^b = {}^{(1)}\mathcal{G}_a{}^b\left[{}^{(p,q)}\mathcal{H}_c{}^d\right] + {}^{(2)}\mathcal{G}_a{}^b\left[{}^{(p,q)}\mathcal{H}_c{}^d, {}^{(p,q)}\mathcal{H}_c{}^d\right], \quad \text{for} \quad (p,q)=(0,2),(2,0). \tag{22}$$

Thus, order by order Einstein equations are necessarily given in terms of gauge invariant variables only.

In summary, we showed the general framework of higher order gauge invariant perturbations of Einstein tensor. We have confirm two facts : First, *if the linear order gauge invariant perturbation theory is well established, its extensions to higher order and multi-parameter perturbation is straight forward.* Second, *Perturbative Einstein equations of each order are necessarily given in gauge invariant form.* The second result is trivial because any equation can be written in the form that the left hand side is equal to "zero" in any gauge, which is gauge invariant. Then the left hand side of this equation should be given in terms of gauge invariant variables. In this sence, the above second result is trivial. However, we have to note that this trivial result implies that our framework is mathematically correct at this level.

Further, we also note that in our framework, we do not specify anything about the background spacetime and physical meaning of the parameters for the perturbations. Our framework is based only on general covariance. Hence this framwork is applicable to any theory in which general covariance is imposed and it has very many applications. Though this framework is not complete, yet, we are planning to apply this to some physical problems. We leave these applications as our future works.

The author would like to thank to Prof. M. Omote (Keio Univ.) and Prof. S. Miyama (NAOJ) for their continuous encouragement.

References

[1] H. Stephani, D. Kramer, M. MacCallum, C. Hoenselaers and E. Herlt, *Exact solutions of Einstein's Field Equations*, (Second Edition, Cambridge: Cambridge University Press, 2003).

[2] J. M. Bardeen, Phys. Rev. D **22** (1980), 1882 ; H. Kodama and M. Sasaki, Prog. Theor. Phys. Suppl. No.78 (1984), 1 ; V. F. Mukhanov, H. A. Feildman, and R. H. Brandenberger, Phys. Rep. **215** (1992), 203.

[3] S. Chandrasekhar, *The mathematical theory of black holes* (Oxford: Clarendon Press, 1983) ; R. J. Gleiser, C. O. Nicasio, R. H. Price and J. Pullin, Phys. Rep. **325** (2000), 41 ; K. D. Kokkotas and B. G. Schmidt, Living Rev. Relativity **2** (1999), 2.

[4] K. Nakamura, A. Ishibashi and H. Ishihara, Phys. Rev. D**62** (2000), 101502(R); K. Nakamura and H. Ishihara, Phys. Rev. D **63** (2001), 127501; K. Nakamura, Class. Quant. Grav. **19** (2002), 783; K. Nakamura, Phys. Rev. D **66** (2002), 084005.

[5] K. Nakamura, Prog. Theor. Phys. **110**, (2003), 201.

[6] K. Nakamura, Prog. Theor. Phys. **110**, (2003), 723.

[7] Y. Kojima, Prog. Theor. Phys. Suppl. No.128 (1997), 251.

[8] R.J. Gleiser, C.O. Nicasio, R.H. Price, and J. Pullin, Phys. Rev. Lett. **77** (1996), 4483.

[9] J. M. Stewart and M. Walker, Proc. R. Soc. London A **341** (1974), 49.
J. M. Stewart, Class. Quantum Grav. **7** (1990), 1169.
J. M. Stewart, *Advanced General Relativity* (Cambridge University Press, Cambridge, 1991).

[10] M. Bruni, S. Matarrese, S. Mollerach and S. Sonego, Class. Quantum Grav. **14**, (1997), 2585; M. Brun and S. Sonego, Class. Quantum Grav. **16** (1999), L29; M. Bruni, L. Gualtieri, and C. F. Sopuerta, Class. Quantum Grav. **20**, (2003), 535; C.F. Sopuerta, M. Bruni, L. Gualtieri, arXiv:gr-qc/0306027.

Deci hertz Laser Interferometer can determine the position of the Coalescing Binary Neutron Stars within an arc minute a week before the final merging event to Black Hole

Takashi Nakamura[1], Ryuichi Takahashi[2]

Department of Physics, Kyoto University, Kyoto 606-8502, Japan

Abstract

It may be possible to construct a laser interferometer gravitational wave antenna in space with $h_{rms} \sim 10^{-23}$ at $f \sim 0.1$Hz in $\sim$ 2020. This deci hertz antenna may be called DECIGO/BBO, which stand for DECi hertz Interferometer Gravitational wave Observatory and Big Bang Observer, respectively. The analysis of 1-10 years observational data of the coalescing binary neutron stars or black holes at the distance of $\sim$ 300Mpc will give us the spatial position within $\sim$ an arc minute and the time of the coalescence within $\sim$ 0.1 sec beforehand. With the knowledge of the accurate position and the time of final merging event, the follow up simultaneous observation using high frequency ($f \sim$ 100Hz) gravitational wave antennae as well as electromagnetic wave antennae from the radio frequency to the ultra high energy gamma ray will reveal the physics in the enigmatic event of the coalescence and the formation of the black hole.

1 Introduction

There are at least four frequency bands where active or planned gravitational wave antennae exist. The resonant bars as well as ground laser interferometers such as TAMA300, LIGO I, VIRGO, and GEO600 are covering the frequency band of 10Hz–kHz while the timing analysis of pulsars is covering $\sim 10^{-8}$Hz band. Laser Interferometer Space Antenna (LISA) will cover $10^{-4} - 10^{-2}$Hz from $\sim$ 2010 [1]. Very recently the space antenna in the deci Hertz band ($10^{-2} - 10$ Hz) comes into the group. According to Seto, Kawamura and Nakamura (2001) [7] it might be possible to construct a laser interferometer gravitational wave antenna in space with $h_{rms} \sim 10^{-27}$ at $f \sim 0.1$Hz in this century. Using this antenna they show that 1) $\sim 10^5$ chirp signals of coalescing binary neutron stars per year may be detected with S/N $\sim 10^4$. 2) The time variation of the Hubble parameter of our universe may be determined for ten years observation of binary neutron stars at $z \sim 1$ so that we can directly measure the acceleration of the universe. 3) the stochastic gravitational wave which is predicted by the inflationary universe paradigm. may be detected.

Seto *et al.* (2001) [7] call the deci Hertz antenna DECIGO(DECi hertz Interferometer Gravitational wave Observatory) while recently in the NASA SEU 2003 Roadmap "Beyond Einstein" the deci Hertz antenna is called as BBO (Big Bang Observer) [3] to stress the detection of the stochastic gravitational waves from inflation. Since DECIGO and BBO are similar antennae, in this Letter we call the deci hertz antenna as DECIGO/BBO. In DECIGO, $h_{rms} \sim 10^{-27}$ around 0.1 Hz is the ultimate goal in the far future, assuming the quantum limit sensitivity for a 100 kg mass.

Let us consider more realistic parameters which might be achieved in $\sim$ 2020 such as 300W laser power, 3.5m mirrors, 5×10^4km arm length and 0.01 LISA acceleration noise, which will give $h_{rms} \sim 10^{-23}$ around 0.1 Hz [5]. In this sensitivity, S/N of the chirp signal from the coalescing binary neutron stars at $z \sim 1$ will be $\sim$ 1 while that of $10M_\odot$ black hole binary will be $\sim$ 10 so that we may directly measure the acceleration of the universe similar to the ultimate DECIGO.

One of the main targets of the ground laser interferometer gravitational wave antennae is the chirp signal from the coalescing binary neutron stars or black holes at the distance of 200 – 400Mpc with the

[1] E-mail:takashi@tap.scphys.kyoto-u.ac.jp
[2] E-mail:takahasi@tap.scphys.kyoto-u.ac.jp
[3] See http://universe.gsfc.nasa.gov/be/roadmap.html

expected event rate of $\sim$1 per year [6]. Since the event rate is $\sim$1 per year, the same binary is in the band of DECIGO/BBO, $1 \sim 10$ years before the ground laser interferometers and bar detectors detect the gravitational waves from the final merging event. This means that in practice we may observe the evolution of the coalescing binary from 10^{-2} Hz band to $\sim$kHz band. The duration in the band of the ground laser interferometer is three minutes or so while the duration in DECIGO/BBO band is $1-10$ years so that we may extract the information of the binary from the DECIGO/BBO band observation first. The point here is that we may know the accurate position and the distance to the binary beforehand so that we can prepare various detectors for the observation of the final merging phase, that is, we can point electro-magnetic antennae from radio to ultra high energy gamma rays and cosmic rays to the direction of the coalescing binary at the expected final merging time. We may also tune the gravitational wave antennae to various sensitivity bands to detect the characteristics of the merging event such as the frequency at the inner most stable circular orbit and the quasi-normal mode of the final black hole.

In this paper using the practical DECIGO/BBO in $\sim$ 2020 we show how accurately we can determine the spatial position and the distance to the coalescing binary neutron stars or black holes [8]. Since the angular resolution of LISA was calculated [2, 4, 9], we apply these methods to the case of DECIGO/BBO. We adopt the Hubble parameter $h \equiv H_0/100\text{km/s/ Mpc}=0.7$ and the units of $c = G = 1$.

2 Gravitational Waveform and Parameter Estimation

2.1 Sensitivity of DECIGO/BBO

DECIGO/BBO would consist of three spacecrafts separated by 5×10^4 km which is 1/100 times smaller than the size of LISA [1]. They would be spaced in an equilateral triangle and be orbiting around the Sun. The change of the detector's orientation and the position enables us to obtain the source position in the following two ways; (i) DECIGO/BBO's orientation rotates with a period of one-year, which imposes the modulation on the measured signal. (ii) DECIGO/BBO's orbital motion around the Sun imposes the periodic Doppler shift on the signal frequency. For the monochromatic signal of the frequency f, (i) the rotational modulation changes the frequency f to $f \pm 2/T$, where $T = 1$ yr ($2/T \sim 10^{-7}$ Hz), (ii) the Doppler modulation changes f to $f(1 \pm v)$, where $v \sim 10^{-4}$. Then for the frequency higher than $\sim 10^{-3}$ Hz like in DECIGO/BBO, the effect of the Doppler modulation is more important for the determination of the source position than the rotational modulation so that we only consider the former effect in the measured signal. The observed waveform h in the frequency domain $\tilde{h}_D(f)$ is given by,

$$\tilde{h}_D(f) = \tilde{h}(f)\, e^{i\phi_D(f)} \tag{1}$$

where $\tilde{h}(f)$ is the waveform at the solar system barycenter. $\phi_D(f)$ is the Doppler phase, which is the difference of the phase between the detector and the Sun; $\phi_D = 2\pi f R \sin\theta_S \cos(2\pi t/T - \phi_S)$, where $R = 1$ AU, $T = 1$ yr and (θ_S, ϕ_S) is the direction to the source. These angular coordinates are defined in a fixed barycenter frame of the solar system [2].

The strain sensitivity of DECIGO/BBO is about 1000 times better than that of LISA (i.e. $10^{-23}\,\text{Hz}^{-1/2}$ at $f = 0.1-1$ Hz), and the acceleration noise is 100 times lower than that of LISA (i.e. $3\times10^{-17}\text{m/s}^2/\text{Hz}^{1/2}$). Adopting these parameters, we show the sensitivity of DECIGO/BBO as compared with LISA and LIGO II in Fig.1 [5]. Note that we are using a smooth curve and neglecting the wavy behavior of the transfer function for simplicity.

2.2 Gravitational Waveform

We consider the equal mass neutron star and black hole binaries as sources of DECIGO/BBO. We only consider a circular orbit since the expected eccentricity is $\sim 10^{-3}$ for the neutron star binary. We use the restricted 1.5 post-Newtonian approximation as the in-spiral waveform [3] for simplicity. The waveform in the frequency domain is given by,

$$\tilde{h}(f) = \mathcal{A} f^{-7/6} e^{i\Psi(f)}, \tag{2}$$

where $\mathcal{A}$ is the amplitude and $\Psi(f)$ is the phase. They depend on six parameters; the red-shifted chirp mass $\mathcal{M}_z = (M_1 M_2)^{3/5}(M_1 + M_2)^{-1/5}(1 + z_S)$, the reduced mass $\mu_z = M_1 M_2 (1 + z_S)/(M_1 + M_2)$, the

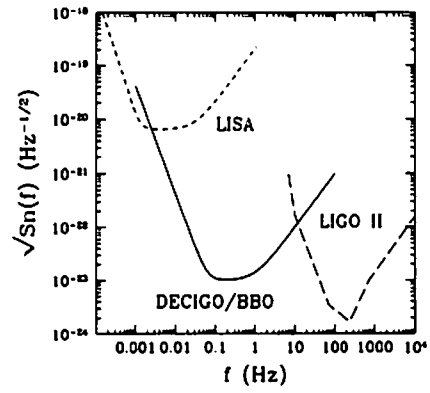

Figure 1: The strain sensitivity of DECIGO/BBO.

spin-orbit coupling constant β, the coalescence time t_c and the phase ϕ_c and the luminosity distance to the source D_S. The amplitude is given by $\mathcal{A} = K\sqrt{5/96}\,\mathcal{M}_z^{5/6}/(\pi^{2/3}D_S)$, where K is the constant determined by the inclination of the source, the relative orientation of the source and the detector. Since the average value of K is about unity [3], we assume $K = 1$ for the following calculation. The phase $\Psi(f)$ in Eq.(2) is a rather complicated function of $\mathcal{M}_z$, μ_z, β, ϕ_c and t_c which is given in Eq.(3.24) of Cutler & Flanagan (1994).

2.3 Parameter Estimation

The signal observed by DECIGO/BBO, $\tilde{h}_D(f)$, can be obtained inserting Eq.(2) to Eq.(1). The signal $\tilde{h}_D(f)$ is characterized by eight parameters ($\mathcal{M}_z$, μ_z, β, ϕ_c, t_c, D_S, θ_S, ϕ_S). In the matched filter analysis with the template, these parameters can be determined. We compute the errors in the estimation of these parameters using the Fisher matrix formalism [3]. The variance-covariance matrix of the parameter estimation error $\Delta\gamma_i$ is given by the inverse of the Fisher information matrix Γ_{ij} as $\langle\Delta\gamma_i\Delta\gamma_j\rangle = \left(\Gamma^{-1}\right)_{ij}$. The Fisher matrix becomes

$$\Gamma_{ij} = 4\mathrm{Re}\int \frac{df}{Sn(f)}\,\frac{\partial\tilde{h}_D^*(f)}{\partial\gamma_i}\,\frac{\partial\tilde{h}_D(f)}{\partial\gamma_j}, \tag{3}$$

where $Sn(f)$ is the noise spectrum. We regard $Sn(f)$ as the instrumental noise in Fig.1, neglecting the binary confusion noise since there are no or little confusion noise for $f \gtrsim 0.1$ Hz [?]. The signal to noise ratio (S/N) is given by

$$(S/N)^2 = 4\int \frac{df}{Sn(f)}\,\left|\tilde{h}_D(f)\right|^2. \tag{4}$$

We integrate the gravitational waveform in Eq.(3) and Eq.(4) from 1 or 10 yr before the final merging to the cut-off frequency f_{cut} when the binary separation becomes $r = 6(M_1 + M_2)$.

The initial frequency is given by $f_{init} = 0.23(\mathcal{M}_z/M_\odot)^{-5/8}(T_{obs}/1\mathrm{yr})^{-3/8}$Hz where $T_{obs} = 1$ or 10 yr, and the cut-off frequency is $f_{cut} = 4.4\times10^3[(M_{1z}+M_{2z})/M_\odot]^{-1}$Hz. The result does not depend on the value of $f_{\rm cut}$ so much, since $Sn(f)$ is large at $f_{\rm cut}$.

3 Results

We consider the neutron star binaries ($1.4M_\odot + 1.4M_\odot$) and the stellar mass BH binaries ($10M_\odot + 10M_\odot$) at $D_S = 200\mathrm{h}^{-1}$ Mpc and the intermediate mass BH binaries of mass ($10^2M_\odot + 10^2M_\odot$) as well as ($10^3M_\odot + 10^3M_\odot$) at $D_S = 3000\mathrm{h}^{-1}$ Mpc (Hubble distance) as the sources. Note here that we adopt $h = 0.7$. For each mass case we randomly distribute 10^4 binaries on the celestial sphere at D_S, and we show the probability distribution of the angular resolution for these sources.

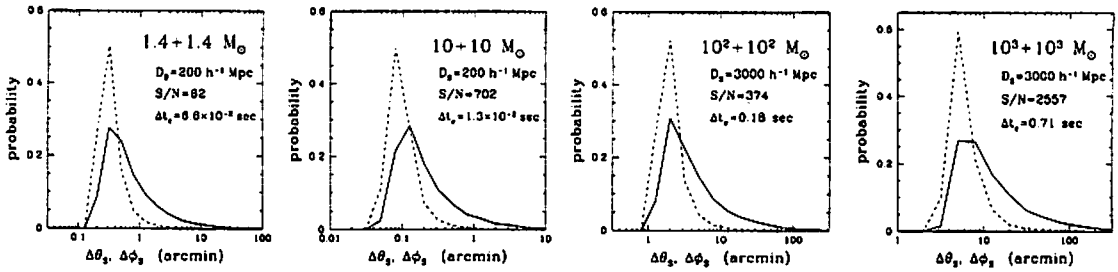

Figure 2: The relative probability distribution of the angular resolution of DECIGO/BBO in the case of 1 yr observation. For each mass case we randomly distribute 10^4 binaries on the celestial sphere at D_S (the Hubble parameter $h = 0.7$), and we show the probability distribution of the angular resolution for these sources. The solid lines and the dashed lines show $\Delta\theta_S$ and $\Delta\phi_S$, respectively. The signal to noise ratio S/N and the estimation error in the coalescence time Δt_c are also shown.

In Fig.2, we show the relative probability distribution of the angular resolution for the various binary masses $M_{1,2z} = 1.4M_\odot, 10^{1-3}M_\odot$ in the case of 1 yr observation. The solid lines and the dashed lines show $\Delta\theta_S$ and $\Delta\phi_S$, respectively. We also show the signal to noise ratio S/N and the estimation error in the coalescence time Δt_c assuming the template is accurate enough. S/N is independent of θ_S and ϕ_S since the phase factor $e^{i\phi_D(f)}$ becomes unity in Eq.(4) while Δt_c is found to depend on θ_S and ϕ_S very weakly. In general, the errors $(\Delta\theta_S, \Delta\phi_S, \Delta t_c)$ simply scale as $(S/N)^{-1}$. As shown in Fig.2, the angular resolutions are typically $\sim 0.1 - 10$ arc minutes for the neutron star binaries and the black hole binaries. This is about $10 - 1000$ times better than that of LISA (~ 1 deg). The Doppler modulation ($\phi_D \propto f$ in Eq.(1)) effect is larger than the rotational modulation for the high frequency band like DECIGO/BBO. It is shown that the angular resolution scales as $\propto f^{-1}(S/N)^{-1}$ for the monochromatic sources. Thus the angular resolution of DECIGO/BBO should be about 100 times better than that of LISA if the S/N is equal. This explains the accuracy of $\sim 0.1 - 10$ arc minute.

We comment the results for 10 yr observation. In this case, the angular resolution is $2-4$ times better than the case for 1 yr observation in Fig.2.

In conclusion DECIGO/BBO in ~ 2020 can determine the angular position of the neutron star binary and the black hole binary at ~ 300 Mpc within an arc minute before the final merging to the black hole. In a sense DECIGO/BBO will truly open gravitational wave astronomy since the positional accuracy is comparable to X-ray telescope on Beppo-SAX.

References

[1] Bender, P.L. *et al.* , 2000, LISA: A Cornerstone Mission for the Observation of Gravitational Waves, System and Technology Study Report ESA-SCI(2000) 11

[2] Cutler, C., 1998, Phys. Rev. D, 57, 7089

[3] Cutler, C. & Flanagan, E.F., 1994, Phys. Rev. D, 49, 2658

[4] Hughes, S. A., 2002, MNRAS, 331, 805

[5] Larson, S.L., Hiscock, W.A. and Hellings, R.W., 2000, Phys. Rev. D, 62, 062001

[6] Phinney, E.S., 1991, Astrophys. J. 380, L17

[7] Seto, N. ,Kawamura, S. & Nakamura, T., 2001, Phys. Rev. Lett., 87, 221103

[8] Takahashi, R. & Nakamura, T., 2003, Astrophys. J. 596, L231

[9] Vecchio, A., 2003, astro-ph/0304051

Effective Search Method for Gravitational Ringing of Black Holes

Hiroyuki Nakano[1(a)], Hirotaka Takahashi[2(b,c,d)], Hideyuki Tagoshi[3(c)], Misao Sasaki[4(d)]

[(a)] *Department of Mathematics and Physics, Graduate School of Science, Osaka City University, Osaka 558-8585, Japan*
[(b)] *Department of Physics, Graduate School of Science and Technology, Niigata University, Niigata 950-2181, Japan*
[(c)] *Department of Earth and Space Science, Graduate School of Science, Osaka University, Toyonaka, 560-0043, Japan*
[(d)] *Yukawa Institute for Theoretical Physics, Kyoto University, Kyoto 606-8502, Japan*

Abstract

We develop a search method for gravitational ringing of black holes. The detection of it will be a direct confirmation of the existence of a black hole. In this paper, we consider matched filtering and develop an optimal method to search for the ringdown waves that have damped sinusoidal waveforms. When we use the matched filtering method, the data analysis with a lot of templates required. It is necessary to keep the detection efficiency as high as possible under limited computational costs. First, we consider the white noise case for which the matched filtering can be studied analytically. We construct an efficient method for tiling the template space. Then, using a fitting curve of the TAMA300 DT7 noise spectrum, we numerically consider the case of colored noise. We find our tiling method developed for the white noise case is still valid even if the noise is colored.

1 Introduction

The gravitational wave detectors in the world; LIGO [1], GEO-600 [2] and TAMA300 [3], and bar detectors are currently in the early stage of their operations. Detection of gravitational waves provides us with not only a direct experimental test of general relativity but also a new window to observe our Universe. To use them as a new tool of observation, it is necessary to know theoretical waveforms. Once we know them, we may appeal to the matched filtering technique to extract source's information from gravitational wave signals. However, because the signals are expected to be very weak and the amount of data will be enormous for long-term continuous observations, it is essentially important to develop efficient data analysis methods.

For the ground-based and future space-based interferometers, the coalescences of compact object binaries are the most important sources of gravitational waves. The process of coalescence can be divided into three distinct phases. During an *inspiral* phase, the gravitational radiation reaction timescale is much longer than the orbital period. The gravitational waves from the inspiral carry the information of the masses and spins of the systems and so on. After the inspiral, compact object binaries encounter the dynamical instability and then would merge. This phase is called as a *merger* phase. The gravitational waves from the merger give us the information about the highly nonlinear dynamics of relativistic gravity. Finally, if a black hole is formed by merger, this system can be describe as oscillations of this final black hole's quasinormal modes and then settles down to a stationary Kerr state. The emitted gravitational waves in this *ringdown* phase carry the information about the mass and spin of the final black hole.

In this paper, we consider gravitational ringing of distorted spinning (Kerr) black holes. The ringdown waves are due to quasi-normal modes of black holes characterized by the central frequency f_c, usually called the (quasi-)normal-mode frequency, and the quality factor Q which is inversely proportional to the

[1]E-mail:denden@sci.osaka-cu.ac.jp
[2]E-mail:hirotaka@vega.ess.sci.osaka-u.ac.jp
[3]E-mail:tagoshi@vega.ess.sci.osaka-u.ac.jp
[4]E-mail:misao@yukawa.kyoto-u.ac.jp

imaginary part of the complex frequency. Here we consider a black hole characterized by its mass M and spin angular momentum J, and use the dimensionless spin parameter $a = J/M^2$ that takes a value in the range $[0, 1)$. Black hole perturbation calculations as well as numerical relativity simulations strongly suggest that the $\ell = m = 2$ least-damped (fundamental) mode is dominated. Hence, we focus on this mode. For this mode, analytical fitting formulas for (f_c, Q) and (M, a) were found by Echeverria [4] as

$$f_c \simeq 32\mathrm{kHz}\,[1 - 0.63(1-a)^{0.3}]\left(\frac{M}{M_\odot}\right)^{-1}, \quad Q \simeq 2.0(1-a)^{-0.45}. \tag{1}$$

The ringdown waveform is expressed as

$$h(f_c, Q, t_0, \phi_0; t) = \begin{cases} e^{-\pi f_c (t-t_0)/Q}\cos(2\pi f_c (t-t_0) - \phi_0) & \text{for } t \geq t_0\ , \\ 0 & \text{for } t < t_0\ , \end{cases} \tag{2}$$

where t_0 and ϕ_0 are the initial time and phase of the ringdown wave, respectively. Methods to search for the ringdown waves were discussed previously by several authors. Creighton [5] reported the results of analyzing data of the Caltech 40m by matched filtering, and emphasized the importance of coincidence event searches to discriminate spurious events from real events. But the search was limited to a single ringdown wave template. In order to treat ringdown waves with unknown parameters, we need to prepare a lot of theoretical templates. It is necessary to keep the loss of the signal to noise ratio (SNR) as small as possible under limited computational costs. So, we should consider an effective template spacing.

2 Template space

When we search ringdown waves in the detector's output, we have to prepare the theoretical template with the parameters (t_0, ϕ_0, f_c, Q). But we have already known the method to maximize the SNR over ϕ_0 [6] and t_0 [7]. So, we may consider the 2-dimensional parameter space, and space the theoretical templates effectively. By using the normalized signal having slightly different sets of the parameters, we can obtain the distance $ds^2_{(2)}$ between the two signals in terms of the metric in the template space,

$$\begin{aligned} ds^2_{(2)} &= \frac{2Q^4}{(2Q^2+1)f_c^2}df_c^2 + \frac{2Q^2(4Q^2+5)}{(4Q^2+1)^2(2Q^2+1)}dQ^2 \\ &\quad - \frac{2Q^3}{f_c(4Q^2+1)(2Q^2+1)}df_c\,dQ\,, \end{aligned} \tag{3}$$

where we assume the detector noise is white. It is noted that the cross term $df_c\,dQ$ arises here. In the following, we discuss a coordinate transformation in the template space that removes the cross term, in order to make our analysis of the template spacing and the error estimation easier. It is also noted that the smaller the volume element of the metric is the fewer the number of required filters is to cover the template space.

Next, let us perform the coordinate transformation by which the two dimensional metric (3) is transformed to a diagonal, conformally flat metric. Although the coordinate transformation involves complicated functions that may not be expressed in terms of elementary functions, we find it is sufficient to use their large Q expansion forms for $Q \geq 2$. Up to $O(1/Q^8)$ inclusive, we have

$$\begin{aligned} X &= \ln f_c + \ln 2 + \frac{1}{8}\frac{1}{Q^2} - \frac{1}{64}\frac{1}{Q^4} + \frac{1}{384}\frac{1}{Q^6} - \frac{1}{2048}\frac{1}{Q^8}\,, \\ Y &= \frac{1}{2}\frac{1}{Q} + \frac{1}{24}\frac{1}{Q^3} - \frac{3}{160}\frac{1}{Q^5} + \frac{1}{128}\frac{1}{Q^7} - \frac{17}{4608}\frac{1}{Q^9}\,. \end{aligned} \tag{4}$$

To the same accuracy, the inverse transformation becomes

$$\begin{aligned} F &= X - \ln 2 - \frac{1}{2}Y^2 + \frac{7}{12}Y^4 - \frac{67}{45}Y^6 + \frac{1769}{360}Y^8\,, \\ Q &= \frac{1}{2}\frac{1}{Y} + \frac{1}{6}Y - \frac{37}{90}Y^3 + \frac{166}{135}Y^5 - \frac{5917}{1350}Y^7\,. \end{aligned} \tag{5}$$

And then, we obtain

$$ds^2 = \Omega(Y)\left(dX^2 + dY^2\right), \tag{6}$$

where the conformal factor $\Omega(Y)$ is given by

$$\Omega(Y) = \frac{1}{4}\frac{1}{Y^2} - \frac{1}{3} + \frac{37}{60}Y^2 - \frac{85}{54}Y^4 + \frac{13069}{2700}Y^6. \tag{7}$$

When $Q = 2$, the errors induced by the above expansion are found to be $\sim 0.1\,\%$. This is accurate enough for our purpose as long as we allow the SNR loss, $ds^2_{\rm max}$, of a few percent.

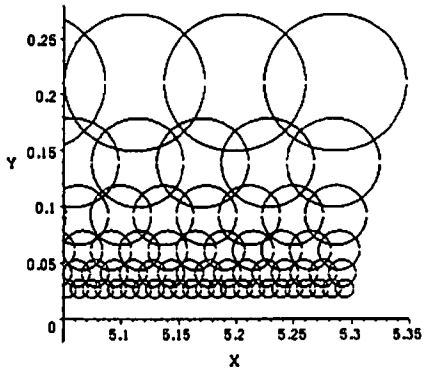

Figure 1: The (X, Y) template space.

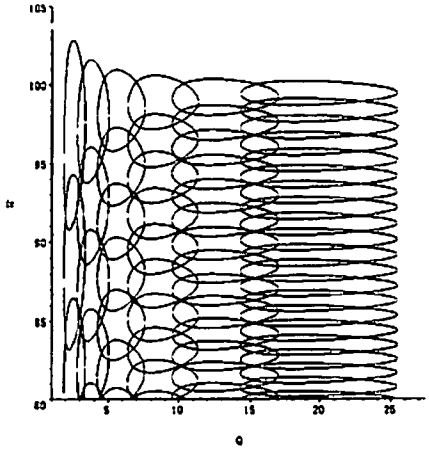

Figure 2: The (f_c, Q) template space.

We have derived the simple, conformally flat metric (6) for the template space. Here, using this metric, we formulate a tiling algorithm which is not only efficient but also quite simple. To develop such a method, we note the following. Because of the conformal flatness, the contour of the fixed maximum distance $ds^2 = ds^2_{\rm max}$ centered at a point on the (X, Y)-plane is a circle for sufficiently small $ds^2_{\rm max}$. Furthermore, along a line of Y =constant, $\Omega(Y)$ is constant. So, we can construct the efficient tiling method by the following procedure.

(A) Put the template points along the first Y =constant line by placing circles of the same radius which show the contour of the fixed maximum distance.

(B) Once the covering of the first line is done, cover the second line.

(C) Repeat until tiling the whole template space.

The detail tiling procedure have been shown in [8]. In Fig. 1, we show the tiling of the template space in the (X, Y) coordinates. Templates are taken at the centers of the circles. The tiling of the template space in the original coordinates (f_c, Q) with f_c measured in units of 100Hz is shown in Fig. 2. Note that the contour of $ds^2_{\rm max} = 0.02$ for each template is warped. When we consider the case of the parameter space (f_c, Q) which has the range, $10^2{\rm Hz} \le f_c \le 10^4{\rm Hz}$, $2 \le Q \le 20$, and the fixed maximum distance $ds^2_{\rm max} = 0.02$, the total number of templates is calculated to be $\mathcal{N} = 1148$ ($\mathcal{N} = 1780$ for $Q_{\rm max} = 34.3$).

3 Discussion

First, we discussed a tiling method assuming the detector noise is white. We found that the $1/Q$-expansion was useful in performing the coordinate transformation of the metric of the template space

because of $Q \geq 2$. We also find an efficient tiling method of the template space which can been formulated analytically[5]. The efficiency of the tiling method is found by the ratio between the sum of the areas of the equal match circles around the templates and the area to be covered. It is 1.57 which is much smaller than the value obtained before [10]. Next, we have discuss the validity of this tiling method in the case of colored noise spectrum. As a model of realistic noise power spectrum, we used the DT7 fitting curve of the noise power spectrum of TAMA300 during 2001 [11]. We prepare a template bank assuming the minimum match 98%. We then examined the loss of SNR of the signals detected in the template bank. We found that, in most case, we do not lose the signal-to-noise ratio no more than 2% which is expected from the pre-assigned minimum match. This shows that the tiling method can be used even in the case of colored noise spectrum.

The tiling method should be tested using the real data of laser interferometers. A study in this direction using the data of TAMA300 is now progressing [12]. In the analysis using real interferometers' data, we have to treat the non-stationary, non-Gaussian noise. It is found [13] that we observe even more fake events than in the case of inspiraling wave, since the ringing wave is usually much shorter than the inspiral waves and can easily be affected by short bursts. In this situation, we would need to introduce some methods to remove such fake events without losing real ringing gravitational wave signals. Coincidence analysis between several detectors would also be needed to reduce the fake event rate. Further, since the ringing waves may be excited by the detector itself, we may need to perform coincidence analysis to reject such spurious events anyway. We will also work on this problem in the future.

Acknowledgments

We would like to thank N. Kanda and Y. Tsunesada for useful discussions and comments. HN is supported by Research Fellowships of the Japan Society for the Promotion of Science for Young Scientists, No. 5919. This work is supported in part by Monbukagaku-sho Grant-in-Aid for Scientific Research No. 14047214 and 12640269.

References

[1] LIGO web page: http://www.ligo.caltech.edu/

[2] GEO600 web page: http://www.geo600.uni-hannover.de/

[3] TAMA300 web page: http://tamago.mtk.nao.ac.jp/

[4] F. Echeverria, Phys. Rev. D **40**, 3194 (1989).

[5] J. D. E. Creighton, Phys. Rev. D **60**, 022001 (1999).

[6] S. D. Mohanty, Phys. Rev. D **57**, 630 (1998).

[7] B. J. Owen, Phys. Rev. D **53**, 6749 (1996).

[8] H. Nakano et al., Phys. Rev. D **68**, 102003 (2003).

[9] H. Nakano et al., in preparation.

[10] N. Arnaud et al., Phys. Rev. D **67**, 102003 (2003).

[11] K. Tsubono eds., "*TAMA Report 2002 (2nd. ed.)*" in Japanese.

[12] Y. Tsunesada et al., in preparation.

[13] Y. Tsunesada and N. Kanda, unpublished work in progress.

[5]There is some improvement of the template space for the initial phase. Investigations in this direction is in progress [9].

Decaying Cold Dark Matter and the High Redshift Cluster Abundance

Masamune Oguri[1], Keitaro Takahashi[2], Kei Kotake[3],

Department of Physics, Graduate School of Science, University of Tokyo, Tokyo 113-0022, Japan

Kiyotomo Ichiki[4], Hiroshi Ohno[5]

Division of Theoretical Astrophysics, National Astronomical Observatory, 2-21-1 Osawa, Mitaka, Tokyo 181-8588, Japan

Abstract

The cluster abundance and its redshift evolution are known to be a powerful tool to constrain the amplitude of mass fluctuations σ_8 and the mass density parameter Ω_{m0}. Recent extensive observations of clusters reveal that the cluster abundance at local and high-redshift universe cannot be explained simultaneously if we assume the mass density parameter $\Omega_{m0} \sim 0.27$ which is obtained from the anisotropy of cosmic microwave background and Type Ia supernovae. We propose that this conflict can be resolved if cold dark matter particles decay into relativistic particles. On the basis of spherical model in decaying cold dark matter universe, we calculate the mass function of clusters and compare it with observed cluster abundance. We find that the lifetime of dark matter particles comparable to the age of the universe lowers the ratio of the local cluster abundance to the high-redshift cluster abundance and can account for the observed evolution of the cluster abundance quite well. The strong dependence of the cluster abundance on the decay rate of dark matter suggests that distant cluster surveys may offer clues to the nature of dark matter. We also investigate how well we can determine the decay rate from Sunyaev-Zel'dovich power spectrum. We find the finite lifetime of dark matter decreases the power at large scale ($l < 4000$) and increases at small scale ($l > 4000$). This is in marked contrast with the dependence of other cosmological parameters such as the amplitude of mass fluctuations σ_8 and the cosmological constant Ω_{m0} which mainly change the normalization of the angular power spectrum. This difference allows one to determine the lifetime and other cosmological parameters rather separately.

1 Introduction

The abundance of cluster of galaxies places a strong constraint on fundamental cosmological parameters such as the amplitude of mass fluctuations on a scale of $8h^{-1}$Mpc, σ_8, and the present mass density parameter, Ω_{m0} [1]. Although the abundance of clusters is strong function of both Ω_{m0} and σ_8, the evolution of the cluster abundance with redshift breaks the degeneracy between Ω_{m0} and σ_8. For instance, [2] pointed out that the relatively high abundance of massive cluster at $z > 0.5$ prefers large mass fluctuations $\sigma_8 = 0.9 - 1$. On the other hand, the local cluster abundance in both optical [3] and X-ray [4] wavebands suggests low mass fluctuations $\sigma_8 = 0.7 - 0.8$ for $\Omega_{m0} \sim 0.3$. The combination of local and high-z cluster abundances yields relatively low matter density in the universe, e.g., $\Omega_{m0} \sim 0.17$ [2]. However, such a low-matter universe conflicts with the results of other observations, $\Omega_{m0} \sim 0.27$, obtained from the anisotropy of cosmic microwave background and Type Ia supernovae. This conflict may be interpreted that underlying models are wrong.

[1] E-mail:oguri@utap.phys.s.u-tokyo.ac.jp
[2] E-mail:ktaro@utap.phys.s.u-tokyo.ac.jp
[3] E-mail:kkotake@utap.phys.s.u-tokyo.ac.jp
[4] E-mail:kiyotomo.ichiki@nao.ac.jp
[5] E-mail:ohno@th.nao.ac.jp

As a possible solution of this discrepancy, we propose decaying cold dark matter scenario in which cold dark matter particles decay into relativistic particles with a decay rate Γ [5]. The decaying cold dark matter model has been studied so far in different contexts, e.g., to reconcile Einstein-de Sitter universe with current low matter universe or to reduce possible over-concentration of dark matter and over-abundance of substructures in cold dark matter model. The cold dark matter with similar property, disappearing dark matter, has been also proposed in the context of the brane world scenario.

We also investigate how well we can determine the decay rate from Sunyaev-Zel'dovich power spectrum [6]. Our finding is that decay of dark matter particles changes the shape of angular power spectrum; thus we will be able to determine decay rate rather separately from other cosmological parameters such as Ω_{m0} and σ_8 which mainly change normalization of angular power spectrum.

2 Mass Function of Dark Halos in Decaying Cold Dark Matter Model

2.1 Cosmology

We assume that dark matter particles decay into relativistic particles and that the radiation component consists only of the decay product of the dark matter. Then rate equations of matter and radiation components are,

$$\dot{\rho}_m + 3H\rho_m = -\Gamma\rho_m, \tag{1}$$

$$\dot{\rho}_r + 4H\rho_r = \Gamma\rho_m, \tag{2}$$

where ρ_m and ρ_r are energy density of matter and radiation, respectively, dot denotes time derivative, and Γ is the decay width of the dark matter. From these equations, we obtain the evolution of the matter and radiation energy density as,

$$\rho_m = \rho_{m0}a^{-3}e^{-\Gamma t}, \tag{3}$$

$$\rho_r = \Gamma\rho_{m0}a^{-4}\int_0^t ae^{-\Gamma t}dt, \tag{4}$$

from which Friedmann equation is obtained as,

$$\frac{H^2(a)}{H_0^2} = \Omega_{m0}a^{-3}e^{-\Gamma(t-t_0)} + \Gamma\Omega_{m0}a^{-4}\int_0^t ae^{-\Gamma(t-t_0)}dt + \Omega_\lambda. \tag{5}$$

Here Ω_{m0} and Ω_λ are the current density parameters of the dark matter and dark energy, respectively. Combining this equation and the definition of the cosmological time,

$$t = \int_0^a \frac{da}{aH(a)}, \tag{6}$$

we obtain the following equation:

$$t'' = -\frac{1}{2}\left(\frac{\Omega_{m0}e^{-\Gamma(t-t_0)}}{a^2} + 4a\Omega_\lambda\right)t'^3 + \frac{t'}{a}, \tag{7}$$

where prime denotes derivative with respect to the scale factor a. It should be noted that the Friedmann equation at $z = 0$ reduces to,

$$1 = \Omega_{m0} + \Gamma\Omega_{m0}\int_0^{t_0} ae^{-\Gamma(t-t_0)}dt + \Omega_\lambda. \tag{8}$$

Thus, the current density parameter Ω_{m0} is uniquely determined by Γ and Ω_λ.

2.2 Mass function

We calculated mass function on the basis of the Press-Schechter theory [7]. We first consider motion of a spherical overdensity with radius R and initial mass M. The equation of motion of the spherical shell is given by,

$$\frac{\ddot{R}}{R} = -\frac{GM}{R^3}e^{-\Gamma t} - H_0^2\Gamma\Omega_{m0}a^{-4}\int_0^t ae^{-\Gamma(t-t_0)}dt + H_0^2\Omega_\lambda. \tag{9}$$

From equations (7) and (9), we can calculate the nonlinear overdensity Δ_c and the extrapolation of the linear fluctuation δ_c at virialization, although we used $\delta_c = 1.58$ for simplicity. It can be interpreted that a region has already been virialized at z if the linearly extrapolated density contrast $\delta_{\rm linear}(M_i, z)$, which is smoothed over the region containing mass M_i, exceeds the critical value δ_c. The evolution of the linear density contrast is determined by,

$$\dot{a}^2\delta'' + \left(\ddot{a} + 2\frac{\dot{a}^2}{a}\right)\delta' - 4\pi G\bar{\rho}_m\delta = 0. \tag{10}$$

If the initial density field is random Gaussian, probability distribution function of the density contrast is given by,

$$P\left[\delta(M_i, z_i)\right] = \frac{1}{(2\pi)^{1/2}\sigma_{M_i}(z_i)}\exp\left[-\frac{\delta^2(M_i, z_i)}{2\sigma^2_{M_i}(z_i)}\right], \tag{11}$$

where $\sigma_{M_i}(z_i)$ is the mass variance. We assume the mass variance for the cold dark matter fluctuation spectrum with the primordial spectral index $n = 1$. Consequently, the probability that the region with mass M has already been virialized is obtained as,

$$f(M, t) = \frac{1}{2}\mathrm{erfc}\left(\frac{\delta_c(z)}{\sqrt{2}\sigma_{M_i}}\right), \tag{12}$$

where $\mathrm{erfc}(x)$ is the complementary error function, $\sigma_{M_i} \equiv \sigma_{M_i}(z = 0)$, and $\delta_c(z) = \delta_c D(z = 0)/D(z)$. Here $D(z)$ is linear growth rate, which can be calculated from equation (10). From this equation, we finally obtain the comoving number density of halos of mass M at redshift z,

$$\begin{aligned}\frac{dn_{\rm PS}}{dM}(M, z) &= e^{2\Gamma t}\sqrt{\frac{2}{\pi}}\frac{\rho_0}{M_i}\frac{\delta_c(z)}{\sigma^2_{M_i}}\left|\frac{d\sigma_{M_i}}{dM_i}\right| \\ &\quad \times \exp\left[-\frac{\delta_c^2(z)}{2\sigma^2_{M_i}}\right]\Bigg|_{M_i = Me^{\Gamma t}},\end{aligned} \tag{13}$$

where $\rho_0 = \rho_{\rm crit}(z = 0)\Omega_{m0}e^{-\Gamma(t-t_0)}$.

3 Evolution of Cluster Abundance

We calculate the redshift evolution of massive clusters, which is shown in Figure 1. As clearly seen, Decay of dark matter particles lowers the ratio of the local cluster abundance to the high-redshift cluster abundance. Since the observed cluster evolution seems to be slow, decaying cold dark matter does explain the observation better.

4 Sunyaev-Zel'dovich Power Spectrum

We also compute the angular power spectrum of Sunyaev-Zel'dovich effect, following [9]. They derived a analytic prediction for the angular power spectrum using the universal gas-density and temperature profile which were developed in [8]. We have found that the finite lifetime of dark matter decreases the power at large scale ($l < 4000$) and increases at small scale ($l > 4000$). This unique feature will allow us to probe the lifetime of dark matter, rather independently with σ_8 and $\Omega_{\rm m}$ which mainly change the normalization of the angular power spectrum.

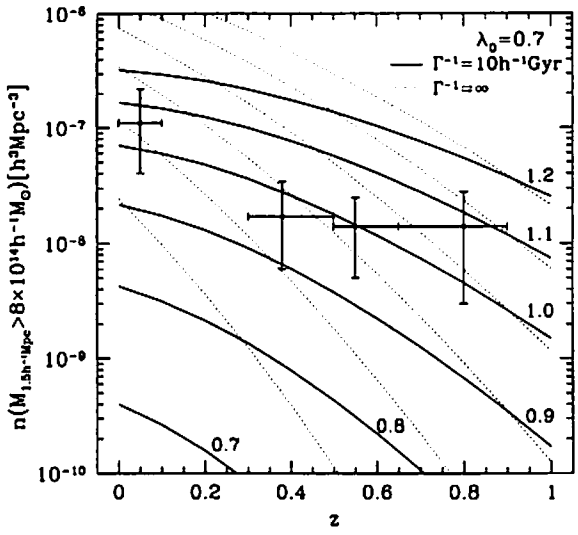

Figure 1: Evolution of the cluster abundance for $\lambda_0 = 0.7$. The number of clusters with mass $M_{1.5h^{-1}\mathrm{Mpc}} > 8 \times 10^{14} h^{-1} M_\odot$, where $M_{1.5h^{-1}\mathrm{Mpc}}$ is the mass within a comoving radius of $1.5h^{-1}$Mpc, is plotted as a function of redshift. The filled circles with errorbars are observed abundance (see text for details). Solid lines are predicted cluster abundance with lifetime of dark matter $\Gamma^{-1} = 10h^{-1}$Gyr, while we assume no decay for the dotted lines. We plot curves with $\sigma_8 = 0.7$, 0.8, 0.9, 1.0, 1.1, and 1.2 (only solid lines are labeled).

References

[1] Kitayama, T., & Suto, Y. 1997, ApJ, **490**, 557

[2] Bahcall, N. A., & Bode, P. 2003, ApJ, **588**, L1

[3] Bahcall, N. A., et al. 2003, ApJ, **585**, 182

[4] Ikebe, Y., Reiprich, T. H., Böhringer, H., Tanaka, Y., & Kitayama, T. 2002, A&A, **383**, 773

[5] Oguri, M., Takahashi, K., Ohno, H., & Kotake, K. 2003, ApJ, **597**, 645

[6] Takahashi, K., Oguri, M., & Ichiki, K. 2004, astro-ph/0312358

[7] Press, W. H., & Schechter, P. 1974, ApJ, **187**, 425

[8] Komatsu, E., & Seljak, U. 2001, MNRAS, **327**, 1353

[9] Komatsu, E., & Seljak, U. 2002, MNRAS, **336**, 1256

Deformed Schwarzschild anti-de Sitter black hole

Tohru Ohba[1], Hirotaka Yoshino[2], and Akira Tomimatsu[3]

Department of Physics, Graduate School of Science,
Nagoya University, Chikusa, Nagoya 464-8602, Japan

Abstract

We study deformed Schwarzschild-anti-de Sitter black hole. We consider static, axisymmetric perturbation from the black hole to second order. The perturbative solutions don't diverge at spatial infinity even if imposing regularity at the event-horizon. The metric is asymptotically weakly AdS spacetimes. We construct the first law of the deformed black hole and discuss the black hole mechanics.

1 Introduction

In the 1990s, new static black-hole solutions with black-hole event horizons of nonspherical spatial topology in spacetimes with a negative cosmological constant were discovered [1, 2, 3, 4] in addition to the well known spherically symmetric black hole (Schwarzschild-anti-de Sitter black hole). In four dimensions, there are the planar [1], the cylindrical [2], so-called toruslike black hole (with the topology $R^2 \times S^1 \times S^1$) [3] and the black holes which have horizon with genus $g > 1$ topology [4].

The existence of the cylindrical and the planar black hole with the horizon of nonspherical spatial topology suggests that there are unknown black holes (deformed black holes) with the horizon of nonspherical geometry. In this paper, as a first step, we consider static, axisymmetric perturbation from a Schwarzschild anti-de Sitter black hole to study the deformed black hole. In asymptotically flat spacetimes, the perturbative solutions diverge at infinity when imposing regularity at the horizon [5]. In spacetimes with a negative cosmological constant, however, we can construct the regular static solutions which converge at infinity even if imposing regularity at the horizon. The metric is not asymptotically AdS spacetimes but asymptotically weakly AdS spacetimes which is defined by Ashtekar and Magnon [6].

Recently, it is proved that the Schwarzschild-anti-de Sitter black hole is a unique solution in asymptotically anti- de Sitter (AdS) vacuum spacetimes [7]. Assuming certain asymptotic conditions, there is a general theorem on the non-existence of static regular black holes [8]. But the deformed black hole solution isn't contradictory to these theorems, because spacelike infinity is also deformed.

We construct the first law of the deformed black hole and discuss the black hole mechanics. The first law of the Schwarzschild-anti-de Sitter black hole can be written as [9]

$$\delta m = \frac{\kappa}{8\pi}\delta A, \tag{1}$$

where κ is the surface gravity, m is the mass, and A is the horizon area of a Schwarzschild-anti-de Sitter black hole. We evaluate the variation of the mass and the horizon area by the deformation of a Schwarzschild-anti-de Sitter black hole to derive the first law of the deformed black hole. We must consider second-order perturbation ($l = 0$) to evaluate the mass and the horizon area because first-order perturbation doesn't change the mass and the horizon area. We use Ashtekar and Magnon's definition [6] for the calculation of the mass.

We find that the first law of the deformed black hole has the following negative work term δW_d as

$$\delta m_d = \frac{\kappa}{8\pi}\delta A_d + \delta W_d, \tag{2}$$

where m_d is the mass and A_d is the horizon area of the deformed black hole.

[1]E-mail:tohba@allegro.phys.nagoya-u.ac.jp
[2]E-mail:hyoshino@allegro.phys.nagoya-u.ac.jp
[3]E-mail:atomi@allegro.phys.nagoya-u.ac.jp

2 Static, axisymmetric perturbation

We consider static, axisymmetric perturbation from a Schwarzschild anti-de Sitter black hole to second order. In the first order perturbation, each function can be written as a product of the radial part and the angular part which is spherical harmonics Y_{lm}, since the background is the spherically symmetric. We take $m = 0$ because the perturbation is axisymmetric. The first order perturbation ($l \geq 2$) deforms a Schwarzschild-anti-de Sitter black hole without changing the mass and the horizon area.

The second order of the Einstein equations has two kinds of terms. There are linear terms of second order quantities and quadratic terms of first order quantities. It is clear that the former terms occur in precisely the same form as the first order equations. Therefore, the second order perturbation ($l = 0$) has the source term that is quadratic in terms of the first order perturbations ($l \geq 2$). It causes the change of the mass and the horizon area by the deformation of the Schwarzschild-anti-de Sitter black hole.

In terms of the usual Schwartzschild-like coordinates t, r, θ, ϕ, and Regge-Wheeler gauge [5] in first order perturbation, we write the perturbation of the black hole metric in the form,

$$g_{tt} = -\left(1 - \frac{2m}{r} - \frac{1}{3}\Lambda r^2\right) \exp\left(-\epsilon H^{(1)} P_l(\theta) - \epsilon^2 \sum_{n=0}^{2l} H_{0n}^{(2)} P_n(\theta)\right), \tag{3}$$

$$g_{rr} = \left(1 - \frac{2m}{r} - \frac{1}{3}\Lambda r^2\right)^{-1} \exp\left(\epsilon H^{(1)} P_l(\theta) + \epsilon^2 \sum_{n=0}^{2l} H_{2n}^{(2)} P_n(\theta)\right), \tag{4}$$

$$g_{\theta\theta} = \sin^{-2}\theta g_{\phi\phi} = r^2 \exp\left(\epsilon K^{(1)} P_l(\theta) + \epsilon^2 \sum_{n=0}^{2l} K_n^{(2)} P_l(\theta)\right), \tag{5}$$

where the functions $H^{(1)}$, $H_{0n}^{(2)}$, $H_{2n}^{(2)}$, $K^{(1)}$, $K_n^{(2)}$ depend only on r and ϵ is the deformation parameter.

Because there is the freedom to choose coordinates in second order perturbation ($l = 0$), we can impose

$$H_{00}^{(2)} = H_{20}^{(2)} \equiv H^{(2)}(l = 0). \tag{6}$$

We derive the following differential equation of $H^{(1)}$ from the Einstein equations,

$$M'' - \frac{f'}{f} M' + \frac{3}{f}\left[2\Lambda r^2 + (l+2)(l-1)\right] M = 0, \tag{7}$$

where $M = f H^{(1)}$, $f = r\left(\Lambda r^3 - 3r + 6m\right)$. $K^{(1)}$ is written in terms of $H^{(1)}$,

$$K^{(1)} = -\frac{2}{3(l+2)(l-1)}\left[\left(\Lambda r^3 - 3m\right) H^{(1)\prime} + \frac{\Lambda^2 r^6 + 3\Lambda r^4 - 24 m\Lambda r^3 + 18 m r - 18 m^2}{f} H^{(1)}\right] + H^{(1)}. \tag{8}$$

We impose regularity of $H^{(1)}$ at the horizon,

$$H^{(1)} = A_1 (r - r_h) + A_2 (r - r_h)^2 + \cdots, \tag{9}$$

where r_h is the radius of the horizon. From Eq. (7), $H^{(1)}$ behaves like

$$H^{(1)} = \frac{a_1}{r} + \frac{a_2}{r^2} + \cdots, \tag{10}$$

at spatial infinity. Therefore, we can construct $H^{(1)}$ which goes to zero at spatial infinity when imposing regularity at the horizon. From Eq. (8) and Eq. (9), $K^{(1)}$ behaves like

$$K^{(1)} = \frac{2 r_h \left(1 - \Lambda r_h^2\right)}{(l+2)(l-1)} A_1 + \left[A_1 + \frac{3 r_h \left(1 - \Lambda r_h^2\right)}{(l+2)(l-1)} A_2\right](r - r_h) + \cdots, \tag{11}$$

near the horizon. From Eq. (8) and Eq. (10), we find that the behavior of $K^{(1)}$ becomes

$$K^{(1)} = \frac{2\Lambda a_2}{3(l+2)(l-1)} - \frac{a_1}{r} + \cdots, \tag{12}$$

for large r. Hence, $K^{(1)}$ is finite from the horizon and spatial infinity. Because $K^{(1)}$ isn't zero at infinity, this spacetime is asymptotically weakly AdS in the sense of Ashtekar and Magnon's definition.

3 Approximate calculation

In this section, we obtain the perturbative solution and evaluate the mass and the horizon area to find the first law of the deformed black hole in the cases of $m\sqrt{-\Lambda} = \alpha \gg 1$ and $\alpha \ll 1$.

Abbott-Deser mass [10] isn't well-defined in second order perturbation because its value diverges by a coordinate transformation $r = R + a\epsilon$. But Ashtekar-Magnon mass [6] is well-defined because its value doesn't change by coordinate transformations. Hence, we evaluate the mass using Ashtekar-Magnon mass.

In the case of $\alpha \gg 1$, the solution of Eq. (7) and Eq. (8) is

$$H^{(1)} = -\frac{(6\alpha)^{-2/3}}{x} + \frac{3(6\alpha)^{-2/3}x}{x^2+x+1}, \tag{13}$$

$$K^{(1)} = -\frac{2}{(l+2)(l-1)} + \mathcal{O}\left(\alpha^{-2/3}\right). \tag{14}$$

where $x = r/r_h$. We find the change in the mass and the horizon area by the deformation of the Schwarzschild-anti-de Sitter black hole as

$$\frac{\delta m_d}{m} \simeq \frac{12\epsilon^2}{(2l+1)(l+2)^2(l-1)^2}, \tag{15}$$

$$\frac{\delta A_d}{A} \simeq \frac{8\epsilon^2}{(2l+1)(l+2)^2(l-1)^2}. \tag{16}$$

Therefore, the first law of the deformed black hole becomes

$$\delta m_d = \frac{\kappa}{8\pi}\delta A_d, \tag{17}$$

where $\kappa = (6\alpha)^{4/3}/12m$. The first law of the deformed black hole is approximately equal to that of a Schwarzschild-anti-de Sitter black hole.

Now we consider the case of $\alpha \ll 1$. The (t,t) component of the background metric is

$$g_{tt}^{(0)} = -\left(1 - \frac{1}{y} + \frac{4}{3}(\alpha y)^2\right), \tag{18}$$

where $y = r/2m$. We find that the spacetime is almost Schwarzschild ($\Lambda = 0$) for $1 \leq y \ll \alpha^{-1}$, flat for $\alpha^{-2/3} \ll y \ll \alpha^{-1}$, and AdS ($m = 0$) for $y \gg \alpha^{-2/3}$. In flat spacetime, we can match the solutions which are constructed in Schwarzschild spacetime and AdS spacetime. We consider only $l = 2$ for simplicity. The solution of Eq. (7) becomes

$$H^{(1)}(\Lambda = 0) = \alpha^2 y(y-1), \tag{19}$$

$$H^{(1)}(m = 0) = \frac{45}{32}\left[\sqrt{3}\left(\frac{1}{z} + \frac{3}{z^3}\right)\arctan\left(\frac{z}{\sqrt{3}}\right) - \frac{5}{z^2} + \frac{6}{z^2(z^2+3)}\right], \tag{20}$$

where $z = \sqrt{-\Lambda}r$. We find the change in the mass and the horizon area by the deformation of the Schwarzschild anti-de Sitter black hole as

$$\frac{\delta m_d}{m} \simeq \frac{27\sqrt{3}\pi}{128}(3\log 2 - 4)\alpha^{-1}\epsilon^2, \tag{21}$$

$$\frac{\delta A_d}{A} \simeq \frac{27\sqrt{3}\pi}{256}(12\log 2 - 11)\alpha^{-1}\epsilon^2. \tag{22}$$

Hence, the first law of the deformed black hole becomes

$$\delta m_d = \frac{\kappa}{8\pi}\delta A_d + \delta W_d, \tag{23}$$

where $\kappa = 1/4m$ and δW_d is the correction term which is given by

$$\delta W_d = -\frac{1}{5}a_1 c_0 < 0. \tag{24}$$

Here c_0 is the value of $K^{(1)}$ at spatial infinity. The first law of the deformed black hole has the negative δW_d.

4 Summary and Discussion

In this paper, we found the existence of deformed black hole solution whose mass and horizon area is finite and constructed the first law of the black hole in the case of $\alpha \gg 1$ and $\alpha \ll 1$. The deformed black hole is asymptotically weakly AdS spacetimes and is consistent with [7] [8]. We can consider larger deformation parameter ϵ in the case of $\alpha \gg 1$ than $\alpha \ll 1$ because the perturbative analysis is reliable for ϵ that satisfy $\epsilon \ll 1$ in the case of $\alpha \gg 1$ and $\epsilon \ll \alpha$ in the case of $\alpha \ll 1$ as we understand from the value of second-order perturbations. Hence the deformation parameter goes to zero in $\alpha \to 0$. In other words, the Schwarzschild black hole can't deform and this is consistent with [5].

We found that the first law of the deformed black hole has the negative work term in $\alpha \ll 1$. This term can be interpreted as the work that is necessary for the deformation of infinity. Hence, it is expected that there is a negative work term for general α. By the existence of the work term, the horizon area of the deformed black hole is larger than that of the Schwarzschild-anti-de Sitter black hole in equal mass. If we assume the area law $\delta A \geq 0$, the deformed black hole may be preferred static configuration after formation of a black hole.

References

[1] J. P. S. Lemos, Class. Quantum Grav. **12**, 1081 (1995).

[2] J. P. S. Lemos, Phys. Lett. B **353**, 46 (1995).

[3] C. G. Huang and C. B. Liang, Phys. Lett. A **201**, 27 (1995).

[4] S. Aminneborg, I. Bengtsson, S. Holst, and P. Peldan, Class. Quantum Grav. **13**, 2707 (1996).

[5] T. Regge and J. A. Wheeler, Phys. Rev. **108**, 1063 (1957).

[6] A. Ashtekar and A. Magnon, Class. Quantum Grav. **1**, 39 (1984).

[7] M. T. Anderson, P. T. Chrusciel, and E. Woolgar, gr-qc/0211006.

[8] G. J. Galloway, S. Surya, and E. Delay, Class. Quantum Grav. **20**, 1635 (2003).

[9] L. Vanzo, Phys. Rev. D **56**, 6475 (1997).

[10] L. F. Abbott and S. Deser, Nucl. Phys. **B195**, 76 (1982).

Dynamics of Brane in 5-Dimensional Bulk and Non-Singular Brane Cosmology

Naoya Okuyama[1], Kei-ichi Maeda[2]

Department of Physics, Waseda University,
3-4-1 Okubo, Shinjuku-ku, Tokyo 169-8555, Japan

Abstract

We study brane cosmology as 4-dimensional domain wall dynamics in 5-dimensional bulk space-time. In general metric as the 5-dimensional bulk, we find that equation of motion of a domain wall depends on mass function of the bulk and conservation law of energy-momentum of the domain wall depends on lapse function of the bulk. Especially in the bulk with non-trivial lapse function, energy of matter field on the domain wall flows out and in from the bulk. We apply the result to the case that SU(2) gauge field is in the bulk and find that domain wall dynamics is corrected to be that singularity-free universe can be realized in brane world scenario.

1 Introduction

Brane world scenario, in which we are living in a hypersurface in a higher dimensional spacetime, attracts our attention as the topic in both unified theory of particle physics and cosmology. In Randall-Sundrum's brane model our universe is regarded as (3+1)-dimensional domain wall in (4+1)-dimensional bulk, whereas only gravitons propagate in the negative curvature spacetime. For brane world cosmological scenario, much research have been extensively studied and found new physics. Among them, the brane cosmology in Randall-Sundrum's model are studied by dynamics of domain wall which have constant curvature in 5-dimensional Schwarzschild-anti de Sitter spacetime [1]. In the result it has been found that the mass of Schwarzschild black hole give a contribution to dark radiation through its tidal force to domain wall.

On the other hand, effective theory of M theory predicts that higher dimensional bulk spacetime has many other fields, such as dilaton scalar field, gauge field, and so on. In its viewpoint bulk spacetime may have various geometries by the effects of bulk other fields. They are studied the dynamics of domain wall in the bulk fields, for example with U(1) gauge field [2], or with higher order term of graviton [3]. Adding their fields, equation of motion of the domain wall changes further. We investigate how the geometries of bulk spacetime contributes to dynamics of domain wall, using general bulk geometry which is not specified. As application of our result we also study dynamics of domain wall in the case that SU(2) gauge field is in the bulk.

2 Dynamics of Brane in 5-Dimensional Bulk

Brane cosmology can be written as dynamics of 4-dimensional domain wall (corresponding to our universe) moving in the 5-dimensional bulk spacetime holding negative cosmological constant. We investigate the dynamics of domain wall in the bulk which have general static metric. Assuming homogeneity and isotropy for spatial component of 4-dimensional domain wall, bulk geometry has to have spherical, plane, or hyperbolic symmetry. So the metric of bulk can be described as

$$ds^2 = -f_k(r)e^{-2\delta(r)}dt^2 + \frac{dr^2}{f_k(r)} + r^2 d\Omega^2_{3,k}, \tag{1}$$

where

$$f_k(r) = k - \frac{\mu(r)}{r^2} + \frac{r^2}{l^2}, \tag{2}$$

[1] E-mail:okuyama@gravity.phys.waseda.ac.jp
[2] E-mail:maeda@gravity.phys.waseda.ac.jp

where $l^2 = -6\Lambda_5^{-1}$ and k takes $0, 1, -1$, corresponding to flat, closed, or open geometries of the spatial part of domain wall. The bulk geometry is represented with lapse function $\delta(r)$ and mass function $\mu(r)$. In this coordinate domain wall is located at $r = a(\tau)$.

We assume the Z_2-symmetry between the two side of the domain wall, and brane tension σ and perfect fluid ρ on the domain wall. Then dynamics of domain wall turns out to be

$$H^2 + \frac{k}{a^2} - \frac{\mu}{a^4} + \frac{1}{\ell^2} - \left[\frac{4\pi G_5}{3}(\sigma + \rho)\right]^2 = 0 \tag{3}$$

and

$$\dot{\rho} + \dot{\sigma} + 3H(p + \rho) = \delta'(\rho + \sigma)\dot{a} \tag{4}$$

by Israel's junction equations at domain wall. The former equation describes modified Friedmann equation which is same form to [1] replacing the mass of Schwarzschild black hole by $\mu(r)$. Quadratic term of ρ and dark radiation term are added to standard Friedmann equation. The latter is the equation corresponding to modified energy conservation law of matter in the standard cosmological model. The equation is same to conservation law in standard cosmological model when $\delta(r) = \text{const.}$, so if U(1) gauge field and negative cosmological constant is in the bulk at the most [1, 2], then lapse function should be trivial by Birkhoff's theorem, thus energy on the domain wall always conserves. In the case when lapse function $\delta(r)$ is non-trivial, energy of matter on the domain wall flows out and in from the bulk, so energy doesn't conserve on the domain wall. Sufficient condition that it is asymptotically recovered at late time ($a \to \infty$) is that bulk geometry is asymptotically anti-de Sitter. In next section we investigate the dynamics of domain wall in the bulk with non-trivial lapse function.

3 Non-Singular Brane Cosmology

As an exercise of non-trivial lapse function, we apply the solutions of 5-dimensional Einstein-Yang-Mills system as bulk. This system has SU(2) gauge field other than gravitational field and negative cosmological constant, whose action is described as

$$S = \frac{1}{16\pi}\int d^5x\sqrt{-g_5}\left[\frac{1}{G_5}(R - 2\Lambda_5) - \frac{1}{g^2}\mathrm{Tr}(\mathrm{F}_{\mathrm{YM}}^2)\right]. \tag{5}$$

In same system in 4-dimension, the black hole solutions that is colored black hole [4] and globally regular solutions that is particle-like solutions [5] are found in spherically symmetric ansatz (that is the case $k = 1$). They are numerical solutions and have non-trivial lapse function. In 5-dimension, it is found that there are similar solutions and they are stable against spherical linear perturbations when $\Lambda_5 < 0$ [6]. In the case $k = 0, -1$, there are no particle-like solutions but are colored black hole solutions.

The Friedmann equation (3) is rewritten in the form of a particle motion with zero energy in a given potential as

$$\frac{1}{2}\dot{a}^2 + U(a) = 0, \tag{6}$$

where the potential $U(a)$ is given by

$$U(a) = \frac{1}{2}\left[k - \frac{\mu(a)}{a^2} - \frac{\Lambda_4}{3}a^2 - \frac{8\pi G_4}{3}\rho(a)a^2\left(1 + \frac{1}{2\sigma}\rho(a)\right)\right]. \tag{7}$$

G_4 and Λ_4 are chosen to adjust to standard cosmological model. If σ is constant and the equation of state of matter on the domain wall is given as $p = (\gamma - 1)\rho$, the integration of (4) gives

$$\rho(a) = \rho_0 a^{-3\gamma}e^{\delta(a)} + \sigma a^{-3\gamma}e^{\delta(a)}\int^a \delta'(a)a^{3\gamma}e^{-\delta(a)}da. \tag{8}$$

In the figure 1 and 2 we show the bulk geometries which are the solutions of (5), and the potential $U(a)$ of domain wall in them. In the figure physical values with scale length are normalized by $\lambda = (G_5/g^2)^{1/2}$.

Figure 1 depicts the bulk geometry for $k = 0$ and the potential $U(a)$. In this case it forms colored black hole, which has an event horizon at $a \sim 1$ and an inner horizon at $a \sim 10^{-7}$. At inner horizon, potential $U(a)$ works as repulsive force. In this case domain wall bounces at there and thus initial singularities can be avoided. However in most of black hole with inner horizon there is Cauchy horizon instabilities such that the effects of domain wall may put out inner horizon, so there is still room of arguments. Figure 2 depicts the bulk geometry for $k = 1$ and the potential $U(a)$. In this case it forms particle-like solution. Potential $U(a)$ also works as repulsive force at finite $a = a_0$, so domain wall bounces at $a = a_0$. In this case it is stable against linear perturbation, so initial singularities can be stably avoided. Moreover there are no singularities in the 5-dimensional bulk, so in this case singularity-free universe in brane world scenario can be realized in the meaning of that both big bang singularities and bulk singularities are avoided [7]. In this case, domain wall solution becomes oscillating universe. In both case energy conservation law recover at large scale factor.

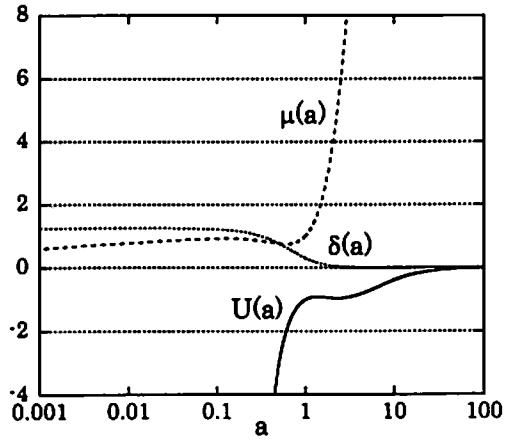

Figure 1: The mass function $\mu(a)$, the lapse function $\delta(a)$ of the 5-dimensional bulk with $k = 0$, and the potential $U(a)$ of the domain wall. We set $l = 1$, $\Lambda_4 = 0$ and $\rho \ll 1$, and all physical values with scale length are normalized by $\lambda = (G_5/g^2)^{1/2}$. The 5-dimensional bulk forms colored black hole spacetime which has inner horizon. Inner horizon is located at $a \sim 10^{-7}$ and in there $U(a)$ works as repulsive force.

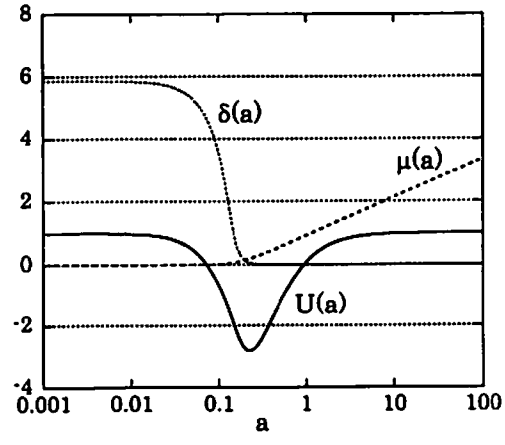

Figure 2: The mass function $\mu(a)$, the lapse function $\delta(a)$ of the 5-dimensional bulk with $k = 0$, and the potential $U(a)$ of the domain wall. We set $l = 1$, $\Lambda_4 = 0$ and $\rho \ll 1$, and all physical values with scale length are normalized by $\lambda = (G_5/g^2)^{1/2}$. The 5-dimensional bulk forms particle-like spacetime.

4 Summary

We investigate the dynamics of domain wall in the bulk which have general static metric. Assuming homogeneity and isotropy for spatial component of (3+1)-dimensional domain wall, bulk geometry has to have spherical, plane, or hyperbolic symmetry. So the metric of bulk can be described with lapse function $\delta(r)$ and mass function $\mu(r)$. By Israel's junction equation at domain wall, we can derive two equations describing dynamics of domain wall, one is Friedmann equation which is same form to [1] replacing mass of Schwarzschild black hole by $\mu(r)$. Another is the equation corresponding to modified energy conservation law of matter in the standard cosmological model. It is worthy of notice that when lapse function $\delta(r)$ is non-trivial, energy of matter on the domain wall flows out and in from the bulk, so energy doesn't conserve on the domain wall.

As an exercise of non-trivial lapse function, we apply 5-dimensional non-trivial black hole spacetime called colored black hole and globally regular spacetime [6], which are solutions with non-Abelian gauge field, as the bulk. In this case energy of the matter on the domain wall escape to the bulk as universe grows by the effect of non-triviality of lapse function, but conservation law asymptotically recovered as $a \to \infty$. On the other hand the mass function works as effects of repulsive forces near $a = 0$, so domain wall solution becomes oscillating universe or bouncing universe with appropriate parameter of bulk spacetime. It is worthy of notice that with globally regular bulk spacetime singularity-free universe in brane world scenario can be realized in the meaning of that both big bang singularities and bulk singularities are avoided [7].

References

[1] P. Kraus, J. High Energy Phys. 12 (1999) 011.

[2] C. Barcelo and M. Visser, Phys. Lett. B482 (2000) 183.

[3] E. Gravanis and S. Willison, Phys. Lett. B562 (2003) 118.

[4] P. Bizon, Phys. Rev. Lett. 64 (1990), 2844.

[5] R. Bartnik and J. McKinnon, Phys. Rev. Lett. 61 (1988), 141.

[6] N. Okuyama and K. Maeda, Phys. Rev. D67 (2003), 104012.

[7] N. Okuyama and K. Maeda, in preparation.

Chiral gravity in higher dimensions

Takayoshi Ootsuka [1,1], Erico Tanaka [1,2], Kousuke Ura [2,3]

[1] *Department of Physics, Ochanomizu University, 2-1-1 Bunkyo Tokyo, Japan*
[2] *Hewlett-Packard Japan,Ltd. Crystal Tower, 1-2-27, Shiromi Chuo Osaka, Japan*

Abstract

We construct a chiral theory of gravity in 7 and 8 dimensions, which are equivalent to Einstein-Cartan theory using less variables [1]. In these dimensions, we can construct such higher dimensional chiral gravity because of the existence of gravitational instanton. The octonionic-valued variables in the theory represent the deviation from the gravitational instanton, and from their non-associativity, prevents the theory to be $SO(n)$ gauge invariant.

1 Introduction

Recently, several researches were made for G_2 and $Spin(7)$ holonomy manifold in 7 and 8 dimensions [2, 3, 4, 5]. Such manifolds have reduced holonomy, i.e., in 7 dimension $SO(7)$ holonomy reduced to G_2, in 8 dimension $SO(8)$ to $Spin(7)$. manifolds, and therefore they have been a plausible candidate for compactification of extra dimensions which shows up in M-theory and superstring theory [6, 7, 8]. For the meanwhile, 4-dimensional quantum loop gravity revealed some non-perturbative effects of gravity, making use of Ashtekar formalism [9, 10, 11]. The Ashtekar formalism used in this case is a 4-dimensional chiral theory [12], which is a theory presented in partial variables (giving the naming of chiral) of Einstein-Cartan theory. For Riemannian manifold, a $SO(4)$-valued spin connection could be decomposed to two $SO(3)$-valued components, and in chiral gravity, the half of $SO(3)$ is used to construct the theory. In the case of Lorentzian, the same decomposition could be achieved by complexification of $SO(1,3)$ to $SO(4)_C$. One specific point of 4-dimensional chiral gravity, is that by setting the connection to zero for the chiral equation of motion, the 4-dimensional special holonomy manifold, $Sp(1)$ holonomy manifold (in other words, HyperKähler manifold; or gravitational instanton) could be derived [13, 14]. It might be said that 4-dimensional chiral gravity states the difference from the gravitational instanton. This is in contrast with Einstein-Cartan theory, whose non-zero connection describes the deviation from flat space-time. In the following discussion, we show in certain higher dimensions, there exists a chiral formalism of gravity. That is, when special holonomy manifold exists, instead of Einstein-Cartan's $SO(n)$ connection, we could use partial ("chiral") variables and construct a theory which is equivalent to Einstein-Cartan theory. We have chosen Euclidean case for presentation, but as in 4 dimension, Lorentzian case could be achieved similarly by complexification of Lie group. However, in higher dimensions, chiral variables could not be understood as connections as in 4 dimension. Still it has local gauge symmetry of G_2 (7-D) and $Spin(7)$ (8-D), which is related to non-associative algebra, octonions.

2 Einstein Cartan theory

We start from the Euclid Einstein-Cartan Lagrangian, which form is valid in any n dimensions,

$$\mathcal{L}_{E.C.}(A,\theta) = \langle F \wedge * (\theta \wedge \theta) \rangle , \tag{1}$$

[1] E-mail: ootsuka@cosmos.phys.ocha.ac.jp
[2] E-mail: erico@cosmos.phys.ocha.ac.jp
[3] E-mail: kousuke.ura@hp.com

where A is the $so(n)$ connection, θ the n-bein 1-form, and F a $so(n)$ curvature. Their explicit definition are given by,

$$A = \frac{1}{2}A^{ab} \otimes M_{ab}, \quad F = dA + \frac{1}{2}[A \wedge A] \quad \theta = \theta^a \otimes P_a,$$
$$\theta \wedge \theta = \frac{1}{2}\theta^a \wedge \theta^b \otimes M_{ab}, \quad *(\theta \wedge \theta) = \frac{1}{2}\frac{1}{(n-2)!}\epsilon_{abc_1 \cdots c_{n-2}}\theta^{c_1 \cdots c_{n-2}} \otimes M_{ab}. \tag{2}$$

Above, $\theta^{c_1 \cdots c_{n-2}}$ is the abbreviation of $\theta^{c_1} \wedge \cdots \wedge \theta^{c_{n-2}}$. Generators M_{ab} and P_c form the Poincaré algebra. There also is a property of killing forms, which we will use frequently in the calculations,

$$\langle P_a, P_b \rangle = \delta_{ab}, \quad \langle M_{ab}, M_{cd} \rangle = \delta_{ac}\delta_{bd} - \delta_{ad}\delta_{bc}. \tag{3}$$

The equation of motion derived from this Lagrangian is,

$$D * (\theta \wedge \theta) = 0, \quad \epsilon_{abc_1 \cdots c_{n-2}} F^{ab} \wedge \theta^{c_1 \cdots c_{n-3}} = 0. \tag{4}$$

The chiral theory we will construct is equivalent to this Einstein-Cartan (E.C.) theory in a certain aspect.

3 Octonions

Before going into the construction of the theory, let us briefly give some outlines of octonions($\mathbb{O}$) [15, 16]. This peculiar algebra appears when one decomposes $so(8)$ and $so(7)$ considering the particular solutions of Einstein equations, the gravitational instantons [17]. Octonions are the biggest alternative division algebra, which are non-commutative and also non-associative. Their basis satisfies the following relations,

$$\begin{aligned}
&a \in \mathbb{O} \quad a = a_0 e_0 + a_1 e_1 + \cdots + a_7 e_7 \quad a_0 \cdots a_7 \in \mathbb{R} \\
&e_0 := 1, \quad e_i e_j := -\delta_{ij} + \varphi_{ijk} e_k, \quad (i,j = 1 \cdots 7) \\
&\varphi_{abc} = 1 \quad \text{if} \quad (abc) = \begin{cases} (123),(516),(624),(435), \\ (471),(673),(572) \end{cases}, \quad \varphi_{abc} = 0 \quad \text{else} \\
&e_a(e_b\, e_c) - (e_a\, e_b)e_c = \psi_{abcd} e_d, \quad \psi_{abcd} = -\frac{1}{3!}\epsilon_{abcdefg}\varphi_{efg}.
\end{aligned} \tag{5}$$

The structure constant φ_{abc} represents non-commutativity, and ψ_{abcd} represents non-associativity. The chiral construction in 8 and 7 dimensions are deeply related to these octonion properties.

4 8-dimensional chiral gravity

The decomposition of $so(8)$ we chose for constructing chiral gravity is

$$so(8) = o \oplus spin(7). \tag{6}$$

This decomposition [17] is $Spin(7)$ invariant, and o is isomorphic to the imaginary part of octonions. The constructed theory should only involve o component of the connection. The algebra for this decomposition are,

$$[spin(7), spin(7)] \subset spin(7), \quad [spin(7), o] \subset o, \quad [o, o] \subset spin(7), \tag{7}$$

and the projection operators,

$$P_{o\mu\nu\rho\sigma} = \frac{1}{8}\{\delta_{\mu\rho}\delta_{\nu\sigma} - \delta_{\mu\sigma}\delta_{\nu\rho} + f_{\mu\nu\rho\sigma}\}, \quad P_{spin(7)\mu\nu\rho\sigma} = \frac{1}{8}\{3(\delta_{\mu\rho}\delta_{\nu\sigma} - \delta_{\mu\sigma}\delta_{\nu\rho}) - f_{\mu\nu\rho\sigma}\}, \tag{8}$$

where Greek subscript runs from 0 to 7. The structure constant $f_{\mu\nu\rho\sigma}$ satisfies the self-duality condition, $f_{\mu\nu\rho\sigma} = \frac{1}{4!}\epsilon_{\mu\nu\rho\sigma\tau\lambda\eta\zeta}f_{\tau\lambda\eta\zeta}$ and could be written in terms of the octonion structure constant,

$f_{abcd} = \psi_{abcd}$, $f_{0abc} = -\varphi_{abc}$. The Latin subscripts run from 1 to 7. We start from the Einstein-Cartan Lagrangian (1). Applying the projection to connection A and $\theta \wedge \theta$,

$$A = A_o + A_{spin(7)}, \quad \theta \wedge \theta = (\theta \wedge \theta)_o + (\theta \wedge \theta)_{spin(7)}. \tag{9}$$

we will construct the 8-dimensional chiral theory with A_o only. Performing some calculations, one could find the relations,

$$*(\theta \wedge \theta)_o = \frac{1}{3}(\theta \wedge \theta)_o \wedge \Psi, \quad *(\theta \wedge \theta)_{spin(7)} = -(\theta \wedge \theta)_{spin(7)} \wedge \Psi, \tag{10}$$

and Ψ is a Cayley 4-form, which is given as $\Psi = \frac{1}{4!} f_{\mu\nu\rho\sigma} \theta^{\mu\nu\rho\sigma}$. Then the Lagrangian could be written,

$$\mathcal{L}_{8E.C.} = \frac{1}{3} \langle F_o \wedge (\theta \wedge \theta)_o \rangle \wedge \Psi - \langle F_{spin(7)} \wedge (\theta \wedge \theta)_{spin(7)} \rangle \wedge \Psi. \tag{11}$$

$F_{spin(7)}$ could be removed by adding an exact term,

$$\mathcal{L}_{8E.C.} + d(\langle T \wedge \theta \rangle \wedge \Psi) = \frac{4}{3} \langle F_o \wedge (\theta \wedge \theta)_o \rangle \wedge \Psi + \langle T \wedge T \rangle \wedge \Psi - \langle T \wedge \theta \rangle \wedge d\Psi, \tag{12}$$

where $T = D\theta$ is the torsion. However, since the decomposition (7) is not a decomposition as a Lie algebra, the curvature component contains both A_o and $A_{spin(7)}$. We could remove the $A_{spin(7)}$ part by using the killing form relation and the torsion-less condition, $D(\theta \wedge \theta) = 2T \wedge \theta = 0$. We define

$$\mathcal{L}_{8chiral}(A, \theta) := \left\{ d \langle A \wedge (\theta \wedge \theta)_o \rangle - \langle [A \wedge A] \wedge (\theta \wedge \theta)_{spin(7)} \rangle \right\} \wedge \Psi, \tag{13}$$

where A_o is replaced by A. This is the chiral Lagrangian, in a sense that is equal to Einstein-Cartan Lagrangian under the torsionless condition.

To check the validity of this Lagrangian, we derive the equation of motion from this Lagrangian and verify that it gives the particular solutions of Einstein equation, gravitational instanton. The equation of motion is,

$$(\theta \wedge \theta)_o \wedge d\Psi - 2[A \wedge (\theta \wedge \theta)_{spin(7)}] \wedge \Psi = 0. \tag{14}$$

Instanton solution is obtained with the condition $A = 0$, and it can be shown that the above equation is equivalent to $d\Psi = 0$, the condition describing the $Spin(7)$ holonomy manifold.

Finally, we show this Lagrangian has $Spin(7)$ gauge symmetry. The $Spin(7)$ gauge transformation is given as,

$$\delta A = [\chi, A], \quad \delta(\theta \wedge \theta)_o = [\chi, (\theta \wedge \theta)_o], \quad \delta(\theta \wedge \theta)_{spin(7)} = [\chi, (\theta \wedge \theta)_{spin(7)}], \tag{15}$$

where χ is $spin(7)$-valued gauge function. It is easy to check that the 4-form Ψ, and therefore the Lagrangian, becomes $Spin(7)$ gauge invariant.

5 7-dimensional chiral gravity

The appropriate decomposition for $so(7)$ and the algebra for them are

$$\begin{aligned} &so(7) = o \ominus g_2, \\ &[g_2, g_2] \subset g_2, \quad [o, g_2] \subset o, \quad [o, o] \subset so(7). \end{aligned} \tag{16}$$

Similar calculation as in the 8 dimensional case applies, and the projection operators also includes the octonion structure constants, ψ_{abcd} and φ_{abc}. Applying the projection to connection A and $\theta \wedge \theta$,

$$A = A_o + A_{g_2}, \quad \theta \wedge \theta = (\theta \wedge \theta)_o + (\theta \wedge \theta)_{g_2}, \tag{17}$$

we construct the 7-dimensional chiral theory with A_o only. The difference between 7 and 8 dimension is that now, by simple calculation, we have the following identity.

$$(\theta \wedge \theta)_o \wedge \varphi = \frac{2}{3}\theta \wedge \psi. \tag{18}$$

where φ and ψ is a Cayley 3-form and 4-form respectively, given by $\varphi = \frac{1}{3!}\varphi_{abc}\theta^{abc}$, $\psi = \frac{1}{4!}\psi_{abcd}\theta^{abcd}$. Using this non-trivial relation, the Einstein-Cartan Lagrangian becomes,

$$\mathcal{L}_{7E.C.} = \frac{1}{3}\left(F_o \wedge \theta\right) \wedge \psi - \left(F_{g_2} \wedge (\theta \wedge \theta)_{g_2}\right) \wedge \varphi, \tag{19}$$

where the decomposed curvature contains both A_o and A_{g_2} components. By the same method used in 8 dimension, we delete A_{g_2} from this Lagrangian. Namely, first add an exact term and modify the Lagrangian in a convenient form, then next delete the remaining A_{g_2} in F_o by the condition $D(\theta \wedge \theta) = 0$, and the property of killing forms. The chiral Lagrangian obtained is:

$$\begin{aligned}\mathcal{L}_{7chiral}(A, \theta) = &\frac{1}{3}\left\{ d\left(A \wedge \theta\right) - \frac{1}{2}\left([A \wedge A] \wedge \theta\right) \right\} \wedge \psi \\ &+ \left\{ d\left(A \wedge (\theta \wedge \theta)\right) - \frac{1}{2}\left([A \wedge A] \wedge (\theta \wedge \theta)_o\right)\left([A \wedge A] \wedge (\theta \wedge \theta)_{g_2}\right) \right\} \wedge \varphi,\end{aligned} \tag{20}$$

which becomes equivalent to Einstein-Cartan Lagrangian under the torsionless condition. The equation of motion becomes,

$$-\frac{1}{3}\theta \wedge \psi + (\theta \wedge \theta)_o \wedge d\varphi - \frac{1}{3}[A \wedge \theta]_o \wedge \psi + [A \wedge (\theta \wedge \theta)_o]_o \wedge \varphi - 2[A \wedge (\theta \wedge \theta)_{g_2}] \wedge \varphi = 0, \tag{21}$$

here A_o replaced by A. Instanton solution is obtained with the condition $A = 0$, and it can be shown that the above equation is equivalent to $d\psi = 0$, $d\varphi = 0$, which is the G_2 manifold, the gravitational instanton of 7 dimension. It could be verified that Lagrangian has G_2 gauge symmetry, defined by,

$$\delta A = [\chi, A], \quad \delta(\theta \wedge \theta)_o = [\chi, (\theta \wedge \theta)_o], \quad \delta(\theta \wedge \theta)_{g_2} = [\chi, (\theta \wedge \theta)_{g_2}], \tag{22}$$

where χ is g_2-valued gauge function.

6 Discussion

We presented the chiral theory of gravity in 7 and 8 dimensions, which are described by less variables than original Einstein-Cartan theory. These chiral variables A also indicates the deviation from the gravitational instantons. However, in these higher dimensions, the chiral variables could not be thought as a connection in comparison to 4-dimensional case. Namely, it does not transform as the usual connection by gauge transformation. It is verified that these chiral theory has G_2 and $Spin(7)$ gauge invariance while they lose $SO(7)$ and $SO(8)$ gauge symmetry. This corresponds to the fact that the chiral variable A must be regarded as the non-associative algebra, octonionic-valued variable. Furthermore, again in contrast to 4 dimension, the chiral Lagrangian is not in the form of BF type, especially the term corresponding to curvature F deviates, and this also comes from the octonionic properties of the chiral variables. It is under question that whether like the BF theory this Lagrangian would be quantizable in this form, but the prospects are that it could be utilized for the higher dimensional quantum gravity as the Ashtekar theory. As the 7 and 8-dimensional chiral gravity reflects the geometric relation of G_2 and $Spin(7)$ manifold, it is hopeful that similar relation as in the case of 3 and 4 dimensions exist and enables one to construct higher dimensional Ashtekar gravity. It is also hoped for the discussion of compactification of 7 or 8 dimensions, as in the Kaluza-Klein scenario of M-theory or 11-dimensional supergravity. In the course of these discussions, we also think it is significant to generalize the theory with supersymmetry. The construction of self-dual supergravity with reduced $Spin(7)$ and G_2 holonomy in 8 and 7 dimensions respectively, are already embodied [5], so one can verify the formulated theory when it is achieved. Finally, in higher dimensions where the special holonomy manifold exists such as $4n\,(n = 1, 2, \cdots)$ or

$2n$ ($n = 2, 3, \cdots$) dimension; namely, $Sp(n)$ holonomy manifold or HyperKähler manifold in $4n$ dimension, and $SU(n)$ holonomy manifold or special Kähler manifold in $2n$ dimension; such chiral gravity should be constructed, and it is now under preparation. As in the dimensions 4, 7 and 8, their chiral variables should represent the deviation from these gravitational instantons. That is, there must be careful tuning to make the chiral variable A represent the projected part of connection of the original E.C. theory. For instance, in 7 dimension, construction of the chiral action was performed that its chiral variable A would be the octonionic part of the original $SO(7)$ connection.

References

[1] Ootsuka T, Tanaka E and Ura K 2004 Chiral Gravity in Higher Dimensions *Class. Quantum Grav.* **21** 975-85

[2] Joyce D D 2000 *Compact Manifolds with Special Holonomy* (New York: Oxford)

[3] Cvetic M, Gibbons G W, Lu H and Pope C N 2002 New Complete Non-compact *Spin*(7) Manifolds *Nucl. Phys.* B **620** 29-54 Cvetic M, Gibbons G W, Lu H and Pope C N 2002 Cohomogeneity One Manifolds of *Spin*(7) and G_2 Holonomy *Phys. Rev.* D **65** 106004

[4] Kanno H and Yasui Y 2002 On *Spin*(7) holonomy metric based on $SU(3)/U(1)$:I,II *J. Geom. Phys.* **43** 293-326

[5] Nishino H and Rajpoot S 2003 Self-Dual $N = (1, 0)$ Supergravity in Eight Dimensions with Reduced Holonomy *Spin*(7) *Phys. Lett.* **564** B 269-79 Nishino H and Rajpoot S 2003 Self-dual supergravity in seven dimensions with reduced holonomy G_2 *Phys. Lett.* **569** B 102-12

[6] Acharya B S 2000 On Realising N=1 Super Yang-Mills in M theory *Preprint* hep-th/0011089

[7] Atiyah M and Witten E 2003 M-Theory Dynamics On A Manifold Of G_2 Holonomy *Adv. Theor. Math. Phys.* **6** 1-106 (Atiyah M and Witten E 2001 *Preprint* hep-th/0107177)

[8] Cvetic M, Gibbons G W, Lu H and Pope C N 2002 Special Holonomy Spaces and M-theory *Preprint* hep-th/0206154

[9] Ashtekar A 2001 Quantum Geometry and Gravity: Recent Advances *Preprint* gr-qc/0112038

[10] Rovelli C 2000 Notes for a brief history of quantum gravity *Preprint* gr-qc/0006061 Rovelli 1998 Loop Quantum Gravity *Living Rev. Rel.* **1** 1-75

[11] Smolin L 2003 How far are we from the quantum theory of gravity? *Preprint* hep-th/0303185

[12] Capovilla R, Dell J, Jacobson T and Mason L 1991 Self-dual 2-forms and gravity *Class. Quantum Grav.* **8** 41-57

[13] Ashtekar A 1987 New Hamiltonian formulation of general relativity *Phys. Rev.* D **36** 1587-602

[14] Ootsuka T, Miyagi S, Yasui Y and Zeze Z 1999 Anti-self-dual Maxwell solutions on hyperkähler manifold and $N = 2$ supersymmetric Ashtekar gravity *Class. Quantum Grav.* **16** 1305-12

[15] Dündarer R, Gürsey F and Tze C H 1964 Generalized vector products, duality, and octonionic identities in $D = 8$ geometry *J. Math. Phys.* **25** No.5 1496-506

[16] Baez J C 2001 The Octonions *Preprint* math.RA/0105155

[17] Bakas I, Floratos E G and Kehagias A 1998 Octonionic gravitational instantons *Phys. Lett.* B **445** 69-76

Stabilization of the hierarchy in brane models

Oriol Pujolàs[1]

Yukawa Institute for Theoretical Physics, Kyoto University
Kitashirakawa-Oiwake-Cho Sakyo-ku, Kyoto 606-8502, Japan

Abstract

We show that the Casimir effect may stabilize the Planck *vs.* electroweak hierarchy naturally in brane models with warped extra dimensions.

1 Introduction

In the Brane world scenario [1], the hierarchy between the electroweak and the Planck scales is a function of the size of the extra dimensions. As in Kaluza Klein theories, this size is dynamical. The corresponding degree of freedom is usually called the *radion*, which is often massless at tree level [2]. Thus, a complete solution to the hierarchy problem in the brane world scenario requires a *stabilization mechanism*, which explains two things [3]. On one hand, it has to give the radion a large enough mass in order that the scalar interactions that it would propagate are not observed. On the other hand, it must explain in a natural way how the radion takes an expactation value that gives rise to the 16 orders of magnitude that separate the Planck and the electroweak scales.

In the context of Kaluza Klein theories, Weinberg and Candelas [4] showed that the quantum effecs from matter fields can stabilize the radion. Here, we investigate whether they can naturally stabilize the hierarchy in brane models.

2 Hierarchy Stabilization

In models of ADD type [1], it seems difficult to generate and stabilize a large hierarchy with quantum effects only [3]. The reason is that in these models, the hierarchy appears as a large volume effect and that the Casimir energy density is a power of the radius. If this energy has to be balanced by, *eg*, curvature terms, generically one does not expect a large radius unless some large number introduced [3]. However, if one introduces a warp factor, the dimensional analysis is not so simple, and the picture changes substantially. Here, we report on some of the examples where the (natural) stabilization by quantum effects is possible.

The Randall Sundrum model

In the RS model [2], the effective potential induced by bulk scalar fields and by the graviton was computed in [5]. This potential cannot generate naturally a large hierarchy. However, the potential induced by bulk gauge fields can generate a large hierarchy and give the radion a sizable mass [6]. This remarkably different behaviour of bulk gauge fields can be understood from the AdS/CFT correspondence [6].

Scalar-tensor model in 5D

In Ref. [7], a family of five dimensional scalar-tensor models are considered, which allow for solutions with a warp factor of the form $a(y) = y^q$, instead of the exponential behaviour in the RS model. These models have two moduli corresponding to the brane locations, $y_\pm$. The effective potential induced by bulk fields contains a logarithmic term (absent in the RS case), which produces a large hierarchy naturally. However, the masses for the moduli $y_\pm$ are too small unless the power in the warp factor is large enough, $q \gtrsim 10$.

[1] E-mail:pujolas@yukawa.kyoto-u.ac.jp

Higher dimensional warped models

The class of models considered in [8] consist of a higher dimensional extension of the RS model with metric

$$ds^2 = e^{-2k|y|}[dy^2 + \eta_{\mu\nu}dx^\mu dx^\nu + ds_\Sigma^2], \quad (1)$$

where Σ is a compact $n-$dimensional space. Two codimension-one branes (with topology $M_4 \times \Sigma$) are located at the orbifold fixed pionts.

The hierarchy arises in these models as a combination of the redshift [2] and large volume [1] effects. The effective potential from bulk fields can be computed without specifying the internal space Σ. This potential can stabilize the two moduli and the hierarchy without fine tuning if Σ is flat but not if it is curved. This can be understood from [7] since these models correspond to a quite small power, $q \leq 4$. It remains to be studied whether models with different warp factors in Eq. (1) can stabilize naturally the hierarchy when Σ is curved.

Factorizable $AdS_5 \times \Sigma$ geometry

The model considered in [9] is the direct product of the RS geometry and some compact manifold Σ of radius R. In contrast with the model of [8], the hierarchy is due to the redshift effect only. Intuitively, this model should reduce to the RS model when R is small. This is explicitly shown in [9], and in particular the potential induced by bulk gauge fields can stabilize a large hierarchy without fine tuning.

We conclude that the Casimir effect may stabilize a large hierarchy naturally in warped brane models. Therefore, the hierarchy problem may be solved without the need to introduce other ingredients in these scenarios.

References

[1] N. Arkani-Hamed, S. Dimopoulos, G. Dvali, Phys. Lett. **B429** (1998) 263; I. Antoniadis, N. Arkani-Hamed, S. Dimopoulos, G. Dvali, *ibid.* **B436** (1998) 257.

[2] L. Randall, R. Sundrum, Phys. Rev. Lett. **83** (1999) 3370.

[3] N. Arkani-Hamed, S. Dimopoulos and J. March-Russell, Phys. Rev. D **63**, 064020 (2001).

[4] P. Candelas, S. Weinberg, Nucl. Phys. **B237** (1984) 397.

[5] J. Garriga, O. Pujolàs, T. Tanaka, Nucl. Phys. **B605** (2001) 192.

[6] J. Garriga and A. Pomarol, Phys. Lett. B **560**, 91 (2003).

[7] J. Garriga, O. Pujolàs, T. Tanaka, Nucl. Phys. B **655**, 127 (2003).

[8] A. Flachi, J. Garriga, O. Pujolàs and T.anaka, JHEP **0308**, 053 (2003)

[9] A. Flachi and O. Pujolàs, Phys. Rev. D **68**, 025023 (2003).

Gauge problem in the gravitational self-force:
- First post-Newtonian force in the Regge-Wheeler gauge -

Norichika Sago[a,b,1], Hiroyuki Nakano[c,2], and Sasaki Misao[d,3]

[a] *Department of Earth and Space Science, Graduate School of Science, Osaka University, Osaka 560-0043, Japan*

[b] *Department of Physics, Graduate School of Science, Kyoto University, Kyoto 606-8502, Japan*

[c] *Department of Mathematics and Physics, Graduate School of Science, Osaka City University, Osaka 558-8585, Japan*

[d] *Yukawa Institute for Theoretical Physics, Kyoto University, Kyoto 606-8502, Japan*

Abstract

We discuss the regularization of the gravitational self-force on a point particle in a Schwarzschild space-time. The metric perturbation induced by a particle can be divided into two parts, the S-part and the-R-part, in the harmonic gauge, and the regularized self-force is derived from the R-part which is regular and satisfies the source-free regularized Einstein equations. In this paper, we consider a gauge transformation from the harmonic gauge to the Regge-Wheeler gauge in which the metric perturbation can be calculated, and present a method of deriving the regularized self-force in the Regge-Wheeler gauge. In addition, as a first application of this method, we calculate the self-force on a particle in circular orbit up to the first post-Newtonian order. We find the correction to the total mass of the system due to the presence of the particle is correctly reproduced in the force at the Newtonian order.

1 Introduction

An inspiral of a compact object into a supermassive black hole, which is expected to exist in the center of many galaxies, is one of the promising targets of the space-based interferometer, LISA. To extract out physical information of such a system from observed gravitational wave signals, it is essential to predict the theoretical waveforms accurately. The black hole perturbation approach is most suited for this purpose. In this approach, one considers gravitational waves emitted by a point particle that represents a compact object orbiting a black hole, assuming the mass of the particle (μ) is much less than that of the black hole (M); $\mu \ll M$. In the lowest order in the mass ratio, μ/M, we can regard the particle as a test particle. Therefore, the particle moves along a geodesic on the background geometry of a black hole. In the next order, however, the orbit deviates from the geodesic on the black hole background because the spacetime is perturbed by the particle. We can interpret this deviation as the effect of the self-force on the particle itself. In order to evaluate this deviation accurately, we have to derive the equation of motion that takes account of the self-force on the particle.

It is known that the gravitational self-force can be derived from the "*tail part*" of the metric perturbation, which has support inside the past null cone of the evaluation point and is regular at the particle's location [1]. However it is difficult to calculate this part directly because it depends on the history of the particle's motion. Therefore, one usually identifies the singular part of the metric perturbation which can be evaluated locally (called the "*direct part*") up to a necessary order and subtract it from the metric perturbation. This identification of the direct part is sometimes called the "*subtraction problem*". In addition, there is another problem, called the "*gauge problem*", which is caused by the gauge dependence of the gravitational self-force.

In this paper, as a first step toward a complete derivation of the gravitational self-force, we consider a particle orbiting a Schwarzschild black hole, and propose a method to calculate the regularized self-force by solving the subtraction and gauge problems simultaneously. Namely, we develop a method to

[1] E-mail:sago@tap.scphys.kyoto-u.ac.jp
[2] E-mail:denden@sci.osaka-cu.ac.jp
[3] E-mail:misao@yukawa.kyoto-u.ac.jp

regularize the self-force in the Regge-Wheeler (RW) gauge based on the "mode decomposition scheme" (or "mode-sum scheme") [2]. In addition, we calculate the regularized self-force on a particle moving along a circular orbit up to the first post-Newtonian (1PN) order, as an application of our method.

The paper is organized as follows. In Sec. 2, we briefly review the situation of the self-force problem and give the regularization prescription under the RW gauge condition. In Sec. 3, at the level of 1PN order, we give the force due to the metric perturbation and its S-part for circular orbit case in the RW gauge. From the results obtained in Sec. 3, we obtain the regularized gravitational self-force in Sec. 4. Finally, we summarize our calculation and discuss the future work in Sec. 5.

2 Self-force in the RW gauge

The Schwarzschild metric is given in the standard Schwarzschild coordinates as

$$g_{\mu\nu}dx^\mu dx^\nu = -f(r)dt^2 + f(r)^{-1}dr^2 + r^2(d\theta^2 + \sin^2\theta d\phi^2)\,, \qquad f(r) = 1 - \frac{2M}{r}\,. \tag{1}$$

We denote the location of the particle at its proper time $\tau = \tau_0$ as $\{z_0^\alpha\} = \{z^\alpha(\tau_0)\}$, where $z^\alpha(\tau)$ is an orbit of the particle parametrized by the background proper time (i.e., $g_{\mu\nu}(dz^\mu/d\tau)(dz^\nu/d\tau) = -1$). We consider the metric perturbation on the background induced by the particle $h^{\rm full}_{\mu\nu} = \tilde{g}_{\mu\nu} - g_{\mu\nu}$, where $\tilde{g}_{\mu\nu}$ is the perturbed metric. According to the works by Mino, Sasaki and Tanaka and Quinn and Wald [1], the gravitational self-force on a particle is given in the harmonic gauge as follows:

$$F^{\rm H}_\alpha(\tau) = \lim_{x\to z(\tau)} F_\alpha[h^{\rm tail,H}(x)] = \lim_{x\to z(\tau)} \left(F_\alpha[h^{\rm full,H}(x)] - F_\alpha[h^{\rm dir,H}(x)]\right)\,. \tag{2}$$

where the superscript H stands for the harmonic gauge. $F_\alpha[\cdots]$ is the differential operator defined by

$$F^\alpha[h_{\mu\nu}] = -\mu P^\alpha_\beta(\bar{h}_{\beta\gamma;\delta} - \frac{1}{2}g_{\beta\gamma}\bar{h}^\epsilon{}_{\epsilon;\delta} - \frac{1}{2}\bar{h}_{\gamma\delta;\beta} + \frac{1}{4}g_{\gamma\delta}\bar{h}^\epsilon{}_{\epsilon;\beta})u^\gamma u^\delta\,, \tag{3}$$

where $P_\alpha{}^\beta = \delta_\alpha{}^\beta + u_\alpha u^\beta$, $\bar{h}_{\alpha\beta} = h_{\alpha\beta} - \frac{1}{2}g_{\alpha\beta}h_\mu{}^\mu$ and $u^\alpha = dz^\alpha/d\tau$.

When we perform this subtraction, the metric perturbation and the direct part must be evaluated in the harmonic gauge because the tail part and the direct part are meaningful only in this gauge. However, it is difficult to obtain the metric perturbation in the harmonic gauge. On the other hand, we can obtain it under the RW gauge condition by using the Regge-Wheeler-Zerilli formalism [3, 4]. Therefore we attempt to regularize the self-force in the RW gauge. But there remains a problem even in this approach. Since the transformation between the harmonic gauge and the RW gauge irregular, except for radial orbit cases, and the tail part of the metric perturbation is not the solution of the linearized Einstein equations, it is not trivial how to define the regularized self-force in the RW gauge [5].

Recent work by Detweiler and Whiting [6] gave an important clue to solve the problem. They introduced a new decomposition of the metric perturbation, improving over the one by Mino, Sasaki and Tanaka and Quinn and Wald. The new singular part, called the S-part, $h^{\rm S,H}_{\mu\nu}$, is constructed to be an inhomogeneous solution of the linearized Einstein equations in the harmonic gauge. The new regular part, called the R-part, $h^{\rm R,H}_{\mu\nu}$, is then a homogeneous solution. Since the S- and R-parts are both the solutions of the Einstein equations, we can define the S- and R-parts in another gauge, which are also the solutions of the Einstein equations, by performing the gauge transformation of each part. Namely, the S- and R-parts are unambiguously defined in any gauge. Therefore, we can consider the subtraction procedure in any gauge we wish to adopt. In the Schwarzschild case, we can formally obtain the self-force in the RW gauge by transforming the R-part of the metric perturbation in the harmonic gauge to the RW gauge. Then the problem is how to calculate the R-part in the RW gauge.

To solve this problem, let us consider the transformation from the harmonic gauge to the RW gauge,

$$x^{\rm H}_\mu \to x^{\rm RW}_\mu = x^{\rm H}_\mu + \xi^{\rm H\to RW}_\mu\,, \quad h^{\rm H}_{\mu\nu} \to h^{\rm RW}_{\mu\nu} = h^{\rm H}_{\mu\nu} - 2\nabla_{(\mu}\xi^{\rm H\to RW}_{\nu)}, \tag{4}$$

where $\xi^{\rm H\to RW}_\mu$ is the generator of the gauge transformation. Using this gauge transformation, the self-force in the RW gauge is formally given by

$$F^{\rm RW}_\alpha(\tau) = \lim_{x\to z(\tau)} F_\alpha\left[h^{\rm R,RW}\right] = \lim_{x\to z(\tau)} \Big(F_\alpha\left[h^{\rm full,RW}\right](x) - F_\alpha\left[h^{\rm S,H} - 2\nabla\xi^{\rm H\to RW}\left[h^{\rm S,H}\right]\right](x)\Big)\,. \tag{5}$$

where we have omitted the spacetime indices of $h_{\mu\nu}$ and $\nabla_{(\mu}\xi_{\nu)}$ for notational simplicity. The full metric perturbation $h^{\rm full.RW}_{\mu\nu}$ can be calculated by using the Regge-Wheeler-Zerilli formalism, while the S-part $h^{\rm S.H}_{\mu\nu}$ can be obtained with sufficient accuracy by the local analysis near the particle location. In addition, we can calculate the gauge generator, $\xi^{\rm H\to RW}\left[h^{\rm S.H}\right]$, once we obtain $h^{\rm S.H}_{\mu\nu}$. In the following section, we shall give the force induced by the metric perturbation (full force) and its S-part, respectively.

3 Full force and its S-part

In this section, we evaluate the full force and its S-part in the RW gauge, respectively.

First, the metric perturbation is calculated by the Regge-Wheeler-Zerilli formalism in which a Fourier-harmonic expansion is used because of the symmetry of the background spacetime. Next, we derive the self-force by acting force operators and represent it in terms of ℓ mode coefficients after summing over ω and m for the Fourier-harmonic series. Here we have calculated it up to 1PN order (The detail is shown in [7]). We shall show only our results:

$$\begin{aligned} F^{r(+)}_{\rm full.RW}\Big|_\ell &= -\frac{(\ell+1)\,\mu^2}{r_0^2} + \frac{1}{2}\,\frac{\mu^2\,(12\,\ell^3+25\,\ell^2+4\,\ell-21)\,M}{r_0^3\,(2\,\ell+3)\,(2\,\ell-1)}\,, \\ F^{r(-)}_{\rm full.RW}\Big|_\ell &= \frac{\ell\,\mu^2}{r_0^2} - \frac{1}{2}\,\frac{\mu^2\,(12\,\ell^3+11\,\ell^2-10\,\ell+12)\,M}{(2\,\ell-1)\,(2\,\ell+3)\,r_0^3}\,, \end{aligned} \tag{6}$$

where the other components of the force vanish. We see that the only non-vanishing component is the radial one as expected because there is no radiation reaction effect at 1PN order. In the above, the indices $(+)$ and $(-)$ denote that the coincidence limit is taken from outside ($r > r_0$) of the orbit and inside ($r < r_0$) of the orbit, respectively.

As for the S-part of the self-force, we first calculate the one in the harmonic gauge by using the local coordinate expansion [2]. After that, we transform the S-part of the metric perturbation from the harmonic gauge to the RW gauge. Our results up to 1PN order are given by:

$$F^{r(\pm)}_{\rm S,RW}\Big|_\ell = \mp\frac{1}{2}\,\frac{\mu^2\,(2\,r_0-3\,M)}{r_0^3}\,L - \frac{1}{8}\,\frac{\mu^2\,(4\,r_0-7\,M)}{r_0^3} + \frac{\mu^2\,M\,(172\,L^4-14784\,L^2+299)}{128\,r_0^3(L^2-1)(L^2-4)(L^2-9)}\,, \tag{7}$$

where $L=\ell+1/2$ and the other components vanish. We now see that the $O(1/L^2)$-term of the S-force in the RW gauge vanishes after summing over ℓ. Note that, the final formula above should be regarded as valid for all ℓ from 0 to ∞ [7].

4 Regularized gravitational self-force

In the previous section, we have calculated the full and S-parts of the self-force in the RW gauge. Now we are ready to evaluate the regularized self-force, though there is one more issue to be discussed, namely, the treatment of the $\ell=0$ and 1 modes.

First, we consider the contributions of $\ell \geq 2$ to the self-force. As noted before, for the 1PN calculation, the only r-component of the full and S-part of the self-force is non-zero. By subtracting the S-part from the full force by each mode and summing over $\ell(\geq 2)$ modes, we obtain

$$F^r_{\rm RW}(\ell \geq 2) = -\frac{3\,\mu^2\,M}{4\,r_0^3}\,. \tag{8}$$

We note that the Regge-Wheeler-Zerilli formalism, which we use to calculate the full force, is valid for $\ell \geq 2$. Although the $\ell=0$ and 1 modes do not contribute to the self-force formally, because of our inability to know the exact form of the S-part, it turns out that we do need to calculate the contributions from the $\ell=0$ and 1 modes. By using the Zerilli's analysis [4] for these modes, we obtain their contribution to the self-force as follows:

$$\delta F^r_{\rm RW}(\ell=0,\,1) = \frac{2\,\mu^2}{r_0^2} - \frac{41\,\mu^2 M}{4 r_0^3}\,. \tag{9}$$

It should be noted that a gauge ambiguity remains in $\ell = 1$ even mode. This is because it is a pure gauge mode which describes a shift of the center of mass coordinates. Nevertheless, we were able to resolve this ambiguity at Newtonian order, and hence to obtain an unambiguous interpretation of the resulting self-force.

Finally, adding Eqs. (8) and (9), we obtain the regularized gravitational self-force up to 1PN order as

$$F^r_{\rm RW} = \frac{2\mu^2}{r_0^2} - \frac{11\mu^2 M}{r_0^3}. \tag{10}$$

Since there will be no effect of the gravitational radiation at the 1PN order, i.e., the t- and ϕ-components are zero, the above force describes the correction to the radius of the orbit that deviates from the geodesic on the background. It is noted that the first term proportional to μ^2 is just the correction to the total mass of the system at the Newtonian order, where r_0 is interpreted as the distance from the center of mass of the system to the particle.

5 Discussion

In this paper, based on the decomposition of the field proposed by Detweiler and Whiting, we have proposed a new approach to solve the gauge problem in the regularization of the gravitational self-force for the Schwarzschild background case. Here we have given the formal expression of the self-force in the RW gauge by using the finite gauge transformation from the harmonic gauge. In addition, taking account of the contribution of $\ell = 0, 1$ modes, we have calculated the self-force on the particle moving along a circular orbit up to 1PN order. We have found that our result recovers the one in the rest frame of the center of mass at the Newtonian level. However, the analysis of the low multipole modes has revealed that there inevitably remains the ambiguity of the gauge due to the $\ell = 1$ even parity mode in the resulting self-force. This is because this mode is a pure gauge mode that corresponds to a dipolar shift of the coordinate. To obtain this mode, we need numerical calculation with some appropriate boundary condition.

Acknowledgements

We would like to thank all participants of the 6th Capra Meeting and the Post-Capra Meeting (YITP-W-03-02) held at Yukawa Institute, Kyoto University. HN is supported by the JSPS Research Fellowships for Young Scientists, No. 5919. This work was supported in part by Monbukagaku-sho Grant-in-Aid for Scientific Research, Nos. 1047214 and 12640269, and by the Center for Gravitational Wave Physics, PSU, which is funded by the National Science Foundation under Cooperative Agreement PHY 0114375.

References

[1] Y. Mino, M. Sasaki and T. Tanaka, Phys. Rev. D **55**, 3457 (1997), T. C. Quinn and R. M. Wald, Phys. Rev. D **56**, 3381 (1997).

[2] Y. Mino, H. Nakano and M. Sasaki, Prog. Theor. Phys. **108**, 1039 (2003), L. Barack, Y. Mino, H. Nakano, A. Ori and M. Sasaki, Phys. Rev. Lett. **88**, 091101 (2002).

[3] T. Regge and J. A. Wheeler, Phys. Rev. **108**, 1063 (1957).

[4] F. J. Zerilli, Phys. Rev. D **2**, 2141 (1970).

[5] L. Barack and A. Ori, Phys. Rev. D **64**, 124003 (2001)

[6] S. Detweiler and B. F. Whiting, Phys. Rev. D **67**, 024025 (2003)

[7] H. Nakano, N. Sago and M. Sasaki, Phys. Rev. D **68**, 124003 (2003)

Paradox between particle number and energy flux for Hawking radiation

Hiromi Saida[1]

Department of Physics, Daido Institute of Technology, Takiharu-cho 10-3, Minami-ku, Nagoya 457-8530, Japan

Hideki Ishihara[2], Ken-ichi Nakao[3]

Department of Mathematics and Physics, Graduate School of Science, Osaka City University, Sugimoto-cho, Sumiyoshi, Osaka 558-8585, Japan

Abstract

For the particle creation along a gravitational collapse (the Hawking radiation), it has already been known that, if the initial quantum state is an excited state for a distant inertial observer, the expectation value of the number operator on the initial state diverges. As far as we know, the effect of a particle detector has not been considered for the calculation of the expectation value. In this talk, we introduce a particle detector and evaluate the Hawking radiation with an excited initial state, and conclude that a particle detector does not resolve the divergence of the expectation value.

1 Introduction

For the particle creation along a gravitational collapse (the Hawking radiation), it has already been known that, if the initial quantum state of a matter field is an excited state for a distant inertial observer, the expectation value of the number operator on the initial excited state diverges. If this is the case, it is implied that a black hole will explode at the moment of its formation. On the other hand, it has also been known that the expectation value of the energy-momentum tensor does not diverge, but it converges to the value of the case with an initial vacuum state [1]. This does not suggest the black hole explosion mentioned above. The latter suggestion by the energy-momentum tensor is more acceptable than the former one by the number operator, because it is expected that the deviation from the initially vacuum case should be smeared out due to the infinite red-shift received by a radiation during propagating from the event horizon to the distant observer.

By the way, a quantum particle has its real meaning after a detection process. Therefore it is better to take a particle detector into account in order to judge whether or not the paradox mentioned above gives rise to some caution in using the particle interpretation. As far as we know, the effect of a particle detector has not been considered for the calculation of the expectation value of the number operator. So, we try introducing a particle detector to evaluate the Hawking radiation with an excited initial state, and extracting some lessons in using the quantum field theory on a curved spacetime.

2 Setting with a detector

Our back ground spacetime is the spherical gravitational collapse to form a Schwarzschild black hole. The observer rests at a constant spatial distance $r = R$ far from the collapsing region (R is a very large constant), and possesses a particle detector. When the matter field contained in the detector is excited through the interaction with the Hawking radiation, the observer recognises the detection of a particle emitted from the collapsing region [2]. To treat this detection process, we set the followings;

[1] E-mail:saida@daido-it.ac.jp
[2] E-mail:ishihara@sci.osaka-cu.ac.jp
[3] E-mail:knakao@sci.osaka-cu.ac.jp

- $\phi\,(=\phi^\dagger)$; a massless scalar field representative of the Hawking radiation.
- ψ ; a matter field contained in the particle detector.
- $x(\tau)$; the orbit of the detector, where τ is its proper time.
- $\mathcal{H}_{int} = -c\,\phi\,\psi$; the interaction Hamiltonian density, where c is the coupling constant.

Hereafter, we set c be small ($c \ll 1$) and consider the detection process up to the first order perturbation about c. Further, in order to avoid the volume divergence, we set the (in-going) mode function f_p of ϕ at the initial time (past null infinity) be a wave packet [3],

$$\begin{aligned} f_{p,l,m} &= \int_0^\infty d\omega\, \frac{W_p(\omega)}{\sqrt{4\pi\omega}\, r}\, e^{-i\,\omega\, v}\, Y_{l,m}(\theta,\varphi) \\ W_p(\omega) &= \frac{1}{\sqrt{\delta\omega}}\, e^{i\,v_0\,\omega}\, \Theta(\omega - p\,\delta\omega)\,\Theta((p+1)\delta\omega - \omega)\,, \end{aligned}$$

where Θ is a step function, p is an integer, v is the in-going null coordinate, v_0 is the peak position of this packet. The frequency of this packet is roughly given by $\Omega = p\,\delta\omega$. We omit the quantum numbers (l,m) due to the spherical symmetry.

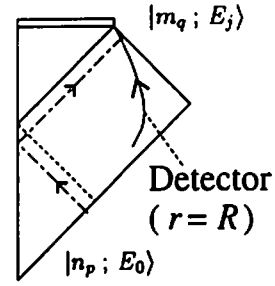

3 Detection probability

At a remote past (initial time), let the detector's field ψ be in its ground state of energy E_0, $|E_0\rangle$, and the radiation field ϕ be in an excited state $|n_p\rangle$ which has n particles at the state of the quantum number p. We denote this initial state as $|n_p\,;\,E_0\rangle$. Then at the remote future (future infinity), the detector field ψ is excited to a state $|E_j\rangle$ due to the interaction $\mathcal{H}_{int}$ while the radiation field ϕ makes a transition to another state $|m_q\rangle$. We denote this final state as $|m_q\,;\,E_j\rangle$. As explained in detail in the reference [2], the amplitude for this detection process is given by

$$A_j = i\langle E_j\,;\,m_q|\, \int_{-\infty}^{\infty} d\tau \int_V d^3x\, \mathcal{H}_{int}(\tau)\ |n_p\,;\,E_0\rangle\,,$$

where V is the volume of the detector, and $\mathcal{H}_{int}(\tau) = -c\,\phi(x(\tau))\,\psi(x(\tau))$. Therefore the detection probability at the energy level E_j becomes

$$P_j(n_p) \;=\; \sum_{\text{all states of }\phi} |A_j|^2 \;=\; c^2\,V^2\,|D_j|^2 \int_{-\infty}^{\infty} d\tau\, d\tau'\, e^{-i\,\Delta E_j\,(\tau-\tau')}\,\langle n_p|\,\phi(\tau)\,\phi(\tau')\,|n_p\rangle\,,$$

where, $D_j = \langle E_j|\,\psi(x(0))\,|E_0\rangle$ and $\Delta E_j = E_j - E_0$. Further note that our interest is in the deviation from the initially vacuum case, so it is enough for us to evaluate the deviation of the detection probabilities, $\Delta P_j(n_p) \equiv P_j(n_p) - P_j(0)$. Then by expanding ϕ with the mode set $\{f_p\}$, we obtain

$$\Delta P_j(n_p) = n_p\, \frac{c^2 V^2\,|D_j|^2\,|Y_{l,m}|^2}{2\pi R^2\, p}\, \Re\left[\int_{-\infty}^{\infty} d\tau\, d\tau'\, e^{-i\,\Delta E_j\,(\tau-\tau') + i\,\Omega\,(v(\tau)-v(\tau'))}\right]\,, \qquad (1)$$

where $\Re[z]$ is the real part of z. Because the detection of the particles has to be carried out at a remote future, we approximate the integrand in eq.(1) by its asymptotic form,

$$v(\tau) = -e^{\kappa(\tau - R^*)} ,$$

where κ is the surface gravity of the black hole, R^* is the tortoise coordinate at the detector and we used $t \simeq \tau$ at future null infinity (t is the Schwarzschild coordinate time). Note that this asymptotic form is derived by connecting the null coordinates at future null infinity and that at the past null infinity along the null geodesic propagating near the event horizon to infinity shown in the above figure [3]. Then, introducing the transformations $T = \tau + \tau'$ and $\delta\tau = \tau - \tau'$ into eq.(1), the integral about $\delta\tau$ can be carried out to give

$$\Delta P_j(n_p) \sim n_p \frac{c^2 V^2 |D_j|^2 |Y_{l,m}|^2}{2\pi R^2 p} \frac{4\, e^{\pi \Delta E_j/\kappa}}{\kappa} \int_{-\infty}^{\infty} dT\, \Re\left[K_{\nu_j}(z(T))\right] , \tag{2}$$

where $K_{\nu_j}(z(T))$ is the modified Bessel function, $\nu_j = i\, 2\, \Delta E_j/\kappa$ and $z(T) = 2\,\Omega\, e^{\kappa(R^* - T/2)}$. Here, for a large T, the integrand in the eq.(2) is approximated as

$$K_{\nu_j}(z(T)) \sim \sqrt{\frac{\pi\,\kappa}{2\,\Delta E_j \sinh(\pi|\nu_j|)}} \cos\left(\Delta E_j\, T + \text{const.}\right) .$$

Consequently, the deviation of the probabilities for the detection of particle at an arbitrary energy level E_j can be evaluated as

$$\int_0^{\infty} d(\Delta E_j)\, \Delta P_j(n_p) \sim \int_0^{\infty} d(\Delta E_j) \frac{1}{\sqrt{\Delta E_j}} \to \infty$$

where it is assumed that the detector has a continuous energy level. This denotes that the divergence of the particle number can not be resolved with introducing a particle detector.

4 Conclusion

As denoted by the previous section, the particle detector does not resolve the divergence of the number of particles in the Hawking radiation with an initially excited state. As mentioned in the section 1, the existence of the event horizon denotes that this divergence should not have physical meaning but should be renormalised to give the same result as the initially vacuum case gives. In fact, the mathematically correct treatment for the resolution of this divergence is explained in the reference [4]. But, without stepping into mathematical complication, we could learn some lessons for the usage of the quantum field theory in the presence of an event horizon;

- The initial state should be taken as the vacuum state with respect to the mode set prepared at the initial time.
- Avoid the particle interpretation but use the energy-momentum tensor for the initially excited case with respect to the mode set prepared at the initial time.

References

[1] R.M. Wald, Phys. Rev. **D13**, 3176 (1976).

[2] N.D. Birrell and P.C.W. Davies, *Quantum fields in curved space* (Cambridge University Press, 1982), §3.3.

[3] S.W. Hawking, Commun. Math. Phys. **43**, 199 (1975)

[4] R.M. Wald, *Quantum Field Theory in Curved Spacetime and Black Hole Thermodynamics* (The University of Chicago Press, 1994), §4.5

Collapse of Differentially Rotating Supermassive Stars

Motoyuki Saijo [1]

Department of Physics. Kyoto University, Kyoto 606-8502, Japan

Abstract

We investigate the gravitational collapse of rapidly rotating relativistic supermassive stars by means of a 3+1 hydrodynamical simulations in conformally flat spacetime of general relativity. We study the evolution of differentially rotating supermassive stars of $q \equiv J/M^2 \sim 1$ (J is the angular momentum and M is the gravitational mass of the star) from $R/M \sim 65$ (R is the circumferential radius of the star) to the point where the conformally flat approximation breaks down. We find that the collapse of the star of $q \gtrsim 1$, a radially unstable differentially rotating star form a black hole of $q \lesssim 1$. The main reason to prevent the formation of a black hole of $q \gtrsim 1$ is that quite a large amount of the angular momentum stays at the surface. We also find that the collapse is coherent and that it likely leads to the formation of a supermassive black hole with no appreciable disk nor bar. In the absence of nonaxisymmetric deformation, the collapse of differentially rotating supermassive stars are the promising sources of burst and quasinormal ringing waves in the Laser Interferometer Space Antenna.

There is increasing evidence that supermassive black holes (SMBHs) exist at the center of all galaxies, and that they are the sources which power active galactic nuclei and quasars. For example, VLBI observations of the Keplerian disk around an object in NGC4258 indicate that the central object has a mass $M \sim 3.6 \times 10^7 M_\odot$ and radius less than ~ 13 pc. Also, large numbers of observations are provided by the Hubble space telescope suggesting that SMBHs exist in galaxies such as M31 ($3 \times 10^7 M_\odot$), M87 ($1 \sim 2 \times 10^9 M_\odot$) and our own galaxy ($2.5 \times 10^6 M_\odot$). Although evidence of the existence of SMBHs is compelling, the actual formation process of these objects is still uncertain [1]. Several different scenarios have been proposed, some based on stellar dynamics, others on gas hydrodynamics, and still others which combine the processes. At present, there is no definitive observation as yet which confirms or rules out any one of these scenarios.

Here we discuss the collapse of a supermassive star (SMS) as one scenario of formation of SMBH. This subject is also interesting from the viewpoint of general relativity. The complete gravitational collapse of a body always results in a black hole (BH) rather than naked singularity, and the final state of the BH should go into the stationary one (the sequence of Kerr BHs) due to the uniqueness theorem. However there are several exceptions to this cosmic censor. BH uniqueness theorem requires that the stationary BH always rotates less than the maximum Kerr limit; i.e. $J/M^2 \lesssim 1$. Therefore, a collapse of a star with the critical value $J/M^2 \sim 1$ (J is the angular momentum, M is the total gravitational energy) may show us a violent phenomenon in general relativity and in gravitational wave physics.

The gravitational collapse of $J/M^2 \sim 1$ has been investigated in several decades. The pioneering study in this field was made by Nakamura [2]. He set up a differentially rotating star with radial velocity to induce the collapse. He found that when the initial star of J/M^2 is less than 0.95, apparent horizon forms, while when J/M^2 is bigger than 0.95, no apparent horizon forms. The following study has been done by Stark and Piran [3]. They set up a uniformly rotating $n = 1$ polytropic star and deplete pressure of 99 % to induce the collapse. They found that when J/M^2 is less than $a_{\rm crit} \pm 0.2$, BH formed. On the other hand, when J/M^2 is larger than $a_{\rm crit} \pm 0.2$, flattened disk formed ($a_{\rm crit} = 1.2$ for the case of 99 % pressure deplete). Finally Shibata [4] performed the collapse of differentially rotating $n = 1$ polytropic star. He also depleted the pressure of the star to induce the collapse. He found that when J/M^2 is less than 0.5, BH is formed when the rest mass is larger than the maximum mass on the J constant sequence, which is formed after the pressure is depleted. When J/M^2 is slightly less than 1, BH formed when

[1] E-mail: saijo@tap.scphys.kyoto-u.ac.jp

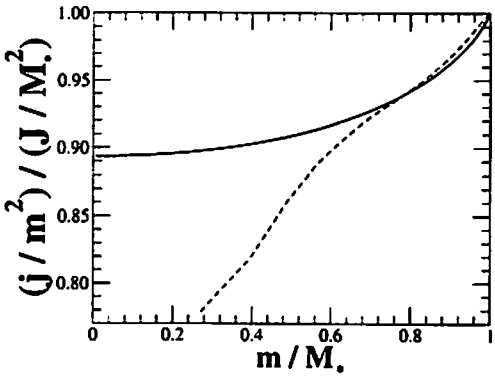

Figure 1: Profile of j/m^2 as a function of cylindrical mass for Model II (Table 2 of Ref. [7]). Solid and dashed line denotes the profile at $t = 0$ and $t = 5.64\ t_{\rm dyn}$, respectively. Note that j is the cylindrical angular momentum, $M_\bullet$ is the rest mass, $t_{\rm dyn}$ is the dynamical time defined in Ref. [7].

the rest mass is sufficiently larger than the maximum allowed mass on the pressure depleted J constant sequence. He also found, by comparing his results from polytropic evolution and from Γ-law evolution of the hydrodynamics, that shock heating prevents the prompt collapse to a BH under the condition of $J/M^2 \sim 1$.

The purpose of this paper is the following threefold. The first is to verify the nature of the gravitational collapse of a differentially rotating equilibrium star from the viewpoint of cosmic censor. If we collapse a star of $J/M^2 \gtrsim 1$, the star cannot directly form a BH of $J/M^2 \gtrsim 1$ because of cosmic censor. Therefore it is important to find the main cause to prevent a BH formation of $J/M^2 \gtrsim 1$. From the previous computational results, shock heating [4] and core bounce [2, 3, 4] are the dominant phenomena to prevent a star from forming a BH. However, all previous calculations have set up violent initial data sets, adding radial velocity or depleting pressure, to induce the collapse, it may cause abrupt transport of the energy. We therefore set up a mild, natural situation, that is the collapse of differentially rotating stars from the onset of radial instability, to focus on a graduate transport of the energy. Also, we compute the collapsing star in 3D to allow shock propagation and bar formation, if it occurs.

The second is to determine the final outcome of the collapse of differentially rotating SMSs. For the collapse of a uniformly rotating SMS from the onset of radially instability, Saijo et al. [5] studied 3D relativistic hydrodynamic simulation and found that the collapse is coherent and that it is likely to form a SMBH with no significant bar nor disk formation. Followup computation has been performed in 2D hydrodynamics in full general relativity and found that approximately 10 % of the total mass can form a disk, while approximately 90 % of that should form a BH [6]. When we consider the collapse of differentially rotating equilibrium stars, the final outcome has the possibility of differing from the collapse of uniform rotation because of the strong centrifugal force at the central core, which may prevent the prompt collapse. What is the final fate of the collapse? Does the star fragment due to the growth of the degree of differential rotation? Does the disk form during the collapse? Relativistic simulation can only answer these questions.

Finally, it is important to probe whether the collapse of differentially rotating SMSs could be promising sources of gravitational waves. Direct detection of gravitational waves by ground based and space based interferometers is of great importance in general relativity, in astrophysics, and in cosmology. The catastrophic collapse is one of the promising sources of gravitational waves. For a gravitational collapse of the star, there are two main reasons that prevent a prompt collapse of the star, which should produce gravitational waves at that time. One reason is core bounce and/or shock heating. Suppose gravitational force is balanced to the centrifugal force ($M/R^2 \sim R\Omega^2$) in Newtonian gravity, and the total mass and the angular momentum ($J \sim MR^2\Omega$) are conserved during the collapse. Note that Ω is the angular velocity,

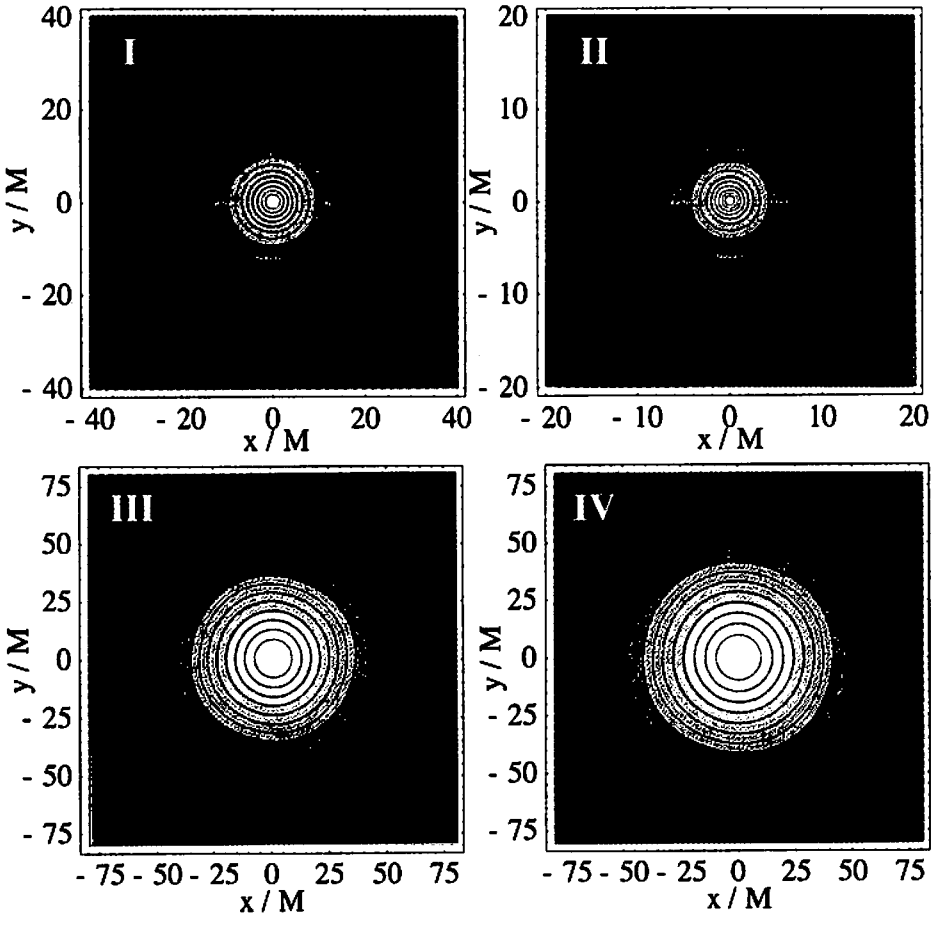

Figure 2: Final density contour in the equatorial plane of 4 differentially rotating stars. Model I, II, III, IV (Table 2 of Ref. [7]) is plotted at the parameter $(t/t_{\rm dyn}, \rho^*_{\rm max}) = (4.38,\ 1.37\times10^{-3})$, $(5.62,\ 2.16\times10^{-2})$, $(5.61,\ 9.13\times10^{-6})$, $(5.60,\ 5.33\times10^{-6})$, respectively. The contour lines denote coordinate densities $\rho^* = \rho^*_{\rm max}\times10^{-0.267(16-i)}(i = 1,\cdots,15)$.

R is the radius. We may estimate the bounce radius of the star in a global sense as $R_{\rm bounce}\approx M(J/M^2)^2$. Since the horizon radius is roughly the order of M, core bounce might take place for the case $J/M^2\gtrsim 1$, which prevents the violation of the cosmic censor. The other is bar formation. From the dimensional analysis, we can describe the rotational kinetic energy T and the gravitational binding energy W as $T\sim MR^2\Omega^2$ and $W\sim M^2/R$. We also accept the assumption that total mass and angular momentum are conserved during the collapse. We could estimate the radius of bar formation in terms of the ratio of the rotational kinetic energy to the gravitational binding energy as $R_{\rm bar}\approx(M/R)(T/W)^{-1}(J/M^2)^2$. Since the dynamical instability for a uniformly rotating, incompressible Newtonian star sets in at $T/W\sim0.27$ and for relativistic gravitation as $T/W\sim0.24-0.26$, bar formation takes place at the radius $R\sim4M$ for the collapse of $J/M^2\sim1$. Therefore, we may expect that the gravitational collapse of $J/M^2\sim1$ is a promising source of quasi-periodic gravitational waves.

We investigate the collapse of differentially rotating SMSs by means of hydrodynamic simulations in conformally flat approximation in general relativity. We start our collapse from $R/M\sim65$, where R is the circumferential radius of the star, to the point where conformally flat approximation breaks down. A more detailed discussion is presented in Ref. [7].

We find that the cosmic censor even holds for the gravitational collapse of radially unstable differentially rotating equilibrium SMS of $J/M^2\gtrsim1$. The main reason to prevent formation of a BH of $J/M^2\gtrsim1$

is that quite a large amount of the angular momentum stays at the surface, not core bounce and/or shock propagation and bar formation in our model. (See Fig. 1 for the final distribution of "J/M^2".) Note that even a thin disk near the surface of the star can hold relatively a large amount of the angular momentum if the radius is large. Although we should stop our numerical integration at the time when the BH is likely to form, it is interesting to investigate the accretion phase of the collapsing SMS. In any case, full general relativistic simulation will enlighten this phase.

The collapse of a differentially rotating, relativistically unstable SMS is coherent and likely leads to the formation of an SMBH. This situation is quite similar to the collapse of a uniformly rotating SMS [5, 6]. Combining these two results, we conclude that the collapse of an SMS is coherent within the order of dynamical time. However, this final outcome may depend on the equation of state of the star.

We cannot find any evidence of bar formation nor significant disk formation from the rotating collapse prior to BH formation. The phenomenon of no bar formation also comes from the fact that mass density collapses first to form a BH. In such case, T/W cannot scale in R^{-1} due to the growth of the degree of differential rotation, and as a fact the star of T/W cannot reach the dynamical instability point of ~ 0.27. (See Fig. 2 for the final coordinate density contour in the equatorial plane.)

Finally, rotating SMS collapse is a promising source of burst gravitational waves and of quasi-normal mode ringing waves. We can estimate the strength and the frequency of the wave burst and the wave quasinormal ringing emitted from this rotating collapse as

$$f_{\rm burst} \sim 3\times 10^{-2}\left(\frac{10^6 M_\odot}{M}\right)\left(\frac{M}{R}\right)^{3/2}[{\rm Hz}], \tag{1}$$

$$h_{\rm burst} \sim 1\times 10^{-18}\left(\frac{M}{10^6 M_\odot}\right)\left(\frac{1{\rm Gpc}}{d}\right)\left(\frac{M}{R}\right), \tag{2}$$

where Q is the quadrupole moment of the star and d is the distance from the observer. We set $R/M = 1$, a characteristic mean radius during BH formation. The characteristic frequency $f_{\rm QNM}$ and strength $h_{\rm QNM}$ of this radiation in rotating star collapse are

$$f_{\rm QNM} \sim 2\times 10^{-2}\left(\frac{10^6 M_\odot}{M}\right)[{\rm Hz}], \tag{3}$$

$$h_{\rm QNM} \sim 6\times 10^{-19}\left(\frac{\Delta E_{\rm GW}/M}{10^{-4}}\right)^{1/2}\left(\frac{2\times 10^{-2}[{\rm Hz}]}{f_{\rm QNM}}\right)^{1/2}\left(\frac{M}{10^6 M_\odot}\right)^{1/2}\left(\frac{1{\rm Gpc}}{d}\right), \tag{4}$$

where $\Delta E_{\rm GW}$ is total radiated energy. Since the main targets of LISA are gravitational radiation sources between 10^{-4} and 10^{-1} Hz, it is possible that LISA can search for the burst waves and the quasinormal ringing waves accompanying rotating SMS collapse and formation of a SMBH.

References

[1] M. J. Rees, in Black Holes in Binaries and Galactic Nuclei, edited by L. Kaper, E. P. J. van den Heurel, and P. A. Woudt (Springer-Verlag, New york, 2001), p. 351.

[2] T. Nakamura, Prog. Theor. Phys. **65**, 1876 (1981).

[3] R. F. Stark and T. Piran, Phys. Rev. Lett. **55**, 891 (1985); erratum ibid **56**, 97 (1986); T. Piran and R. F. Stark, in Dynamical Spacetimes and Numerical Relativity, edited by J. M. Centrella (Cambridge Univ. Press, Cambridge, 1986), p. 40.

[4] M. Shibata, Prog. Theor. Phys. **104**, 325 (2000).

[5] M. Saijo, T. W. Baumgarte, S. L. Shapiro, and M. Shibata, Astrophys. J. **569**, 349 (2002).

[6] M. Shibata and S. L. Shapiro, Astrophys. J. **572**, L39 (2002).

[7] M. Saijo, Submitted to Astrophys. J. (2003).

A criterion for direct black hole formation in rapidly rotating stellar collapse

Yu-ichirou Sekiguchi[1], Masaru Shibata

Graduate School of Arts and Sciences.
University of Tokyo, Komaba, Meguro-ku, Tokyo, 163-8092, Japan

Abstract

We study the process of the gravitational collapse of rotating relativistic polytropes ($\Gamma = 1.5$) which have a spin parameter of $q \equiv J/M^2 > 1$ in full general relativity. We predict the process of gravitational collapse the final outcome after the collapse, investigating an initial spin parameter distribution inside stars. Then we perform fully general relativistic simulations on assumption of axial and equatorial symmetry, in order to confirm our predictions. As a result of simulations we find that in contrast with the previous belief, even for stars with $q > 1$, the collapse proceeds to form an seed black hole at central region, and the seed black hole grows as ambient fluids accrete onto it. Thus we suggest a new criterion for direct black hole formation. Possible reasons for this discrepancy between our results and the previous results are also discussed. Furthermore we find that growth of J and M of the seed black hole proceeds approximately along the initial J-M distribution. Unfortunately, however, we cannot follow the final state of the collapse; for this, a black hole excision technique is absolutely necessary.

1 Introduction

One of the fundamental problems in numerical relativity is to explore the final fate after gravitational collapse of rotating stars. If mass of the stars is sufficiently large, the collapse will proceed completely, and a spacetime singularity will be formed according to singularity theorems. If the cosmic censorship conjecture suggested by Penrose is correct, any singularity should be surrounded by event horizon. Then the black hole uniqueness theorems of Carter and Robinson tell that a collapsed star may consequently settle down to a Kerr black hole. It is well known that in the Kerr spacetime, the singularity is covered by event horizon only if non-dimensional rotational parameter or spin parameter $q \equiv J/M^2$, where J and M are the angular momentum and the gravitational mass of the system, does not exceed unity. Otherwise the singularity is naked. This means that any black hole cannot have spin parameter of $q > 1$. The realistic progenitor of black holes, however, can have $q > 1$. Now, it is interesting to explore the final fate after gravitational collapse of rotating stars with $q > 1$. Numerical relativity is required to resolve this problem.

There are some studies concerned with the above problem on the assumption of axial symmetry[1]. These studies seem to suggest that $q \sim 1$ is a critical value for the black hole formation, and the final state after gravitational collapse of rotating stars with $q < 1$ is a rotating Kerr black hole with a negligible disk. The problem, however, is not sufficiently investigated for wide range of stiffness of the equations of state and for $q > 1$. In this article, therefore, we study the rotating stellar collapse with a *moderately* soft equations of state in full general relativity.

2 Initial Conditions and Predictions

Initial conditions are prepared in the following manner. First we give a spherical star in the marginally stable state using the polytropic equations of state with $\Gamma = 1.5$. Second an angular momentum distribution is imposed according to the rotation law $u^\varphi/u^t = \Omega = \Omega_0 \exp[-\varpi^2/(2R_0^2)]$, where $\varpi = \sqrt{x^2 + y^2}$.

[1] E-mail:sekig@provence.c.u-tokyo.ac.jp

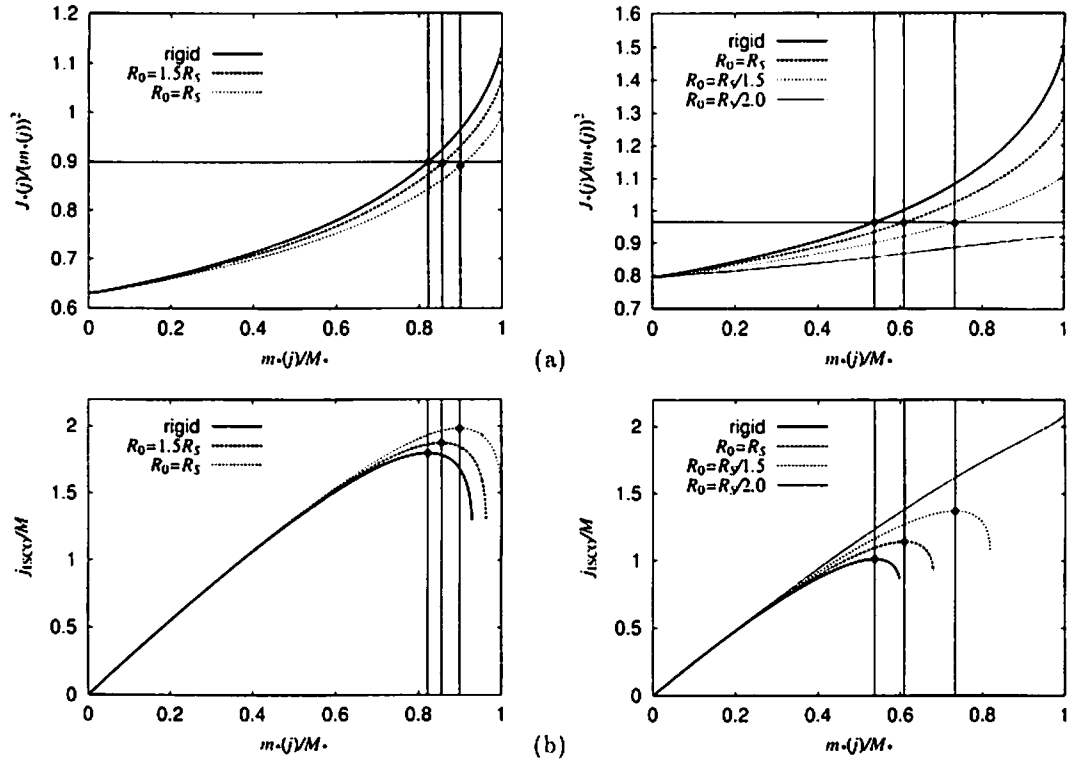

Figure 1: (a) The distribution of $q_*(j)$ as a function of $m_*(j)/M_*$. (b) $j_{\rm ISCO}/M$ as a function of $m_*(j)/M_*$. The Left figures are for $\Omega_0 = 7.0 \times 10^{-2}$, and the right for $\Omega_0 = 9.0 \times 10^{-2}$

Third, we reduce the pressure to a choose fraction f_P of its equilibrium pressure. Forth, the Hamiltonian constraint and the momentum constraint are reimposed and then the time evolution is set out.

Since a viscous effect is negligible during the collapse by assumption, the specific angular momentum $j \equiv hu_\varphi$ of each fluid element is conserved in an axisymmetric system. Then we define a rest mass distribution $m_*(j)$ and a specific angular momentum distribution as :

$$m_*(j) = 2\pi \int_{j'<j} \rho_* r^2 dr d(\cos\theta), \quad J_*(j) = 2\pi \int_{j'<j} \rho_* j' r^2 dr d(\cos\theta). \tag{1}$$

Now, we define a spin parameter

$$q_*(j) \equiv \frac{J_*(j)}{(m_*(j))^2}, \tag{2}$$

which may be approximately regarded as the parameter q of total fluid elements with the specific angular momentum less than j. Figure 1(a), which denote $q_*(j)$ as a function of $m_*(j)/M_*$, shows that the values of $q_*(j)$ at the center of stars (hereafter denoted as $q_{*,c}$) are smaller than unity although the whole values of $q_*(j)$ (hereafter denoted as $q_{*,w}$) are larger than unity. The collapse of rotating stars initially proceeds in a homologous manner. As collapse proceeds, however, inner region of stars collapse faster. Taking this and the distribution of $q_*(j)$ into account, we conjecture that it is possible that a seed black hole is formed at inner region, in which $q_*(j) \leq 1$, and subsequently grows as ambient fluids accrete onto it .

Now let us consider the innermost stable circular orbit (ISCO) around a black hole formed at the center. In order to estimate the value of $j_{\rm ISCO}$ and investigate the growth of the black hole, we assume that the spacetime metric can be instantaneously approximated by that of Kerr spacetime and regard $m_*(j)$ and $q_*(j)$ as mass and spin parameter of Kerr spacetime. On these approximation we can compute $j_{\rm ISCO}$ of the seed black holes [2] In figure 1(b) we show $j_{\rm ISCO}[m_*(j), q_*(j)]$ as a function of $m_*(j)/M_*$

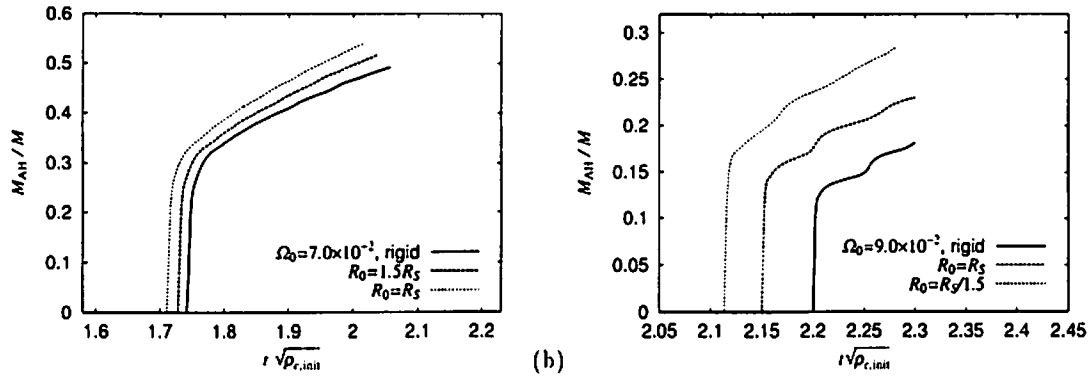

Figure 2: Evolution of apparent horizon mass $M_{\rm AH}$ for models of (a) $\Omega_0 = 7.0 \times 10^{-2}$ and (b) $\Omega_0 = 9.0 \times 10^{-2}$.

for our models. This figure shows that $j_{\rm ISCO}$ have a maximum (hereafter denoted as $j_{\rm ISCO,max}$). Thus a seed black hole will grow until j reaches $j_{\rm ISCO,max}$.

It should be addressed that for a fixed value of $q_{*,c}$ the corresponding value of $q_*(j_{\rm ISCO,max})$ is almost independent of the differential rotation parameter R_0, i.e., the value of $q_{*,w}$. This immediately indicates that the spin parameter of the final black hole is determined by the value of $q_{*,c}$ and independent of $q_{*,w}$. Furthermore it may suggest that whether black hole is formed or not is determined by $q_{*,c}$ independent of $q_{*,w}$ or q.

3 Results

To confirm the conjectures suggested the previous section, we performed simulations in full general relativity for various initial models we prepared, adopting a so-called Γ-law equation of state of the form

$$P = (\Gamma - 1)\rho\epsilon, \tag{3}$$

and set the adiabatic constant as $\Gamma = 1.5$. As a result of numerical simulations, we found that if $q_{*,c} \lesssim 0.9$, the collapse proceeds almost monotonically to form an apparent horizon irrespective of the value of $q_{*,w}$ even though $q_{*,w} > 1$. On the other hand, for $q_{*,c} \gtrsim 0.95$, we found that no black hole is formed, and the stars experience bounce and oscillation instead. For $0.9 \lesssim q_{*,c} \lesssim 0.95$, we cannot obtain accurate, well-converged results. From these results we suggest that $q \approx 1$ is inappropriate for a criterion for black hole formation and $q_{*,c} \approx 1$ will be more appropriate.

In figures 2 we show time evolution of apparent horizon mass $M_{\rm AH} \equiv \sqrt{A/16\pi}$, where A denotes the area of the apparent horizon. These figures indicate that process of black hole formation can be divided into two phases. One is a phase in which a seed black hole is formed (almost vertical part of the graphs). The other is a phase in which the seed black hole grows as the ambient fluid falls into it (the following monotonically increasing part). We have tried to reveal the final fate but we can not since computations crash in a duration $\sim 20M$ after an apparent horizon is first formed, due to the grid stretching around the black holes. To carry out a simulation beyond this, black hole excision techniques are absolutely necessary.

We also compute the total baron rest mass and the total angular momentum inside the apparent horizon (denoted as $m_{*,\rm AH}(j)$ and $J_{*,\rm AH}(j)$ respectively) and compare these with the initial $m_*(j)$-$J_*(j)$ distribution for $\Omega_0 = 5.0 \times 10^{-2}$ in figure 3(a). This figure shows that the initial distribution is an approximate evolutionary track of black hole and confirms the above conjecture.

Finally let us explain why $q \approx 1$ can be regarded as an threshold for black hole formation in previous works. Stark and Piran used an stiff ($\Gamma = 2$) equations of state. First note that since the configuration of stars with such a stiff equations of state is less centrally condensed and more homologous, the collapse of

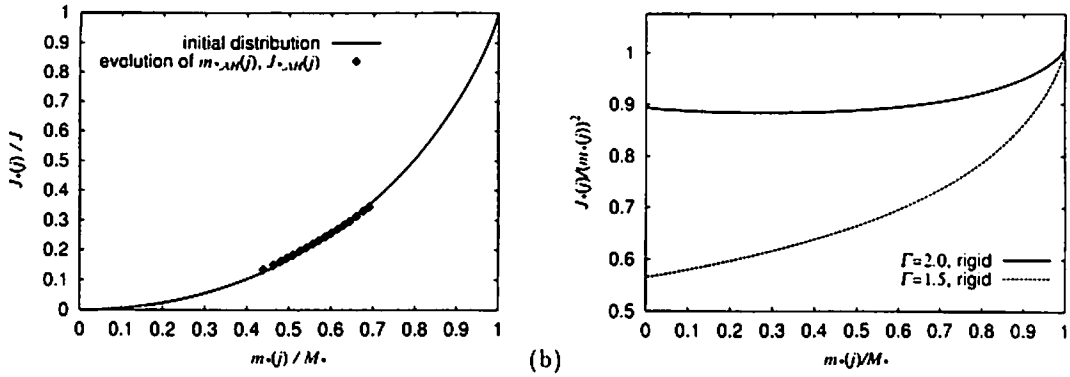

Figure 3: (a) Evolution of the baryon rest mass $m_{*,\mathrm{AH}}(j)$ and the angular momentum $J_{*,\mathrm{AH}}(j)$ inside the apparent horizon (filled diamonds) together with the initial $m_*(j)$-$J_*(j)$ distribution for $\Omega_0 = 5.0 \times 10^{-2}$, rigidly rotating case. (b) Comparison between the distribution of $q_*(j)$ for $\Gamma = 1.5$ spherical polytrope with rigid rotation imposed and for $\Gamma = 2.0$ spherical polytrope with rigid rotation imposed

rotating stars proceeds in a more homologous manner. Furthermore the distribution of $q_*(j)$ expressed as a function of $m_*(j)$ inside the star with stiff equations of state is rather flatter as indicated in figure3(b). indeed the difference between $q_{*,c}$ and $q_{*,w}$ is only $\approx 10\%$ in contrast with $\Gamma = 1.5$ case. These two lead them to their result that $q \approx 1$ is an threshold for black hole formation. Nakamura and his collaborators performed simulation for a highly differentially rotating star. The higher the degree of differential rotation becomes, the flatter the the distribution of $q_*(j)$ becomes, as indicated in figure1(a). This is why the global parameter q is regarded as the black formation criterion. Abrahams *et. al.* performed simulations for toroidal star clusters. Because of their toroidal nature, there is no central region to collapse first to form a black hole.

4 Summary

In summary, we have conjectured and then confirmed the followings : (I) Inner region of star which has $q_{*,c} < 1$ collapses first to form a seed black hole even if the whole value q exceeds unity. (II) The ambient fluids accrete onto the formed seed black hole. (III) The mass $m_*(j)$ and angular momentum $J_*(j)$ inside the black hole evolve along the initial $m_*(j)$-$J_*(j)$ distribution. (IV) Whether black hole is formed or not is determined by $q_{*,c}$ independent of q or $q_{*,w}$. We have conjectured but cannot confirmed : (V) The final outcome of dynamical collapse is a black hole surrounded by an appreciable disk.

We also suggest that $q_{*,c} \sim 1$ is a more appropriate threshold for black hole formation.

References

[1] T. Nakamura, Prog. Theor. Phys. **65**, 1876 (1981); **70**, 1144 (1983); T. Nakamura, K. Oohara, and Y. Kojima, Prog. Theor. Phys. Suppl. **90**, 1 (1987); R. F. Stark and T. Piran, Phys. Rev. Lett. **55**, 891 (1985); T. Piran and R. F. Stark in *Dynamical Spacetimes and Numerical Relativity*, edited by J. M. Centrella (Cambridge University Press, Cambridge, 1986); A. Abrahams, G. B. Cook, S. L. Shapiro, and S. A. Teukolsky, Phys. Rev. D **49**, 5153; M. Shibata, Prog. Theor. Phys. **104**, 325 (2000); M. Shibata, Astrophys. J. **595**, 992 (2003); M. Shibata and S. L. Shapiro, Astrophys. J. **572**, L39.

[2] J. M. Bardeen, W. H. Press, and S. A. Teukolsky, Astrophys. J. **178**, 347 (1972); S. L. Shapiro and S. A. Teukolsky, *Black Holes, White Dwarfs, and Neutron Stars* (Jon Wiely & Sons, New York, 1983).

Cosmic-ray antiprotons from primordial black holes in the braneworld

Yuuiti Sendouda[1][a], Kazunori Kohri[b], Shigehiro Nagataki[a,c], Katsuhiko Sato[a,c]

[a] *Department of Physics, Graduate School of Science, University of Tokyo, Bunkyo, Tokyo 113-0033, Japan*
[b] *Department of Earth and Space Science, Graduate School of Science, Osaka University, Toyonaka, Osaka 560-0043, Japan*
[c] *Research Center for the Early Universe, School of Science, University of Tokyo, Bunkyo, Tokyo 113-0033, Japan*

Abstract

We investigate cosmic-ray antiprotons emitted from the galactic primordial black holes (PBHs) in the Randall-Sundrum type-2 (RS2) braneworld. The BESS 1997 observation of cosmic-ray antiproton flux favors a large extra-dimension and particularly in the cases of large PBH abundance, it sets lower bounds on the size of the extra dimension above $\sim 10^{20}$ times the four-dimensional Planck length.

1 The PBH mass spectrum

The mass spectrum of PBHs formed by the inflationary density perturbation in the RS2 braneworld is deformed in comparison with that in the 4D case. The points are (i) slowing cosmological expansion in the so-called five-dimensional *ρ-square* era before the ordinary radiation-dominated phase, (ii) mass increase caused by *accretion* in the ρ-square phase, and (iii) slowing evaporation of 5D PBHs [1]. In short, forms of the mass spectrum are determined as follows.

(a) Initial spectrum is

$$\frac{\mathrm{d}n}{\mathrm{d}M_\mathrm{i}} = \begin{cases} \dfrac{3}{2^{17/4}\pi} \dfrac{a_\mathrm{eq}^3}{t_\mathrm{eq}^{3/4}(t_\mathrm{eq}+t_\mathrm{c})^{3/4}} \alpha_\mathrm{i}(M_\mathrm{i}) f^{1/8} l^{-3/8} M_\mathrm{i}^{-17/8} & \text{for } M_\mathrm{i} \lesssim f M_\mathrm{c} \\ \dfrac{3}{32\pi} \dfrac{a_\mathrm{eq}^3}{t_\mathrm{eq}^{3/4}(t_\mathrm{eq}+t_\mathrm{c})^{3/4}} \alpha_\mathrm{i}(M_\mathrm{i}) f^{1/2} M_\mathrm{i}^{-5/2} & \text{for } M_\mathrm{i} \gtrsim f M_\mathrm{c}, \end{cases} \tag{1}$$

where M_i is the initial mass of PBHs and α_i denotes the ratio of the mass density of PBHs with mass $\mathcal{O}(M_\mathrm{i})$ at their formation to the radiation energy density, l is the bulk AdS curvature radius, f is an $\mathcal{O}(1)$ parameter related with gravitational collapse of the density perturbation [1], and t_eq and a_eq are the time of matter-radiation equality and cosmological scale-factor at that time, respectively. A time $t_\mathrm{c} \sim l$ characterizes the end of the ρ-square phase and $M_\mathrm{c} \sim l$ is the horizon mass at that time. PBHs with mass below M_c are essentially five-dimensional objects. Note that hereafter all quantities are represented in the 4D Planck units.

(b) After accretion ends, the spectrum of lighter PBHs is deformed as

$$\frac{\mathrm{d}n}{\mathrm{d}M_\mathrm{p}} = \begin{cases} \dfrac{3}{2^{17/4}\pi} \dfrac{a_\mathrm{eq}^3}{t_\mathrm{eq}^{3/4}(t_\mathrm{eq}+t_\mathrm{c})^{3/4}} \alpha_\mathrm{i}[M_\mathrm{i}(M_\mathrm{p})] \left(1+8\mathcal{F}/9\right) 4^{\mathcal{F}} f^{1/8+\mathcal{F}} l^{-3/8+\mathcal{F}} M_\mathrm{p}^{-17/8-\mathcal{F}} & \text{for } M_\mathrm{p} \lesssim f M_\mathrm{c} \\ \dfrac{3}{32\pi} \dfrac{a_\mathrm{eq}^3}{t_\mathrm{eq}^{3/4}(t_\mathrm{eq}+t_\mathrm{c})^{3/4}} \alpha_\mathrm{i}(M_\mathrm{p}) f^{1/2} M_\mathrm{p}^{-5/2} & \text{for } M_\mathrm{p} \gtrsim f M_\mathrm{c}, \end{cases} \tag{2}$$

where $M_\mathrm{p} = (4fl)^{F/\pi} M_\mathrm{i}^{(\pi-F)/\pi}$ for $M_\mathrm{p} \lesssim fl$ (otherwise $M_\mathrm{p} = M_\mathrm{i}$), $M_\mathrm{i}(M)$ is its inverse, $F \in [0,1]$ is the accretion efficiency, and $\mathcal{F} \equiv 9F/[8(\pi - F)]$.

[1] E-mail:sendouda@utap.phys.s.u-tokyo.ac.jp

(c) Finally, taking their evaporation into consideration, we obtain the spectrum at present as

$$\frac{\mathrm{d}n}{\mathrm{d}M} = \begin{cases} \dfrac{3}{2^{17/4}\pi}\dfrac{a_{\rm eq}^3}{t_{\rm eq}^{3/4}(t_{\rm eq}+t_{\rm c})^{3/4}}\alpha_{\rm i}[M_{\rm i}(M_{\rm p})]\,(1+8\mathcal{F}/9)\,4^{\mathcal{F}} f^{1/8+\mathcal{F}} l^{-3/8+\mathcal{F}} & \\ \quad \times M\left[M^2+g_{\rm eff.5}t_0/l\right]^{-25/16-\mathcal{F}/2} & \text{for } M^* \gtrsim M \\ \dfrac{3}{32\pi}\dfrac{a_{\rm eq}^3}{t_{\rm eq}^{3/4}(t_{\rm eq}+t_{\rm c})^{3/4}}\alpha_{\rm i}[M_{\rm i}(M)] f^{1/2} & \\ \quad \times M\left[(g_{\rm eff.4}/g_{\rm eff.5})\,l\,(M^2-M_{\rm c}^2)+M_{\rm c}^3+g_{\rm eff.4}t_0\right]^{-3/2} & \text{for } fM_{\rm c} \gtrsim M \gtrsim M^* \\ \dfrac{3}{32\pi}\dfrac{a_{\rm eq}^3}{t_{\rm eq}^{3/4}(t_{\rm eq}+t_{\rm c})^{3/4}}\alpha_{\rm i}[M_{\rm i}(M)] f^{1/2} M^2\left[M^3+g_{\rm eff.4}t_0\right]^{-3/2} & \text{for } M \gtrsim fM_{\rm c}, \end{cases} \tag{3}$$

where M denotes PBH mass at present, M^* is defined as $M^* \equiv \sqrt{M_{\rm c}^2 - g_{\rm eff.5}t_0/l}$, $t_0 \approx 13.7$ Gyr is the present age of the Universe, and $g_{{\rm eff}.D}$'s are the degrees of freedom of the massless particles for each dimensionality.

2 Antiprotons

2.1 Primaries from the galactic PBHs

Let us consider *primary* antiprotons emitted from PBHs distributed over the Milky-Way halo. We apply the same form of the PBH density profile as a particular one of dark matter: $\rho_{\rm PBH}(r,z) = \rho_{\rm PBH}(R_\odot,0)(R_{\rm core}^2+R_\odot^2)/(R_{\rm core}^2+r^2+z^2)$, where $R_{\rm core} = 3$ kpc is the so-called core radius, $R_\odot$ is the distance from the galactic center to the solar system [2], and $\rho_\odot$ is the normalization at the Solar neighborhood. Quantities are expressed in the cylindrical coordinates (r,z,ϕ). We define the effective mass spectrum in the Galaxy as

$$\frac{\mathrm{d}\tilde{n}}{\mathrm{d}M}(r,z,M) = \mathcal{G}\frac{\rho_{\rm PBH}(r,z)}{\rho_{\rm PBH}(R_\odot,0)}\frac{\mathrm{d}n}{\mathrm{d}M}, \tag{4}$$

where $\mathcal{G} \sim 10^5$ represents the enhancement factor of matter density measured at the solar neighborhood relative to the extragalactic value [3], which is expected to be also valid for dark matter. As for hadron emission processes, we make use of PYTHIA/JETSET [4]. We denote the effective differential emission rate of antiprotons as $\mathrm{d}^2\tilde{N}_{\bar{p}}/\mathrm{d}E\mathrm{d}t$ defined in the following manner:

$$\frac{\mathrm{d}^2\tilde{N}_{\bar{p}}}{\mathrm{d}E\mathrm{d}t} = 2\sum_j \int_{E'=E}^{\infty} g_j \frac{\sigma_j(M,E')}{\exp(E'/T_{\rm H})\pm 1}\frac{\mathrm{d}g_{j\bar{p}}(E',E)}{\mathrm{d}E}\frac{E'^2}{2\pi^2}\mathrm{d}E', \tag{5}$$

where subscript j stands for quark or gauge boson species emitted from a black hole and runs $j = q,\bar{q},g,Z^0,W^\pm$. $\mathrm{d}g_{j\bar{p}}/\mathrm{d}E$ is the differential fragmentation ratio into antiproton for a particle j. We multiplied it by 2 taking antineutrons into account. We are now able to write down the differential antiproton emission rate from primordial black holes with the effective emission rate and mass spectrum as

$$q^{\rm pri}(r,z,E) = \int \frac{\mathrm{d}^2\tilde{N}_{\bar{p}}}{\mathrm{d}E\mathrm{d}t}(M.E)\frac{\mathrm{d}\tilde{n}}{\mathrm{d}M}(r,z,M)\mathrm{d}M. \tag{6}$$

It is almost obvious that $\bar{p}$'s are only emitted from PBHs with typical temperature $T_{\rm H} \gtrsim m_{\bar{p}} \sim 1$ GeV even though we took into consideration the hadronization processes in the quark-gluon jets. From now, we denote the mass corresponding with $T_{\rm H} \sim 1$ GeV as $M_{\rm GeV}$. We find $M_{\rm GeV} \sim 10^{15}\,(l/10^{19})^{-1}$ g for $l \gtrsim 10^{19}$, otherwise it retains the 4D value $\sim 10^{15}$ g. PBHs which have primordial mass $M_{\rm p} < M_{\rm GeV}$ have all evaporated away by now, so contributions to the antiproton flux are all from "evaporating tail" in the present mass spectrum. Thus we find that no braneworld signature in the antiproton flux is expected when $l \lesssim 10^{19}$ because then the shape of present mass spectrum around $M_{\rm GeV}$ does not deviate from that in the 4D case at all. On the other hand, when $l \gtrsim 10^{20}$, $M_{\rm GeV}$ is five dimensional and the effect of

the braneworld will be strongly reflected in the $\bar{p}$ flux. Under such a condition, the mass spectrum obeys a simple power-law in the range of our interest. Combining with another fact that the $\bar{p}$ emission rate per a PBH is completely determined by its Hawking temperature only, one reaches the conclusion: The spectral shape such as peak location of the resultant antiproton flux is unchanged even if l or F varies; the only possible modification is over-all fluctuation. We can write down the dependence of the $\bar{p}$ flux, $\Phi_{\bar{p}}$, on the mass spectrum as

$$\begin{aligned}\Phi_{\bar{p}} &\propto \int^{M_{\rm GeV}} \mathrm{d}M \frac{\mathrm{d}^2\tilde{N}}{\mathrm{d}E\mathrm{d}t}\frac{\mathrm{d}\tilde{n}}{\mathrm{d}M} \approx \int^{M_{\rm GeV}} \mathrm{d}M \frac{\mathrm{d}^2\tilde{N}}{\mathrm{d}E\mathrm{d}t}\frac{M}{M_{\rm GeV}}\frac{\mathrm{d}\tilde{n}}{\mathrm{d}M}\bigg|_{M_{\rm GeV}} \propto M_{\rm GeV}\frac{\mathrm{d}\tilde{n}}{\mathrm{d}M}\bigg|_{M_{\rm GeV}} \\ &\propto \mathcal{G}\alpha_{\rm i} l^{-13/16+3\mathcal{F}/2}\left[g_{\rm eff,5}t_0\right]^{-\mathcal{F}/2}. \end{aligned} \tag{7}$$

This is a decreasing function of l because the index p runs $-0.81 < p < -0.018$ according to $0 \leq \mathcal{F} \leq 0.53$. Thus we find that abundant PBHs set a *lower boundary* on the bulk curvature radius l. Taking a logarithm of Eq. (7), we obtain: $\log\Phi_{\bar{p}} \propto \log\left[\mathcal{G}\alpha_{\rm i}\right] - (13/16 - 3\mathcal{F}/2)\log l - (\mathcal{F}/2)\log\left[g_{\rm eff,5}t_0\right]$. When the flux reaches some upper bound, which means that $\alpha_{\rm i}$ also reaches its upper limit $\mathrm{LIM_i}$, l has the minimum value $l_{\rm min}$. Then the above proportionality becomes $\log\left[\mathrm{U.L.}\right] = \log\left[\mathcal{G}\mathrm{LIM_i}\right] - (13/16 - 3\mathcal{F}/2)\log l_{\rm min} - (\mathcal{F}/2)\log\left[g_{\rm eff,5}t_0\right]$, where U.L. is an undetermined constant which corresponds with upper limit flux. In principle U.L. cannot be determined unless propagation is solved. However, even without the knowledge of propagation, we can find more about the above relation. What is important is the fact that the only difference for each case is the over-all fluctuation of the antiproton flux. Therefore we can understand that U.L. is a universal value. Keeping it in mind, we modify the relation as

$$\log l_{\rm min} = \frac{\log[g_{\rm eff,5}t_0]}{3}\left[1 + \frac{48\log[\mathcal{G}\mathrm{LIM_i}/\mathrm{U.L.}]/\log[g_{\rm eff,5}t_0] - 13}{13 - 24\mathcal{F}}\right]. \tag{8}$$

Although we cannot determine in general the sign of the numerator in the right hand side, we are particularly interested in the cases of large PBH abundance, which means that the numerator is positive. For the same reason as the flux is a decreasing function of l, the denominator is always positive for $0 \leq \mathcal{F} \leq 0.53$. Therefore we finally find that the lower boundaries for l draw a family of hyperbolas expressed in Eq. (8).

2.2 Secondaries as the background

Besides exotic primaries, there is a firm background component for the cosmic-ray antiproton flux, i.e., the *secondaries*. The secondary antiprotons are produced in the galactic disc by reactions between nuclei in cosmic ray and interstellar gas such as $p\mathrm{H} \to \bar{p}X$ or $p\mathrm{He} \to \bar{p}X$. The high-energy cosmic-ray proton flux above a few GeV have been measured by observations [5] and their table-top result is well fitted by [6] $\Phi_p(R_\odot, E_p) = N\left(T_p/1\ \mathrm{GeV}\right)^{-\gamma}\ \mathrm{m^{-2}sr^{-1}s^{-1}GeV^{-1}}$ with parameterizations $N = 13249$ and $\gamma = 2.72$, where $T_p \equiv E_p - m_p$ is kinetic energy of protons. The radial distribution of the proton flux in the Galaxy may be crucial in the later analysis, but unfortunately we have little knowledge of it. So we assume it is constant of r and use the value at $r = R_\odot$. Finally we obtain the production rate of the secondary antiprotons in the galactic disc as

$$q^{\rm scc}(r, z=0, E_{\bar{p}}) = \int_{E_{\rm th}}^{\infty} \mathrm{d}E_p \left(4\pi\Phi_p(r, E_p)\right) \sum_{A=\mathrm{H,He}} n_A \frac{\mathrm{d}\sigma_{pA\to\bar{p}X}}{\mathrm{d}E_{\bar{p}}}(E_p, E_{\bar{p}}), \tag{9}$$

where the threshold of these interactions $E_{\rm th}$ is $8m_p$. We use $n_{\rm H} = 1\ \mathrm{cm^{-3}}$ and $n_{\rm He} = 0.1\ \mathrm{cm^{-3}}$ for the number densities of the targets [3].

2.3 Propagation of antiprotons in the Galaxy

At the beginning, we write down the full diffusion equation in the steady-state for the differential number density $N(r, z, E) \equiv \mathrm{d}n_{\bar{p}}/\mathrm{d}E$:

$$0 = \frac{\partial N}{\partial t} = \vec{\nabla}\cdot\left[K(E)\vec{\nabla} - \vec{V}_{\rm c}(r,z)\right]N(r,z,E) + \frac{\vec{\nabla}\cdot\vec{V}_{\rm c}(r,z)}{3}\frac{\partial}{\partial E}\left[\frac{p^2}{E}N(r,z,E)\right] - \Gamma(E)N(r,z,E)$$

$$+Q(r,z,E)+\frac{\partial}{\partial E}\left[-\{b_{\rm reacc}(E)+b_{\rm coll}(E)\}+\beta^2 K_{pp}(E)\frac{\partial}{\partial E}\right]N(r,z,E). \quad (10)$$

Undetermined quantities are the diffusion coefficient K_0, the Alfvén velocity $V_{\rm A}$, velocity of the convective wind $V_{\rm c}$, and the hight of the so-called diffusion halo L. We take into account the following energy gain/loss processes: Fermi acceleration, Coulomb scattering, ionization, adiabatic expansion, ant the so-called tertiary source. Throughout the analysis, cylindrically symmetric geometry of the Galaxy allows us to take a semi-analytical method. For detailed treatment, see [6, 7].

3 Result – allowed regions of braneworld parameters

The final project is to obtain upper limits on the abundance of PBHs for each braneworld parameter set (l, F). For each situation, we obtain the best-fit PBH abundance using BESS '97 data [8]. We show an example of spectra with brane parameters $l = 10^{31} l_4$ and $F = 1.0$ in the left panel of Fig. 1, and allowed regions for each $\mathcal{G}\alpha_{\rm i}$ in the right panel. The way of interpretation of the allowed regions are the same as that presented in our previous paper [9]; they are all lower limits on l.

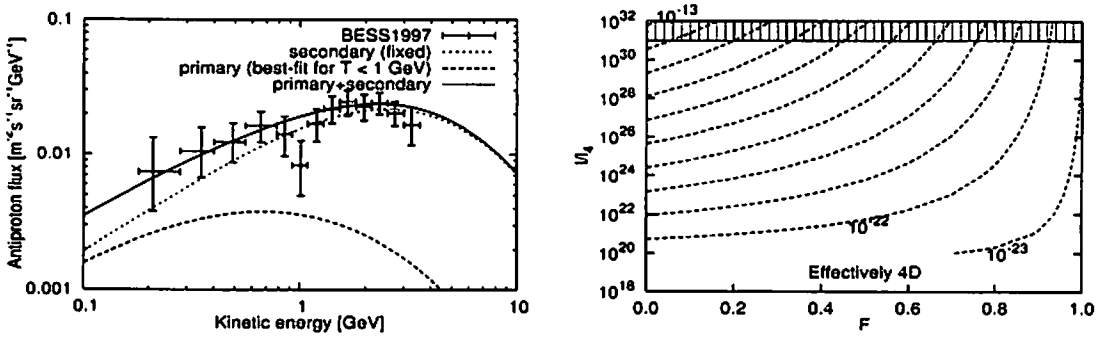

Figure 1: Left panel: Total antiproton flux with a typical braneworld parameter set $l = 10^{31} l_4$ and $F = 1.0$. Right panel: Boundaries of (l, F) in the braneworld-parameter plane for PBH abundance $\mathcal{G}\alpha_{\rm i} = 10^{-13}$–$10^{-23}$ (from top to bottom) using best-fit parameters. They are all lower boundaries of l, i.e., left-hand-side regions are allowed for each PBH abundance. l_4 is the 4D Planck length.

References

[1] R. Guedens, D. Clancy, and A.R. Liddle, Phys. Rev. D **66**, 043513 (2002); 083509 (2002); A.S. Majumdar, Phys. Rev. Lett. **90**, 031303 (2003).

[2] J.F. Navarro, C.S. Frenk, and S.D.M. White, Astrophys. J. **462**, 563 (1996); B. Moore *et al.*, Astrophys. J. **524**, L19 (1999).

[3] M.A. Gordon and W.B. Burton, Astrophys. J. **208**, 346 (1976).

[4] T. Tjöstrand, Comput. Phys. Commun. **82**, 74 (1994).

[5] W. Menn *et al.*, Astrophys. J. **533**, 281 (2000); T. Sanuki *et al.*, Astrophys. J. **545**, 1135 (2000); J. Alcaraz *et al.*, Phys. Lett. B**472**, 215 (2000); **490**, 27 (2000).

[6] F. Donato *et al.*, Astrophys. J. **563**, 172 (2001).

[7] D. Maurin, F. Donato, R. Taillet, and P. Salati, Astrophys. J. **555**, 585 (2001).

[8] S. Orito *et al.*, Phys. Rev. Lett. **84**, 1078 (2000).

[9] Y. Sendouda, S. Nagataki, and K. Sato, Phys. Rev. D **68**, 103510 (2003).

Effect of the Rotational Pressure on the Cylindrical Shell Collapse: A Model Analysis

Masafumi Seriu[1]

Department of Applied Physics, Faculty of Engineering, University of Fukui, Bunkyo 3-9-1, Fukui 910-8507, Japan

Abstract

We consider the dynamics of a cylindrical shell in the spacetime with cylindrical symmetry. We investigate a particular model of a cylindrical shell-collapse with rotational pressure, accompanying the radiation of gravitational waves and massless particles. The model has been introduced previously by other authors but has been awaiting for proper analysis. It is proved that, as far as the weak energy condition is satisfied outside the shell, the collapsing shell bounces back at some point irrespective of the initial conditions, and escapes from the singularity formation. This result of bouncing behavior is, contrary to the claim by the preceding authors, compatible with the behavior of other cylindrical shell-collapse models and confirms once again the essential importance of the rotational effect in the gravitational collapse.

1 Introduction

There are two possibilities for the fate of the gravitational contraction; (i) gravitational collapses (i.e. singularity formations) and (ii) regular evolutions (e.g. bouncing). The case (i) is further sub-classified into (i-a) black-hole formations and (i-b) naked-singularity formations.

Due to its highly nonlinear nature, investigations of the process as well as the fate of gravitational evolutions are not easy tasks, both conceptually and technically. Recent development of numerical methods is contributing to our deeper understanding on gravitational dynamics. It does not mean, however, the analytical investigations are becoming less important. On the contrary, the more the numerical results are obtained, the more variety of analytical model investigations is required for interpreting the numerical results and for attaining the whole understanding of the phenomena.

Just spherical collapses already show unexpectedly rich features, and investigations are still going on [1]. As the next natural direction of investigations, cylindrical collapses have also been analyzed considerably [2, 3, 4]. Evolutions of the elongated matter, such as cylindrical cases, are worth studying in view of the so-called "hoop conjecture" [2] along with the cosmic-censorship conjecture [5]. Indeed, logical consequence of the combination of both the conjectures implies that cylindrical models with reasonable matter content and natural initial conditions should evolve regularly without singularity formations.

In this respect, a particular cylindrical shell model recently discussed by Pereira and Wang [6, 7] cannot be overlooked. The model can be interpreted as indicating a shell filled with massless particles yielding rotational pressure. They claimed that there is a special class of solutions in which the shell develops into line-like singularity, which could possibly be naked. However their argument was not sophisticated enough and has been awaiting for proper analysis. Here we reanalyze their model and prove rigorously that, contrary to their claim, the shell always bounces back and never forms singularities as far as the weak energy condition is satisfied outside the shell [8]. This bouncing behavior is similar to the one found in the case of a cylindrical shell of counter-rotating dust particles [4] and suggests that the two conjectures [5, 2] mentioned above do not show any flaw as far as the present model is concerned.

2 The cylindrical shell model

Let us first consider a general metric of a cylindrical spacetime,

$$ds^2 = -T(t,r)^2dt^2 + R(t,r)^2dr^2 + Z(t,r)^2dz^2 + \Phi(t,r)^2d\phi^2 \ . \tag{1}$$

[1] E-mail:mseriu@edu00.f-edu.fukui-u.ac.jp

Suppose we study the dynamics of a shell Σ described by $r = \rho(t)$ in the spacetime defined by Eq.(1). Then the proper-time for an observer sitting on the shell is given by

$$d\tau^2 = T^2\,(1 - \frac{R^2}{T^2}\,\dot{\rho}^2)\,dt^2 = X^{-2}dt^2 \quad , \tag{2}$$

where the symbols $X := dt/d\tau$ and $^\circ := \partial_\tau$ frequently appear below. We note that $e_\tau := \partial_\tau$, $e_z := 1/Z\,\partial_z$ and $e_\phi := 1/\Phi\,\partial_\phi$ form a set of orthonormal bases on the shell Σ. Then the components of the extrinsic curvature of the shell are given by [8]

$$\begin{aligned} K_{e_\tau e_\tau} &= -\frac{R}{XT}\,\overset{\circ\circ}{\rho} - \frac{R}{2XT}\,\overset{\circ}{\rho}\,(\ln R^2)^\circ + \frac{1}{2}(T^2X^2 - 1)\,\partial_n(\ln R^2) + \frac{X^2T^2}{2}(X^2T^2 - 1)\,\partial_n(\ln T^2/R^2) \\ &\quad -\frac{XTR}{2}\,\overset{\circ}{\rho}\,(X^2T^2 - 1)\,(\ln T^2/R^2)^\circ \quad , \\ K_{e_z e_z} &= \partial_n \ln Z \quad , \quad K_{e_\phi e_\phi} = \partial_n \ln \Phi \quad , \quad \text{others} = 0 \quad . \end{aligned} \tag{3}$$

Let us now consider a particular model previously discussed by Pereira and Wang [6, 7]. In this model an interior flat spacetime (described by ds_-) and an exterior cylindrical spacetime (ds_+) are matched together at a timelike shell Σ ($r_\pm = \rho_\pm(t_\pm)$):

$$ds_-^2 = -dt_-{}^2 + dr_-{}^2 + dz_-{}^2 + r_-{}^2 d\phi_-{}^2 \tag{4}$$

$$ds_+^2 = e^{2\gamma(\xi)}(-dt_+{}^2 + dr_+{}^2) + dz_+{}^2 + r_+{}^2 d\phi_+{}^2 \quad , \tag{5}$$

where γ is a function of $\xi := t_+ - r_+$ only. It is seen that the C-energy [9] C and the Einstein tensor G_{ab} outside the shell are given by

$$C = \frac{1}{8\kappa}(1 - e^{-2\gamma}) \quad , \quad \mathrm{G}_{ab} = \frac{\gamma'}{\alpha^2 r_+} k_a k_b \quad ,$$

where $k_\mu = (\alpha,\ -\alpha,\ 0,\ 0)_{(tr z\phi)}$ is a null-vector and $\kappa := 8\pi G$ is the Einstein's gravitational constant. The formula for G_{ab} suggests that the model may be interpreted as describing a contracting shell accompanied by outward radiation of massless particles and gravitational waves [6]. Postulating the positivity of the C-energy and the weak energy condition, then, *the function γ is required to satisfy $\gamma \geq 0$ and $\gamma' \geq 0$.* We also note that the quantity X (see Eq.(2)) in the present model becomes $X := \frac{dt_+}{d\tau} = \frac{e^{-\gamma_+}}{\sqrt{1-\dot{\rho}_+^2}}$ so that $\dot{\rho}_+^2 < 1$. Looking at Eq.(5), it means that the radial velocity of the shell should be less than the light-velocity.[2]

Imposing the standard junction conditions [10], we get $\frac{dt_-}{dt_+} = \left\{(1 - e^{2\gamma_+})\dot{\rho}_+^2 + e^{2\gamma_+}\right\}^{1/2} =: \Delta$ along with

$$\kappa\epsilon = e^{-\gamma_+}\frac{\Delta - 1}{\rho_+\sqrt{1 - \dot{\rho}_+^2}} \tag{6}$$

$$\kappa p_z = \frac{e^{-\gamma_+}}{\Delta(1 - \dot{\rho}_+^2)^{3/2}}\left\{(\Delta - 1)\ddot{\rho}_+ - \gamma'_+\dot{\rho}_+(1 - \dot{\rho}_+)[(\Delta + 1)\dot{\rho}_+ + 1] - \Delta(\Delta - 1)\frac{1 - \dot{\rho}_+^2}{\rho_+}\right\} \tag{7}$$

$$\kappa p_\phi = \frac{e^{-\gamma_+}}{\Delta(1 - \dot{\rho}_+^2)^{3/2}}\left\{(\Delta - 1)\ddot{\rho}_+ - \gamma'_+\dot{\rho}_+(1 - \dot{\rho}_+)[(\Delta + 1)\dot{\rho}_+ + 1]\right\} \quad . \tag{8}$$

Here ϵ is identified with the energy density of the shell; p_z and p_ϕ are the pressures of the shell in the z- and ϕ-direction, respectively. It should be noted that $\gamma_+ > 0 \Longrightarrow \Delta > 1 \Longrightarrow \epsilon > 0$.

Now, setting in Eq.(7), $P_0 := \kappa p_z$ (constant), we finally get the *dynamical equation for the shell*,

$$\ddot{\rho}_+ = \Delta\frac{1 - \dot{\rho}_+^2}{\rho_+} + \gamma'_+\frac{\dot{\rho}_+}{\Delta - 1}(1 - \dot{\rho}_+)[(\Delta + 1)\dot{\rho}_+ + 1] + \frac{\Delta}{\Delta - 1}(1 - \dot{\rho}_+{}^2)^{3/2}e^{\gamma_+}P_0 \quad . \tag{9}$$

[2]Hereafter, the suffix + implies that the quantity is evaluated on the shell from the viewpoint of the exterior observer.

First of all, to get a rough idea for the behavior described by the above highly nonlinear dynamical equation, it may be helpful to show a typical numerical result. *Figure 1* indicates the evolutions of the shell-radius and the rotational pressure p_ϕ for the case $\gamma_+(r_+ - t_+) = \frac{1}{10^6}(r_+ - t_+ + 100)^3$ and $P_0 = 0$ with the initial conditions $\rho_+(0) = 0.1$ and $\dot{\rho}_+(0) = -0.999$ (i.e. very close to the light-velocity). We see that the rotational pressure prevents the shell from collapsing; the shell bounces back and its velocity approaches to the light-velocity after the bouncing.

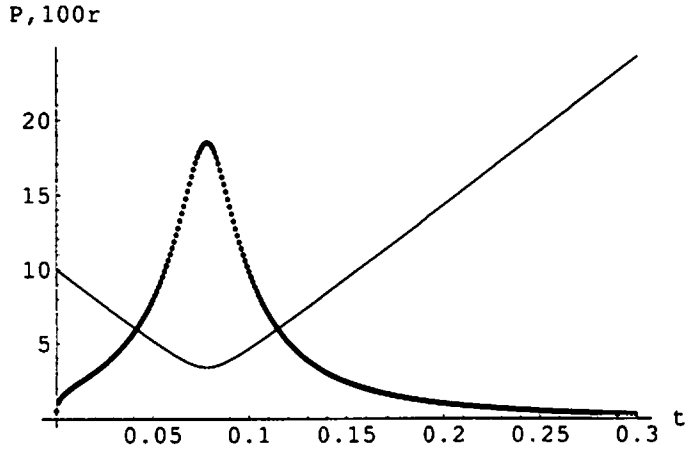

Figure 1: Typical evolutions of the shell-radius (thinner curve) and the rotational pressure p_ϕ (thicker curve). We have set $\gamma_+(r_+ - t_+) = \frac{1}{10^6}(r_+ - t_+ + 100)^3$. Initial conditions are $\rho_+(0) = 0.1$ and $\dot{\rho}_+(0) = -0.999$. The vertical line indicates $100\rho_+$ and p_ϕ, while the horizontal line indicates t_+.

The above typical numerical result arouses doubts for the claim by Pereira and Wang that a line-like singularity can form in this model. Indeed we can rigorously prove that the shell always bounces back and never forms a singularity in this model.

To avoid any confusion, let us set $V := -\dot{\rho}_+$ which takes the value $0 < V < 1$ in the contracting phase. Then Eq.(9) is rewritten as

$$\ddot{\rho}_+ = \Delta\frac{1-V^2}{\rho_+} + \gamma'_+\frac{V}{\Delta-1}(1+V)[(\Delta+1)V-1] + \frac{\Delta}{\Delta-1}(1-V^2)^{3/2}e^{\gamma_+}P_0 \ ,$$

where $\Delta = \left[V^2 + e^{2\gamma_+}(1-V^2)\right]^{1/2}$. Investigating the behaviors of the three terms on the right hand side (let us call them [[1]], [[2]] and [[3]] for brevity), we observe the following:

(i) The first term [[1]] produces a strong repulsive force, which prevents the shell from collapsing. The only possible exception may arise when V approaches to 1 faster than $\rho_+ \to 0$. Only in this case the term [[1]] can be negligible. Let us call, then, the phase-point $(V\ ,\ \rho_+) = (1,0)$ the *singularity-prone point.* However, it turns out that the other two terms become dominant near the singularity-prone point.

(ii) Indeed, the second term [[2]], which is an attractive force when V is small, turns to a repulsive force as $V \to 1$. (The function $f(V) := [(\Delta+1)V - 1]$ is a monotonic, increasing and continuous function; $f(0) = -1$, $f(1) = 1$; then $f(V)$ has only zero in (0,1). It means $f(V)$ turns from negative to positive as $V \to 1$.)

(iii) The third term [[3]] always causes a repulsive force; when $P_0 > 0$ (pressure in z-direction), it causes more acceleration in the expanding direction, and while $P_0 < 0$ (tension) causes less acceleration. (The term [[3]] does not change the whole dynamics so much.)

Setting $V = 1 - \delta$ ($\delta > 0$), it is easy to see that the three terms behave as [[1]] $\sim \frac{\delta}{\rho_+}$, [[2]] $\sim \frac{1}{\delta}$ and [[3]] $\sim \delta^{1/2}$. Thus even near the singularity-prone point, the shell always feels a very strong repulsive force and never collapses. We can refine the above argument to prove the following statements [8];

Lemma

Once the shell enters the core-region at $t = t_*$, it bounces back without reaching zero-radius. Indeed, $\rho_+(t)$ is bounded from below as

$$\rho_+(t) > \rho_+(t_*)\sqrt{1 - \dot{\rho}_+(t_*)^2} \quad .$$

(We define the *core-region* as a connected region in phase-space which contains a neighborhood of the singularity-prone point and where $[[2]] + [[3]] > 0$ is satisfied [8].)

Proof:

The claim follows from the fact that

$$\ddot{\rho} = \frac{1 - \dot{\rho}^2}{\rho} \quad , \text{with } \rho(0) = a \ , \ \dot{\rho}(0) = -b \ \ (a > 0, 1 > b > 0)$$

is exactly solved as $\rho(t) = ((t - ab)^2 + +a^2(1 - b^2))^{1/2}$, so that $\rho_+(t) > \rho(t) \geq a\sqrt{1 - b^2} > 0$.

Theorem

The shell never reaches $\rho_+ = 0$ irrespective of its initial conditions.

Proof:

If the shell could have ever reached $\rho_+ = 0$, it should have been through the core-region. However, *Lemma* indicates that this never happens.

3 Summary

We have investigated a particular model of a cylindrical shell-collapse with rotational pressure. Contrary to the claim by the preceding authors, as far as the weak energy condition is satisfied outside the shell, the collapsing shell always bounces back at some point irrespective of the initial conditions, and escapes from the singularity formation. This bouncing behavior is compatible with the results of other cylindrical shell-collapse models and confirms once again the essential importance of the rotational effect in the gravitational collapse.

This work has been supported by the Japan Ministry of Education, Culture, Sports, Science and Technology with the grant #14740162.

References

[1] For the basic accounts on the spherical collapses, see, e.g. P.S. Joshi, *Global Aspects in Gravitation and Cosmology* (Clarendon, Oxford, 1993).

[2] K. S. Thorne, in *Magic Without Magic: John Archibald Wheeler* (J. Klauder (ed.), Freeman, San Francisco, 1972), p.1.

[3] S. L. Shapiro and S. A. Teukolsky, Phys. Rev. Lett. **66**, 994 (1991).

[4] T. A. Apostolatos and K. S. Thorne, Physical Review D**46**, 2435 (1992).

[5] R. Penrose, Riv. Nuovo Cimento 1 (Numero Special), 252 (1969).

[6] P. R. C. T. Pereira and A. Wang, Physical Review D**62**, #124001 (2000).

[7] P. R. C. T. Pereira and A. Wang, Physical Review D**67**, #129902(E) (2003).

[8] M. Seriu, submitted for publication.

[9] K. S. Thorne, Phys. Rev. **138**, B251 (1965).

[10] W. Israel, Il Nuovo Cimento **B44**, 1 (1966); **B48**, 463(E) (1967).

A Novel Approach to Braneworld

Jiro Soda [1], Sugumi Kanno [2]

Department of Physics, Kyoto University, Kyoto 606-8501, Japan

Abstract

Evaluating Kaluza-Klein (KK) corrections is indispensable to test the braneworld scenario. In this report, we propose a novel symmetry approach to an effective 4-dimensional action with KK corrections for the Randall-Sundrum two-brane system.

1 Introduction

It is generally believed that the singularity problem of the cosmology can be resolved in the context of the superstring theory. It seems that the most clear prediction of the superstring theory is the existence of the extra-dimensions. This apparently contradicts our experience. Fortunately, the superstring theory itself provides a mechanism to hide extra-dimensions, which is the so-called braneworld scenario where the standard matter lives on the brane, while only the gravity can feel the bulk space-time. In the seminal paper by Randall and Sundrum, this scenario has been realized in a two-brane model [1]. Needless to say, it is important to test this new picture by the cosmological observations in the context of this model.

As the observable quantities are usually represented by the 4-dimensional language, it would be advantageous if we could find purely 4-dimensional description of the braneworld which includes the enough information of the bulk geometry, i.e. KK effects. In the case of the single-brane model, it is known that AdS/Conformal Field Theory (CFT) correspondence is a useful description of the braneworld [2]. There, KK effects are interpreted as the contribution of CFT matter. In the case of two-brane system, no such argument can be found in the literature. What we need for the two-brane system is a 4-dimensional description including KK effects like the AdS/CFT correspondence.

The purpose of this paper is to present a novel approach that utilize the conformal symmetry as a principle to determine the effective action. Our new method not only gives a simple re-derivation of known results [3], but also leads to a new result, i.e. the effective action with KK corrections.

The organization of this paper is as follows. In sec.II, we explain our method and re-derive known result. In sec.III, we derive new result, i.e. the KK corrected effective action. In the final section, we summarize our results and discuss possible applications and extension of our results. Throughout this paper, we take the unit $8\pi G = 1$.

2 Symmetry Approach

For simplicity, we concentrate on the vacuum two-brane system. Let us start with the 5-dimensional action for this system

$$S[\gamma_{AB}, g_{\mu\nu}, h_{\mu\nu}] \tag{1}$$

where γ_{AB}, $g_{\mu\nu}$ and $h_{\mu\nu}$ are the 5-dimensional bulk metric, the induced metric on the positive and the negative tension branes, respectively. Now, suppose to solve the bulk equations of motion and the junction condition on the negative tension brane, then formally we get the relation

$$\gamma_{AB} = \gamma_{AB}[g_{\mu\nu}] \ , \quad h_{\mu\nu} = h_{\mu\nu}[g_{\mu\nu}] \ . \tag{2}$$

By substituting relations (2) into the original action, in principle, the 4-dimensional effective action can be obtained as

$$S_{\rm eff} = S[\gamma_{AB}[g_{\mu\nu}], g_{\mu\nu}, h_{\mu\nu}[g_{\mu\nu}]] \ . \tag{3}$$

[1] E-mail:jiro@tap.scphys.kyoto-u.ac.jp
[2] E-mail:sugumi@tap.scphys.kyoto-u.ac.jp

Unfortunately, the above calculation is not feasible in practice. In the following, we propose a novel method to deduce the effective action.

Let us take the gradient expansion approach at the action level. At low energy, it seems legitimate to assume that the action can be expanded by the local terms with increasing orders of derivatives if one includes all of the relevant degrees of freedom [3]. In the two-brane system, the relevant degrees of freedom are nothing but the metric and the radion which can be seen from the linear analysis [4]. Hence, we assume the general local action constructed from the metric $g_{\mu\nu}$ and the radion Ψ as an ansatz. Therefore, we can write the action as

$$\begin{aligned} S_{\rm eff} &= \frac{1}{2}\int d^4x\sqrt{-g}\left[\Psi R - 2\Lambda(\Psi) - \frac{\omega(\Psi)}{\Psi}\nabla^\mu\Psi\nabla_\mu\Psi\right] \\ &+ \int d^4x\sqrt{-g}\left[A(\Psi)\left(\nabla^\mu\Psi\nabla_\mu\Psi\right)^2 + B(\Psi)\left(\Box\Psi\right)^2 + C(\Psi)\nabla^\mu\Psi\nabla_\mu\Psi\Box\Psi + D(\Psi)R\,\Box\Psi\right. \\ &\left. + E(\Psi)R\nabla^\mu\Psi\nabla_\mu\Psi + F(\Psi)R^{\mu\nu}\nabla_\mu\Psi\nabla_\nu\Psi + G(\Psi)R^2 + H(\Psi)R^{\mu\nu}R_{\mu\nu} + I(\Psi)R^{\mu\nu\lambda\rho}R_{\mu\nu\lambda\rho} + \cdots\right] \end{aligned} \tag{4}$$

where we have listed up all of the possible local terms which have derivatives up to fourth-order. This series will continue infinitely. We have the freedom to redefine the scalar field Ψ. In fact, we have used this freedom to fix the functional form of the coefficient of R. To determine other coefficient functions, we use the geometric method which yields, instead of the action, directly the effective equations of motion [5]

$$G_{\mu\nu} = T_{\mu\nu} + \pi_{\mu\nu} - E_{\mu\nu} \tag{5}$$

where $T_{\mu\nu}$ is the energy-momentum tensor of the matter and

$$\pi_{\mu\nu} = -\frac{1}{4}T_{\mu\lambda}T^{\lambda}{}_{\nu} + \frac{1}{12}TT_{\mu\nu} + \frac{1}{8}g_{\mu\nu}\left(T^{\alpha\beta}T_{\alpha\beta} - \frac{1}{3}T^2\right) . \tag{6}$$

Note that the projection of Weyl tensor $E_{\mu\nu}$ represents the effect of the bulk geometry. For the vacuum brane which we are considering, this reduces to

$$G_{\mu\nu} = -E_{\mu\nu} - \lambda g_{\mu\nu} , \tag{7}$$

where we have renormalized the cosmological constant λ so that it includes the quadratic part of the energy-momentum tensor. One defect of this approach is that $E_{\mu\nu}$ is not known except for the following property

$$E^{\mu}{}_{\mu} = 0 . \tag{8}$$

For the isotropic homogeneous universe, Eq. (8) has sufficient information to deduce the cosmological evolution equation. For general spacetimes, however, this traceless condition is not sufficient to determine the evolution of the braneworld. However, combination of the geometric approach and the gradient expansion approach determines the effective action. Now, we explain our method. We have introduced the radion explicitly in the gradient expansion approach. While the radion never appears in the geometric approach, instead $E_{\mu\nu}$ is induced as the effective energy-momentum tensor reflecting the effects of the bulk geometry. Notice that the property (8) implies the conformal invariance of this effective matter. Clearly, both approaches should agree to each other. Hence, the radion must play a role of the conformally invariant matter $E_{\mu\nu}$. This symmetry requirement gives a stringent constraint on the action, more precisely, the conformal symmetry (8) determines radion dependent coefficients in the action (4).

Let us illustrate our method using the following truncated action

$$S_{\rm eff} = \frac{1}{2}\int d^4x\sqrt{-g}\left[\Psi R - 2\Lambda(\Psi) - \frac{\omega(\Psi)}{\Psi}\nabla^\mu\Psi\nabla_\mu\Psi\right] , \tag{9}$$

which is nothing but the scalar-tensor theory with coupling function $\omega(\Psi)$ and the potential function $\Lambda(\Psi)$. Note that this is the most general local action which contains up to the second order derivatives

and has the general coordinate invariance. First, we must find $E_{\mu\nu}$. The above action gives the equations of motion for the metric as

$$G_{\mu\nu} = -\frac{\Lambda}{\Psi}g_{\mu\nu} + \frac{1}{\Psi}\left(\nabla_\mu\nabla_\nu\Psi - g_{\mu\nu}\Box\Psi\right) + \frac{\omega}{\Psi^2}\left(\nabla_\mu\Psi\nabla_\nu\Psi - \frac{1}{2}g_{\mu\nu}\nabla^\alpha\Psi\nabla_\alpha\Psi\right) . \tag{10}$$

The right hand side of this Eq. (11) should be identified with $-E_{\mu\nu} - \lambda g_{\mu\nu}$. Hence, the condition $E^\mu{}_\mu = 0$ becomes

$$\Box\Psi = -\frac{\omega}{3\Psi}\nabla^\mu\Psi\nabla_\mu\Psi + \frac{4}{3}\left(\Lambda - \lambda\Psi\right) . \tag{11}$$

This is the equation for the radion Ψ. However, we also have the equation for Ψ from the action as

$$\Box\Psi = \left(\frac{1}{2\Psi} - \frac{\omega'}{2\omega}\right)\nabla^\alpha\Psi\nabla_\alpha\Psi + \frac{\Psi}{2\omega}R - \frac{\Psi}{\omega}\Lambda' , \tag{12}$$

where the prime denotes the derivative with respect to Ψ. In order for these two Eqs. (12) and (13) to be compatible, Λ and ω must satisfy

$$\frac{1}{2\Psi} - \frac{\omega'}{2\omega} = -\frac{\omega}{3\Psi} , \quad \frac{4}{3}\left(\Lambda - \lambda\Psi\right) = \frac{\Psi}{\omega}\left(2\lambda - \Lambda'\right) , \tag{13}$$

where we used $R = 4\lambda$ which comes from the trace part of Eq. (7). Eqs. (14) and (15) can be integrated as

$$\Lambda(\Psi) = \lambda + \lambda\beta\left(1-\Psi\right)^2 , \quad \omega(\Psi) = \frac{3}{2}\frac{\Psi}{1-\Psi} , \tag{14}$$

where the constant of integration β represents the ratio of the cosmological constant on the negative tension brane to that on the positive tension brane [3]. Here, one of constants of integration is absorbed by rescaling of Ψ. In doing so, we have assumed the constant of integration is positive. The case of negative signature corresponds to the negative tension brane. In other words, we can also describe the negative tension brane in this method.

Thus, we get the effective action

$$S_{\rm eff} = \int d^4x\sqrt{-g}\left[\frac{1}{2}\Psi R - \frac{3}{4(1-\Psi)}\nabla^\mu\Psi\nabla_\mu\Psi - \lambda - \lambda\beta(1-\Psi)^2\right] . \tag{15}$$

This completely agrees with the previous result [3]. Surprinsingly, our simple symmetry approach has determined the action completely.

3 KK corrections

Let us extend the result in the previous section to the higher order case. We have already determined the functions $\Lambda(\Psi)$ and $\omega(\Psi)$. From the linear analysis, the action in the previous section is known to come only from zero modes. Hence, one can expect the other coefficients in the action (4) represent the effects of KK-modes.

Now we impose the conformal symmetry on the fourth order derivative terms in the action (4) as we did in the previous section. Starting from the action (4), one can read off the equation for the metric and hence $E_{\mu\nu}$ can be identified. The compatibility condition between $E^\mu{}_\mu = 0$ and the equation for the radion Ψ leads to a set of equations which seems to be over constrained. Nevertheless, one can find solutions consistently. Thus, we find the 4-dimensional effective action with KK corrections as [6]

$$\begin{aligned} S_{\rm eff} \;=\; & \int d^4x\sqrt{-g}\left[\frac{1}{2}\Psi R - \frac{3}{4(1-\Psi)}\nabla^\mu\Psi\nabla_\mu\Psi - \lambda - \lambda\beta(1-\Psi)^2\right] \\ & + \ell^2\int d^4x\sqrt{-g}\left[\frac{1}{4(1-\Psi)^4}\left(\nabla^\mu\Psi\nabla_\mu\Psi\right)^2 + \frac{1}{(1-\Psi)^2}\left(\Box\Psi\right)^2 + \frac{1}{(1-\Psi)^3}\nabla^\mu\Psi\nabla_\mu\Psi\Box\Psi\right. \\ & \left. + \frac{2}{3(1-\Psi)}R\Box\Psi + \frac{1}{3(1-\Psi)^2}R\nabla^\mu\Psi\nabla_\mu\Psi + gR^2 + hR^{\mu\nu}R_{\mu\nu}\right] . \end{aligned} \tag{16}$$

Because of the existence of the Gauss-Bonnet topological term, we can omit the square of Riemann tensor without losing the generality. The constants g and h can be interpreted as the variety of effects of the bulk gravitational field.

4 Conclusion

We have established a novel symmetry approach to an effective 4-dimensional action with KK corrections. This is done by combining the low energy expansion of the action and the geometric approach. Our result supports the smoothness of the collision process of two branes advocated in the ekpyrotic (cyclic) model and born-again model. Not only our result can be used to assess the validity of the low energy approximation, but also has a potential to make concrete predictions to be compared with observations.

As to the cosmological applications, it is important to recognize that our action can describe the inflation. Cosmological perturbations [7] are now ready to be studied. In fact, our result provides the basis of the prediction of CMB spectrum with KK corrections.

The black hole solutions with KK corrections are also interesting subjects. If we truncate the system at the lowest order, the static solution is Schwartzshild black hole with a trivial radion which corresponds to the black string in the bulk. The Gregorry-Laflamme instability occurs when the wavelength of KK modes exceeds the gravitational length of the black hole [8]. Clearly, the lightest KK mode is important and this mode is already included in our action, hence it would be interesting to investigate if the Gregory-Laflamme instability occurs or not within our theory [9, 10].

Acknowledgements
The authors would like to thank Kei-ichi Maeda for useful comments. This work was supported in part by Grant-in-Aid for Scientific Research Fund of the Ministry of Education, Science and Culture of Japan No. 155476 (SK) and No.14540258 (JS).

References

[1] L. Randall and R. Sundrum, Phys. Rev. Lett. **83**, 3370 (1999) [arXiv:hep-ph/9905221].

[2] S. S. Gubser, Phys. Rev. D **63**, 084017 (2001) [arXiv:hep-th/9912001];

[3] S. Kanno and J. Soda, Phys. Rev. D **66**, 083506 (2002) [arXiv:hep-th/0207029]; S. Kanno and J. Soda, Phys. Rev. D **66**, 043526 (2002) [arXiv:hep-th/0205188].

[4] J. Garriga and T. Tanaka, Phys. Rev. Lett. **84**, 2778 (2000) [arXiv:hep-th/9911055].

[5] T. Shiromizu, K. Maeda and M. Sasaki, Phys. Rev. D **62**, 024012 (2000) [arXiv:gr-qc/9910076].

[6] S. Kanno and J. Soda, arXiv:hep-th/0312106.

[7] D. Langlois, Phys. Rev. Lett. **86**, 2212 (2001) [arXiv:hep-th/0010063]; H. Kodama, A. Ishibashi and O. Seto, Phys. Rev. D **62**, 064022 (2000) [arXiv:hep-th/0004160]; C. van de Bruck, M. Dorca, R. H. Brandenberger and A. Lukas, Phys. Rev. D **62**, 123515 (2000) [arXiv:hep-th/0005032]; K. Koyama and J. Soda, Phys. Rev. D **62**, 123502 (2000) [arXiv:hep-th/0005239]; D. Langlois, R. Maartens, M. Sasaki and D. Wands, Phys. Rev. D **63**, 084009 (2001) [arXiv:hep-th/0012044]; K. Koyama and J. Soda, Phys. Rev. D **65**, 023514 (2002) [arXiv:hep-th/0108003].

[8] R. Gregory and R. Laflamme, Phys. Rev. Lett. **70**, 2837 (1993) [arXiv:hep-th/9301052].

[9] T. Tamaki, S. Kanno and J. Soda, arXiv:hep-th/0307278.

[10] S. Kanno and J. Soda, arXiv:gr-qc/0311074.

Constraint on the EOS of quark matter by gravitational observation

Hajime Sotani[1], Kazunori Kohri[2], Tomohiro Harada[3]

[1] *Department of Physics, Waseda University, Okubo 3-4-1, Shinjuku, Tokyo 169-8555, Japan*

[2] *Department of Earth and Space Science, Graduate School of Science, Osaka University, Toyonaka, Osaka 560-0043, Japan*

[3] *Astronomy Unit, School of Mathematical Sciences, Queen Mary, Mile End Road, London E1 4NS, UK*

Abstract

We consider possibilities for obtaining information about the equation of state for quark matter by using future direct observational data on gravitational waves. We study the nonradial oscillations of both fluid and spacetime modes of pure quark stars. If we observe the f and the lowest $w_{\rm II}$ modes from quark stars, by using the simultaneously obtained radiation radius we can constrain the bag constant B with reasonable accuracy, independently of the s quark mass.

1 Introduction

Gravitational wave observation projects, such as the Laser Interferometric Gravitational Wave Observatory (LIGO), TAMA300, GEO600 and VIRGO, are making remarkable progress in sensitivity [1]. Among them, several interferometers are steadily developing today. Thus it will be possible for us to detect gravitational waves directly in the near future. It is believed that mergers of binary NS/NS, NS/BH, and BH/BH, or supernovae, and so on, can become strong sources of gravitational waves. After these violent events occur, compact objects may be left and may be turbulent. Then gravitational waves are emitted from them. At this time, these gravitational waves convey information on the source object. If these gravitational waves are directly detected on the Earth, it is possible to obtain some information about the sources. This research field is called "gravitational wave astronomy". In this field, there is an attempt to obtain information about properties of the equation of state (EOS) of the high density matter. This is one of the most important purposes of gravitational wave astronomy.

Gravitational waves are emitted by the nonspherical oscillation of compact objects. The oscillations are damped out as gravitational waves carry away the oscillational energy. Such oscillations are called quasinormal modes (QNMs). The QNMs have complex frequencies whose real and imaginary parts correspond to oscillational frequency and damping rate, respectively. For the QNMs of neutron stars, so far many authors have argued possibilities for determining the EOS in the high density region and/or for restricting the properties of neutron stars, such as radius R or mass M, by employing the observed gravitational wave of several nonradial modes [2]. On the other hand, recently, the radiation radius of the compact star RX J1856.5−3754 was estimated to be very small ($R_\infty = 3.8 - 8.2$ km) based on the deep Chandra LETG+HRC-S observations [3]. That is smaller than typical neutron star radii [4]. Thus they suggested that the X-ray source may be a quark star. As for gravitational waves emitted from quark stars, Sotani and Harada showed that the f and the lowest $w_{\rm II}$ modes depend strongly on the EOS of quark matter and the properties of quark stars, where the lowest $w_{\rm II}$ mode is the one which has the largest frequency among all $w_{\rm II}$ modes [5]. Then they pointed out the possibility of determining the EOS and/or the stellar properties. Furthermore, although w modes are also calculated, it was showed that w modes have little dependence on the EOS of quark matter. In their work, however, they assumed that the star is a pure quark star and that the EOS is described by a simple bag model which has only one parameter, i.e., the bag constant B. In general, there are a variety of parameters even within bag

[1]E-mail:sotani@gravity.phys.waseda.ac.jp
[2]E-mail:kohri@vega.ess.sci.osaka-u.ac.jp
[3]E-mail:T.Harada@qmul.ac.uk

models, e.g., the bag constant B, the strange quark mass m_s, the fine structure constant in QCD α_c, and so on. In particular, if the effects of nonvanishing strange quark mass m_s are taken into account, the structure of quark stars can be affected considerably [6]. In this situation, we compute the QNMs in the bag model used in [6] and investigate the possibility of restricting the model parameters by the observations of QNMs. In this study, we deal with only f and the lowest $w_{\rm II}$ modes in consideration of the results of [5].

2 Numerical Results

The QNMs are determined by solving the perturbation equations with appropriate boundary conditions. The details of the perturbation equations and the boundary conditions and the method of determination of QNMs are given in [5].

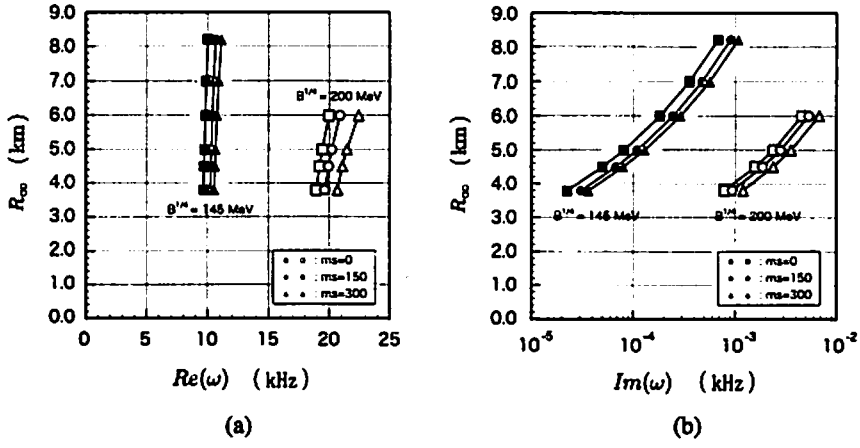

Figure 1: Radiation radius as a function of (a) frequency Re(ω) and (b) damping rate Im(ω) of f mode for $l = 2$. In each figure, the filled and open marks denote $B^{1/4} = 145$ MeV and 200 MeV, respectively.

2.1 f mode

Compared with the other QNMs, we might relatively easily detect the f mode, because its frequency and damping rate are approximately within the sensitivity band of gravitational wave interferometers, e.g., LIGO and so on. Therefore, first we discuss the possibility of constraining parameters of bag models by using the f mode data. From Fig. 1 (b) we see that the damping rate is very sensitive to the radiation radius, unlike the frequency in Fig. 1 (a). If we observe the damping rate of the f mode within 20 percent, the radiation radius can be determined within 10 percent as a function of B, independently of the value of m_s. On the other hand, from Fig. 1 (a) we see that if we observe the frequency within about 20 percent, for example, we can determine the value of B with reasonable accuracy by using the simultaneously obtained radiation radius from Fig. 1 (b). To demonstrate that, we investigate the dependence of the f mode on both the bag constant and the s quark mass when we fix the radiation radius as $R_\infty = 6.0$ km. In Fig. 2, we plot the contours of (a) frequency Re(ω) and (b) damping rate Im(ω) of the f mode for $l = 2$ in the ($B^{1/4}$, m_s) plane. The numbers on the curves denote the value of frequency Re(ω) or damping rate Im(ω) in units of kHz. We should note that each contour line is nearly parallel to the vertical axis in both Figs. 2(a) and (b). This implies that we can obtain a stringent constraint on the bag constant. Indeed, Fig. 2(a) shows that if the frequency of the f mode is detected within 20 percent, then we can determine the value of the bag constant within about 15 percent independently of the value of the s quark mass.

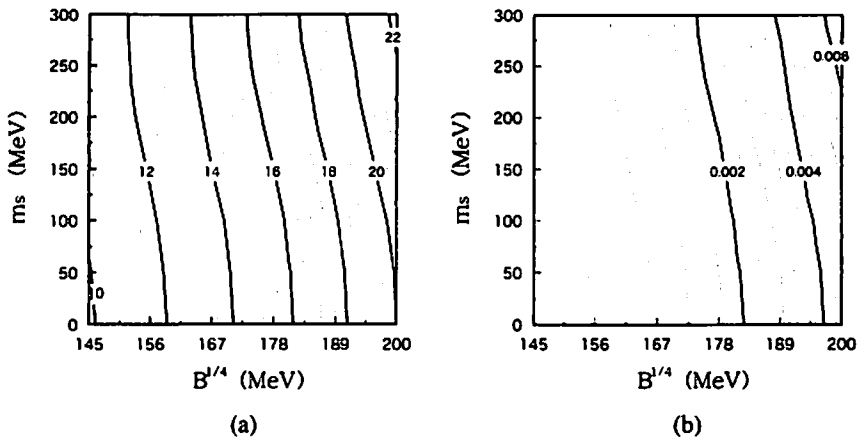

Figure 2: (a) Contours of frequency Re(ω) and (b) damping rate Im(ω) of f mode for $l = 2$ in ($B^{1/4}$, m_s) plane. Here we adopt the radiation radius as $R_\infty = 6.0$ km. The numbers with the curve denote the value of frequency Re(ω) or damping rate Im(ω) in units of kHz.

2.2 The lowest $w_{\rm II}$ mode

In general, there exist infinite number of w modes and several $w_{\rm II}$ modes for each l. However, because the lowest $w_{\rm II}$ mode is the one that is the most sensitive to parameters in a bag model, as was shown by numerical analysis in Ref. [5], we deal with only in the lowest $w_{\rm II}$ mode. Along with the case of the f mode, we plot the contour of the frequency and the damping rate of the lowest $w_{\rm II}$ mode in the ($B^{1/4}$, m_s) plane in Fig. 3. By using the lowest $w_{\rm II}$ mode, we are able to develop a similar argument as that discussed in the case of the f mode and get on independent constraint on the bag constant and s quark mass.

However, we should keep in mind that even if a large amount of energy is released through these modes, the accurate observation of the w and $w_{\rm II}$ modes may be difficult. That is because both the frequency and the damping rate of these modes are larger than the sensitivity ranges of gravitational wave interferometers [7]. Thus we would mainly use the observational data of the f mode to obtain information about the bag model parameters. Then we could subsidiarily use the data on the lowest $w_{\rm II}$ mode. It should be noted that, since Fig. 3 has similar features found in the f mode, even if we combine it with information from the f mode, we may not have strict constraints on both m_s and B, independently. There exist an essential degeneracy in f and the lowest $w_{\rm II}$ mode QNMs because the configuration of the contour of Fig. 2 is very similar to that of Fig. 3.

3 Conclusion

We have discussed how we can obtain information about the EOS of quark matter by using future observations of gravitational waves emitted from quark stars. In particular we have studied the EOS in bag models and assumed that the star is a pure quark star. We have computed the QNMs, i.e., the f and the lowest $w_{\rm II}$ modes, in the several quark star models. We have demonstrated that by comparing the results of theoretical computations with the observational data of the f mode and the lowest $w_{\rm II}$ modes we can obtain constraints on the bag constant B and s quark mass m_s.

If we have the damping rate, i.e., Im(ω), of the f mode within 20 percent, the radiation radius of the quark star can be determined within about 10 percent including the uncertainty of the s quark mass. Furthermore if we also obtain the frequency, i.e., Re(ω), of the f mode within 20 percent, the value of bag constant can be determined within about 15 percent, independently of the uncertainty of the s quark mass by using the simultaneously obtained radiation radius. Concerning the lowest $w_{\rm II}$ mode, we can also develop a similar argument as in the case of the f mode and get independent constraints

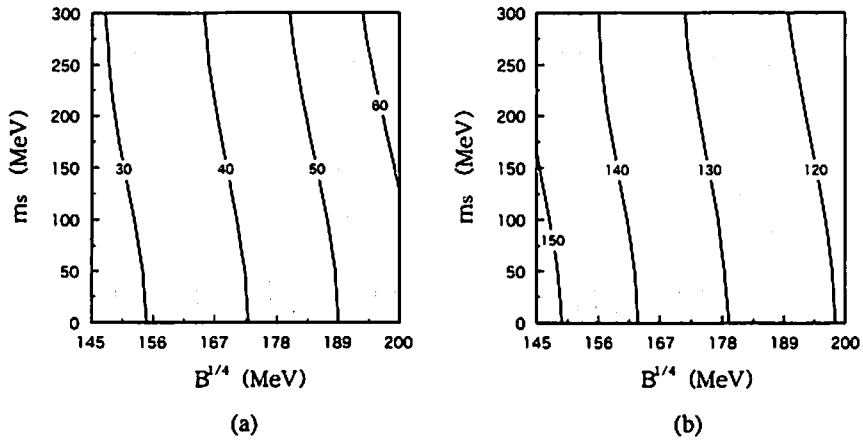

Figure 3: (a) Contours of frequency Re(ω) and (b) damping rate Im(ω) of the lowest $w_{\rm II}$ mode for $l = 2$ in ($B^{1/4}$, m_s) plane. Here we adopt the radiation radius as $R_\infty = 6.0$ km. The numbers with the curve denote the value of frequency Re(ω) or damping rate Im(ω) in units of kHz.

on the model parameters. However, note that it is relatively difficult to detect the lowest $w_{\rm II}$ mode by the future planned gravitational wave interferometers whose frequency ranges are not very sensitive to the lowest $w_{\rm II}$ mode. Therefore, such data will be subsidiarily used in statistical analyses. It should be also noted that there is a degeneracy in the dependence of f and the lowest $w_{\rm II}$ mode QNM complex frequencies on the bag model parameters, m_s and B. As for high-frequency gravitational waves, a dual type detector has been proposed, which would reach very good spectral strain sensitivities ($\sim 2\times10^{-23}$Hz) in a considerable broadband (between 1kHz and 3kHz) [8] and then open a new interesting window to the QNMs of compact objects.

As long as we have data with tolerable accuracy in future, we will be able to perform statistical analyses to fit them, and get constraints on both the bag constant and the s quark mass. If we have further information about the bag constant or the s quark mass by utilizing the EOS models based on future developments in an effective theory of QCD, such as perturbation theories or finite-temperature lattice data, we can constrain them more strictly. Including independent observations of radiation radius, e.g., sorts of X-ray observations, would also support us in infering the bag model parameters. QNMs from compact stars will be observed in the near future and deepen our understanding of hadron physics and QCD.

References

[1] C. Cutler and K. S. Thorne, in Proceedings of GR16, Durban, South Africa (World Scientific, Singapore, 2001)

[2] K. D. Kokkotas, and B. G. Schmidt, in *Living Rev. Rel.* **2**, 2 (Potsdam, Max Planck Inst., 1999).

[3] J. J. Drake, *et al.*, Astrophys. J. **572**, 996 (2002).

[4] J. M. Lattimer and M. Prakash, Astrophys. J. **550**, 426 (2001).

[5] H. Sotani and T. Harada, Phys. Rev. D **68**, 024019 (2003).

[6] K. Kohri, K. Iida and K. Sato, Prog. Theor. Phys. **109**, 765 (2003)

[7] N. Andersson, and K. D. Kokkotas, Phys. Rev. Lett. **77**, 4134 (1996).

[8] M. Cerdonio, *et al.*, Phys. Rev. Lett. **87**, 031101 (2001).

Spontaneous Baryogenesis in Flat Directions

Fuminobu Takahashi[1],

Research Center for the Early Universe (RESCEU), School of Science, The University of Tokyo, 7-3-1 Hongo, Bunkyo-ku, Tokyo 113-0033, Japan

Abstract

We present a new mechanism of spontaneous baryogenesis. Usually such mechanisms require a derivative coupling between a scalar field and baryon current. In our model, the scalar field instead derivatively couples to a current associated with some global symmetry $U(1)_Q$. In this case, baryogenesis is still possible provided that an interaction exists, which violates the baryon and $U(1)_Q$ symmetries simultaneously. As a concrete example, we discuss baryogenesis in a flat direction with neither baryon nor lepton charge.

Baryogenesis is one of the most important challenges in cosmology and particle physics. Sakharov proposed three conditions to realize baryogenesis [1]: (i) an interaction which actually violates baryon conservation, (ii) violation of C and CP symmetries, (iii) deviation from thermal equilibrium. Thus far many scenarios, which have been proposed, satisfy the above requirements. However, a spontaneous baryogenesis mechanism, which was proposed by Cohen and Kaplan, works even in thermal equilibrium [2] contrary to the above conditions. This is because, while Sakharov's conditions apply for the case where CPT symmetry is conserved, CPT symmetry is violated in the context of any spontaneous baryogenesis mechanism.

A spontaneous baryogenesis mechanism requires a derivative coupling between a scalar field a and a baryon current J_B^μ,

$$\mathcal{L}_{eff} = -\frac{\partial_\mu a}{f} J_B^\mu, \tag{1}$$

where f is a cut-off scale. The baryon current J_B^μ is given by

$$J_B^\mu = \sum_i B_i j_i^\mu, \tag{2}$$

where B_i and j_i^μ are respectively the baryon number and the usual number current of the i-th field. A nonzero value of $\partial_\mu a$ leads to spontaneous CPT violation since $\partial_\mu a$ is odd under CPT transformations. This enables spontaneous baryogenesis mechanisms to evade Sakharov's conditions. Assuming that a is homogeneous, the derivative interaction becomes

$$\mathcal{L}_{eff} = -\frac{\dot{a}}{f} n_B \equiv \sum_i \mu_i n_i, \tag{3}$$

where the dot denotes differentiation with respect to time, n_B is the baryon number density, and n_i is the number density of the i-th field. $\mu_i \equiv -\dot{a}B_i/f$ is an effective chemical potential for the i-th field, which creates a bias between baryons and anti-baryons. Then, according to the effective chemical potential, the baryon number density is induced while in thermal equilibrium,

$$n_B(t) = \sum_i B_i \frac{g_i \kappa_i T^3}{6} \left(\frac{\mu_i}{T} + O\left[\left(\frac{\mu_i}{T} \right)^3 \right] \right), \tag{4}$$

where g_i represents the degree of freedom of the corresponding fields, κ_i is 1 for fermions and 2 for bosons, and the summation should be taken for light fields in thermal equilibrium. In fact, baryon asymmetry is generated only when a baryon number violating interaction actually exists and is in thermal equilibrium. Thus, the final baryon asymmetry is determined at decoupling of the baryon number violating interaction.

[1] E-mail:fumi@resceu.s.u-tokyo.ac.jp

In the above example, a scalar field derivatively couples to the baryon current. However, in this Letter, we show that baryogenesis is still possible even if a scalar field derivatively couples not to baryon current, but to other currents such as the lepton current and/or the PQ current. Our basic idea is very simple. Assume that a scalar field derivatively couples to some global $U(1)_Q$ current which is not necessarily related to baryon current. Then, if an interaction exists and is in thermal equilibrium, which violates $U(1)_Q$ and baryon symmetries simultaneously, baryon asymmetry is generated in addition to the $U(1)_Q$ asymmetry through the spontaneous mechanism. This is because the ratio of $U(1)_Q$ charge to baryon charge must follow the ratio of violations of the interaction. Therefore generation of $U(1)_Q$ asymmetry always involves generation of baryon asymmetry.

The above idea has a lot of implications. For example, if a scalar field derivatively couples to lepton current and an interaction violating both lepton and baryon symmetries is in thermal equilibrium, baryon asymmetry is generated without resort to sphaleron effects. More amazingly, even if a scalar field has an interaction with neither baryon nor lepton charge but only derivatively couples to some global $U(1)_Q$ current like PQ current, baryon asymmetry is generated provided that an interaction which violates both $U(1)_Q$ and baryon symmetries is in thermal equilibrium.

To make our ideas clear and concrete, we consider spontaneous baryogenesis in the context of flat directions with neither baryon nor lepton charge. The characteristics of flat directions enable spontaneous baryogenesis to be realized. First of all, due to its flatness, a flat direction can easily acquire a large vacuum expectation value, which yields a derivative interaction between its phase and the symmetry current under which the flat direction is charged. Second, by virtue of a charge violating term (a so-called A-term), the phase starts rotating, thus acquiring a nonzero velocity. Thus, flat directions are suitable for realizing spontaneous baryogenesis. In this Letter, we show that baryogenesis is still possible for a flat direction with $B = L = 0$ by applying the spontaneous mechanism with our new idea stated above, that is, baryon and/or lepton asymmetries generated thermodynamically instead of through condensation. Further implications and details of our ideas is discussed in the future publication [3].

Now let us go into some details of our scenario. First off, we show that if a flat direction with neither baryon nor lepton number is charged under another global symmetry and has a nonzero expectation value, its phase (more precisely, the Nambu-Goldstone (NG) boson associated with breaking of the global symmetry) derivatively couples to the corresponding current. One of the famous examples of such a global symmetry is the PQ symmetry, which is introduced to solve the strong CP problem of quantum chromodynamics. For definiteness, we adopt the supersymmetric DFSZ axion model [4], but it is trivial to extend it to the case with general global $U(1)$ symmetries.

Though a flat direction is specified by a holomorphic gauge-invariant polynomial, it is often described by a single complex scalar field $\Phi \equiv \phi/\sqrt{2}\, e^{i\theta}$. Assuming that a flat direction has only PQ charge, its phase is given by

$$\theta = \frac{1}{N}\mathcal{R}\alpha_R, \tag{5}$$

where N is the number of constituent fields, $\mathcal{R} \equiv \sum_i R_i$ is the sum of the PQ charges, R_i is the PQ charge of each field, and α_R is the angle conjugate to the generator of the PQ symmetry. If the flat direction has a nonzero expectation value, the PQ symmetry is spontaneously broken and a NG boson a_R appears, which is given by

$$a_R \equiv v_a \alpha_R, \tag{6}$$

where $v_a \sim \langle\phi\rangle$ is a decay constant. Then, the NG mode a_R transforms as $a_R \to a_R + v_a\epsilon$ under the PQ transformation $\alpha_R \to \alpha_R + \epsilon$. The effective Lagrangian is given as

$$\mathcal{L}_{\rm eff} = -\sum_m \frac{R_m}{v_a}\left(\partial_\mu a_R\right) j^\mu_m, \tag{7}$$

which yields the derivative interactions between the NG mode a_R and the other charged fields.

Next, we show that a flat direction has a nonzero expectation value during and after inflation, and the corresponding NG boson rolls down along the potential, that is, it acquires a nonzero velocity. Although there are no classical potentials along flat directions in the supersymmetric limit, they are lifted by both supersymmetry breaking effects and non-renormalizable operators. Adopting gravity-mediated supersymmetry breaking, a flat direction has a soft mass $m_\phi \sim 1$TeV. Moreover, assuming a

non-renormalizable operator in the superpotential of the form

$$W = \frac{1}{nM^{n-3}}\Phi^n\,, \tag{8}$$

the flat direction is further lifted by the potential

$$V_{NR} = \frac{|\Phi|^{2n-2}}{M^{2n-6}}\,, \tag{9}$$

where M is a cutoff scale. During the inflationary epoch, there is another contribution to the potential. A flat direction has a negative mass squared proportional to the Hubble parameter squared, which is derived from a four-point coupling to the inflaton in the Kähler potential. Then, this negative mass squared term destabilizes the flat direction at the origin and the flat direction rolls down toward the minimum of the potential. The minimum of the potential $\phi_{\rm min}$ is determined by the balance between the negative mass squared term and the non-renormalizable potential V_{NR}, and is given by

$$\phi_{\rm min} \sim \left(HM^{n-3}\right)^{\frac{1}{n-2}}\,. \tag{10}$$

In fact, the above non-renormalizable superpotential not only lifts the potential but also gives the charge-violating A-terms of the form

$$V_A = a_m \frac{m_{3/2}}{nM^{n-3}}\Phi^n + \text{h.c.} = M_A^4 \cos\left[k\mathcal{R}a_R/v_a\right], \tag{11}$$

where $m_{3/2}$ is the gravitino mass, a_m is a complex constant of order unity, M_A is the energy scale of the A-term, $k \equiv n/N$, and we have assumed a vanishing cosmological constant. By virtue of this A-term, the NG boson a_R begins rotating and acquires a nonzero velocity given by

$$|\dot{a}_R| \sim \frac{k\mathcal{R}}{Hv_a}M_A^4, \tag{12}$$

where we used the slow-roll approximation because the inverse curvature scale of the potential is roughly $\sqrt{m_{3/2}H} \ll H$. We have also assumed that a_R sits far from the extremum of the potential by $O(v_a)$.

The final ingredient to realize the spontaneous mechanism is an interaction which actually breaks the relevant symmetry. In this Letter, as stated in the introduction, we consider an interaction which violates multiple symmetries simultaneously, that is, PQ and lepton symmetries. Such an violating interaction is characterized by the amounts of violation of the PQ and lepton symmetries, that is, δ_R and δ_L. Then, since the produced asymmetries n_R and n_L should be proportional to the amount of each violation, the simple relation $n_R\delta_L = n_L\delta_R$ must be satisfied, or equivalently,

$$\sum_m \Xi_m n_m = 0, \tag{13}$$

where we have defined $\Xi_m = R_m\delta_L - L_m\delta_R$ and L_m is the lepton charge of the m-th field. Then, the resultant lepton number density at decoupling is given by [3]

$$n_L(t_D) = \sum_m L_m n_m = -\delta_R\delta_L\frac{C}{D}\frac{T_D^2}{6}\frac{\dot{a}_R}{v_a}, \tag{14}$$

where we have defined

$$C = R^2L^2 - (R\cdot L)^2\,, \quad D = \delta_L^2R^2 + \delta_R^2L^2 - 2\delta_L\delta_R\,(R\cdot L)\,, \tag{15}$$

with $R\cdot L \equiv \sum_m \kappa_m g_m R_m L_m$. From this result, we can easily reconfirm that an interaction which has $\delta_R \neq 0$ and $\delta_L \neq 0$, that is, which violates both PQ and lepton symmetries simultaneously, is indispensable for the final generation of a lepton asymmetry.

As a concrete example of such a violating interaction, we consider the following dimension five operator,

$$\mathcal{L}_{\not L} = \frac{2}{v}l\,l\,H_uH_u + \text{h.c.}, \tag{16}$$

where v is a scale characterizing the interaction and may be identified with the heavy Majorana mass for the right-handed neutrino in the context of the see-saw mechanism. Note that the above interaction breaks both PQ and lepton symmetries by $\delta_R = 2(R_l + R_{H_u}) \neq 0$ and $\delta_L = 2$. The violating rate of this interaction is given by $\Gamma \sim 0.04T^3/v^2$. Then, the decoupling temperature is calculated as

$$T_D \sim 5 \times 10^{11}\text{GeV} \left(\frac{g_*}{200}\right)^{\frac{1}{2}} \left(\frac{v}{10^{14}\text{GeV}}\right)^2 . \tag{17}$$

where g_* counts the effective degrees of freedom for relativistic particles.

A part of the produced lepton asymmetry is converted into baryon asymmetry through sphaleron effects, which is estimated as

$$\frac{n_B}{s} = \frac{120k\mathcal{R}(R_L + R_{H_u})}{23\pi^2 g_*} \frac{C}{D} \frac{m_{3/2}}{T_D} \sim 3 \times 10^{-10} \left(\frac{m_{3/2}}{3\text{TeV}}\right) \left(\frac{T_D}{10^{12}\text{GeV}}\right)^{-1} , \tag{18}$$

where we have assumed that $\dot{a}_R > 0$ and that PQ charges are of order unity.

Finally we discuss the constraint on the reheating temperature due to the gravitino problem. For $m_{3/2} = 3 \sim 10$ TeV, the reheating temperature is constrained as $T_{RH} \lesssim 10^{12}$ GeV, assuming that the mass of the LSP is $O(100$ GeV). If we take this bound seriously, the decoupling temperature T_D must be less than 10^{12} GeV so that the violating interaction is in thermal equilibrium. For $m_{3/2} \sim 100$ GeV, the reheating temperature must be smaller than $T_{RH} \lesssim 10^9$ GeV. However, these constraints on the reheating temperature are evaded by the introduction of a supersymmetric partner with a mass much lighter than 100 GeV. One such particle is the axino, which naturally exists in our scenario. In fact, it was shown that the reheating temperature is constrained rather loosely as $T_{RH} < 10^{15}$ GeV for $m_{3/2} \simeq 100$ GeV, if the axino is the LSP and the gravitino is the NLSP [5].

In summary, we have discussed a spontaneous baryogenesis mechanism with an interaction violating another global symmetry in addition to baryon (lepton) symmetry. We have shown that even if a scalar field derivatively couples not to baryon current but to another current associated with some global symmetry $U(1)_Q$, baryogenesis is still possible by virtue of such a violating interaction. As a concrete realization of our idea, we have discussed baryogenesis in the context of a flat direction with neither baryon nor lepton charge. First, we have shown that the phase of such a flat direction, strictly speaking, the NG boson associated with breaking of the symmetry, derivatively couples to the global current if it is charged under another global $U(1)_Q$ symmetry, such as the PQ symmetry. The A-term gives this NG boson a nonzero velocity, which leads to the CPT violation. By virtue of the interaction violating $U(1)_Q$ and baryon (lepton) symmetries simultaneously, CPT violation is transmitted to the baryon (lepton) sector, which makes it possible to generate baryon (lepton) asymmetry for this flat direction. In the case of a lepton asymmetry production, a part of the lepton asymmetry is converted into the baryon asymmetry through sphaleron effects.

References

[1] A. D. Sakharov, Zh. Eksp. Teor. Fiz. Pis'ma **5**, 32 (1967); JETP. Lett. **91B**, 24 (1967).

[2] A. G. Cohen and D. B. Kaplan, Phys. Lett. B **87**, 251 (1987).

[3] T. Chiba, F. Takahashi and M. Yamaguchi, Phys. Rev. Lett. **92**, 011301 (2004) [arXiv:hep-ph/0304102]; F. Takahashi and M. Yamaguchi, arXiv:hep-ph/0308173 (to be published in Phys. Rev. D).

[4] M. Dine, W. Fischler and M. Srednicki, Phys. Lett. B **104**, 199 (1981); A. R. Zhitnitsky, Sov. J. Nucl. Phys. **31**, 260 (1980) [Yad. Fiz. **31**, 497 (1980)]; E. Ma, Phys. Lett. B **514**, 330 (2001).

[5] T. Asaka and T. Yanagida, Phys. Lett. B **494**, 297 (2000).

Search for gravitational waves from inspiraling compact binaries using TAMA300 data

Hirotaka Takahashi[a,b,c,1] , Hideyuki Tagoshi[a] and the TAMA Collaboration

[a] *Department of Earth and Space Science , Graduate School of Science, Osaka University, Toyonaka, Osaka 560-0043, Japan*
[b] *Graduate School of Science and Technology, Niigata University, Niigata, Niigata 950-2181, Japan*
[c] *Yukawa Institute for Theoretical Physics, Kyoto University, Kyoto 606-8502, Japan*

Abstract

We analyze the data from the TAMA300 detector taken in 2001 and 2003. We search for gravitational waves from inspiraling compact binaries using matched filtering. The mass region searched is from $1M_\odot$ to $2M_\odot$. The preliminary results of analysis are reported.

1 Introduction

Several laser interferometric gravitational wave detectors are constructed and have started observation runs. These include LIGO [1] , VIRGO [2], GEO [3] and TAMA300 [4] .

TAMA300 is an interferometric gravitational wave detector with 300 m baseline length located at Mitaka campus of the National Astronomical Observatory of Japan in Tokyo ($35.68°N, 139.54°E$). TAMA300 began to operate in 1999. It had performed observations for 8 times by July 2003. In particular, during the period from 1 August to 20 September 2001, TAMA300 performed an observation, which is called Data Taking 6 (DT6), and about 1039 hours of data were taken. The best sensitivity was about $5 \times 10^{-21}/\sqrt{\text{Hz}}$ around 800Hz. More recently, a longest observation was performed by TAMA300 during 14 February to 15 April. 2003, and about 1163 hours of data were taken. This observation is called Data Taking 8 (DT8). The best sensitivity was about $3 \times 10^{-21}/\sqrt{\text{Hz}}$ around 1kHz.

We consider gravitational waves from inspiraling compact binaries, consisting of neutron stars or black holes. Since their wave forms are well known by post-Newtonian approximation of general relativity, we can use the matched filtering. In this paper, we report preliminary results of the inspiraling compact binaries event search.

2 Matched filtering

In this section, we briefly describe a method of matched filtering search. We assume that the time sequential data of the detector output $s(t)$ consists of a signal plus noise $n(t)$. We denote the one-sided power spectrum density of noise by $S_n(f)$.

The gravitational wave strain amplitude $h(t)$ is calculated by combining two independent modes of the gravitational wave and antenna pattern of interferometer as

$$h(t) = \mathcal{A}[h_c(t - t_c)\cos\phi_0 + h_s(t - t_c)\sin\phi_0], \tag{1}$$

where $h_c(t)$ and $h_s(t)$ are two independent templates whose phase are different to $\pi/2$ from each other and $\mathcal{A}$ is amplitude. The parameters which characterize the templates are the coalescence time t_c, the chirp mass $\mathcal{M}(\equiv M\eta^{3/5})$ $(M = m_1 + m_2)$, non-dimensional reduced mass $\eta(\equiv m_1 m_2/M^2)$ and the phase ϕ_0. The details of the wave form can be found in [5]. We use the restricted post-Newtonian wave forms in which the phase evolution is calculated to 2.5 post-Newtonian order, but the amplitude evolution

[1] E-mail:hirotaka@vega.ess.sci.osaka-u.ac.jp

contains only the lowest Newtonian quadrupole contribution. The effects of spin angular momentum are not taken into account here.

The two wave forms, h_c and h_s, are transformed into the Fourier domain by the stationary phase approximation. We use templates for matched filtering defined in the Fourier domain as $\tilde{h}(f) = \tilde{h}_c(f)\cos\phi_0 + \tilde{h}_s(f)\sin\phi_0$, where $\tilde{h}(f)$ denotes the Fourier transform of $h(t)$. Here, $\tilde{h}_c$ and $\tilde{h}_s$ are normalized as $(h_c|h_c) = (h_s|h_s) = 1$, where

$$(a|b) \equiv 2\int_{-\infty}^{\infty} df \frac{\tilde{a}(f)\tilde{b}^*(f)}{S_n(|f|)}, \tag{2}$$

and * means the operation to take the complex conjugate. The filtered output is then defined by

$$\rho(t_c, M, \eta, \phi_0) \equiv (s|h). \tag{3}$$

In the matched filtering, we look for the maximum of ρ over the parameter t_c, M, η, and ϕ_0. In Eq. (3), we can take the maximization over ϕ_0 analytically which gives

$$\rho(t_c, m_1, m_2) = \sqrt{(s|h_c)^2 + (s|h_s)^2}. \tag{4}$$

We see that ρ^2 has an expectation value 2 in the presence of only Gaussian noise. Thus, we can define the normalized signal-to-noise ratio by $SNR = \rho/\sqrt{2}$.

In the TAMA300 analysis, we have found that the noise contained a large amount of non-stationary and non-Gaussian noise [6]. In order to remove the influence of such noise, we introduce a χ^2 test [8]. First we divide each template into n mutually independent pieces in the frequency domain, chosen so that the expected contribution to ρ from each frequency band is approximately equal, as

$$\tilde{h}_{c,s}(f) = \tilde{h}^{(1)}_{c,s}(f) + \tilde{h}^{(2)}_{c,s}(f) + \cdots + \tilde{h}^{(n)}_{c,s}(f). \tag{5}$$

The χ^2 is defined by

$$\chi^2 = n\sum_{i=1}^{n}\left[(z^{(i)}_{(c)} - \bar{z}^{(i)}_{(c)})^2 + (z^{(i)}_{(s)} - \bar{z}^{(i)}_{(s)})^2\right], \tag{6}$$

where

$$z^{(i)}_{(c,s)} = (\tilde{s}|\tilde{h}^{(i)}_{c,s}), \qquad \bar{z}^{(i)}_{(c,s)} = \frac{1}{n}(\tilde{s}|\tilde{h}_{c,s}). \tag{7}$$

This quantity must satisfy the χ^2-statistics with $2n-2$ degrees of freedom, as long as the data consists of Gaussian noise plus inspiraling signals. For convenience, we use the reduced χ-square defined by $\chi^2/(2n-2)$. In this paper, we chose $n = 16$ (hereafter, χ^2 means the reduced χ-square).

The value of χ^2 is independent of the amplitude of the signal as long as the template and the signal have an identical wave form. However, in reality, since the template and the signal have different value of parameters because of the discrete time step and discrete mass parameters we search, the value of χ^2 becomes larger when the amplitude of signal becomes larger. In such situation, if we reject events simply by the value of χ^2, we may lose real events with large amplitude. In order to avoid this, we have been introducing a statistic, $\rho/\sqrt{\chi^2}$, in the TAMA300 data analysis [9].

The mass parameters considered in this paper is $1.0M_\odot \leq m_1, m_2 \leq 2.0M_\odot$, which is a typical mass region of neutron stars. In this region, a discrete mass parameter space is determined so that the maximum loss of SNR due to discretization becomes less than 3%. The parametrization of mass parameters are done based on [7].

The mass parameter space depends on the power spectrum of noise. Averaged power spectrum of noise for each continuously locked segment was used to define the mass parameter space in each segments. This parameter space is not changed within the continuously locked segment. However, in order to take into account of the variation of the noise power spectrum with time, we use a different mass parameter space for different locked segments. The mass parameter space turned out to contain about $200 \sim 1000$ templates for the DT6 data, and about $200 \sim 800$ templates for the DT8 data. The typical value of the number of template is about 700 for DT6, and 600 for DT8.

3 Matched filtering algorithm

In this section, we briefly describe the matched filtering algorithm which are used for TAMA300 analysis.

The time sequential voltage data from the interferometer data are divided into small length of data with length of 52 seconds. Each peace of data have overlap portion with 4.0 seconds. The data are Fourier transformed into frequency domain and are multiplied by transfer function to transfer into strain equivalent data. We calculate eqn. (8) for a mass parameter on the mesh point. For each interval of coalescence time with Δt_c = 25m seconds, we search for t_c which realize the maximum value of ρ.@If $\rho > 7$, we calculate the value of χ^2 which correspond to the t_c. The same calculations are perform for the other parameters. The results are stored in an event list file.

4 Results and Discussion

Our analysis was done with 9 Compaq Alpha machines and also 16 Intel Pentium4 machines in our laboratory at Osaka University. The matched filtering codes are written in C language and are MPI paralleled.

We present results of matched filtering analysis including preliminary results of DT6 and DT8 analysis. We plot the number of events as a function of $\rho/\sqrt{\chi^2}$. The solid line of Fig.1 shows histogram for DT8. In order to compare the results, we also plot the same figure using DT6 results. In these histograms, only events with $\rho > 7$ are plotted.

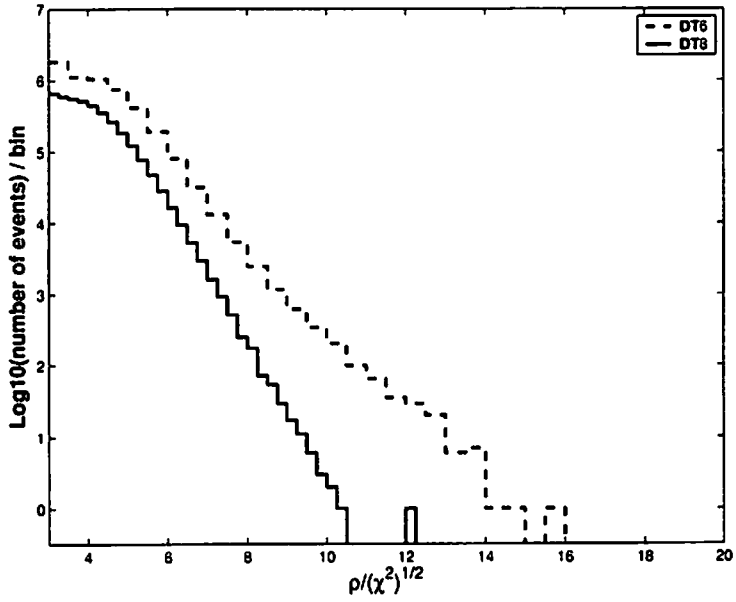

Figure 1: The number of events as a function of $\rho/\sqrt{\chi^2}$. The dot and solid lines show histograms for DT6 and DT8 respectively.

We find from the distribution of $\rho/\sqrt{\chi^2}$, we have a shorter tail in DT8 than in DT6. If we determine threshold of $\rho/\sqrt{\chi^2}$ for a given false alarm rate, the threshold of DT8 becomes lower than that of DT6. This fact will help us to improve the detection efficiency of the Galactic events in DT8 further. These facts suggest that the DT8 data have much better quality than the DT6 data in the sense that it is easier to discriminate the non-Gaussian noise events.

After the observation of DT6, the configuration of TAMA300 has been changed very much. One of the major changes is the installation of the power recycling system. Thus, it will be important and

interesting to investigate the origin of the different property of data between DT6 and DT8. We will work on such analysis in the future.

Much more details of the analysis using the data of TAMA300 DT6 and DT8 will be discussed elsewhere [9].

This work was supported in part by Grant-in-Aid for Scientific Research, Nos. 14047214 and 12640269, of the Ministry of Education, Culture, Sports, Science, and Technology of Japan.

References

[1] A. Lazzarini et al, in this volume.
LIGO web page: http://www.ligo.caltech.edu/

[2] VIRGO web page: http://www.virgo.infn.it/

[3] GEO600 web page: http://www.geo600.uni-hannover.de/

[4] R. Takahashi et al, in this volume.
M. Ando et al., Phys. Lett., **86**, 3950 (2001).
See also TAMA300 web site for the latest information, http://tamago.mtk.nao.ac.jp/tama.html/.

[5] L. Blanchet et al., Phys. Rev. Lett. **74**, 3515 (1995).

[6] H. Tagoshi et al., Phys. Rev. **D63**, 062001 (2001).

[7] T. Tanaka and H. Tagoshi, Phys. Rev. **D62**, 082001 (2000).

[8] B. Allen et al., Phys. Rev. Lett. **83**, 1489 (1999).

[9] H. Tagoshi, H. Takahashi et al., in preparation.

Quasi-geometrical Optics Approximation in Gravitational Lensing

Ryuichi Takahashi[1],

Department of Physics, Kyoto University,
Kyoto 606-8502, Japan

Abstract

We study the gravitational lensing in the quasi-geometrical optics approximation which is the geometrical optics including the corrections arising from the effects of the finite wavelength. Theses correction terms can be obtained analytically by the asymptotic expansion of the diffraction integral in powers of the wavelength λ. The first term, arising from the short wavelength limit $\lambda \to 0$, corresponds to the geometrical optics limit. The second term, being of the order of λ/M (M is the Schwarzschild radius of the lens mass), is the first correction term arising from the diffraction effect. By analyzing this correction term, we find that (i) the lensing magnification μ is modified to $\mu(1+\delta)$, where δ is of the order of $(\lambda/M)^2$, and (ii) if the lens has cuspy (or singular) density profile at the center $\rho(r) \propto r^{-\alpha}$ $(0 < \alpha \leq 2)$, the diffracted image is formed at the lens center with the magnification $\mu \sim (\lambda/M)^{3-\alpha}$.

1 Introduction

The gravitational lensing of light is usually treated in the geometrical optics approximation, which is valid in all the observational situations [1],[2]. Lensing quantities (the deflection angle, the image positions, its brightness, the number of images, etc.) are calculated in the geometrical optics. However for the gravitational lensing of gravitational waves, the wavelength is long so that the geometrical optics approximation is not valid in some cases. For example, the wavelength λ of the gravitational waves for the space interferometer is ~ 1 AU which is extremely larger than that of a visible light ($\lambda \sim 1\mu$ m). If the wavelength λ is larger than the Schwarzschild radius of the lens mass M, the diffraction effect is important and the magnification is small [1],[2].

From the above discussion, for $\lambda \gtrsim M$ the diffraction effect is important, and for $\lambda \ll M$ the geometrical optics approximation is valid. In this paper, we consider the case for $\lambda \lesssim M$, i.e. the quasi-geometrical optics approximation which is the geometrical optics including corrections arising from the effects of the finite wavelength. We can obtain these correction terms analytically by an asymptotic expansion of the diffraction integral in powers of the wavelength λ. It is important to derive these correction terms for the following two reasons: (i) calculations in the wave optics are based on the diffraction integral, but it is time consuming to numerically calculate this integral especially for high frequency. Hence, it is a great saving of computing time to use the analytical expressions. (ii) We can understand clearly the difference between the wave optics and the geometrical optics.

This paper is organized as follows: In §2 we briefly review the wave optics in gravitational lensing of gravitational waves. In §3 we show that in the short wavelength limit $\lambda \to 0$, the wave optics is reduced to the geometrical optics limit. In §4 we expand the diffraction integral in powers of the wavelength λ, and derive the leading correction terms arising from the effect of the finite wavelength. We use units of $c = G = 1$.

2 Wave Optics in Gravitational Lensing

We briefly review the wave optics in gravitational lensing of gravitational waves [1], [2] [4]. We consider gravitational waves propagating under the gravitational potential of a lens object. The background metric is given by,

$$ds^2 = -(1+2U)\,dt^2 + (1-2U)\,d\mathbf{r}^2 \equiv g^{(\mathrm{B})}_{\mu\nu} dx^\mu dx^\nu, \tag{1}$$

[1] E-mail:takahasi@tap.scphys.kyoto-u.ac.jp

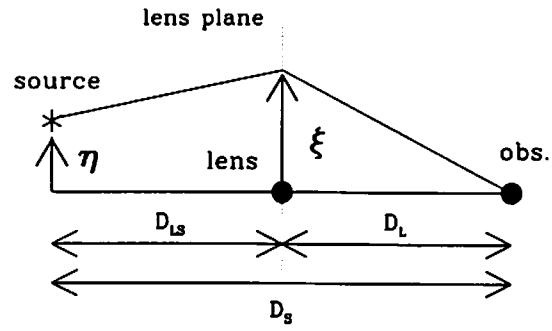

Figure 1: Gravitational lens geometry for the source, the lens and the observer. D_L, D_S and D_{LS} are the distances between them. η is the displacement of the source from the line of sight to the lens, while ξ is the impact parameter. We use the thin lens approximation in which the gravitational waves are scattered only on the thin lens plane.

where $U(\mathbf{r})$ ($\ll 1$) is the gravitational potential of the lens object. The propagation equation for the gravitational waves $h_{\mu\nu}$ in the curved background is given by [3],

$$h_{\mu\nu;\alpha}{}^{;\alpha} + 2R^{(B)}_{\alpha\mu\beta\nu}h^{\alpha\beta} = 0, \tag{2}$$

where the semicolon denotes the covariant derivative with respect to $g^{(B)}_{\mu\nu}$ and $R^{(B)}_{\alpha\mu\beta\nu}$ is the background Riemann tensor. $h_{\mu\nu}$ satisfies the transverse traceless Lorentz gauge condition of $h^{\nu}_{\mu;\nu} = 0$ and $h^{\mu}{}_{\mu} = 0$. The above equation (2) can be solved by using the Kirchhoff diffraction integral [2].

In Fig.1, we show the gravitational lens geometry of the source, the lens and the observer. Here, D_L, D_S and D_{LS} are the distances to the lens, the source and from the source to the lens, respectively. η is the displacement of the source from the line of sight to the lens, while ξ is the impact parameter in the lens plane. We use the thin lens approximation in which the lens is characterized by the surface mass density $\Sigma(\xi)$ and the gravitational waves are scattered only on the thin lens plane. Then, the lensed wave $\tilde{h}^L_{\mu\nu}(\omega)$ at the observer in the frequency domain is given by the product of the amplification factor F and the unlensed wave $\tilde{h}_{\mu\nu}(\omega)$ ($U = 0$):

$$\tilde{h}^L_{\mu\nu}(\omega) = F(\omega, \eta)\ \tilde{h}_{\mu\nu}(\omega). \tag{3}$$

The amplification factor F is given by [2],

$$F(\omega, \eta) = \frac{D_S}{D_L D_{LS}} \frac{\omega}{2\pi i} \int d^2\xi\ \exp\left[i\omega t_d(\xi, \eta)\right], \tag{4}$$

where the time delay t_d from the source position η through ξ is given by,

$$t_d(\xi, \eta) = \frac{D_L D_S}{2D_{LS}} \left(\frac{\xi}{D_L} - \frac{\eta}{D_S}\right)^2 - \hat{\psi}(\xi) + \hat{\phi}_m(\eta). \tag{5}$$

The deflection potential $\hat{\psi}(\xi)$ is determined by, $\nabla^2_\xi \hat{\psi} = 8\pi\Sigma$, where ∇^2_ξ denotes the two-dimensional Laplacian with respect to ξ and $\Sigma(\xi)$ is the surface mass density of the lens. $\hat{\phi}_m$ is the additional phase in F, and we choose $\hat{\phi}_m$ so that the minimum value of the time delay is zero. The amplification factor F is normalized such that $|F| = 1$ in no lens limit ($U = \hat{\psi} = 0$).

It is useful to rewrite the amplification factor F in terms of dimensionless quantities. We introduce ξ_0 as the normalization constant of the length in the lens plane. The impact parameter ξ, the source position η and the frequency ω are rewritten in dimensionless form,

$$\mathbf{x} = \frac{\xi}{\xi_0}, \quad \mathbf{y} = \frac{D_L}{\xi_0 D_S}\eta, \quad w = \frac{D_S}{D_{LS}D_L}\xi_0^2\,\omega. \tag{6}$$

Then, the dimensionless time delay is given by,

$$T(\mathbf{x},\mathbf{y}) = \frac{D_L D_{LS}}{D_S}\,\xi_0^{-2}\,t_d(\boldsymbol{\xi},\boldsymbol{\eta}) = \frac{1}{2}\,|\mathbf{x}-\mathbf{y}|^2 - \psi(\mathbf{x}) + \phi_m(\mathbf{y}), \tag{7}$$

where $\psi(\mathbf{x})$ and $\phi_m(\mathbf{y})$ correspond to $\hat{\psi}(\boldsymbol{\xi})$ and $\hat{\phi}_m(\boldsymbol{\eta})$ in equation (5): $\psi = D_L D_{LS}/(D_S\xi_0^2)\,\hat{\psi}$ and $\phi_m = D_L D_{LS}/(D_S\xi_0^2)\,\hat{\phi}_m$, respectively. Using the above dimensionless quantities, the amplification factor is rewritten as,

$$F(w,\mathbf{y}) = \frac{w}{2\pi i}\int d^2x \exp\left[iwT(\mathbf{x},\mathbf{y})\right]. \tag{8}$$

We use the Einstein radius ($\sim (MD)^{1/2}$) as the arbitrary scale length ξ_0 for convenience. The Einstein radius is the typical scale length of the impact parameter in the gravitational lensing, and hence the dimensionless quantities $\mathbf{x},\mathbf{y}$ become of the order of one. The dimensionless potential $\psi(\mathbf{x})$ and time delay $T(\mathbf{x},\mathbf{y})$ are also of the order of one. Then, the dimensionless frequency w is roughly $\sim M/\lambda$ from Eq.(6).

3 Geometrical Optics Approximation

In the geometrical optics limit ($w \gg 1$), the stationary points of the $T(\mathbf{x},\mathbf{y})$ contribute to the integral of Eq.(8) so that the image positions $\mathbf{x}_j$ are determined by the lens equation, $\nabla_x T(\mathbf{x},\mathbf{y}) = 0$. This is just the Fermat's principle. We expand $T(\mathbf{x},\mathbf{y})$ around the j-th image position $\mathbf{x}_j$ as,

$$T(\mathbf{x},\mathbf{y}) = T(\mathbf{x}_j,\mathbf{y}) + \frac{1}{2}\sum_{a,b}\partial_a\partial_b T(\mathbf{x}_j,\mathbf{y})\tilde{x}_a\tilde{x}_b + \mathcal{O}(\tilde{x}^3) \tag{9}$$

where $\tilde{\mathbf{x}} = \mathbf{x} - \mathbf{x}_j$ and the indices a,b,... run from 1 to 2. Inserting Eq.(9) to (8), we obtain the amplification factor in the geometrical optics limit as [1], [2],

$$F_{geo}(w,\mathbf{y}) = \sum_j |\mu_j|^{1/2}\exp\left[\,iwT_j - i\pi n_j\right], \tag{10}$$

where the magnification of the j-th image is $\mu_j = 1/\det(\partial\mathbf{y}/\partial\mathbf{x}_j)$, $T_j = T(\mathbf{x}_j,\mathbf{y})$ and $n_j = 0, 1/2, 1$ when $\mathbf{x}_j$ is a minimum, saddle, maximum point of $T(\mathbf{x},\mathbf{y})$.

4 Quasi-geometrical Optics Approximation

4.1 Effect on the Magnification of the Image

We expand the amplification factor $F(w,\mathbf{y})$ in powers of $1/w$ ($\ll 1$) and discuss the behavior of the order of $1/w$ term. We expand $T(\mathbf{x},\mathbf{y})$ in Eq.(7) up to the fourth order of $\tilde{x}$ as,

$$\begin{aligned} T(\mathbf{x},\mathbf{y}) \;=\; & T_j + \frac{1}{2}\sum_{a,b}\partial_a\partial_b T(\mathbf{x}_j,\mathbf{y})\tilde{x}_a\tilde{x}_b + \frac{1}{6}\sum_{a,b,c}\partial_a\partial_b\partial_c T(\mathbf{x}_j,\mathbf{y})\tilde{x}_a\tilde{x}_b\tilde{x}_c \\ & + \frac{1}{24}\sum_{a,b,c,d}\partial_a\partial_b\partial_c\partial_d T(\mathbf{x}_j,\mathbf{y})\tilde{x}_a\tilde{x}_b\tilde{x}_c\tilde{x}_d + \mathcal{O}(\tilde{x}^5). \end{aligned} \tag{11}$$

After inserting the above equation (11) into (8), we expand the amplification factor in powers of $1/w$. Then we obtain,

$$F(w,\mathbf{y}) = \sum_j |\mu_j|^{1/2}\left(1 + \frac{i}{w}\Delta_j\right)e^{iwT_j - i\pi n_j} + \mathcal{O}(w^{-2}), \tag{12}$$

where Δ_j is a real number. Δ_j is given for the axially-symmetric lens model as,

$$\Delta_j = \frac{1}{16}\left[\frac{1}{2\alpha_j^2}\psi_j^{(4)} + \frac{5}{12\alpha_j^3}\psi_j^{(3)^2} + \frac{1}{\alpha_j^2}\frac{\psi_j^{(3)}}{|x_j|} + \frac{\alpha_j - \beta_j}{\alpha_j\beta_j}\frac{1}{|x_j|^2}\right], \tag{13}$$

where $\alpha_j = (1 - \psi_j'')/2$, $\beta_j = (1 - \psi_j'/|x_j|)/2$ and $\psi_j^{(n)} = d^n\psi(|\mathbf{x}_j|)/dx^n$. The first term of the above equation (12) is the amplification factor in the geometrical optics limit F_{geo} in equation (10). The second term is the leading correction term, being proportional to $1/w$, arising from the diffraction effect. Thus the deviation from the geometrical optics is of the order of $1/w \sim \lambda/M$.

We rewrite F in above equation (12) as,

$$F(w,\mathbf{y}) = \sum_j \left| \mu_j \left[1 + \left(\frac{\Delta_j}{w} \right)^2 \right] \right|^{1/2} e^{iwT_j + i\delta\varphi_j - i\pi n_j} + \mathcal{O}(w^{-2}). \tag{14}$$

where $\delta\varphi_j = \arctan(\Delta_j/w)$. Thus in the quasi-geometrical optics approximation, the magnification μ_j is modified to $\mu_j[1 + (\Delta_j/w)^2]$, where $(\Delta_j/w)^2$ is of the order of $(\lambda/M)^2$. The phase is also changed by $\delta\varphi_j$, which is of the order of λ/M.

4.2 Central Cusp of the Lens

We consider the correction terms in the amplification factor F arising at the central cusp of the lens. For the inner density profile of the lens $\rho \propto r^{-\alpha}$ $(0 < \alpha \leq 2)$, the deflection potential at small radius is given by,

$$\psi(\mathbf{x}) \propto x^{-\alpha+3} \tag{15}$$

For example, if the inner density profile is $\rho \propto r^{-2}$ (e.g. the singular isothermal sphere model), the deflection potential is given by $\psi(\mathbf{x}) = \psi_0 x$ (ψ_0 is a constant) from equation (15). Inserting this potential ψ into equation (8), we obtain,

$$F(w,y) = \frac{e^{iw[y^2/2+\phi_m(y)]}}{2\pi i w} \int dx'^2 \exp\left[-i \left\{ yx_1' + \psi_0 \sqrt{x_1'^2 + x_2'^2} + \mathcal{O}(1/w) \right\} \right], \tag{16}$$

where we changed the integral variable from $\mathbf{x}$ to $\mathbf{x}' = w\mathbf{x}$. We denote $dF_c(w,y)$ as the leading term of the above integral which is proportional to $1/w$. dF_c is obtained by integrating the above equation as,

$$dF_c(w,y) = \frac{e^{iw[y^2/2+\phi_m(y)]}}{w} \frac{1}{(y^2 - \psi_0^2)^{3/2}} \quad \text{for } |y| > |\psi_0|, \tag{17}$$

$$= \frac{e^{iw[y^2/2+\phi_m(y)]}}{w} \frac{i}{(\psi_0^2 - y^2)^{3/2}} \quad \text{for } |y| < |\psi_0|. \tag{18}$$

Thus, the contributions to the amplification factor F at the lens center is of the order of $1/w \sim \lambda/M$. This is because of the singularity in the density profile at the lens center. The correction terms dF_c in equations (17) and (18) represent a diffracted image which is formed at the lens center by the diffraction effect. The magnification of this image is of the order of $\sim \lambda/M$.

For the general value of α, the diffracted image is formed at the lens center for the inner density profile $\rho \propto r^{-\alpha}$ $(0 < \alpha \leq 2)$. The magnification of this central image is roughly given by, $\mu \sim (\lambda/M)^{3-\alpha}$.

References

[1] Nakamura, T.T. & Deguchi, S., Prog. Theor. Phys. Suppl., **133**, 137, (1999).

[2] Schneider, P., Ehlers, J. & Falco, E.E., Gravitational Lenses, 1992, (New York : Springer).

[3] Misner, C.W., Thorne, K.S. & Wheeler, J.A., 1973, Gravitation, Freeman, San Francisco

[4] Takahashi, R. & Nakamura, T., ApJ, **595**, 1039, (2003).

Radionic Non-uniform Black Strings

Takashi Tamaki[1], Sugumi Kanno[2] and Jiro Soda[3]

Department of Physics. Kyoto University. 606-8501. Japan

Abstract

Non-uniform black strings in the two-brane system are investigated using the effective action approach. It is shown that the radion acts as a non-trivial hair of black strings. The stability of solutions is demonstrated using the catastrophe theory. The black strings are shown to be non-uniform.

1 Introduction

In the Randall-Sundrum 1 model [1], the black hole can be regarded as a section of the black string as long as the distance between two branes is less than the radius of the black hole on the brane. As the radion controls the length of the black string, it can trigger the transition from the black string to localized black hole through the Gregory-Laflamme instability. The purpose of this work is to reveal the role of the radion in the black string system with the hope to understand this phenomena. We take the specific model that the dilaton field coupled to the electromagnetic field on the $\oplus$-brane. In the case of stable black string, we can use the low energy approximation that the curvature on the brane is smaller than the curvature in the bulk. Foutunately, the effective action is known in this case as [2]

$$S_{\oplus} = \frac{1}{2\kappa^2}\int d^4x\sqrt{-h}\left[\Psi R(h) - \frac{3(\nabla\Psi)^2}{2(1-\Psi)}\right] - \int d^4x\sqrt{-h}\left(\frac{(\nabla\phi)^2}{2} + \frac{e^{-2a\phi}}{4}F^2\right),$$

where we defined $\Psi := 1 - \exp(-2d/\ell)$. Here, d and ℓ are the proper distance between the branes and the curvature radius in AdS_5, respectively. The point is that the bulk metric is completely determined by the 4-dimensional theory through the holographic relation as [2]

$$g_{\mu\nu} = (1-\Psi)^{y/\ell}\left[h_{\mu\nu}(x) + g^{(1)}_{\mu\nu}(h_{\mu\nu}, \Psi, T^{\oplus}_{\mu\nu}, T^{\ominus}_{\mu\nu}, y)\right] . \tag{1}$$

Here, we have used the following coordinate system to describe the geometry of the brane model:

$$ds^2 = e^{2\eta(x^\mu)}dy^2 + g_{\mu\nu}(y, x^\mu)dx^\mu dx^\nu . \tag{2}$$

We place the branes at $y = 0$ ($\oplus$-brane) and $y = \ell$ ($\ominus$-brane) in this coordinate system. Using this fact, we have investigated the bulk geometry of this system and found stable non-uniform black strings for which the radion plays an important role [3]. We consider the static and spherically symmetric metric in the Einstein frame on the $\oplus$-brane as

$$ds^2 = -f(r)e^{-2\delta(r)}dt^2 + f(r)^{-1}dr^2 + r^2d\Omega^2, \tag{3}$$

where $f(r) := 1 - \kappa^2 m(r)/4\pi r$. We assume the existence of a regular event horizon at $r = r_H$ and asymptotically flatness. We consider solutions with a magnetic charge Q_m. In the following, we provide views both from the brane and from the bulk.

[1] E-mail:tamaki@tap.scphys.kyoto-u.ac.jp
[2] E-mail:sugumi@tap.scphys.kyoto-u.ac.jp
[3] E-mail:jiro@tap.scphys.kyoto-u.ac.jp

2 View from the Brane

2.1 Radion as a Hair

We obtain the first law of black hole thermodynamics, from which we can find that the radion field is a hair of black strings. We can prove that Ψ is monotonically decreasing function of r. In Fig. 1 (a), as an example, Ψ for a solution $\tilde{a} := \sqrt{2}a/\kappa = \sqrt{3}$, $\Psi_\infty := \Psi(\infty) = 0.25$ and the horizon radius $\lambda_H := \sqrt{2}r_H/\kappa Q_m = 0.119$ is depicted.

2.2 Stability of the Black String

In the single brane limit $\Psi \to 1$, the effect of the radion ceases. Hence, the solution approaches GM-GHS solution [4]. In the close limit $\Psi \to 0$, we have $\phi(r) = 0$. Thus, only Reissner-Nordström (RN) solutions are possible in this limit because of the no-hair theorem. Therefore, the non-trivial radion ($\Psi \neq 0, 1$) interpolates RN and GM-GHS solutions as in Fig. 1 (b) where the relation between the inverse temperature $1/\tilde{T}_H$ and $\tilde{M}$ are plotted.

We can prove that there is no inner horizon for $\Psi \neq 0$. Thus, the causal structure is the same as that of Schwarzschild black hole. This suggests that our solutions are stable as the GM-GHS solutions. We can also argue stability of our solutions using the catastrophe theory. According to the catastrophe theory, the stability changes at $d(1/T_H)/dM = \infty$ [5, 6]. Since we cannot find the point $d(1/T_H)/dM = \infty$ in the graph for various parameters, our solutions are stable in the catastrophic sense.

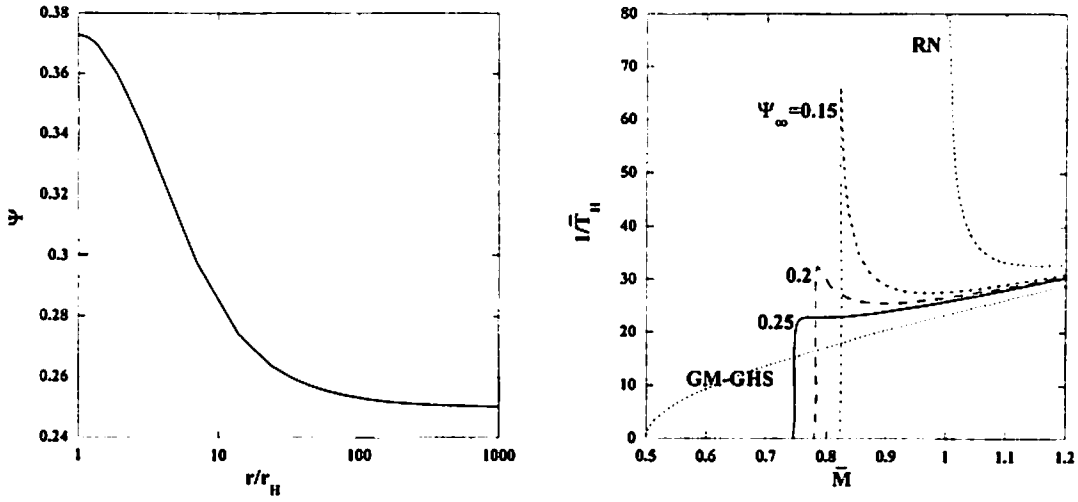

Figure 1: (a) The behavior of Ψ (b) $\tilde{M}$-$1/\tilde{T}_H$.

3 View from the bulk

Our interest here is the y-dependence of the horizon which had not been investigated so far in the RS1 model. The hologram (1) can be used to see the shape of the black strings. To see the non-uniformity of the horizon, let us investigate the change of the circumference radius along y direction. The procedure to obtain a circumference radius of the horizon is summarized as follows: (i) seek for the radius $r = r_+(y)$ which satisfies $h_{00} + g^{(1)}_{00} = 0$ (or equivalently $h_{11} + g^{(1)}_{11} = \infty$ as we denote below.) (ii) evaluate the

circumference radius in the Einstein frame as

$$R_H := \sqrt{r_+^2 + \Psi(r_+) g_{22}^{(1)}(r_+)} \,. \tag{4}$$

Note that we subtracted the effect of the AdS background in the above expression (See, Eq. (1)).

First, let us find $r_+(y)$. Writing $g_{00}^{(1)} =: h_{00} f_0(r,y)$ and $g_{11}^{(1)} =: h_{11} f_1(r,y)$, we can verify that $f_0 = f_1$ and they have finite values at $r = r_H$. Hence, the coordinate value of the horizon does not change $r_+(y) = r_H$ even at this order. Thus, we can evaluate the circumference radius (4) using the expression

$$g_{22}^{(1)}(r_H) = -\frac{\ell^2 w}{2}\left[R_{22} - \frac{1}{6}h_{22}R + (w+2)\chi_{22}\right] \,. \tag{5}$$

Here, we introduced the variable $w := (1-\Psi)^{-y/\ell} - 1$ which increases toward the $\ominus$-brane.

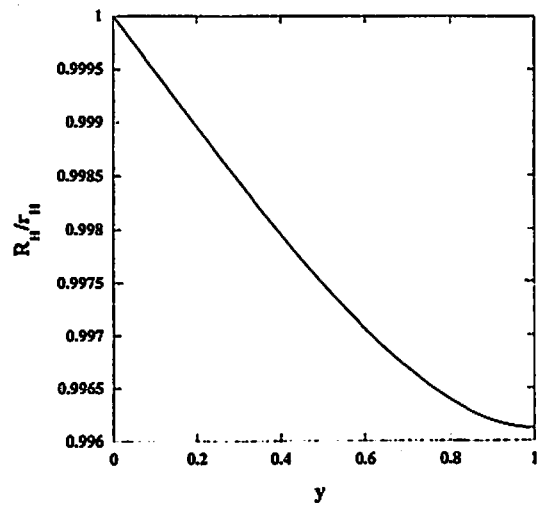

Figure 2: Deformation of the horizon for $\Psi_\infty = 0.25$, $\lambda_H = 1.11 \times 10^{-2}$, $\tilde{a} = \sqrt{3}$ and $\ell/r_H = 0.5$.

As an example, we show the ratio of the horizon R_H/r_H as a function of y in Fig. 2. We find that the circumference radius of the horizon monotonically shrinks toward the $\ominus$-brane even if we subtract the background effect. Although, we showed only one example, we can easily confirm that this is general by differentiating (5) with respect to w since the fields satisfy the conditions

$$T_{22} = \frac{\Psi Q_m^2}{2r^2} e^{-2a\phi} > 0 \,, \quad T^\mu_{\ \mu} = 0 \,, \tag{6}$$

at $r = r_H$. In fact, by rewriting Eq. (5) as

$$K := -\frac{2}{\ell^2} g_{22}^{(1)}(r_H) = w\left[\frac{h_{22}}{3}R + \frac{\kappa^2}{\Psi}T_{22}\left\{1 - (w+2)\,\frac{1-\Psi}{2}\right\}\right] \,, \tag{7}$$

we obtain

$$\frac{dK}{dw} = \frac{h_{22}}{3}R + \frac{\kappa^2}{\Psi}T_{22}\left\{1 - (w+1)\,(1-\Psi)\right\}, \tag{8}$$

$$\frac{d^2K}{dw^2} = -\frac{\kappa^2}{\Psi}(1-\Psi)T_{22} < 0. \tag{9}$$

From Eq.(9), we see dK/dw takes minimum value at the $\ominus$-brane. On the $\ominus$-brane, we have

$$\frac{dK}{dw} = \frac{1}{3}h_{22}R = -\frac{1}{3}h_{22}T^\mu_{\ \mu} = 0 \,. \tag{10}$$

Therefore, dK/dw is always positive in the bulk. This means $dg_{22}^{(1)}/dw < 0$. As the horizon has non-trivial y-dependence, the black strings are non-uniform.

Finally, we comment on the zeroth law of the non-uniform black string. Using the metric (3), the Hawking temperature is

$$T_H = \frac{2\pi - \kappa^2 m'_H}{8\pi^2 r_H} e^{-\delta_H} \sqrt{\frac{1 + f_0(r_H, y)}{1 + f_1(r_H, y)}}\,, \tag{11}$$

Since $f_0 = f_1$ at $r = r_H$, T_H does not depend on y. Therefore, the zeroth law of black hole thermodynamics holds.

4 Conclusion

Non-uniform black strings in the two-brane system are investigated using the effective action approach. We considered the dilaton field coupled to the electromagnetic field on the $\oplus$-brane. It is shown that the radion acts as a non-trivial hair of the black strings. From the brane point of view, the black string appears as the deformed GM-GHS black hole which becomes GM-GHS black hole in the single brane limit and reduces to the RN black hole in the close limit of two-branes. In view of the catastrophe theory, our solutions are stable. From the bulk point of view, the black strings are proved to be non-uniform. Nevertheless, the zeroth law of black hole thermodynamics holds.

We established the picture that the event horizon shrinks toward the $\ominus$-brane (even if we subtract the effect of the AdS background) and the distance between branes decreases toward the asymptotically flat region.

However, we cannot apply our present analysis if the distance between branes exceeds the horizon radius. This is because the Kaluza-Klein effect becomes significant. It is the point that Gregory-Laflamme instability commences. The transition to the localized black hole may occurs. The AdS/Conformal field theory correspondence argument suggests the classical evaporation of the resultant black hole. Moreover, there is also a possibility that the shape of the horizon becomes complicated. To get a hint, we need to proceed to the next order calculations corresponding to Kaluza-Klein corrections. We want to investigate it in the future.

References

[1] L. Randall and R. Sundrum, Phys. Rev. Lett. **83**, 4690 (1999) [arXiv:hep-th/9906064]; *ibid.*, 3370 (1999) [arXiv:hep-th/9905221].

[2] S. Kanno and J. Soda, Phys. Rev. D **66**, 083506 (2002) [arXiv:hep-th/0207029]; *ibid.*, 043526 (2002) [arXiv:hep-th/0205188].

[3] T. Tamaki, S. Kanno and J. Soda, arXiv:hep-th/0307278.

[4] G. W. Gibbons and K. Maeda, Nucl. Phys. B **298**, 741 (1988); D. Garfinkle, G. T. Horowitz and A. Strominger, Phys. Rev. D **43**, 3140 (1991).

[5] O. Kaburaki, I. Okamoto, and J. Katz, Phys. Rev. D **47**, 2234 (1993).

[6] K. Maeda et al., Phys. Rev. Lett. **72**, 450 (1994) [arXiv:gr-qc/9310015].

Gravitational Wave Propagation in Static Brane Universe

Izumi Tanaka[1] and Hideki Ishihara

Department of Mathematics and Physics, Graduate School of Science, Osaka City University, Sugimoto-cho, Sumiyoshi, Osaka 558-8585, Japan

Abstract

We investigate the gravitational waves propagation in the Einstein static brane universe. We define the phase velocity and the group velocity on the brane by boundary values of the waves on the brane. It is shown that both the phase velocity and group velocity of the gravitational waves are larger than the light velocity.

1 Introduction

The string or M-theory suggests the idea of brane world, i.e., our universe is a 4-dimensional sub-manifold, brane, embedded in a higher dimensional spacetime where the matter fields live only on the brane while the gravity can access the bulk spacetime[1]. Randall and Sundrum [2] proposed a flat brane model realized in the 5-dimensional anti-de Sitter bulk. Remarkably, in this model, usual 4-dimensional gravity is recovered at first approximation because of the existence of zero-mode gravitons effectively confined on the brane. Cosmological extension of this model have been investigated by many authors (see references in [3]).

Towrds verification of the brane world, it might be important to investigate the gravitaional wave propagation in the brane universe and clarify difference from the usual 4-dimensional universe because only gravitational waves can travel directly in the bulk. It is pointed out that there exists apparent causality violation: gravitons which travel along null geodesics in the anti-de Sitter bulk can carry information faster than the light on the brane[4],[5].

For the apparent causality violation, the existence of non-vanishing null component of the extrinsic curvature of the brane, which is in proportion to the matter energy on the brane, is essential. Since it is very complicate to study the propagation of gravitational waves in a realistic expanding brane universe, where the brane plays a role of the moving boundary for the waves[6], we consider, here, the Einstein static brane universe for the first step. The Einstein static brane has also desirable extrinsic curvature, and its static property make the problem very simple.

2 Einstein static brane universe

The metric of the 5-dimensional anti-de Sitter(AdS) spacetime is given by

$$ds^2 = -\cosh^2 \chi/l \, dt^2 + d\chi^2 + l^2 \sinh^2 \chi/l \, d\Omega^2_{S^3}, \tag{1}$$

where $d\Omega^2_{S^3}$ is the metric of S^3. The Einstein static brane with a radius $\chi = \chi_b$ solves the 5-dimensional Einstein equation,

$$R_{AB} - \frac{1}{2} g_{AB} R + \Lambda g_{AB} = 0, \quad \Lambda := -\frac{6}{l^2}, \tag{2}$$

and the junction condition at the brane with Z_2 symmetry,

$$K_{ab} = -\frac{1}{2}\kappa^2 (S_{ab} - \frac{1}{3} S \gamma_{ab}), \tag{3}$$

where γ_{ab}, K_{ab}, S_{ab} and κ^2 are the induced metric, the extrinsic curvature, the stress tensor of the perfect fluid on the brane and the five-dimensional gravitational constant, respectively. The energy density of a perfect fluid is determined by the junction condition when the radius of the brane is given.

[1] E-mail:itanaka@sci.osaka-cu.ac.jp, E-mail:ishihara@sci.osaka-cu.ac.jp

n	ω for $\chi_b = 5$	ω for $\chi_b = 10$
1	1000.272521	1000.000052
2	1003.351441	1003.000522
3	1005.535308	1005.000540

Table 1: Eigenvalues are listed for the modes $n = 0, 1, 2$ and $k = 1000$ in the cases $\chi_b = 5$ and $\chi_b = 10$.

Since the bulk is negatively curved, the circumference radius of the spherical brane $r_b = l \sinh \chi_b/l$ is larger than 2π times the proper radius χ_b. When $l \sim 0.1$mm, the present size of the universe $r_b \sim 3000$Mpc is much larger than the corresponding value $\chi_b \sim 1$cm.

3 Bulk perturbation equation

We consider gravitational wave perturbations on the background spacetime (1). In this report, we consider a massless scalar field, Φ, living in the bulk spacetime which mimics the gravitational wave, for simplicity.

The wave equation for the scalar field in the bulk is

$$-(\cosh^2 \chi/l)^{-1}\partial_t^2\Phi + \partial_\chi^2\Phi + \frac{1}{l}(3\coth\chi/l + \tanh\chi/l)\partial_\chi\Phi + \frac{1}{l^2\sinh^2\chi/l}\Delta\Phi = 0, \tag{4}$$

where Δ is the Laplacian on S^3. The Z^2 symmetry with respect to the brane requires the Neumann boundary condition for Φ at the brane. Setting $\Phi = \phi(\chi)Y(x^a)e^{-i\omega t}$, we obtain

$$\frac{d^2}{d\chi^2}\phi + \frac{1}{l}(3\coth\chi/l + \tanh\chi/l)\frac{d}{d\chi}\phi + \left(-\frac{k^2}{l^2\sinh^2\chi/l} + \frac{\omega^2}{\cosh^2\chi/l}\right)\phi = 0, \tag{5}$$

where $Y(x^a)$ are the harmonics on S^3 which satisfy the eqation

$$(\Delta + k^2)Y = 0, \quad k^2 = (m-1)(m+1), \ (m = 1, 2, \cdots). \tag{6}$$

The boundary conditions for ϕ are

$$\partial_\chi\phi|_{\chi=\chi_b} = 0 \quad \text{and} \quad \phi|_{\chi=0} = 0, \tag{7}$$

where the second one is regurality condition at the center $\chi = 0$ for the modes $k \neq 0$.

If k is given, the problem we should solve is the eigenvalue problem for ω in the ordinary differential equation (5) with the boundary conditions (7). The eigenfunction $\phi(\chi)$ is specified by the number of nodes n, and the eigenvalue is obtained as a function in the form $\omega = \omega(k, n)$.

The background spacetime has three typical scales: l, χ_b and r_b. When we consider the massless scalar wave of its wave length λ is much less than l, n takes a large number and the wave propagates along a null geodesic[5] since the approximation of the geometrical optics is valid. In this report, we concentrate on the wave with $\lambda \gtrsim \chi_b$, so it is natural that n possibly takes zero or a non-large number.

4 Results

We solve the problem by shooting method using Runge-Kutta routine, where we set $l = 1$. First, we show typical shape of the eigenfunctions in Fig.1. The boundary value of the eigenfunction, $\phi(\chi = \chi_b)$, is large for $n = 0$ mode and very small for $n = 1, 2$ modes. It means that $n = 0$ mode is dominant for the gravitational phenomena on the brane.

In the case $\chi_b = 10$, the eigenfunctions for $n = 0, 1, 2$ in the region $0 \leq \chi \leq 5$ resemble the counterparts in the case $\chi_b = 5$. While those are almost constant in the region $5 \leq \chi \leq 10$. It might suggest that the expansion of the universe causes small modification for the eigenvalues.

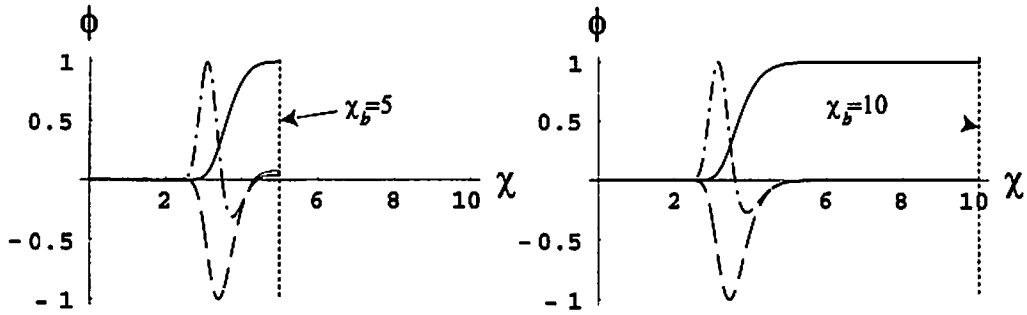

Figure 1: Eigenfunctions for $n = 0, 1, 2$ and $k = 1000$ are plotted in the case $\chi_b = 5$ (left) and $\chi_b = 10$ (right). The eigenfunctions are normalized by the maximal values.

Next, we consider the difference of the gravitational waves propagation on the brane from the one in the usual 4-dimensional universe. In the usual Einstein static universe with the metric $ds^2 = -d\tau^2 + r_b^2 d\Omega^2$, the wave equation for a massless scalar field is

$$-\partial_\tau^2 \Phi + \frac{1}{r_b^2}\Delta\Phi = 0. \tag{8}$$

The solutions in separation variables in the form $\Phi = Y(x^a)e^{-i\tilde{\omega}\tau}$ lead the dispersion relation $\tilde{\omega}^2 = \tilde{k}^2$, where $\tilde{\omega}$ and $\tilde{k} := k/r_b$ are frequency and wavenumber, respectively. Then the phase velocity, v_p, and the group velocity, v_g, are

$$v_p := \frac{\tilde{\omega}}{\tilde{k}} = 1, \quad \text{and} \quad v_g := \frac{\delta\tilde{\omega}}{\delta\tilde{k}} = 1. \tag{9}$$

If $d^2\phi/d\chi^2$ vanishes on the brane, equation (5) with the first condition in (7) leads (8) at the brane. However, this means constancy of $\phi(\chi)$ and make a contradiction to the second condition in (7) for $k \neq 0$, then the term can not be zero on the brane even for $n = 0$ mode. Therefore, the propagation of the waves on the brane is surely different from the one in the 4-dimensional universe.

For the brane case, defining frequency on the brane and wavenumber on the brane as

$$\tilde{\omega} := \frac{\omega}{\cosh\chi_b/l} \quad \text{and} \quad \tilde{k} := \frac{k}{l\sinh\chi_b/l}, \tag{10}$$

we can naturally introduce the phase velocity on the brane and the group velocity on the brane as

$$v_p(\tilde{k}; n) := \frac{\tilde{\omega}(\tilde{k}; n)}{\tilde{k}}, \quad \text{and} \quad v_g(\tilde{k}; n) := \frac{\delta\tilde{\omega}(\tilde{k}; n)}{\delta\tilde{k}}. \tag{11}$$

By numerical calcurations the dispersion relation $\tilde{\omega} = \tilde{\omega}(\tilde{k}; n)$ for $n = 0, 1, 2$ are obtained. According to the numerical results, the phase velocity on the brane for each mode exceeds the light velocity and approaches to the light velocity as $\tilde{k} \to \infty$. For each mode, $v_p - 1$ depends on $\tilde{k}$ as a power function with a negative power (see Fig. 2). Furthermore, the group velocity v_g is shown as a function of $\tilde{k}$ in Fig.3. We can see that the group velocity on the brane for each $n = 0, 1, 2$ mode is larger than the light velocity in the range $\lambda \gtrsim \chi_b$.

How much amount of the excess does the gravitatinal wave velocity have over the light velocity? From the numerical results, we see

$$\frac{v_g|_{\chi_b=10} - 1}{v_g|_{\chi_b=5} - 1} \sim \left(\frac{r_b|_{\chi_b=5}}{r_b|_{\chi_b=10}}\right)^2. \tag{12}$$

The right hand side of (12) is in proportion to the ratio of the null component of extrinsic curvature of the brane in $\chi_b = 10$ to the one in $\chi_b = 5$. It means that the non-vanishing of the quantity[5]. Since the

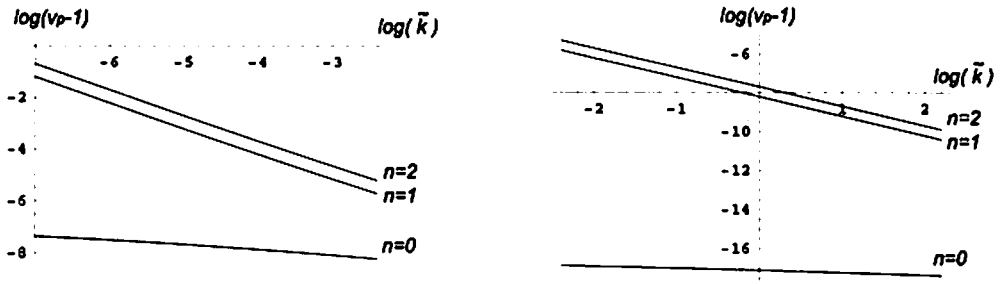

Figure 2: The phase velocity for $n = 0, 1, 2$ modes are plotted as functions of $\tilde{k}$ in cases of $\chi_b = 5$(left) and $\chi_b = 10$ (right).

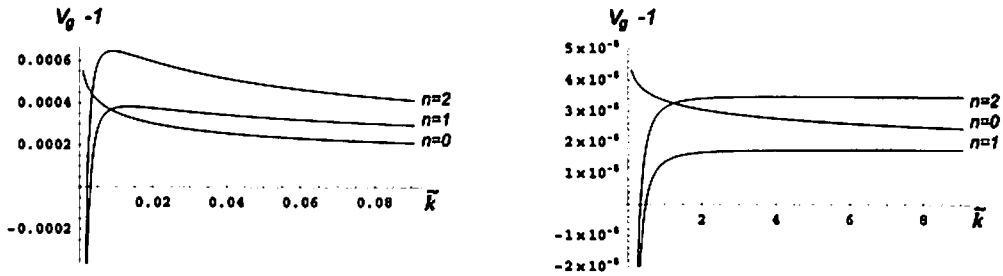

Figure 3: The group velocity for $n = 0, 1, 2$ modes are plotted as functions of $\tilde{k}$ in cases of $\chi_b = 5$(left) and $\chi_b = 10$ (right).

radius of the present universe is enormously large then the null component of extrinsic curvature of the brane takes a tiny value. Then the excess of the gravitational wave velocity over the light velocity might be too small to observe. However, if the gravitational waves propagate long distance or penetrate high density regions, where the extrinsic curvature are large, we would be able to detect some phenomena concerning to the excess.

In the present report, we only treat an over simplified static brane universe model. As noted before, since the radial dependence of the wave functions does not change so much when the radius of the brane increases, then the results obtaind in the static model would hold in the present stage of the realistic expanding universe where the expantion rate is moderate.

In the early stage of the universe, gravitational waves consist of a number of different n-modes. In such a situation, it is expected that the amplitude on the brane changes in its value depending on time and place. Further, it is intresting to study the velocity on the brane for modes mixed waves.

References

[1] P. Horava and E. Witten, Nucl. Phys. B **475**, 94 (1996).

[2] L.Randall, R.Sundrum, Phys. Rev. Lett. **83**, 4690 (1999).

[3] R.Maartens, arXiv:gr-qc/0312059

[4] D.J.H.Chung and K.Freese, Phys. Rev. **D61** (2000) 023511.

[5] H. Ishihara, Phys. Rev. Lett. **86**, 063513 (2001);
H.Ishihara, Phys. Rev. **D66** (2002) 023513.

[6] T. Hiramatsu, K. Koyama, and A. Taruya, Phys.Lett.**B578** (2004)269;
K. Ichiki , K. Nakamura, arXiv:hep-th/0310282.

The AdS/CFT correspondence in Friedmann braneworld

Takahiro Tanaka[1]

Department of Physics, Graduate School of Science,
Kyoto University, Kyoto 606-8502, Japan

Abstract

If the AdS/CFT correspondence conjecture holds, the Randall-Sundrum infinite braneworld is equivalent to four dimensional Einstein gravity with $\mathcal{N} = 4$ super Yang-Mills fields at low energies. Here we derive a four dimensional effective equation of motion for tensor-type perturbations on a Friedmann brane background in two different pictures, and demonstrate their equivalence.

1 Introduction

Randall and Sundrum proposed very interesting braneworld scenarios[1, 2]. Especially the second model[2] (RS II) has attracted a lot of attention as a toy model which realizes a new scheme of compactification of an extra dimension[3, 4]. The model assumes five dimensional spacetime. The five dimensional bulk dynamics is governed by the vacuum Einstein equations with a negative cosmological constant. Ordinary matter fields are confined to a four dimensional brane located at a boundary of the bulk. Across the brane Z_2-symmetry is imposed. The simplest solution of the bulk is a five dimensional AdS spacetime

$$ds^2 = -\frac{\ell}{z^2}\left(-dt^2 + \delta_{ij}dx^i dx^j + dz^2\right),$$

where ℓ is the AdS curvature length. Latin indices are used for 3-dimensional spatial coordinates and are raised and lowered by using the Kronecker delta δ_{ij}. A brane which moves in z-direction represents a flat Friedmann universe. The scale factor on the brane is read as $a = \ell/z(t)$, and the Hubble parameter H is related to the brane motion as $H = -\dot{z}/\ell\sqrt{1-\dot{z}^2}$, where dot represents diffenciation with respect to t. From the junction condition on the brane, the motion of the brane is determined, and we obtain a modified Friedmann equation

$$\mathcal{H}^2 = \frac{8\pi G}{3}a^2\left(\rho + \frac{\rho^2}{2\sigma}\right), \tag{1}$$

where $\mathcal{H} \equiv aH$ and ρ is the total energy density of matter fields localized on the brane.

According to the AdS/CFT conjecture[5, 6], the RS II model is thought to be equivalent to four dimensional Einstein gravity with correction due to CFT fields at low energies. Here low energies mean that typical length scales are longer than the bulk curvature scale ℓ. The conjecture in this form is directly confirmed in the case of linear perturbations on a Minkowski brane[7]. Also in the case of Friedmann homogeneous cosmology the correspondence holds[8].

In this talk we give another example for the equivalence between two pictures. One is the RS II model and the other is four dimensional Einstein gravity with CFT. We consider tensor-type perturbations on a Friedmann brane. We derive the leading order deviations from the conventional four dimensional gravity at low energies in both pictures independently, and show the equivalence of two results.

2 Five dimensional RS picture

First we discuss tensor-type perturbations on a Friedmann brane in the five dimensional RS picture. The bulk metric with tensor type perturbations will be given by

$$ds^2 = \frac{\ell^2}{z^2}\left(-dt^2 + (\delta_{ij} + h_{ij})dx^i dx^j + dz^2\right). \tag{2}$$

[1] E-mail:tama@scphys.kyoto-u.ac.jp

By using Y_k^{ij}, a transverse traceless tensor harmonics normalized as $\int d^3x\, Y_{kij}(\mathbf{x})Y_{k'}^{ij}(\mathbf{x}) = \delta^3(\mathbf{k}-\mathbf{k}')$, we expand perturbations as $h_{ij} = Y_{kij}\Phi$. In these coordinates the five dimensional perturbation equation reduces to

$$\left(-\partial_z^2 + \frac{3}{z}\partial_z + \partial_t^2 + k^2\right)\Phi = 0. \tag{3}$$

The general solution to this equation is given by

$$\begin{aligned}\Phi &= \int d\omega\, \tilde{\Psi}(\omega)e^{-i\omega t}2(pz)^2K_2(pz) \\ &= \int d\omega\, \tilde{\Psi}(\omega)e^{-i\omega t}\left[1 - \frac{(pz)^2}{4} + \frac{(pz)^4}{16}\left(b - \ln(pz)\right) + \cdots\right],\end{aligned} \tag{4}$$

where $p^2 = -(\omega + i\epsilon)^2 + k^2$, $b = \frac{1}{2}\left(\frac{3}{2} - 2\gamma\right) + \ln 2$, and γ is Euler's constant. The problem is solved, if we can find $\tilde{\Psi}$ so as for Φ to satisfy the perturbed junction condition $n^\rho\partial_\rho\Phi = 0$, where n^ρ is the unit normal to the brane.

In this paper we use an alternative approach to derive the correction from the conventional four dimensional gravity. In Ref. [9] effective Einstein equations

$${}^{(4)}G^\mu_{\ \nu} - 8\phi G_4 T^\mu_{\ \nu} = (8\pi G_5)^2\pi^\mu_{\ \nu} - E^\mu_{\ \nu}, \tag{5}$$

were derived, where $\pi^\mu_{\ \nu}$ is a tensor quadratic in the matter energy momentum tensor $T^\mu_{\ \nu}$ and $E^\mu_{\ \nu}$ is a projected Weyl tensor defined by $n^\rho n^\sigma C^\mu_{\ \rho\nu\sigma}$. From Eq. (5) the effective four dimensional equation for tensor perturbations is deduced as

$$\left(\partial_\eta^2 + 2\mathcal{H}\partial_\eta + k^2\right)\phi = -2E, \tag{6}$$

where $\phi \equiv \Phi|_{z=z(t)}$, η is the conformal time coordinate for the geometry induced on the brane and the correction due to $E_{\mu\nu}$ is explicitly given as

$$-2E = \left\{(H\ell)^2\left(\partial_t^2 + \partial_z^2\right) - 2H\ell\sqrt{1+(H\ell)^2}\partial_t\partial_z + \left(\partial_z^2 - \frac{1}{z}\partial_z\right)\right\}\Phi\Big|_{z=z(t)}, \tag{7}$$

At low energies (when $H^2\ell^2 \ll 1$ and $(pz)^2 = p\ell/a \ll 1$), z and t derivatives are rather straight forward by using the expression (4). However, if we try to write E in terms of ϕ, we must rewrite ω (or p) somehow. $-i\omega$ is very close to but slightly different from η derivative. But if we neglect higher order terms of $O(\ell^4)$, further reduction is possible like

$$\begin{aligned}&\partial_t^2\Phi \approx \partial_\eta^2\Phi, \\ &\partial_z^2\Phi \approx -\frac{1}{2}\int d\omega\, \tilde{\Psi}e^{-i\omega\eta}p^2 \approx -\frac{1}{2}\left(\partial_\eta^2 + k^2\right)\Phi, \\ &\partial_t\partial_z\Phi \approx -\frac{\ell}{2a}\partial_\eta\left(\partial_\eta^2 + k^2\right)\Phi.\end{aligned} \tag{8}$$

Only the last term $\left(\partial_z^2 - \frac{1}{z}\partial_z\right)\Phi$ does not allow such a simple reduction because the third term in the expansion of $K_2(pz)$, which is not a polynomial in p^2, contributes to this term. This term does not have explicit ℓ^2 suppression at first sight. However, first two terms in the expansion of $K_2(pz)$ vanish for this combination of differentiation. As a result, a factor of $z^2 = \ell^2/a^2$ arises. We finally obtain

$$\begin{aligned}&\left(\partial_\eta^2 + 2\mathcal{H}\partial_\eta + k^2\right)\phi \\ &\quad\approx \frac{\ell^2}{a^2}\left[\left(3\mathcal{H}^3 - 2\mathcal{H}\mathcal{H}'\right)\partial_\eta + k^2\mathcal{H}^2\right]\phi \\ &\qquad + \frac{\ell^2}{2a^2}\int d\omega\, \tilde{\phi}e^{-i\omega\eta}p^4\left(b - \frac{3}{4} - \ln\left[\frac{p\ell}{a}\right]\right),\end{aligned} \tag{9}$$

where we used the lower order equation obtained by setting the left hand side equal to zero to simplify the right hand side. A similar equation was derived for scalar-type perturbations in Ref. [10]. All the corrections are suppressed by ℓ^2 or $\ell^2\ln\ell$.

3 Four dimensional CFT picture

Next we discuss the same problem in the four dimensional CFT picture. The equation for tensor-type perturbations will be given in the form of

$$\partial_\eta a^2 \partial_\eta \phi + a^2 k^2 \phi = 16\pi G a^2 \tau, \tag{10}$$

where the perturbation variable ϕ has the same meaning as before, and $\tau(\eta) \equiv \int d^3x\, T^{(CFT)}_{ij}(\eta, \mathbf{x}) Y^{ij}_k(\mathbf{x})$ is the contribution from the effective energy momentum tensor of CFT. In order to evaluate the energy momentum tensor due to vacuum polarization of CFT, we can make use of the fact that the metric of flat perturbed FLRW universe is related via conformal transformation to Minkowski spacetime with the corresponding perturbations as

$$ds^2_{(1)} = g_{\mu\nu} dx^\mu dx^\nu = a^2(\eta) ds^2_{(0)}, \tag{11}$$

where $ds^2_{(0)} = g^{(0)}_{\mu\nu} dx^\mu dx^\nu = (\eta_{\mu\nu} + h_{\mu\nu}) dx^\mu dx^\nu$. We consider one parameter family of conformally related metrics $g^{(\theta)}_{\mu\nu} = a^{2\theta} g^{(0)}_{\mu\nu}$ connecting $g_{\mu\nu} \equiv g^{(1)}_{\mu\nu}$ with $g^{(0)}_{\mu\nu}$. The action for CFT is invariant under conformal transformation except for $T^{(A)}_{\mu\nu}$, the contribution from the conformal anomaly. Hence, the energy momentum tensor of CFT excluding the anomaly contribution transforms in a trivial manner under a conformal transformation. Thus we have

$$T^{(CFT)}_{\mu\nu} = a^{-2} T^{(0)}_{\mu\nu} + T^{(A)}_{\mu\nu}, \tag{12}$$

where $T^{(0)}_{\mu\nu}$ is the CFT energy momentum tensor evaluated on the metric $g^{(0)}_{\mu\nu}$. Correspondingly, τ is given as a sum of two pieces, $\tau^{(0)}$ and $\tau^{(A)}$.

By using the results in Ref.[7], $\tau^{(0)}$ is found to be given by

$$-16\pi G a^2 \tau^{(0)} = 2 \int d\omega\, e^{-i\omega\eta} \Pi_2(p^2)\, p^4 \tilde{\phi}(\omega), \tag{13}$$

with

$$\Pi_2(p^2) = \frac{\ell^2}{8} \ln \frac{p^2}{\mu^2}, \tag{14}$$

where we used the properties of tensor-type perturbations, $h^{0\alpha} = 0$, $h_j{}^j = 0$, and $h^{ij} k_j = 0$. Constant part in $Pi_2(p^2)$ was absorbed by the renormalization scale μ. Here $\tilde{\phi}(\omega)$ is the Fourier transform of $\phi(\eta)$.

Next we consider the anomaly contribution $\tau^{(A)}$. The anomaly contribution to the effective action, $S^{(A)}$, is given by an integral of the trace anomaly from $\theta = 0$ to 1 as[11]

$$S^{(A)} = -\int_0^1 d(\ln\Omega) \int d^4x \sqrt{-g^{(\theta)}} < T_\rho{}^\rho[g^{(\theta)}] > \equiv -\frac{1}{16\pi^2} \int_0^1 a_2^\theta \ln a\, d\theta. \tag{15}$$

From Ref. [6] we find $a_2^\theta = \int d^4x \frac{N^2}{6} \sqrt{-g^{(\theta)}} (3R_{\mu\nu}R^{\mu\nu} - R^2)[g^{(\theta)}]$, and $N^2 = \pi\ell^2/G$ is the number of degrees of freedom of CFT. The anomaly contribution to the energy momentum tensor is obtained by taking variation of $S^{(A)}$ as $T^{(A)}_{\mu\nu} = -(1/2\sqrt{-g})(\delta S^{(A)}/\delta g^{\mu\nu})$. Expanding the action up to second order in $h_{\mu\nu}$, we obtain

$$S^{(A)} = \frac{\ell^2}{64\pi G} \int d\eta \left(2\mathcal{H}^4 + \sum_k \phi \left[\ln a \left(\partial_\eta^2 + k^2 \right)^2 + \mathcal{O} \right] \phi \right), \tag{16}$$

where

$$\mathcal{O} = 2\mathcal{H}\partial_\eta^3 + \left(\mathcal{H}' + \mathcal{H}^2\right)\partial_\eta^2 + \left((\mathcal{H}^2)' + \mathcal{H}k^2\right)\partial_\eta + k^2\left(\mathcal{H}' - \mathcal{H}^2\right) + 4\mathcal{H}'\mathcal{H}^2 - \mathcal{H}^4. \tag{17}$$

The first term in the round brackets in Eq. (16) gives a correction to the background Friedmann equation. Variation of the action with setting $\phi = 0$ leads to

$$aa'' = \frac{4\pi G}{3} a^4(\rho - 3P) + \frac{\ell^2}{2} \mathcal{H}^2 \mathcal{H}'. \tag{18}$$

Using the continuity equation $\rho' = -3\mathcal{H}(\rho + P)$, we can integrate Eq. (18) once to obtain

$$\mathcal{H}^2 = \frac{8\pi G}{3}a^2\rho + \frac{\ell^2}{4a^2}\mathcal{H}^4 + \frac{C}{a^2}. \tag{19}$$

Here C arises as an integration constant. This term represents the so-called dark radiation. It is easy to verify the equivalence between Eqs. (1) and (18) up to $O(\ell^2)$ when $C = 0$.

The ϕ-dependent part of the anomaly contribution is given by

$$16\pi G a^2 \delta\tau^{(A)} = 16\pi G \frac{\delta S^{(A)}}{\delta\phi} = \frac{\ell^2}{2}\left[\ln a \left(\partial_\eta^2 + k^2\right)^2 + \mathcal{O}\right]\phi. \tag{20}$$

Combining two contributions $\tau^{(0)}$ and $\delta\tau^{(A)}$, using the background equation and the lower order perturbations equation, we can write down the modified equation of motion for ϕ as

$$\left(\partial_\eta^2 + 2\mathcal{H}\partial_\eta + k^2\right)\phi \approx \frac{\ell^2}{a^2}\left[\left(3\mathcal{H}^3 - 2\mathcal{H}\mathcal{H}'\right)\partial_\eta + k^2\mathcal{H}^2 + \frac{2C}{a^2}\right]\phi - \frac{\ell^2}{2a^2}\int d^4p\,\tilde{\phi}e^{-i\omega\eta}p^4 \ln\left(\frac{p}{a\mu}\right). \tag{21}$$

Hence, we find that the above equation for tensor-type perturbations is identical to Eq. (9) obtained in the five dimensional RS II picture, as far as the dark radiation term, which we neglected in deriving Eq. (9), is set to zero. Therefore a proof of equivalence of two pictures in the problem of tensor-type perturbations in a Friedmann brane is established.

The author would like to thank Roy Maartens, Shinji Mukohyama and Tsutomu Kobayashi for valuable discussions. This work was supported in part by the Monbukagakusho Grant-in-Aid Nos. 12740154 and 14047212 and by the Inamori Foundation.

References

[1] L. Randall and R. Sundrum, Phys. Rev. Lett. **83**, 3370 (1999).

[2] L. Randall and R. Sundrum, Phys. Rev. Lett. **83**, 4690 (1999).

[3] D. Langlois, Prog. Theor. Phys. Suppl. **148**, 181 (2003).

[4] R. Maartens, arXiv:gr-qc/0312059.

[5] J. M. Maldacena, Adv. Theor. Math. Phys. **2**, 231 (1998).

[6] S.W. Hawking, T. Hertog and H.S. Reall Phys. Rev. D **62** 043501 (2000).

[7] M. J. Duff and J. T. Liu, Phys. Rev. Lett. **85**, 2052 (2000).

[8] T. Shiromizu and Daisuke Ida Phys. Rev. D **64** 044015 (2001).

[9] T. Shiromizu, K. i. Maeda and M. Sasaki, Phys. Rev. D **62**, 024012 (2000).

[10] K. Koyama and J. Soda, Phys. Rev. D **65**, 023514 (2002);
K. Koyama and J. Soda, JHEP **0105**, 027 (2001).

[11] Birrel and Davis, *Quantum field in curved space*, p181, Cambridge univeristy press.

Various features of quasiequilibrium sequences of binary neutron stars in general relativity

Keisuke Taniguchi[1]

Department of Earth Science and Astronomy, Graduate School of Arts and Sciences, University of Tokyo, Komaba, Meguro, Tokyo 153-8902, Japan

Eric Gourgoulhon[2]

Laboratoire de l'Univers et de ses Théories, UMR 8102 du C.N.R.S., Observatoire de Paris, F-92195 Meudon Cedex, France

Abstract

Quasiequilibrium sequences of binary neutron stars are numerically calculated in the framework of the Isenberg-Wilson-Mathews (IWM) approximation of general relativity. The results are presented for both rotation states of synchronized spins and irrotational motion, the latter being considered as the realistic one for binary neutron stars just prior to the merger. We assume a polytropic equation of state and compute several evolutionary sequences of binary systems composed of different-mass stars as well as identical-mass stars with adiabatic indices $\gamma = 2.5, 2.25, 2$, and 1.8. From our results, we propose as a conjecture that if the turning point of binding energy (and total angular momentum) locating the innermost stable circular orbit (ISCO) is found in Newtonian gravity for some value of the adiabatic index γ_0, that of the ADM mass (and total angular momentum) should exist in the IWM approximation of general relativity for the same value of the adiabatic index.

1 Introduction

The final stage of coalescing binary neutron stars is one of the most promising sources of gravitational waves for ground-based laser interferometers, and is also considered as one of the candidates for short-duration gamma-ray burst sources. With accurate templates of gravitational waves from coalescing binary neutron stars, it may be possible to extract informations from signals observed by the interferometers through the matched filtering technique. Therefore, it is essential to theoretically predict the wave form of gravitational radiation as well as to understand the details of the physics of binary neutron stars. With such a motivation, many efforts have been invested in this topic (some recent reviews can be found in [1])

In the present article, we focus on the *intermediate* phase (or *hydrodynamical inspiral* phase) of the evolution of binary neutron stars, in which the separation between the two components is as small as a few times of the radius of one star. This phase is also inspiraling, the time scale of the orbital shrink being still larger than the orbital period, hence the qualifier of *quasiequilibrium* given to it. What differs this phase from the pointlike inspiral is that the tidal deformation of the stars is no longer negligible, making necessary a hydrodynamical treatment, in addition to general relativity. This phase is interesting because one might get informations on the equation of state of nuclear matter [2]. Furthermore, the most realistic initial data for computing the merger are given at the end point of sequences in the hydrodynamical inspiral [3, 4].

Binary neutron stars gradually decrease their orbital separations as a result of the emission of gravitational radiation. However, it is still impossible to integrate the Einstein's equations for the thousands of orbits of the hydrodynamical inspiral. Fortunately the time scale of the orbit shrink being much longer than the orbital period, the hydrodynamical inspiral phase can be approximated by a sequence

[1] E-mail:keisuke@provence.c.u-tokyo.ac.jp
[2] E-mail:Eric.Gourgoulhon@obspm.fr

of steady-state (quasiequilibrium) configurations. In order to combine general relativity and quasiequilibrium, we adopt the conformal-flatness condition for the spatial part of the metric — the so-called Isenberg-Wilson-Mathews (IWM) approximation of general relativity [5, 6, 7] (see [8] for a discussion). This treatment postpones one of the goals of the study of the hydrodynamical inspiral, i.e. the theoretical prediction of the wave form of gravitational radiation. Accordingly, we focus on the evolution of various physical parameters during the hydrodynamical inspiral and investigate the nature of the innermost orbit (mass-shedding or orbital instability).

To get a quasiequilibrium configuration of binary neutron stars, we have to specify the rotation state of the system. About ten years ago, Kochaneck [9] and Bildsten and Cutler [10] concluded that the irrotational flow is much more realistic than the synchronized rotation, because the shear viscosity of nuclear matter is far too low to synchronize the spins of the stars with the orbital motion by the dynamical merging. The formulation for solving quasiequilibrium configurations of irrotational binary neutron stars in general relativity has been proposed by several authors [11, 12, 13, 14]. In the present work, we have calculated not only irrotational configurations but also synchronized ones in order to exhibit the differences between these two extreme states. Beside the type of rotation, some equation of state for neutron star matter must be specified to get a binary model. Although some realistic equation of state arising from nuclear physics has to be used, we adopt here the polytropic one for simplicity. Nevertheless we vary the adiabatic index in the range $\gamma = 1.8$ to 3 to cover the large range of nuclear equations of state published in the literature.

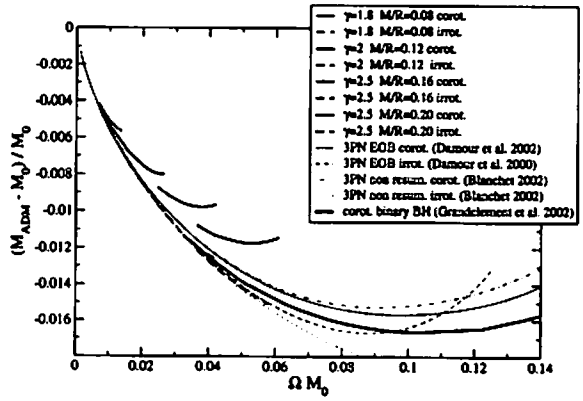

Figure 1: Relative binding energy along evolutionary sequences of equal-mass binary neutron stars, compared with (i) analytical results at the 3rd post-Newtonian order for point-masses by Damour et al. 2000 [19], Damour et al. 2002 [20] and Blanchet 2002 [21], and with (ii) numerical results for corotating binary black holes by Grandclément et al. 2002 [22]. Ω is the orbital angular velocity and M_0 is twice the gravitational mass of a single static neutron star (resp. black hole) of the same baryon number (resp. same horizon area) as that defining the considered sequence.

Under the above assumptions, we have computed quasiequilibrium sequences of binary systems composed of neutron stars with different masses. Until now, all studies on quasiequilibrium sequences of binary neutron stars in the framework of general relativity have dealt with only identical-mass binary systems, except for our previous work [15]. In that article we have also presented quasiequilibrium sequences of binary neutron stars with a polytropic equation of state. However, we limited ourselves to the adiabatic index $\gamma = 2$, because it was the first step to relativistic different-mass binary systems. In the present article, we enlarge the range of adiabatic index, investigating softer equations of state ($\gamma = 1.8$) and stiffer ones ($\gamma = 2.25$, 2.5 and 3), and show some selected results based on the recent paper [16].

2 Formulation

The details about our method and basic equations have been already given in previous papers of this series (Refs. [17] and [18]). We refer the interested reader to those articles.

3 Numerical results

The spirit of the quasiequilibrium approach is to model the (gravitational-radiation driven) evolution of a neutron star binary by a sequence of steady-state circular-orbit configurations. Along the sequence the

baryon number is kept constant, since no matter loss occurs during the evolution of each star, until the end of the inspiral stage. Such constant-baryon-number sequences are called *evolutionary sequences*.

We have computed numerous evolutionary sequences, for different values of the adiabatic index γ and various compactness. We have used 5 (resp. 4) domains for each star and the space around it in the case of a large (resp. small) separation. In each domain, the number of collocation points of the spectral method is chosen to be $N_r \times N_\theta \times N_\varphi = 25 \times 17 \times 16$ or $33 \times 25 \times 24$, where N_r, N_θ, and N_φ denote the number of collocation points in respectively the radial, polar, and azimuthal directions.

In Fig. 1, we present the ADM mass as a function of the orbital angular velocity with a scaling defined by twice the gravitational mass of the single static neutron star of the same baryon number as that of the sequence M_0. Note that M_0 can also be viewed as the ADM mass at infinite separation. This enables us to compare with third order post-Newtonian results for point-mass particles obtained in the Effective One Body (EOB) approach by Damour et al. [19, 20] or in the standard non-resummed post-Newtonian framework by Blanchet [21]. This also enables us to compare with corotating binary black holes, according to the numerical results by Grandclément et al. [22]. We note from these figures that the irrotational binary neutron star sequences are very close to the 3PN irrotational ones (dashed and dotted fine curves). Moreover, all curves converges at large separation (small value of ΩM_0), which can be considered as a check of our numerical computations, especially the way Ω is determined.

Another interesting feature shown in Fig. 1 is the good agreement between the irrotational binary neutron star sequence with high compactness ($M/R = 0.20$) and the binary black hole sequence. The latter is made of corotating black holes, but for $\Omega M_0 \leq 0.06$, the spin effects are not very important, so that it is meaningful to compare the corotating black hole sequence up to $\Omega M_0 \leq 0.06$ with the irrotational neutron star sequence.

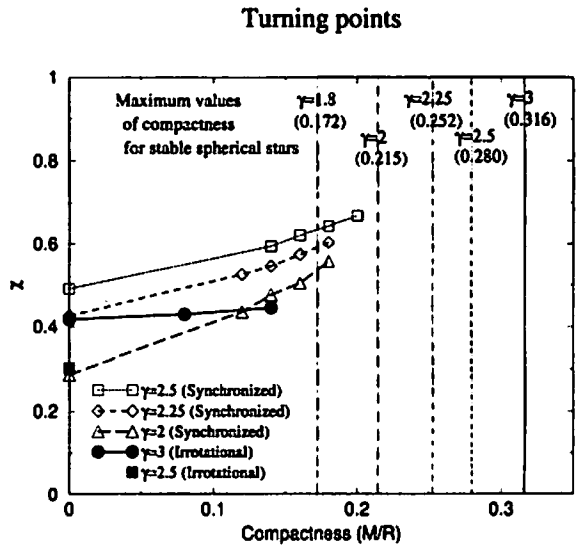

Figure 2: Positions of the turning points of the ADM mass (and total angular momentum) in the sequence as a function of the compactness parameter. Solid curve with filled circle is for the irrotational binary system with $\gamma = 3$. Dotted with open square, dashed with open diamond, and long-dashed with open triangle denote the results of synchronized binary systems with $\gamma = 2.5$, 2.25, and 2, respectively. Vertical solid, dotted, dashed, and long-dashed lines are maximum values of compactness for stable spherical stars (at $\chi = 1$) for $\gamma = 3$, 2.5, 2.25, 2, and 1.8, respectively. Here, the quantity χ denotes the equatorial to polar ratio of the radial derivative of the enthalpy ($\chi := (\partial H/\partial r)_{\rm eq,comp}/(\partial H/\partial r)_{\rm pole}$).

4 Summary

We have developed a numerical code for computing quasiequilibrium sequences of binary neutron stars through the series of works [17, 18, 23, 15]. In the present article, we have presented the results of relativistic computations of both synchronized and irrotational rotation states, for polytropic equations of state with several adiabatic indices based on the recent paper [16]. We have considered not only binary systems composed of identical-mass stars but also different-mass systems. We have investigated the behaviors of various physical quantities along constant baryon number sequences (evolutionary sequences): the relative change in central energy density, the ADM mass, the total angular momentum, the shape of the figures, as well as the location of the end point and that of the turning point in the ADM mass and angular momentum.

As one of interesting results, we propose, as a conjecture, that if the turning points defining the ISCO are found for the Newtonian calculations for some adiabatic index γ, they should exist in the general relativistic computations for the same value of γ. Of course, this conjecture is derived from the results of non-realistic cases such as synchronized

binary systems or irrotational ones with $\gamma = 3$. Furthermore, since the inclination of lines in Fig. 2 is positive, it is not possible to exactly predict whether or not a turning point appears in the IWM approximation when there is no turning point in the Newtonian calculation. However, if the computations of irrotational binary systems for $\chi < 0.2$ could be obtained in the future with sufficient accuracy in Newtonian gravity, which is easier to be calculated than in the relativistic framework, it would be possible to speculate about the turning points in the IWM approximation without computations.

Acknowledgments

KT acknowledges a Grant-in-Aid for Scientific Research (No. 14-06898) of Japan Society for the Promotion of Science.

References

[1] T.W. Baumgarte and S.L. Shapiro, Phys. Rep. **376**, 41 (2003).

[2] J.A. Faber, P. Grandclément, F.A. Rasio, and K. Taniguchi, Phys. Rev. Lett. **89**, 231102 (2002).

[3] M. Shibata and K. Uryu, Phys. Rev. **D61**, 064001 (2000); Prog. Theor. Phys., **107**, 265 (2002).

[4] M. Shibata, K. Taniguchi, and K. Uryu, Phys. Rev. **D68**, 084020 (2003).

[5] J. A. Isenberg : *Waveless approximation theories of gravity*, preprint University of Maryland, unpublished (1978).

[6] J. Isenberg and J. Nester, in *General Relativity and Gravitation*, edited by A. Held (Plenum, New York, 1980), Vol. 1.

[7] J.R. Wilson and G.J. Mathews, in *Frontiers in numerical relativity*, edited by C.R. Evans, L.S. Finn and D.W. Hobill (Cambridge University Press, Cambridge, England, 1989).

[8] J.L. Friedman, K. Uryu, and M. Shibata, Phys. Rev. **D65**, 064035 (2002).

[9] C.S. Kochaneck, Astrophys. J. **398**, 234 (1992).

[10] L. Bildsten and C. Cutler, Astrophys. J. **400**, 175 (1992).

[11] S. Bonazzola, E. Gourgoulhon, and J.-A. Marck, Phys. Rev. **D56**, 7740 (1997).

[12] H. Asada, Phys. Rev. **D57**, 7292 (1998).

[13] M. Shibata, Phys. Rev. **D58**, 024012 (1998).

[14] S.A. Teukolsky, Astrophys. J. **504**, 442 (1998).

[15] K. Taniguchi and E. Gourgoulhon, Phys. Rev. **D66**, 104019 (2002).

[16] K. Taniguchi and E. Gourgoulhon, Phys. Rev. **D68**, 124025 (2003).

[17] E. Gourgoulhon, P. Grandclément, K. Taniguchi, J.-A. Marck, and S. Bonazzola, Phys. Rev. **D63**, 064029 (2001).

[18] K. Taniguchi, E. Gourgoulhon, and S. Bonazzola, Phys. Rev. **D64**, 064012 (2001).

[19] T. Damour, P. Jaranowski, and G. Schäfer, Phys. Rev. D **62**, 084011 (2000).

[20] T. Damour, E. Gourgoulhon, and P. Grandclément, Phys. Rev. D **66**, 024007 (2002).

[21] L. Blanchet, Phys. Rev. D **65**, 124009 (2002).

[22] P. Grandclément, E. Gourgoulhon, and S. Bonazzola, Phys. Rev. D **65**, 044021 (2002).

[23] K. Taniguchi and E. Gourgoulhon, Phys. Rev. **D65**, 044027 (2002).

Gravothermal Catastrophe and Quasi-equilibrium Structure in N-body Systems

Atsushi Taruya[1], Masa-aki Sakagami[2]

[1] *Research Center for the Early Universe(RESCEU), School of Science, University of Tokyo, Tokyo 113-0033, Japan*

[2] *Graduate School of Human and Environmental Studies, Kyoto University, Kyoto 606-8501, Japan*

Abstract

We discuss the the quasi-equilibrium and the quasi-attractive properties of self-gravitating N-body systems found in the previous numerical study. In particular, a systematic N-body simulations starting from the various initial conditions are presented, which reveals that for moderate range of the dimensionless energy, $0.3 \lesssim \lambda(\equiv -Er_e/GM^2) \lesssim 0.8$, the quasi-attractive behavior generally appears for systems with shallow slope of the central density profile. Based on this numerical results, physical reason for quasi-attractive feature is discussed.

1 Introduction

Self-gravitating N-body system as prototypical long-range system has several distinctive features from the short-range systems. Among these, the negative specific heat is an essential ingredient to understand the late-time phase of the self-gravitating systems. In presence of this, the thermal equilibrium of the stellar system cannot be always stable and most of the system finally undergoes core-collapse. This phenomenon is the so-called *gravothermal catastrophe*, originally named by Lynden-Bell & Wood[1], which has been first investigated by Antonov[2] in a very idealistic situation, i.e., stellar self-gravitating system confined in an adiabatic wall of the radius r_e.

Previously, we have numerically studied the long-term evolution of N-body system confined in an adiabatic wall[3]. In this study, we were especially interested in the quasi-equilibrium behavior away from the thermal equilibrium, which might have to do with the thermostatistics beyond standard Boltzmann-Gibbs theory. The major findings of our previous study is summarized as follow:

Quasi-equilibrium behavior : In stellar system confined in a spherical container, no stable equilibrium configuration exists except for the Boltzmann-Gibbs state(isothermal distribution). Thus, any systems starting from the non-isothermal distribution gradually change in time, on the timescale of two-body relaxation time. However, focusing on the transient states, we found that the evolutionary sequence can be remarkably fitted by a sequence of *stellar polytropic distribution* satisfying the polytropic equation of state $P \propto \rho^{1+1/n}$, with varying polytrope index n.

Quasi-attractive feature : The above quasi-equilibrium feature can be seen even when the initial state is not the stellar polytropic distribution. In the case starting from the Hernquist model[4], which has a cuspy density profile $\rho(r) \propto 1/r/(r+a)^3$, the central cusp is smeared and flat core is eventually formed. Then the transient state can be approximately characterized by a sequence of stellar polytrope for a long time.

These results are remarkable and amazing in a sense that the stellar polytropic distribution as a possible dynamical equilibrium state might have a special meaning in characterizing the transient state of the stellar system, which is completely different from the standard view of stellar dynamics. Further, the results even suggest a possible connection with non-extensive thermostatistics [5, 6, 7].

To understand these numerical findings, we should further study the quasi-equilibrium and the quasi-attractive properties in details, from the physical point of view. In this article, especially focusing on the transient state from the various initial distributions, we numerically investigate the physical reason for quasi-attractive property.

[1] E-mail:ataruya@utap.phys.s.u-tokyo.ac.jp

[2] E-mail:sakagami@phys.h.kyoto-u.ac.jp

2 N-body Simulations and Results

In order to investigate the quasi-attractive feature numerically, we perform a series of N-body simulations starting from the various initial conditions. Without loss of generality, we set the units $G = M = r_e = 1$. Here, we briefly mention the initial distribution. The setup of the N-body simulation together with some important parameters is given in [3].

The initial distribution we adopt here is so-called Tremaine's family of stellar models(TFSM)[8], which are the two-parameter family of spherical stellar distribution whose density profile is given by:

$$\rho(r) \propto \frac{1}{(r/a)^{3-\eta}(1+r/a)^{1+\eta}}. \tag{1}$$

Note that the above family of models includes some popular models: the Hernquist model ($\eta = 2$) and the Jaffe model ($\eta = 1$). In Fig.1, the equilibrium properties of the TFSM are summarized in the (a, λ)-plane, where a is the scale-radius of the system and λ is the dimensionless energy given by $\lambda = -r_e E/GM^2$. For a system with isotropic velocity distribution, the one-particle distribution function $f(\varepsilon)$ can be reconstructed from the density profile $\rho(r)$ through the Eddington formula. Then, using $f(\varepsilon)$, one can easily generate the random initial data set. To perform the simulation, we have made use of different realization of the initial data in each model parameter.

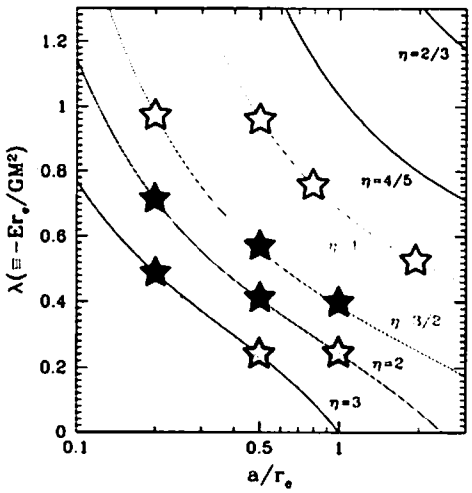

Figure 1: Equilibrium sequence of Tremaine's family of stellar models in (a, λ)-plane. The *filled-stars* represent the initial distribution of the simulation whose transient state can be well-fitted by a sequence of stellar polytropes, while no such quasi-attractive transients have appeared in the *open-stars*. The *shaded-stars* indicate the initial state of the simulations which finally approaches stable isothermal distribution.

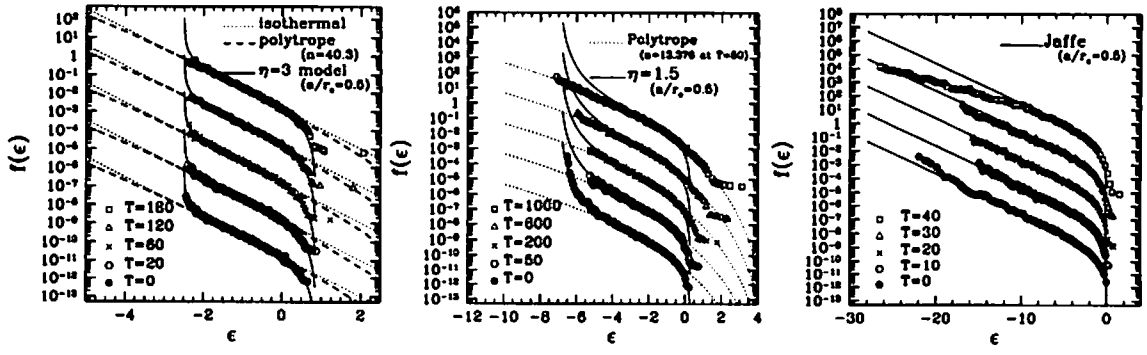

Figure 2: Evolution of one-particle distribution function from Tremaine's family of stellar models in cases with scale-radius $a/r_e = 0.5$. For illustrative purposes, each output result is artificiality shifted to the two digits below. In each panel, solid lines represent the theoretical curve for initial distribution, while the dotted and the dashed lines are the fitting result of the N-body data to the stellar polytropic and the isothermal distributions. *Left*: $\eta = 3$; *Middle*: $\eta = 1.5$; *Right*: $\eta = 1$(Jaffe model)

Let us now mention the main results of our N-body runs. In Fig.1, the survey results of the N-body simulation are marked by the *open-*, *filled-* and *shaded-stars*, which reveal the fact that the appearance of the quasi-attractive behavior is forbidden for some model parameters, a and η. Fig.2 shows the snapshots of the one-particle distribution $f(\varepsilon)$ as typical examples in absence/presence of the quasi-attractive behavior. Roughly speaking, the quasi-attractive feature appears in a moderate range of the energy ($0.3 \lesssim \lambda \lesssim 0.8$) when the slope of the central density profile is shallow, $\eta > 1$. In the energy range with $\lambda \lesssim 0.3$, there exists the stable isothermal distribution(Boltzmann-Gibbs state) and any of the initial distribution finally approaches the isothermal state. Hence, the isothermal distribution acts as a role of the attractor and the quasi-attractor characterized by the stellar polytropic distribution does not appear (*left-panel* of Fig.2). On the other hand, for the energy with $\lambda \gtrsim 0.3$, the isothermal distribution ceases to exist and there appears a possibility to have the quasi-attractive features. The *middle-panel* in Fig.2 represents a typical example of quasi-attractive behavior, while the *right-panel* shows the result that the system undergoes core-collapse without passing through the stellar polytropic state.

3 Physical Reasons for Quasi-attractivity

The presence or the absence of quasi-attractive property seen in the N-body simulations can be qualitatively explained as follows. First notice the fact that the velocity dispersion profile $\sigma_v^2(r)$ of the TFSM shows non-monotonic behavior when $\eta > 1$. That is, as decreasing the radius from $r = r_e$, the quantity $\sigma_v^2(r)$ first increases, but it eventually turns to decrease. From a thermodynamical point of view, this fact implies that the inward heat flow (i.e., exchange of the kinetic energy in each particle via two-body encounter) occurs. In presence of the negative specific heat, the inward heat flow makes the central part cool and conversely the outer part hot. Thus, the depth of the central potential becomes shallower. As a consequence, the cusped density profile is smeared out and the flatter core is formed. This is known as *gravothermal expansion*. The important point is that the gravothermal expansion occurs when $\eta > 1$. Recalling the fact that the stellar polytropic distribution has also flat core, one can deduce that $\eta > 1$ is the necessary condition for the quasi-attractive behavior. Note further that the size of the flat core after the gravothermal expansion depends on the depth of the potential or λ. This fact indicates that quasi-attractive behavior appears only for a moderate range of the energy λ, consistent with the results in Fig.1. Fig.3 shows the snapshots of one-dimensional velocity dispersion profile for $\eta = 1.5$(*left-panel*) and $\eta = 1$(*right-panel*). As anticipated, the inward heat flow occurs in the $\eta = 1.5$ case, while it does not occur when $\eta = 1$.

Another important condition for quasi-attractivity is the relaxation timescale. For the relaxation process driven by the two-body encounter, the relaxation timescale is locally estimated as [9]:

$$t_r = 0.065 \, \frac{\sigma_v^3}{G^2 m \rho \ln \Lambda} \tag{2}$$

with Λ being the Coulomb logarithm. That is, the local relaxation time is sensitive to the underlying local density and is inversely proportional to ρ. This implies that the relaxation in the central part tends to become faster than that in the outer part. This is the reason why the gravothermal expansion takes place in an earlier phase of the evolution. Since a subsequent evolution follows from the local relaxation given by (2), it seems natural that once the flat core is formed, the one-particle distribution function maintains the power-law form long before entering the core-collapse phase.

4 Discussion & Summary

In this article, we focused on the quasi-attractive behavior in self-gravitating N-body system. Adopting Tremaine's family of stellar models as initial distribution, a systematic survey of N-body simulation with various model parameters is presented. The resultant simulation data implies that the quasi-attractive feature appears in a moderate range of the energy, $0.3 \lesssim \lambda \lesssim 0.8$ when the slope of the central density profile is shallow, $\eta > 1$. Based on this result, the physical reason for quasi-attractive behavior is discussed. The key ingredients for quasi-attractivity are (i) gravothermal expansion arising from the long-range nature of attractive gravity and (ii) local relaxation time inversely proportional to the density.

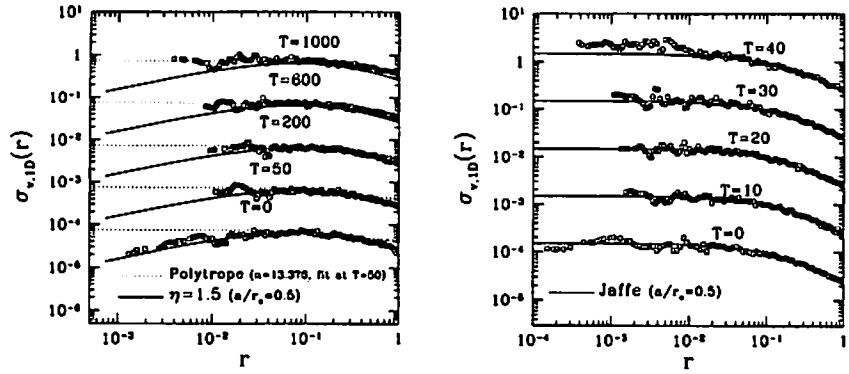

Figure 3: Evolution of one-dimensional velocity dispersion profile in models with $(\eta, a/r_e) = (1.5, 0.5)$ *Left* and $(\eta, a/r_e) = (1, 0.5)$ *Right*. Similar to Fig.2, each output result is shifted to the two digits below. In each panel, solid lines represent the theoretical curve for initial distribution and the dotted lines are the fitting results of N-body data to the stellar polytropes.

Therefore, the quasi-equilibrium and the quasi-attractive features seen in the N-body system might be considered as unique feature in a variety of the long-range system.

Of course, the physical reason and the condition for quasi-attractivity described here is only qualitative and still far from complete. For further quantitative statement, a more detailed N-body study is required. Simultaneously, analytic approach to clarify the quasi-equilibrium state should be developed. In this respect, the Fokker-Planck model of stellar dynamics provides various useful information. This issue will be tackled near future.

References

[1] D. Lynden-Bell, R. Wood, Mon.Not.R.Astr.Soc. **138** (1968) 495.

[2] V.A. Antonov, Vest. Leningrad Gros. Univ., 7 (1962) 135 (English transl. in *IAU Symposium 113, Dynamics of Globular Clusters*, ed. J. Goodman and P. Hut [Dordrecht: Reidel], pp. 525–540 [1985]).

[3] A. Taruya, M. Sakagami, Phys. Rev. Lett. **90**, 181101 (2003).

[4] L. Hernquist, Astrophys. J. **356** (1990) 359

[5] A. Taruya, M. Sakagami, Physica A **307** (2002) 185.

[6] A. Taruya, M. Sakagami, Physica A **318** (2003) 387.

[7] A. Taruya, M. Sakagami, Physica A **322** (2003) 285.

[8] S. Tremaine et al., Astron. J. **107** (1994) 634.

[9] J. Binney, S. Tremaine, *Galactic Dynamics* (Princeton Univ. Press, Princeton 1987)

Expansion law and fractal structure in one-dimensional self-gravitating system

Takayuki Tatekawa[1], Kei-ichi Maeda[2]

Department of Physics, Waseda University,
3-4-1 Ohkubo, Shinjuku-ku, Tokyo 169-8555, Japan

Abstract

In one-dimensional sheet model with cosmic expansion, scale-free or fractal structure forms spontaneously during evolution. Furthermore, they seem stable. On the other hand, in one-dimensional sheet model without cosmic expansion, Scale-free correlation function appears during evolution. Is the cosmic expansion important for the formation of scale-free structure? Here we analyzed one-dimensional sheet model which expansion rate is given by power-law of time. We derived self-similar solution for arbitrary expansion rate, and calculated long-time evolution. From numerical analysis, we show that the fractal dimension of structure converges and it can be described with simple equation of expansion rate.

1 Introduction

In self-gravitating systems, scale-free or fractal structure is observed. For example, two-point correlation function of galaxy distribution obeys power-law with respect to separation distance. How such a structure is formed in the evolution of the Universe? One of the most plausible explanations is that the nonlinear dynamics of the perturbations will provide such a scale-free structure during the evolution of the Universe.

Davis and Peebles [1, 2] explained the power-law behavior in nonlinear stage. They assume a self-similar evolution of density fluctuation and some additional condition. Then they showed a relation between the power index γ of two-point correlation function and that of initial power spectrum n as $\gamma = 3(n+3)/(n+5)$. Since their additional condition is not trivial and might not be appropriate, Padmanabhan [4] and Yano and Gouda [5, 6] extended their model. Since we do not know the stability of their solution, we should study dynamical evolution.

For dynamical evolution, one-dimensional sheet model with cosmic expansion has been analyzed. Although the interaction in one-dimensional sheet model is differ from that in three-dimensional model, there is advantage to describe the motion of matter exactly. Gouda and Nakamura [3] and Yano and Gouda [6] analyzed the time evolution of density fluctuation with scale-free spectrum. They showed scale-free spectrum which index is independent of initial condition appears during evolution. We [7] also analyzed the time evolution of fractal density perturbations in Einstein-de Sitter universe. We assume a one-dimensional collisionless sheet model with initial Cantor-type fractal perturbations. The nonlinear structure seems to approach some attractor with a unique fractal dimension, which is independent of the fractal dimensions of initial perturbations.

On the other hand, one-dimensional model without cosmic expansion has been analyzed. Recently Koyama and Konishi [8] analyzed two-point correlation function of sheets. If special initial condition, such as cold collapse (initial virial ratio is given by 0), is given, the two-point correlation function obeys power-law of distance temporary. Although the situation appears only from special initial condition, the results seem remarkable.

2 Self-similar solution of two-point correlation function

According to recent galaxy survey, two-point correlation function of galaxy distribution obeys power-law with respect to separation distance. How such a structure is formed in the evolution of the Universe?

[1]E-mail:tatekawa@gravity.phys.waseda.ac.jp
[2]E-mail:maeda@gravity.phys.waseda.ac.jp

How do we explain the formation of this scale-free structure? Davis and Peebles [1, 2] derived self-similar solution from BBGKY equations. They assumed self-similarity for two-point correlation function.

In d-dimensional space, when we give scale-free spectrum $P(k) \propto k^n$ as initial condition, the two-point correlation in linear region is written as

$$\xi(x) \propto x^{-(d+n)}. \tag{1}$$

Here we give scale factor and linear growth rate of density fluctuation as $a(t) \propto t^p$ and $D^+(t) \propto t^q$ respectively. In linear region, the correlation function is written as

$$\xi(x,t) \propto x^{-(d+n)} t^{2q}. \tag{2}$$

If we suppose self-similarity in the correlation function;

$$\xi(x,t) = \tilde{\xi}\left(\frac{x}{t^{\alpha_L}}\right), \tag{3}$$

the exponent α_L becomes

$$\alpha_L = \frac{2q}{d+n}. \tag{4}$$

On the other hand, in strongly nonlinear region, we obtain evolution equation of the two-point correlation function from BBGKY equations.

$$\frac{\partial \xi}{\partial t} + \frac{1}{ax^{d-1}} \frac{\partial}{\partial x}\left(x^{d-1} v \xi\right) = 0, \tag{5}$$

where v means peculiar velocity. Here we assume following relation:

$$v = -ha\dot{x}. \tag{6}$$

If $h = 1$, the structure does not change the size. Davis and Peebles [1] introduced 'stable condition' $h = 1$. After that, Padmanabhan [4] and Yano and Gouda [5] considered the case of general h. Using this relation, we obtain the solution of two-point correlation function:

$$\xi(x,t) \propto a^{(d-\gamma)/h} x^{-\gamma} \propto t^{p(d-\gamma)/h} x^{-\gamma}. \tag{7}$$

γ means integration constant. Here we suppose self-similarity in the correlation function.

$$\xi(x,t) = \tilde{\xi}\left(\frac{x}{t^{\alpha_{NL}}}\right). \tag{8}$$

Finally, we think that the exponent of self-similarity in linear region and strongly nonlinear region is the same:

$$\alpha_L = \alpha_{NL}. \tag{9}$$

From this relation, we obtain the two-point correlation function in strongly nonlinear region.

$$\xi \propto x^{\frac{dp(d+n)}{(d+n)p+2h_q}}. \tag{10}$$

3 Fractal dimension of structure

We investigated long-time evolution in one-dimensional case. The equation of motion is given as follows:

$$\ddot{S} + 2\frac{\dot{a}}{a}\dot{S} + \frac{2}{3}\left(\frac{\dot{a}}{a}\right)^2 S = 0, \tag{11}$$

$$x = x_0 + S(x_0, t), \tag{12}$$

where x_0 and S mean initial position in comoving coordinates and displacement respectively. From eq. 11, we obtain exact solutions:

$$S \propto t^q, \quad q = \frac{1}{2}\left(1 - 2p \pm \sqrt{10p^2 - 4p + 1}\right). \tag{13}$$

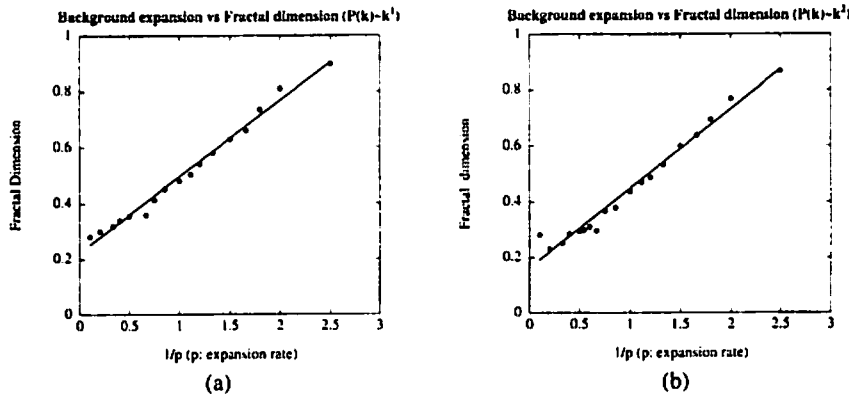

Figure 1: The relation between expansion rate p and the fractal dimension D. The relation between p and D can be fitted by simple equation. (a) The case of $P(k) \propto k^1$. (b) The case of $P(k) \propto k^2$.

When two sheets cross, we exchange the velocities of just crossed two sheets. From eq.(10), we can discuss correspondence between self-similar solution and numerical calculation.

Through these analyses, we use 2^{13} sheets for numerical calculation. Then the periodic boundary condition is given. The scale free initial power spectrum is given by

$$P(k) \propto k^n \quad (n = 1, 2). \tag{14}$$

We used the box-counting method to calculate the fractal dimension of the structure. When we choose $p > 1/3$, the fractal structure appears and its dimension converges. Furthermore, we found simple relation between the expansion rate p and the fractal dimension D:

$$D = \frac{A}{p} + B, \tag{15}$$

where A and B means constant (Fig. 1). In our analysis, A is independent of initial condition.

$$A \simeq 0.27\,. \tag{16}$$

We also compare self-similar solution and numerical calculation. Here we adjust h and check the correspondence between both calculation (Fig. 2). Unfortunately, in our calculation, parameter h which conformed to all the models could not be found. We will reconsider assumption to derive the self-similar solution, or analyze the relation between peculiar motion and Hubble flow.

4 Summary

We analyzed one-dimensional sheet model which expansion rate is given by power-law of time. When the expansion rate is larger than 1/3, the fractal structure forms spontaneously. The fractal dimension converges during evolution. Furthermore we can write the relation between the expansion rate and the fractal dimension with simple equation.

We also derived self-similar solution of two-point correlation function for generic expansion case. Because there is relationship between the exponent of two-point correlation function and the fractal dimension, we can ascertain correspondence between the self-similar solution and numerical calculation. We found that it was difficult to explain the correspondence from this result. We need reconsider assumption to derive the self-similar solution, or analyze the relation between peculiar motion and Hubble flow.

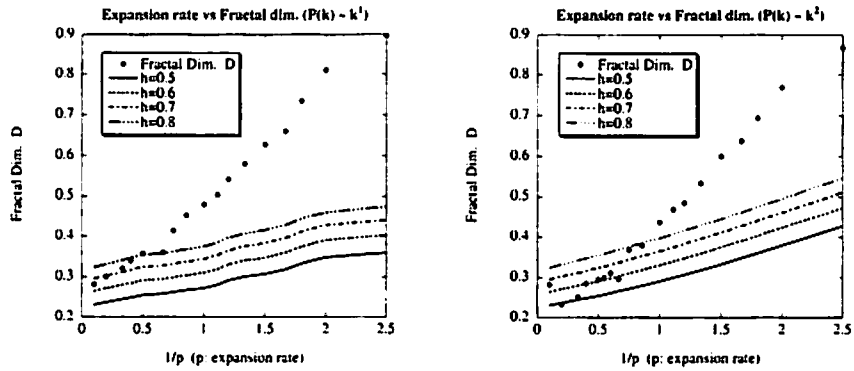

(a) (b)

Figure 2: The comparison between self-similar solution and numerical calculation. In our analysis, parameter h which conformed to all the models could not be found. (a) The case of $P(k) \propto k^1$. (b) The case of $P(k) \propto k^2$.

References

[1] M. Davis and P. J. E. Peebles, Astrophys. J. Supple. **34**, 425 (1977).

[2] P. J. E. Peebles, "The Large-scale Structure in the Universe" (1980, Princeton University Press).

[3] N. Gouda and T. Nakamura, Prog. Theor. Phys. **79**, 765 (1988); **81**, 633 (1989).

[4] T. Padmanabhan, Mon. Not. R. Astron. Soc. **279**, L29 (1996).

[5] T. Yano and N. Gouda, Astrophys. J. **487**, 473 (1997).

[6] T. Yano and N. Gouda, Astrophys. J. Supple. **118**, 267 (1998).

[7] T. Tatekawa and K. Maeda, Astrophys. J. **547**, 531 (2001).

[8] H. Koyama and T. Konishi, Phys. Lett. A **279**, 226 (2001); Europhys. Lett. **58**, 356 (2002); Phys. Lett. A **295**, 109 (2002).

[9] T. Suginohara, A. Taruya, and Y. Suto, Astrophys. J. **566**, 1 (2002).

Quantum Poincare Algebra and Ultra High Energy Cosmic Rays

Ken-Ichi Tezuka[1]

Graduate School of Science and Technology,
Chiba University, 1-33 Yayoi-cho Inage-ku, Chiba 263-8522, Japan

Abstract

We investigate description of the Poincare symmetry by a quantum group. It does not have unique mathematical definition. We define the Poincare quantum group by demanding some physical requirements with respect to its coproduct. The quantum group is applied to ultra high energy cosmic rays.

1 Introduction

In cosmic ray physics, the following problem is not solved yet; anomalous detection of extremely high energy cosmic rays [1] above the GZK cutoff (5×10^{19} eV) [2]. It was suggested that the absence of the GZK cutoff is closely related to violation of the Lorentz invariance [3]. If the Lorentz invariance is violated or deformed, there is the possibility to explain that there is not the GZK cutoff at $E = 5 \times 10^{19}$ eV. Therefore we have to consider a violation or a deformation of the symmetry.

The doubly special relativity [4] was introduced as a deformed special relativity which has two observer independent scales; the velocity c and a mass κ. This is explicitly realized by the κ-Poincare algebra [5, 6]. It is defined by replacing the Poincare algebra with a quantum group (Hopf algebra) with the parameter κ [7]. In the limit $\kappa \to \infty$, the Hopf algebra is reduced to the ordinary Lie algebra.

It is known that the κ-deformation of the Poincare algebra is not unique. The purpose of this article is to define the κ-Poincare algebra by imposing some physical requirements. In the final section, the resulting Hopf algebra is applied to ultra high energy cosmic rays.

2 Review of Hopf algebra

In this section, we briefly review the general definition of Hopf algebra. A Hopf algebra $(H, +, m, \eta, \Delta, \epsilon, S; k)$ over k is a vector space $(H, +; k)$ over k with coproduct $\Delta : H \to H \otimes H$, counit $\epsilon : H \to k$, and antipode $S : H \to H$ which satisfy

$$(\Delta \otimes id) \circ \Delta = (id \otimes \Delta) \circ \Delta$$
$$(\epsilon \otimes id) \circ \Delta(h) = h = (id \otimes \epsilon) \circ \Delta(h)$$
$$m(S \otimes id) \circ \Delta = m(id \otimes S) \circ \Delta = \eta \circ \epsilon$$

with $h \in H$. Here m means product $m : H \otimes H \to H$. The coproduct satisfies also the relations

$$\Delta(hg) = \Delta(h)\Delta(g), \qquad \Delta(1) = 1 \otimes 1.$$

Let us define a term relating to coproduct. We permutate two elements in the vector space $V \otimes W$ by the map

$$\tau : v \otimes w \mapsto w \otimes v,$$

which is called transposition map. If a coproduct is invariant under the map, it is called cocommutative coproduct.

[1] E-mail:tezuka@graduate.chiba-u.jp

3 κ-Poincare algebra

It is known that we cannot uniquely determine κ-Poincare group, since the Poincare algebra is not a semi-simple Lie algebra. One way to obtain a κ-Poincare algebra is to use contraction of the AdS algebra $o(3,2)$. Since it is a semi-simple Lie algebra, we can define $U_q(o(3,2))$ uniquely. A κ-Poincare algebra is obtained through the contraction of $U_q(o(3,2))$. Some κ-Poincare algebras are obtained by redefining translation's generators P_μ.

What they have in common is that coproduct $\Delta(P_i)$ is non-cocommutative. For instance, in the bicrossproduct basis, the coproduct is given by

$$\Delta(E) = E \otimes 1 + 1 \otimes E$$
$$\Delta(P_i) = P_i \otimes 1 + \exp\left(-\frac{E}{\kappa}\right) \otimes P_i.$$

The second one means that the composition law of two three-momenta $P_i^{(1)}$ and $P_i^{(2)}$ is given by

$$P_i^{(1+2)} = P_i^{(1)} + \exp\left(-\frac{E^{(1)}}{\kappa}\right) P_i^{(2)}.$$

The total momenta is not invariant under the exchange $P_\mu^{(1)} \leftrightarrow P_\mu^{(2)}$, even if they are momenta of particles of a kind. We would like, however, a composition law of momenta that is symmetric under the exchange. It is physically more realistic. It is possible to get such the composition law, if $\Delta(P_\mu)$ is cocommutative. If a quantum group, however, does not have non-cocommutative coproduct, it may be a trivial one as a quantum group. So we should have our sights on acquiring a composition law $P_i^{(1+2)}$ which is not symmetric under the exchange only in a case that $P_\mu^{(1)}$ and $P_\mu^{(2)}$ are momenta of two different particles. So $\Delta(P_\mu)$ should be dependent not only on the parameter κ, but also physical quantities which characterize particles. When we calculate the threshold energy of ultra high energy cosmic rays, we use basically only partilcles' masses in order to distinguish between two particles. So let us construct a composition law $P_i^{(1+2)}$ which is invariant under $P_\mu^{(1)} \leftrightarrow P_\mu^{(2)}$, only if $m_1 = m_2$, where m_α $(\alpha = 1, 2)$ are masses of particles. It is equivalent to the fact that $\Delta(P_\mu)$ is dependent on m_α, and is cocommutative, only if $m_1 = m_2$. It means that the κ-Poincare group is influenced by particles that exist in spacetime.

Since the above requirement to $\Delta(P_\mu)$ is not enough to determine a basis of k-Poincare algebra, we need to impose additional conditions. The Poincare algebra has $o(3)$ subalgebra. We assume that it is not deformed by κ. Deformation of rotational symmetry means that there is a preferred direction in the universe. By the assumption, for the generators of rotation M_i, we have

$$\Delta(M_i) = M_i \otimes 1 + 1 \otimes M_i, \qquad [M_i, M_j] = i\epsilon_{ijk} M^k.$$

We also suppose that the κ-Poincare algebra is a non-semi-simple algebra. It makes us possible to construct a dispersion relation through a Casimir operator of the κ-Poincare algebra. Then translation generators have to be commutative with each other

$$[P_\mu, P_\nu] = 0.$$

Let us actually adopt one coproduct of P_μ. We use the ansatz

$$\Delta(E) = E \otimes 1 + 1 \otimes E \tag{1}$$
$$\Delta(P_i) = P_i \otimes f(\kappa, m_\alpha, E) + \tilde{f}(\kappa, m_\alpha, E) \otimes P_i, \tag{2}$$

where $f(\kappa, m_\alpha, E)$ and $\tilde{f}(\kappa, m_\alpha, E)$ are undetermined functions. The coassociativity of $\Delta(P_i)$ requires that

$$\Delta(f(\kappa, m_\alpha, E)) = f(\kappa, m_\alpha, E) \otimes f(\kappa, m_\alpha, E), \qquad \Delta(\tilde{f}(\kappa, m_\alpha, E)) = \tilde{f}(\kappa, m_\alpha, E) \otimes \tilde{f}(\kappa, m_\alpha, E). \tag{3}$$

We must determine $\Delta(N_i)$. We introduce the ansatz

$$\begin{aligned}\Delta(N_i) \;=\; & N_i \otimes g(\kappa, m_\alpha, E) + \tilde{g}(\kappa, m_\alpha, E) \otimes N_i \\ & + \omega_1 \epsilon_{ijk} M_j \tilde{g}(\kappa, m_\alpha, E) \otimes P_k - \omega_2 \epsilon_{ijk} P_j \otimes M_k g(\kappa, m_\alpha, E),\end{aligned} \tag{4}$$

where $g(\kappa, m_\alpha, E)$, $\tilde{g}(\kappa, m_\alpha, E)$, and ω_α are unknowns. The coproduct (4) is coassociative, if

$$\Delta(g(\kappa, m_\alpha, E)) = g(\kappa, m_\alpha, E) \otimes g(\kappa, m_\alpha, E), \qquad \Delta(\tilde{g}(\kappa, m_\alpha, E)) = \tilde{g}(\kappa, m_\alpha, E) \otimes \tilde{g}(\kappa, m_\alpha, E).$$

The commutator between $\Delta(N_i)$ and $\Delta(E)$ is

$$[\Delta(N_i), \Delta(E)] = [N_i, E] \otimes g(\kappa, m_\alpha, E) + \tilde{g}(\kappa, m_\alpha, E) \otimes [N_i, E].$$

Since coproduct is an algebra map, the right hand side have to be equivalent to $\Delta(h(P_\mu))$, where $h(P_\mu)$ is an unknown function. From the o(3) invariance, $[N_i, E]$ have to be proportional to P_i. In general we have the algebra $[N_i, E] = iP_iL(P_\mu)$, where $L(P_\mu)$ is $o(3)$ invariant unknown factor. $L(P_\mu)$, however, can be eliminated by redefinition of P_i. Then we adopt

$$[N_i, E] = iP_i.$$

This is implemented in the choice

$$g(\kappa, m_\alpha, E) = f(\kappa, m_\alpha, E), \qquad \tilde{g}(\kappa, m_\alpha, E) = \tilde{f}(\kappa, m_\alpha, E).$$

The most simplest choice of $f(\kappa, m_\alpha, E)$ and $\tilde{f}(\kappa, m_\alpha, E)$ that makes $\Delta(P_i)$ be cocommutative only for $m_1 = m_2$ is

$$f(\kappa, m_\alpha, E) = \exp\left(-\frac{m_1 E}{\kappa^2}\right), \qquad \tilde{f}(\kappa, m_\alpha, E) = \exp\left(-\frac{m_2 E}{\kappa^2}\right).$$

They satisfy (3). In the following, we construct a basis of κ-Poincare algebra for the selection.

We have assumed that P_μ are elements of the ideal of the κ-Poincare algebra. Furthermore, we also assume that P_i is invariant under a boost transformation along a direction which is orthogonal to P_i. In other words,

$$[N_i, P_j] = i\delta_{ij} R(P_\mu), \tag{5}$$

where $R(P_\mu)$ is a function depending only on P_μ. Under the postulations we construct a quantum Poincare algebra. From the condition (5) we have $\omega_1 = \frac{m_2}{\kappa^2}$ and $\omega_2 = \frac{m_1}{\kappa^2}$. So we have the commutator

$$[N_i, P_j] = -i\delta_{ij}\left[\frac{\kappa^2}{2(m_1 - m_2)}\left[\exp\left(-\frac{2m_1}{k^2}E\right) - \exp\left(-\frac{2m_2}{\kappa^2}E\right)\right] - \frac{m_1 + m_2}{\kappa^2}P_k P^k\right]$$

that is consistent with the coproduct (2) and (4). The dispersion relation is defined by a Casimir operator of the Hopf algebra. It is given by

$$M(m) = \frac{\kappa^2}{2(m_1 - m_2)}\left[\frac{\kappa^2}{m_1}\left(\exp\left(\frac{2m_1}{\kappa^2}E\right) - 1\right) - \frac{\kappa^2}{m_2}\left(\exp\left(\frac{2m_2}{\kappa^2}E\right) - 1\right)\right] - P_j P^j \exp\left(\frac{2(m_1 + m_2)}{\kappa^2}E\right).$$

We have defined the κ-Poincare algebra by demanding that the coproduct $\Delta(P_\mu)$ gives a composition law $P_i^{(1+2)}$ that is not symmetric under the exchange only in a case that $P_\mu^{(1)}$ and $P_\mu^{(2)}$ are momenta of two different particles.

4 Application to UHECRs

In the previous section, we have constructed the quantum Poincare algebra. We would like to apply it to cosmic rays above the GZK cutoff. The highest energy observed by AGASA is 2×10^{20}eV. By using our formalism, we would like to make the threshold energy of cosmic rays be larger than 2×10^{20}eV.

Let us consider head-on collision of a proton and a CMB photon that produces π^0 and a proton. Then we set $m_1 = m_p$ that is the mass of a proton. m_2 is zero, since a photon is massless. The process will occur, if the proton's energy E_p satisfies the inequality

$$\left(\frac{\kappa^2}{2m_p}\right)\left[\left(\frac{\kappa^2}{2m_p}\right)\left(\exp\left(\frac{2m_p(E_p+E_\gamma)}{\kappa^2}\right)-1\right)-(E_p+E_\gamma)\right]$$
$$-\left(P_p\exp\left(-\frac{m_pE_\gamma}{\kappa^2}\right)-P_\gamma\right)^2\exp\left(\frac{2m_p(E_p+E_\gamma)}{\kappa^2}\right)\geq M_{p\pi}(m_p+m_\pi),$$

where $E_\gamma \sim 10^{-3}$eV. The left hand side is a quantum Poincare invariant value in the system with a proton and a photon. If the collision does not occur, ultra high energy cosmic rays can reach the earth. The proton's threshold energy is larger than 2×10^{20}eV which is the highest energy observed by AGASA, if $\kappa \lesssim 10^{15}$eV.

References

[1] M. Takeda *et al.*, "Extension of the cosmic-ray energy spectrum beyond the predicted Greisen-Zatsepin-Kuzmin cutoff", Phys. Rev. Lett. **81**, 1163 (1998), astro-ph/9807193.

[2] K. Greisen, "End to the Cosmic-ray spectrum?", Phys. Rev. Lett. **16**, 748 (1966); G. T. Zatsepin and V. A. Kuzmin, "Upper limit of the spectrum of cosmic rays", Sov. Phys. JETP Lett. **4**, 78 (1966).

[3] H. Sato and T. Tati, "Hot Universe, Cosmic Rays of Ultrahigh Energy and Absolute Reference System", Prog. Theor. Phys. **47**, 1788 (1972), T. Kifune, "Invariance violation extends the cosmic ray horizon?" Astrophys. J. **518**, L21 (1999), astro-ph/9904164; S. R. Coleman and S. L. Glashow, "High-energy tests of Lorentz invariance", Phys. Rev. D **59**, 116008 (1999), hep-ph/9812418; G. Amelino-Camelia and T. Piran, "Planck-scale deformation of Lorentz symmetry as a solution to the UHECR and the TeV-gamma paradoxes", Phys. Rev. D **64**, 036005 (2001), astro-ph/0008107, T. Tamaki, T. Harada, U. Miyamoto and T. Torii, "Have we already detected astrophysical symptoms of space-time noncommutativity?", gr-qc/0111056; "Particle velocity in noncommutative space-time", Phys. Rev. D **66**, 105003 (2002), gr-qc/0208002.

[4] G. Amelino-Camelia, "Relativity in space-times with short-distance structure governed by an observer-independent (Planckian) length scale", Int. J. Mod. Phys. D **11**, 35 (2002), gr-qc/0012051; "Testable scenario for relativity with minimum-length," Phys. Lett. B **510**, 255 (2001), hep-th/0012238.

[5] J. Kowalski-Glikman, "Observer independent quantum of mass", Phys. Lett. A **286**, 391 (2001), hep-th/0102098; N. R. Bruno, G. Amelino-Camelia and J. Kowalski-Glikman, "Deformed boost transformations that saturate at the Planck scale", Phys. Lett. B **522**, 133 (2001), hep-th/0107039.

[6] K. I. Tezuka, "Uncertainty of velocity in kappa-Minkowski spacetime," hep-th/0302126.

[7] J. Lukierski, H. Ruegg, A. Nowicki and V. N. Tolstoi, "Q deformation of Poincare algebra", Phys. Lett. B **264**, 331 (1991).

Possibilities to Suppress the Low Multipoles in the CMB Anisotropies
— Review —

Kenji Tomita[1]

Yukawa Institute for Theoretical Physics, Kyoto University, Kitashirakawa, Kyoto 606-8502, Japan

Abstract

The Cosmic Microwave Background (CMB) anisotropies on the largest angular scales observed by WMAP and COBE appear to be lower than the ones predicted by the standard cosmological model with scale free primordial perturbations arising from the inflationary period. Various possible mechanisms to suppress such low l multipoles have been proposed, including the change in the initial power spectrum induced by the inflation, the cut-off of long-wavelength perturbations in special topologies, and special structures arising from the late-time evolution of the universe. Main mechanisms of these three types are shown and discussed.

1 Introduction

The Cosmic Microwave Background (CMB) anisotropies on the largest angular scales observed by the Wilkinson Microwave Anisotropy Probe (WMAP) are very lower than the ones predicted by the standard cosmological model with scale free primordial perturbations, though those on the moderate scales are consistent with the predicted ones. This discrepancy on the largest scales is the same as that found by COBE observation and was confirmed by the WMAP observation. It is important that the cross correlation of the temperature anisotropy and the polarization on the largest scales is comparable with the one which is theoretically predicted in the above model. This situation is very curious, because the probability for it to be realized is very small according to simulation analyses. Recently many mechanisms have been proposed for suppressing the low multipoles of the CMB anisotropies. In this short review I show first the result of WMAP, and then classify the mechanisms and discss their significance.

2 Observational results on low multipoles with $l = 2$ and 3

The WMAP observational data of the temperature anisotropies was obtained for the multipole moment $l \lesssim 900$ and compared with theoretical values in the homogeneous cosmological models (Bennet et al. 2003 and Spergel et al. 2003). The best-fit cosmological parameters are shown in Table 1.

The temperature fluctuations for l is defined by

$$(\delta T_l)^2 = l(l+1)C_l/2\pi, \tag{1}$$

where we have $C_l = 1/(2l+1) \cdot \sum_m |a_{lm}|^2$ and

$$T(\mathrm{n}) = \sum_{l,m} a_{lm} Y_{lm}(\mathrm{n}) \tag{2}$$

with the unit directional vector n.

The predicted values of $(\delta T_l)^2$ in units of $\mu\mathrm{K}^2$ in the concordant model are shown in the first line of Table 2, where the concordant model has the parameters consistent with the above best-fit ones. The observed values of multipoles determined from the original map with the cut sky (corresponding to the Galactic plane) are shown in the second line (Hinshow et al. 2003) of Table 2. From these lines we find that for $l = 2$ the observed value is by a factor of about 10 smaller than the predicted value. The corrected

[1]E-mail:tomita@yukawa.kyoto-u.ac.jp

Table 1: The bets-fit parameters in homogeneous cosmological models.

$\Omega_{\rm tot} = 1.02 \pm 0.02$	
$\Omega_{\rm b} = 0.047 \pm 0.006$	
$\Omega_{\rm m} = 0.29 \pm 0.07$	
$h = 0.72 \pm 0.05$	Hubble constant
$z_{\rm r} = 17 \pm 5$	Reionization epoch
$n_{\rm s} = 0.99 \pm 0.04$	Spectral index
$\tau = 0.166{+}0.076/-0.071$	Optical depth

Table 2: WMAP measurements of the CMB quadrupole and octopole.

	$(\delta T_2)^2\ \mu{\rm K}^2$	$(\delta T_3)^2\ \mu{\rm K}^2$	P
Concordant model (theory)	1140	1060	
Hinshow et al. (cut sky)	123.4	611.8	0.0035
Bennett et al.'s ILC map (all sky)	195.1	1053.4	
Tegmark et al.'s map (all sky)	201.6	866.1	0.017
Efstathiou (b)(c), Max. Likelihood	$176-250$	$794-1183$	

maps for all sky were derived by Bennet et al.(2003) and Tegmark et al.(2003). The values determined by them are shown in Table 2 for comparison and it is found that the latter values of $(\delta T_l)^2$ are a little larger than the original ones. Moreover, Efstathiou (a)(2003) derived the values in another method of the maximum likelihood using Tegmark et al's all-sky map. His values are shown in the last line of Table 2, which are consistent with the corrected ones of Bennet et al.(2003) and Tegmark et al.(2003) In this Table, P denotes the frequentist estimate of the probability in which the observed values of $(\delta T_l)^2$ arise in the concordant model.

Together with the temperature anisotropies, the temperature-polarization correlation (TE) was observed and shown by WMAP. It is interesting and important that this observed cross correlation is comparable with the predicted one in the concordant model, contrary to the case of temperature anisotropies. By Doré, Holder and Loeb (2003), it was shown using the numerical simulation that, if current cosmological models for the generation of large angle anisotropy are correct and the WMAP data are not significantly contaminated by non-CMB signals, then the $C_l^{\rm TE}$ amplitude on the largest scales is discrepant at the $\sim 99.8(98.5)\%$ level with the observed $C_l^{\rm TT}$ for the concordant LCDM model with optical depth $\tau = 0.11(0.17)$, respectively.

3 Various mechanisms for suppressing low multipole moments

Various mechanisms which have been proposed for suppressing low multipoles are classified into following three types. Here let us discuss each of them.

(1) Cut-off of the primordial power spectrum $P(k)$ at low wavenumbers

First by taking simply the cut-off of the power spectrum at low wavenumbers $k = k_*$, the dependence of C_l on k_* was considered in the concordant (flat) model (Cline et al. 2003 and Bridle et al. 2003). The concordant model is usually regarded as spatially flat. However the best-fit spaces are degenerate and tend to be closed ($\Omega_{\rm tot} > 1.0$), as in Table 1. So the similar dependence in closed models also was analyzed (Efstathiou 2003(a)). In all of them we find that the temperature anisotropies can be suppressed, but at the same time the cross correlation of temperature and polarization also is suppressed, in the inverse ways to the observational result. So it is concluded that the standard LCDM model and the low-k cut-off models are rather poor fits to the observed quadrupole, and to do better one should find a way to more effectively suppress the theoretical value of the quadrupole moment.

The mechanisms for causing the cut-off of the power spectrum were studied by Contaldi et al. (2003) by reforming inflationary scenarios in the form of fine-tuning the functional form of the inflaton potential $V(\phi)$ and considering the departure from the slow roll approximation. Hybrid new inflation was pro-

posed by Kawasaki and F. Takahashi (2003), and the role of the correlated isocurvature fluctuations in quintessence to cancel the adiabatic fluctuations was considered by Moroi and T. Takahashi (2003).

The possibility of inflation in closed universes was examined by Uzan, Kirchner and Ellis (2003) and Linde (2003). It was, moreover, found by Kesden et al.(2003) that the cut-off increases significantly the cross correlation between the large-scale CMB and cosmic-shear patterns. What the origin of the suppression is will be made clearer through the observational study of this correlation.

(2) Compact topology

If we are in a compact space and the size of the fundamental domain (L) is smaller than the present horizon size, the density fluctuations longer than this size do not appear, so that the primordial power spectrum is effectively cut-off at the largest scales. The spaces with compact topology are classified into Euclidean, spherical and hyperbolic spaces.

Recently the observational evidences such as ghost images and matching circles of the last scattering surfaces have been examined. At present, however, no observational evidences for the compact topology have not been detected. If L is large enough to make the evidences invisible, this compact topology cannot suppress the low multipoles. Accordingly the suppression due to compact topology seems to be rather pesimistic, though its various spaces of compact topology (especially closed topology) have been analyzed and studied observationally (Cornish et al. 2003, Uzan et al. 2003, Luminet et al. 2003).

(3) Special structures in the late-time evolution of the universe

In the third type, the suppression due to special structures in the late-time or in the neighborhood of us is considered. First of the various mechanisms is the possible cancellation of the integral Sachs-Wolfe effect in the process of integration for $(\delta T_l)^2$, proposed by Contaldi et al. (2993).

Second is the Sunyaev-Zeldovich Effect (SZE) of the Local Supercluster (LSC). It was found by Abramo and Sodré (2003) that the temperature distortion due to SZE can be as high as $\delta T \approx 30\mu K$, so that the result at $\nu < 218$ GHz is a suppression of the multipoles in the direction of LSC, and for small scales the effect decays, and for $\nu > 218$ GHz the effect is inverse.

Moreover the suppression in inhomogeneous cosmological models can be taken into consideration in principle. Linde et al. (1995, 1996) proposed a model with spherical structure in the neighborhood. This comes from that under certain assumptions concerning the choice of measure in the theory of eternal inflation, we should live in a center of a spherically symmetric distribution of matter. This may lead to suppression of the large-scale anisotropy without affecting the small-angle effects.

In the inhomogeneous model with a local void (Tomita 2000, 2003), low multipole moments consist of two components: One is the multipole moments caused by the density fluctuations mainly through the inverse Sachs-Wolfe effect. The other is the component observed by an observer whose position in the void region is off-center. By the relative motion to the last scattering surface, additional low multipoles with $l > 1$ are caused geometrically together with the dipole moment ($l = 1$), but with the increase of l, their moments decrease rapidly. The total moments are the sums of these two components. If both components can cancel each other for $l = 2, 3$, their sufficient suppression may appear.

Finally the following two points are remarked. First is that there is a possibility of Galactic contamination from unknown radio emissions within the Galactic plane which give moments in non-cosmological origin, as was indicated by Doré et al.(2003). If its existence will be found, the corrected moments of low multipoles may be larger and so their discrepancy with the theoretical values in the concordant model may decrease.

Second it should be noted that at present there is the discrepancy ($\approx$ about 28%) between the observed dipole moment of CMB anisotropies and the corresponding dipole moment which is theoretically estimated from the galactic distribution (Rowan-Robinson 2000, Tomita 2003). This latter puzzle also will have to be studied in the form of the late-time evolution.

References

[1] L. Abramo and L. Sodré, astro-ph/0312124 (2003).

[2] C. Bennett et al., ApJ Suppl. **148**, 97 (2003).

[3] S. Bridle, et a., astro-ph/0302306 (2003).

[4] J. Cline, et al., astro-ph/0304558 (2003).

[5] C. Contaldi, et al., J. Cosm. Astro. Phys. **07**, 002 (2003).

[6] N. Cornish, et al., astro-ph/0310233 (2003).

[7] O. Doré, G. Holder and A. Loeb, astro-ph/0312124 (2003).

[8] G. Efstathiou (a), Mon. Not. R.A.S., **343**, L95 (2003).

[9] G. Efstathiou (b), astro-ph/0306431 (2003).

[10] G. Efstathiou (c), astro-ph/0310207 (2003).

[11] G. Hinshow, et al., ApJ Suppl. **148**, 135 (2003).

[12] M. Kawasaki and F. Takahashi, Phys. Lett., **B570**, 151 (2003).

[13] M. Kesden, et. al., astro-ph/0306597 (2003).

[14] A. Linde, Phys. Rev. **D54**, 2504 (1996); Phys. Lett., **B345**, 20 (1995).

[15] A. Linde, J. Cosm. Astro. Phys. **0305**, 002 (2003)

[16] J. Luminet, et al., Nature **425**, 1593 (2003).

[17] T. Moroi and T. Takahashi, astro-ph/0308208 (2003).

[18] A. de Oliviera-Costa, et al., astro-ph/0307282 (2003).

[19] M. Rowan-Robinson, et al., Mon. Not. R.A.S., **314**, 375 (2000).

[20] D. Spergel, et al., ApJ Suppl. **148**, 175 (2003).

[21] M. Tegmark et al., astro-ph/0302496 (2003).

[22] K. Tomita, ApJ **529**, 26 (2000).

[23] K. Tomita, ApJ **584**, 580 (2003).

[24] J. Uzan. U. Kirchner, et al., astro-ph/0302597 (2003).

[25] J. Uzan, A. Riazauelo, et al., astro-ph/0303580 (2003).

Covariant Gravitational Equations on Brane World with Gauss-Bonnet term in bulk spacetime

Takashi Torii[1]

Advanced Research Institute for Science and Engineering, Waseda University. 3-4-1 Okubo, Shinjuku-ku, Tokyo 169-8555, Japan

Kei-ichi Maeda[2]

Department of Physics, School of Science, Waseda University. 3-4-1 Okubo, Shinjuku-ku, Tokyo 169-8555, Japan

Abstract

We present the covariant gravitational equations to describe a 4-D brane world in the case with the Gauss-Bonnet term in a bulk spacetime, assuming that gravity is confined on the Z_2 symmetric brane. It contains some components of 5-D Weyl curvature which describes all effects from the bulk spacetime as in the Randall-Sundrum second model. Applying this formalism to cosmology, we derive the generalized Friedmann equation and calculate the Weyl curvature term, which is directly obtained from a black hole solution.

1 Introduction

Among many brane models, ones proposed by Randall and Sundrum[1, 2] are very important. They are motivated by superstring/M-theory, i.e., the orbifold compactification of higher-dimensional string theory by the dimensional reduction of 11-D supergravity in $R^{10} \times S^1/Z_2$[3]. RSII type model[1] provides us an alternative compactification of extra dimensions. However, this model may inevitably expect a singular spacetime just as in general relativity, although they are based on a string theory[4]. One of the ways to evade this argument is adding the higher curvature corrections to the bulk Lagrangian. The higher curvature terms naturally arise as a next leading order of the α'-expansion of a superstring theory[5]. One may expect that they are described by the so-called Gauss-Bonnet combination, which is shown to be a ghost-free combination. It was shown that the graviton zero mode is localized at law energies in the Gauss-Bonnet brane system as in the RS II model[6] and that the correction of the Newton's law becomes milder by including the Gauss-Bonnet term[7].

In order to understand the higher curvature model, it may be convenient for us to extend the covariant gravitational equations on a brane[8] to the case with the Gauss-Bonnet term. When we have a system with quadratic curvature terms in a bulk spacetime, we expect terms such as $(\pounds_n K_{AB})^2$ in the field equations which could be described by the square of the δ-function. This is the breakdown is our thin-wall ansatz. In the case with the Gauss-Bonnet term, however, the basic equations show a quasi-linear property[9], which guarantees a thin-wall ansatz because it contains only linear terms of $\pounds_n K_{AB}$. With this fact, here we derive the covariant gravitational equations on a brane in the case with the Gauss-Bonnet term. We see more detailed analysis in Ref. [10].

2 Effective equation on brane

We consider a 5-D bulk spacetime with a single 4-D brane world, on which gravity is confined.

$$S_{\rm bulk} = \int_{\mathcal{M}} d^5X\sqrt{-g}\left\{\frac{1}{2\kappa_5^2}\left[\mathcal{R} + \alpha(\mathcal{R}^2 - 4\mathcal{R}_{AB}\mathcal{R}^{AB} + \mathcal{R}_{ABCD}\mathcal{R}^{ABCD})\right] + \mathcal{L}_{\rm m}\right\}, \tag{1}$$

[1]E-mail:torii@gravity.phys.waseda.ac.jp
[2]E-mail:maeda@gravity.phys.waseda.ac.jp

where α is a coupling constant. The brane action is assumed to be given by the most generic action:

$$S_{\rm brane} = \int_{\mathcal{B}} d^4x\sqrt{-h}\left[L_{\rm surface} + L_{\rm brane}(h_{\alpha\beta}, \psi)\right]. \tag{2}$$

$L_{\rm brane}(h_{\alpha\beta}, \psi)$ is the effective 4-D Lagrangian, which is given by a generic functional of the brane metric $h_{\alpha\beta}$ and matter fields ψ. The surface term[11] is

$$L_{\rm surface} = \frac{1}{\kappa_5^2}\left[K + 2\alpha(J - 2G^{\rho\sigma}K_{\rho\sigma})\right], \tag{3}$$

where $K_{\mu\nu}(= h^A_{\ \mu}h^B_{\ \nu}\nabla_A n_B)$, K, J and $G^{\rho\sigma}$ in the surface term are the extrinsic curvature of $\mathcal{B}$, its trace, its cubic combination defined later, and the Einstein tensor of the induced metric $h_{\mu\nu}$, respectively.

Using the similar method as the Shiromizu-Maeda-Sasaki formalism[8], we can obtain the 4D effective gravitational equations on the brane. After rather long calculations we obtain

$$M + \alpha\left(\frac{1}{6}M^2 - 2\tilde{M}_{\alpha\beta}\tilde{M}^{\alpha\beta} + L_{\alpha\beta\gamma\delta}L^{\alpha\beta\gamma\delta}\right) = -2\kappa_5^2\mathcal{T}_{MN}n^M n^N, \tag{4}$$

$$\begin{aligned}&\frac{3}{2}\left(\tilde{M}_{\mu\nu} + E_{\mu\nu}\right) + \alpha\left[\tilde{H}^{(1)}_{\mu\nu} + \tilde{H}^{(2)}_{\mu\nu} + \tilde{H}^{(3)}_{\mu\nu}\right]\\ &\qquad = \kappa_5^2\left[\mathcal{T}_{MN}h^M_{\ \mu}h^N_{\ \nu} - \frac{1}{4}h_{\mu\nu}\mathcal{T}_{MN}h^{MN} + \frac{\alpha}{3+\alpha M}\tilde{M}_{\mu\nu}\mathcal{T}_{MN}h^{MN}\right],\end{aligned} \tag{5}$$

Here we have divided the Einstein equation into two parts: its trace and the trace free equation by introducing trace free variables as

$$\tilde{M}_{\mu\nu} := M_{\mu\nu} - \frac{1}{4}Mh_{\mu\nu}, \qquad L_{\mu\nu\rho\sigma} := M_{\mu\nu\rho\sigma} + h_{\mu[\sigma}\tilde{M}_{\rho]\nu} + h_{\nu[\rho}\tilde{M}_{\sigma]\mu} - \frac{1}{6}Mh_{\mu[\rho}h_{\sigma]\nu}, \tag{6}$$

where

$$M_{\alpha\beta\gamma\delta} := R_{\alpha\beta\gamma\delta} - K_{\alpha\gamma}K_{\beta\delta} + K_{\alpha\delta}K_{\beta\gamma}, \qquad M_{\alpha\beta} := h^{\rho\sigma}M_{\alpha\rho\beta\sigma}, \qquad M := h^{\alpha\beta}M_{\alpha\beta}, \tag{7}$$

$$N_{\mu\nu\rho} := D_\mu K_{\nu\rho} - D_\nu K_{\mu\rho}, \qquad N_\mu := h^{\rho\sigma}N_{\rho\mu\sigma} = D_\nu K_\mu^{\ \nu} - D_\mu K, \tag{8}$$

$$\begin{aligned}\tilde{H}^{(1)}_{\mu\nu} &:= 2\left(L_{\mu\alpha\beta\gamma}L_\nu^{\ \alpha\beta\gamma} - \tilde{M}^{\alpha\beta}L_{\mu\alpha\nu\beta} - \tilde{M}_\mu^{\ \alpha}\tilde{M}_{\alpha\nu}\right) - \frac{3-\alpha M}{6(3+\alpha M)}M\tilde{M}_{\mu\nu} + \frac{2\alpha}{3+\alpha M}\tilde{M}_{\alpha\beta}\tilde{M}^{\alpha\beta}\tilde{M}_{\mu\nu}\\ &\quad - \frac{1}{2}h_{\mu\nu}\left(L_{\alpha\beta\gamma\delta}L^{\alpha\beta\gamma\delta} - \tilde{M}_{\alpha\beta}\tilde{M}^{\alpha\beta}\right),\\ \tilde{H}^{(2)}_{\mu\nu} &:= -3\left(\tilde{M}_{\mu\rho}E^\rho_{\ \nu} + \tilde{M}_{\nu\rho}E^\rho_{\ \mu} + 2L_{\mu\rho\nu\sigma}E^{\rho\sigma}\right) + \frac{3}{2}h_{\mu\nu}\tilde{M}_{\rho\sigma}E^{\rho\sigma} + \frac{1}{2}ME_{\mu\nu} + \frac{6\alpha}{3+\alpha M}\tilde{M}_{\rho\sigma}E^{\rho\sigma}\tilde{M}_{\mu\nu},\\ \tilde{H}^{(3)}_{\mu\nu} &:= -4N_\mu N_\nu + 8N^\rho N_{\rho(\mu\nu)} + 2N_{\rho\sigma\mu}N^{\rho\sigma}_{\ \ \ \nu} + 4N_{\mu\rho\sigma}N_\nu^{\ \rho\sigma} + 3h_{\mu\nu}\left(N_\alpha N^\alpha - \frac{1}{2}N_{\alpha\beta\gamma}N^{\alpha\beta\gamma}\right)\\ &\quad + \frac{4\alpha}{3+\alpha M}\left(N_\alpha N^\alpha - \frac{1}{2}N_{\alpha\beta\gamma}N^{\alpha\beta\gamma}\right)\tilde{M}_{\mu\nu}.\end{aligned} \tag{9}$$

$\mathcal{T}_{AB}$ and $\tau_{\mu\nu}$ are the energy-momentum tensor of bulk matter field and the "effective" energy-momentum tensor localized on the brane.

The junction condition[12]

$$B_{\mu\nu} = -\frac{\kappa_5^2}{2}\tau_{\mu\nu}, \tag{10}$$

where

$$B_{\mu\nu} := K_{\mu\nu} - Kh_{\mu\nu} + 2\alpha\left(3J_{\mu\nu} - Jh_{\mu\nu} - 2P_{\mu\rho\nu\sigma}K^{\rho\sigma}\right), \tag{11}$$

$$J_{\mu\nu} := \frac{1}{3}\left(2KK_{\mu\rho}K^\rho_{\ \nu} + K_{\rho\sigma}K^{\rho\sigma}K_{\mu\nu} - 2K_{\mu\rho}K^{\rho\sigma}K_{\sigma\nu} - K^2K_{\mu\nu}\right), \tag{12}$$

$$P_{\mu\nu\rho\sigma} := R_{\mu\nu\rho\sigma} + 2h_{\mu[\sigma}R_{\rho]\nu} + 2h_{\nu[\rho}R_{\sigma]\mu} + Rh_{\mu[\rho}h_{\sigma]\nu}, \tag{13}$$

is also decomposed into two parts:

$$B := B^{\mu}_{\ \mu} = -3K + \alpha\left(4\tilde{M}_{\rho\sigma}\tilde{K}^{\rho\sigma} - KM - \frac{1}{2}K^3 + 2K\tilde{K}_{\rho\sigma}\tilde{K}^{\rho\sigma} - \frac{8}{3}\tilde{K}^{\rho}_{\ \sigma}\tilde{K}^{\sigma}_{\ \kappa}\tilde{K}^{\kappa}_{\ \rho}\right) = -\frac{\kappa_5^2}{2}\tau, \quad (14)$$

$$\begin{aligned}\tilde{B}_{\mu\nu} &:= B_{\mu\nu} - \frac{1}{4}Bh_{\mu\nu} \\ &= \tilde{K}_{\mu\nu} - 12\alpha\tilde{J}_{\mu\nu} - \alpha\left[4L_{\mu\rho\nu\sigma}\tilde{K}^{\rho\sigma} + 4\tilde{K}_{(\mu}^{\ \ \rho}\tilde{M}_{|\rho|\nu)} - h_{\mu\nu}\tilde{K}_{\rho\sigma}\tilde{M}^{\rho\sigma} - K\tilde{M}_{\mu\nu} - \frac{1}{3}M\tilde{K}_{\mu\nu}\right] \\ &= -\frac{\kappa_5^2}{2}\left(\tau_{\mu\nu} - \frac{1}{4}\tau h_{\mu\nu}\right), \end{aligned} \quad (15)$$

where

$$\tilde{K}_{\mu\nu} := K_{\mu\nu} - \frac{1}{4}Kh_{\mu\nu}, \quad \tilde{J}_{\mu\nu} := J_{\mu\nu} - \frac{1}{4}Jh_{\mu\nu}. \quad (16)$$

In this decomposition, our basic equations are (4) and (5) with the junction conditions (14) and (15). This form may be better to describe some symmetric spacetime such as the Friedmann-Robertson-Walker (FRW) universe, which we shall study next.

The remaining component of the Einstein equation is

$$D_{\nu}\left[K_{\mu}^{\ \nu} - K\delta_{\mu}^{\ \nu} + 2\alpha(3J_{\mu}^{\ \nu} - J\delta_{\mu}^{\ \nu} - 2P_{\mu}^{\ \rho\nu\sigma}K_{\rho\sigma})\right] = \kappa_5^2\mathcal{T}_{MN}h_{\mu}^{M}n^{N}, \quad (17)$$

which gives the constraint on the brane matter fields through the junction condition (10), i.e.

$$D_{\nu}\tau_{\mu}^{\ \nu} = -2\mathcal{T}_{MN}h_{\mu}^{M}n^{N}. \quad (18)$$

If there is no energy-momentum transfer from the bulk, we find the energy-momentum conservation of brane matter fields as

$$D_{\nu}\tau_{\mu}^{\ \nu} = 0. \quad (19)$$

Although the obtained equations are very complicated, any effects from a bulk spacetime to a brane world are described only by the Weyl curvature ($E_{\mu\nu}$). The basic equations are not given in a closed form because of this term. Giving the energy-momentum tensor of the brane, which is shown to be conserved, the extrinsic curvature ($K_{\mu\nu}$) of a brane satisfies a cubic matrix equation. Since it is not explicitly given by the energy-momentum tensor, we have to solve a couple of equations for the induced metric and the extrinsic curvature. If the brane action includes the induced gravity term, which may be expected from quantum effects of matter fields on the brane, we have to replace the energy-momentum tensor with its generalization just as in Ref. [13].

3 Friedmann equation

We apply the present reduction to the FRW cosmology. We assume spacetime as

$$ds^2 = -dt^2 + a^2(t)\,\gamma_{ij}\,dx^i dx^j, \quad (20)$$

where γ_{ij} denotes the metric of maximally symmetric 3-dimensional space. We also assume that only a cosmological constant exists in the bulk. By the Eq. (4) and the junction condition (14), we obtain the generalized Friedmann equation

$$\left[X - \bar{X}_{\pm}(a)\right]\left[1 + \frac{8}{3}\alpha X + \frac{4}{3}\alpha\bar{X}_{\pm}(a)\right]^2 = \frac{\kappa_5^4}{36}\left(\tau^0_{\ 0}\right)^2, \quad (21)$$

where

$$X := H^2 + \frac{k}{a^2}, \quad \bar{X}_{\pm}(a) := \frac{1}{4\alpha}\left[-1 \pm \sqrt{1 + 8\alpha\left(\frac{\Lambda}{6} + \frac{C}{a^4}\right)}\right]. \quad (22)$$

and C is the integration constant, which corresponds to the mass of the black hole solution in bulk spacetime. The Eq. (5) and the junction condition (15) gives the value of E^0_0, i.e.

$$E^0_0 = -\frac{3}{2}\bar{Y}_\pm(a)\left[1+\frac{8\alpha\bar{Y}_\pm(a)}{3(1+4\alpha\bar{X}_\pm(a))}\right], \quad \bar{Y}_\pm(a) = -2C\left(1+4\alpha\bar{X}_\pm(a)\right)^{-1}a^{-4}. \tag{23}$$

The "dark radiation" E^0_0 is not a radiation but depends complicatedly on the scale factor. But our cosmological model has only one unknown parameter C and the system is described in a closed form. The advantage of our description of the basic equations (4) and (5) is that the former gives the generalized Friedmann equation, while the latter is an algebraic equation for E^0_0.

4 Concluding Remarks

We have derived the covariant gravitational equations of a brane world model with the Gauss-Bonnet curvature-squared term in a bulk spacetime. Although the obtained equations are very complicated, any effects from a bulk spacetime to a brane world are described only by the Weyl curvature ($E_{\mu\nu}$). The basic equations are not given in a closed form because of this term.

Giving the energy-momentum tensor of the brane, which is shown to be conserved, the extrinsic curvature ($K_{\mu\nu}$) of a brane satisfies a cubic matrix equation. Since it is not explicitly given by the energy-momentum tensor, we have to solve a couple of equations for the induced metric and the extrinsic curvature. If the brane action includes the induced gravity term, which may be expected from quantum effects of matter fields on the brane, we have to replace the energy-momentum tensor with its generalization just as in Ref. [13].

References

[1] L. Randall and R. Sundrum, Phys. Rev. Lett. **83**, 3370 (1999).

[2] L. Randall and R. Sundrum, Phys. Rev. Lett. **83**, 4690 (1999).

[3] P. Hořava and E. Witten, Nucl. Phys. **B475**, 94 (1996).

[4] G. W. Gibbons, *Supersymmetry, Supergravity and Related Topics* eds. F. del Aguila, et al., World Scientific, Singapore (1985);
J. Maldacena and C. Nunez, Int. J. Mod. Phys. **A16**, 822 (2001).

[5] See, for example, D. J. Gross and J. H. Sloan, Nucl. Phys. **B291**, 41 (1987).

[6] Y. M. Cho and I. P. Neupane, Int. J. Mod. Phys. **A18**, 2703 (2003);
Y. M. Cho, I. P. Neupane and P. S. Wesson, Nucl. Phys. **B621**, 388 (2002).

[7] N. Deruelle and M. Sasaki, Prog. Theor. Phys. **110**, 441 (2003).

[8] T. Shiromizu, K. Maeda and M. Sasaki, Phys. Rev. **D62**, 024012 (2000);
M. Sasaki, T. Shiromizu and K. Maeda, Phys. Rev. **D62**, 024008 (2000).

[9] Y. Choquet-Bruhat, C. R. Acad. Sci., **I 306**, 445 (1988);
Y. Choquet-Bruhat, J. Math. Phys., **29**, 1891 (1988).

[10] K. Maeda and T. Torii, hep-th/0309152, to appear in Phys. Rev. **D**.

[11] R. C. Myers, Phys. Rev. **D36**, 392 (1987).

[12] S. C. Davis, Phys. Rev. **D67**, 024030 (2003);

[13] K. Maeda, S. Mizuno and T. Torii, Phys. Rev. **D68**, 024033 (2003).

Dilaton Dynamics in Type IIB Supergravity

Kunihito Uzawa[1]

Graduate School of Human and Environmental Studies,
Kyoto University, Kyoto 606-8501, Japan

Abstract

We investigate the dynamics of extra dimension in ten-dimensional type IIB supergravity model. The background geometry is assumed to be a product of five-dimensional anti-de Sitter spacetime (AdS_5) and five sphere (S^5). We calculate quantum effects of Neveu-Schwartz scalar field in order to stabilize the extra dimension and find an effective potential for the radius of internal space. The effective potential has a minimum and the internal space S^5 stays to be small and its radius becomes constant even if AdS_5 spacetime evolves. In our model, we assume the gauge fields with classically vacuum expectation value. The 4-form gauge field is role of ten-dimensional cosmological constant. The local minimum of the effective potential is generated by the contribution of gauge field, curvature of internal space, and Casimir effect.

1 Introduction

The idea that our universes may consist of more than four-dimensional spacetime, with extra spatial dimension compactified on some small scale, is motivated by supergravity and superstring theory. In general strategy, it is considered that obvious difference between the usual four dimensions and the extra dimension could result from a process of spontaneous breakdown of the vacuum symmetry, which is often called "spontaneous compactification" of the extra dimensions.

Recently, the Randall & Sundrum (RS) brane world model[1] has been investigated by many authors in the cosmological and gravitational points of view. This model shows that the hierarchy problem may be solved by the warp factor or the gravity can be confined in non-compact spacetime. However, a higher-dimensional realistic model including RS setup is not so far known. The most plausible candidate is the $AdS_5 \times S^5$ compactification of the ten-dimensional type IIB supergravity theory. The scale of S^5 is determined by the dilaton arising from a spontaneous compactification and is generally dynamical variable in the cosmological point of view. Moreover, the scale of internal space is expected to be much smaller than that of AdS_5. The dilaton in type IIB supergravity model has not ever been discussed as a dynamical variable but assumed to be a constant parameter. In order to discuss whether such a background is realized in the universe, we have to derive a potential for the dilaton, and analyze its stability. Unfortunately, in a pure gravitational system without quantum effects, there is no solution to stabilize a dilaton. We thus see that the stabilization of the dilaton is a crucial issue. The purpose of this paper is to investigate a stabilization mechanism of the internal space via quantum effects in the ten-dimensional type IIB supergravity model. We assume that the vacuum ten-dimensional spacetime is compactified into the direct product of five-dimensional anti-de Sitter spacetime and compact five-dimensional sphere, i.e $AdS_5 \times S^5$. We consider the quantum fluctuations associated with Neveu-Schwartz(NS) scalar fields in order to stabilize the scale of internal space S^5. Many works suggest that quantum correction of higher-dimensional matter field might provide a physical mechanism which is capable of accounting for extreme smallness of the extra dimensions. In our previous work[2], we have discussed the stabilization mechanism of dilaton in terms of the quantum correction in the ten-dimensional type IIB supergravity. The background contains only gravity, NS scalar and 4-form fields. We have showed that the dilaton potential has a local minimum resulting from contributions of the gauge field, the curvature of the internal spacetime and quantum effects of the background scalar, vector, spinor, and tensor fields. The dilaton settles down to the local minimum, and the scale of the extra dimensions eventually become time independent. The five-dimensional universe evolves from dS_5 into AdS_5 after stabilization of the extra dimension. The

[1] E-mail:uzawa@phys.h.kyoto-u.ac.jp

background solution contains a 3-brane because the background geometry has the 5-form gauge field strength. Hence, the ten-dimensional (A)dS$_5 \times$ S^5 compactification may provide a realistic model of the RS brane world.

Here we consider more general set up including not only 5-form gauge field strength but also taking into account the contribution of 1-form and 3-form gauge field strength. In this model, there is a new contribution to the dynamics of extra dimension because the dilaton exponentially couples to the gauge fields. The low energy effective action in our model is obtained by the integration of internal space, which is often called dimensional reduction. In the sphere compactification of higher-dimensional theory, in order to obtain the lower-dimensional effective action, the field is expanded by the spherical harmonics. The field depending only on the lower-dimensional coordinate is obtained by integrated out the spherical harmonics on the internal space. However, there is the exponential function of NS scalar field Φ in the ten-dimensional type IIB action. The spherical harmonics in the NS scalar field can not be naively integrated on the internal space. Therefore, above mentioned procedure can not be simply used in our model. Then, we use the following method in order to avoid the problem. First, we consider the perturbation of NS scalar field around $\Phi = \Phi_c$ and substitute this perturbation into the ten-dimensional action. Second, the action is expanded with respect to the perturbation of NS scalar field around $\Phi = \Phi_c$ up to second order. We assume that the value of Φ_c is constant and the perturbation of NS scalar field around $\Phi = \Phi_c$ depends on the ten-dimensional coordinate. By above procedure, the exponential functions of NS scalar field does not appear in the ten-dimensional type IIB supergravity action, and lower-dimensional action is obtained by using the spherical harmonics of NS scalar field.

After the dimensional reduction, the dilaton couples the matter fields in external spacetime. The quantum fluctuations around a classical solution are computed in the form of quantum effective potential as a function of dilaton. Then the quantum correction of the matter field naturally contributes to the dilaton potential. Since the quantum correction is dominant effect at the small scale of internal space, this correction at nearly Planck scale is expected to be very important. We also consider the quantum effect of dilaton around the stable point. The dilaton potential contains the exponential function. Then it is ordinary difficult to calculate the effective potential including the quantum effect of dilaton. Fortunately, using the our method that we have mentioned above, we can treat the quantum correction of dilaton.

2 Dilaton dynamics in Type IIB supergravity

Let us consider ten-dimensional type IIB supergravity action. If we assume the $B_2 = 0$ and consider the conformal transformation $\bar{g}_{MN} = \mathrm{e}^{\Phi/2}\bar{g}_{MN}$, the type IIB supergravity action is given by

$$I_{\mathrm{IIB}}[\bar{g}, \Phi] = \frac{1}{2\bar{\kappa}^2}\int d^{10}X\sqrt{-\bar{g}}\left\{\bar{R} - \bar{g}^{MN}\partial_M\Phi\partial_N\Phi - \frac{1}{2}\left(\mathrm{e}^{2\Phi}|F_1|^2 + \mathrm{e}^{\Phi}|F_3|^2 + \frac{1}{2}|F_5|^2\right)\right\}, \tag{1}$$

where $\bar{R}$ is a Ricci scalar of the ten-dimensional metric tensor $\bar{g}_{MN}$, $\bar{\kappa}$ is positive constant, and F_1, F_3, F_5 etc denote the rank of tensor fields. We consider the constant solution as gauge field strength. These field strengths are wrapped around the S^5. We then set $|F_5|^2 \equiv 8\bar{\Lambda}$, $|F_3|^2 \equiv 4A$, $|F_1|^2 \equiv 4B$ and redefine the NS scalar $\varphi = \Phi/\bar{\kappa}$. The ten-dimensional action (1) is now rewritten by

$$I_{\mathrm{IIB}}[\bar{g}, \varphi] = \int d^{10}X\sqrt{-\bar{g}}\left[\frac{1}{2\bar{\kappa}^2}\left(\bar{R} - 2\bar{\Lambda}\right) - \frac{1}{2}\bar{g}^{MN}\partial_M\varphi\partial_N\varphi - \frac{1}{\bar{\kappa}^2}\left(A\,\mathrm{e}^{\bar{\kappa}\varphi} + B\,\mathrm{e}^{2\bar{\kappa}\varphi}\right)\right]. \tag{2}$$

Now we take a dimensional reduction. Our ansatz for the metric is the following;

$$\bar{g}_{MN}dX^M dX^N = \left(\frac{b_0}{b}\right)^{-10/3} g_{\mu\nu}dx^\mu dx^\nu + b^2(x^\mu)\Omega^{(5)}_{ij}dy^i dy^j, \tag{3}$$

where $g_{\mu\nu}$ is metric of five-dimensional anti-de Sitter spacetime, b is the scale of a five-dimensional sphere (i.e. a radius of S^5), a constant b_0 is an initial value of b, and $\Omega^{(5)}_{ij}dy^i dy^j$ is the line element of a unit five-dimensional sphere. The five-dimensional metric $g_{\mu\nu}$ and b depend only on the five-dimensional coordinate $\{x^\mu\}(\mu = 0, 1, 2, \cdots)$. To write down the five-dimensional effective action, it is convenient to

expand the field in terms of harmonics on the five-dimensional sphere:

$$\varphi = b_0^{-5/2} \sum_{l,m} \varphi_{lm}(x^\mu) Y_{lm}^{(5)}(y^i) , \tag{4}$$

where $Y_{lm}^{(5)}$ are real harmonics on the 5-sphere, and $\varphi_{lm}(x^\mu)$ is a real function depending only on the five-dimensional coordinate $\{x^\mu\}$. Unfortunately, the spherical harmonics for exponential potential of the NS scalar field in the action (2) cannot be integrated on the internal space. Then we consider the perturbation $\varphi = \varphi_c + \delta\varphi$, where the value of φ_c is assumed to be constant. In the following, we investigate the dilaton dynamics around $\varphi = \varphi_c$. Substituting the perturbation $\varphi = \varphi_c + \delta\varphi$, the metric (3) and the scalar harmonics (4) into the action (2), we get the five-dimensional effective action

$$\begin{aligned} I_{\rm IIB}[g\,,\,\varphi_{lm}] \;=\; & \int d^5x\sqrt{-g}\left[\frac{1}{2\kappa^2}R - \frac{1}{2}g^{\mu\nu}\partial_\mu\sigma\partial_\nu\sigma - U(\sigma)\right. \\ & \left. - \sum_{l,\,m}\frac{1}{2}\left(g^{\mu\nu}\partial_\mu\varphi_{lm}\partial_\nu\varphi_{lm} + M_\varphi^2\varphi_{lm}^2\right) + O\left((\varphi_{lm})^3\right)\right] , \end{aligned} \tag{5}$$

where R is Ricci scalar of five-dimensional metric tensor $g_{\mu\nu}$, κ is a positive constant defined by $\kappa^2 = \bar{\kappa}^2/(2^5 b_0^5 \pi)$, the field σ is defined by $\kappa_\sigma\sigma = \ln(b/b_0)$, $\kappa_\sigma = \kappa\sqrt{2/(35)}$, the mass M_φ^2 of five-dimensional NS scalar field φ is given by

$$M_\varphi^2 = \left(\bar{A} + 4\bar{B}\right) {\rm e}^{-10\kappa_\sigma\sigma/3} + \frac{l(l+4)}{b_0^2}\,{\rm e}^{-16\kappa_\sigma\sigma/3} , \tag{6}$$

and the dilaton potential $U(\sigma)$ is given by

$$U(\sigma) = \frac{1}{\kappa^2}\left(\bar{\Lambda} + \bar{A} + \bar{B}\right) {\rm e}^{-10\kappa_\sigma\sigma/3} - \frac{10}{\kappa^2 b_0^2}\,{\rm e}^{-16\kappa_\sigma\sigma/3} . \tag{7}$$

The parameters $\bar{A}\,,\bar{B}$ are defined by $\bar{A} \equiv A{\rm e}^{\bar{\kappa}\varphi_c}$, $\bar{B} \equiv B{\rm e}^{2\bar{\kappa}\varphi_c}$, respectively. Since this potential does not have any local minimum, there is no stable compactification by S^5. The five-dimensional NS scalar field potential contains the term which is proportional to φ_{lm}^2. This term is derived from the kinetic term of NS scalar field after the dimensional reduction. Note that the local minimum of $V(\varphi_{lm})$ is located at $\varphi_{lm} = 0$.

Now we compute the quantum correction of the NS scalar field in 1-loop level. The quantum correction arising from matter field is very important to stabilize the scale of extra dimension. If this correction does not exist in our model, it is impossible of dilaton to stabilize. Then the extra dimension finally collapses to singularity or expands forever. Here we adopt the path integral to compute the dilaton effective potential. Any divergence appeared in calculation must be removed by regularization technique. We use the zeta function regularization, which was developed for performing the path integral in curved spacetime[3]. To calculate the quantum correction, we consider the 1-loop quantum correction for NS scalar field. The calculation of the effective potential is carried out using path integral method. The field φ_{lm} is split into a classical part $\varphi_{lm\,c}$ and quantum part $\varphi_{lm\,q}$. The action is then expanded in the quantum fields around arbitrary classical background field. We expand the fields to second order to calculate all 1-loop diagrams with any number of lines of external fields. We go over to Euclidiean space in the action and calculate the Gaussian functional integrals, which can be expressed as functional determinants. In order to evaluate the functional integrals, we introduce the generalized zeta function $\zeta_\varphi(s)$ which is the sum of the operator eigenvalues. We adopt this method to determine the 1-loop effective potential in anti-de Sitter spacetime. If the condition of a(the curvature scale of AdS_5) $\gg b$ and $b^2(\bar{A}+4\bar{B}) \ll 1$ are satisfied, we easily calculate the value of $\zeta_\varphi(0)$ and $\zeta'_\varphi(0)$. Then the effective potential is given by

$$\begin{aligned} V_{\rm eff}(\sigma) \;=\; & \frac{1}{\kappa^2}\left(\bar{\Lambda} + \bar{A} + \bar{B}\right) {\rm e}^{-10\kappa_\sigma\sigma/3} - \frac{10}{\kappa^2 b_0^2}\,{\rm e}^{-16\kappa_\sigma\sigma/3} + \frac{1}{b_0^5}\,{\rm e}^{-40\kappa_\sigma\sigma/3} \\ & \times\left[-\ln(\mu^2 a^2) + \frac{\pi^2}{2211840}\left\{\frac{5}{2} + b^2(\bar{A}+4\bar{B})\right\}\ln\left\{\left(\frac{a}{b_0}\right)^2 {\rm e}^{-16\kappa_\sigma\sigma/3}\right\}\right] . \end{aligned} \tag{8}$$

Setting $\bar{\Lambda} = 1.6 \times 10^{-5} M_\kappa^2$, $b_0 = 10^2 L_\kappa$, $\bar{A} = \bar{B} = 10^{-10} M_\kappa^2$, and $\mu = (10^4 b_0)^{-1}$, we find the stable minimum point $\sigma_s = -4.29337 M_\kappa^{-3}$ where $V_{\rm eff}(\sigma_s) = -0.142633 M_\kappa^5$ for $a = 10^6 L_\kappa$. L_κ and M_κ denote the five-dimensional Planck length and mass, respectively. Note that the contribution of gauge field $b^2(\bar{A} + 4\bar{B})$ in the effective potential (8) can be negligible as $b \to 0$ because the gravity is most dominant contribution near the Planck scale.

3 Summary

We have calculated quantum effects in the $AdS_5 \times S^5$ background of the ten-dimensional type IIB supergravity and discussed its stability using the effective potential. In their pure gravity systems, a curvature term of the internal space gives a dominant contribution to the dilaton potential at small b, while gauge field terms become dominant for large b. Hence the dilaton potential is unbounded from below as $b \to 0$ and drops as $b \to \infty$. Then the extra dimension either shrinks to zero volume or is decompactified. However, if we include quantum effects, we find a stable minimum for the dilaton potential.

The energy-momentum tensor in our model consists of the matter and quantum effects of dilaton and NS scalar field. This quantum correction is often called the Casimir effect. The quantum effective potential associated with the NS scalar field is similar power to the part of dilaton potential arising from the curvature and the cosmological constant (or gauge field). A local minimum is created by their combination due to their signs being opposite. In ten-dimensional type IIB supergravity model, the scale of extra dimension is stabilized by balancing the gauge field strength wrapped around the S^5, the curvature term of S^5 and quantum correction term induced by the NS scalar. The NS scalar is originally characterized by the direction of eleventh dimension in the eleven-dimensional supergravity. Thus the quantum effect of NS scalar becomes important if the eleventh dimension is compactified near the Planck scale. In the large b, gauge fields mainly contribute to the dynamics of dilaton. In our model, the gauge fields are wrapped around the direction of extra dimension while these look like scalar field in the AdS_5 spacetime. The scale of extra dimension decreases as the flux density of gauge fields increase. Then the gauge field strength acts the repulsive force to the dynamics of b because the magnitude of the force is proportional to the flux density. On the other hand, the gravitational contribution becomes dominant near the Planck scale. First, the classical effect of the gravity is dominant, which is the curvature of the internal space. Since S^5 is compact space, the curvature effect make the scale of extra dimension collapse as the dilaton approaches to the Planck scale. Next, in the more small b, the quantum gravitational effect such as radiative correction of moduli field becomes important in the dilaton effective potential. It can be considered that the quantum effect of NS scalar is the kind of quantum correction of gravity. It is expected that the higher loop correction of NS scalar field becomes dominant as $b \to 0$.

Finally, we have discussed the quantum correction of NS scalar and dilaton field in the ten-dimensional type IIB supergravity. If the model that we have considered keeps the maximal supersymmetry, the cancellation between the bosonic and the fermionic contribution with respect to the quantum correction occurs. However, the maximal supersymmetry is broken by the dynamics of dilaton in our model. Therefore, we can discuss the stabilization mechanism of internal space via the quantum correction.

References

[1] L. Randall and R. Sundrum, Phys. Rev. Lett. **83** (1999) 3370; *ibid.* **83** (1999) 4690.

[2] K. Uzawa and K. i. Maeda, Phys. Rev. D **68** (2003) 084017.

[3] K. Uzawa, Prog. Theor. Phys. **110** (2003) 457.

Power Spectrum Analysis to Explore the Nature of the Dark Energy

Kazuhiro Yamamoto[1]

Graduate School of Science, Hiroshima University, Higashi-Hiroshima, 739-8526, Japan

Abstract

We investigate the power spectrum analysis as a probe of the nature of the dark energy with large redshift surveys. By developing an optimal weighting scheme for the power spectrum analysis in redshift-space, we demonstrate that the luminous red galaxy (LRG) sample in the Sloan Digital Sky Survey (SDSS) is useful as a probe of the equation of state of the dark energy w. As a practice of the power spectrum analysis, we revisit the complete sample of the two degree field (2dF) QSO redshift (2QZ) survey. A power spectrum consistent with that of the 2QZ group is obtained. Fitting of the power spectrum is investigated incorporating the nonlinear effects, the geometric distortion and the light-cone effect. It is shown that the QSO power spectrum is consistent with the Λ cold dark matter (CDM) model with the matter density parameter $\Omega_m = 0.2 \sim 0.4$. The constraint on w from the QSO power spectrum is demonstrated, though it is not very tight due to shotnoise contribution. We also mention future prospect of such power the spectrum method. With future redshift survey, the method might become competitive with the supernovae method in order to constrain w.

1 Introduction

The origin of the today's cosmic acceleration is an open question. It can be explained by introducing the dark energy. Recently, it is argued that modifying gravity also explains the acceleration. In order to explore the origin, it will be important to test theoretical predictions of these models with cosmological observations. Here, we investigate the power spectrum method as a probe of the nature of the cosmic acceleration, based on the framework of the model introducing a time-variable cosmological constant with the equation of state $w(z)$.

This paper is organized as follows: In section 2, by developing a useful formulation of the optimal weighting scheme for redshift-space power spectrum analysis, we assess the feasibility of the power spectrum analysis with the luminous red galaxy sample in the SDSS as a probe of the equation of state of the dark energy. In section 3, we revisit the power spectrum analysis of the 2dF QSO redshift (2QZ) survey. Cosmological constraint from the 2QZ sample is investigated. Section 4 is devoted to conclusions.

2 Optimal weighting scheme in redshift-space power spectrum analysis and a prospect for measuring w

In usual power spectrum analysis, many authors base their methods on the optimal weighting scheme developed by Feldman, Kaiser & Peacock [1]. In this section, we present the formulation of the optimal weighting scheme incorporating the light-cone effect and the redshift-space distortions. See [2] for details. The method introduces the weight factor that minimizes the error of the power spectrum estimator $w(\mathbf{s},\mathbf{k})$, where $\mathbf{s}$ and $\mathbf{k}$ are the coordinate of a map and the wave number, respectively. The Fourier coefficient of the density fluctuation $n(\mathbf{s})$ is obtained by

$$\mathcal{F}(\mathbf{k}) = \frac{\int d\mathbf{s} w(\mathbf{s},\mathbf{k})[n(\mathbf{s}) - \alpha n_s(\mathbf{s})]e^{i\mathbf{k}\cdot\mathbf{s}}}{[\int d\mathbf{s}\bar{n}(\mathbf{s})^2 w(\mathbf{s},\mathbf{k})^2]^{1/2}},$$

[1] E-mail:kazuhiro@hiroshima-u.ac.jp

where $\bar{n}(\mathbf{s})$ is the mean number density and $n_s(\mathbf{s})$ is a random density field that has a mean number density $1/\alpha$ times that of $n(\mathbf{s})$. The estimator of the power spectrum $\mathcal{P}_0(k)$ is given as follows: First define

$$\mathcal{P}(\mathbf{k}) = |\mathcal{F}(\mathbf{k})|^2 - \frac{(1+\alpha)\int d\mathbf{s}\bar{n}(\mathbf{s})w(\mathbf{s},\mathbf{k})^2}{\int d\mathbf{s}\bar{n}(\mathbf{s})^2 w(\mathbf{s},\mathbf{k})^2},$$

and average it over a thin shell in k-space with radius k,

$$\mathcal{P}_0(k) = \frac{1}{\Delta V_k}\int_{\Delta V_k} d\mathbf{k}\mathcal{P}(\mathbf{k}),$$

where ΔV_k denotes the volume of the shell. Next we evaluate the ensemble average $\langle\mathcal{P}_0(k)\rangle$ and the variance $\langle\Delta\mathcal{P}_0(k)^2\rangle \equiv \langle[\mathcal{P}_0(k) - \langle\mathcal{P}_0(k)\rangle]^2\rangle$. The optimal weighting scheme is determined so that it minimizes $\langle\Delta\mathcal{P}_0(k)^2\rangle$. After some calculations, we have $w(\mathbf{s},k) = 1/\bar{n}(\mathbf{s})Q(k,\mathbf{s})$ with

$$Q^2(k,\mathbf{s}) = \frac{1}{\Delta V_k}\int_{\Delta V_k} d\mathbf{k}\Big[P\Big(\mathbf{k},|\mathbf{s}|\Big) + \frac{\alpha+1}{\bar{n}(\mathbf{s})}\Big]^2. \tag{1}$$

Once the minimal variance of the power spectrum is evaluated, one can construct the probability distribution function of the power spectrum, assuming the Gaussian distribution. By employing the Fisher matrix approach, it is possible to estimate the accuracy to which one can constrain cosmological parameters with a measurement of the power spectrum. The Fisher matrix is approximately expressed as

$$F_{ij} = \frac{1}{4\pi^2}\int_{k_{\rm min}}^{k_{\rm max}} \kappa(k)\frac{\partial\langle\mathcal{P}_0(k)\rangle}{\partial\theta_i}\frac{\partial\langle\mathcal{P}_0(k)\rangle}{\partial\theta_j}k^2dk \tag{2}$$

with

$$\kappa(k) = \frac{[\int d\mathbf{s}\bar{n}(\mathbf{s})^2 w(\mathbf{s},k)^2]^2}{\int d\mathbf{s}\bar{n}(\mathbf{s})^4 w(\mathbf{s},k)^4[P_0(k,\mathbf{s}),+1/\bar{n}(\mathbf{s})]^2}. \tag{3}$$

Next we investigate the prospect of the power spectrum analysis using the luminous red galaxy (LRG) sample in the SDSS. The LRG is intrinsically luminous early-type galaxy and the SDSS spectroscopic survey will provide a sample of 10^5 LRGs of the redshift to $z \sim 0.5$. In the analysis of the clustering statistics of such sample, the light-cone effect and the geometric distortion can be substantial. Here we assume the final sample of the LRG in the SDSS of the survey area $10^4\mathrm{deg}^2$. In this analysis we assume that $w(z)$ can be parameterized by

$$w(z) = \bar{w}\left(\frac{1+z}{1+z_*}\right)^{\nu}, \tag{4}$$

where z_* is a constant. The Fisher matrix analysis demonstrates that the LRG sample has a potential for constraining the equation of state $\bar{w}$ around $z_* = 0.13$ with 1σ errors at the 10% level, if other fundamental parameters are determined in an independent fashion.

3 Power spectrum analysis of the 2dF QSO sample revisited

In this section we report on our analysis of the power spectrum of the 2dF QSO sample. (See also [3]) Recently, Outram et al. have reported the power spectrum analysis of the complete 2QZ sample [4]. They have shown that the QSO power spectrum is consistent with the ΛCDM model and obtained a constraint on the cosmological density parameters. However, in the modeling of the QSO power spectrum, they have not taken the light-cone effect, the geometric distortions and the non-linear effect into account. As a complementary test of the work by Outram et al., we independently determine the power spectrum in the clustering of the 2dF QSO sample. Then we fit the QSO power spectrum with theoretical models incorporating these effects properly.

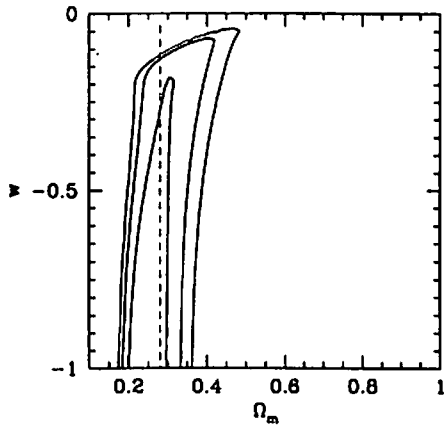

Figure 1: Contours of the likelihood function on the Ω_m and w plane. Contours are confidence of 65%, 95% and 99%. Here we assume $\Omega_b = 0.045$, $h = 0.7$, $n = 1$ and $\sigma_8 = 0.9$. The dashed line is $\Omega_m = 0.28$.

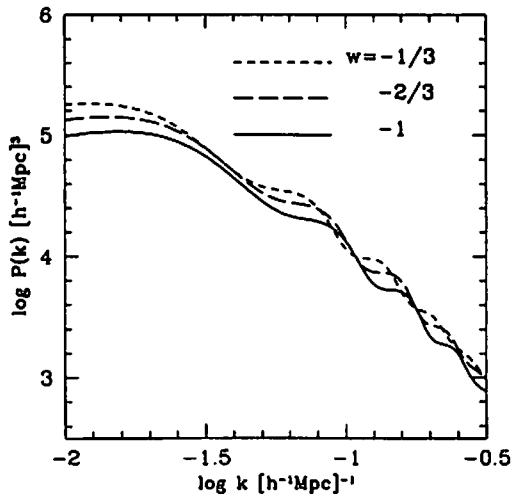

Figure 2: Theoretical power spectra with $w = -1$ (solid curve), $w = -2/3$ (long dashed curve) and $w = -1/3$ (dashed curve). The other cosmological parameter is fixed as $\Omega_m = 0.28$, $\Omega_b = 0.1$, $h = 0.7$, $\sigma_8 = 0.9$ and $n = 1$. The amplitude is normalized as $P(k) = 10^4 (h^{-1}\mathrm{Mpc})^3$ at $k = 0.1h\mathrm{Mpc}^{-1}$. Note that the model of large baryon fraction is adopted to emphasize the scaling effect of the geometric distortion.

In our power spectrum analysis we use the complete sample of the full 2QZ survey publicly available. The 2QZ survey covers two area of 5×75 deg^2, one in the South Galactic Cap (SGC) and the other in the North Galactic Cap (NGC), respectively. The redshift is distributed up to 3. The survey area is defined by the equatorial coordinates from $\alpha = 21^h40$ to $\alpha = 3^h15$ and $-32.5° \leq \delta \leq -27.5°$ in the SGC, and $9^h50 \leq \alpha \leq 14^h50$ and $-2.5° \leq \delta \leq 2.5°$ in the NGC, respectively. We use 10713 and 8443 QSOs in the SGC and the NGC, respectively, in the range of redshift $0.2 \leq z \leq 2.2$.

We have obtained a power spectrum consistent with the result by the 2QZ group. The error bar of our power spectrum is larger than that of the 2QZ group. We have fitted the power spectrum with theoretical model introduced the time-variable cosmological constant with the constant equation of state w. Figure 1 shows the contour of the likelihood function when different values of Ω_m and w are used in the modeling the power spectrum, where we fixed $\Omega_b = 0.045$, motivated from the WMAP result. It is shown that the density parameters in the range $0.2 \lesssim \Omega_m \lesssim 0.4$ is preferable, which is not very sensitive to the value of w. Therefore the constraint on w is not very tight, and $w \gtrsim -0.2$ (-0.1) is only excluded at the one (two) sigma level.

It is useful to show how the theoretical power spectrum depends on the equation of state w of the dark energy. Curves in Figure 2 are theoretical power spectra with the various equation of state $w = -1$(solid curve), $w = -2/3$(long dashed curve) and $w = -1/3$(dashed curve). The theoretical curves scale from right to left as w becomes larger, which traces back to the geometric distortion effect. The oscillating feature comes from the baryonic contribution. Thus, because of the fine structure in the matter power spectrum, a precise measurement of the power spectrum has a potential to constrain the equation of state.

4 Conclusions

We have presented a generalized formula of the optimal weighting scheme for the power spectrum analysis as an extension of the work by Feldman et al. [1], incorporating the redshift distortions and the light-cone effect. Using the Fisher matrix approach, we have shown that the LRG sample in SDSS will provide a useful constraint on w, 1 sigma errors at the 10% level, if other cosmological parameters are well determined independently. I have re-analyzed the power spectrum of the 2dF QSO sample. It is shown that the QSO spatial power spectrum is consistent with the ΛCDM model with $\Omega_m = 0.2 \sim 0.4$. The result of our analysis is effectively consistent with that of the 2QZ group. The constraint on w from the QSO power spectrum is demonstrated. No tight constraint on w is obtained, $w \gtrsim -0.2$ (-0.1) is only excluded at the one (two) sigma level. However, the redshift-space power spectrum analysis of high-redshift objects can be a useful probe of the dark energy. The geometric distortion effect and the baryonic contribution in the matter power spectrum play a key role. The power spectrum method will provide useful constraints on $w(z)$ when applied to the SDSS LRG sample and future redshift survey such as the KAOS project [5] (see also http://www.noao.edu/kaos). It will be complementary to the method with the supernovae to constrain the nature of the dark energy and the cosmic acceleration.

Acknowledgment: The author thanks B. A. Bassett for the useful conversations on the KAOS project.

References

[1] H. A. Feldman, N. Kaiser, & J. A. Peacock, ApJ, 426, 23 (1994)

[2] K. Yamamoto, ApJ, 595, 577 (2003)

[3] K. Yamamoto, ApJ (2004) in press, (astro-ph/0401039)

[4] P. J. Outram, et al., MNRAS, 342, 483 (2003)

[5] H-J. Seo & D. J. Eisenstein, ApJ, 598, 720 (2003)

Chaotic preheating

Yoshida Jin[1]

Department of Physics, Waseda University,
Okubo 3-4-1, Shinjuku, Tokyo 169-8555, Japan

Shinji Tsujikawa[2]

Institute of Cosmology and Gravitation, University of Portsmouth,
Portsmouth PO1 2EG, United Kingdom

Abstract

We study the chaotic dynamics of reheating after inflation in which the self-coupling inflaton field, ϕ, couples to another scalar field, χ, through an interaction, $\frac{1}{2}g^2\phi^2\chi^2$. When the background field χ is not dynamically suppressed during inflation, reheating proceeds in a chaotic way due to a non-negligible mixing term between two fields. This also provides us an interesting possibility to lead to a tachyonic-type instability in addition to the standard parametric resonance.

1 Introduction

The preheating scenario has been proposed to consider a reheating stage more realistically, that is considering the decay of the classical inflaton field ϕ into ϕ particle or into other bosons by a parametric resonance [1], [2]. The parametric resonance was calculated to solve Mathieu equation. Another model was studied in which the action is

$$S = \int dx^4\sqrt{-g}\left(\frac{1}{2}M_p^2R - \frac{1}{2}\partial^\mu\phi\partial_\mu\phi - \frac{1}{4}\lambda\phi^4 - \frac{1}{2}g^2\phi^2\chi^2\right), \tag{1}$$

where ϕ and χ are an inflaton and another scalar field respectively [3]. A stability-instability chart was derived to solve the Lamé equation (see figure 1). This figure shows that the darker the shade is, the

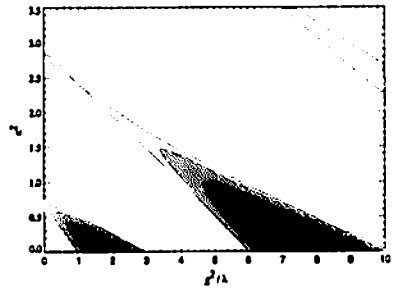

Figure 1: A stability-instability chart for the fluctuation $\delta\chi_K$ in the parameter g^2/λ and K^2, where K is a normalized wave number [3].

stronger the fluctuation $\delta\phi_k$ and $\delta\chi_k$ grow. To derive the Lamé equation, the condition that χ dumps during the inflation era is needed. Without this condition a new kind of instability, named "tachyonic instability", has been found by D.I.Podolsky and A.A.Starobinsky [4]. However, their analysis has been done only around a special solution. In this article we study numerically whether the tachyonic instability occurs around general solutions.

Units are used in which $c = \hbar = 1$, $M_p^2 = G/8\pi$.

[1] E-mail:jin@gravity.phys.waseda.ac.jp
[2] E-mail:shinji.tsujikawa@port.ac.uk

2 "Chaotic reheating" scenario

In this section, we review the "chaotic reheating" scenario [4]. The action was presented in equation (1).

In order to inflate the universe, the assumption is necessary that χ is never dynamically important. The following condition makes sure of the assumption, $m_\chi^2 = g^2\phi^2 \geq H^2 = \frac{2\pi}{3M_p^2}\frac{\lambda}{4}\phi^4$. That means $\kappa \gg 1$. Unless $\kappa \gg 1$, it also makes sure of the above assumption that $g^2\chi^2 \leq \lambda\phi^2$. In this case χ is not suppressed during inflation as we mention below. The new time variable is defined $\tau \equiv \ln(a(t)/a_f)$, where a_f is the value of the scale factor at the end of inflation. ϕ can be solved with slow-roll approximation,

$$\phi^2 = -\frac{\tau}{8\pi^2 M_p^2}, \ |\tau| \gg 1. \tag{2}$$

The Gaussian approximation is imposed to χ, and z is defined as following, $z \equiv 8\pi^2 M_p^2\langle\chi^2\rangle$. Using Fokker-Planck equation and slow-roll approximation, the equation for z is derived,

$$\frac{dz}{d\tau} = -\frac{2m_\chi^2 z}{3H^2} + \frac{1}{2}M_p^2 H^2 = \frac{g^2 z}{\lambda\tau} + \frac{\lambda\tau^2}{6\pi^2}. \tag{3}$$

With the initial condition that $z = 0$, this equation is solved,

$$z = \frac{\lambda}{6\pi^2(3-\kappa)}(\tau_0^{3-\kappa}|\tau|^\kappa - |\tau|^3), \ |z| \geq 1. \tag{4}$$

The second term shows that z is growing in inflationary stage. That means χ is not dynamically suppressed during inflation.

Conformal time and conformal variables are defined as $d\eta \equiv \frac{dt}{a}$, $\tilde{\phi} \equiv a\phi$, $\tilde{\chi} \equiv a\chi$. Because $a \propto \eta$ at the radiation dominant era, $\frac{a'}{a}$, $\frac{a''}{a} \to 0$ at the end of inflation. As a result the field equations become integrable,

$$\tilde{\phi}'' + \lambda\tilde{\phi}^3 + g^2\tilde{\chi}^2\tilde{\phi} = 0, \tag{5}$$

$$\tilde{\chi}'' + g^2\tilde{\phi}^2\tilde{\chi} = 0, \tag{6}$$

$$(a')^2 = \frac{8\pi}{3M_p^2}\left(\frac{1}{2}\left(\tilde{\phi}'\right)^2 + \frac{1}{2}(\tilde{\chi}')^2 + \frac{\lambda}{4}\tilde{\phi}^4 + \frac{g^2}{2}\tilde{\phi}^2\tilde{\chi}^2\right) = \frac{8\pi}{3M_p^2}E. \tag{7}$$

The behavior of $\tilde{\phi}$, $\tilde{\chi}$ is interpreted as the particle motion in the potential which is $V = \frac{\lambda}{4}\tilde{\phi}^4 + \frac{g^2}{2}\tilde{\phi}^2\tilde{\chi}^2$. It is known that a particle motion with the Hamiltonian that $H = \frac{1}{2}\dot{x}^2 + \frac{1}{2}\dot{y}^2 + \frac{1}{8}x^4 + \frac{1}{2}x^2y^2$ is chaotic [3].

Introducing the Fourier mode decomposition, we get

$$\delta\tilde{\chi}_k'' + (k^2 + g^2\tilde{\phi}^2)\delta\tilde{\chi}_k + 2g^2\tilde{\chi}\tilde{\phi}\delta\tilde{\phi}_k = 0, \tag{8}$$

$$\delta\tilde{\phi}_k'' + (k^2 + 3\lambda\tilde{\phi}^2 + g^2\tilde{\chi}^2)\delta\tilde{\phi}_k + 2g^2\tilde{\chi}\tilde{\phi}\delta\tilde{\chi}_k = 0. \tag{9}$$

The $\delta\tilde{\chi}_k$ term of equation (9) and the $\delta\tilde{\phi}_k$ term of equation (8) are the mixing terms. These mixing terms do not exist in [3], because χ is neglected in [3]. The special background solution [4] is considered that $\tilde{\phi} = \alpha\tilde{\chi}$, where $\alpha^2 = \frac{g^2}{g^2-\lambda} = \frac{\kappa}{\kappa-1}$. The new decoupled perturbations are introduced: $\Sigma_k \equiv A\delta\tilde{\chi}_k + B\delta\tilde{\phi}_k$, $\Delta_k \equiv C\delta\tilde{\chi}_k + D\delta\tilde{\phi}_k$, where A, B, C, D are some constants. The fluctuation equations are

$$\Sigma_k'' + (k^2 + 3g^2\tilde{\phi}^2)\Sigma_k = 0, \ \ \Delta_k'' + (k^2 + \frac{2-\kappa}{\kappa}g^2\tilde{\phi}^2)\Delta_k = 0. \tag{10}$$

The field Σ_k can be interpreted as the inflaton, because the structure of equation (10) is the same as that of (9) if $\tilde{\chi} = 0$. The equation (10) results in the tachyonic instability of Δ_k in case of $K^2 + (2-\kappa)\frac{\tilde{\phi}^2}{\tilde{\phi}_0^2} < 0$, where $K^2 \equiv \frac{k^2}{\lambda\phi_0^2}$ and ϕ_0 is the initial value of ϕ at inflationary phase.

[3] e.g. Yang-Mills field behavior in the axi-symmetric Bianchi I spacetime .

[4] This special solution is unstable. Thus the following results may not make sense well.

3 Chaotic preheating scenario

We study the "chaotic reheating" scenario precisely and we call our study "chaotic preheating" scenario [7] to distinguish our study from theirs. The following three topics are mainly studied; the first is the estimation of z at the end of inflation, the second is the chaotic behavior of background field $\tilde{\phi}$ and $\tilde{\chi}$ and the third is the verification of tachyonic instability in general cases.

We estimate numerically $z \equiv 8\pi^2 M_p^2 \langle \chi^2 \rangle$ at the end of inflation, using Fokker-Planck equation (3) and field equation with $\chi = \dot{\chi} = 0$. After that we estimate $\sqrt{\langle \chi_i^2 \rangle}$, where χ_i is the value of χ at the end of inflation. It is found that the smaller κ is, the larger $\sqrt{\langle \chi_i^2 \rangle}$ becomes, and the larger ϕ_0 is, the larger $\sqrt{\langle \chi_i^2 \rangle}$ becomes. One may say $\sqrt{\langle \chi_i^2 \rangle}$ is at most $O(10^{-2})$ with the assumption that χ is not dynamically important. The following numerical studies in a reheating stage are based on this estimation.

We show the behavior of $\tilde{\phi}$ and $\tilde{\chi}$ in figure 2. This figure shows that only if $1 < \kappa < 3$, $\tilde{\phi}$, $\tilde{\chi}$ behave

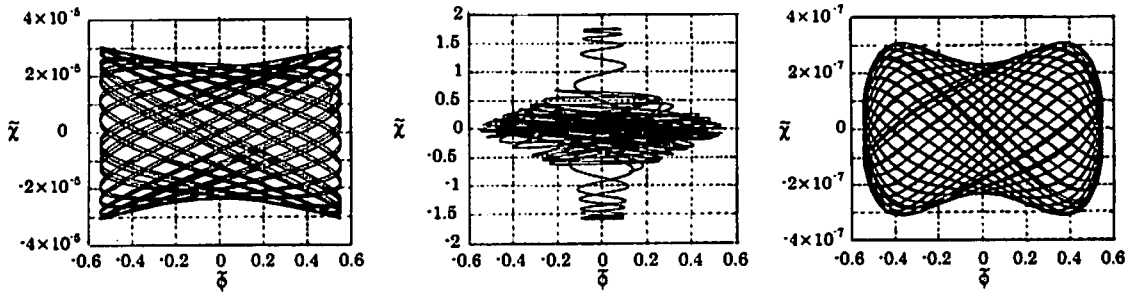

(a) $0 < \kappa \leq 1$ (b) $1 < \kappa < 3$ (c) $3 < \kappa \leq 6.5$

Figure 2: Typical behavior of $\tilde{\phi}$ and $\tilde{\chi}$: (a) $0 < \kappa \leq 1$, (b) $1 < \kappa < 3$, (c) $3 < \kappa \leq 6.5$. The initial value of $\tilde{\chi}$ is $10^{-5} M_p$

chaotically. There are non-chaotic cases in spite of the results of [5], [6]. It is, however, consistent with the results of [5], [6], because the results are same as in case of $\kappa = 2$. This figure also shows that a necessary and sufficient condition for chaotic behavior of $\tilde{\phi}$ and $\tilde{\chi}$ is almost same as that for instability of $\tilde{\chi}$ at $K = 0$ mode, see figure 1.

Figure 3 shows the difference between two cases, one is with the mixing term and the other is without the mixing term. With the mixing term, growth of $\delta\tilde{\chi}$ enhances $\delta\tilde{\phi}$ by the mixing term and growth of

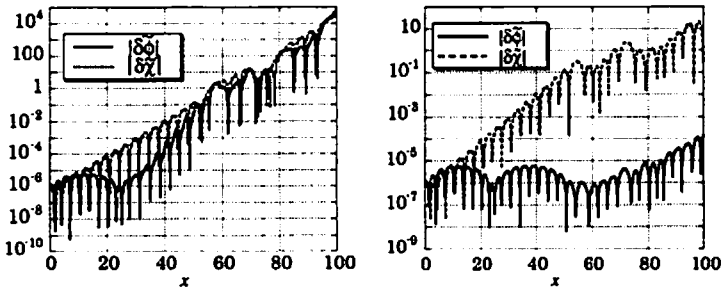

(a) (b)

Figure 3: Typical behavior of $\delta\tilde{\phi}$ and $\delta\tilde{\chi}$ when $\kappa = 2$ and $K^2 = 0.2$: (a) with the mixing term, (b) without the mixing term, where x is the new time variable which is defined as $x \equiv \sqrt{\lambda}\phi_0 \eta$

$\delta\tilde{\phi}$ also enhances $\delta\tilde{\chi}$. In short, growth of $\delta\tilde{\phi}$ and $\delta\tilde{\chi}$ enhance each other by the mixing term. Without the mixing term growth of $\delta\tilde{\chi}$ has no effect on $\delta\tilde{\phi}$. The above enhancements may explain the tachyonic instability. Figure 4 shows that any enhancements, however, do not occur when $\kappa = 3.1$ and $K^2 = 0.1$.

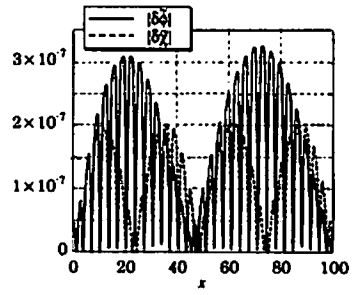

Figure 4: Typical behavior of $\delta\tilde{\phi}_K$ and $\delta\tilde{\chi}_K$ when $\kappa = 3.1$ and $K^2 = 0.1$ with the mixing term

Numerical studies make it clear when the enhancements occur. If and only if κ and K^2 are the values in which $\delta\tilde{\phi}_K$ and $\delta\tilde{\chi}_K$ grow, the enhancements occur. It follows from what has been said that the tachyonic instability does not extend the parametric region where fluctuations will grow.

4 Conclusion

We study the model precisely in which the action is equation (1). Three topics are studied. First we estimate z at the end of inflation. It is confirmed that z is not negligible at the end of inflation and $\sqrt{\langle\chi_i^2\rangle}$ is at most $O(10^{-2})M_p$. Second it is studied whether behavior of $\tilde{\phi}$ and $\tilde{\chi}$ is chaotic in a reheating stage. It is found that if $1 < \kappa < 3$, $6.5 < \kappa < 10$, $\cdots$, then $\tilde{\phi}$ and $\tilde{\chi}$ behave chaotically and if not chaotically their behavior is quasi-periodic in bounded region. The parameter region where $\tilde{\phi}$ and $\tilde{\chi}$ behave chaotically is almost same with that where the fluctuations of $K^2 = 0$ mode grow (see figure 1). We should study further to explain what this difference mean. Third it is studied whether the tachyonic instability occur generally. We interpret the enhancement of the $\delta\tilde{\phi}_K$ and $\delta\tilde{\chi}_K$ growth by the mixing term as the tachyonic instability. In this respect the tachyonic instability does not occur generally in spite of expectation in [4]. It occurs, however, in the parameter region where fluctuations $\delta\tilde{\phi}_K$ and $\delta\tilde{\chi}_K$ are unstable in figure 1. Finally we mention the relation between the chaotic behavior of ϕ and χ and the tachyonic instability. There is the parameter region where the chaotic behavior of ϕ and χ and the tachyonic instability do not coexist. This means that the chaotic behavior is not the necessary condition for the tachyonic instability.

We conclude that the effect of mixing term results in the stronger instability of $\delta\tilde{\chi}_K$ only if $\delta\tilde{\chi}_K$ is unstable and does not expand the parameter region where $\delta\tilde{\chi}_K$ is unstable. It follows from what has said that the mixing term does not make drastic change to the reheating model.

This work was partially supported by a Grant for The 21st Century COE Program (Holistic Research and Education Center for Physics Self-organization Systems) at Waseda University.

References

[1] J. H. Traschen and R. H. Brandenberger, Phys. Rev. D **42**, 2491 (1990).

[2] L. A. Kofman, A. D. Linde, A. A. Starobinsky, Phys. Rev. Lett. **73**, 3195 (1994).

[3] P. B. Green et.al., Phys. Rev. D **56**, 6175 (1997).

[4] D. I. Podolsky and A. A. Starobinsky, Grav. Cosmol. Suppl. **8N1**, 13 (2002).

[5] B. K. Darian, H. P. Künzle, Class. Quantum Grav. **13**, 2651 (1996).

[6] J. D. Barrow, J. Levin, Phys. Rev. Lett. **80** 656 (1998).

[7] Y. Jin, S. Tsujikawa, in preparation

Aichelburg-Sexl boost of Kerr black holes in higher-dimensions

Hirotaka Yoshino[1]

Department of Physics, Graduate School of Science,
Nagoya University, Chikusa, Nagoya 464-8602, Japan

Abstract

We calculate the lightlike boost of the higher-dimensional Kerr black holes. According to recent discussions in the string theory, these solutions have possibilities to describe the gravitational fields around the high-energy fundamental strings. We consider two cases: the boost in the direction parallel to the spin and in the direction transverse to the spin. The resulting spacetime contains a singularity propagating at the speed of light, which is ring or disk-like in the former case and is segment-like in the latter case. We discuss the implication of our results for the black hole formation in accelerators in the brane world scenario.

1 Introduction

The brane world scenario [1] is recently paid much attentions. In this scenario, our 3-dimensional space is the 3-brane in large extra-dimensions and the fundamental Planck energy M_P could be as low as O(TeV). In this TeV-scale gravity, a small black hole becomes higher-dimensional and its gravitational radius is far larger than the four-dimensional gravitational radius with the same mass. This indicates that we might be able to produce black holes in future-planned accelerators [2]. In our previous paper, we investigated the high-energy two-point-particle system and calculated the cross section for the black hole production [3]. We derived that the maximal impact parameter for the black hole production is given by $b_{\max} \simeq 1.5 r_h(p)$, where $r_h(p)$ denotes the gravitational radius of each incoming particle's energy p. We used the lightlike limit of the boosted D-dimensional Schwarzschild black hole for the model of a high-energy particle, where we fixed the energy p in the boosting. The resulting spacetime is flat except for a lightlike point singularity accompanied by a gravitational shock wave which is distributed in the transverse direction of motion. This system was originally developed by Aichelburg and Sexl [4].

In this paper, we would like to consider the lightlike limit of the boosted D-dimensional Kerr black holes. This analysis have two meanings. First, this system might provide the gravitational field around a high-energy particle with spin. Although the spin angular momentum is not the same as the orbital angular momentum, the particle spin would affect the spacetime structure because the sum of the spin and the orbital angular momentum is the conserved quantity. Although the gravitational field around a spinning particle is an unsolved problem, some authors discussed that the Kerr-Newman black hole might provide the classical model for a spinning particle [5], especially motivated by the fact that the gyromagnetic ratio of a Kerr-Newman black hole is exactly the same as that of the Dirac electron. The second meaning, which we consider to be a more natural motivation, is that the Kerr black hole might provide the gravitational field of a fundamental string. In the recent string theory, there are some discussions that some black holes should be regarded as elementary particles [6], or the Kerr black holes are the classical model for the gravitational field of a closed string [7]. If this is the case, the boosted Kerr black holes provide a model for the high-energy string. Hence, we might be able to understand the stringy feature of the black hole formation in the high-energy collisions by analyzing the boosted Kerr black hole systems.

In the boosting of Kerr black hole, we usually fix the mass m and the Kerr parameter a. If we fix the energy p, we should impose $m = p/\gamma \to 0$ and $a = a_0/\gamma \to 0$ in the boost, where a_0 is a constant. However if we assume that the Kerr black hole is the elementary string, a has the same order as the fundamental string scale, which in turn is expected to be the order of the Planck length. Because the gravitational radius of energy $p \simeq$ (few) TeV is similar to the Planck length in the TeV scale gravity, a has the same order as the length that is characteristic to the particle energy. Hence in this case, we should fix both energy p and the Kerr parameter a when we calculate the boost.

[1] E-mail:hyoshino@allegro.phys.nagoya-u.ac.jp

2 Boosting Kerr black holes

The lightlike limit of the Kerr black hole with fixing p and a has been investigated by several authors in four-dimensional case [8], and they found consistent results using different techniques. The resulting metrics of the boost in the direction parallel to the spin and transverse to the spin are represented as follows;

$$ds^2 = -dt^2 + dx^2 + dy^2 + dz^2 + \Phi(\rho)\delta(z-t)(dz-dt)^2, \tag{1}$$

$$\Phi(\rho) = -8p\log\rho + p\theta(a-\rho)\left(8\log\left[\rho/(a+\sqrt{a^2-\rho^2})\right] + 4\sqrt{a^2-\rho^2}/a\right), \tag{2}$$

where $\rho \equiv (x^2+y^2)^{1/2}$ for the parallel case, and

$$ds^2 = -dt^2 + dx^2 + dy^2 + dz^2 + \Phi(y,z)\delta(x-t)(dx-dt)^2, \tag{3}$$

$$\Phi(y,z) = -4p\log\left[(y-a)^2+z^2\right] \tag{4}$$

for the transverse case. The term with δ-function indicates the existence of a gravitational shock wave, and the function Φ, which we call the potential, characterizes the shock wave structure. In the parallel case, the gradient of Φ is discontinuous at $\rho = a$ although Φ is finite everywhere. Hence the shock wave contain a mild ring singularity. In the transverse case, Φ diverges at $(y,z) = (a,0)$. This is almost the same as the boosted Schwarzschild case except for the location of the singularity. We generalize these results for higher-dimensional cases.

First we consider the boost in the parallel direction to the spin. The metric of the higher-dimensional Kerr black hole [9] is given by

$$ds^2 = ds_0^2 + \frac{\mu r^{7-D}}{r^4 + a^2(z^2+\sum_i y_i^2)}\left(dt + \frac{r(x_1dx_1+x_2dx_2)}{r^2+a^2} + \frac{a(x_1dx_2-x_2dx_1)}{r^2+a^2} + \frac{zdz+\sum_i y_i dy_i}{r}\right)^2, \tag{5}$$

where ds_0^2 is the flat metric $ds_0^2 \equiv -dt^2 + dx_1^2 + dx_2^2 + dz^2 + \sum_i dy_i^2$, μ and a are related to the mass m and the angular momentum J as are shown in [9], and r is defined by

$$\frac{X^2}{r^2+a^2} + \frac{z^2+Y^2}{r^2} = 1, \tag{6}$$

with $Y^2 \equiv \sum_i y_i^2$ and $X^2 \equiv x_1^2 + x_2^2$. The ring singularity is rotating in (x_1,x_2)-plane, and the other spatial directions are specified by z and y_i. By boosting in the z-direction and taking the limit $v \to 1$ with fixing a and $P \equiv \gamma\mu$ (or equivalently $p \equiv \gamma m$), we find the metric

$$ds^2 = ds_0^2 + \Phi(X,Y)\delta(t-z)(dt-dz)^2. \tag{7}$$

The function $\Phi(X,Y)$ is expressed by the elliptic integrals, although we don't show explicitly here.

Figure 1 shows the behavior of $\Phi(X,Y)$ for $D = 5,...,8$ in the parallel case. In the case of $D = 5$, the function Φ logarithmically diverges at $X = a$. Hence the shock wave contains a one-dimensional ring-like singularity. For $D \geq 6$, the function Φ diverges at $Y = 0, -a \leq X \leq a$. Hence the singularity is a two-dimensional disk in these cases. This is interpreted as follows: For $D = 5$, the black hole horizon doesn't exist in the resulting spacetime because we fixed a in the boosting. The singularity becomes naked and the potential Φ diverges on the singularity. However for $D \geq 6$, the horizon exists for arbitrarily m and a. Hence the resulting gravitational shock wave contains an extremely oblate horizon and the potential Φ diverges on it. The function Φ behaves like $\log Y$ for $D = 6$, and $1/Y^{D-6}$ for $D \geq 7$. One can understand these behaviors of the potential using a Newtonian analogue. The Newtonian potential of n-dimensional distribution of matter in N-dimensional space is given by $\sim 1/r^{N-n-2}$. Because the shock wave is $(D-2)$-dimensional, the power of the potential Φ and the dimensionality of the singularity have the same relation as the Newtonian gravity.

Next we consider the boost in the transverse direction to the spin. In this case, we span the coordinate as follows:

$$ds^2 = ds_0^2 + \frac{\mu r^{7-D}}{r^4 + a^2\sum_i z_i^2}\left(dt + \frac{r(xdx+ydy)}{r^2+a^2} + \frac{a(xdy-ydx)}{r^2+a^2} + \frac{z_i dz_i}{r}\right)^2, \tag{8}$$

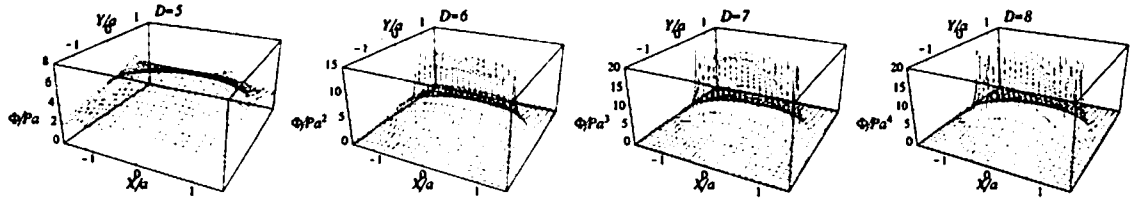

Figure 1: The behavior of the function Φ for $D = 5, ..., 8$ in the parallel case. The unit of X and Y is a, and the unit of Φ is Pa^{D-4}. In the case of $D = 5$, Φ diverges at $Y = 0, X = \pm a$, which indicates that the singularity is a one-dimensional ring. In other cases, Φ diverges at $Y = 0, -a < X < a$. This implies that the singularity is a two-dimensional disk.

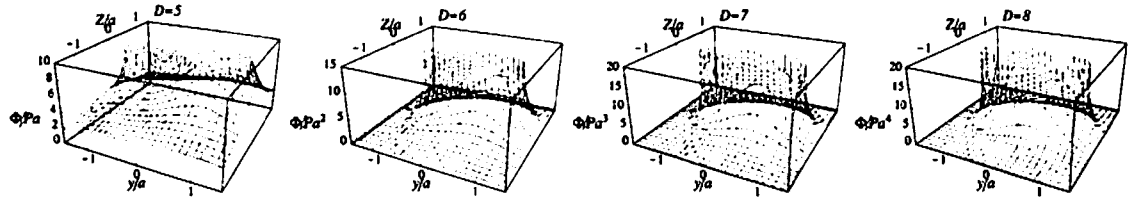

Figure 2: The behavior of the function Φ for $D = 5, ..., 8$ in the transverse case. The unit of y and Z is a, and the unit of Φ is Pa^{D-4}. For all D, Φ diverges at $Z = 0, -a \leq y \leq a$, which indicates that the singularity is a one-dimensional segment.

where $ds_0^2 \equiv -dt^2 + dx^2 + dy^2 + \sum_i dz_i^2$. In this coordinate, the ring singularity rotates in (x, y)-plane, and the other spatial directions are specified with z_i. We boost this metric in the x-direction. The resulting metric becomes

$$ds^2 = ds_0^2 + \Phi(y, Z)\delta(t - x)(dt - dx)^2, \tag{9}$$

where we have set $Z^2 \equiv \sum_i z_i^2$. The function Φ can be expressed in terms of the elementary functions for even D and the elliptic integrals for odd D.

Figure 2 shows the potential Φ of the shock wave in the transverse case. For all D, the potential diverges at $Z = 0, -a \leq y \leq a$. Hence in the transverse case, the singularity is a one-dimensional segment for all $D \geq 5$. This is interpreted as follows: in the boosting, the ring singularity becomes naked for $D = 5$ and the horizon becomes extremely oblate for $D \geq 6$. This singularity or the horizon is infinitely Lorentz-contracted in the direction of the motion. This leads to the segment shape of the singularity in the gravitational shock wave. The behavior of the potential Φ around the singularity is $\sim \log Z$ for $D = 5$, and $\sim 1/Z^{D-5}$ for $D \geq 6$. Similarly to the parallel case, we see that the relation between the potential behavior near the singularity and the dimensionality of the singularity is the same as the Newtonian gravity.

3 Summary and discussion

In this paper, we have investigated the lightlike limit of the boosted Kerr black holes. If we boost the Kerr black hole in the parallel direction to the spin, the resulting spacetime contains a gravitational shock wave which has a ring-like singularity for $D = 5$, and a disk-like singularity for $D \geq 6$. In the case of the boost in the transverse direction to the spin, the resulting gravitational shock wave has a segment-like singularity. The behavior of the potential Φ of the shock wave can be interpreted using the Newtonian analogue. Because there are some discussions that the Kerr black hole might provide the gravitational field of the fundamental string, these solutions have possibilities to be a good model for the high-energy elementary strings in the brane world scenario.

Now we would like to discuss the properties of the black hole formation in the collisions of two lightlike Kerr black holes. Although we have not yet completed the calculation of the apparent horizon for this

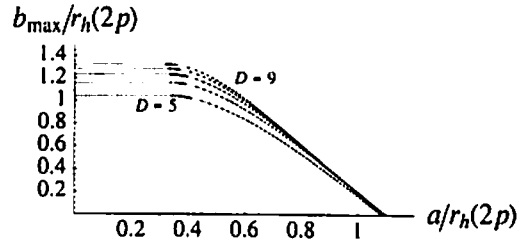

Figure 3: The expected relation between a and the maximal impact parameter $b_{\rm max}$ for the black hole production in the collision of two lightlike Kerr black holes boosted in the parrallel direction to the spin. The unit of axis is $r_h(2p)$. We see that $b_{\rm max} = 0$ in the case of $a \gtrsim r_h(2p)$ for all D.

system, we can discuss the condition for the black hole formation as follows, using the fact that the incoming shock wave has a singularity with characteristic scale a. For some impact parameter b, we write the horizon shape in the case of the two particle collision which is calculated in [3]. Then we draw on it the shape of the singularity of the boosted Kerr black holes with Kerr parameter a. If the singularity crosses the horizon, the apparent horizon would not form for such b and a. Under this assumption, we can calculate the maximal impact parameter of the black hole production as a function of a.

Figure 3 shows the maximal impact parameter $b_{\rm max}$ in the collision of two Kerr black holes which are boosted in the direction of the spin. If the Kerr parameter is small, it doesn't affect the black hole formation. But $b_{\rm max}$ decreases with the increase in a, and becomes zero at $a \sim r_h(2p)$. We can write a similar figure for the case of two lightlike Kerr black holes which are boosted in the transverse direction to the spin. Hence, the condition for $b_{\rm max} \neq 0$ is written as $a \lesssim r_h(2p)$. If the Planck energy is O(TeV) and the string length is $l_s \sim a \sim 1/M_P$, the gravitational radius for the two particle system becomes $r_h(2p) \sim l_s$ if the incoming energy is (few) TeV. Hence the string length might have an effect on the black hole formation. If this is the case, we would be able to determine the string length from the experiment, or whether the gravitational field of the elementary particle is described by the Kerr black hole or not.

References

[1] N. Arkani-Hamed, S. Dimopoulos and G. R. Dvali, Phys. Lett. B **429**, 263 (1998); L. Randall and R. Sundrum, Phys. Rev. Lett. **83**, 3370-3373 (1999).

[2] S. Dimopoulos and G. Landsberg, Phys. Rev. Lett. **87**, 161602 (2001); S. B. Giddings and S. Thomas, Phys. Rev. **D65**, 056010 (2001).

[3] H. Yoshino and Y. Nambu, Phys. Rev. **D67**, 024009 (2003).

[4] P. Aichelburg and R. Sexl, Gen. Rel. Grav. **2**, 303 (1971).

[5] W. Israel, Phys. Rev. **D2**, 641 (1970); C. A. Lòpez, Phys. Rev. **D30**, 313 (1984); J. Kim, J. Korean Phys. Soc. **27**, 479-483 (1994).

[6] A. Sen, Phys. Rev. Lett. **69**, 1006(1992); G. T. Horowitz and A. Sen, Phys. Rev. **D53**, 808 (1996); A. Dabholkar, J. Gauntlett, J. Harvey, and D. Waldram, Nucl. Phys. **B474**, 85 (1996).

[7] A. Burinskii, Phys. Rev. **D52**, 5826 (1995); H. Nishino, Phys. Lett. B359, 77-86 (1995); H. Nishino and S. Rajpoot, Phys. Lett. B540, 125-136 (2002).

[8] C. O. Loustó and N. Sánchez, Nucl. Phys. **B383**, 377-394 (1992); H. Balasin and H. Nachbagauer, Class. Quantum Grav. **11**, 1453-1461 (1994); **12**, 707-713 (1995); **13**, 731-737 (1996); A. Burinskii and G. Magli, Phys. Rev. **D61**, 044017 (2000); C. Barrabès and P. A. Hogan, Phys. Rev. **D67**, 084028 (2003).

[9] R. C. Myers and M. J. Perry, Annals Phys. **172**, 304 (1986).